SHEAR RESISTANCE OF REINFORCED CONCRETE BEAMS WITH AND WITHOUT STEEL FIBRES

by

CHIAM TOU PING
(B.Eng. (Hons))

November, 1981

A thesis presented to the University of Sheffield for the degree of Doctor of Philosophy.


1TL-1
1TLF-1
2TL-1
2TLF-1
3TL-1
3TLF-1
1TL-2
1TLF-2
2TL-2

To my parents

CONTENTS

CHAPTER THREE

CHAPTER FOUR

CHAPTER FIVE

CHAPTER SIX

LIST OF FIGURES

LIST OF TABLES

CHAPTER SIX

CHAPTER SEVEN

CHAPTER NINE

LIST OF PLATES

NOTATIONS

A_f	Fibre cross-sectional area
A_s	Area of tension reinforcement or total area of stirrups crossing shear plane
A_{sv}	Cross-sectional area of the two legs of a link
a_v	Shear span
a_1, a_2	Localization parameters of bar element ends
bd	Area of shear plane
b_w	Breadth of web or rib of a member
b_1,b_2	Localization parameters of bar element ends
C	Compressive force
c	Cohesion
d	Effective depth of beam
d_f	Diameter of fibre
E	Elastic modulus
E_c	Elastic modulus of concrete
E_f	Fibre elastic modulus
E_s	Elastic modulus of steel reinforcement
F	Yield function
f_{bs}	Local bond stress
f_c'	Cylinder compressive strength
f_{ct}	Split cylinder tensile strength
f_{cu}	Cube Strength of concrete
f_t'	Uniaxial tensile strength
f_{tm}	Flexural tensile strength
f_{tw}	Post-cracking tensile resistance of the web
f_y	Yield stress of steel
G	Shear modulus
G_m	Shear modulus of matrix
G_s	Shear transfer stiffness
gd	Distance between stringers

I_1	First stress invariant
J_2	Second invariant of deviatoric stresses
K	Dimensional constant with stress units
K_L	Bond length coefficient
K_o	Effectiveness factor
l_c	Critical fibre length
l_f	Fibre length
M_{Exp}	Experimental ultimate moment of resistance
M_F	Flexural Capacity of beam
N_i	Shape functions
R	Mean interfibre spacing
r	$r = \frac{A_{sv}}{sb_w}$ or $r = \frac{A_s}{bd}$
S	Average fibre spacing
S_e	Effective fibre spacing
s	Spacing of stirrups
T	Tensile Force
ΣU	Bar perimeter
u, v, w	Components of displacement
V, M	Shear force and bending moment at the section considered
V_a	Shear component of the friction and aggregate interlock in the cracked oncrete
V_c	Shear carried by compression zone
V_d	Dowel action of the longitudinal reinforcement
V_{Exp}	Experimenal ultimate shear force
V_f	Fibre volume fraction
V_m	Matrix volume fraction
V_u	Ultimate shear force
V_w	Shear carried by web reinforcement

v	Shear stress transmitted across the crack
v_u	Ultimate shear stress
W_i	Weighting coefficients
w	crack width
x,y,z	Cartesian co-ordinate system
Z	Lever arm
β	Shear retention factor
$\sigma_1,\sigma_2,\sigma_3$	Principal stresses
σ_c	Composite stress
σ_{cu}	Post-cracking tensile strength of fibre concrete
σ_{fu}	Ultimate strength of fibre
σ_m	Matrix stress
σ_N	Externally applied direct stress acting across the shear plane
$\sigma_x,\sigma_y,\sigma_z$	Normal stresses in cartesian co-ordinate system
γ_f	Partial safety factor for load
γ_m	Partial safety factor for strength
$\gamma_{xy},\gamma_{yz},\gamma_{zx}$	Shear strains in the cartesian co-ordinate system
ε_1	Fictitious tensile strain in the direction of normal to crack.
ε_s	Strain in Steel bar
ε_t	Limiting uniaxial tensile strain
ε_u'	Ultimate strain in the uniaxial compression
$\varepsilon_x,\varepsilon_y,\varepsilon_z$	Normal strains in cartesian co-ordinate system
Δs	Shear displacement
ψ	$\psi = \frac{A_{sv}\ fy}{s\ b_w}$
ρ_w	$\rho_w = \frac{A_s}{b_w d}$
λ	Proportionality constant

α	Angle between inclined stirrups and longitudinal axis of member
ν	Poisson's ratio
ϕ	Diameter of main bar
η_o	Orientation factor
η_L	Length efficiency factor
τ	Average fibre-matrix bond strength
τ_R	$\tau_R \simeq 0.035(f_c')^{2/3}$
$\tau_{xy}, \tau_{yz}, \tau_{zx}$	Shear stresses in cartesian co-ordinate system
ξ, η, ζ	Local co-ordinate system of element
$[A]$	Normalized nodal matrix
$[B]$	Strain Matrix
$[C_{mn}]$	Expansion coefficient matrices
$[D]$	Composite material matrix
$[D_c]$	Material matrix of concrete
$[D_s]$	Material matrix of steel reinforcement
$[J]$	Jacobian matrix
$[K]$	Global structural stiffness matrix
$[K_e]$	Concrete element stiffness matrix
$[K^b]$	Bar element stiffness matrix
$[K^{bh}]$	Equivalent hexahedron stiffness matrix of bar element
$[T]$	Transformation matrix
$\{R\}$	Global load vector
$\{\sigma\}$	Stress vector
$\{\Delta\sigma\}$	Incremental stress vector
$\{\varepsilon\}$	Strain vector
$\{\Delta\varepsilon\}$	Incremental strain vector
$\{\Delta\varepsilon\}_e$	Incremental elastic strain vector
$\{\Delta\varepsilon\}_p$	Incremental plastic strain vector
$\{\delta\}$	Displacement vector

Acknowledgement

Foremost, the author would like to thank the University of Sheffield for awarding him the Grouped Scholarship in Engineering and Materials. He acknowledges his gratitude to Prof. D. Bond, former Head of the Department of Civil and Structural Engineering, for allowing him to use the facilities of the department.

The author would like to express his profound thanks to his supervisors, Mr. R. Jones and Dr. R. N. Swamy, for their assistance and guidance throughout the period of the project.

The completion of this work would not have been possible without the assistance of the following people:

a) the technical and clerical staff of the Department of Civil and Structural Engineering,

b) the staff of the Computer Services and

c) the staff of the Applied Science Library.

The consultation and discussion with friends and colleagues had been most useful. In particular, the assistance of Dr. T. A. Ooi and Dr. N. S. Mahmoud is gratefully acknowledged.

Thanks are due to Mrs. Parkes for her efficient typing of the thesis.

The author would like to thank his family for their concern and unfailing encouragement throughout his education in England.

Last but not least, the author would like to express his gratitude and appreciation to Jee for her assistance and encouragement during the course of the research.

SUMMARY

The fabrication and placement of conventional shear reinforcement are time consuming and costly and its use in thin structural concrete members is often impractical. Fibre reinforcement is known to control flexural and shear cracking and can therefore be used to replace conventional shear reinforcement. This investigation consists of experimental and theoretical studies into the use of crimped steel fibres as shear reinforcement in reinforced concrete beams.

Eighteen reinforced lightweight concrete beams with thin web were fabricated and tested under four point loading. The parameters studied were the fibre content, the shear span/effective depth ratio and the amount of main steel. Subsidiary tests on concentric pull-out specimens and shear transfer specimens were carried out to study the influence of steel fibres on the bond stress-slip characteristics of a deformed bar (Tor Bar) and the stiffness and ultimate strength of the shear transfer mechanism across a definite plane respectively.

The inclusion of fibres increased the ultimate strength of the beams by 63 to 211.5%. Fibre concrete beams had more flexural and shear cracks and showed substantially greater ductility at failure than their plain concrete counterparts. The fibres in the pull-out specimens were effective in controlling the splitting cracks and transforming a sudden bond failure into a gradual one. The fibres increased the ultimate shear strength of the shear transfer specimens by 9.9 to 101.8%. The stiffness of the shear transfer mechanism was not, however, significantly affected.

A simple approach based on the Standard Method of the CEB-FIP Model Code is proposed to determine the ultimate shear resistance of fibre reinforced concrete beams. It predicts adequately the ultimate shear strength of steel fibre reinforced

concrete beams.

A nonlinear 3-dimensional finite element model was developed to predict the entire structural response up to failure of both plain and fibre reinforced concrete beams subjected to short-term monotonically increasing loading. The concrete is represented by 8-node isoparametric hexahedra and the tension steel by bar elements. The finite element model predicts satisfactorily the structural behaviour of both plain and fibre reinforced concrete beams.

CHAPTER ONE

INTRODUCTION

1.1 Introduction

Recent developments in analysis, design and construction have resulted in the tendency to use more slender structures which possess lower factors of safety. This demands properties of materials other than strength and requires greater flexibility and stability of not only the material but also of the structure as a whole. The engineer is therefore constantly engaged in the search for new materials and improved methods of utilising existing materials.

The trend towards slender concrete structures and the increasing scarcity of good quality natural aggregates have led to the use of structural lightweight aggregates. These aggregates are made artificially by expanding, foaming or sintering clays, shales and slate or industrial by-products such as pulverised fuel ash and blast furnace slag. There is considerable evidence to show that structural lightweight concrete is a technically sound material with good structural behaviour. It offers the benefits of lighter weight and lower elastic modulus in seismic conditions and it reduces the susceptibility to thermal effects. However, it generally has higher creep and shrinkage, greater deflection and lower tensile strength than normal weight concrete.

Plain concrete has some inherent limitations. It has low tensile strength, limited ductility and low resistance to crack control. The need to improve these inherent weak properties has led to the development of fibre reinforced concrete. The concept of using fibres to reinforce weak and brittle matrices is not new. The use of straw in sun-dried mud bricks and heavy walls and that of horse hair or sisal in gypsum plaster have been

known for many centuries. The use of fibre reinforcements in cement-based matrices is however relatively new. Many types of materials have been used as fibre reinforcement to brittle cement matrices, such as asbestos, glass, ceramics, polymers, etc, but the one type of fibre which has found considerable application in mortar and concrete is steel.

In the last twenty years or so, much attention has been given to the material side of fibre reinforced concrete technology. It is now well established that the inclusion of fibres in concrete improves the tensile strength, ductility, energy absorption and crack control characteristics of the matrix. The fibres arrest any advancing cracks by applying pinching forces at the crack tips, thus delaying their propagation across the matrix, and creating a distinct slow crack propagation stage (1).

Research into the structural behaviour of fibre reinforced concrete is comparatively scarce and therefore the need to carry out investigations in this direction cannot be overemphasised. The limited experimental data indicate the potential of steel fibres for structural applications. Investigations on the flexural behaviour of reinforced concrete beams have shown that the presence of steel fibres improves the ultimate strength, stiffness, ductility and resistance to cracking. Tests on reinforced concrete beams and slab-column connections have also shown the effectiveness of steel fibres as shear reinforcement.

The use of steel fibres as shear reinforcement in thin structural members is attractive. In such members, conventional stirrups will be difficult to place and often impractical. Furthermore, a better alignment of the fibres in the principal tensile stress direction may be achieved in members with thin webs.

The use of slender structures with low safety factors demands a sound knowledge of the internal structural behaviour of such structures. In the case of reinforced concrete, this requirement often can be met only if the nonlinear response of the structure can be traced throughout its entire load range. The finite element method has been shown to be capable of this type of analysis.

1.2 Purpose and Scope

The research programme is divided into two parts: experimental studies and theoretical studies.

1.2.1 Experimental Studies

To date, there is no reported investigation on the use of steel fibres as shear reinforcement in lightweight concrete beams. Because of the reduced modulus of elasticity and lower tensile strength of lightweight concrete, the effect of adding a relatively high modulus fibre, such as steel, on the strength and deformation characteristics may be more pronounced than for normal weight concrete. Therefore the purpose of the main experimental investigation is to assess the effectiveness of steel fibres as shear reinforcement in lightweight concrete beams.

Eighteen full size I -beams were cast and tested under four point loading system. The parameters studied were the fibre percentage, amount of tension reinforcement and the shear span/ effective depth ratio. The deflection at mid span, end rotations, steel strains and concrete strains of all the beams were measured at various stages of loading.

Conventional stirrups slow the propagation of a splitting crack and keep this crack width small, thus delaying

the degeneration of the bond at the interface between deformed steel reinforcement and concrete. If surplus stirrups are present, ultimate bond stress is increased. If, however, stirrups are simply adequate for the expected shear, ultimate bond strength is little influenced, although toughness is considerably improved (2). A subsidiary experimental investigation was therefore carried out to study the effect of steel fibres on the ultimate bond strength and the bond stress-slip relations at the interface between a deformed bar and concrete. The bond stress-slip relations obtained will be useful in analytical studies of reinforced concrete structures.

Concentric pull-out specimens with short embedded length were cast and tested under a constant rate of loading. The applied load and the endslip were monitored continuously during each test. The main parameters studied were concrete type, fibre type, fibre percentage and cover to reinforcing bar. The reinforcing bar was a 16 mm diameter deformed bar (TorBar).

Another subsidiary experimental investigation was carried out to study the effect of steel fibres alone or in conjunction with conventional stirrups on the shear transfer across a definite plane. Tests were carried out using both initially uncracked and precracked push-off specimens. The parameters studied were the concrete type, fibre percentage, and amount of conventional stirrups. The reasons for carrying out this investigation are twofold:

1. To provide information on the stiffness of the shear transfer mechanism across a crack. This information will be useful in analytical studies of reinforced concrete structures.
2. Because of the greater efforts generally required in mixing,

placing and compacting fibre reinforced concrete, its structural application may be more appropriate in precast construction. In such constructions there are instances where shear transfer across a definite plane must be considered in the design (3, 4).

1.2.2 Theoretical Studies

The objectives of the theoretical studies are:

1. To derive a simple method which can adequately predict the ultimate shear strength of fibre reinforced concrete beams.
2. To formulate an analytical model which can adequately predict the entire structural response up to failure of both plain and fibre reinforced concrete beams subjected to monotonically increasing loading.

A method based on the Standard Method of the CEB - FIP Model Code (5) was proposed to meet the first objective. The accuracy of the proposed method was studied using results obtained from the main experimental investigation of this research and from test data of other investigators.

The second objective was met by adopting a 3-dimensional nonlinear finite element model for reinforced concrete. The model takes into account material nonlinearity arising from tensile cracking of concrete, yielding of concrete, crushing of concrete or yielding of main reinforcement or a combination of two or more of these effects. The accuracy of the model was checked against the test results of the present main experimental investigation and those reported by Bahia (6).

1.3 Layout of Thesis

Chapter 2 gives a general review of the mechanics of fibre reinforced concrete, past research into the use of steel fibres as shear reinforcement in reinforced concrete beams, and

the behaviour and methods of analysis of reinforced concrete beams with and without conventional web reinforcement failing in shear.

In Chapter 3 the properties of the materials used in the experimental investigations are given. The mix proportions used are also presented. The influence of steel fibres on the material properties of concrete are discussed.

The experimental studies are reported in Chapters 4, 5 and 6. The bond tests are presented in Chapter 4 and the shear transfer tests are given in Chapter 5. Chapter 6 is devoted to the main experimental investigation. The strengths of the plain concrete beams obtained experimentally and analytically using the methods given in several structural codes were compared. A simple method based on the Standard Method of CEB-FIP Model Code (5) was proposed to analyse the ultimate shear strength of fibre reinforced concrete beams. The accuracy of the method was checked using the results of the present investigation and those of other investigators.

Chapters 7, 8 and 9 deal with the analytical study using the finite element method. The finite element model adopted is described in Chapter 7. The computer program is briefly described in Chapter 8. The accuracy of the finite element model is reported in Chapter 9.

In Chapter lO the limitations, general conclusions and suggestions for future work are presented.

CHAPTER TWO

LITERATURE SURVEY

2.1 Introduction

In this chapter, the main literature survey is reported. First a review of the mechanics of fibre reinforced concrete is given. This is followed by a review of the past research into the use of steel fibres as shear reinforcement in reinforced concrete beams. Finally, a review of the behaviour and strength of reinforced concrete beams with and without conventional web reinforcement failing in shear is presented. Some methods of analysis of the shear strength of these beams are also given.

2.2 Fibre Reinforced Concrete

2.2.1 Introduction

Fibre reinforced concrete can be defined as concrete made from hydraulic cements containing fine or fine and coarse aggregate and discontinuous discrete fibre reinforcements (7). Fibres that are currently being investigated as reinforcement for concrete include steel, glass, polymer, carbon, mineral wool and natural vegetable.

Concrete is inherently weak in tension and possesses limited ductility and little resistance to cracking. The concept of fibre reinforcement is to use the deformation of the matrix under stress to transfer load to the fibres. The fibres act as crack arrestors and slow down the propagation of the cracks across the matrix. Consequently the ultimate cracking strain of the composite is increased to many times greater than that of the unreinforced matrix. The fibres impart to the composite qualities of crack control, toughness, ductility and impact resistance.

Because of their high tensile strength and elastic modulus, and adequate durability (8, 9), steel fibres are best suited for structural applications. They may be plain, crimped, duoform or hooked amd have either round or rectanular cross-section. Their length and aspect ratio (i.e, length/diameter or equivalent diameter) generally range from 20 to 65 mm and from 40 to 150 respectively.

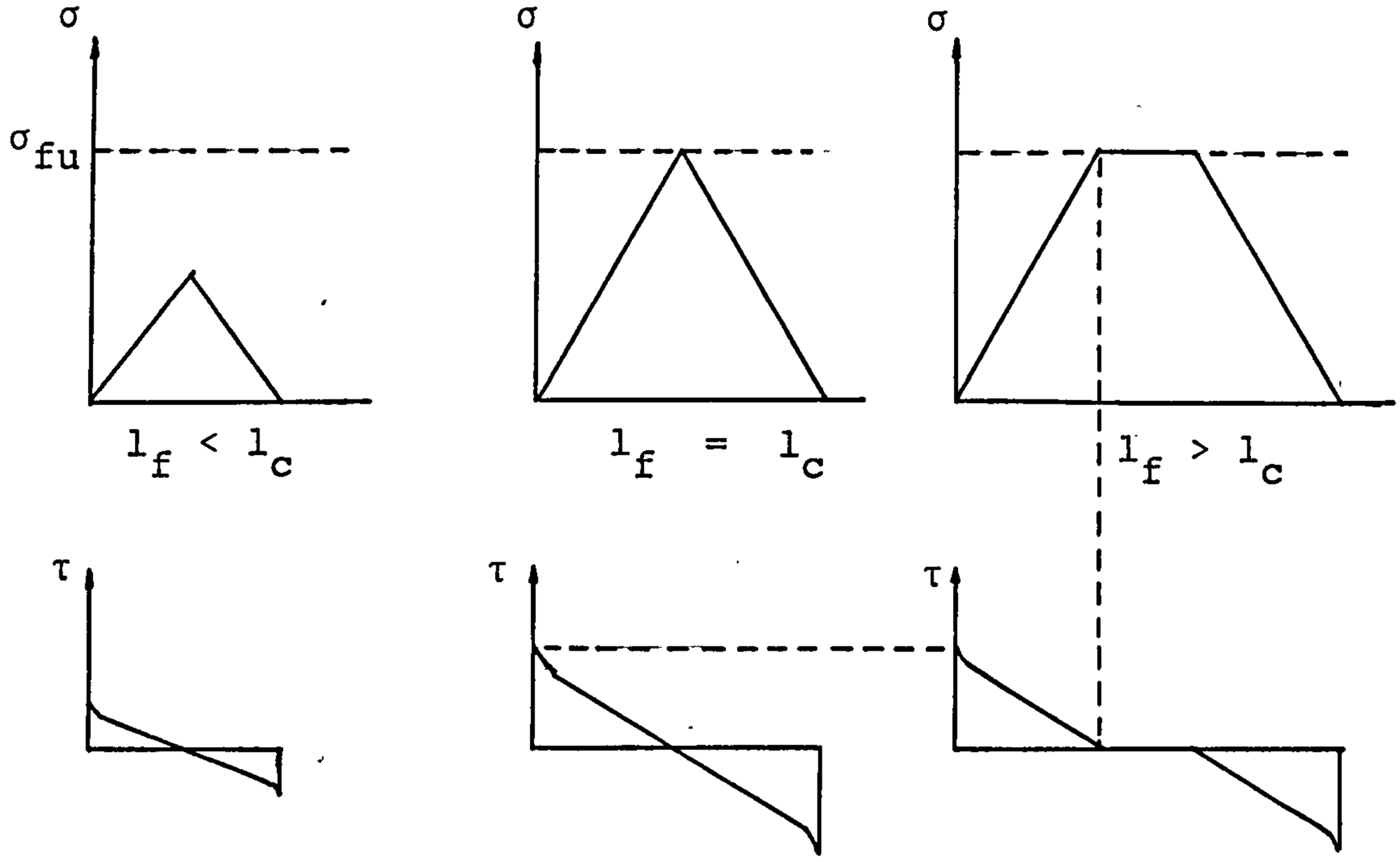

Fig. 2.1 Schematic Variation of Interfacial Shear Stress and Fibre Tensile Stress

2.2.2 Critical Fibre Length and Efficiency Factors

2.2.2.1 Critical Fibre Length (l_c)

Failure in fibre reinforced concrete occurs either by the simultaneous yielding of fibres and matrix or by fibre-matrix interfacial bond failure. The length of the fibre determines the mode of failure of the composite. If the fibre length is greater than the critical length, fibres will yield at the failure of the composite and if it is less than the critical length, composite failure will occur by fibre pull-out.

The stresses in fibres with length greater than, equal to and less than the critical value and the corresponding interface shear stresses are shown in Fig. 2.1. The critical fibre length l_c can be established from equilibrium consideration, and can be shown to be

$$l_c = \sigma_{fu} \cdot \frac{d_f}{2\tau} \qquad (2.1)$$

where σ_{fu} = the ultimate strength of the fibre

d_f = the diameter of the fibre, and

τ = the average interfacial shear stress.

2.2.2.2 Orientation Factor (η_o)

The orientation factor η_o describes the effect of fibre orientation on the composite strength. With discrete randomly orientated fibres only those fibres which are parallel or nearly parallel to the tensile stress trajectories are effective in strengthening the composite.

Romualdi and Mandel (10) have demonstrated that for the case of randomness in which the fibres can be orientated in any direction with equal probability, the orientation factor is 0.41.

2.2.2.3 Length Efficiency Factor (η_L)

The length efficiency factor η_L describes the effect of the fibre length on the efficiency of the reinforcement i.e., takes into account the variation of the fibre tensile stress along its length. Various values have been suggested for this correction term.

Cox (11) has proposed a value

$$\eta_L = 1 - \frac{\tanh\left(\beta \frac{l_f}{2}\right)}{\left(\beta \frac{l_f}{2}\right)} \qquad (2.2)$$

where

$$\beta = \left[\frac{2\pi \, G_m}{E_f A_f \ln(\frac{2R}{d_f})} \right]^{\frac{1}{2}}$$

l_f = fibre length

E_f = fibre elastic modulus

G_m = shear modulus of matrix

A_f = fibre cross sectional area

and R = mean interfibre spacing.

Krenchel (12) has used a value

$$\eta_L = 1 - \frac{l_c}{l_f} \qquad (2.3)$$

Laws (13) has suggested the following values for length efficiency factor:

$$\eta_L = \frac{l_f}{2l_c} \qquad \text{if } l_f < l_c \qquad (2.4)$$

$$\eta_L = 1 - \frac{l_c}{2l_f} \qquad \text{if } l_f > l_c \qquad (2.5)$$

2.2.3 Composite Mixture Rule for Fibre Concrete

For continuous fibres the basic composite mixture rule gives

$$\sigma_c = \sigma_m V_m + \sigma_f V_f \qquad (2.6)$$

where σ_c - composite stress

σ_m - matrix stress

σ_f - fibre stress

V_m - matrix volume fraction

V_f - fibre volume fraction

In the case of a discontinuous fibre composite, the length efficiency factor and the orientation factor have to be introduced into the mixture rule as follows:

$$\sigma_c = \sigma_m V_m + \eta_o \eta_L \sigma_f V_f \quad (2.7)$$

where η_o - orientation factor

η_L - length efficiency factor

2.2.4 Fibre-Matrix Interfacial Bond Stress

For a discontinuous fibre composite, the fibre-matrix interfacial bond stress is of critical importance in determining the composite strength.

With steel fibres the bond is a combination of adhesion and friction and mechanical interlocking, although some chemical interaction could also occur due to surface reactions (14). Because of the complex nature of the interfacial bond and its dependency on many parameters, a true assessment of the bond strength is difficult if not impossible. Nevertheless, there are various direct and indirect methods which can be used to determine the approximate bond strength in a fibre composite.

In the direct methods, a single fibre model or a group of fibres embedded in a block of the matrix material is used. The matrix is either in compression or tension depending on the test system used. The value of the bond strength is calculated directly from the measured failure load. Many researchers have used the single or group model to determine the fibre-matrix interfacial bond strength (15, 16, 17, 18) and typical values obtained are tabulated in Table 2.1. The large scatter of test results generally associated with such tests can be seen from the table. It must be noted that apart from the properties of the matrix and fibre geometry, the bond strength is also influenced by the proximity of adjacent fibres and the consequent stress distribution in the matrix between fibres. Thus some of the exceedingly high pull-out bond values reported (for example in

Table 2.1 Steel Fibre-Matrix Interfacial Bond Strength

Matrix	Fibre Type	Fibre Diameter mm	Embedded Length mm	Mean Bond Strength N/mm^2	Method	Ref No
Mortar	Plain	0.30	13.7	4.17 (22.4)†		
Mortar	Indentations	0.50	12.5	8.10 (20.4)		
Mortar	Hooked ends	0.40	21.8	4.93 (28.1)	Direct	(15)
Mortar	Weak crimped	0.35	15.2	5.23 (22.5)		
Mortar	Heavy crimped	0.40	12.0	13.40 (2.6)		
Mortar	Enlarged ends	0.3x0.4	6.0	7.27 (20.0)		
Mortar	Brass coated	0.38	51.0	2.21 (25.8)	Direct	(16)
Mortar	Plain	0.38	17.5	1.24		
Mortar	Duoform	0.38	17.5	6.94	Direct	(17)
Mortar	Looped end	0.38	17.5	>9.38		
Cement Paste	Plain	0.38	17.5	2.48		
Concrete	Plain	-	-	3.57* 4.15**	Indirect	(20)

Note: † Figures in brackets are coefficients of variation in %
* First crack
** Failure

Ref (17)) may not be reflected in the flexural or tensile strength of the composites made with such fibres.

In the indirect methods, the bond strength value is obtained from the material properties of the composite material. Aveston et al (19) calculated the interfacial bond stress from crack spacing and obtained a bond strength of 6.8 N/mm^2 for continuous steel fibre reinforced cement paste and bond values ranging from 6.0 to 10.6 N/mm^2 for discontinuous steel fibre reinforced cement paste. The point to be noted here is that cracking is a random phenomenon and wide variations in crack spacing and crack width could be obtained under apparently similar conditions.

Swamy and Mangat (20) analysed the results of their own flexural tests and those of other investigators by using a combined crack arrest-composite material theory to obtain quantitative values for the bond strength in plain steel fibre composites at first crack and at ultimate load. The bond strength was found to be 3.57 N/mm^2 at first crack and 4.15 N/mm^2 at ultimate load. In a subsequent paper (21) they analysed the results for individual groups of tests and obtained interfacial bond strength values ranging from 2.0 to 5.30 N/mm^2. They observed that there is a progressive reduction in the bond strength as the size of the aggregate inclusion increases.

2.2.5 Fibre Strengthening Mechanisms

Two approaches have been proposed to explain the behaviour of fibre reinforced concrete. One is based on the spacing concept and the other the composite material concept.

2.2.5.1 Spacing Concept

The mechanism of fibre reinforcement of cement materials

was first explained by Romualdi and Batson (22, 23). Based on crack arrest action by the fibres and linear elastic fracture mechanics concept, they showed that the first crack tensile strength was inversely proportional to the geometrical spacing of fibres for a given fibre volume content. Romualdi and Mandel (10) subsequently showed that the results of closely spaced wires could be achieved by mixing short discrete fibres directly into the matrix. Variations in spacing were accomplished by varying fibre diameter in accordance with the following expression for geometric fibre spacing,

$$S = 13.8\, d_f \sqrt{\frac{1.0}{V_f}} \qquad (2.8)$$

where S = average fibre spacing.

In deriving the above equation Romualdi and Mandel (10) took into account the overlapping effect of the fibres but the bond deficiency of short fibres was ignored. They further assumed that the shear forces at the fibre-matrix interface are absent until the occurrence of a crack, when the additional concrete displacement caused by the extensional strains in the vicinity of the crack cause a distribution of shear forces along the fibre that act to close the crack. This assumption is valid for long, continuous fibres where the shear stress distribution in the absence of a crack extends only up to half the critical length from each end of the fibre, leaving the rest of the fibre length free from any shear stresses. It is, however, not valid for short fibres where the shear stresses distribution in the absence of a crack extends along the whole length of the fibre.

Kar and Pal (24) considered the bond deficiency of short fibres and derived the following expression for the effective fibre spacing

$$S_e = 8.85\, d_f \sqrt{\frac{1.0}{V_f\, \eta_o \frac{l_f}{K_1 d_f} \left(1 - \frac{l_f}{3K_1 d_f}\right)}} \qquad (2.9)$$

where S_e = effective fibre spacing

η_o = average orientation factor

K_1 = bond length coefficient

However, the shear stress distribution at the fibre-matrix interface in the absence of a crack was overlooked. The effective fibre spacing was correlated to the ultimate tensile strength.

By considering the interfacial bond stress distribution due to load transfer and the presence of a crack and taking into account the bond deficiency by introducing bond efficiency factors for both the length and diameter of fibres, Swamy et al (1) proposed an effective spacing equation of the form:

for first crack modulus of rupture

$$S_e = 27 \sqrt{\frac{d_f}{V_f\, l_f}} \qquad (2.10)$$

for ultimate modulus of rupture

$$S_e = 25 \sqrt{\frac{d_f}{V_f\, l_f}} \qquad (2.11)$$

The randomness of the short fibres was taken by considering an orientation factor of 0.41.

2.2.5.2 Composite Materials Concept

Shah and Rangan (25) analytically predicted the reinforcing action of fibres by using the composite materials approach based on knowledge of the properties of individual components.

Swamy et al (1) adopted a combined crack control-composite mechanics approach to predict the first crack modulus of rupture and the ultimate modulus of rupture of concrete reinforced with randomly orientated short discontinuous fibres. When the composite strain exceeds the cracking strain of the matrix, first crack in the composite occurs . On further loading, the stiffer fibres act as crack arrestors and a period of slow crack propagation with progressive debonding of fibres occurs. Final composite failure occurs simultaneously due to unstable crack propagation and bond failure.

The derived equation for the flexural strength of the composite takes the general form

$$\sigma_c = A\sigma_m (1 - V_f) + 0.82 \tau V_f \frac{l_f}{d_f} \qquad (2.12)$$

where σ_c = stress in the composite

σ_m = flexural strength of the unreinforced matrix

and A = constant.

From regression analysis of their own test results and of other investigators, Swamy et al obtained the following equations:

for the first crack modulus of rupture

$$\sigma_c = 0.843\ \sigma_m(1 - V_f) + 2.93\ V_f \frac{l_f}{d_f} \qquad (2.13)$$

for ultimate modulus of rupture

$$\sigma_c = 0.97\ \sigma_m\ (1 - V_f) + 3.41\ V_f \frac{l_f}{d_f} \qquad (2.14)$$

2.2.6 Practical Applications of Fibre Reinforced Concrete

There have been significant worldwide applications of steel fibre reinforced concrete since the renewal of interest in this field in the 1960's (7, 8, 14, 26, 27). It has been used

in pavement and airfield construction, marine applications, heavy duty floors, pipes, thin wall sections, refractory concrete, rock stablization and underground applications such as tunnel lining.

2.3 Steel Fibres as Shear Reinforcement in Beams

The use of steel fibres in concrete can be considered not only as a way to improve the properties of the concrete itself but also as a way to replace conventional reinforcement. In the latter context, a limited amount of experimental data is now available on the feasibility of using steel fibres to replace conventional shear reinforcement in concrete beams.

2.3.1 Batson, Jenkins and Spatney's Tests (28)

They pointed out that steel fibres have two advantages over vertical stirrups or bent-up flexural steel. First the fibres are randomly distributed through the volume of the concrete at much closer spacing than can be obtained by the smallest reinforcing rods. Secondly, the first crack tensile strength and the ultimate tensile strength are increased by the steel fibres.

To determine the effectiveness of steel fibres as web reinforcement, they carried out tests on 96 rectangular mortar beams. The beams were 100 mm wide x 150 mm deep and 1980 mm long, and were tested in flexure under two point loading on a simple span. The main variables were the types of steel fibres (round, flat and crimped), percentages of fibres (0.22, 0.44, 0.88, 1.76 and 2.88) and the shear span/effective depth ratio.

The main conclusions of their investigation were that the replacement of vertical stirrups by steel fibres provided effective reinforcement against shear failure and that the shear span ratio at which shear failure was possible decreased with increasing fibre content.

2.3.2 Williamson and Knab's Tests (29)

With the objective of determining the effectiveness of steel fibres as shear reinforcement in full scale structures, Williamson and Knab carried out tests on four full scale rectangular beams. The dimensions of the beams were 305 x 546 x 7010 mm. One beam was fabricated without shear reinforcement, one beam contained stirrups as shear reinforcement and two beams were made with 1.5% by volume of steel fibres as shear reinforcement.

They reported that the steel fibres increased the shear strength of the concrete by 39% over the beam unreinforced in shear. They observed that the steel fibres were not effective in preventing catastrophic shear failures and that the load-deflection relationships of the steel fibre concrete beams were similar to the beams with stirrups.

2.3.3 La Fraugh and Moustafa's Tests (30)

They carried out tests on ten small scale rectangular beams and six full scale T-beams. Percentages by volume of steel fibres used were 1.0 and 1.5 and fibre type included melt extract, duoform, crimped and round fibres.

They reported that a dramatic improvement in ultimate capacity of beams containing steel fibres was observed over the performance of beams without any web reinforcement. Also the beams containing steel fibres sustained greater loads than the conventional beam without web reinforcement before cracking. They found that crack widths were significantly less in fibre concrete beams and that the use of steel fibres in conjunction with welded wire fabric stirrups produced the best results. The latter was attributed to the fact that the presence of the stirrups helped in developing the full strength of the fibre concrete in shear by bridging the areas where less fibres may have been

present and which would have triggered earlier failure. They concluded that steel fibres can be used to produce beams with thinner webs resulting in overall weight savings.

Finally they proposed a design method for fibre concrete as shear reinforcement in flexural members identical to the ACI-318-71 Code Recommendations for lightweight concrete.

$$v_u = 0.28 f_{ct} + 2500 \frac{A_s}{bd} \frac{V_d}{M} \qquad (2.15)$$

w

where v_u = nominal shear stress of steel fibre concrete

f_{ct} = split cylinder tensile strength

b_w = width of beam

d = effective depth

V, M = shear force and bending moment at the section considered.

2.3.4 Bahia's Tests (6)

He carried out three series of specialized beam like tests to study the fundamental shear transfer mechanism in fibre reinforced concrete T-beams and a series of full T-beam tests to study the use of steel fibres as shear reinforcement to replace fully or partially conventional vertical stirrups. The main variables were fibre content (0 to 1.2% by volume), percentage of main steel (1.95, 3.05 and 4.0%) and amount of conventional web reinforcement (rfy = 0, 0.54, 0.83 N/mm^2). The fibre type used was 0.5 x 50 mm crimped steel.

Some of the main conclusions were:

1. The effect of fibres was dominant after cracking. The fibres preserved the stiffness of the beams to carry higher loads with ductility until complete collapse
2. The distribution of the contribution of shear components at ultimate load was in the proportions:

Concrete Compression zone = 55 - 60%

Combined dowel action and

aggregate interlock = 40 - 45%

3. In fibre concrete beams with web reinforcement, although the shear strength increased by 27.2% as rfy value increased from 0 to 0.83 N/mm^2, there was a transfer of forces from fibres to stirrups at failure.

4. The performance of steel fibre reinforcement in resisting shear appeared to be better than in flexure.

2.3.5 Muhidin and Regan's Tests (31)

They reported tests on a series of twenty-five simply supported I-section beams. Three of the beams were without web reinforcement, four had conventional stirrups amd the remaining eighteen were reinforced with duoform fibres. The main variables were the percentage of fibre reinforcement (0 - 3.0% by volume), the aspect ratio of the fibres (62.5, 80 and 93.8), the concrete cube strength (25 - 75 N/mm^2), the shear span/effective depth ratio (3.24 and 4.68) and the web breadth.

It was observed that the beams without shear reinforcement failed soon after the appearance of web shear cracks. But those with stirrups or fibre reinforcement sustained higher loads and developed similar crack patterns. There was an increase in shear strength with high strength concrete butthe rate of increase was small. The reduction of the web thickness from 70 to 30 mm caused an increase of nominal shear stress of about 38%. This was attributed possibly to a better alignment of fibres in the direction of principal stresses and to the higher relative contribution from the compression zone. Finally there was an increase in strength as the aspect ratio of the fibres increased

for low percentage by volume.

The Refined Method of the European code for concrete structures (5) was adapted to predict shear strength of fibre reinforced beams. The proposed method of analysis based on truss analogy takes the form:

$$V_u = V_w + V_c \qquad (2.16)$$

$$V_w = 0.9 f_{ct}\, b_w d \cot\theta \qquad (2.17)$$

$$f_{tw} = 0.125\, V_f \cdot \frac{l_f}{d_f} \left(1 + 0.57 \frac{l_f}{b_w}\right) \sqrt{f_{cu}} \qquad (2.18)$$

$$\cot\theta = 1 + 0.25 \sqrt{f_{cu}} / f_{ct} \qquad (2.19)$$

$$V_c = 0.2 \sqrt{f_{cu}}\, b_w d \quad \text{when } V_w = 0 \qquad (2.20)$$

$$V_c = 0 \quad \text{when } V_w \geq 0.6 \sqrt{f_{cu}}\, b_w d$$

and V_c varies linearly between these values.

In the above equations

V_u = ultimate shear strength

V_w = shear force carried by truss action in web (inclined concrete struts + fibre reinforcement)

V_c = shear forces carried by the compression flange

f_{tw} = post-cracking tensile resistance of the web

θ = inclination of web compression diagonals

and f_{cu} = cube strength of concrete.

The above method was proposed for the analysis of duoform fibre reinforced normal weight concrete beams. The

applicability of the method to other types of steel fibre reinforced concrete beams has not been demonstrated. Equation (2.19) must be used with caution as it can give strut inclinations less than the inclination of the line joining the point load to the support. Furthermore, the final form of equation (2.19) was obtained from experimental data on initially cracked plain normal weight concrete push-off specimens and hence it is not applicable to lightweight concrete beams.

2.4 Behaviour and Strength of Reinforced Concrete Beams With and Without Conventional Web Reinforcement Failing in Shear

Many approaches have been proposed for the analysis of reinforced concrete beams subjected to shear. These approaches can be classified into three categories:

1. Empirical methods
2. Semi-empirical methods
3. Methods based on physical models.

A detailed survey of the various approaches is beyond the scope of the present work. Such appraisal can be found in many references (32, 33, 34, 35). Instead a brief review of the behaviour of reinforced concrete beams failing in shear and some of the methods of analysis of the shear strength of these beams is given in the following sections.

2.4.1 Modes of Inclined Cracking and Shear Failure

Shear failures of reinforced concrete beams are characterized by the formation of inclined cracks. These cracks develop at approximately mid-depth when the tensile principal stresses become greater than the tensile strength of the concrete. They may either appear suddenly in regions where there is

no flexural cracking, or, as it is often the case, they may develop as extensions of previously developed flexural cracks. The first type of inclined crack is often referred to as a "web shear crack" and the second type is often identified as "flexural-shear crack". The two types of cracks are shown in Fig. 2.2.

In addition to the primary cracks (flexural and the two types of inclined cracks), secondary cracks often result from splitting forces developed by the deformed bars when slip between concrete and steel reinforcement occurs, or from dowel action of the longitudinal bars.

The manner in which inclined cracks develop and grow and the type of failure that subsequently develops are strongly dependent on the relative magnitudes of the shear and flexural stresses. These are in turn dependent on several variables including the geometry of the beam, the type of loading, the amount and arrangement of reinforcement, the type of steel and the interaction between steel and concrete (32). The principal failure modes of rectangular beams in shear are shown in Fig. 2.3. Typical modes of shear failure in I-beams are shown in Fig.2.4.

In slender beams ($\frac{a_v}{d} > 2.5$ to 3) without web reinforcement, failure occurs soon after the formation of the inclined cracks. For short beams ($\frac{a_v}{d} < 2.5$ to 3) it leads to additonal shear strength due to arching action.

In beams with web reinforcement it has been observed that the web reinforcement has little effect on the load at which inclined cracking first occurs. But once inclined cracking has started, the web reinforcement begins to deform gradually as the load increases, until it yields. Yielding does not cause the failure of a member except if the member has only a small amount of web reinforcement.

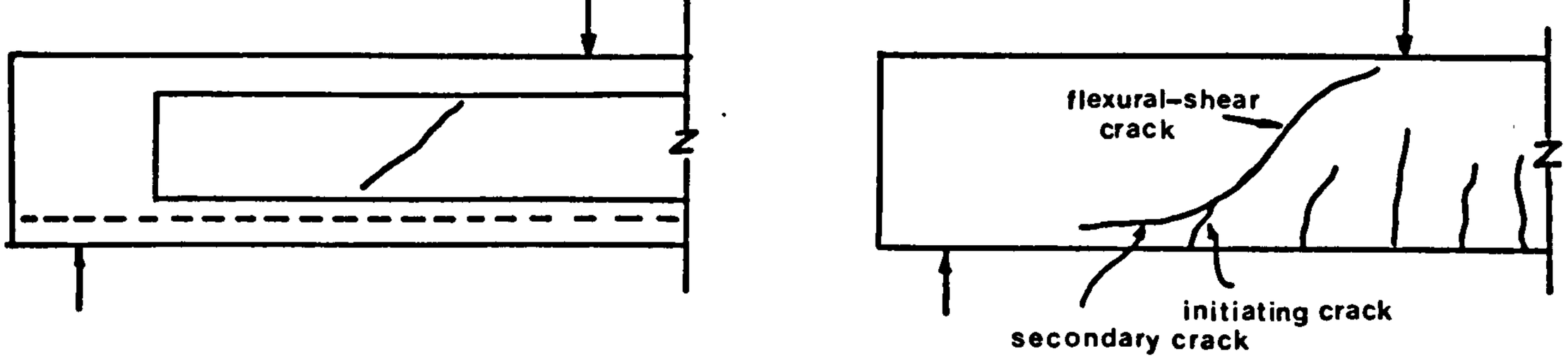

WEB SHEAR CRACK

FLEXURAL-SHEAR CRACK

FIG·2·2 TYPES OF INCLINED CRACKS(AFTER REF.(32))

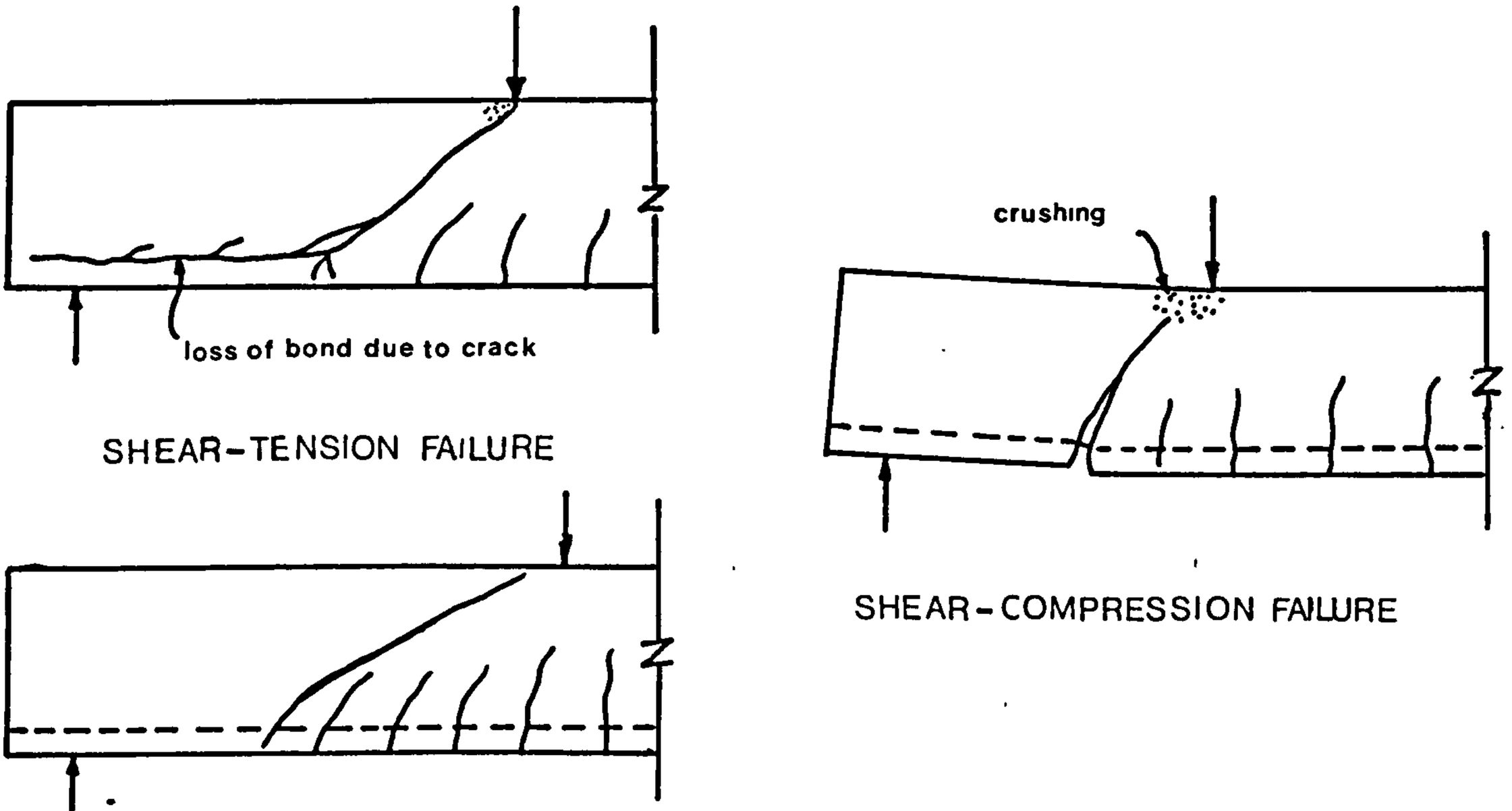

SHEAR-TENSION FAILURE

SHEAR-COMPRESSION FAILURE

DIAGONAL TENSION FAILURE

FIG·2·3 PRINCIPAL SHEAR FAILURES IN RECTANGULAR BEAMS

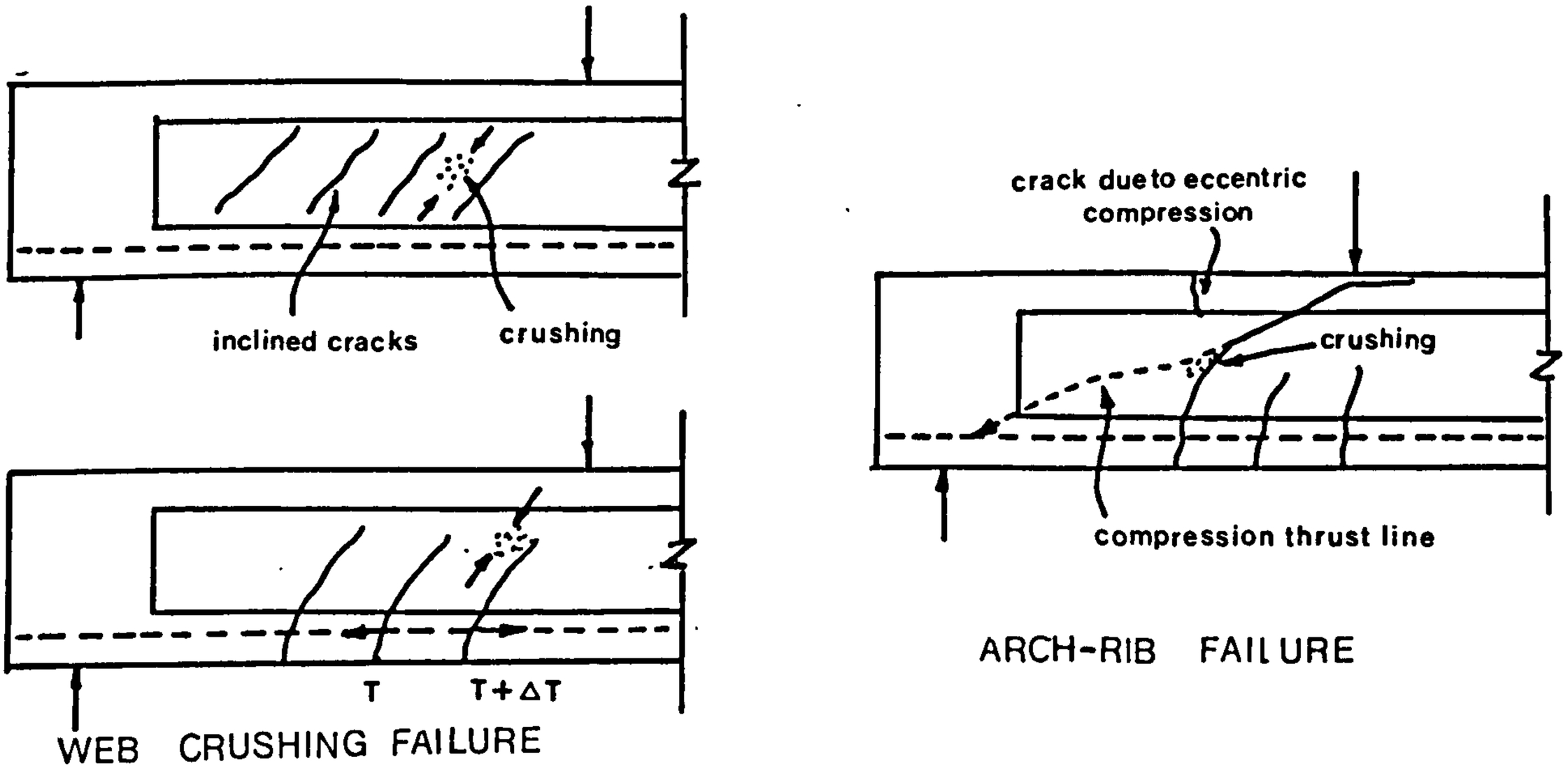

ARCH-RIB FAILURE

WEB CRUSHING FAILURE

FIG·2·4 TYPICAL SHEAR FAILURES IN I-BEAMS(AFTER REF·(32))

2.4.2 Shear Strength

Shear strength, V, in reinforced concrete beams without web reinforcement has three components (Fig. 2.5):

1. The shear component of the stress resultant in the uncracked concrete compression zone, V_c
2. The shear component of the friction and aggregate interlock in the cracked concrete, V_a
3. The dowel action of the longitudinal reinforcement, V_d.

At the point of failure of the beam, the shear force is carried in the approximate proportions (34, 36):

Compression zone shear	20 - 40%
Aggregate interlock	33 - 50%
Dowel action	15 - 25%

The ultimate shear capacity of the compression zone is affected by the concrete strength. Aggregate interlock shears depend on the surface roughness of the cracks, aggregate type and the displacements across the cracks, whereas dowel action depends on the layout of tension steel, the width of the dowel failure surface and the tensile strength of the concrete. The ultimate shear strength of the beam depends also on its size and $\frac{a_v}{d}$ ratio. The shear strength reduces with the beam size (37, 38, 39), probably because in practice the aggregate interlock capacity does not increase in the same proportion as the beam size. The CEB - FIP Model Code (5) takes into account this effect for normal weight concrete beams. All things equal, an increase in $\frac{a_v}{d}$ ratio results in a decrease of shear strength.

In addition to the three shear components mentioned above, part of the shear force of beams with web reinforcement is carried by the web bars crossed by the inclined cracks. This shear component is designated V_w in Fig. 2.6. The web reinforcement also

aids the shear carrying capacity of the beam by resisting the growth of the shear crack width thereby delaying the degeneration of aggregate interlock action. It holds the longitudinal bars and slows the propagation of splitting cracks along the main reinforcement.

2.4.3 Some Methods of Analysis of the Shear Strength of Reinforced Concrete Beams

2.4.3.1 Tooth Mechanism of Inclined Cracking

For $\frac{a_v}{d}$ ratios greater than about 3 to 4, inclined cracks develop in the shear span as an extension of a flexural crack which progressively bends over until the inclined crack is formed, see Fig. 2.7. Several authors have idealized this mechanism as the breaking off of a concrete "tooth" between two flexural cracks (40, 41).

The variation in steel stress from crack to crack sets up forces on the teeth between the flexural cracks, which tend to cause bending and shearing deflections of the teeth. As the teeth deflect dowel forces and aggregate interlock stresses developed between the teeth tend to prevent relative deflections of the teeth, thus delaying the formation of further cracks (this effect was ignored in Ref. (40)). Failure of a tooth occurs when the tensile stress at the root of the tooth exceeds the tensile strength of concrete.

2.4.3.2 Truss Analogies

For beams with web reinforcement, a more familiar and generally more useful model for the designer is based on the truss analogy. In this model the beam is represented by a pin-jointed truss in which the concrete compression zone is represented by the compression chord, the tensile reinforcement is represented by

tension chord, the web reinforcement is represented by the web tension members, and the concrete between inclined cracks is represented by compression web members.

In the classical truss model introduced by Ritter and Morsch, the chords are assumed to be parallel to each other and the slope of the compression diagonals is taken to be 45^{o}, see Fig. 2.8(a). This model is extremely oversimplified, ignoring the shear contribution from the compression zone, aggregate interlock action and dowel action. A number of researchers have tried to improve it by sloping the compression chord or by changing the slope of the compression diagonals, see Fig. 2.8(b).

In a variable angle truss model, the main difficulty lies in choosing the appropriate value for the angle of inclination of the compression diagonals. Rabbat and Collins (42) established this angle by incorporating compatibility of strains in the truss members. Grob and Thurlimann (43) introduced limits of this angle in their truss model by kinematic considerations and assuming at ultimate load uniaxial yielding of the reinforcing bars and opening of the final cracks perpendicular to the crack direction. Within the limits, the longitudinal and web reinforcement have to yield in order to form a collapse mechanism and beyond the limits yielding of the web or longitudinal reinforcement alone produces a mechanism.

2.4.3.3 Equilibrium Analysis

In short beams or beams with web reinforcement, the mode of failure may be shear compression, as shown in Fig. 2.3. The usual approach to the analysis of this type of failure is by summing moments about a point in the compression zone above the end of the inclined cracks. Generally the effect of the shearing stresses in the strength of the compression zone is considered.

Swamy and Qureshi (44) adopted a similar approach to predict the ultimate shear strength of T-beams of long shear span without web reinforcement. Failure occurs in the compression zone above the inclined crack when the combined shearing and compressive stresses satisfy Mohr's failure criterion. The shear force due to dowel action of the longitudinal reinforcement was considered by assuming that it is 10% of the total shear force. This approach was subsequently extended to predict the shear resistance of T-beams with vertical stirrups (45).

2.4.3.4 Statistical Estimates of Shear Strength

Some researchers have presented statistical studies of the factors affecting the shear failure capacity of reinforced concrete beams. Zsutty (46) derived an empirical equation for the prediction of ultimate shear strength of rectangular beams with $\frac{a_v}{d}$ greater than 2.5 by using a combination of the techniques of dimensional analysis and multiple regression analysis.

2.4.3.5 Theory of Plasticity Model

Nielson and Braestrup (47) applied the theory of plasticity in the study of the shear capacity of reinforced concrete beams. They assumed a failure mechanism for a simply supported beam loaded by two symmetrical point loads, V , as shown in Fig. 2.9. The mechanism consists of a vertical deformation in a yield line inclined at an angle θ to the longitudinal axis of the beam. This mechanism implies the existence of tangential shearing forces in the yield zone. It assumes:

1. The main reinforcement at the bottom of the beam and the compression zone at the top act as stringers, carrying uniaxial tensile force and compressive force respectively. Thus any dowel action of the reinforcement and shear in the compression zone are neglected.

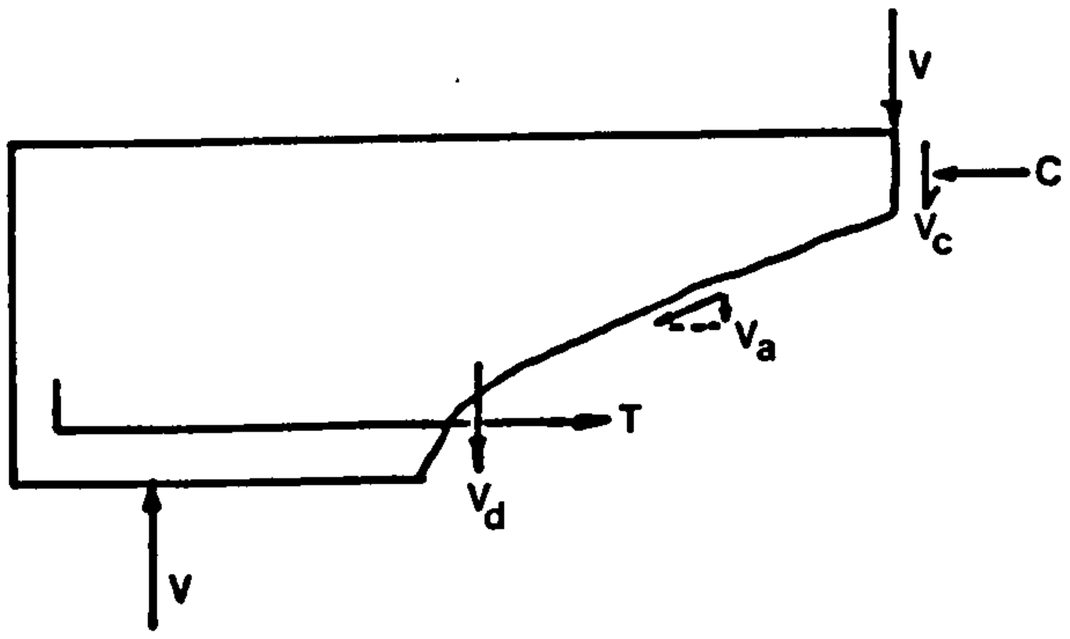

FIG·2·5 COMPONENTS OF SHEAR STRENGTH– WITHOUT WEB REINFOCEMENT

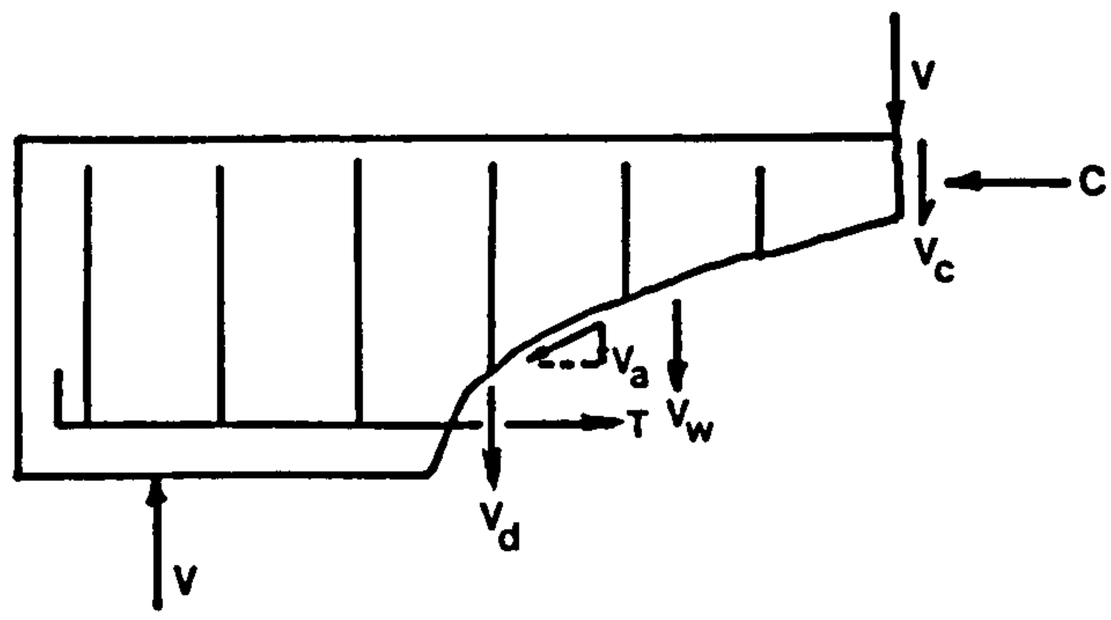

FIG·2·6 COMPONENTS OF SHEAR STRENGTH– WITH WEB REINFORCEMENT

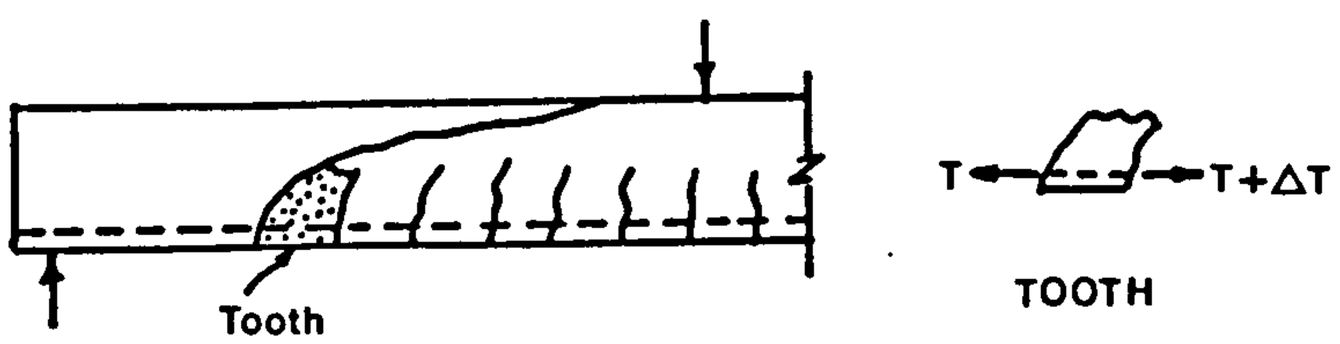

FIG·2·7 TOOTH MECHANISM OF INCLINED CRACKING

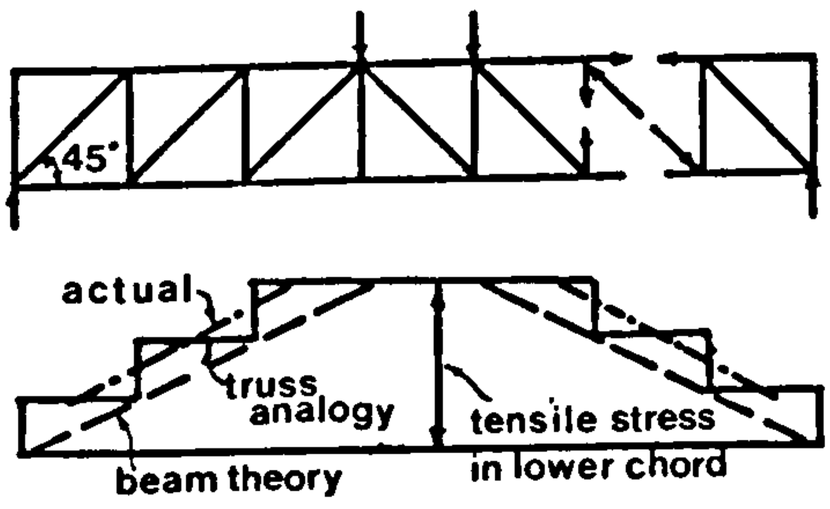

(a) DISTRIBUTION OF FORCES IN CLASSICAL TRUSS ANALOGY

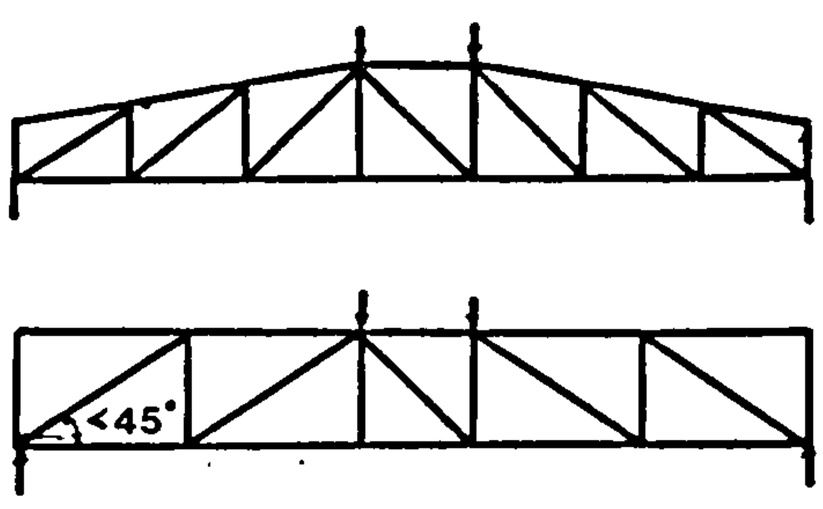

(b) MODIFIED TRUSS ANALOGIES

FIG·2·8 TRUSS ANALOGIES (AFTER REF·(34))

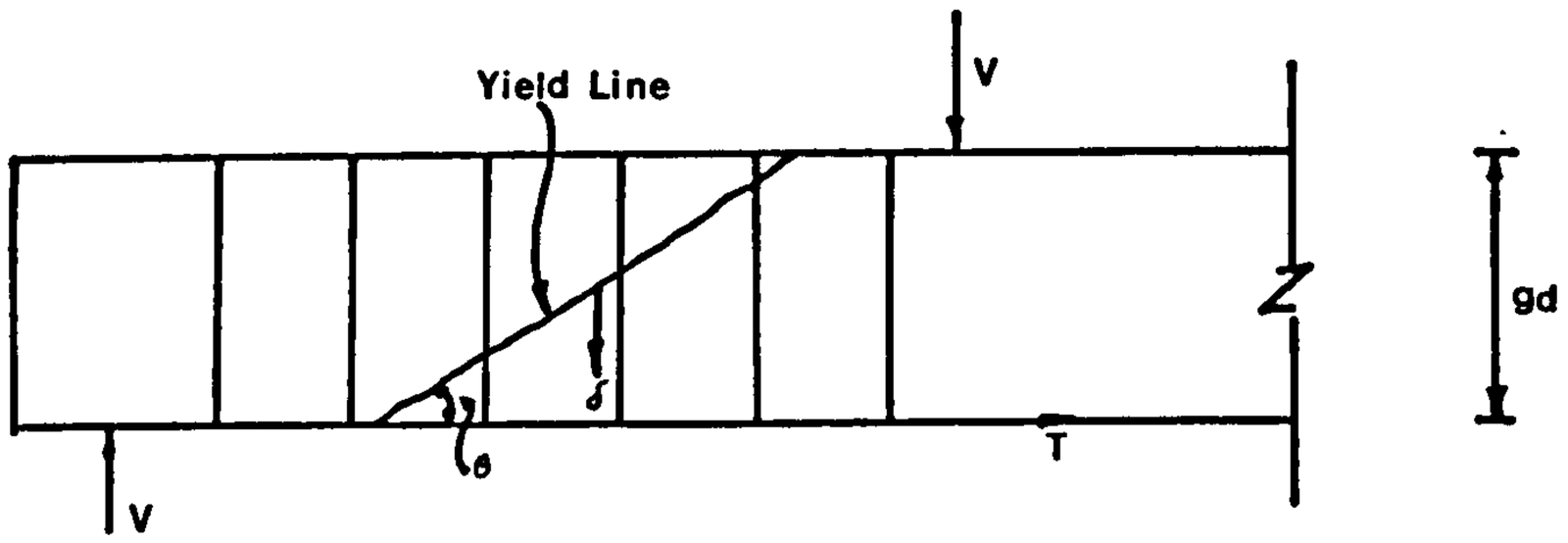

FIG·2·9 FAILURE MECHANISM ASSUMMED IN UPPER-BOUND SOLUTION (AFTER REF·(47))

2. The web concrete is rigid, perfectly plastic obeying the modified Coulomb failure criterion with a zero tensile cut off and the associated flow rule of plasticity. The compressive strength is $K_o f'_c$ where f'_c is the cylinder strength and K_o is an effectiveness factor.
3. The stirrups are rigid, perfectly plastic and are able to resist axial forces only.
4. The longitudinal tensile reinforcement does not yield at failure and, consequently, failure is due to crushing of the concrete, which may or may not be accompanied by yielding of the web reinforcement.

By equating internal and external work of the beam for the deformation in the above mode, Nielson and Braestrup showed that, at failure,

$$\frac{v_u}{f'_c} = \sqrt{\psi\ (K_o - \psi)} \qquad \text{for } 0 < \psi \leq \frac{K_o}{2}$$

$$\frac{v_u}{f'_c} = \frac{K_o}{2} \qquad \text{for } \psi > \frac{K_o}{2} \qquad (2.21)$$

$$v_u = \frac{V}{b_w gd}$$

and $$\psi = \frac{Asv\ f_y}{s\ b_w}$$

where v_u - ultimate shear stress

V - applied shear force

gd - distance between stringers

Asv - area of stirrups crossing the concrete of area sb_w

b_w - web width

s - spacing of stirrups

and f_y - yield stress of stirrups

The effectiveness factor, K_o, having value less than unity, is introduced to account for the limited deformability of the concrete and to allow for the reduction in the strength of the concrete due to the presence of stirrups in tension. K_o is obtained by correlation with experimental data.

Equation (2.21) is an upper bound solution. Nielson and Braestrup also derived an identical expression from a lower bound solution, indicating that equation (2.21) is an exact solution according to the assumptions made. In a subsequent study of the effect of main steel strength of the shear capacity of reinforced concrete beams, Braestrup (48) considered the displacement vector to be at an angle, α, to the beam normal. Yielding of main reinforcement occurs if α is greater than zero.

2.4.3.6 Finite Element Approach

The versatility of the finite element method provides a sophisticated tool for the analysis of reinforced concrete structures. Concrete and steel may be represented by appropriate types of elements, nonlinear material behaviour can be taken into account with general solution logarithms, and slip occurring at the interface between concrete and reinforcement can be introduced through linkage elements. Furthermore aggregate interlock action of cracked concrete and dowel action of the reinforcement may be considered in the analysis. The basic formulations of the finite element approach and a brief review of the various finite element models of reinforced concrete will be given in Chapter 7.

Several investigators have applied the finite element approach to the study of the problem of shear in reinforced concrete structures. Scordelis et al (49) and Houde et al (50) analysed reinforced concrete beams with predefined shear cracks.

Aggregate interlock across the shear cracks was considered by the use of linkage elements. Hammad (51) investigated the shear contribution from the compression flange of reinforced concrete T-beams using a 3-dimensional finite element analysis. Cedolin et al (52) demonstrated the possibility of predicting shear failures of reinforced concrete beams through a nonlinear 2-dimensional finite element model.

2.4.4 Lightweight Concrete Beams

The shear resistances of lightweight concrete beams are generally lower than those of corresponding normal weight concrete beams. The reduction in strength is due mainly to the lower aggregate interlock capacity and the lower tensile strength of lightweight concrete.

In normal weight concrete fracture surfaces are locally rough as the cracks go round rather than through the aggregate particles. In lightweight concrete, on the other hand, the surfaces are smoother as the fractures run through the aggregate. The degree of smoothness of the crack surfaces depends on the type of aggregate. The stronger lightweight aggregates generally provide rougher surfaces while the weaker types can give very smooth surfaces. Consequently, the aggregate interlock stresses that can be transferred across the cracks will be reduced in lightweight concrete.

The lower tensile strength results in a reduction of the inclined or shear cracking load.

CHAPTER THREE

MIX DESIGN AND MATERIAL PROPERTIES

3.1 Introduction

Extensive research work over the last two decades has shown that the introduction of short, discrete steel fibres into normal weight or lightweight concrete mixes is not only possible, but it also results in marked improvement in the material properties of the resulting composite. For example, an increase in the flexural strength of 1.5 to 3 times is not uncommon.

In addition to the water-cement ratio and cement content, the rheological and material properties of fibre concrete depends on the geometry, type and amount of fibres; the proportion of fine materials, the size, shape and volume fraction of coarse aggregates and the fibre distribution in the matrix. These factors must be considered in the mix design of fibre concrete.

Generally, more energy is required to compact fibre concrete than conventional concrete. The length and diameter of the fibre in relation to the size of the mould and the method of compaction have a major influence on the orientation of the fibres in the matrix.

In this chapter, the properties of the various materials used are given first. Then the mix design of both the gravel and Lytag-sand concretes used in the investigation is explained. Based on the experimental data obtained, the influence of steel fibres on workability, compressive strength, dry density, flexural strength, static elastic modulus and Poisson's ratio is discussed.

3.2 Materials

The materials used in this investigation are given below. The same type of materials was used throughout the investigation but, unavoidably, they were from different deliveries.

3.2.1 Cement

Ordinary Portland cement which was considered to comply with B.S. 12 (53) was used.

3.2.2 Pulverised Fly Ash (PFA)

The pulverised Fly Ash used was obtained from Ferry Bridge power station. Its chemical composition and grading, as quoted by the supplier, are shown in Table 3.1. The chemical composition of the PFA complied with B.S. 3892 (54)

Table 3.1 Chemical Composition of the PFA

Constituents	% by weight	B.S. 3892 Limits
Silica as SiO_2	56.2	-
Alumina as Al_2O_3	26.2	-
Iron as Fe_2O_3	7.3	-
Titanium as TiO_2	1.0	-
Phosphate as P_2O_5	0.3	-
Calcium as CaO	1.6	-
Magnesium as MgO	0.7	4% Max
Potassium as K_2O	2.5	-
Sodium as Na_2O	1.3	-
Sulphate as SO_3	0.7	2.5% Max
Loss on ignition	2.2	7% Max

Specific Surface = 3690 cm^2/gm
Density = 2170 kg/m^3

3.2.3 Sand

Washed natural river sand was used. The grading curve for the sand as shown in Fig. 3.1 lies within zone 2 of the grading limites of B.S. 882: Pt 2: 1973 (55). All sand was dried thoroughly in a mechanical sand drier before use.

3.2.4 Coarse aggregates

Two types of coarse aggregates were used: 10 mm nominal size crushed gravel and lightweight aggregate (Lytag) of 14 mm maximum size. The grading curves for both types of aggregates are shown in Fig. 3.2 and they fall in the zones defined by B.S. 882: 1973 (55) and B.S. 3797 (56) respectively. Plate 3.1 shows the two types of coarse aggregates. The loose bulk density and the total water absoption of the Lytag aggregate, as specified by the manufacturer, were 800 kg/m^3 and 12% respectively. The gravel aggregates were dried before use. The Lytag aggregates were partially soaked by rain or by water in the stockpile and the water content of the aggregates was determined by the "Speedy Moisture Tester" (0 to 20% model) prior to each casting.

3.2.5 Water Reducing Agent

Febflow was used as a water reducing agent to increase the workability of the concrete. The dosage used was 4.5 c.c./kg of fines (cement + PFA) for all mixes except for that with 1.2% by volume of crimped fibres, where a dosage of 5.6 c.c/kg of fines was used instead. The Febflow was added to the mixing water first before adding to the dry mix.

3.2.6 Steel Fibres

Crimped steel fibres of 0.5 mm in diameter and 50 mm long were the main type of fibres used in this investigation.

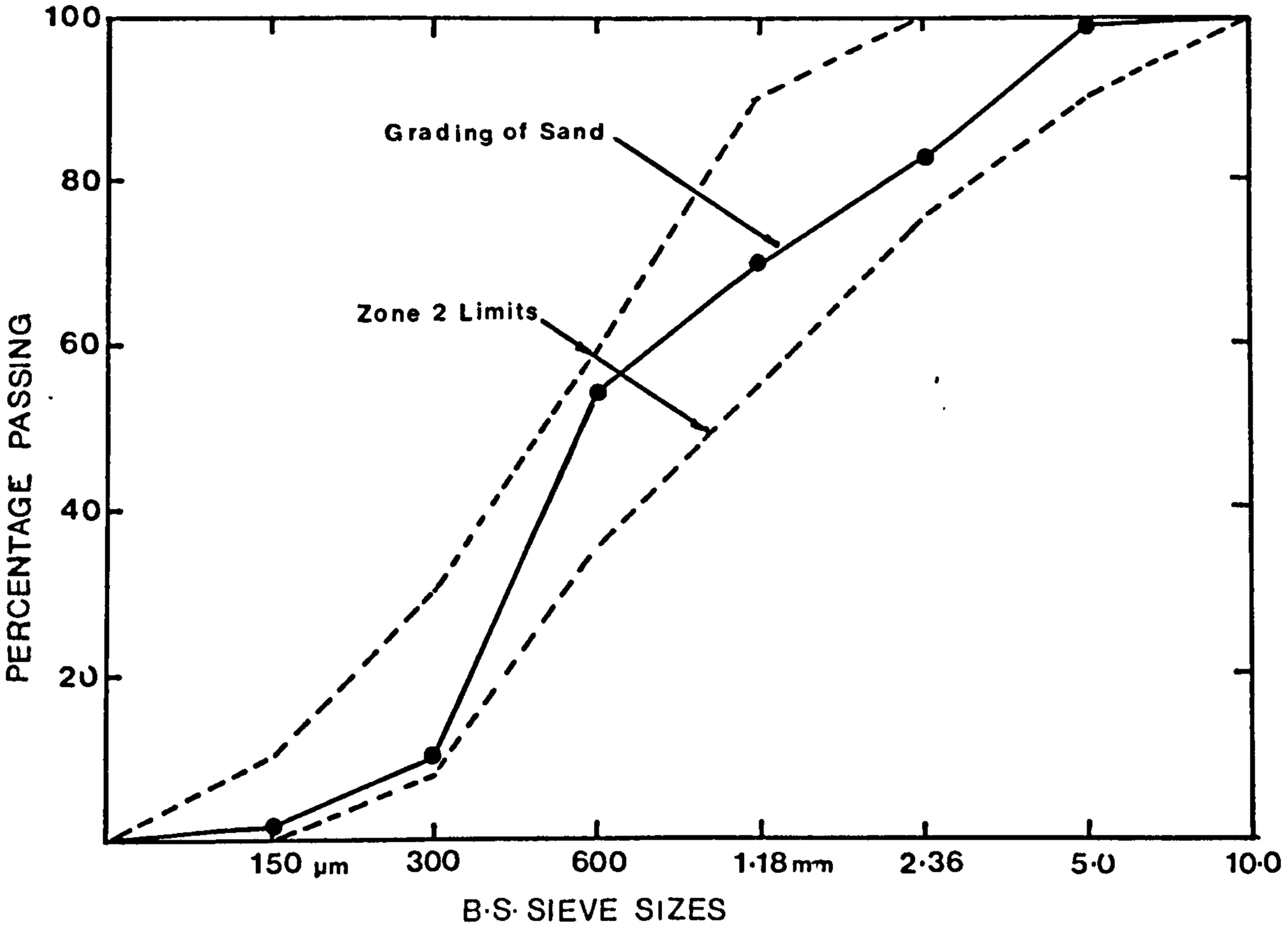

Fig.3·1 B·S· Sieve Analysis For Sand

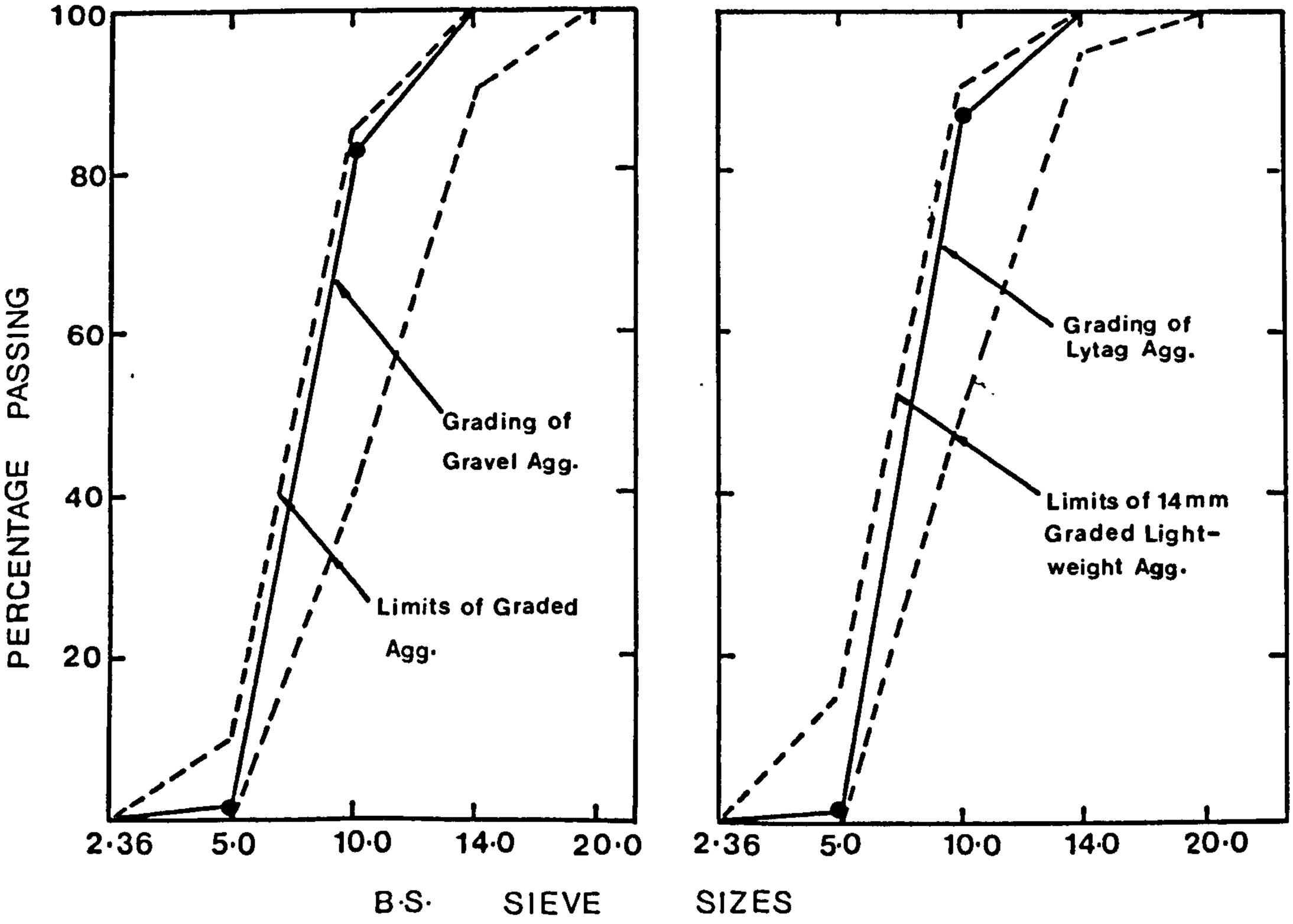

Fig.3·2 B·S· Sieve Analysis For Coarse Aggregates

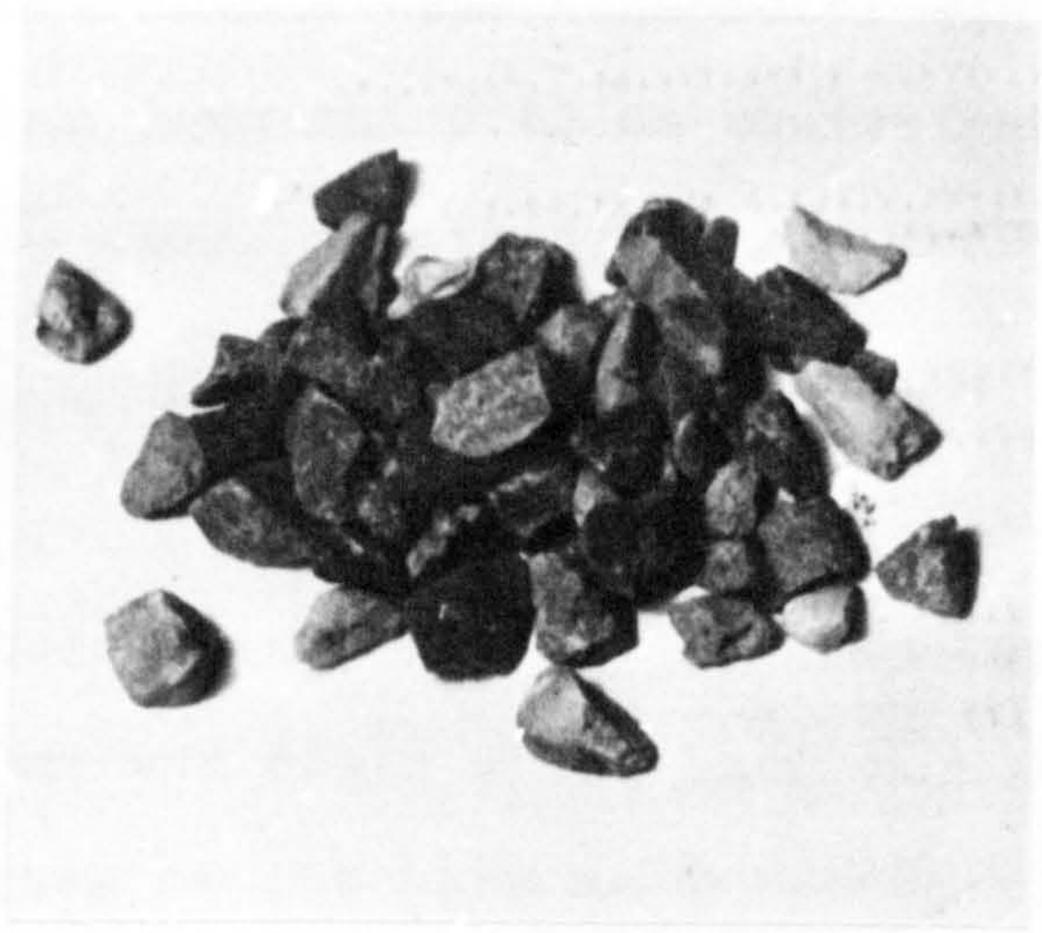

. Gravel

Lytag

PLATE 3·1 COARSE AGGREGATES

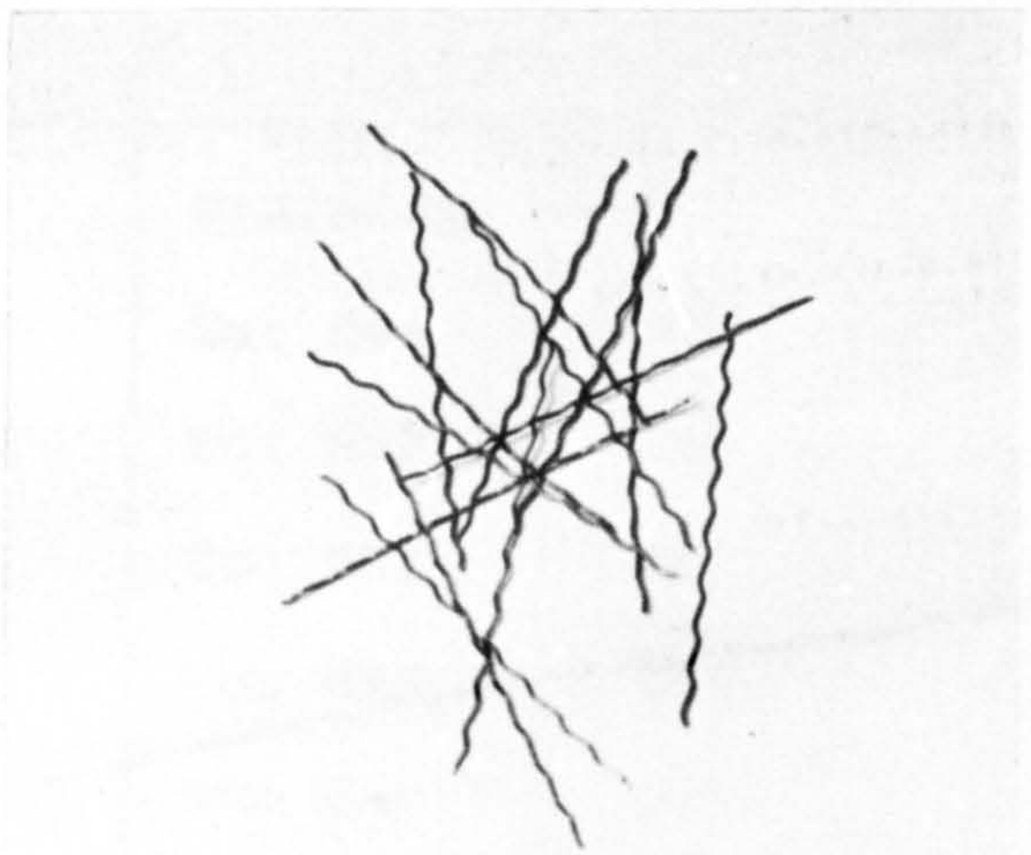

Crimped

Japanese

PLATE 3·2 STEEL FIBRES

The average ultimate stress determined by the tensile test using Hounsfield W type tensometer was 1570 N/mm^2. In addition, 25 mm long and 0.42 mm equivalent diameter Japanese fibres were also used. Plate 3.2 shows the two types of fibres.

3.2.7 Steel Reinforcement

The types of steel reinforcement used were cold worked ribbed bars (Tor Bar) of diameter 8 mm, 10 mm, 12 mm, 16 mm and 20 mm and plain steel bars of 6 mm diameter. The stress-strain curves of the bars as determined by extensometers of 50 mm gauge length are shown in Fig. 3.3 while the average tensile strength and Young's modulus obtained are tabulated in Table 3.2. The characteristic strength as quoted by the manufacturer is also given in the same table.

Table 3.2 Properties of Steel Reinforcement

Bar Size mm	Type	Es kN/mm^2	0.2% proof stress, fy N/mm^2	Specifield Characteristic 0.2% proof stress N/mm^2	Ultimate Tensile Stress N/mm^2
6	Plain Bar	200	353	350	485
8	Tor Bar	200	505	460	590
10	Tor Bar	203	500	460	580
12	Tor Bar	195	470	460	585
16	Tor Bar	195	465	460	530
20	Tor Bar	200	455	425	575

3.3 Mix Design

The aim was to achieve a satisfactory workable gravel and Lytag-sand concrete mixes having a 28 day cube strength of about 40 N/mm^2.

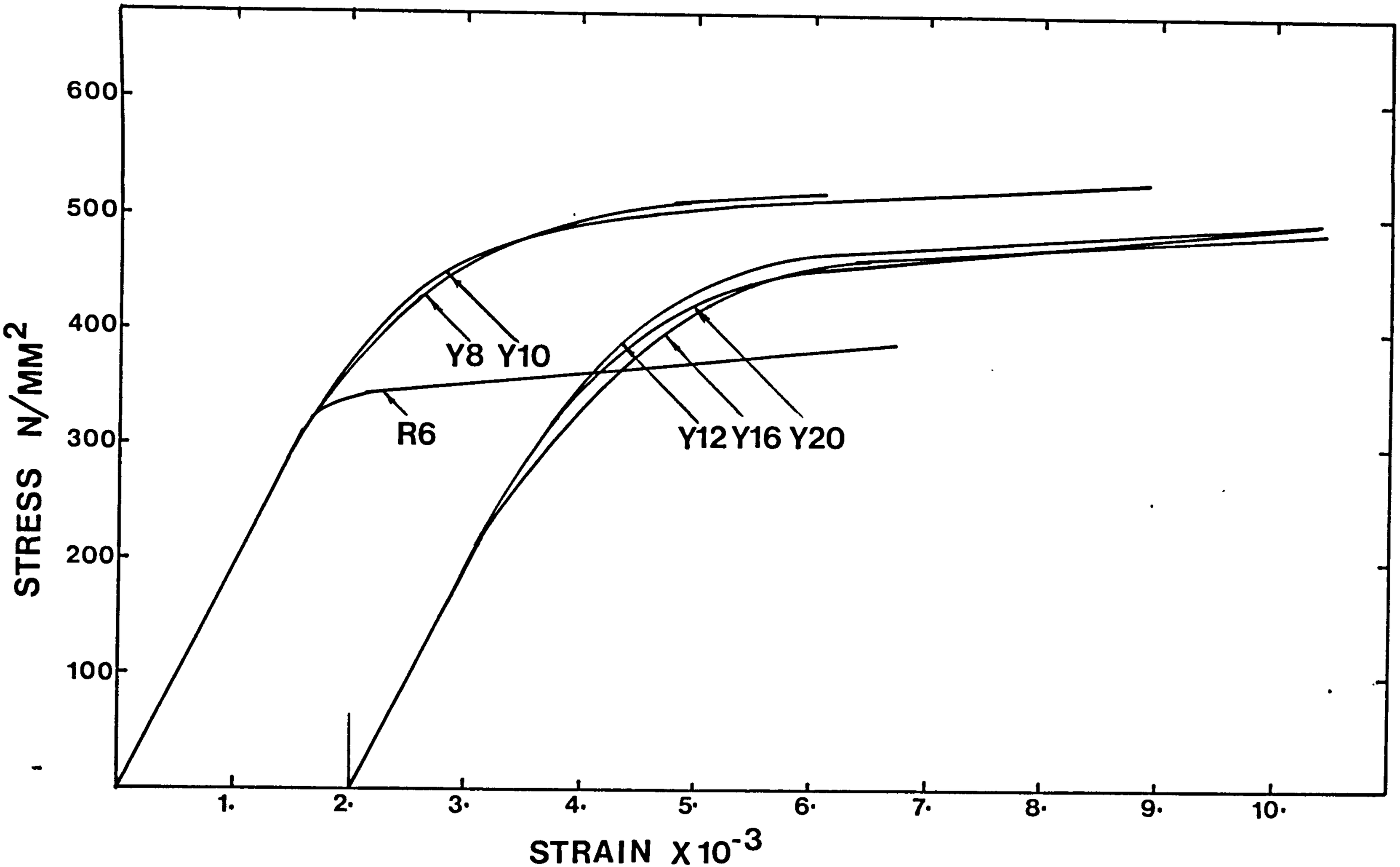

FIG·3·3 STRESS-STRAIN CURVES FOR STEEL REINFORCEMENT

3.3.1 Normal Weight Concrete Mix

Past experience in the design of fibre concrete mix has shown that good quality fibre concrete can be made by using 10 mm maximum size of aggregate and fly ash as a straight forward substitute of 30% of the cement by weight (6, 57, 58). The mix proportions adopted were a slight modification to those used by Bahia (6) and the proportions by weight are as follows:

PFA/(cement + PFA) = 0.3

Cement/(cement + PFA) = 0.7

Sand/(cement + PFA) = 1.7

Gravel/(cement +PFA) = 2.2

Water/(cement + PFA) = 0.45

Febflow = 4.5 → 5.6 c.c./kg of fines (cement + PFA)

Fibre percentage by volume of the matrix = 0 → 1.20

3.3.2. Lytag - sand Concrete Mix

Basically the mix design was a trial and error process, although the method put forward by Jackson and Goodridge (59) for the design of PFA normal weight concrete mix served as a general guide. In this method good early strength is achieved by both sand and cement replacement.

The basic mix proportions used were those due to Lambert (60). Four modifications to this basic mix were carried out. The proportions of each of the mixes are tabulated in Table 3.3. The compressive strengths of 100 mm cubes cured in uncontrolled laboratory conditions at various ages are tabulated in Table 3.4. Mix ML5 was adopted for subsequent experimental work as it gave good early strength and was close to the desired cube strength of about 40 N/mm^2.

3.3.3 Mixing Procedure

All concrete was made in a horizontal type pan mixer

Table 3.3 Proportions of Trial Mixes of Lytag-sand Concrete

Mix No	PFA : C : S : LA : W	*kg per m^3			Slump mm	REMARKS
		OPC	PFA	EFF WATER		
ML1†	0 :1.0 :1.89:2.11:.53	330	-	175	-	Basic mix
ML2	0.3 :0.7 :1.89:2.11:.45	234	100	150	COLLAPSED	30% OPC Replacement
ML3	0.2 :0.8 :1.89:2.11:.45	267	67	150	160	20% OPC Replacement
ML4	0.29:0.71:1.32:1.77:.38	289	118	155	COLLAPSED	OPC + Sand Replacement
ML5	0.28:0.72:1.50:1.90:.40	272	106	152	160	OPC + sand Replacement

NOTE: (i) * Based on an average 28-day dry density of 1820 kg/m^3.
(ii) † Basic mix for grade 40 concrete (after Lambert (60))
(iii) Febflow dosage for all modified mixes was 2.8 cc/kg of fines (PFA + Cement)

Table 3.4 Cube Strength of Modified Mixes at Various Ages

Mix No	1-day N/mm^2	3-day N/mm^2	7-day N/mm^2	14-day N/mm^2	28-day N/mm^2
ML2	3.0	13.7	22.9	29.3	33.5
ML3	5.9	16.8	29.0	33.3	40.8
ML4	7.3	21.1	32.0	41.0	46.3
ML5	7.0	20.2	31.3	35.8	41.8

NOTE: (i) All cubes were 100 x 100 x 100 mm
(ii) Internal vibration was used
(iii) All cubes cured in uncontrolled laboratory conditions

of 0.1 m^3 capacity. The aggregates, cement and PFA were first mixed for about 90 seconds, then water with the reducing agent (Febflow) was added and mixing continued further for about 60 seconds. In the case of fibre concrete, the fibres were subsequently added through a mechanical dispenser (but during the later part of the research, a one inch-sieve had to be used to break up the fibres as the mechanical dispenser was considered unsafe) and the mixer was stopped when a reasonably homogeneous mix was produced. Balling of fibres was experienced during mixing although not very significantly.

After mixing, the concrete was poured into lightly oiled moulds in two layers and compacted well using either a 25 mm diameter internal poker vibrator or a 3.05 x 1.20 m table vibration system. The specimens were left under polythene sheets in the laboratory generally for 24 hours before they were demoulded and stored in the laboratory under uncontrolled conditions until they were tested.

3.3.4 Properties of Fresh Concrete

Characteristically a steel fibre mix will experience a decrease in workability with increasing volume of fibres. In this investigation, pulverised fly ash (PFA) and a water reducing agent (Febflow) were used to improve the workability of the mixes. The workability was measured by the slump test. The results of the different types of mixes used are given in Table 3.5. Where used the fibres were crimped steel. It should be mentioned that the slump test, at best, can only provide qualitative information on the workability of fibre concrete mixes because of the difficulty in rodding the concrete in the cone.

Table 3.5 Properties of Fresh Concrete

Mix	Type of Agg.	% fibre volume	Febflow cc/kg of (opc + PFA)	Slump mm
1	Gravel	0	4.5	120
2	Gravel	0.4	4.5	80
3	Gravel	0.8	4.5	40
4	Gravel	1.2	5.6	20
5	Lytag	0	2.8	160
6	Lytag	1.0	4.5	35

3.3.5 Properties of Hardened Concrete

The following discussion is based mainly on the average values obtained from standard tests on the numerous control specimens cast along with the shear transfer specimens and beams. However , in addition two series of 18 cubes and 18 prisms each were conducted to study the strength development of plain and crimped fibre Lytag-sand concrete over a period of 180 days.

3.3.5.1 Compressive Strength

The size of all the test cubes was 152 x 152 x 152 mm and the stress rate applied was approximately 15 N/mm^2 per minute according to B.S. 1881:Part 4 (61). Table 3.6 shows the 28-day compressive strength of the control cubes cast together with the shear transfer specimens. Table 3.7 shows those cast along with the beams. The former were externally vibrated using a table vibration system while the latter were internally vibrated using a 25 mm diameter poker vibrator. Table 3.8 shows the average values and the percentage increase of the compressive strength of the fibre concrete relative to the plain concrete. It can be

Table 3.6 Compressive and Flexural Test Results of Shear Transfer Secimens

Specimen Number	Aggregate Type	% Fibre Volume	Compressive Strength N/mm^2	Modulus of Rupture	
				1st crack N/mm^2	Ultimate N/mm^2
1SN-1	Gravel	0	39.0	-	-
2SN-1	Gravel	0	37.0	-	3.80
2SN-2	Gravel	0	43.2	-	-
2SNP-1	Gravel	0	36.2	-	3.48
2SNP-2	Gravel	0	37.0	-	3.74
1SN-2	Gravel	0.4	42.4	4.01	4.90
1SNP-2	Gravel	0.4	43.1	3.92	5.04
3SN-1	Gravel	0.4	37.1	-	-
3SN-2	Gravel	0.4	38.8	-	-
3SN-3	Gravel	0.4	39.4	3.85	4.92
3SNP-2	Gravel	0.4	41.6	3.75	4.40
1SN-3	Gravel	0.8	43.0	4.71	6.00
1SNP-3	Gravel	0.8	43.5	4.82	6.08
4SN-1	Gravel	0.8	40.1	4.84	6.30
4SN-2	Gravel	0.8	39.3	-	-
4SN-3	Gravel	0.8	40.3	-	-
4SNP-2	Gravel	0.8	41.6	4.15	5.48
1SN-4	Gravel	1.2	42.4	5.08	6.54
1SL-1	Lytag	0	39.8	-	3.49
2SL-1	Lytag	0	41.0	-	3.20
2SL-2	Lytag	0	38.0	-	3.10
2SL-3	Lytag	0	36.8	-	3.05
2SLP-1	Lytag	0	37.0	-	3.72
2SLP-2	Lytag	0	41.4	-	3.24
2SLP-3	Lytag	0	39.8	-	3.50
1SL-2	Lytag	1.0	40.3	4.0	6.52
3SL-1	Lytag	1.0	46.1	4.57	6.64
3SL-2	Lytag	1.0	40.0	4.35	6.36

NOTE (1) All specimens were externally vibrated using a table vibrator.
(2) All fibres were 0.5 x 50 mm crimped fibres.
(3) All specimens were cured in uncontrolled laboratory conditions.
(4) All specimens were tested at 27 - 29 days.
(5) The 1st crack was detected visually.

Beam Number	% Fibre Volume	Compressive Strength N/mm^2	Modulus of Rupture		Static Modulus kN/mm^2	Poisson's Ratio
			1st crack N/mm^2	Ultimate N/mm^2		
1TL-1	0	44.3	-	3.60	19.4	0.20
1TL-2	0	42.0	-	3.59	19.4	0.20
1TL-3	0	42.6	-	3.44	19.6	0.20
2TL-1	0	45.6	-	3.80	20.0	0.19
2TL-2	0	41.7	-	3.56	19.3	0.19
2TL-3	0	45.1	-	3.60	19.6	0.18
3TL-1	0	46.7	-	3.76	20.2	0.19
3TL-2	0	41.0	-	3.04	19.6	0.19
3TL-3	0	42.3	-	3.36	18.7	0.17
1TLF-1	1.0	44.5	4.67	7.00	20.8	0.18
1TLF-2	1.0	51.1	4.96	7.35	22.0	0.18
1TLF-3	1.0	45.0	4.58	6.73	21.5	0.19
2TLF-1	1.0	47.2	4.93	7.00	21.6	0.17
2TLF-2	1.0	41.4	4.59	6.60	21.0	0.17
2TLF-3	1.0	44.9	4.60	6.90	21.4	0.17
3TLF-1	1.0	44.6	4.84	6.85	-	-
3TLF-2	1.0	43.1	4.56	6.73	-	-
3TLF-3	1.0	40.6	4.10	6.00	-	-

NOTE (1) All specimens were of Lytag-sand concrete and were internally vibrated using poker vibrator.
(2) All fibres were 0.5 x 50 mm crimped fibres.
(3) All specimens were cured in uncontrolled laboratory conditions.
(4) All specimens were tested at 27 - 29 days.

Table 3.8 Influence of Fibre Percentage on Average Compressive Strength of the Control Specimens

Aggregate Type	% Fibre Volume	Method of Vibration	Average Compressive Strength N/mm^2	Standard Deviation N/mm^2 (%)	% Increase Relative to plain Concrete
Gravel	0 0.4 0.8 1.2	Table Vibrator	38.5 40.4 41.3 42.4	2.53(6.58 2.13(5.27) 2.38(3.73) -	- 4.9 7.3 10.1
Lytag	0 1.0	Table Vibrator	39.1 42.1	1.72(4.41) 2.81(6.67)	- 7.7
Lytag	0 1.0	Poker Vibrator	43.5 44.7	1.88(4.32) 2.94(6.57)	- 2.8

seen that the fibre concrete shows a small consistent increase in the average compressive strength over the plain concrete. The increase was 4.9%, 7.3% and 10.1% for externally vibrated gravel concrete with 0.4%, 0.8% and 1.2% of crimped steel fibres by volume respectively. The increase for Lytag-sand concrete with 1% of crimped fibres by volume was 7.8% and 2.8% for externally vibrated and internally vibrated concrete respectively. This seems to suggest that external vibration is a better way of compacting fibre concrete. Ali (58) also reported the same observation.

For normal weight concrete, Bahia (6) reported a variation range of ±4.5% in the compressive strength by using 0.6 to 1.2% by volume of crimped fibres, Al-Ta'an (62) reported an increase of about 6% by using 1.0% and Ali (58) reported a variation range of -10.0 to 5.0% by using 0.6 to 1.2%. For Lytag-sand concrete, Sittampalan (63) reported an increase of 10.3% in the compressive strength by using 1% by volume of crimped steel fibres while Theodorakopoulos (64) reported a decrease of 3.3% and an increase of 4.0% by using 0.5 and 1.0% respectively. Thus the published results and the results of this investigation seem to contradict each other. It is a well known fact that the compressive strength of concrete is strongly related to the presence of voids. Fibre concrete mixes may have more voids than plain concrete mixes if they are not properly compacted. Therefore, the reported reduction in compressive strength was possibly due to insufficient compaction. Although a final conlcusion cannot be drawn as to the effect of crimped steel fibres on the 28-day compressive strength, it can be expected that this effect will not be significant.

Fig. 3.4 shows the development of the compressive strength of both plain and crimped fibre Lytag -sand concrete

cured in uncontrolled laboratory conditions over a period of 180 days. It can be seen that the compressive strength development of both the plain and the fibre concrete seems to follow the same pattern except that the fibre concrete shows consistently a slightly higher strength (percentage increase ranged from 5.9% at 1 day to 16.4% at 7 days). Both strength development seem to stablize after about 90 days. The percentage increase of the strength at 180 days over that at 28 days was 8.8% for plain concrete and 13.6% for fibre concrete.

3.3.5.2 Dry Density

The 28-day dry density of plain and crimped fibre Lytag-sand concrete determined as an average of three 152 x 152 x 152 mm cubes was 1820 and 1860 kg/m^3 respectively. Inclusion of 1.0% crimped fibres effected an increase of 2.2%. Theodorakopoulos (64) reported an increase of 4.0% for Lytag-sand concrete with an inclusion of 1.0% by volume of similar type of fibres.

3.3.5.3 Flexural Tensile Strength (Modulus of Rupture)

The flexural test was carried out on 100 x 100 x 500 mm prisms with a loaded span of 400 mm under third point loading and at a stress rate of 1.6 N/mm^2 per minute according to B.S. 1881 Part 4 (61). The first crack (detected visually) and the ultimate modulus of rupture of the control prisms of the shear transfer specimens and the beams are shown in Tables 3.6 and 3.7 respectively. The average values and the percentage increase of the flexural strength of the fibre concrete over the plain concrete are shown in Tables 3.9 and 3.10. It can be seen that, for externally vibrated gravel concrete, the inclusion of crimped steel fibres of 0.4 to 1.2% by volume increased the first crack strength by 5.7 to 38.4% and the ultimate strength by 31.3 to 78.2%.

Table 3.9 Influence of Fibre Percentage on First Crack Modulus of Rupture of the Control Specimens

Aggregate Type	% Fibre Volume	Method of Vibration	Average 1st crack M.O.R. N/mm^2	Standard Deviation N/mm^2 (%)	%Increase Relative to Plain Concrete
Gravel	0	Table Vibrator	3.67	0.14(3.78	-
	0.4		3.88	0.10(2.45)	5.7
	0.8		4.63	0.28(6.08)	26.2
	1.2		5.08	-	38.4
Lytag	0	Table Vibrator	3.33	0.23(6.84)	-
	1.0		4.31	0.23(5.44)	29.4
Lytag	0	Poker Vibrator	3.53	0.22(6.10)	-
	1.0		4.65	0.24(5.23)	31.7

Table 3.10 Influence of Fibre Percentage on Ultimate Modulus of Rupture of the Control Specimens

Aggregate Type	% Fibre Volume	Method of Vibration	Average Ultimate M.O.R. N/mm^2	Standard Deviation N/mm^2 (%)	% Increase Relative to Plain Concrete
Gravel	0	Table Vibrator	3.67	0.14(3.78)	-
	0.4		4.82	0.25(5.09)	31.3
	0.8		5.97	0.30(5.04)	62.7
	1.2		6.54	-	78.2
Lytag	0	Table Vibrator	3.33	0.23(6.84)	-
	1.0		6.51	0.12(1.76)	95.5
Lytag	0	Poker Vibrator	3.53	0.22(6.10	-
	1.0		6.80	0.35(5.11)	92.6

This agrees with that of Ali (58) who reported an increase in the ultimate strength from 27.9 to 73.7% by using crimped fibres of 0.6 to 1.2% by volume.

For externally vibrated Lytag-sand concrete, the inclusion of 1.0% of crimped fibres increased the first crack strength by 29.4% and the ultimate strength by 95.5%. Whereas for internally vibrated Lytag-sand concrete this increase was 31.7 and 92.6% respectively. Thus both methods of compaction gave about the same percentage increases in the flexural strength. However, Swamy and Stavrides (65) and Ali (58) reported that external vibration increased the flexural strength significantly compared to internal vibration. Sittampalam (63) reported an increase of about 100% in the ultimate strength by using 1.0% by volme of crimped fibres while Theodorakopoulos (64) reported an increase of 75.9 and 107.4% for a crimped fibre content of 0.5 and 1.0% respectively.

Fig. 3.5 shows the development of the flexural stength of both plain and crimped steel fibre reinforced Lytag-sand concrete cured in uncontrollable laboratory conditions over a period of 180 days. It can be seen that there is a distinct difference in the stength development of the two types of concrete. The fibre concrete showed a gradual increase in the flexural strength up to 28 days and beyond this, there was very little increase in strength. The increase in the flexural strength at 90 days and 180 days over that at 28 days was 4.7 and 0.2% respectively. The plain concrete, on the other hand, showed a slower rate of increase in the flexural strength up to 28 days, then there was a significant increase at 90 days and stabilization occurred beyond this. The increase in the flexural strength at 90 days and 180 days relative to that at 28 days was 46.3

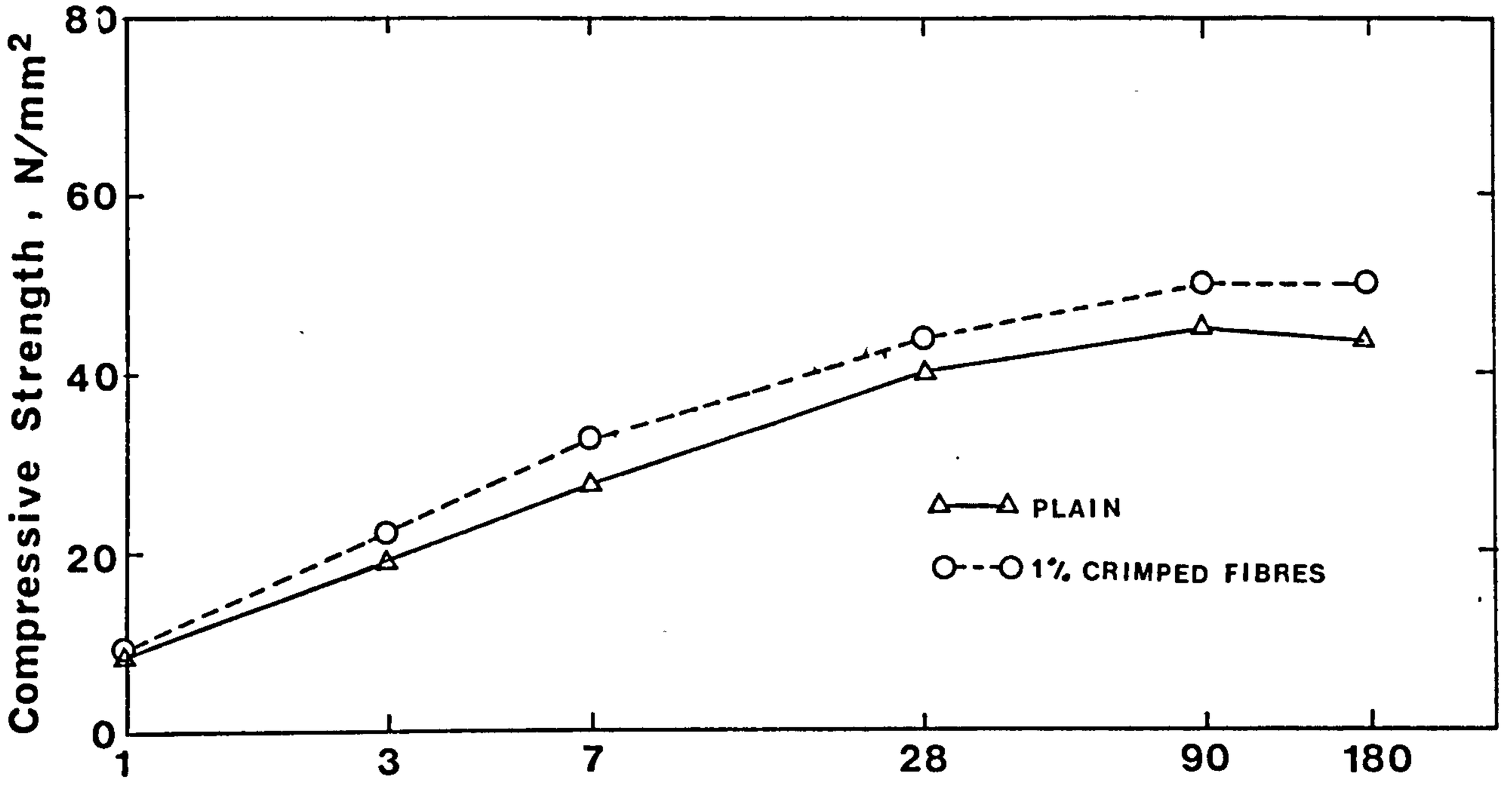

FIG·3·4 COMPRESSIVE STRENGTH DEVELOPMENT IN LYTAG-SAND CONCRETE

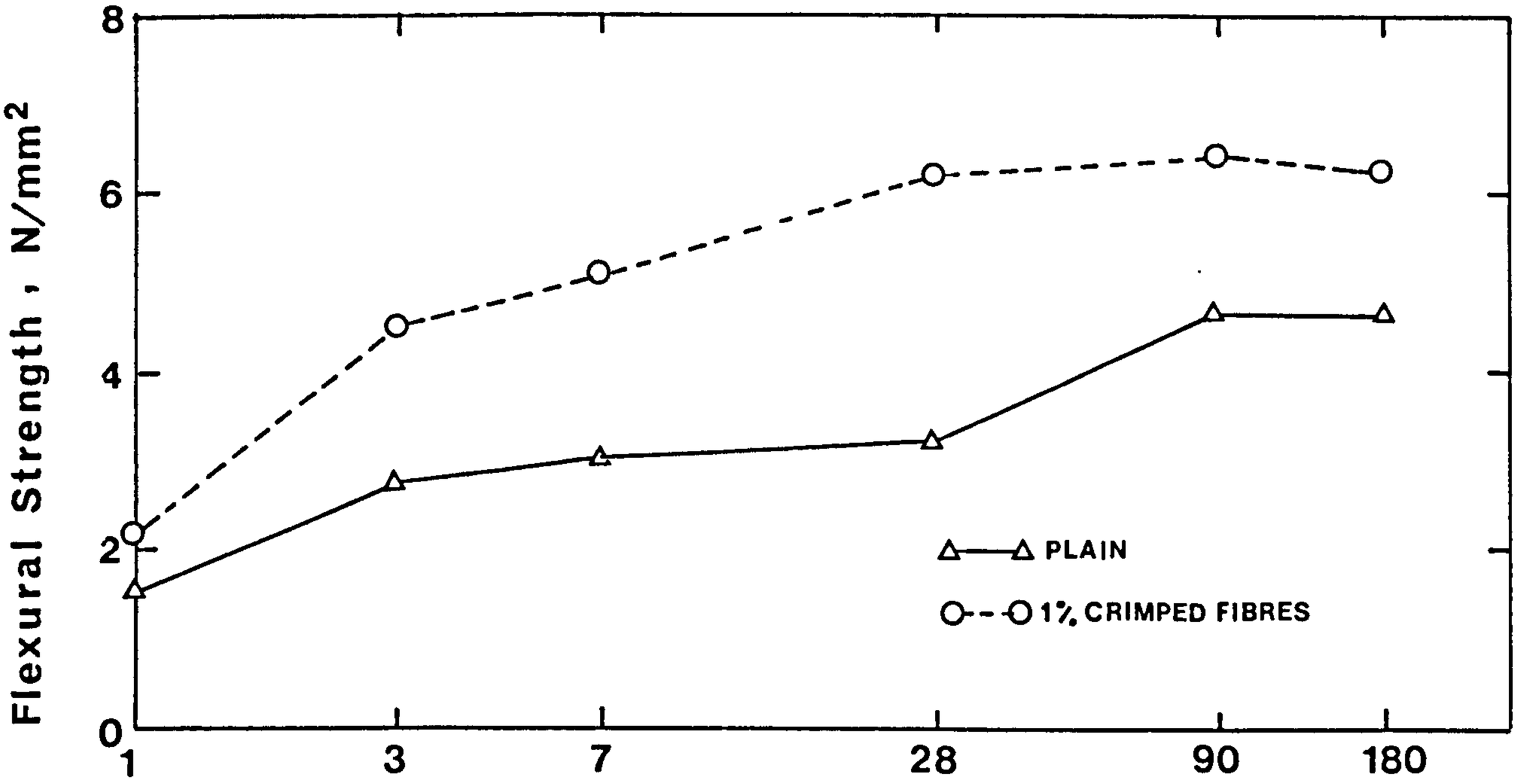

FIG·3·5 FLEXURAL STRENGTH DEVELOPMENT IN LYTAG-SAND CONCRETE

and 44.1% respectively. This observation confirmed that observed by Theodorakopoulos (64) who reported no significant increase in the flexural strength of crimped fibre reinforced Lytag-sand concrete after 28 days but a 49.4% increase in the flexural strength at 90 days over that at 28 days for plain Lytag-sand concrete. Both types of prisms were cured under uncontrolled laboratory conditions. The possible explanation of this is because of the tensile stresses induced in the outer 'fibres' of the specimens due to differential drying at earlier ages (66). As the specimens were already in a state of stress without a load, lower flexural strength was obtained. The specimens became uniformly dry with time, thus relieving the self-induced stresses and resulting in higher flexural strength. The presence of crimped fibres reduced shrinkage and this coupled with the fact that the ultimate flexural strength of fibre concrete depends substantially on the geometry and surface deformation and volume concentration of the fibres resulted in a different strength development pattern from that of plain concrete.

The plain concrete specimens had a brittle mode of failure and the crack was through the aggregates in the case of the Lytag -sand concrete and through the matrix and around the aggregates in the case of gravel concrete. This is not unexpected since the bond between the matrix and aggregate in the former was higher and the Lytag aggregates were weaker. The fibre concrete specimens showed a higher degree of ductility before failure. Several cracks usually occurred and final failure happened at the position of the first crack or at the position of a later crack. Fibre pull-out commenced as the maximum load was reached.

3.3.5.4 Bond Strength of Crimped Fibres

From the results of the modulus of rupture tests reported above, the average bond strength of the crimped fibres used in this investigation can be determined by adopting the method proposed by Swamy et al (1, 20, 21). The method was based on a dual criterion of crack control and composite mechanics and the general form of the derived equation is

$$\sigma_c = \sigma_m(1 - V_f) + 0.82\,\tau\,V_f \cdot \frac{l_f}{d_f} \qquad (3.1)$$

where σ_c = ultimate modulus of rupture of composite

σ_m = modulus of rupture of matrix

$\frac{l_f}{d_f}$ = aspect ratio of fibres

V_f = % fibre content by volume

and τ = bond strength

The average bond strength values obtained are tabulated in Table 3.11. A certain degree of balling occurred in the normal weight concrete mix with 1.2% of fibres by volume and this is reflected in the lower bond value obtained. From the analysis of their own test results and of others, Swamy and Mangat (20) obtained an average bond strength of 4.15 N/mm^2 for plain round fibres embedded in normal weight concrete or mortar. Theodorakopoulos (64) reported values of 4.53 and 4.11 N/mm^2 for crimped fibres (identical to those used in this investigation) embedded in normal weight and Lytag-sand concrete respectively. One of the reasons for the lower values obtained in this investigation is probably the lower grade of concrete used. Therefore, the values quoted in Table 3.11 are applicable only to the type of crimped fibres, mix proportions and methods

of vibration adopted in this investigation.

Table 3.11 Values of Bond Strength (τ) of Crimped Fibres Used in this Investigation

% Fibre Volume	Concrete	Method of Vibration	No. of Results	Average τ for M.O.R. tests, N/mm^2
0.4	Normal Wt	Table Vibrator	12	3.55
0.8	Normal Wt	Table Vibrator	12	3.54
1.2	Normal Wt	Table Vibrator	3	3.00
1.0	Lytag-sand	Table Vibrator	9	3.92
1.0	Lytag-sand	Poker Vibrator	27	4.04

3.3.5.5 Static Modulus of Elasticity

The test was carried out on 100 x 100 x 300 mm prisms according to B.S. 1881:Part 5(10). The longitudinal strains were measured with a Demec gauge over a gauge length of 100 mm in the middle third on two opposite sides of each specimen. The test was conducted only on Lytag-sand concrete specimens.

The results of static modulus of elasticity test on all the control prisms of the beams are shown in Table 3.7 while Table 3.12 gives the average values and the percentage increase of the crimped fibre concrete relative to the plain concrete. It can be noted that an increase of 9.7% was achieved when 1.0% fibre content by volume was used. Theodorakopoulos (64) reported an increase in the static modulus of 12.0% for Lytag-sand concrete when using 1.0% of crimped fibres by volume. Ritche and Al-Kayyali (67) reported an increase of about 3.9% for Lytag concrete when 0.6% of Duoform fibres by volume were

used. For normal weight concrete, the increase was 18.2% (58) and 20.6% (6) when 0.9% and 1.2% respectively of crimped fibres by volume were used.

The average static modulus for the plain Lytag-sand concrete (Table 3.12) was 19.5 kN/mm^2. Application of the method in section 2.4.2.2 of CP110 (68) for lightweight concrete yielded a value of 20.0 kN/mm^2, an overestimation of only 2.5%

Table 3.12 Average Static Modulus of Elasticity and Poisson's Ratio

	Concrete	% Fibre Volume	No. of Specimens	Mean Value	Standard Deviation	% Increase relative to plain
Static Elastic Modulus kN/mm^2	Lytag-sand	0	27	19.5	0.40 (2.05%)	-
		1.0	18	21.4	0.39 (1.82%)	9.7
Poisson's Ratio	Lytag-sand	0	27	0.19	0.009 (4.96%)	-
		1.0	18	0.18	0.007 (4.21%)	-6.8

3.3.5.6 Poisson's Ratio

The test was carried out in conjunction with the static modulus test on 100 x 100 x 300 prisms. The longitudinal strains were measured as described in the previous section. The lateral strains were measured with a Demec gauge over a gauge length of 50 mm at the centre on two opposite sides of the specimens. Again the test was only carried out on Lytag-sand concrete specimens.

The results of the Poisson's ratio test on all the control prisms of the beams are shown in Table 3.7 while Table 3.12 gives the average values and the percentage increase of

of the fibre concrete relative to plain concrete. The average value for plain Lytag -sand concrete was 0.19 and this is within the range of 0.15 to 0.20 generally quoted for normal weight concrete (68, 69). Inclusion of 1.0% of crimped fibres by volume effected a decrease of 6.8%. For normal weight concrete, Ali (58) reported a decrease of 21.1, 31.6, and 21.1% when crimped fibre contents of 0.6, 0.9 and 1.2% by volume were used respectively.

3.4 Conclusions

1. PFA replacement of cement and sand can be successfully carried out to obtain Lytag-sand concrete mixes of good early strength.

2. Fibres can be introduced and successfully incorporated in both gravel and Lytag-sand concrete mixes.

3. Inclusion of crimped steel fibres effected a small increase in the 28-day compressive strength. For externally vibrated gravel concrete, an increase of 4.9 to 10.1% was achieved when 0.4 to 1.2% by volume of fibres were used. For Lytag-sand concrete with 1.0% by volume of fibres, the increase was 7.8% and 2.8% for externally and internally vibrated concrete respectively.
The compression strength development of both plain and fibre Lytag-sand concrete cured in uncontrolled laboratory conditions seems to follow similar pattern and both seem to stabilize after about 90 days.

4. The 28-day dry density of plain Lytag-sand concrete was 1820 kg/m^3. The use of 1.0% by volume of crimped steel fibres caused an increase in the density of about 2.2%

5. For externally vibrated gravel concrete, the inclusion of

crimped steel fibres of 0.4 to 1.2% by volume increased the 28-day first crack modulus of rupture by 5.7 to 38.4% and the ultimate strength by 31.3 to 78.2%. The corresponding increases in Lytag-sand concrete with 1.0% of fibres were 29.4 and 95.5% respectively for externally vibrated concrete and 31.7 and 92.6% respectively for internally vibrated concrete.

Plain Lytag-sand concrete, cured under uncontrolled laboratory conditions, exhibited a 49.4% increase in the ultimate flexural strength at 90 days over that at 28 days. Fibre reinforced Lytag-sand concrete, on the other hand, showed no significant increase in strength after about 28 days.

6. Inclusion of 1.0% by volume of crimped fibres caused a 9.7% increase in the static elastic modulus of Lytag-sand concrete.

7. A decrease of 6.8% in the Poisson's ratio of Lytag-sand concrete was achieved by the use of 1.0% by volume of crimped fibres.

CHAPTER FOUR

BOND STRESS-SLIP CHARACTERISTICS IN FIBRE CONCRETE

4.1 Introduction

One of the most important factors that affects the behaviour of reinforced concrete structures is the bond stress-slip characteristics at the interface between concrete and reinforcement. It has a major influence on the spacing and width of tensile cracks and on the distribution of concrete stresses in cracked concrete members.

The basic nature of bond is a complex phenomenon and, despite the numerous experimental and analytical studies that have been carried out thus far, is not yet fully understood. This is not surprising as there are many factors influencing bond and it is not always possible to isolate them in tests. Measurement of bond stress distribution and particularly slip along the interface betwen concrete and steel is complicated and because of the small magnitude involved, local slip measurement is highly sensitive to experimental errors. Furthermore, bond in actual structures exists under a wide variety of complex stress conditions which are unlikely to be simulated in simple bond test specimens.

Deformed bars with high yield strength are of common usage in the modern construction industry. Bond failure of such bars is generally associated with longitudinal splitting in the concrete cover of the bars. Longitudinal splitting occurs when the principal tensile stress, generated by bearing under the ribs, exceeds the tensile strength of the concrete. The presence of stirrups in conventional reinforced concrete structures slows the propagation of the splitting crack and keeps its width small. However, whether the ultimate bond stress is increased or not depends on the amount of stirrups used (2,70).

Therefore in this subsidiary experimental investigation, the effectiveness of steel fibres in containing the longitudinal splitting crack and their influence on the ultimate bond strength and bond stress-slip characteristics are investigated. A limited number of tests were carried out using concentric pull-out specimens with short embedded length. The reinforcing bars were 16 mm diameter deformed bars (Tor Bar) and both normal weight and lightweight concrete were used. The bond stress-slip relationships obtained from these tests may be useful in analytical studies of reinforced concrete.

4.2 Bond Action

Bond can be considered as the shearing stress or force between a bar and the surrounding concrete. The force in the bar is transmitted to the concrete by bond, or vice versa. Basically, bond is made up of three components (2):

(i) Chemical adhesion

(ii) Friction

(iii) Mechanical interaction between concrete and steel.

Bond for plain bars depends mainly upon chemical adhesion and after slip upon friction. There is also some interlocking due to roughness of the bar surface. Deformed bars, however, depend primarily on mechanical interlocking for superior bond qualities. The effect of chemical adhesion and friction are still there but they are secondary.

According to Rehms (71) and Lutz and Gergely (70), slip of deformed bars can occur in two ways:

(i) The ribs can push the concrete away from the bar (wedging action) and

(ii) The ribs can crush the concrete.

They have also observed that ribs with a face angle greater than 40^{o} (the face angle of ribs is measured with respect to the bar axis) produce the same movement. This suggests that, for these angles, the friction between the rib face and the concrete is sufficient to prevent relative movement at the interface and consequently, slip is due almost entirely to the crushing of the concrete in front of the ribs. Wedging action does not appear until considerable crushing has occurred, at which time a wedge of crushed concrete becomes lodged in front of the rib and moves along with it. However, extensive crushing and wedge action in front of every rib cannot occur without transverse and longitudinal cracking in the surrounding concrete. For bars with ribs having face angles less than about 30^{o}, the friction between the rib face and the concrete is not sufficient to prevent relative movement. Slip is then due primarily to the relative movement between the concrete and steel along the face of the rib, and secondarily to some crushing of the mortar.

Recent analytical and experimental studies on internal cracking associated with the development of bond stresses in concrete tension prisms (72, 73, 74) have established the existence of inclined cracks originating at the steel-concrete interface and terminating within the prism, i.e., not extending to the concrete surface and therefore not visible to the outside observer. With the formation of such inclined cracks, the concrete round the reinforcing bar takes a comb-like appearance as shown in Fig. 4.1. The deformation of the teeth of the comb-like concrete serves to tighten the concrete around the reinforcing bar and increases the frictional resistance between concrete and steel. The reaction of this tightening force also produces ring tension in the concrete around the bar, which can be another cause

of the formation of longitudinal cracks (74).

4.3 Review of Past Research

A summary of only some of the more important work is given.

4.3.1 Bond Stress Distribution

The local bond stress at any point on the interface between an embedded bar and the surrounding concrete can be determined by using the following equation:

$$f_{bs} = \frac{A_s}{\Sigma U} \cdot \frac{df_s}{dx} \qquad (4.1)$$

where f_{bs} = local bond stress at the point considered

ΣU = bar perimeter

A_s = bar cross sectional area

df_s = change in steel stress in the bar over an infinitesimal length dx.

Equation (4.1) can be rewritten in terms of the steel strain by:

$$f_{bs} = \frac{A_s \cdot E_s}{\Sigma U} \cdot \frac{d\varepsilon_s}{dx} \qquad (4.2)$$

where ε_s = strain in the bar at the point considered

E_s = elastic modulus of steel bar.

Thus at any load, the bond stress at any point along a bar embedded in concrete is proportional to the slope of the steel stress or steel strain distribution curve at the point considered.

The bond stress distribution along a bar can be obtained through measurements of the steel strain distribution along the embedded bar. Several techniques have been adopted to measure the steel strain distribution and each has its limitations.

Watstein (75) measured steel strains at intervals

along an embedded bar using external dial gauges in conjunction with access slots through the conrete permitting access to small holes drilled in the side of the embedded bar. This method has the disadvantage that the bond distribution around the holes is modified.

Some investigators have used electrical resistance strain gauges bonded to the outer surface of the steel bar, but this is objectionable since the presence of properly waterproofed gauges at the desired close spacing modifies the distribution of steel strain and bond. A slightly improved version is to mount the strain gauges on either side of a small slot cut into the bar from one side.

A better technique perhaps is the one introduced by Mains (76). He used electrical strain gauges mounted internally at close spacing in a hollow core formed by sawing one bar longitudinally in a diametrical plane, milling a slot along the centre line of each cut surface, and tack welding the bar together in its original position, after bonding the gauges in the slots. Many subsequent investigators adopted this method to measure the steel strain distribution of a bar embedded in plain concrete (50, 77, 78) or fibre concrete (79).

4.3.2 Slip Between Reinforcing Bar and Concrete

The measureement of local slip at the steel-concrete interface is a formidable problem. Several techniques have been attempted. Evans and Robinson (80) used a radiographic technique in which thin strips of lead were inserted into holes drilled in the bar. The carefully placed markers projected about 1 mm into the concrete. Before-and-after X-ray photographs indicated the amount of relative movement or slip. This method is unsatisfactory because of artificial constraints in proportioning

the test specimens and the need of expensive equipment and stringent safety precautions.

Attempts to measure directly the local slip between steel and concrete in realistic specimens were initiated at Cornell University by Ruiz in 1968 (cited in (78)). He developed a slip gauge using a standard electric resistance strain gauge installed with the central portion unbonded. One end of the gauge was bonded to the reinforcing bar, the other bonded to a small cube of mortar later to be embedded in the concrete. The gauges were placed parallel to the axis of the bar, and after pretensioning and calibrating were waterproofed and completely encased by the poured concrete. Encouraging results were claimed to have been obtained. However, these gauges required great care in their placement and calibration and, most importantly, their presence interfered with the bonding surface to a possibly significant degree.

Wahla et al (81), in addition to using Ruiz's technique also used miniaturized differential transducer gauges to measure slip directly at internal locations in several types of reinforced concrete specimens. But the fixing pin attached to the transducer casing and placed in a positioning hole drilled into the reinforcing bar interfered with the normal bond distribution.

The more recent attempt at Cornell University, under the direction of Nilson (78), made use of internal strain gauges for concrete. Each consisted of a wire resistance strain gauge cemented between two thin polyester resin blocks. The outer surface of the resin was coated with a coarse grit material to provide good bonding with the concrete. Several of such gauges were embedded in the concrete along the length of the specimen, about 12 mm from the surface of the reinforcement. The variation

of the slip along the steel-concrete interface was obtained from the internal measurements of concrete strain and steel strain by integrating the steel and concrete strains along the length of the bar. This technique of obtaining local slip has two advantages. The embedded strain gauges did not interfere with the normal distribution of bond stresses at the interface. They could be regarded as the equivalent of pieces of aggregate. The slip along the entire interface could be found. However, the calculations required were labourious since strain, displacement and slip functions must be determined at each increment of applied load. Slip was indirectly obtained from concrete and steel strain measurements which were both subject to experimental error. In additon, the concrete strains were measured about 12 mm from the surface of the bar.

4.3.3 Bond Stress-Slip Relations

Rehm (71) appears to be the first investigator to get directly the relationship betwen bond stress and the associated displacement on a localized basis. He conducted pull-out tests of plain and specially-made bars having a single projecting annular rib of different shapes which were centrally embedded in 100 mm and 200 mm cubes. The length of embedment used varied between 3 and 67 mm. The bond stress-slip relationships were obtained directly from the load indicated on the testing machine and the displacements measured at the free end of the specimens. These relationships constitute what Rehm termed a 'fundamental law for bond'. The applicability of his results to real bar reinforcement is open to question because of the highly idealized bars used. Further studies of this nature were conducted by Lutz and Gergeley (70).

Edwards and Picard (82) conducted tests on short

length pull-out specimens to obtain bond-stress-slip curves for a 12.7 mm diameter strand. The embedded length was 38.1 mm and three covers of 12.7, 25.4 and 38.1 mm were used. The load in the bar was measured by calibrated measuring bars passing through holes provided in the specimen and both loaded and free end slips were measured by linear displacement transducers. The bond stress-slip curves obtained could be idealized as elastic-plastic and the average value of the maximum bond strength decreased when the concrete cover was increased. This was attributed possibly to the settlement of concrete under the strand which was held in a horizontal position during casting.

Edwards and Yannopoulos (83) later adopted the same method to obtain statistically dependable bond stress-slip curves for 16 mm diameter hot rolled deformed bars (Welbond) and mild steel plain bars. Two concrete covers of 25 and 35 mm, two directions of bar pull relative to the settlement of concrete, and different magnitudes of bar back load were used. A concrete embedment length of 38 mm was adopted. The scatter in the bond stress-slip curves obtained was considerable. However, there was no appreciable difference in the mean initial slope of the bond stress-slip curves (slip modulus) obtained from specimens of different concrete cover, different bar back load values or different direction of bar pull relative to the direction of settlement of concrete. The maximum bond stress was not significantly affected by the magnitude of the bar back load and hence by influence by distance from a crack face, or a loaded end, in a concrete member. But it increased with increasing concrete cover and increased to a less extent when the bar was pulled in the opposite direction to that of casting as compared to pulling it in the same direction. This was attributed to

the settlement and pore formation in the concrete below every bar deformation.

Nilson (84), in his finite element analysis of reinforced concrete structures, derived a bond stress-slip relationship indirectly from experimental data obtained by Bresler and Bertero (85). The latter carried out tests on concentrically reinforced concrete cylinders. Tensile load was applied axially on both ends of the steel bar and the strain along the embedded length was measured using the technique developed by Mains (section 4.3.1). From these strain measurements, the local bond stress was determined. However, slip between steel and concrete was measured only at the end faces. Therefore, local slip had to be obtained indirectly by estimating the concrete displacement on the basis of the measured end slips. Nilson then fitted a third degreee polynomial to the resulting data. The reliability of the bond stress-slip curve obtained is questionable because of the simplifying assumption that had to be made in estimating the concrete displacement.

More recently, Nilson (78) attempted to establish bond stress-slip relationships in reinforced concrete by carrying out direct measurements. He used concentric tension specimens reinforced with a 25 mm deformed bar. The variation of steel strain along the length of the bar was measured using Main's technique. The local slip between steel and concrete was determined using the technique as described in section 4.3.2 (Nilson's technique). Tedious calculations had to be done before the bond stress-slip curves could be plotted. Nilson found that both the peak local bond stress and the slip modulus varied with distance from the loaded end of the specimens tested (and, by analogy with distance from a crack face in typical members).

These bond stress-slip curves have been applied by several investigations in their finite element analysis of reinforced concrete structures (52, 62). Typical curves are shown in Fig. 4.2.

Houde and Mirza (50) conducted concentric tension tests on specimens with varying cross sections and reinforced with a single steel bar of diameter 12, 19 or 25 mm. The tensile stress variation along the bar was measured using a technique similar to that of Mains. Slip was measured at the end faces, being 406 or 838 mm apart. First, they derived an empirical expression for the endslip in terms of the applied steel stress at the face, the steel bar cross-sectional area and the area of surrounding concrete in tension. Local bond stresses at known points along the bar were calculated at each load level using the bar tensile stress curve. Slips of the bar, at the same locations, for known bar tensile stress levels, were evaluated using the derived expression. The applicability of the empirical slip expression derived solely from end slip measurements to determine local slip within the specimen is open to question.

4.4 Test Specimens and Parameters Studied

Noting the limitations of all types of simple bond test specimens (section 4.1) and the fact that this study formed only a minor part of the overall investigation, a concentric pull-out specimen as shown in Fig. 4.3 was adopted. Theoretically the embedded length should be as small as possible, so that the local bond stress-slip relation is determined. However, practical considerations limit the size, and the length of embedment chosen was 50 mm. This was the same as that used by Tepfers (86).

The reinforcing bar used was a 16 mm diameter cold twisted and high yield type 2 deformed bar (Tor Bar). The

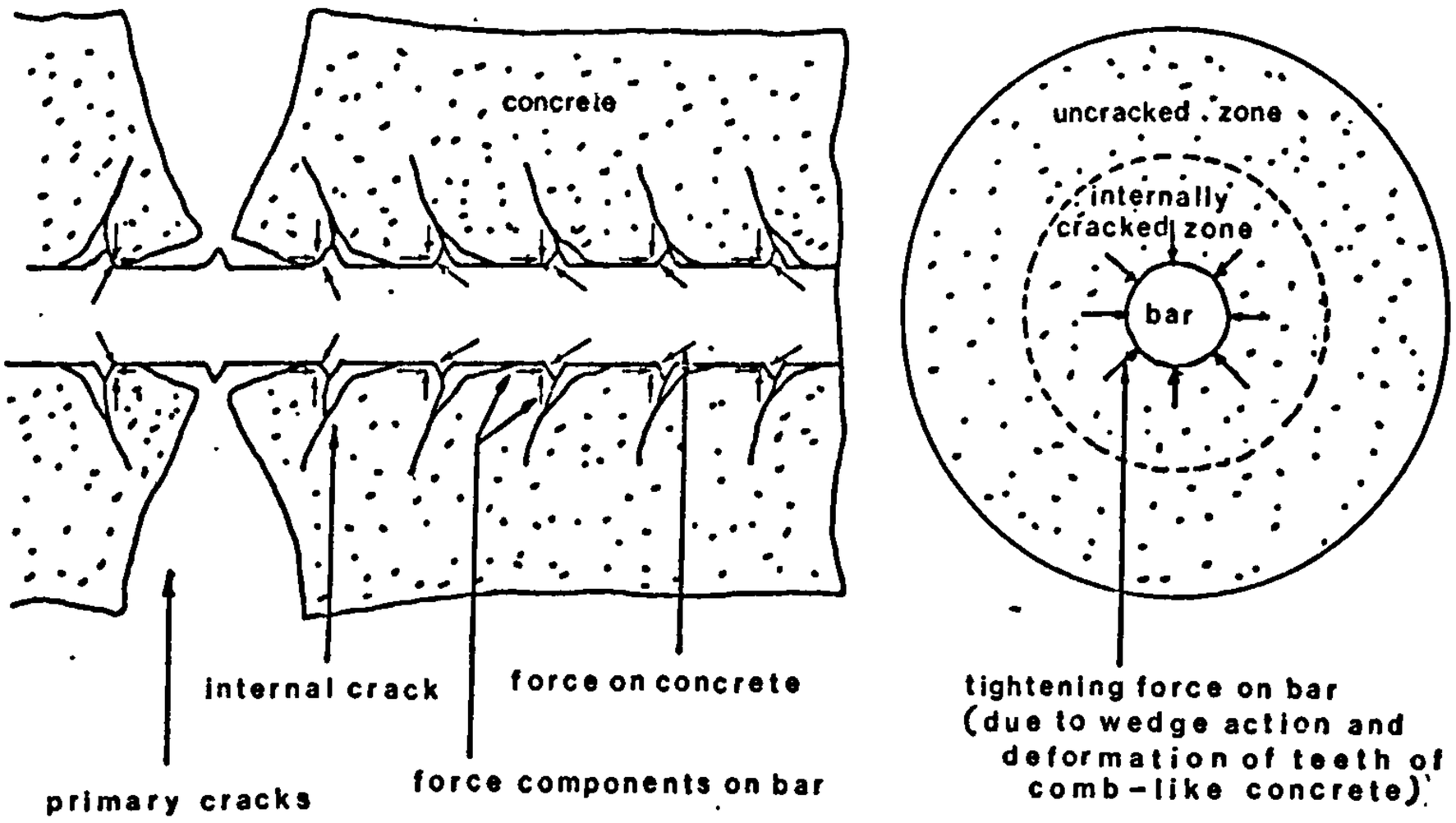

Fig. 4·1 Deformation of Concrete Around Reinforcing Steel After Formation of Internal Cracks (after Goto (74))

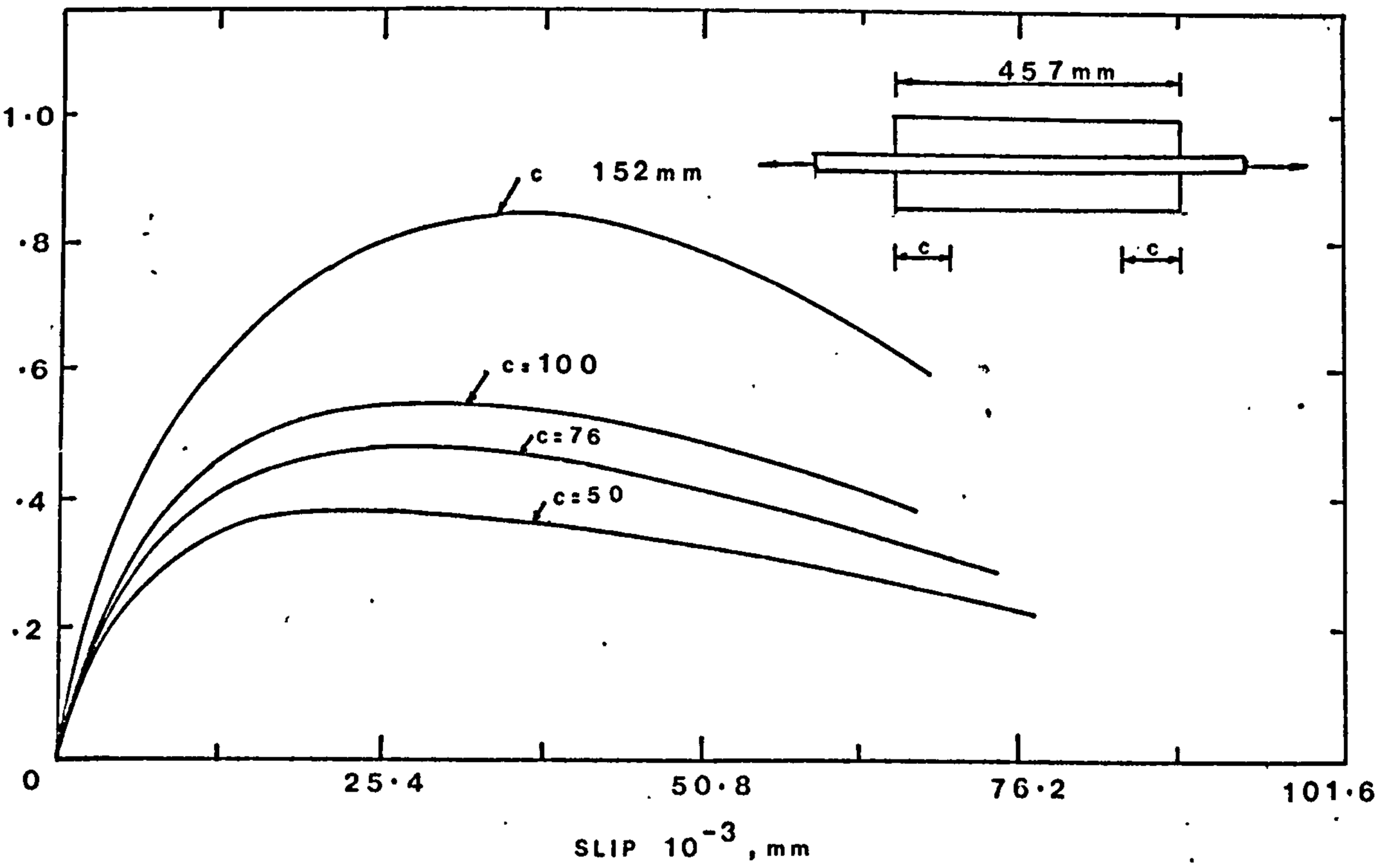

FIG. 4·2 BOND STRESS VS. SLIP-CONCENTRIC TENSION TESTS (AFTER NILSON (78))

specified characteristic strength was 460 N/mm^2 and the stress-strain curve and strength properties obtained by extensometer tests are given in Fig. 3.3 and Table 3.2 respectively. The bar consisted of a circular core with two continuous helical longitudinal ribs and transverse ribs on opposite sides of the bar. The spacing of the transverse ribs was 10.7 mm and thus the embedment length used was 4.67 times the rib spacing. Detailed information on Tor Bar can be found in Ref. (87).

Two concrete covers of 42 and 67 mm were chosen. This choice of cover enabled the use of standard cylinder moulds of 100 and 150 mm in diameter respectively for casting the specimens.

Two types of coarse aggregates were used and these were 10 mm maximum crushed gravel and Lytag lightweight aggregates. The physical properties of these aggregates are given in section 3.2.4. The mix proportions used are given in sections 3.3.1 and 3.3.2.

The steel fibres used were 0.5 x 50 mm crimped fibres and 0.418 mm equivalent diameter and 25 mm long Japanese fibres. The properties of the fibres are given in section 3.2.6. For the crimped fibres, fibre percentages by volume of 0, 0.4, 0.8 and 1.2 were used for gravel concrete and 0 and 1.0 for Lytag-sand concrete. For Japanese fibres, a volume percentage of 0.8 was used.

4.5 Casting of Specimens

First the standard cylinder mould was cleaned thoroughly and a thin layer of oil was applied. A solid cylinder was placed at the base of the mould to give the required height to the specimen. The reinforcing bar with rubber tubes correctly held in place by blu-tack was then lowered into the mould, centred carefully and then clamped in position as shown in Fig. 4.4. The centering

process was facilitated by the use of a transparent perspex sheet with marking and a hole drilled at the centre of the solid cylinder.

The concrete was then poured into the mould in two layers, and compacted well by using a table vibrator.

At least three specimens and three 100 x 100 x 100 mm control cubes were cast for each test. All specimens were left under polythene sheets in the laboratory for 24 hours before they were demoulded and stored in the laboratory under uncontrolled conditions until they were tested at 28-days.

4.6 Instrumentation and Testing Procedure

The test set-up is shown in Fig. 4.5. The test specimen was mounted centrally in a specially-made test frame. Each bar of the frame was fixed with 2 strain gauge rosettes (Kyowa Type FCA-2-11) and when carefully calibrated, served as a load cell with a sensitivity of ±0.06kN. The top face of the lower plate was machined. A hard board was placed between the bearing face of the test specimen and this machined face. This was necessary as the end of the reinforcing bar at which the pull was applied was that which projected from the top end of the concrete cylinder as cast. Vertical movement was confined to the upper grip of the standard Avery test machine (100 kN maximum capacity). The upper grip was also free to rotate.

Slip was monitored at the free end of the test specimen by using an induction type linear displacement transducer (LVDT) with a sensitivity of ±0.001 mm.

The test specimen was subject to monotonically increasing load at a rate of approximately 0.1 kN/sec and the load in each of the calibrated bars and slip were monitored continuously by a portable data logger.

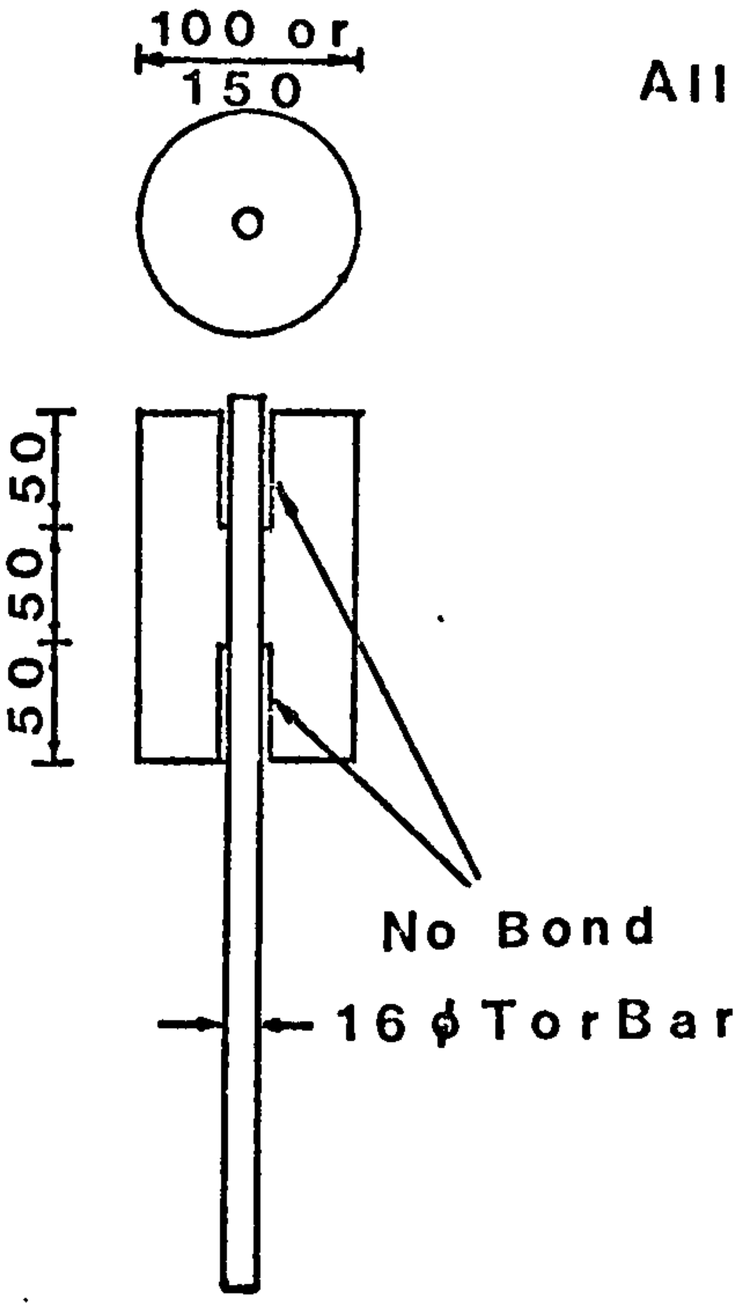

Fig. 4·3 Details of Pull-out Specimen

All dimensions in mm

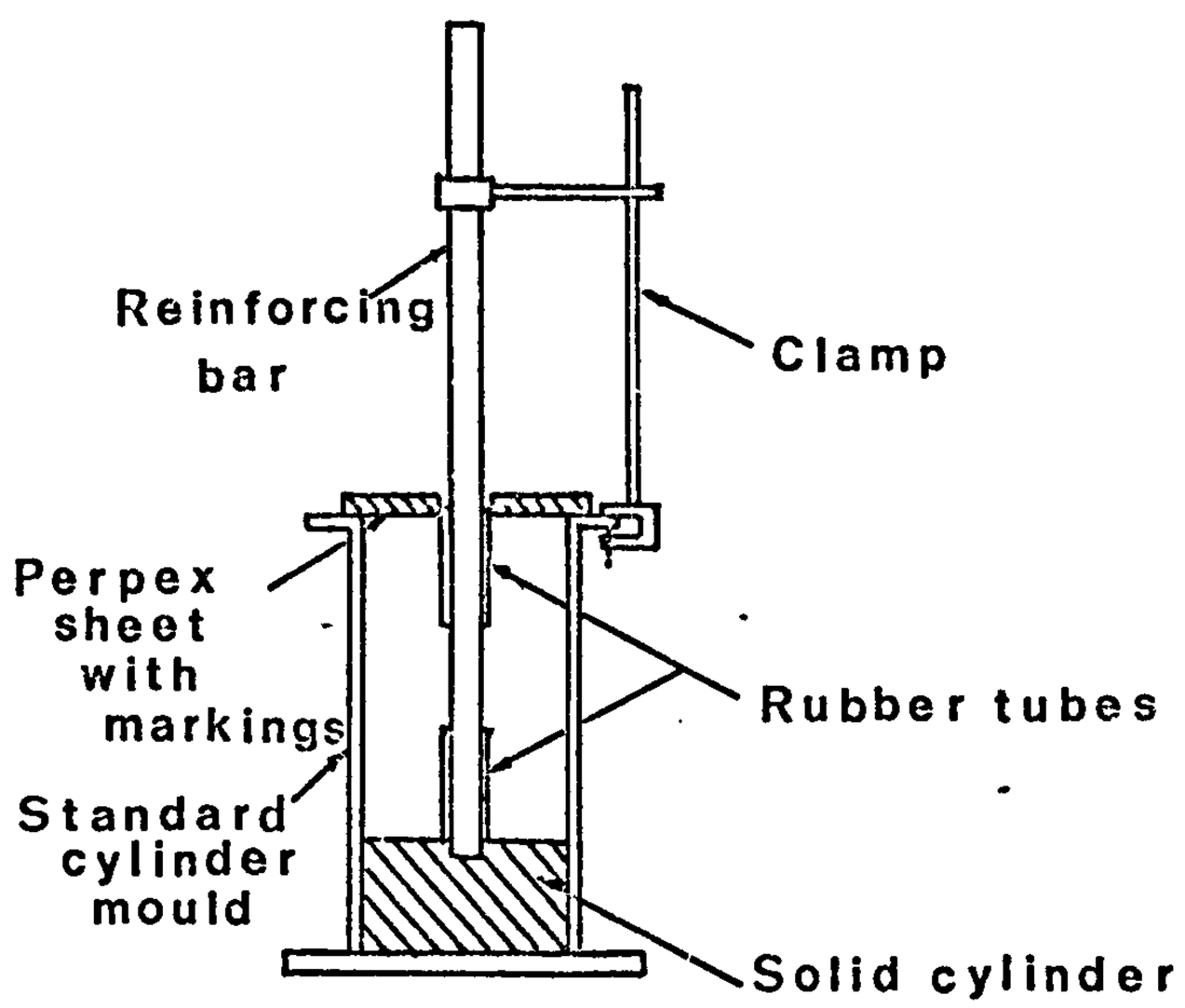

Fig. 4·4 Casting of Pull-out Specimen

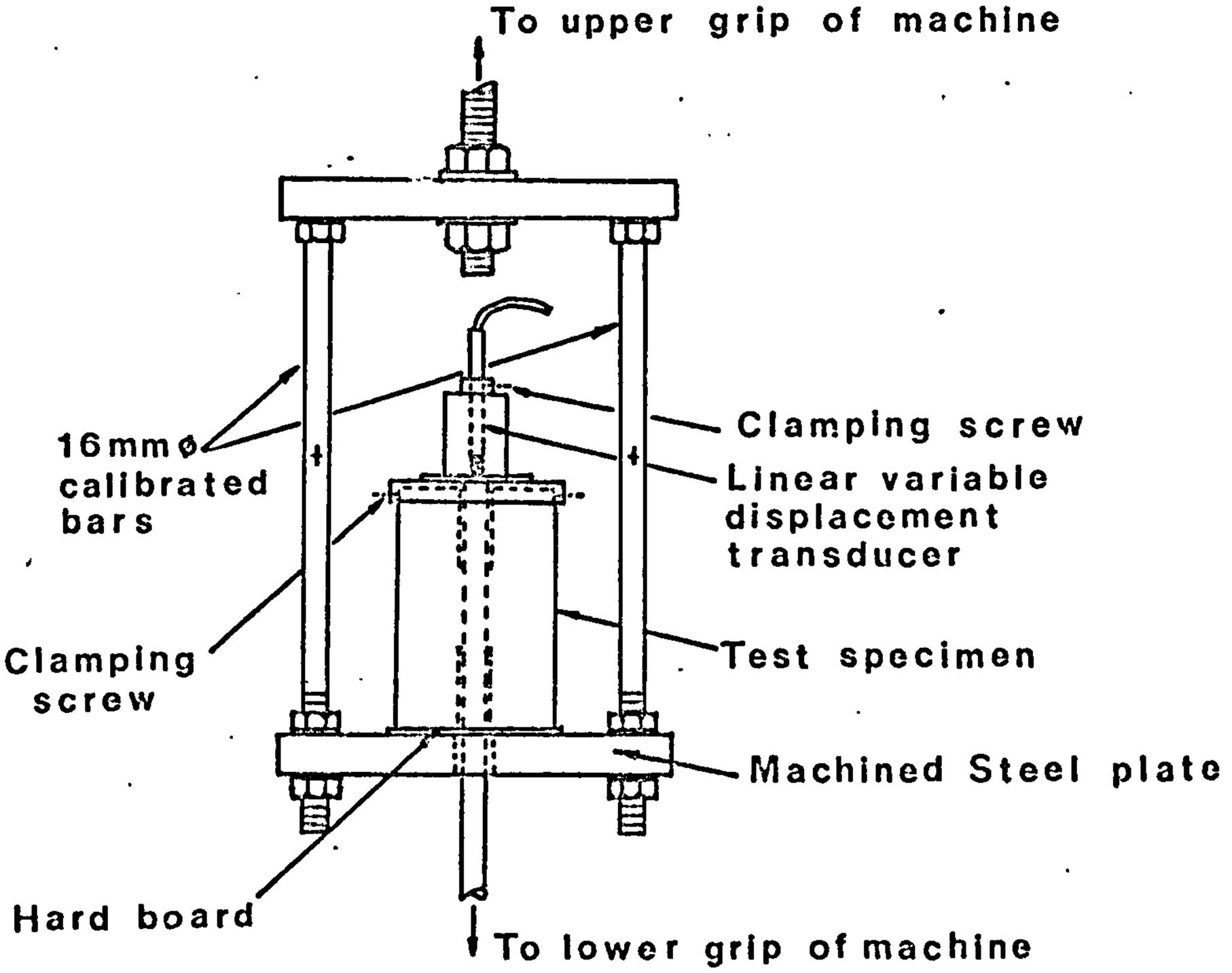

Fig. 4·5 Test Set-up of Pull-out Specimen

4.7 Test Results and Discussion

4.7.1 Mode of Failure

The failure of all the 100 mm diameter specimens was associated with the formation of longitudinal and transverse cracks. For the plain concrete specimens, failure occurred immediately after the formation of these cracks. The failure was sudden and the specimens broke into several pieces. The imprint of the bar ribs could be seen clearly in the split concrete pieces. For the fibre specimens, on the other hand, failure was gradual but a greater number of finer longitudinal and transverse cracks were present. In almost all the fibre cases, the longitudinal cracks did not extend throughout the whole length of the specimens. Complete pulling out of the bar was possible without the disintegration of the surrounding concrete. Plate 4.1 shows some of the specimens after failure.

In almost all the 100 mm diameter specimens, the transverse cracks appeared at the same instant as the longitudinal cracks. However in the test with 1.2% of crimped fibres, one longitudinal crack appeared first at peak load and more longitudinal and transverse cracks appeared later. This seems to suggest that the formation of the transverse cracks could possibly be as a result of stress distribution after the formation of longitudinal cracks.

Longitudinal splitting was less dominant in the 150 mm diameter specimens. Indeed most of them had no visible longitudinal or transverse cracks at failure. Failure in all the specimens was gradual and complete pulling out of the bar was possible without the break-up of the surrounding concrete. Bond failure resulted mainly from concrete crushing at the bearing face of the ribs and by shearing of the concrete around the

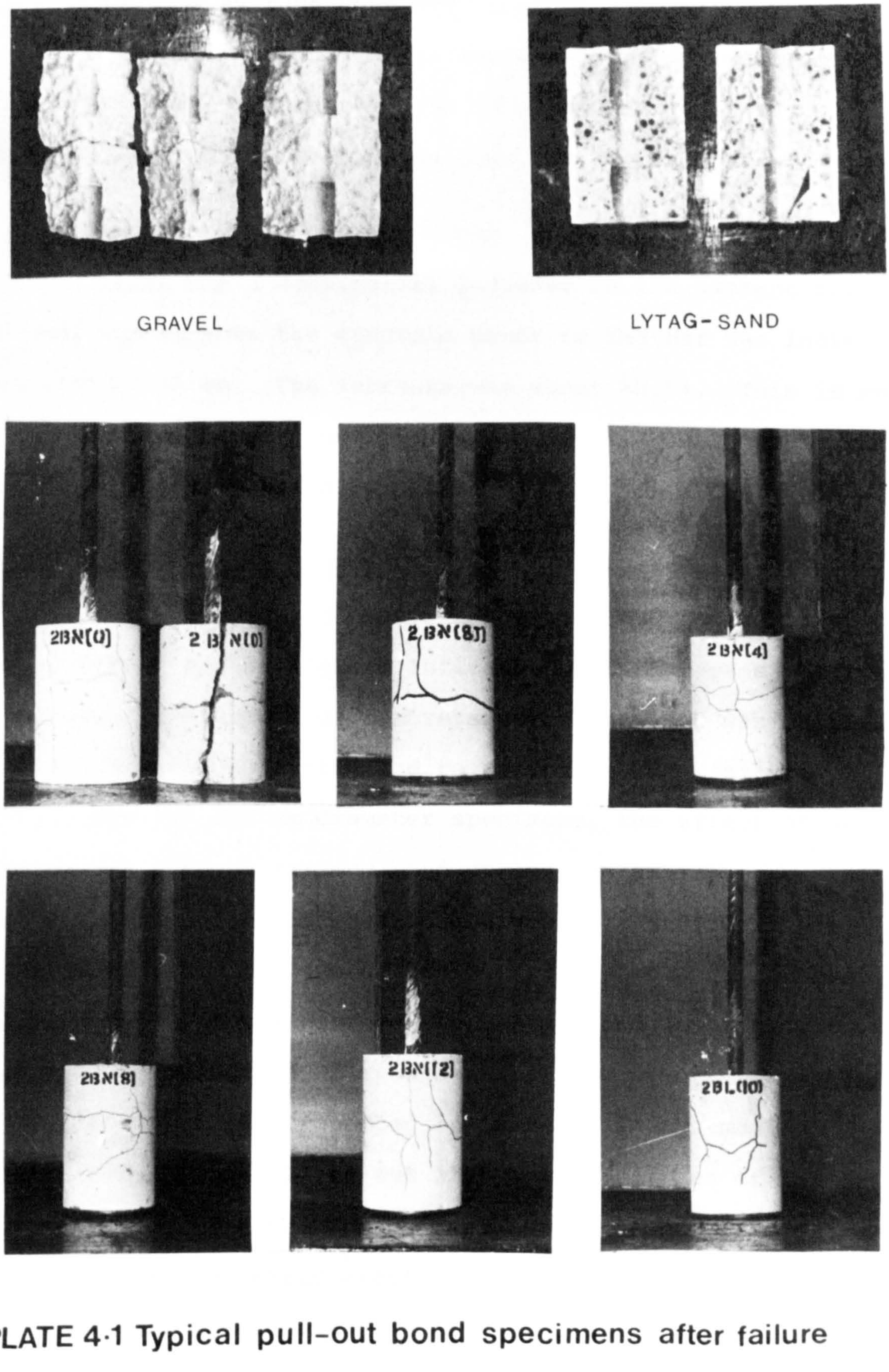

PLATE 4·1 Typical pull-out bond specimens after failure

extremities of the bar.

4.7.2 Maximum Average Bond Stresses

The maximum bond stress and the compressive strength of the control cubes of each test are tabulated in Table 4.1. The bond stress quoted is the average over the 50mm embedment length.

4.7.2.1 Influence of Concrete Cover

There was a substantial increase in the average maximum bond stress when the concrete cover to the bar was increased from 42 mm to 67 mm. The increase was about 80.5%. This is not unexpected since bigger concrete cover offers greater confinement to the bar against tensile splitting.

4.7.2.2 Influence of Fibres

For the 150 mm diameter specimens, the inclusion of Japanese fibres had negligible influence on the average maximum bond stress. The amount of concrete cover provided was sufficient to contain tensile splitting and to prevent sudden failure.

For the 100 mm diameter specimens, the effect of steel fibres on the average maximum bond stress was small. For gravel concrete specimens, an increase of between 2.2 and 10.1% was achieved when fibre content of 0.4 to 1.2% by volume was used. An increase of 4.5% was achieved for Lytag-sand concrete with the use of 1.0% by volume of crimped steel fibres.

Al-Noori (88) reported an increase in the maximum bond stress of between 26 to 60% when crimped fibres of 1.0 and 2.0% by volume were used. He carried out pull-out tests on 150 mm diameter concentric gravel concrete specimens of 100 and 150 mm embedment length and the diameters of the deformed bars ranged from 12 mm to 25 mm. In addition, each specimen was

reinforced with a helix of 6 mm diameter plain mild steel at 25 mm pitch. The discrepancy betwen Al-Noori's results and those of the author is possibly due to the larger embedded length and the use of helical reinforcement in the former case.

4.7.2.3 Influence of Aggregate Type

The average maximum bond stress of Lytag-sand concrete pull-out specimens was marginally less than that of corresponding gravel concrete specimens. The difference was only about 4.5% for plain 100 mm diameter specimens.

4.7.3 Bond Stress-Slip Relations

The bond stress-slip relations obtained from the various tests are shown in Figs. 4.6 through 4.14. The average slip modulus for each test is given in Table 4.1. The bond stress-slip curves were produced by a computer plotter. All replications of the same test are shown on the same figure for ease of comparison.

4.7.3.1 Influence of Concrete Cover

The bond stress-slip curves of plain concrete specimens with 67 mm cover were quite different from those of corresponding specimens with 42 mm cover. Though the initial slip moduli for both cases were more or less the same, in the former case, maximum bond stress was reached after a substantial amount of slip while in the latter, maximum bond stress was reached after a slip of about 0.4 mm. This difference in behaviour was due to the different nature of bond failure as explained in section 4.7.2.

4.7.3.2 Influence of Fibres

Inclusion of steel fibres had a negligible influence on the bond stress-slip relations of test specimens with 67 mm concrete cover.

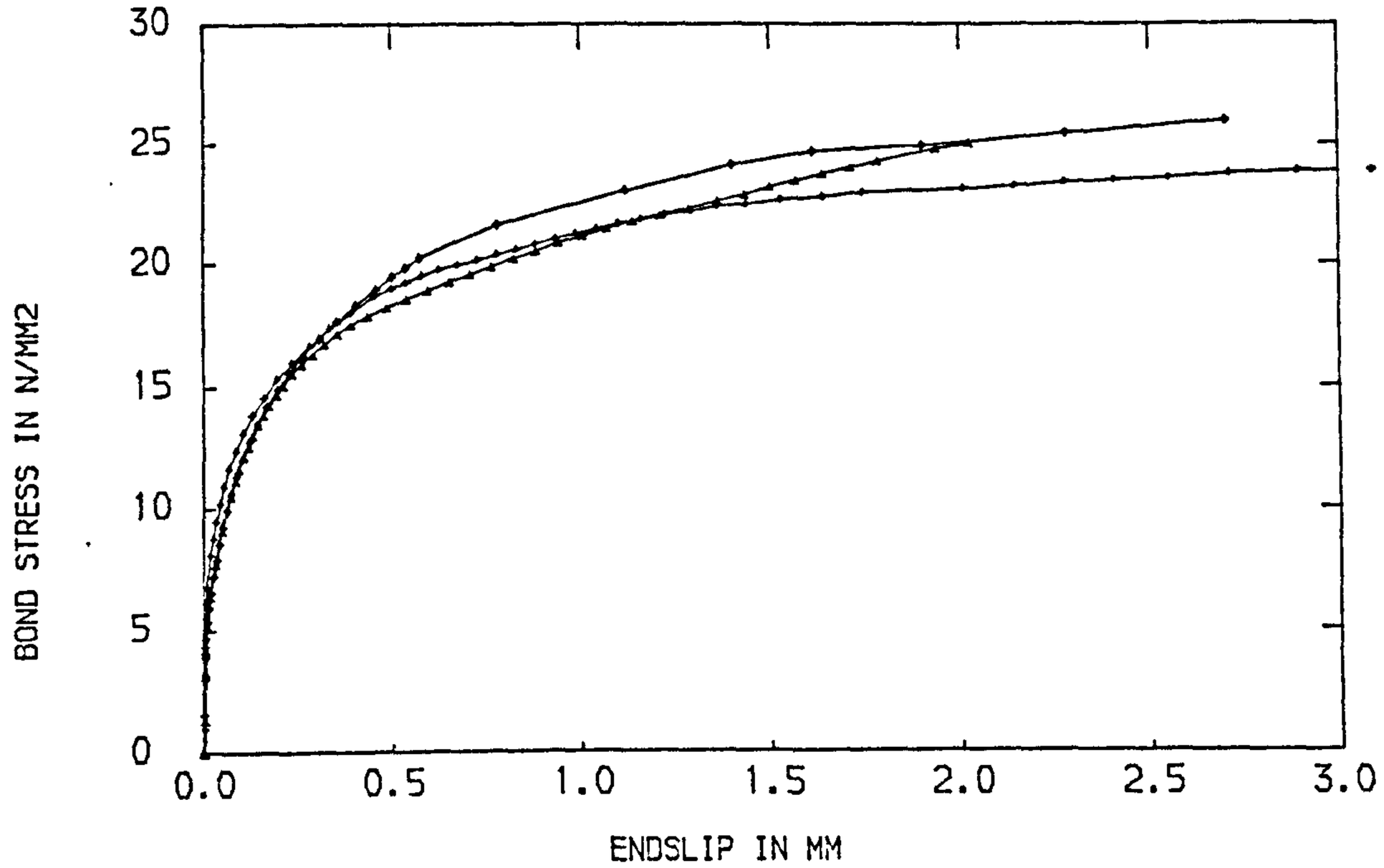

FIG.4.6 BOND STRESS-ENDSLIP CURVES OF 1BN(0)

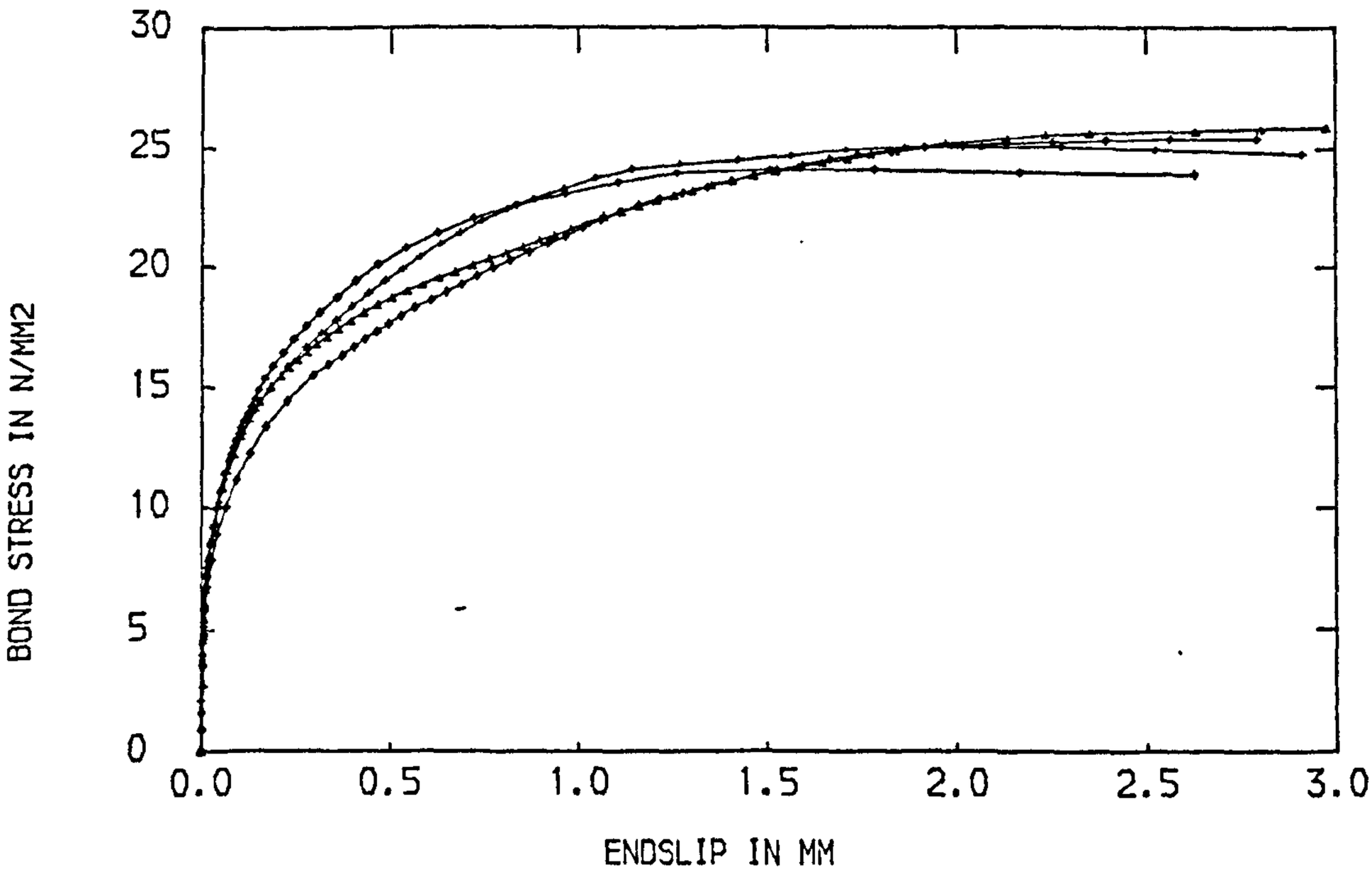

FIG.4.7 BOND STRESS-ENDSLIP CURVES OF 1BN(8J)

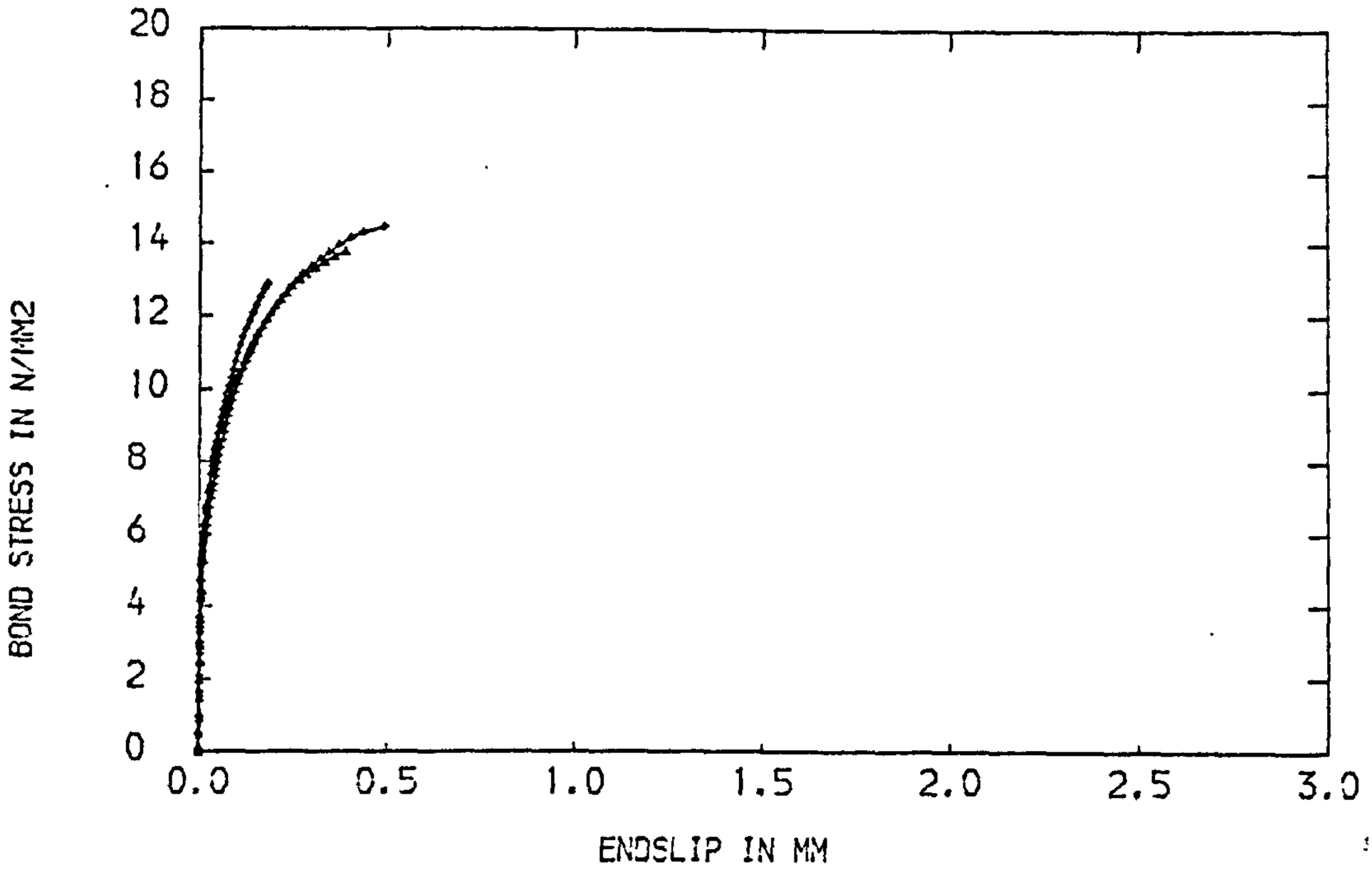

FIG.4.8 BOND STRESS-ENDSLIP CURVES OF 2BN(0)

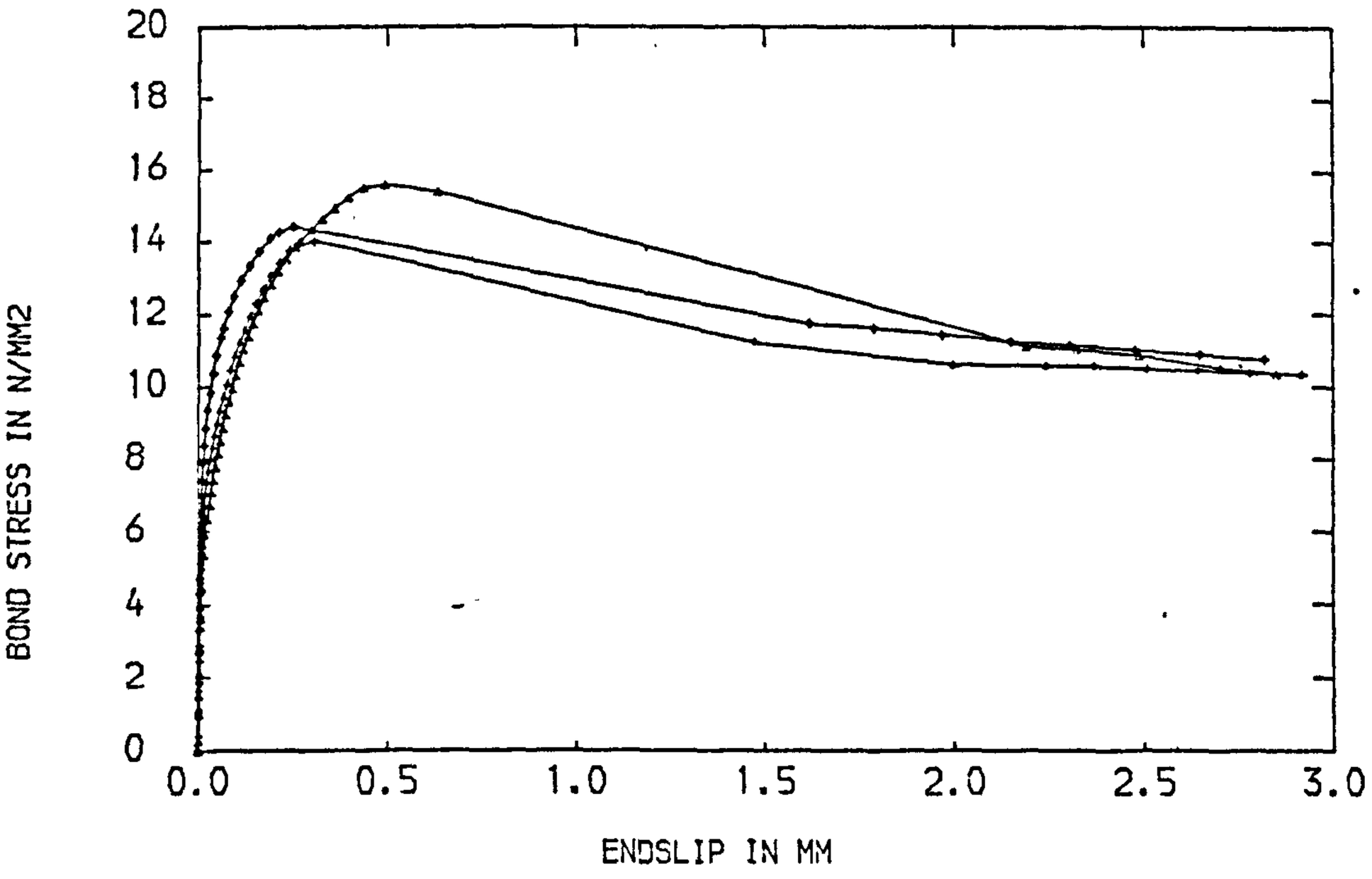

FIG.4.9 BOND STRESS-ENDSLIP CURVES OF 2BN(4)

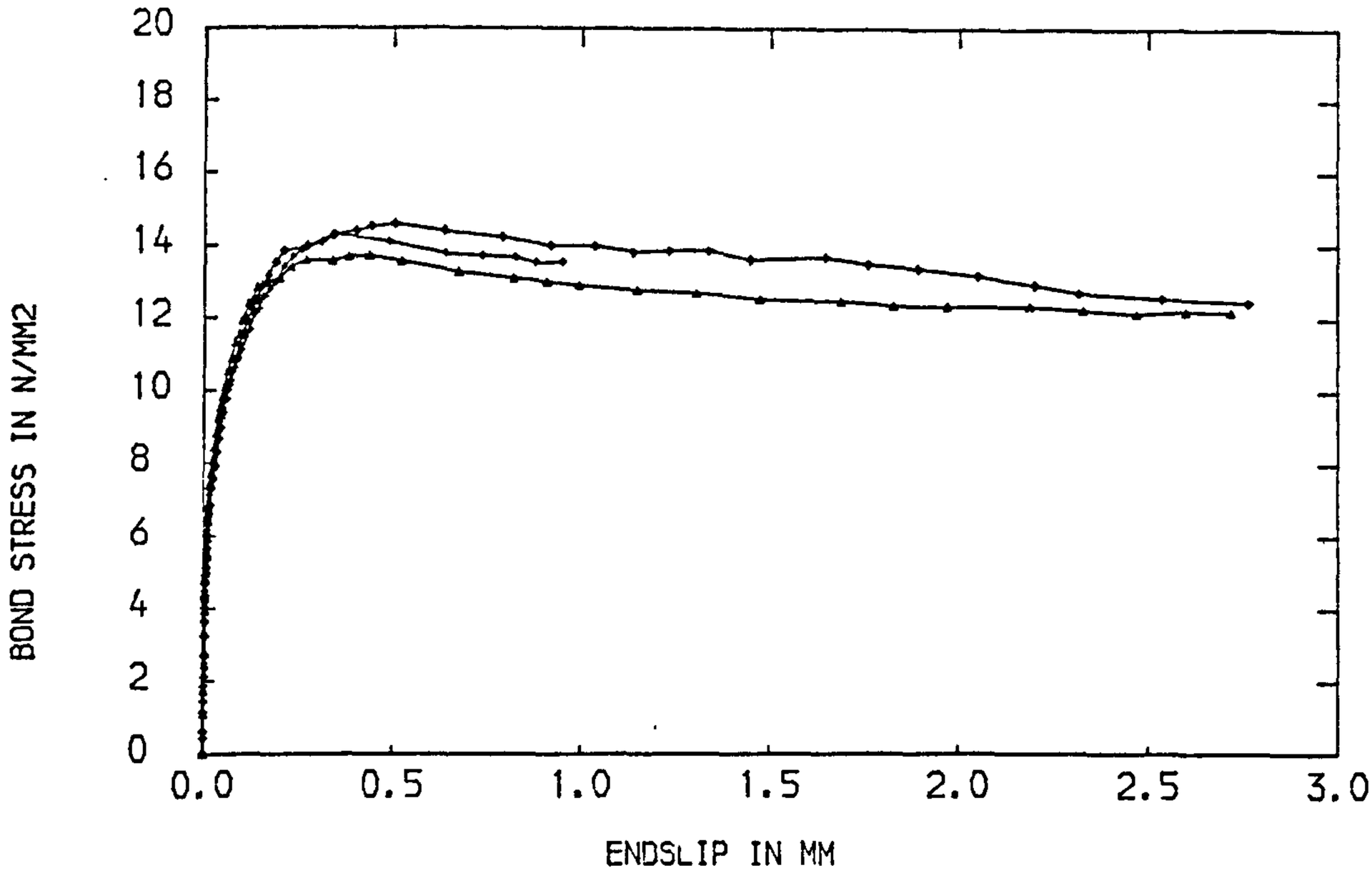

FIG.4.10 BOND STRESS-ENDSLIP CURVES OF 2BN(8)

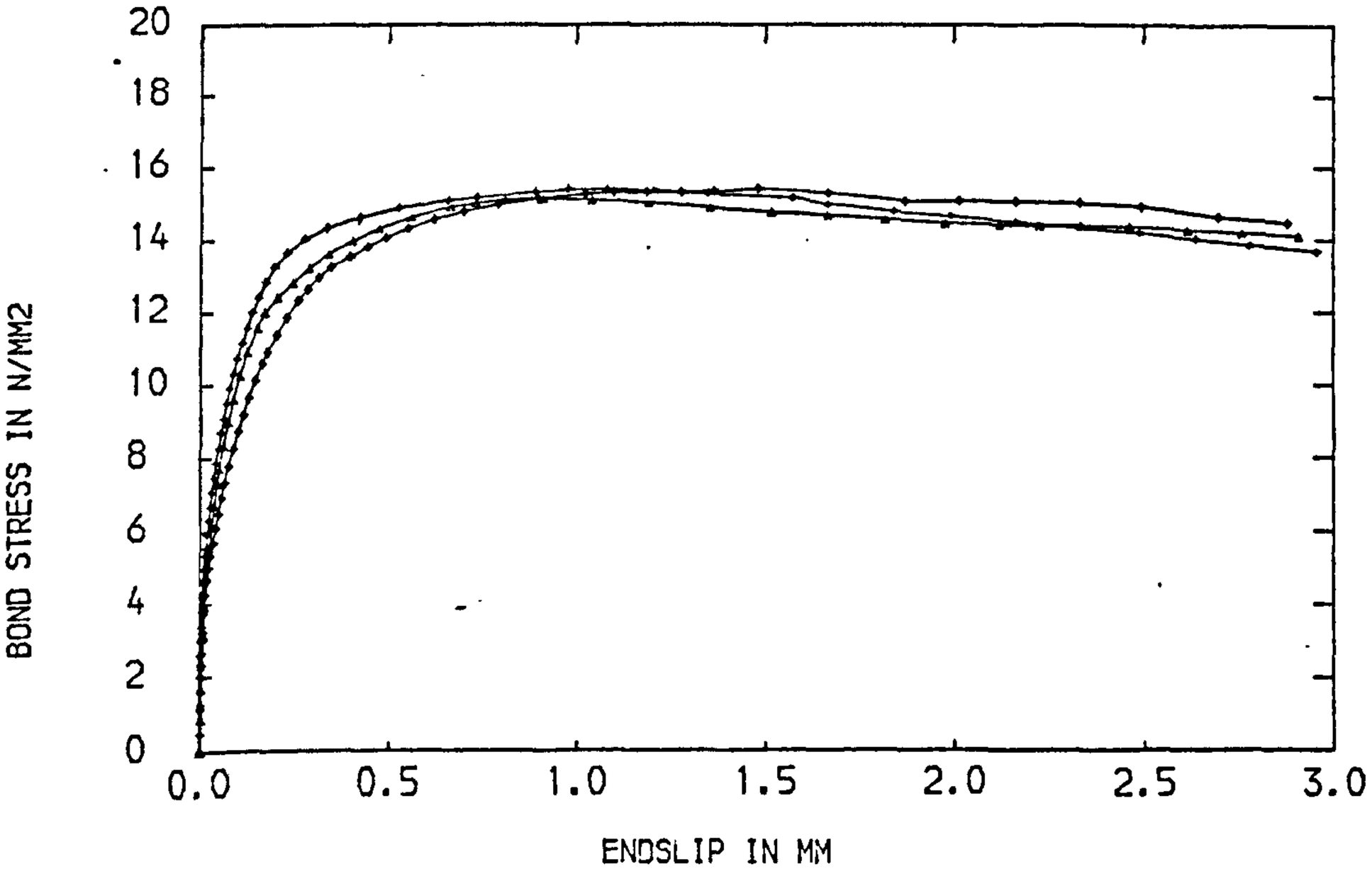

FIG.4.11 BOND STRESS-ENDSLIP CURVES OF 2BN(12)

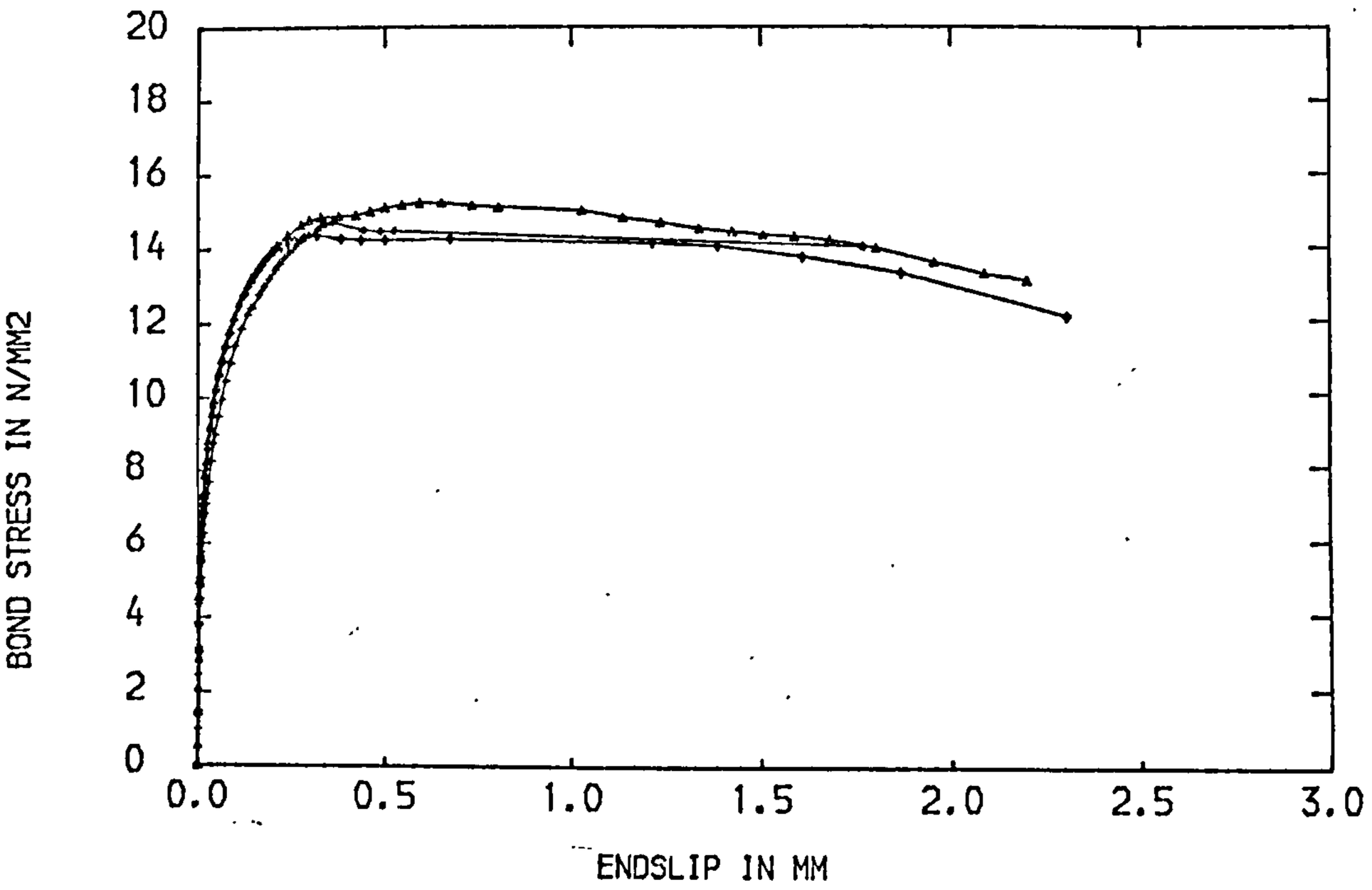

FIG.4.12 BOND STRESS-ENDSLIP CURVES OF 2BN(8J)

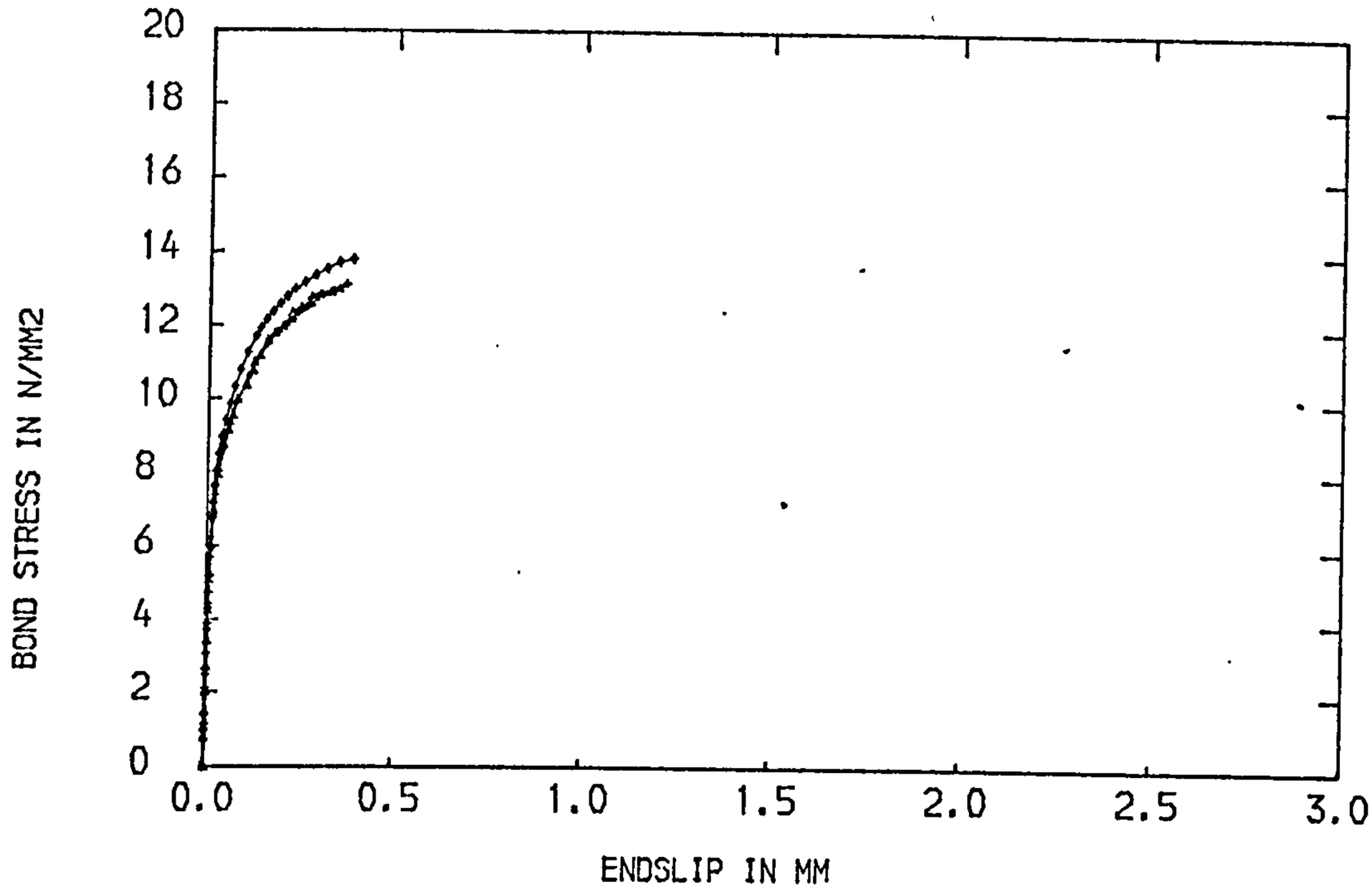

FIG.4.13 BOND STRESS-ENDSLIP CURVES OF 2BL(0)

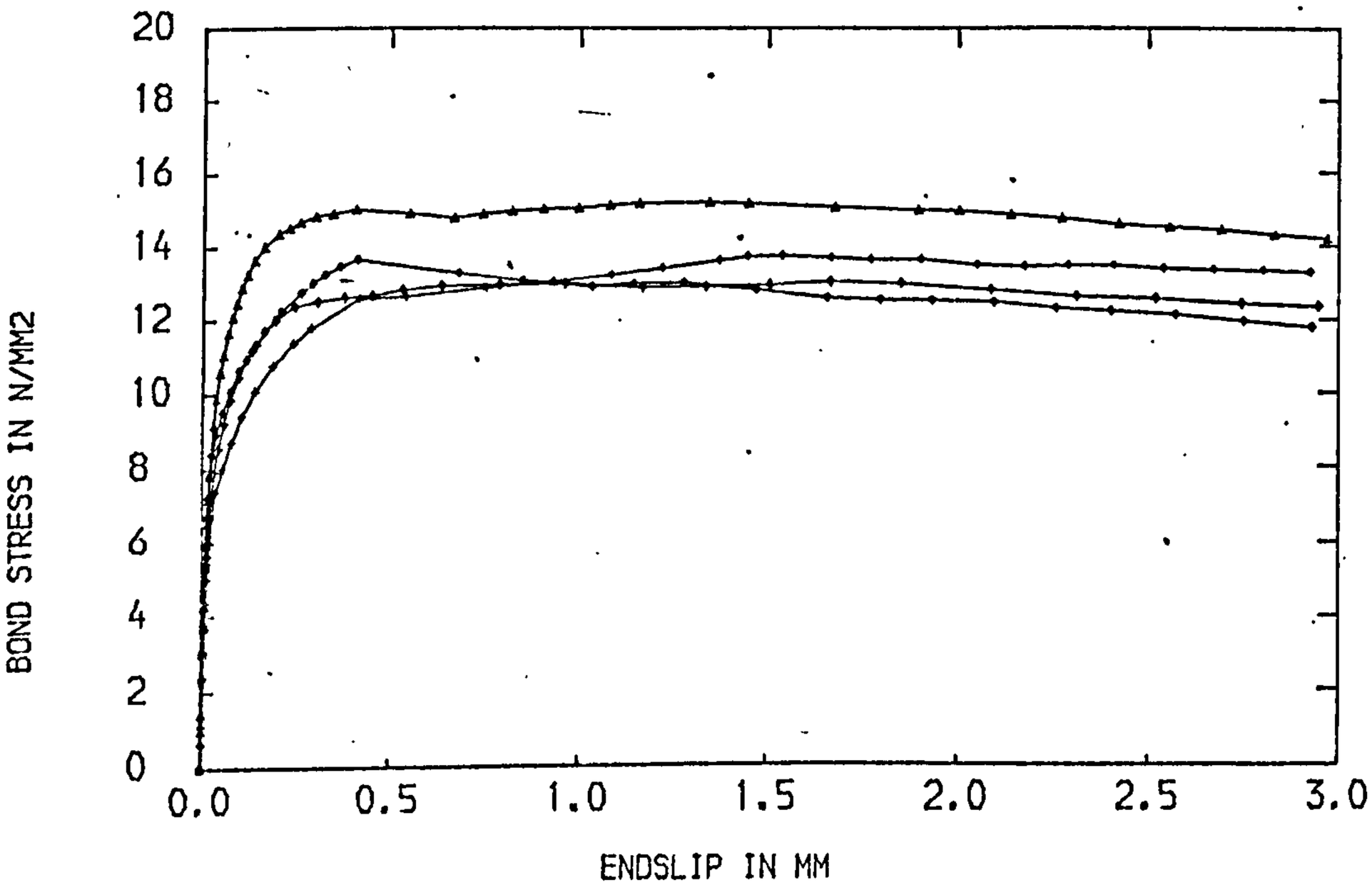

FIG.4.14 BOND STRESS-ENDSLIP CURVES OF 2BL(10)

Table 4.1 Results of Pull-out Tests

Specimen No.	Aggregate Type	Concrete Cover mm	Fibre Type	% Fibre Volume	Cube Strength f_{cu} N/mm^2	Av. Slip Modulus $N/mm^2/mm$	Max. Bond Stress N/mm^2	Av. Max Bond Stress N/mm^2
1BN(0)	Gravel	67	-	-	42.0	730	24.0 26.1 25.2	25.1
1BN(8J)	Gravel	67	Japanese	0.8	43.0	750	25.1 25.4 26.0 24.1	25.2
2BN(0)	Gravel	42	-	-	35.1	800	14.5 13.1 14.0	13.9
2BN(4)	Gravel	42	Crimped	0.4	37.5	825	14.0 14.4 15.6	14.7
2BN(8)	Gravel	42	Crimped	0.8	37.2	810	14.3 14.6 13.7	14.2
2BN(8J)	Gravel	42	Japanese	0.8	36.7	890	14.7 14.4 15.2	14.8
2BN(12)	Gravel	42	Crimped	1.2	35.2	710	15.4 15.3 15.2	15.3
2BL(0)	Lytag	42	-	-	37.6	670	13.1 13.8 13.0	13.3
2BL(10)	Lytag	42	Crimped	1.0	37.0	610	13.5 13.0 15.2 13.7	13.9

Inclusion of steel fibres in specimens with 42 mm concrete cover, however, had a pronounced affect on the bond stress-slip relations after the formation of longitudinal and transverse cracks. For plain concrete specimens, once the longitudinal and transverse cracks appeared, the specimens became unstable and the bond stress dropped quickly to zero. The situation was different for fibre concrete. The steel fibres were able to slow down the propagation and opening of these cracks. This ability to hold cracked matrix together enabled the bond stress to be maintained at more or less the maximum value (depending on the amount of fibres) over a considerable amount of slip.

The initial slip moduli were not significantly affected by the use of steel fibres.

4.7.3.3 Influence of Aggregate Type

Both gravel concrete specimens and the corresponding Lytag-sand concrete specimens generally had the same bond stress-slip relations. However, the latter seemed to have a lower initial slip modulus. This can be attributed to the fact that Lytag aggregates are invariably weaker than gravel aggregates.

4.7.3.4 Initial Slip Modulus

The average initial slip modulus for all tests on gravel concrete specimens was 785 $N/mm^2/mm$. The corresponding value for Lytag-sand concrete specimens was 640 $N/mm^2/mm$.

Edwards and Yannopoulos (83) obtained a slip modulus value of 500 $N/mm^2/mm$ for 16 mm diameter Welbond deformed bar embedded in gravel concrete. The rib pattern of a Welbond bar is different from that of a Tor Bar. This difference in rib pattern possibly accounts for the difference in the slip modulus values.

4.7.4 Idealization of Bond Stress-Slip Relations of Fibre Concrete

The bond stress-slip relationship of a 16 mm diameter Tor Bar embedded in fibre reinforced concrete may be idealized as elastic-plastic. The slope of the elastic portion is the initial slip modulus and the horizontal portion correspnds to the maximum bond stress.

4.8 Conclusions

1. In the 100 mm diameter concentric pull-out specimens, both longitudinal and transverse cracks were observed at failure.
2. Steel fibres slowed down the propagation and opening of the longitudinal and transverse cracks. This ability to contain the splitting cracks transformed a sudden bond failure to a gradual one.
3. The maximum bond stress was not significantly affected by the inclusion of steel fibres or types of concrete. Inclusion of steel fibres effected an increase of between 2.2 and 10.1%. Lytag-sand concrete showed a marginally lower bond stress value than that of gravel concrete. Nevertheless, the maximum bond stress increased with increasing concrete cover to steel.
4. Inclusion of steel fibres or increasing the concrete cover to steel had no appreciable effect on the average initial slope (slip modulus) of the bond stress-slip relations. However, Lytag-sand concrete seemed to have a lower slip modulus than that of gravel concrete.
5. Fibre concrete has a distinctive post-cracking characteristic and this is reflected in the bond stress-slip relations.

The fibres were able to hold the split specimens together so that the bond stress could be maintained at more or less the maximum value over a considerable amount of slip.

6. Finally, the bond stress-slip relationship of a 16 mm diameter deformed bar (Tor Bar) embedded in fibre concrete could be idealized as elastic-plastic.

CHAPTER FIVE

SHEAR TRANSFER IN FIBRE REINFORCED CONCRETE

5.1 Introduction

In this study, shear transfer is defined as the transfer of shear stress across a definite plane in reinforced concrete members (as in (89)).

There are two ways in which the shear transfer strength can develop, depending on the nature of the shear plane before the shear is applied. If no weakness exists along the shear plane, the strength development is by truss action after the formation of short inclined cracks (89, 90, 91). See Fig. 5.1.

In the presence of a crack along the shear plane prior to loading, the main way of developing shear is through the friction that arises when one element tends to slip with regards to the other one. Slippage causes the irregular faces of the crack to separate slightly. Tensile stresses created in the transverse reinforcement by crack opening induce clamping forces between the crack faces that in turn develop shear resistance. See Fig. 5.2. This is the basis of shear friction principle and the application of which depends on the correct selection of an assumed crack. Dowel action of the transverse reinforcement also plays a part in shear strength development.

The post-cracking resistance or tensile ductility of fibre concrete should aid in shear transfer. The randomly orientated steel fibres serve as small dispersed shear friction reinforcement and possibly enhance the roughness of the crack surface.

The scope of this part of the investigation was to study the influence of steel fibres alone or in conjunction with conventional stirrups on shear transfer. In particular the influence on its strength and stiffness was closely examined. The

study was carried out using both initially uncracked and initially cracked push-off specimens. The reasons for carrying out this study are given in section 1.2.1.

5.2 Review of Past Research

In order to establish a shear force displacement relationship, Fenwick and Paulay (41) carried out shear tests on 100 x 100 x 350 mm concrete blocks with a groove across the centre of each block (Fig. 5.3). This groove was used to initiate a crack which passed right through the specimen. The variables considered in the tests were crack width and concrete strength. Each test was carried out with a constant crack width, the crack width being adjusted after each application of shear force. Their results indicate that:

(1) Large shear stresses up to 1.8 N/mm^2 are possible with small crack widths. There is a drastic reduction of the shear that can be transmitted across the shear plane when the crack width is increased.

(2) Concrete strength affects the interface shear strength though the effect becomes less marked as the concrete strength is increased.

(3) The stiffness of the shear transfer mechanisms decreases with increasing crack width and decreasing concrete strength.

From a regression analysis of their test results, Fenwick and Paulay proposed a shear stress-displacement relationship as given below:

$$v = \left(\frac{467}{w} - 8410\right)\left(0.0225\sqrt{f_c'} - 0.409\right)(\Delta s - 0.0436\ w) \qquad (5.1)$$

where v = shear stress transmitted across the crack, psi

w = crack width, inches

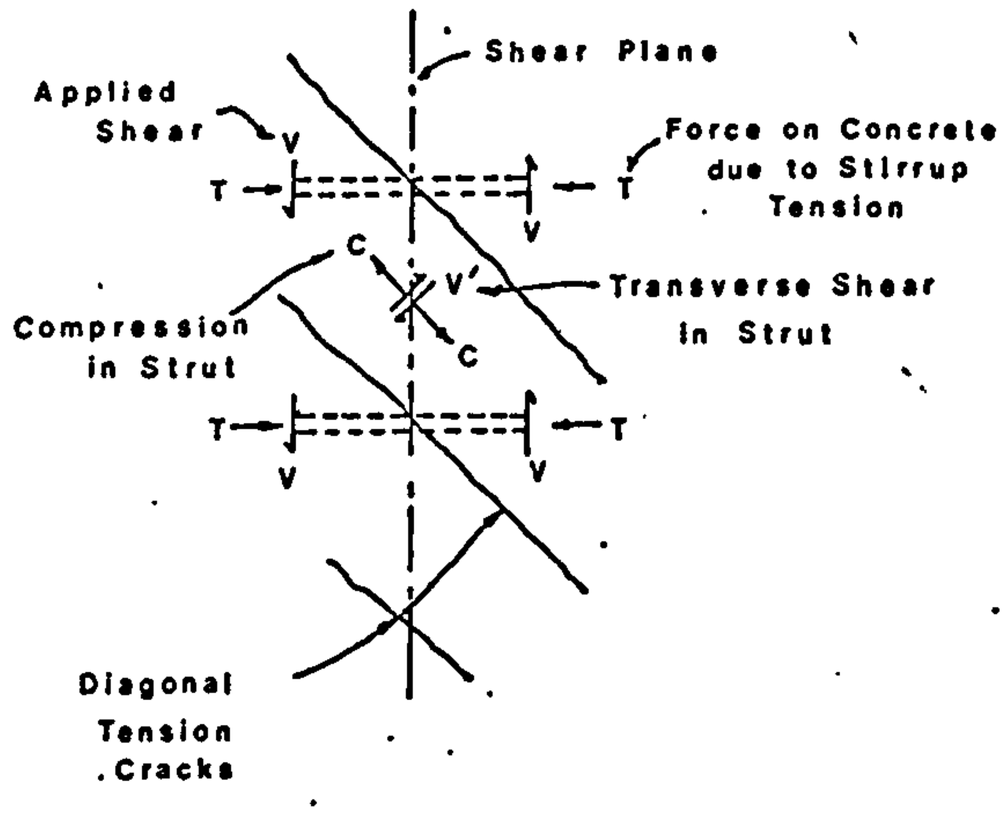

FIG. 5·1 SHEAR TRANSFER IN INITIALLY UNCRACKED CONCRETE (AFTER MATTOCK et al (90))

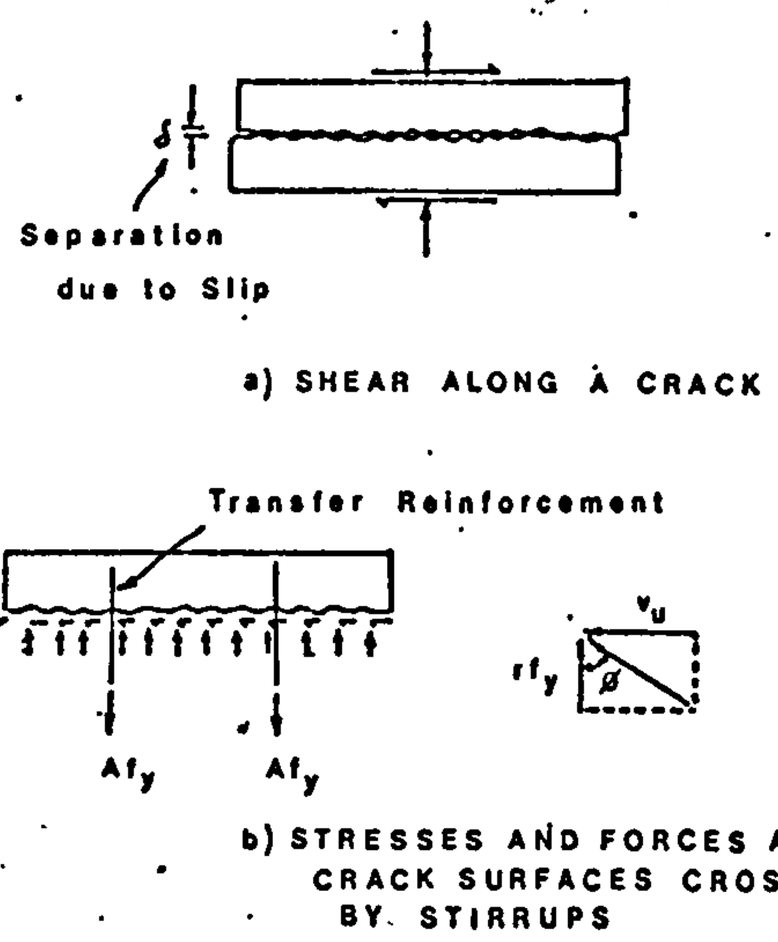

FIG. 5·2 SHEAR FRICTION CONCEPT (AFTER MAST(4))

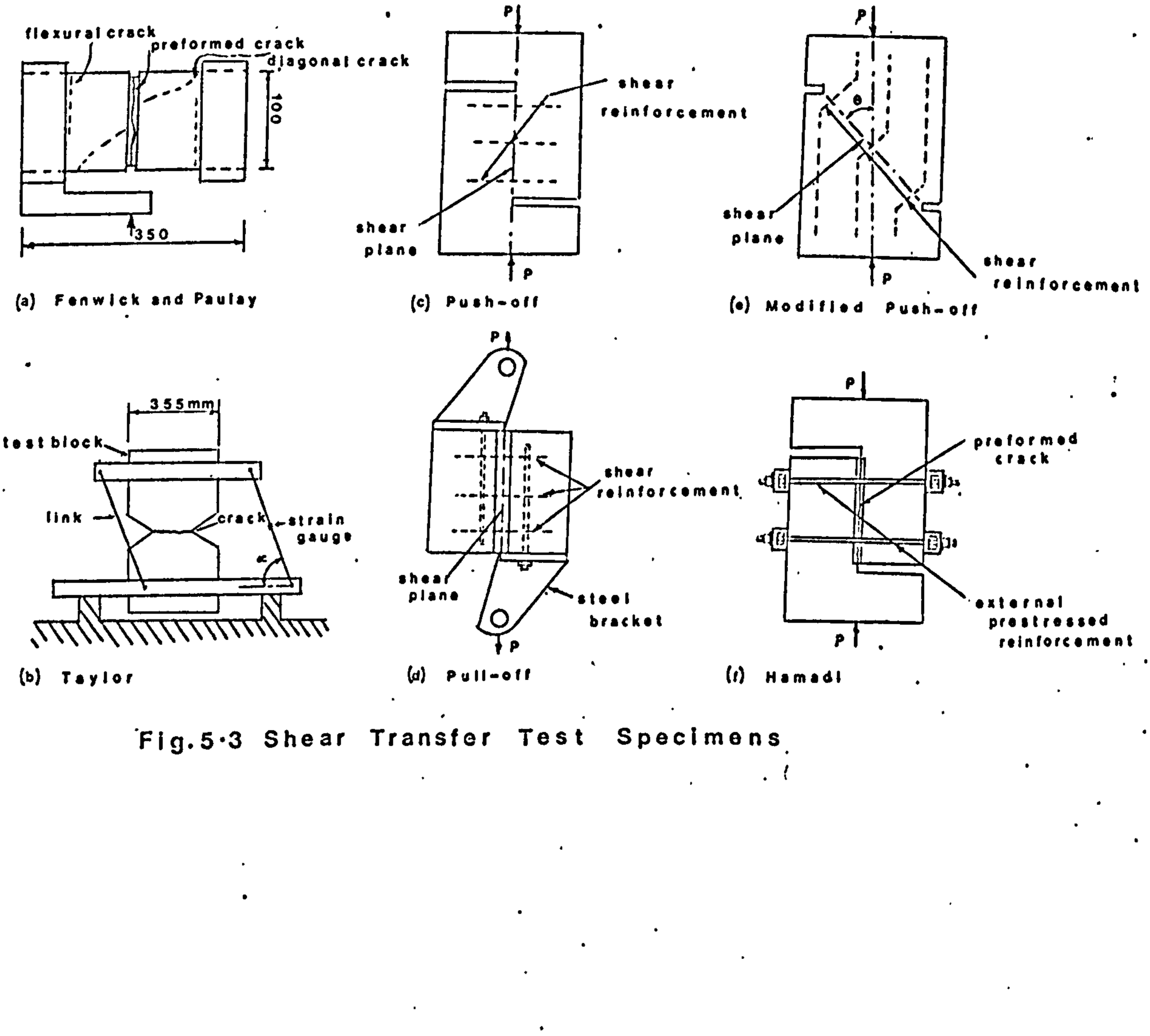

Fig.5·3 Shear Transfer Test Specimens

f_c' = Cylinder crushing strength, psi

Δs = Shear displacement, inches

These tests have been criticized for the unrealistic displacement pattern selected. In real concrete members, the cracks open and shear simultaneously, i.e., they do not shear with constant crack width.

Taylor (92) carried out a number of tests on concrete blocks in which the ratio of crack opening to the shear movement was maintained constant during testing. The shape of the test specimen and the special rig he devised are shown in Fig. 5.3. The ratio of the normal to shear displacement was varied by varying the value of the angle α. The test specimen had a precracked section of 127 mm long and 140 mm wide. The major variables considered were normal to shear displacement ratio, concrete strength, aggregate size and aggregate type. In addition a few tests were carried out with the shear plane reinforced by a stirrup. Taylor reported that the interface shear strength decreased linearly as the normal to shear displacement ratio was increased. The shear strength was also dependant on the concrete strength and the type of aggregate. However the effect of aggregate size did not appear to be significant and this was attributed to the small displacements used. The presence of a stirrup increased the interface shear strength considerably. Because no direct shear displacement was measured by Taylor, he did not propose an analytical expression to relate shear stress to shear displacement.

Much research work has been done on the strength of shear transfer across a definite plane in normal weight reinforced concrete by Mattock and his co-workers (89, 90) at the University of Washington. The factors included in their study were:

(1) The characteristics of the shear plane, i.e., initially

uncracked or initially cracked

(2) The characteristics of the reinforcement

(3) The concrete strength

(4) Direct stresses acting parallel and transverse to the shear plane.

The influence of the first three factors was studied in tests of monolithically cast push-off specimens, each having a shear plane of 250 mm long and 130 mm wide and with transverse reinforcement at 90^{o} to the shear plane. Tests to study the influence of the fourth factor were made on pull-off and modified push-off specimens, having shear areas of 300 x 130 mm and 300 x 150 mm respectively. Again the transverse reinforcement was at 90^{o} to the shear plane. Fig. 5.3 shows the various types of specimens used. Mattock et al concluded that:

(1) A pre-existing crack along the shear plane will both reduce the ultimate shear transfer strength and increase the slip at all levels of load.

(2) The shear transfer strength is a function of the reinforcement parameter rf_y^+. See Fig. 5.4a. Changes in strength, size, and spacing of reinforcement affect the shear strength only insofar as they change the value of rf_y for $f_y < 456$ N/mm^2.

(3) In initially cracked concrete, the concrete strength sets an upper limit value for rf_y, below which the relationship between the shear transfer stength and rf_y is the same for concretes of strength equal to or greater than that of the concrete being considered, and above which the shear transfer strength increases at a much reduced rate. See Fig. 5.4b.

+ $r = \frac{A_s}{bd}$ where A_s is total area of stirrups crossing the shear plane of area bd.

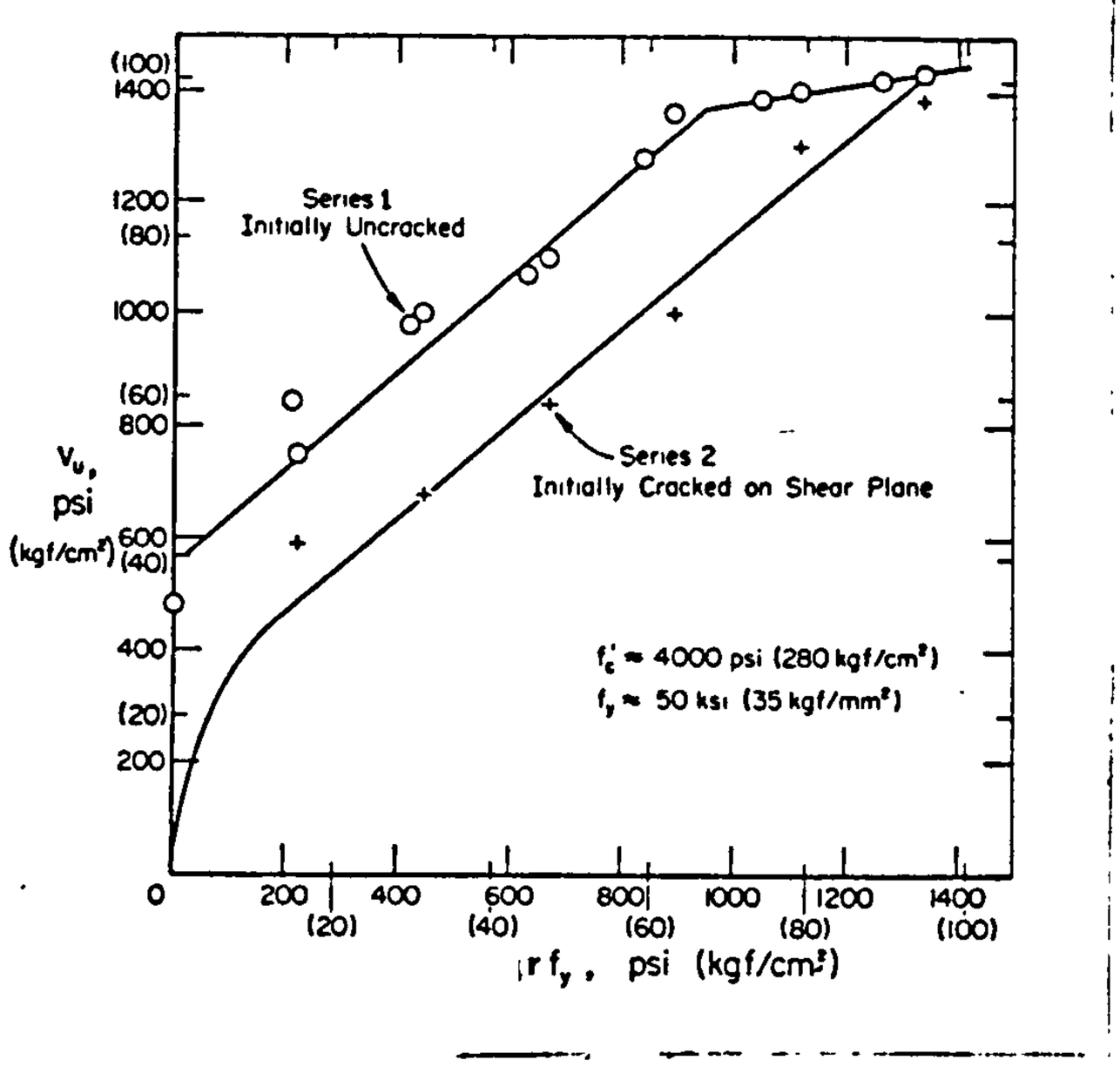

FIG. 5·4a VARIATION OF SHEAR STRENGTH WITH REINFOCEMENT PARAMETER rf_y WITH AND WITHOUT A CRACK ALONG THE SHEAR PLANE (after MATTOCK et al (89))

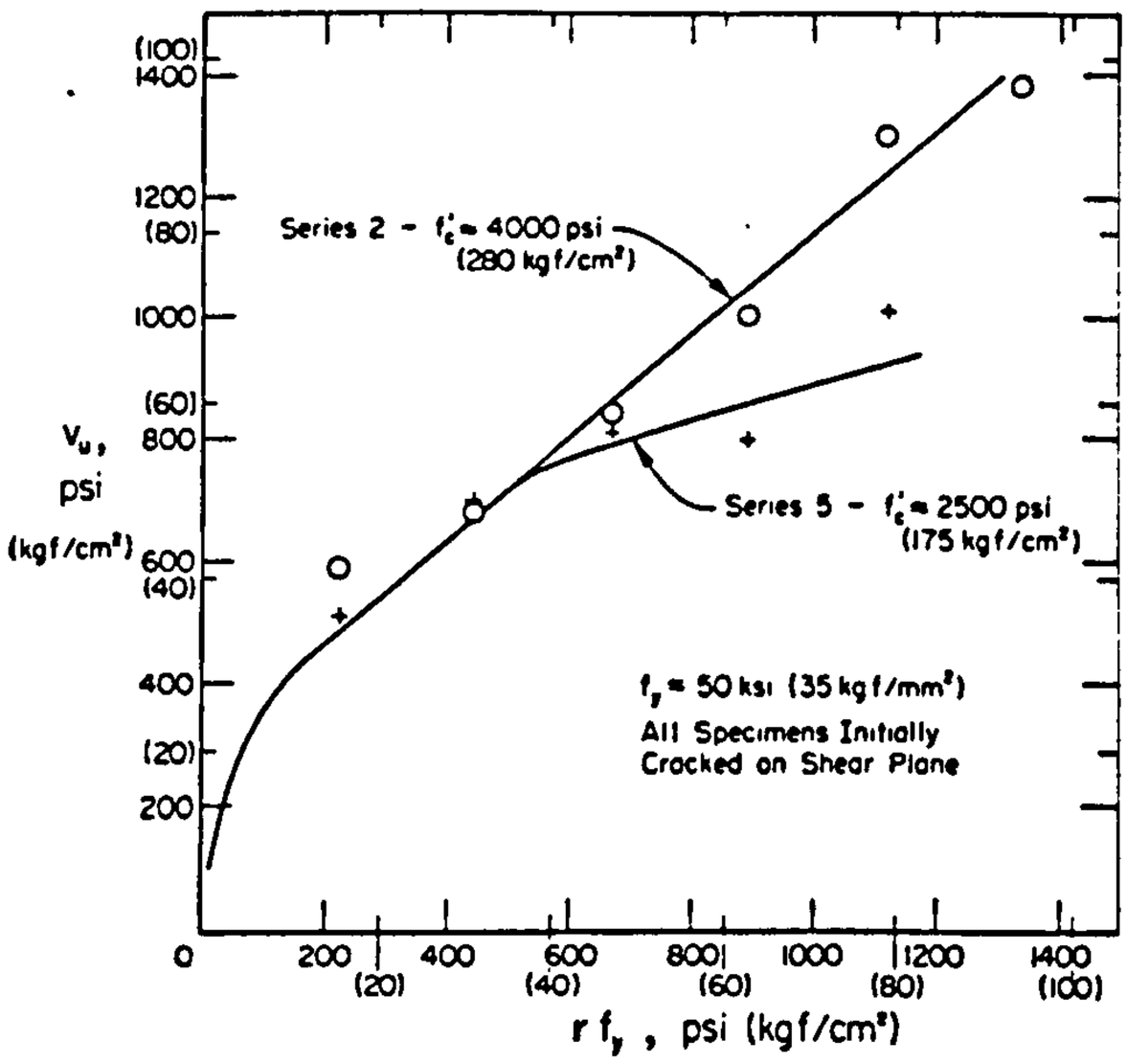

FIG. 5·4b EFFECT OF CONCRETE STRENGTH ON THE SHEAR STRENGTH OF INITIALLY CRACKED SPECIMENS (after MATTOCK et al (89))

(4) Direct tension stresses parallel to the shear plane reduce the shear transfer strength of initially uncracked concrete, but do not reduce the shear transfer strength of precracked concrete.

(5) An externally applied compressive stress acting transversely to the shear plane is additive to rf_y in calculations of the ultimate shear transfer strength of both initially cracked and uncracked concrete.

From the test results of the initially cracked specimens, Mattock and Hawkins (90) proposed a design equation for shear transfer across a crack in monolithic concrete as given below:

$$v_u = 1.38 + 0.8(rf_y + \sigma_N); \qquad (5.2)$$

providing $v_u \nmid 0.3f_c'$ and $(rf_y + \sigma_N) \nmid 1.38$ N/mm^2

where v_u = ultimate shear transfer strength, N/mm^2

rf_y = shear reinforcement parameter

σ_N = the externally applied direct stress acting across the shear plane, taken as positive for a compressive stress and negative for a tensile stress

In a subsequent paper Mattock (93) proposed an analytical equation for the ultimate shear transfer strength of sand gravel concrete:

$$v_u = 2.76 + 0.8\ rf_y; \qquad (5.3)$$

providing $V_u \nmid 0.3\ f_c'$ and $rf_y \nmid 1.38$ N/mm^2

Mattock et al (91) also carried out tests to study the shear transfer strength of lightweight concrete. The primary variable in the tests was the type of aggregate, four types being used:

(1) Naturally occurring gravel and sand

(2) A predominantly coated, rounded lightweight aggregate

(3) A predominantly crushed angular lightweight aggregate

(4) A 'sand lightweight' aggregate, in which most of the lightweight fine particles were replaced with normal weight sand.

Both initially uncracked and initially cracked push-off specimens each having a shear plane of 125 x 300 mm were used. The reinforcement crossing the shear plane at 90^{o} was in the form of welded stirrup. Their results indicate that the shear transfer strength of lightweight concrete is less than that of sand and gravel concrete of the same compressive strength and it is not significantly affected by the type of lightweight aggregate, i.e., by whether the aggregate is a "coated aggregate" or "crushed aggregate". They proposed two analytical expressions for calculating the ultimate shear transfer strength of lightweight concrete:

For sanded lightweight concrete having a unit weight not less than 1680 kg/m^3,

$$v_u = 1.72 + 0.8\ rf_y; \qquad (5.4)$$

providing $v_u \nmid 0.2\ f_c'$ or 6.89 N/mm^2

and $rf_y \nmid 1.38\ N/mm^2$

For all lightweight concrete having a unit weight not less than 1470 kg/m^3,

$$v_u = 1.38 + 0.8\ rf_y; \qquad (5.5)$$

providing $V_u \nmid 0.2\ f_c'$ or 5.51 N/mm^2 and

$rf_y \nmid 1.38\ N/mm^2$.

Paulay and Loeber (94) tested a number of initially

cracked push-off specimens which were not reinforced in the shear plane. Each specimen had a shear plane of 190 mm x 114 mm. Among the variables considered were the effect of aggregate shape and size and crack width. Bolt inserts were used to introduce a controlled tension force to form the crack width required. In the first series the crack width was maintained constant at a pre-selected value during testing. They reported that the shear stress-displacement relation did not seem to be affected by either the size or shape of the coarse aggregate used in making the concrete. For a constant crack width, the shear stress-displacement relation could be satisfactorily represented by a bilinear relationship up to a shear stress of about 6.8 N/mm^2. The few tests in which the crack width was increased proportionally with the applied load verified that the stiffness of the shear transfer mechanism decreased as the shear stress across the interface increased. Finally tests, in which the restraining stress required to prevent the opening of a preformed crack was monitored while interface shear was being transferred, revealed that this restraining stress was independent of aggregate shape and size and also of crack width.

In order to get a simplified load-displacement relationship for the aggregate interlock springs in their finite element model, Houde and Mirza (95) carried out tests on 32 concrete blocks similar to those of Fenwick and Paulay (41). The influence of crack width, concrete strength and maximum aggregate size was considered. They concluded that the variation of the shear transfer stiffness with concrete strength was proportional to $\sqrt{f_c'}$. The influence of the aggregate size was reported to be negligible. They proposed a shear stress-displacement relationship for a unit crack length as:

$$v_u = 9.98 \left(\frac{1}{w}\right)^{1.5} \Delta s \qquad N/mm^2 \qquad (5.6)$$

for f_c' = 34.5 N/mm^2 and in the range of crack widths tested (0.05 - 0.51 mm)

Hamadi (96) carried out an extensive study on the shear transfer across cracks. He carried out tests on 45 initially cracked push-off specimens. Each specimen had a shear plane of 350 x 120 mm. The main variables studied were the type of aggregate (gravel, expanded slate and expanded clay) and the normal force across the shear plane. In the first series, the specimens were tested with zero normal force across the shear plane. In the second series, the specimens were restrained by external bolts during testing. See Fig. 5.3. The test specimens were reinforced in the shear plane with bonded reinforcement in the final series. He reported that aggregate type influenced both the strength and stiffness of shear transfer primarily as a function of roughness of the fracture surface. He arranged the aggregate types he investigated in ascending order of roughness, stiffness and strength as expanded clay, expanded slate and natural gravel. The effect of crack width on the shear transfer stiffness was significant but was less pronounced on the shear transfer strength if significant normal forces were present. Compressive normal force increased shear transfer strength but did not have much effect on the shear transfer stiffness. Hamadi expressed the shear transfer stiffness as:

$$G_s = \frac{k}{w} \qquad (5.7)$$

where G_s = shear transfer stiffness, N/mm^3

w = crack width, mm

k = dimensional constant with stress unit, N/mm^2

He gave the following range of values for k:

If $\sigma_N = 0$:

$k = 1.2$ for gravel concrete

$= 1.1$ for expanded-slate concrete

$= 0.4$ for expanded-clay concrete

If $0.5 < \sigma_N < 7.0$ N/mm^2:

$k = 5.4$ for gravel concrete

$= 2.7$ for expanded-slate and expanded-clay concretes.

He expressed the ultimate shear transfer strength in terms of Coulomb's criterion:

$$v_u = c + \mu\sigma_N \qquad (5.8)$$

where c = cohesion, N/mm^2

μ = coefficient of friction

He gave a range of c-values and μ-values and these are summarized in Table 5.1. Note that the average cylinder compressive strength was 25.0 N/mm^2.

Table 5.1 c and μ values as given by Hamadi (96)

Concrete	$\sigma_N < 2.0$ N/mm^2		$\sigma_N > 2.0$ N/mm^2	
	c	μ	c	μ
Gravel	0.3	2.7	4.0	0.7
Expanded -slate	0.2	1.5	2.6	0.4
Expanded -clay	0.1	1.3	2.0	0.3

With the ultimate aim of developing a model for shear transfer in cracked concrete to be used in finite element analysis of concrete structures. Walraven et al (97) carried out

a number of tests on initially cracked push-off specimens. Among the parameters studied were the influence of restraining force in the form of bonded reinforcement or external restraining bars and concrete type. They reported that neither the concrete type nor the amount of reinforcement appeared to have a significant influence on the displacement path in the loading range from zero to maximum shear stress. For greater crack widths, after yielding of the reinforcement, the displacement path seemed to be affected by the type of concrete but not by the reinforcement ratio. For the same separation, gap graded concrete exhibited a smaller, and high strength concrete a greater shear displacement than normal concrete. Analytical study by considering equilibrium of forces on the crack plane revealed that the frictional resistance decreases with increasing normal force. This was attributed to the continuing deterioration of the mortar in the crack plane.

5.2.2 Fibre Concrete

Criswell (98), in his feasibility study of the use of steel fibres as shear reinforcement, carried out tests on seven push-off specimens. Each specimen had a shear plane of 152 x 100 mm. These included those with and without stirrups, with and without fibres and initially cracked or uncracked. The type of fibre used was 0.26 x 0.56 x 25.4 mm steel fibres and the volume percentage of fibre was 1.0. He reported that the use of 1.0% by volume of fibres alone was nearly as efficient in increasing the single direction interface shear strength as a slightly smaller area percentage of stirrups. For initially uncracked specimens, addition of fibres to plain concrete gave a 70% strength increase. The strength contributions of the two reinforcement types were nearly but not completely additive. The residual resistance of the specimens with fibres only was however less than that achieved with the use of stirrups.

5.2.3 General Conclusions

It may be concluded from the above literature review that:

(1) The existence of a crack in the shear plane, before the application of shear, reduces significantly the ultimate shear transfer strength and increases slip at all stress levels.

(2) The ultimate shear transfer strength of initially cracked concrete is affected significantly by the type of aggregate, the crack width (in the absence of significant normal forces), the restraining force and to a lesser extent the concrete strength. It can be adequately represented by using Coulomb's criterion.

(3) The stiffness of the shear transfer mechanism of initially cracked concrete is affected by the crack width, the type of aggregate and concrete strength. For a given concrete strength and concrete type, it can be adequately represented by:

$$G_s = k\left(\frac{1}{w}\right)^n \qquad (5.9)$$

where G_s = shear transfer stiffness

k, n = constants

w = crack width

(4) There is at present, very little experimental data on the influence of steel fibres on shear transfer. The ultimate strength and the stiffness of shear transfer of fibre concrete are yet to be determined quantitatively.

5.3 Experimental Study

5.3.1 Parameters Studied

The primary objective of this part of the investigation was to study the influence of short discrete steel fibres alone and in conjunction with conventional stirrups on the strength and behaviour of single direction shear transfer in both gravel and Lytag-sand concrete. The fibre type used was 0.50 x 50 mm crimped fibres and the properties of which are given in section 3.2.6. The fibre percentage by volume used ranged from 0 to 1.2. The physical properties of the coarse aggregate and the mix proportions used are given in section 3.2.4 and sections 3.3.1 and 3.3.2 respectively. Both initially uncracked and initially cracked specimens were used.

The properties of each of the thirty-five specimens tested are shown in Table 5.2.

5.3.2 The Test Specimens

The test specimens were of the push-off type shown in Fig. 5.5 with a shear plane of 220 x 125 mm for an initially uncracked specimen and 220 x 100 mm for an initially cracked specimen. The conventional reinforcement crossing the shear plane at 90^{o} was in the form of closed stirrups, anchored by wrapping around longitudinal reinforcement. The number and types of stirrups are given in Table 5.2. The properties and stress-strain curves for the various types of shear reinforcement are given in Table 3.2 and Fig. 3.3 respectively. Auxilliary reinforcement was used to ensure failure along the shear plane.

5.5.3 Casting and Curing

Each specimen was cast with the mould placed horizontally and resting on the wide face (300 x 520 mm). Generally, two

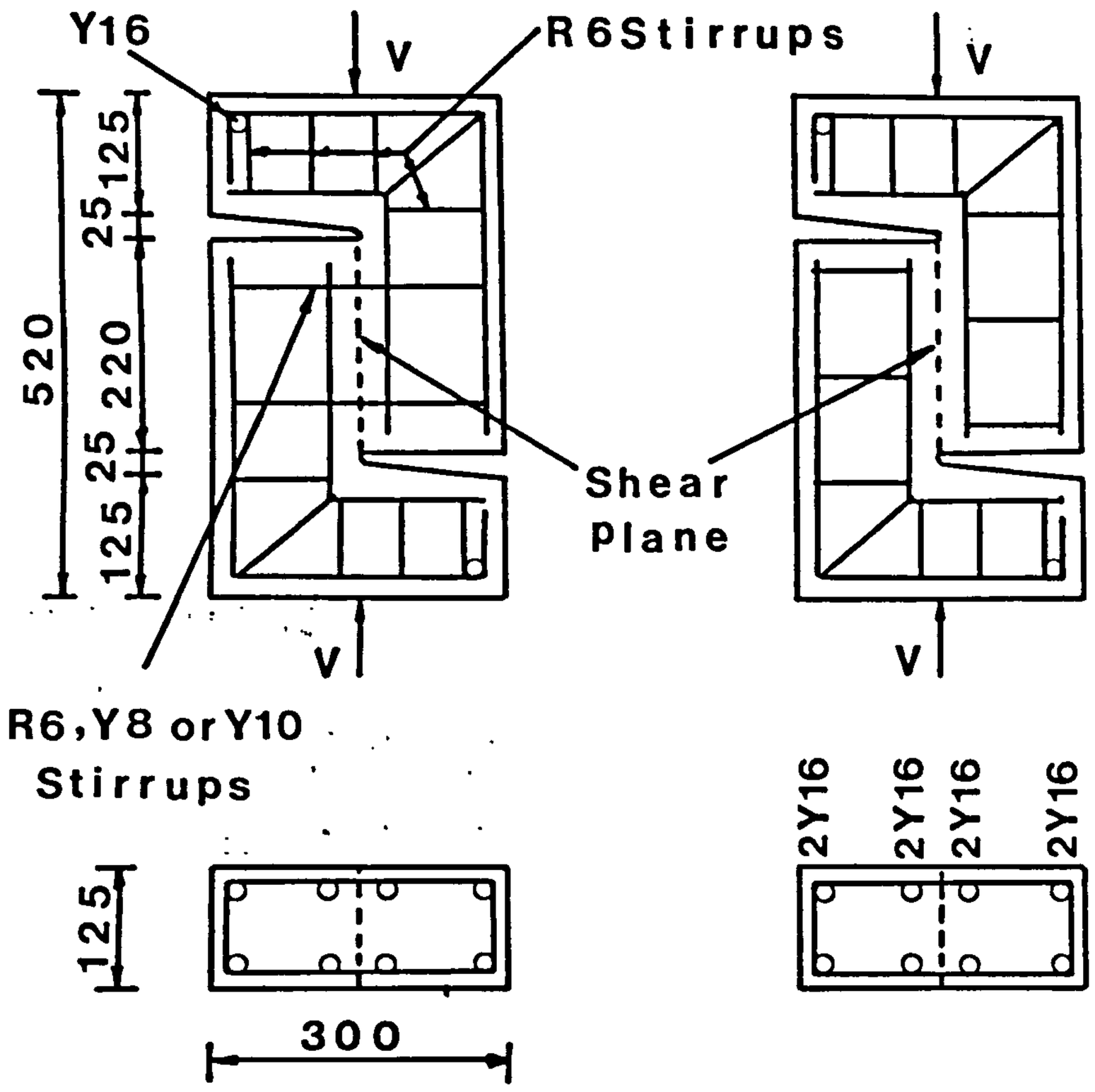

a) Initially Uncracked

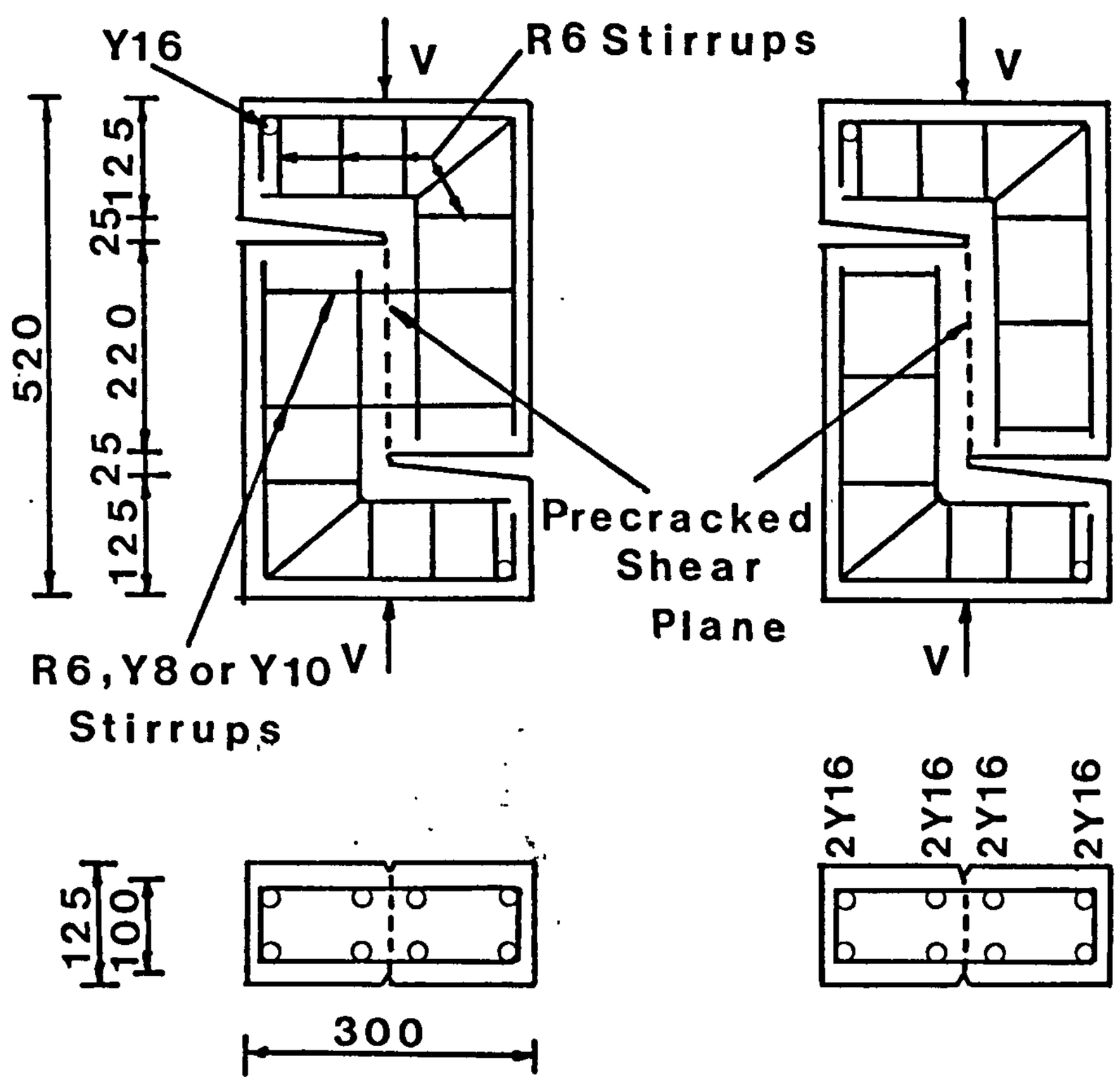

b) Initially Cracked

Fig. 5·5 Details of Push-off Specimens

Table 5.2 Test Specimen Properties

Specimen No.	Size & No. of Stirrups	Spacing of Stirrups s (mm)	Stirrup Yield Stress f_{y_2} N/mm^2	Fibre by Volume %	Cube Strength f_{cu} N/mm^2	Modulus of Rupture N/mm^2		Initial Cond-itions
						1st crack	ultimate	
Gravel Concrete								
1SN-1	-	-	-	0	39.0	-	-	
1SN-2	-	-	-	0.4	42.4	4.01	4.90	Not
1SN-3	-	-	-	0.8	43.0	4.71	6.00	Cracked
1SN-4	-	-	-	1.2	42.4	5.08	6.54	
2SN-1	2R6	115	350	0	37.0	-	3.80	Not
2SN-2	2Y8	115	505	0	43.2	-	-	Cracked
2SN-3	2Y10	115	500	0	43.2	-	-	
3SN-1	2R6	115	350	0.4	37.1	-	-	Not
3SN-2	2Y8	115	505	0.4	38.8	-	-	Cracked
3SN-3	2Y10	115	500	0.4	39.4	3.85	4.92	
4SN-1	2R6	115	350	0.8	40.1	4.84	6.30	Not
4SN-2	2Y8	115	505	0.8	39.3	-	-	Cracked
4SN-3	2Y10	115	500	0.8	40.3	-	-	
1SNP-1	-	-	-	0.4	43.1	3.92	5.04	
1SNP-3	-	-	-	0.8	43.5	4.82	6.08	Cracked
1SNP-4	-	-	-	1.2	42.4	5.08	6.54	
2SNP-1	2R6	115	350	0	362	-	3.48	Cracked
2SNP-2	2Y8	115	505	0	37.0	-	3.74	
3SNP-1	2R6	115	350	0.4	43.1	3.92	5.04	Cracked
3SNP-2	2Y8	115	505	0.4	41.6	3.75	4.40	
4SNP-1	2R6	115	350	0.8	43.5	4.82	6.08	Cracked
4SNP-2	2Y8	115	505	0.8	41.6	4.15	5.48	
Lytag-sand Concrete								
1SL-1	-	-	-	0	39.8	-	3.49	Not
1SL-2	-	-	-	1.0	40.3	4.0	6.52	Cracked
2SL-1	2R6	115	350	0	41.0	-	3.20	Not
2SL-2	2Y8	115	505	0	38.0	-	3.10	Cracked
2SL-3	2Y10	115	500	0	36.8	-	3.05	
3SL-1	2R6	115	350	1.0	46.1	4.57	6.64	Not
3SL-2	2Y8	115	505	1.0	40.0	4.35	6.36	Cracked
1SLP-2	-	-	-	1.0	40.3	4.35	6.52	Cracked
2SLP-1	2R6	115	350	0	37.0	-	3.72	
2SLP-2	2Y8	115	505	0	41.4	-	3.24	Cracked
2SLP-3	2Y10	115	500	0	39.8	-	3.50	
3SLP-1	2R6	115	350	1.0	46.1	4.57	6.64	Cracked
3SLP-2	2Y8	115	505	1.0	40.0	4.35	6.36	

test specimens, three 152 x 152 x 152 mm cubes and three 100 x 100 x 500 mm prisms were cast at one time.

Concrete was poured into the lightly oiled moulds in two layers and compacted well using a vibrating table system. As the end pieces of each test specimen were quite heavily reinforced, fibre concrete was only used in the middle section. Plain concrete of similar mix proportions was used in the end pieces. The surface of each of the specimens was levelled and finished with a steel trowel.

The specimens were left under a polythene sheet for 24 hours. They were then stripped from the moulds and stored in the laboratory atmósphere until the day of testing, which was between 27 and 29 days after casting.

5.3.4 Instrumentation and Testing Procedure

Fifteen of the test specimens were cracked along the shear plane before testing. The rest of the specimens were tested in an initially uncracked condition.

The initially cracked specimens were cast with top and bottom grooves along the shear plane. The crack along the shear plane was formed by applying line loads along these grooves. The average crack width achieved was measured using 3 pairs of Demec discs at 50 mm separation on both sides of the specimen and is given in Table 5.3. See Fig. 5.6(a).

In all the specimens which were reinforced in the shear plane by stirrups, the steel strain was measured by gluing two strain gauges (Kyowa, Type KFC-5-C1-11L30) on diametrically opposed sides of one of the legs of the top stirrup, at a small distance away from the shear plane. This was to avoid false reading resulting from the bar's own bending. Each strain gauge was protected with Kyowa's C5 protective coating. The steel strain

was monitored during the initial cracking process (for initially cracked specimens) and subsequent application of shear.

Both vertical displacement along the shear plane and lateral displacement across it were measured on both faces of the test specimen. This was done by using linear variable displacement transducers (LVDT) mounted in steel blocks attached to the specimen, on one side of the shear plane, with their tips resting on brackets secured to the specimen on the opposite side of the shear plane.* The vertical and lateral displacements in initially uncracked specimens were monitored up to near maximum load, when surface spalling prevented further readings being taken. The type of LVDT used had a sensitivity of $\pm$ 0.001 mm. For initially cracked specimen, the displacement readings were monitored well past the maximum load. The type of LVDT used in this case had longer travel and a sensitivity of $\pm$ 0.003 mm.

Each specimen was loaded along the shear plane as shown in Fig. 5.5 by placing it vertically and centrally between the platens of an Amsler hydraulic testing machine. The upper platen was free to rotate in any plane. A specially fabricated sliding bearing was placed centrally between the top face of the specimen and the upper platen to ensure that separation of the two halves of the test specimen was not restrained by the testing machine. A load cell having a sensitivity of $\pm$ 0.3 kN was placed centrally betwen the sliding bearing and the top platen of the testing machine.

The specimens were subjected to a continuously increasing load until failure occurred, with short pauses to mark the crack development in the case of initially uncracked specimens. Each test was generally completed within 15 minutes.

* See Fig. 5.6(b) for details.

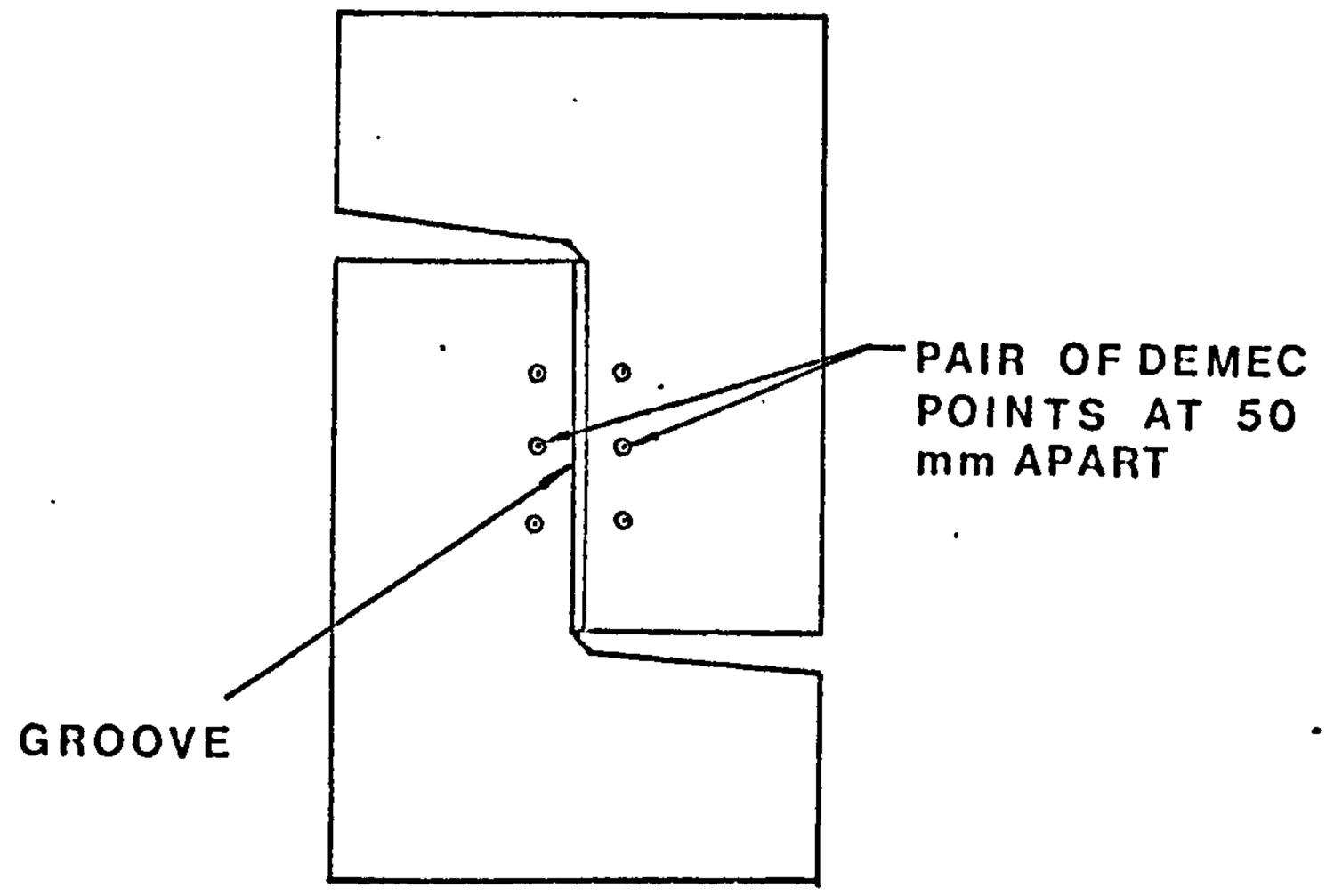

FIG·5·6(a) DETAILS OF INITIAL CRACK WIDTH MEASUREMENT

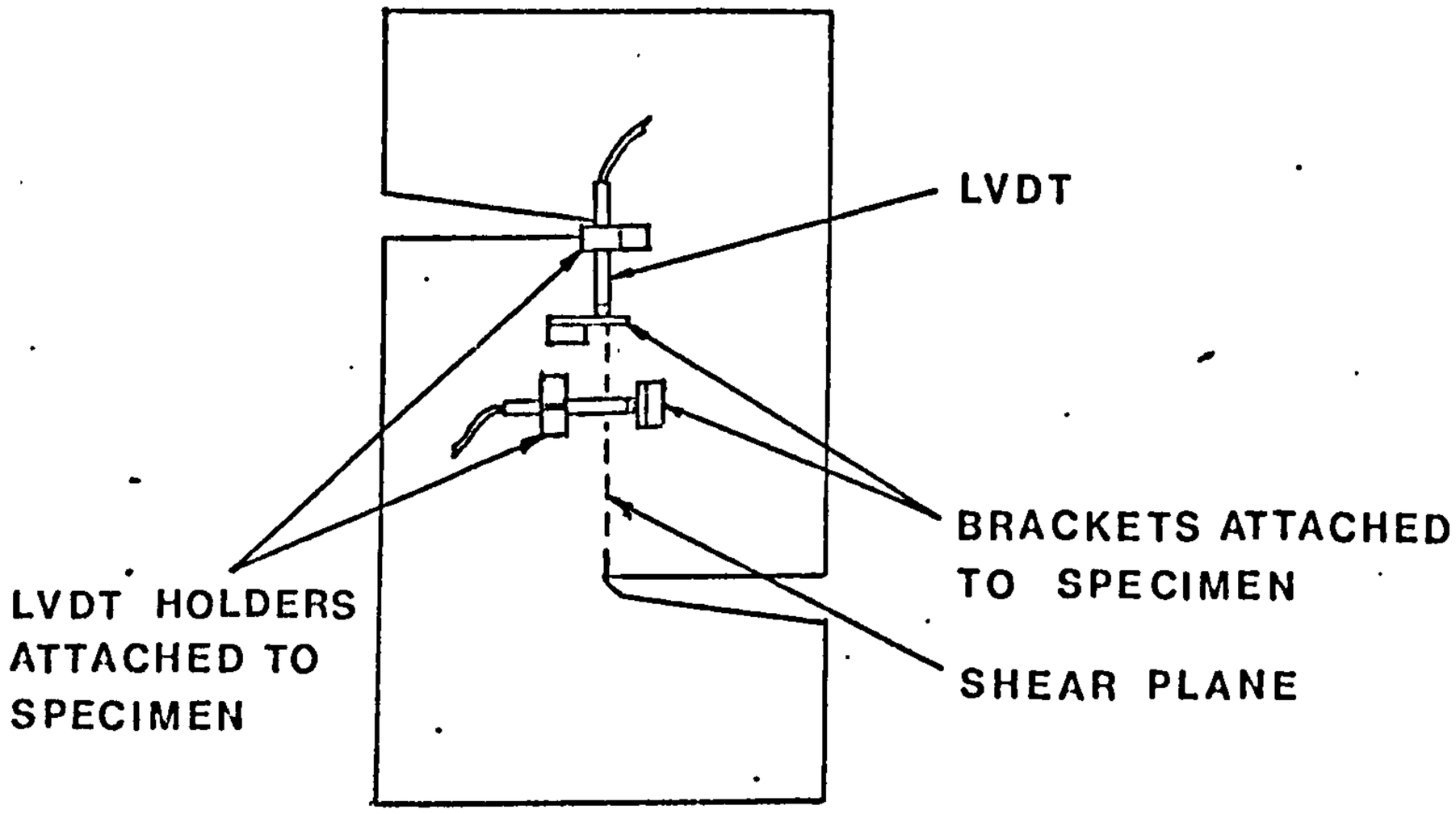

FIG·5·6(b)DETAILS OF VERTICAL AND LATERAL DISPLACMENT MEASUREMENTS

5.3.5 Mode of Failure

5.3.5.1 Initially Uncracked Specimens

All specimens failed along the shear plane although a few with high shear reinforcement showed signs of distress in the vicinity of the sliding bearing and in the corners of the two halves of the specimens.

The general behaviour was very similar to that reported by Mattock (89, 90). Diagonal tension cracks became visible at shear stresses between 3.0 and 6.0 N/mm^2. These short inclined cracks cross the shear plane at an angle of from 15^o to 40^o to the shear plane. As the load increased, some of the cracks lengthened and new cracks appeared. In general, at failure more cracks at closer spacing were formed in fibre concrete specimens than in corresponding plain concrete specimens. See Plate 5.1.

Final failure was characterized by the formation of additional cracks joining the diagonal tension cracks together and by compression spalling in the region of diagonal tension cracks adjacent to the shear plane.

5.3.5.2 Initially Cracked Specimens

All specimens failed along the precracked plane and were allowed to deform well beyond the maximum load. Inclined cracks crossing the shear plane occurred at high loads in two of the more highly reinforced gravel concrete specimens. In all the specimens, a certain amount of spalling of the concrete was observed along the crack plane at failure. Generally, the gravel concrete specimens showed a much larger amount of spalling than the Lytag-sand concrete specimens.

After the devlopment of large displacements, the local bending of the stirrups adjacent to the shear plane and fibre pull-out were clearly evident.

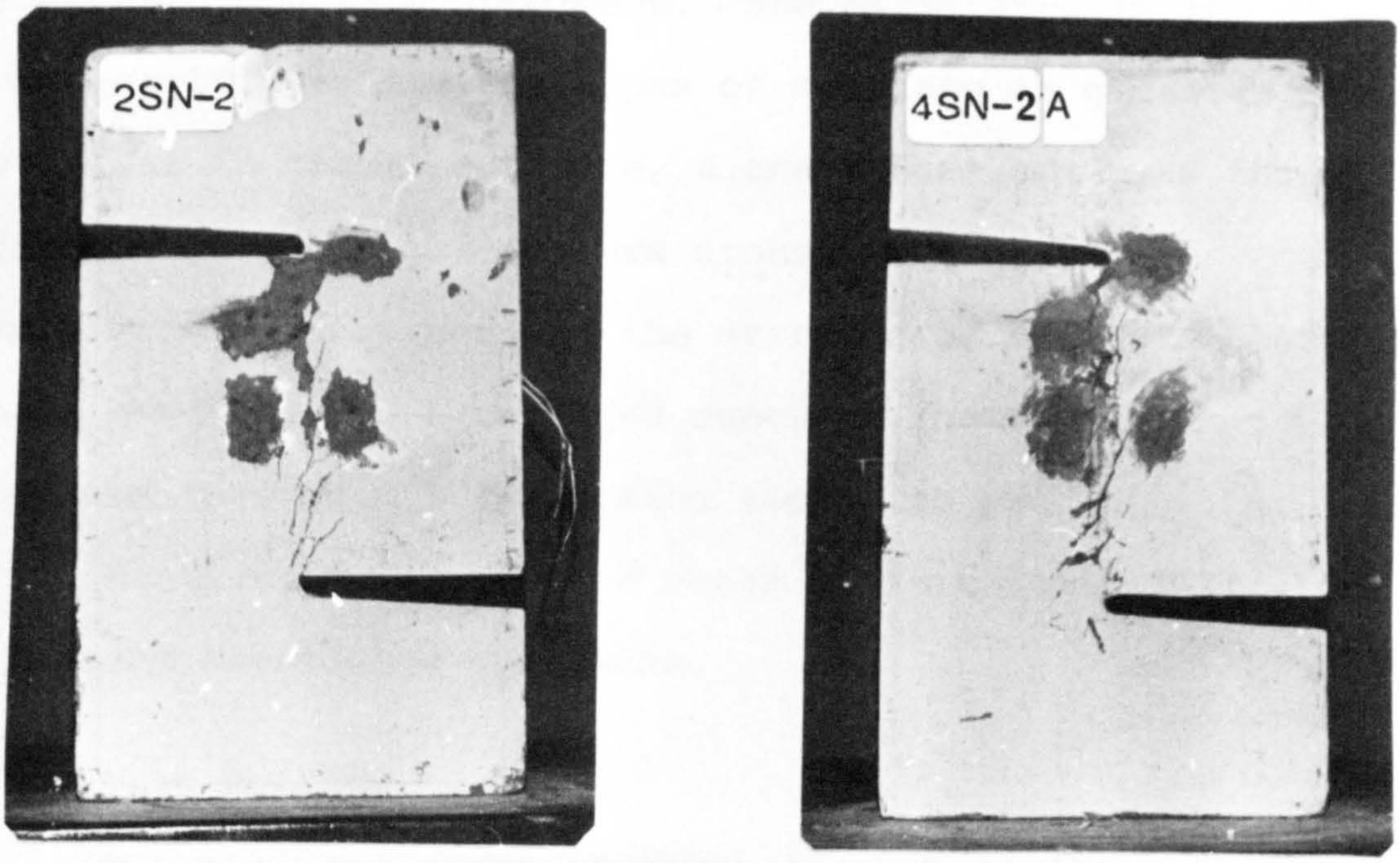

PLAIN FIBRE

a) Gravel Concrete(with 2Y8 stirrups)

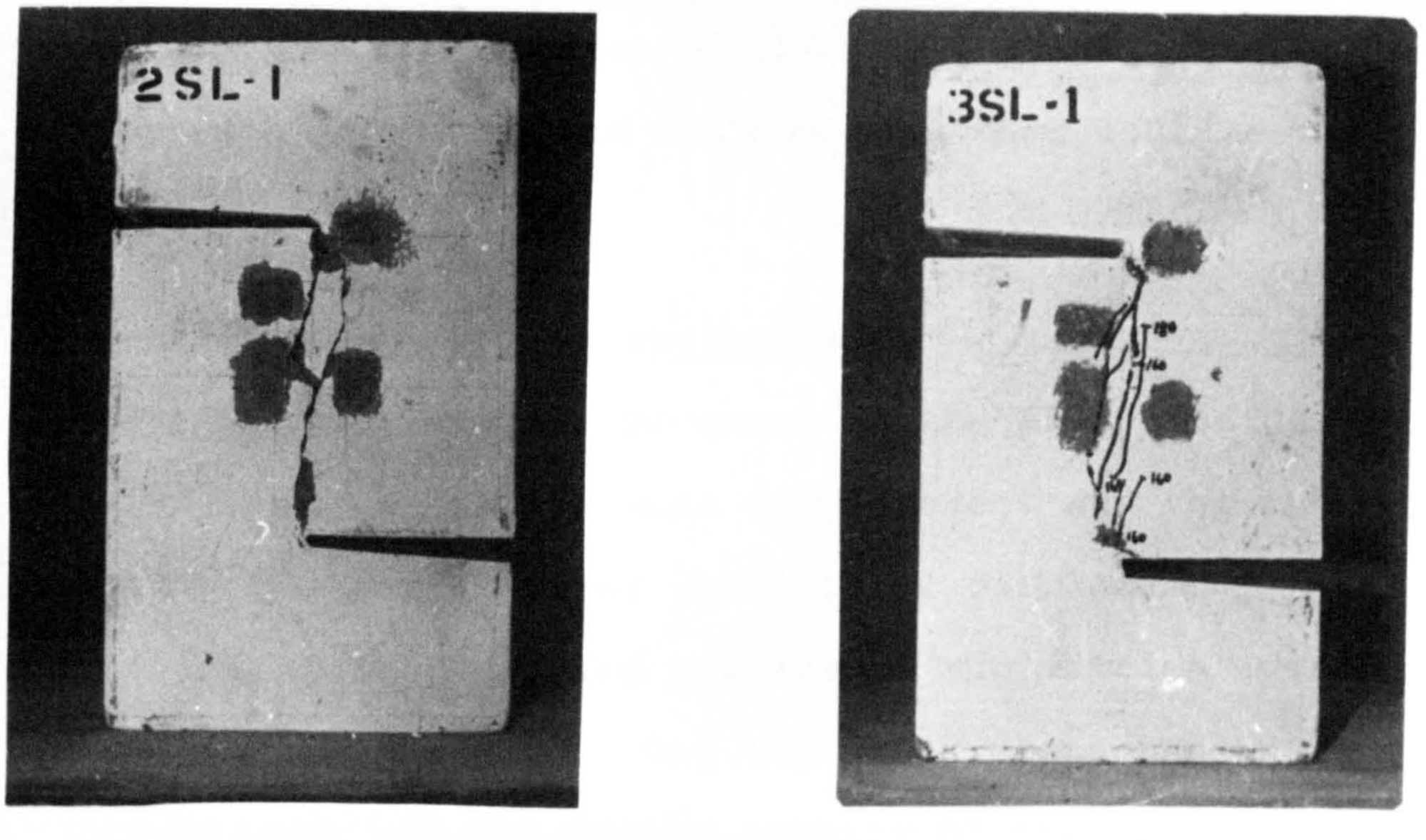

PLAIN FIBRE

b) Lytag–Sand Concrete(with 2R6 stirrups)

PLATE 5·1 Modes of failure of initially uncracked concrete specimens

Plate 5.2 shows the fracture surfaces of both gravel and Lytag-sand concrete specimens. The difference in the degree of roughness between the two types of concrete is quite apparent. It shows that in gravel concrete, a crack does not pass through the gravel aggregates and failure around each gravel aggregate is simply bond failure between the surrounding matrix and the aggregate surface. In Lytag-sand concrete, however, a tensile crack passes through all aggregates along its path.

Plate 5.3 compares the modes of failure in initially uncracked and precracked specimens.

5.3.6 Test Results

The ultimate shear strength of each of the test specimens is given in Table 5.3. The ultimate shear strength is expressed as average shear stress v_u, obtained by dividing the ultimate shear force by the area of the shear plane. The ultimate shear force was taken to be the maximum load that could be carried by the specimen.

5.3.6.1 Load-displacement Characteristics

For convenience, the movement in the direction of the shear plane was called the vertical displacement and the movement at right angles to it was termed the lateral displacement. Obviously, for initially cracked specimens, the vertical displacement was due to the slip along the shear plane and the lateral displacement was due to the opening of the preformed crack. For initially uncracked specimens, these displacements were due to elastic deformation initially and then due to the rotation of the inclined concrete struts after the formation of diagonal tension cracks.

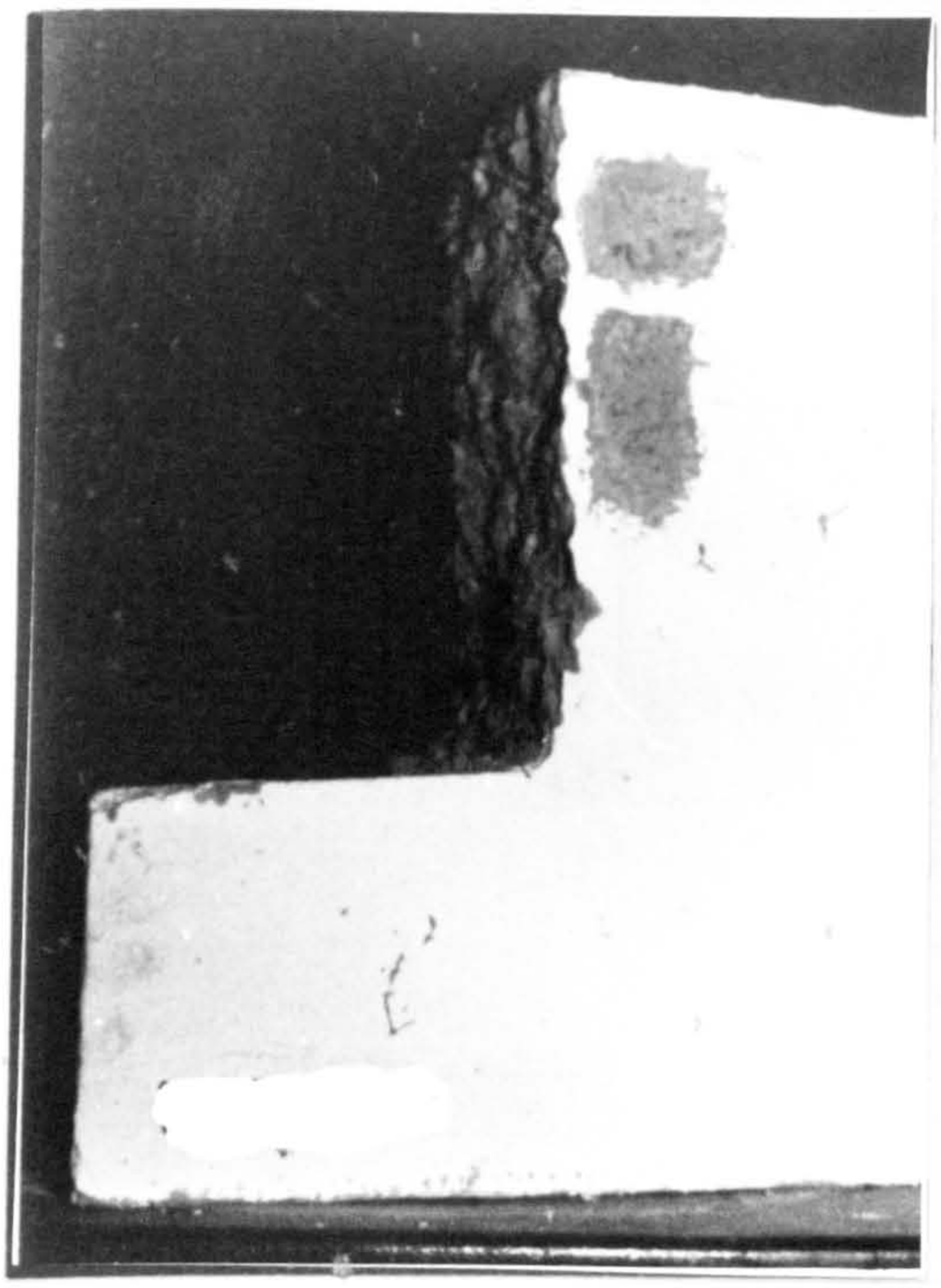

GRAVEL

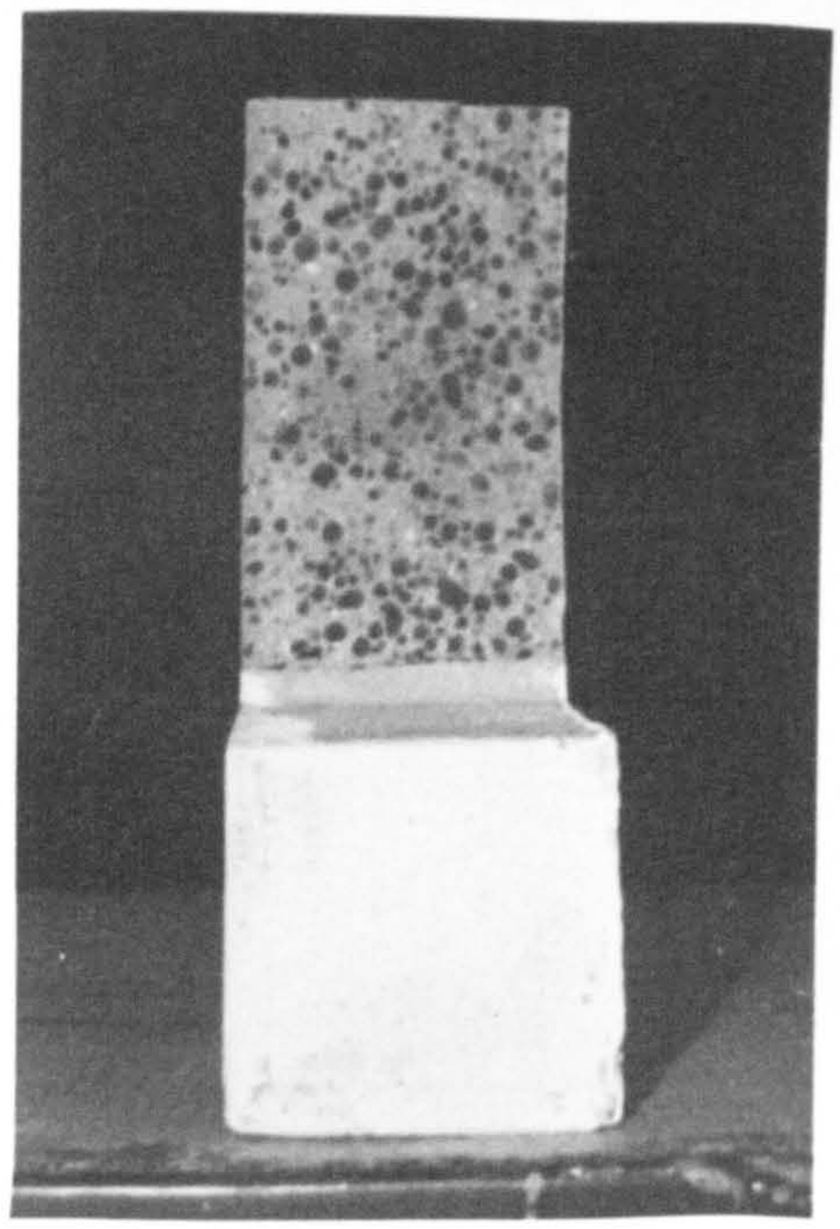

LYTAG-SAND

PLATE 5·2 Fracture surfaces of gravel & lytag-sand concretes

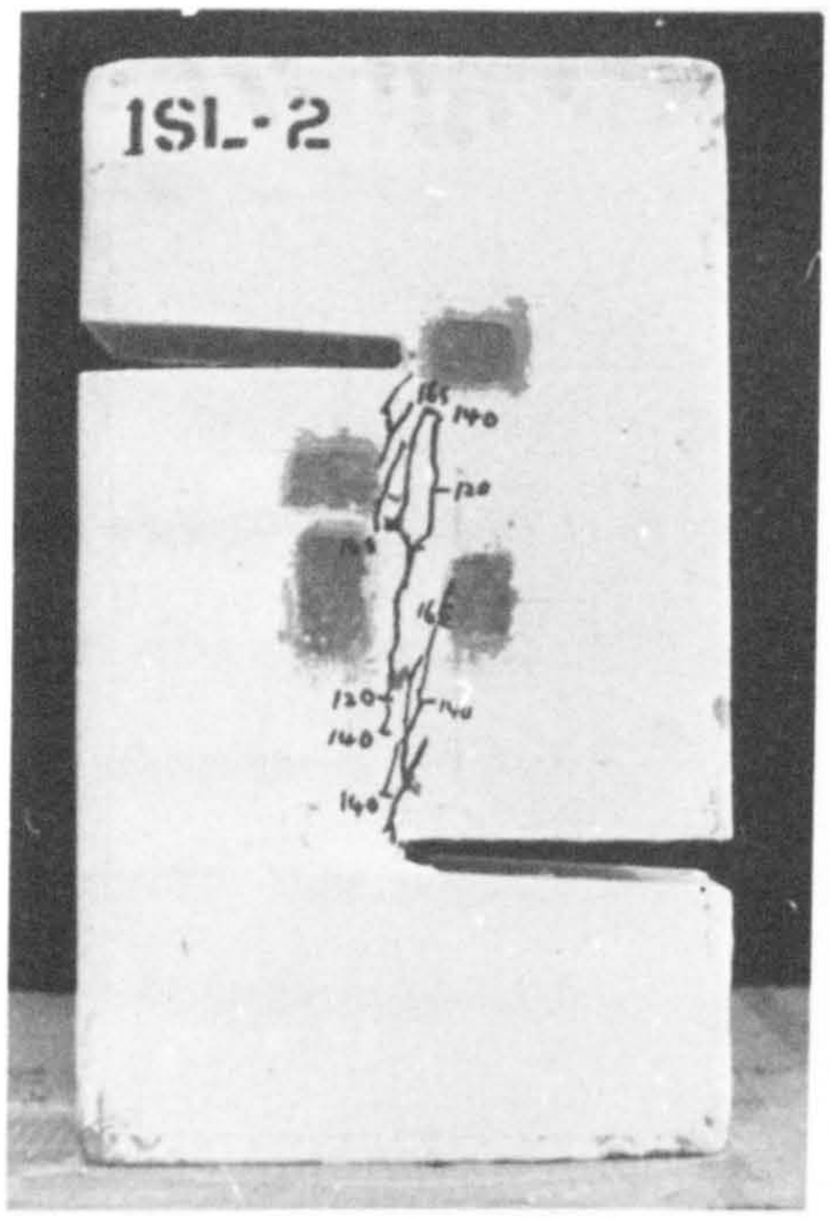

INITIALLY UNCRACKED

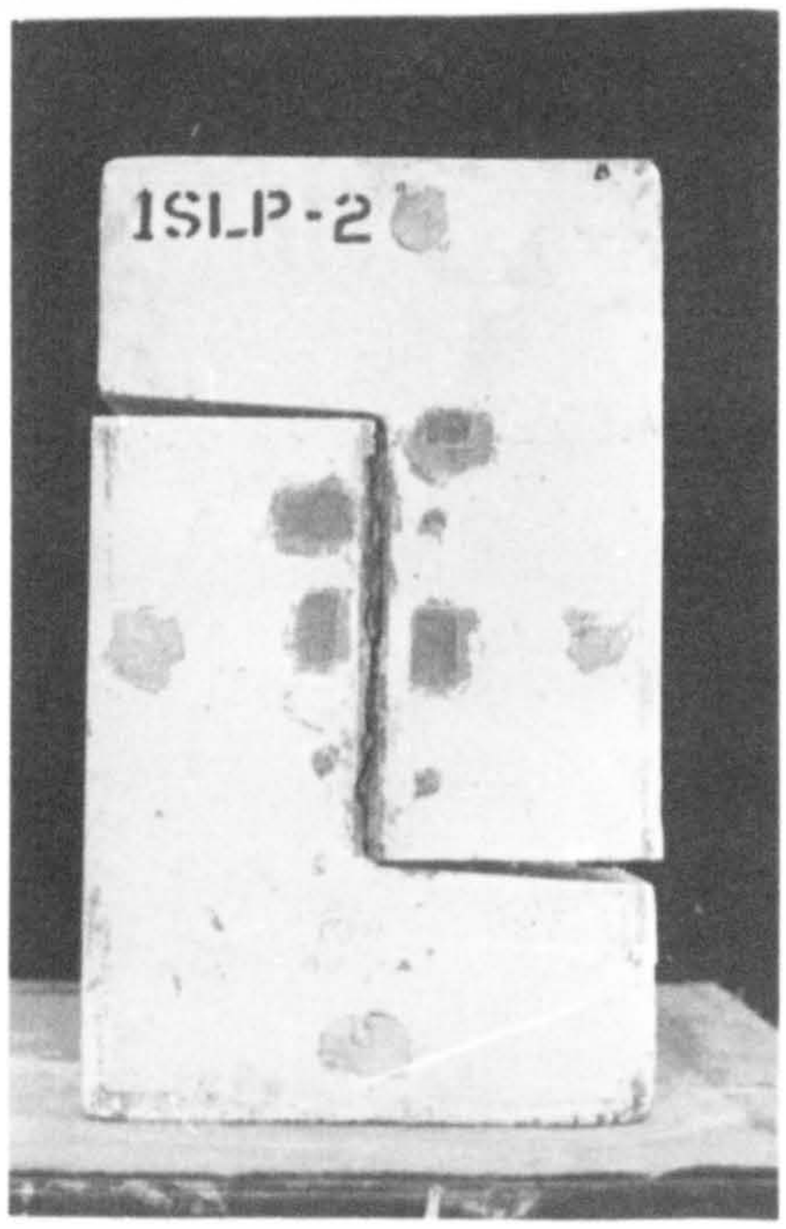

PRECRACKED

PLATE 5·3 Typical initially uncracked & precracked specimens after failure

Shear stress-vertical displacement and shear stress-lateral displacement curves were produced using a computer plotter for each of the thirty-five specimens tested. The vertical and lateral displacement values used were the averages of those of the top and bottom faces.

Typical shear stress-displacement curves of initially uncracked specimens with different types of shear reinforcement and concrete are shown in Figs 5.7 through 5.10. The formation of inclined cracks across the shear plane was reflected in the sudden increase in the lateral displacement and, though less obviously for high amount of shear reinforcement, in the jump in the vertical displacement. The rate of increase of the lateral displacement with the shear stress was less than that of the vertical displacement before the formation of inclined cracks. Once such cracks were formed, the rate of increase of both displacements was generally about the same. Also the rate of increase of both displacements depended on the amount of shear reinforcement provided.

Typical shear stress-displacement curves of initially cracked specimens with different types of shear reinforcement and concrete are given in Figs. 5.11 through 5.14. Generally, the rate of change of the lateral displacement (crack width) with the shear stress was less than that of the vertical displacement (slip or shear displacement)

5.3.6.2 Steel Strains

Typical shear stress-steel strain curves of the initially uncracked specimens are shown in Fig. 5.15. A large increase in the steel strain was observed at the formation of inclined cracks across the shear plane. After this the steel strain increased at

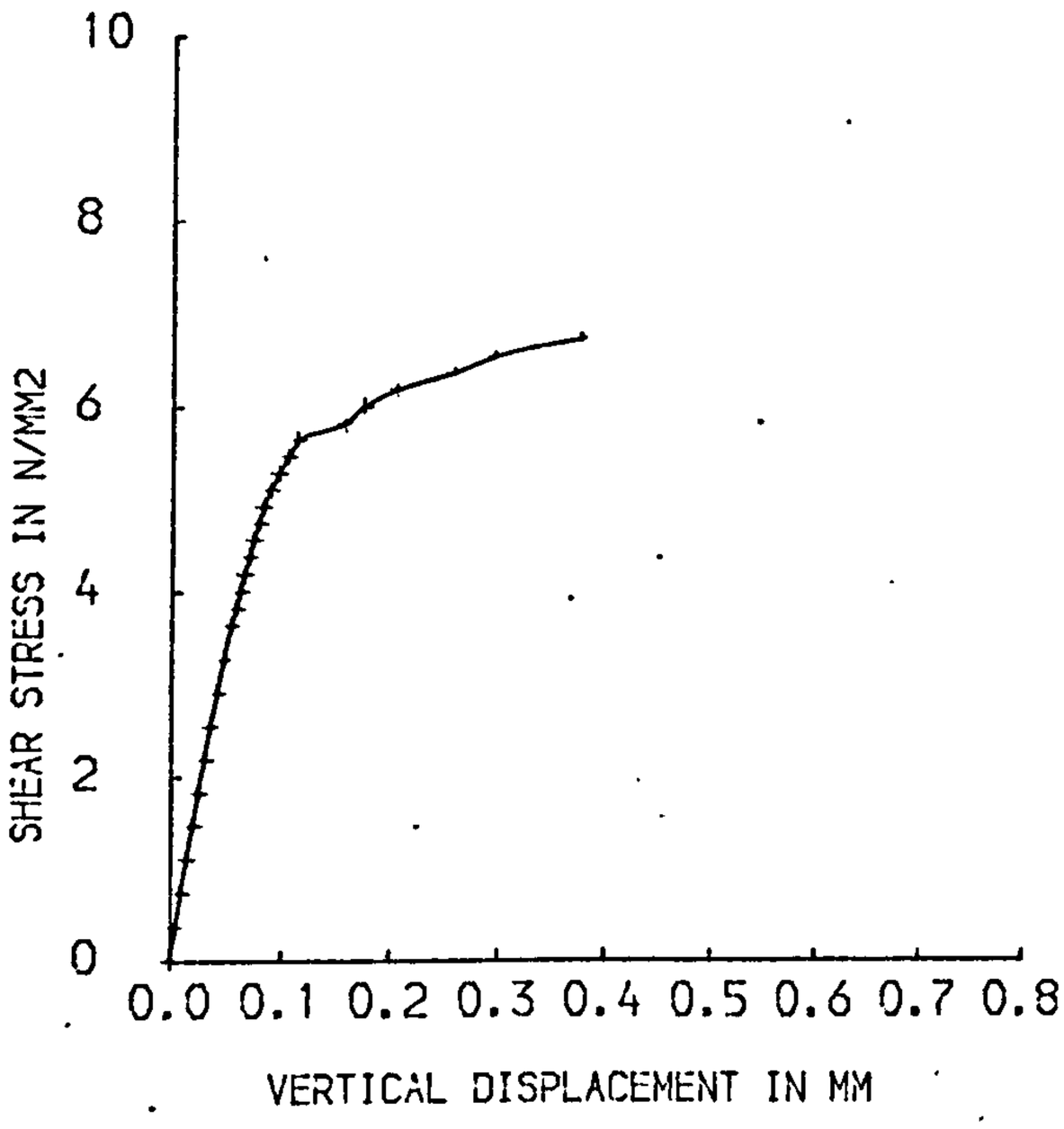

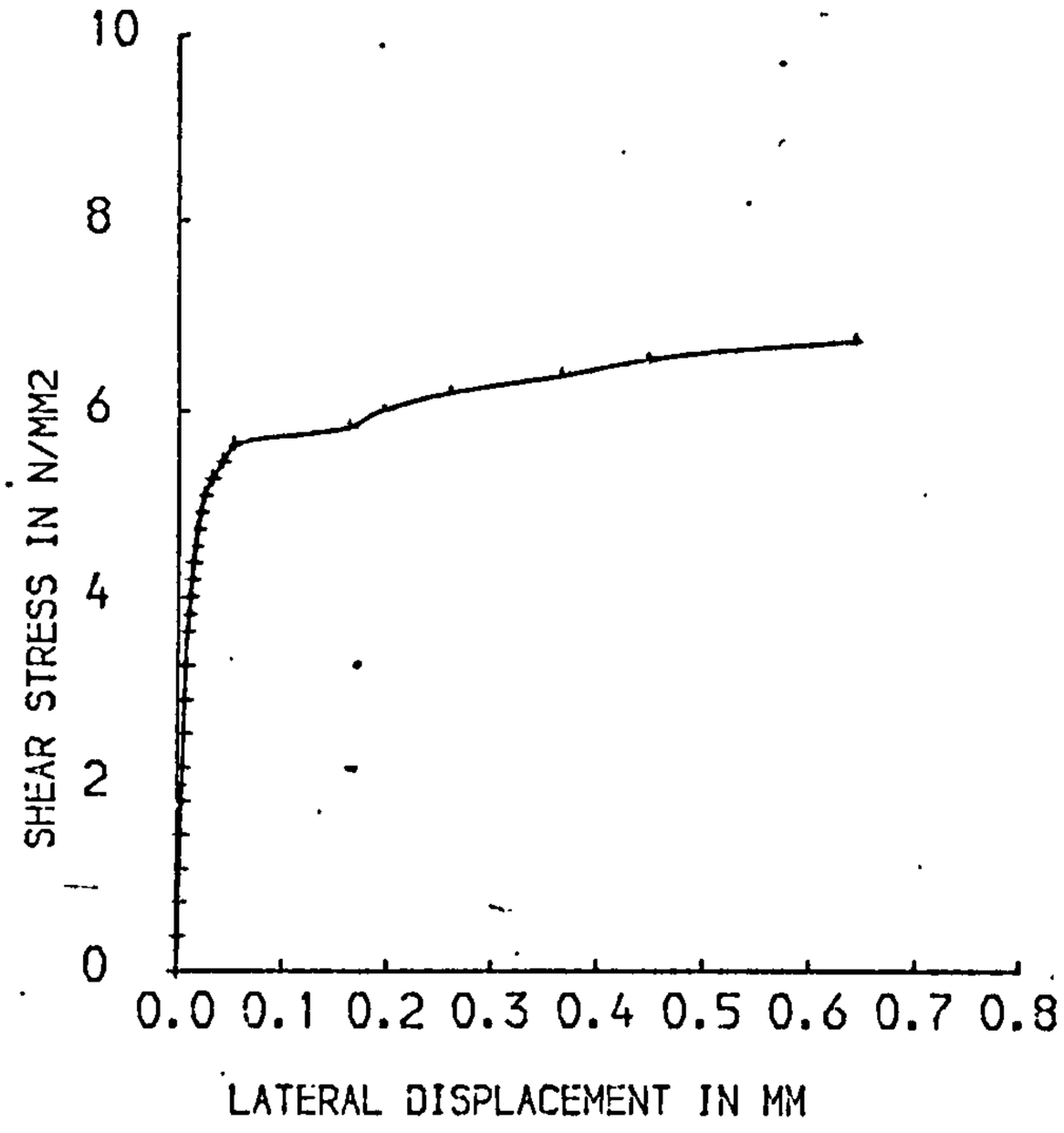

FIG. 5·7 DISPLACEMENT CURVES OF 1SN-3

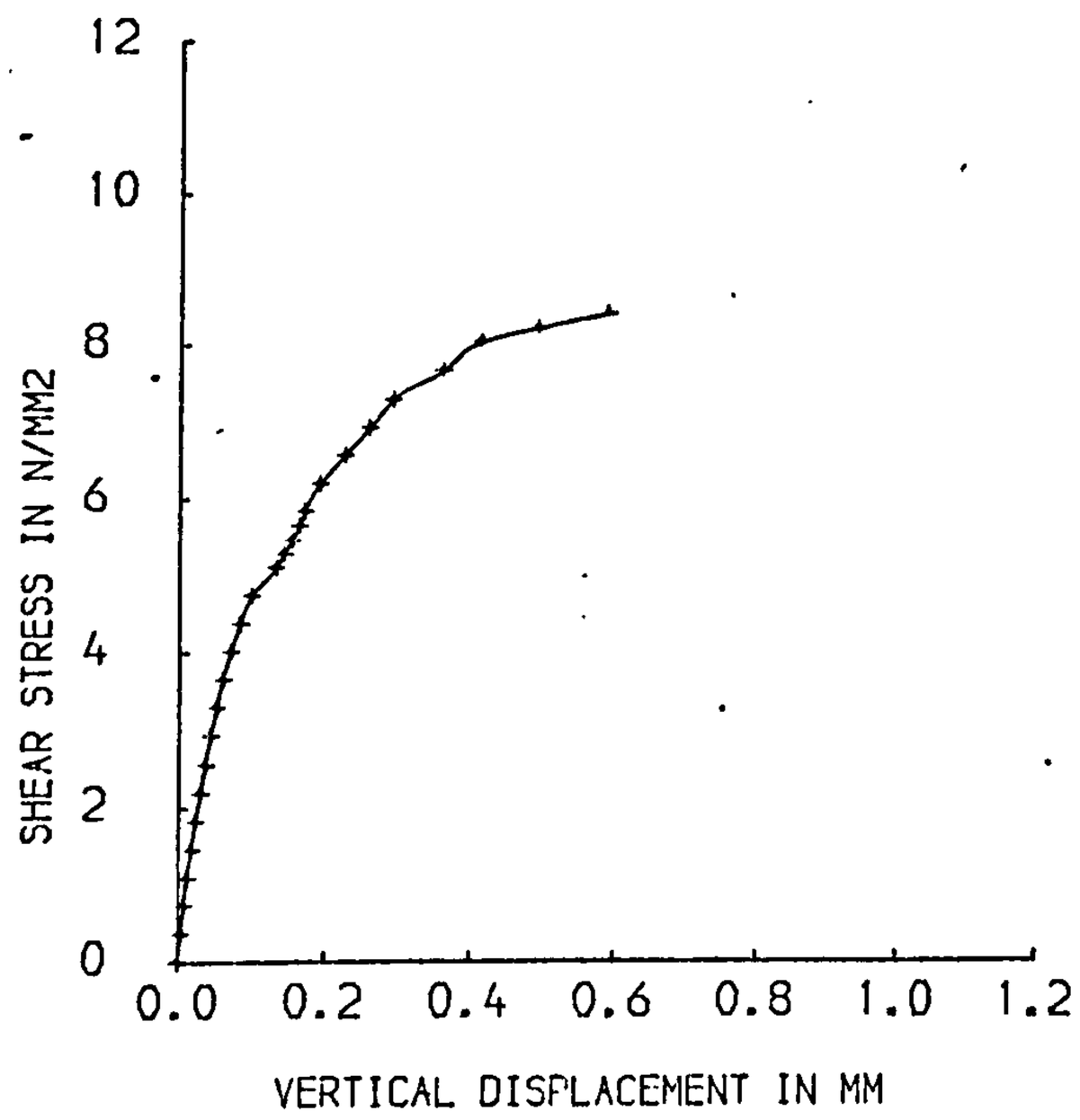

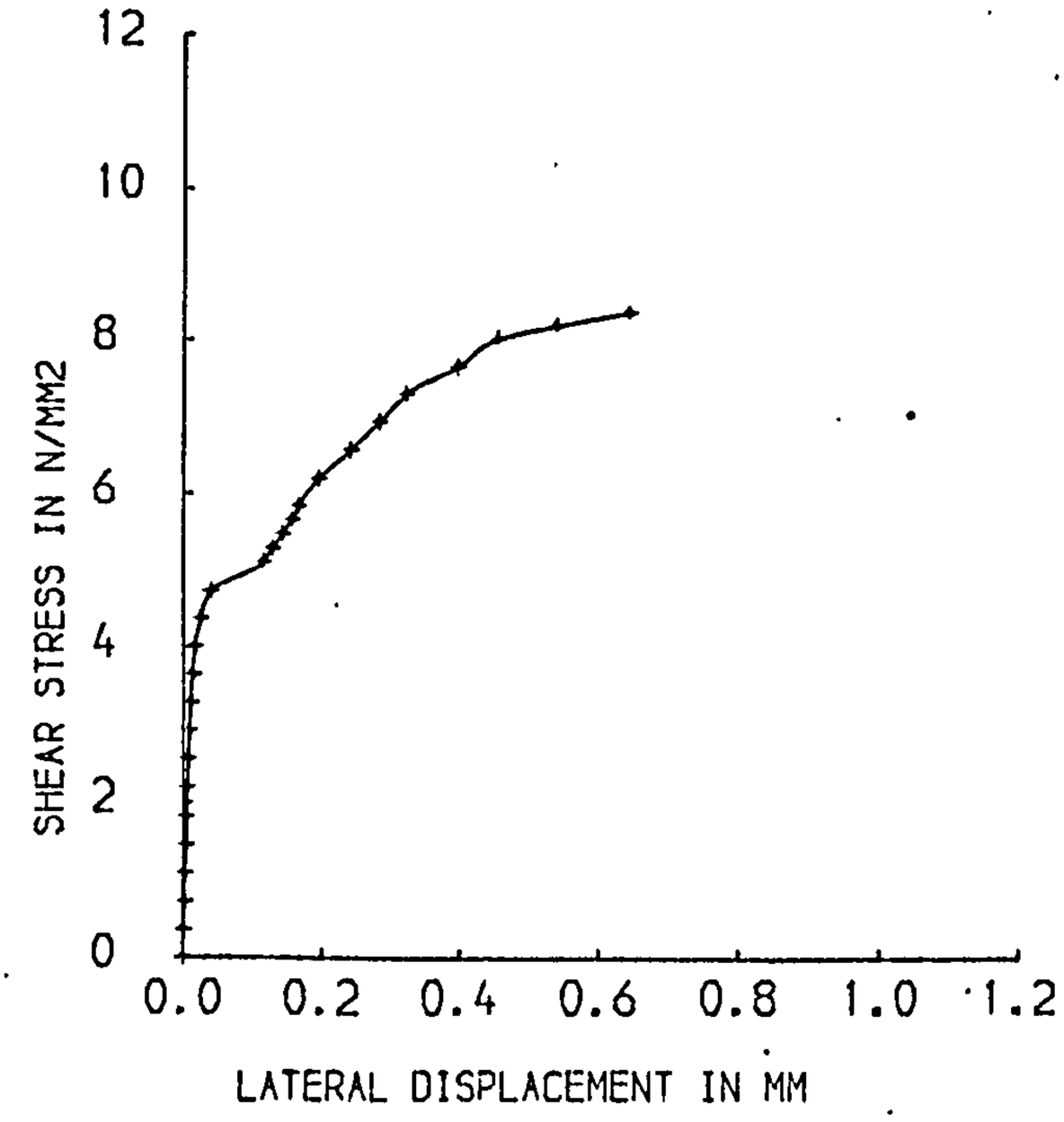

FIG. 5·8 DISPLACEMENT CURVES OF 3SN-2

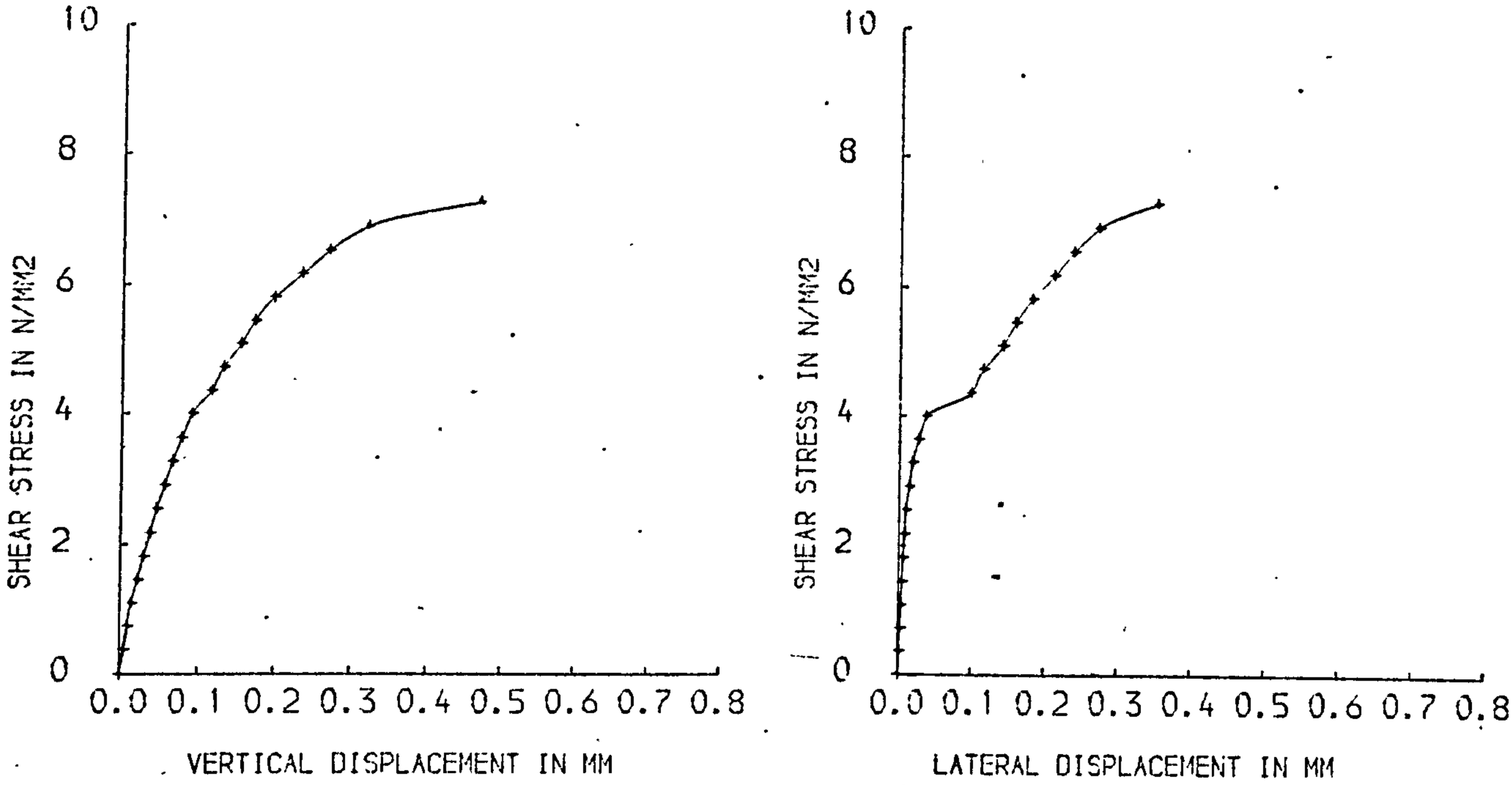

FIG. 5·9 DISPLACEMENT CURVES OF 2SL-3

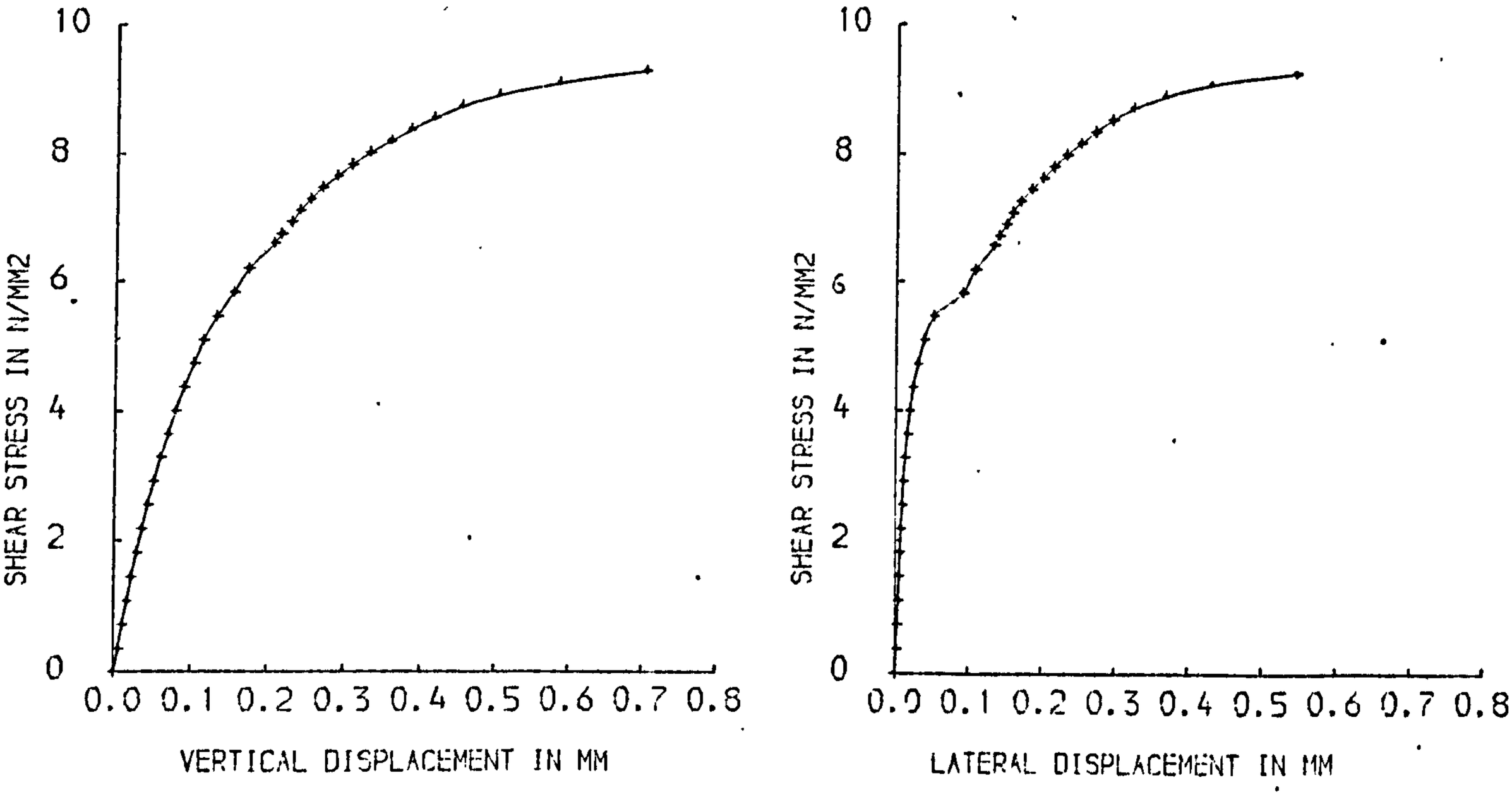

FIG.5·10 DISPLACEMENT CURVES OF 3SL-2

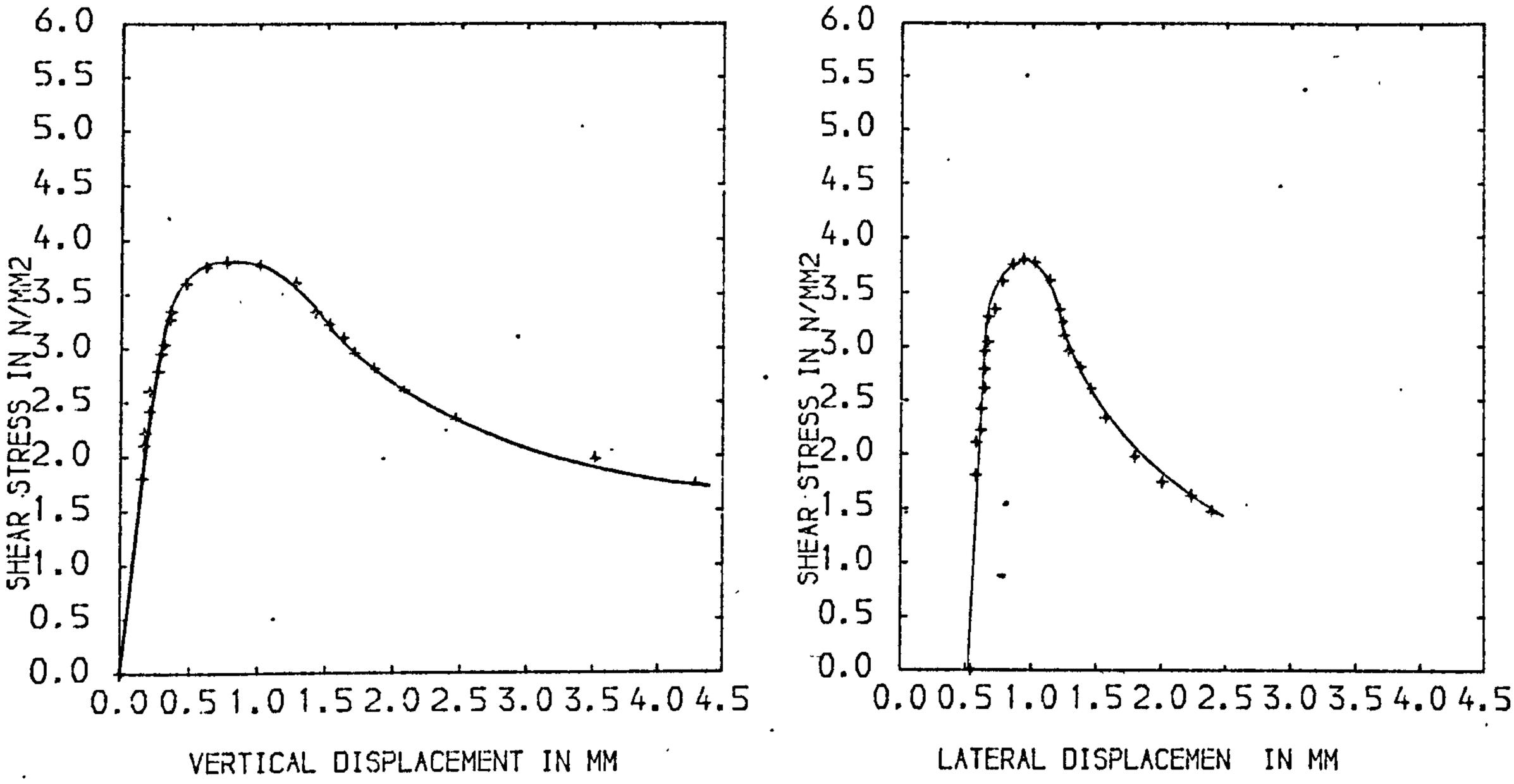

FIG. 5·11 DISPLACEMENT CURVES OF 1SLP-2

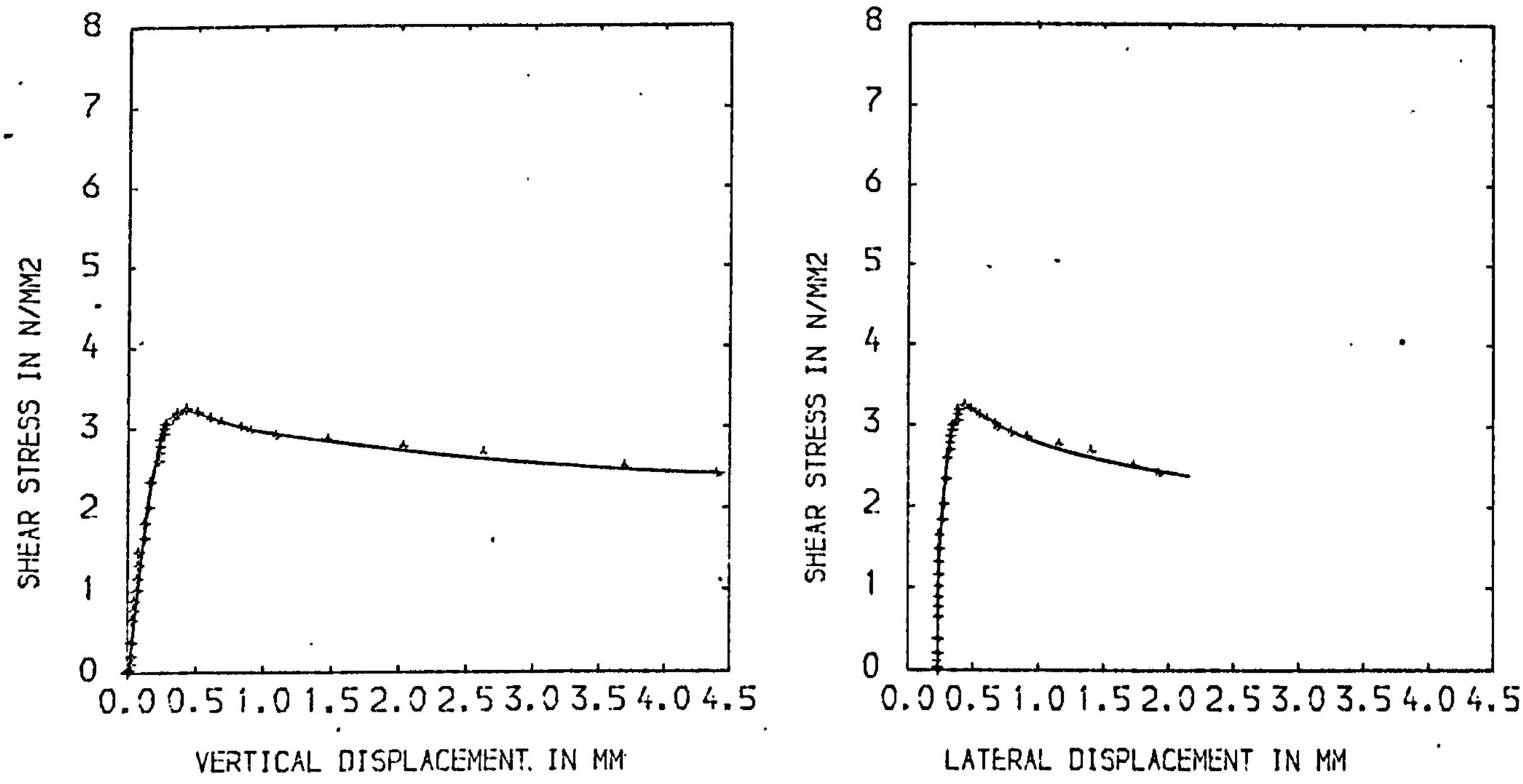

FIG. 5·12 DISPLACEMENT CURVES OF 2SNP-1

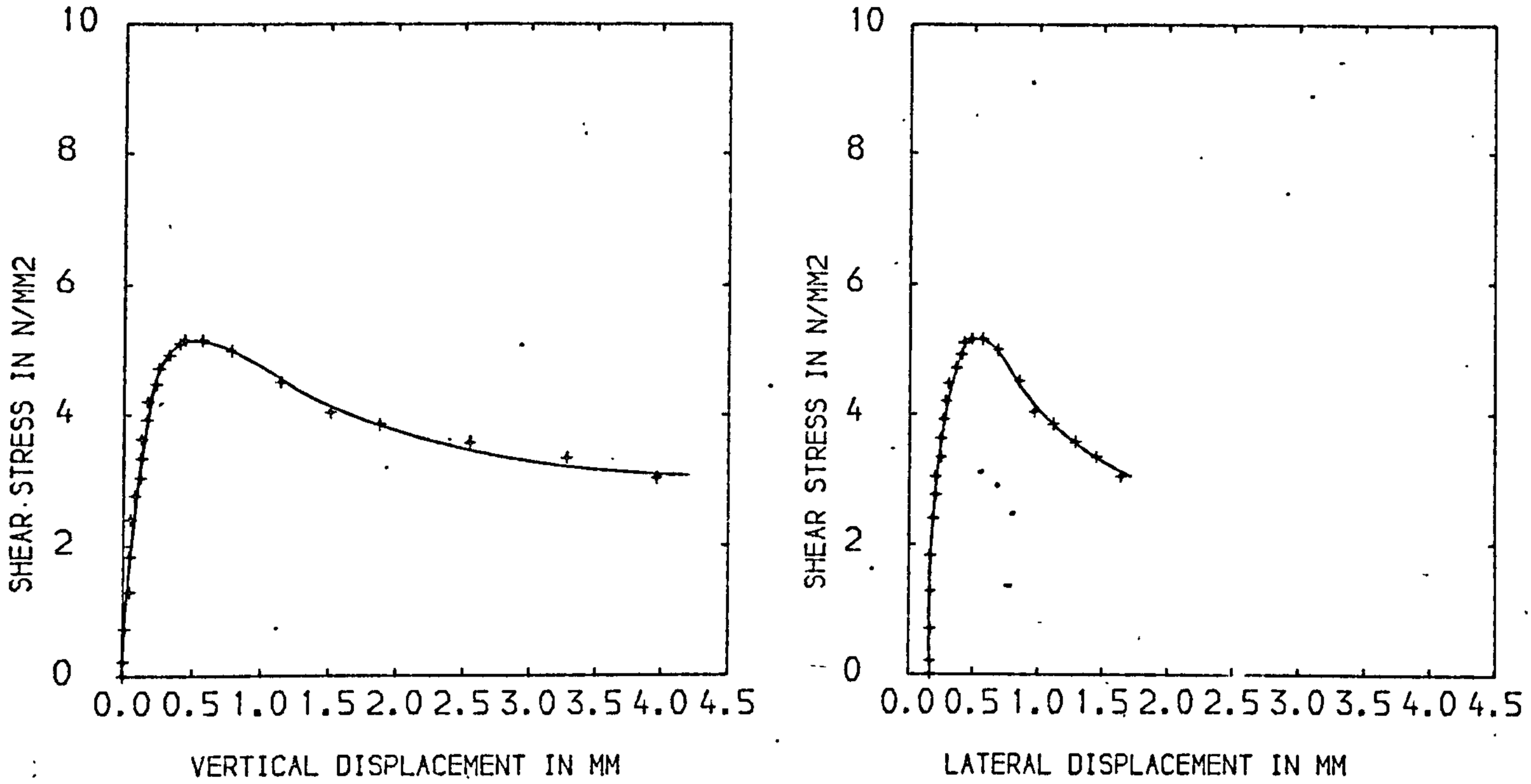

FIG. 5·13 DISPLACEMENT CURVES OF 3SNP-1

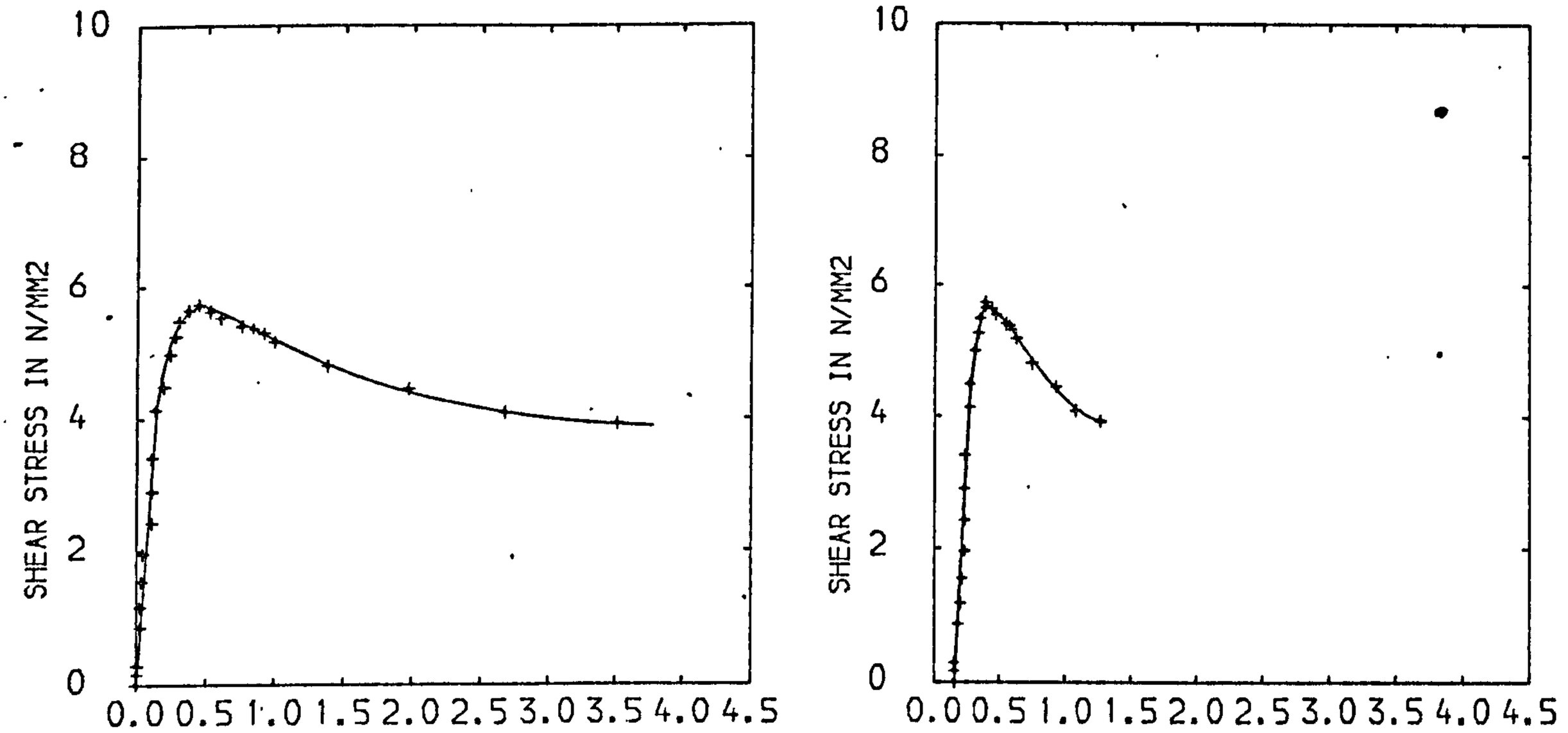

FIG. 5·14 DISPLACEMENT CURVES OF 3SLP-1

an increasing rate with the shear stress.

Typical shear stress-steel strain curves of the initially cracked specimens are shown in Fig. 5.16. Generally, the steel strain increased with increasing shear stress and there was a rapid increase in the steel strain near and beyond the maximum load.

5.4 Discussion and Analysis of Test Results

First the influence of crimped steel fibres on the ultimate shear transfer strength will be discussed and analysed. Then their effect on the load-deformation behaviour is discussed. Finally the variation of the stiffness of the shear transfer with crack widths will be discussed and analysed.

5.4.1 Ultimate Strength of Shear Transfer

The term 'total shear reinforcement parameter' will be encountered frequently in the discussion. It is defined as the sum of the conventional shear reinforcement (stirrup) parameter rf_y and the post-cracking tensile strength of fibre reinforced concrete σ_{cu}. The calculation of the post-cracking tensile strength of the various fibre concretes used in this investigation is shown in Appendix A.

5.4.1.1 Initially Uncracked Gravel Concrete

The total shear reinforcement parameter, the shear stress at the appearance of diagonal tension cracks and the ultimate shear strength of all the initially uncracked gravel concrete specimens are shown in Table 5.3. The percentage increase of the fibre concrete specimens over that of corresponding plain concrete specimens is also shown in the same table.

It can be seen that the inclusion of 0.4% by volume of crimped fibres increased the ultimate shear strength by 9.9 to

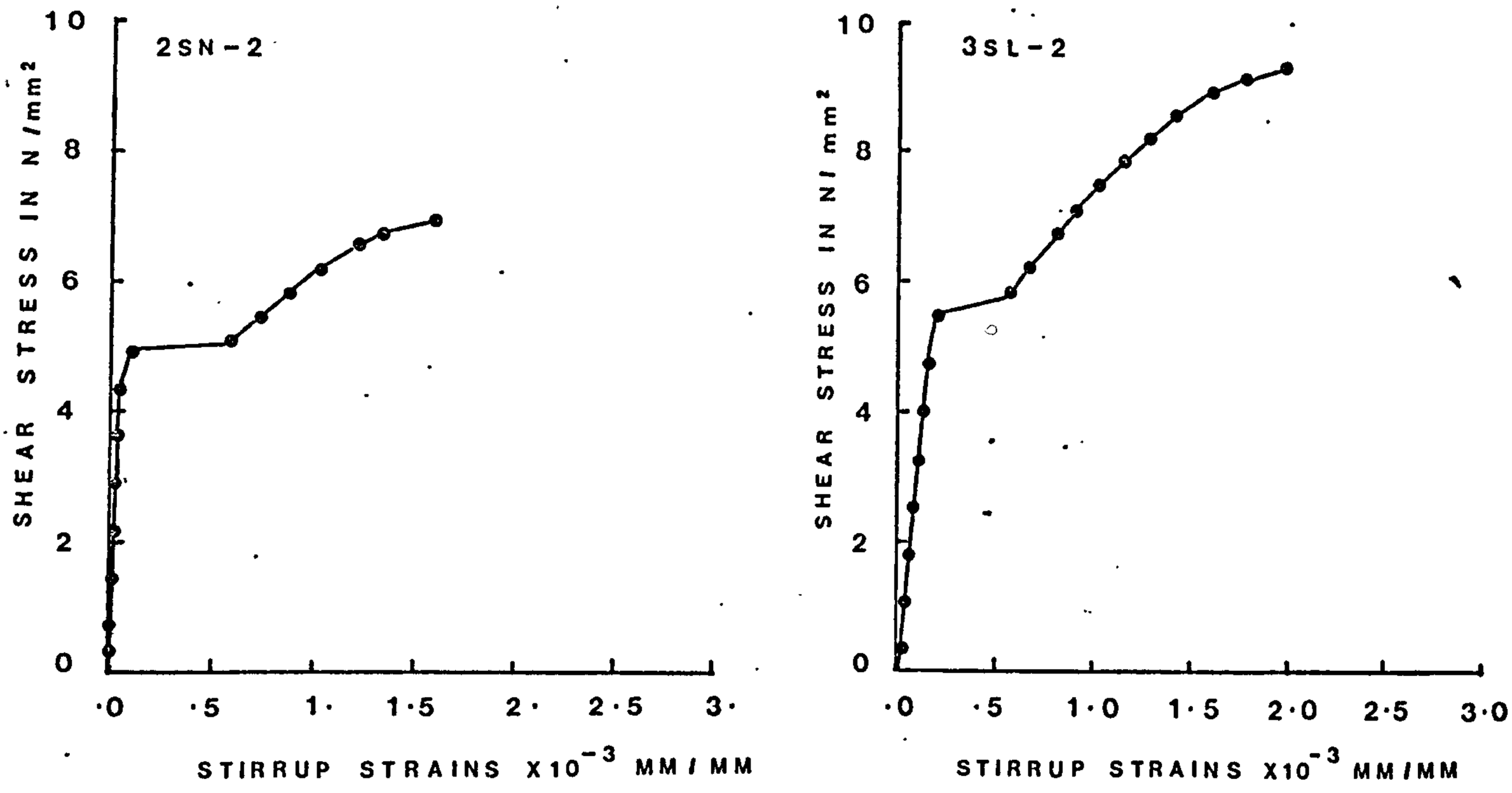

FIG. 5·15 TYPICAL SHEAR STRESS VERSUS STIRRUP STRAIN CURVES OF INITIALLY UNCRACKED SPECIMENS

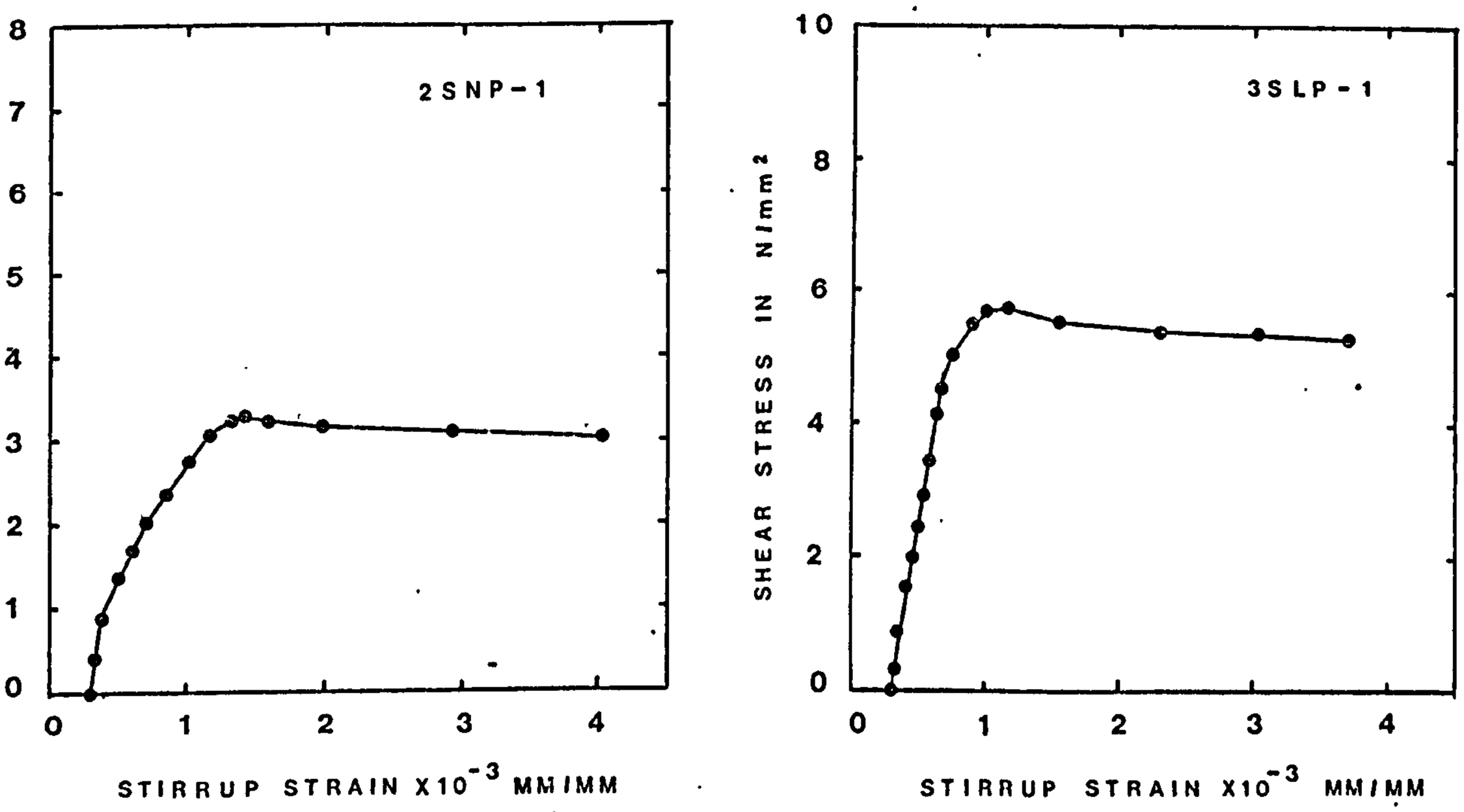

FIG. 5·16 TYPICAL SHEAR STRESS VERSUS STIRRUP STRAIN CURVES OF INITIALLY CRACKED SPECIMENS

Table 5.3 Test Results

Specimen No.	rf_y * N/mm^2	σ_{cu} † N/mm^2	$(rf_y + \sigma_{cu})$ N/mm^2	Initial Crack Width mm	Shear** Stress at 1st crack N/mm^2	Ultimate Shear Stress N/mm^2	Percentage Increase %
Gravel Concrete							
1SN-1	-	-	-	-	4.36	4.36	-
1SN-2	-	0.58	0.58	-	4.83	5.28	21.1
1SN-3	-	1.16	1.16	-	5.50	6.70	53.7
1SN-4	-	1.48	1.48	-	5.50	6.75	54.8
2SN-1	1.44	-	1.44	-	4.64	5.28	-
2SN-2	3.69	-	3.69	-	4.95	7.00	-
2SN-3	5.71	-	5.71	-	5.0	9.10	-
3SN-1	1.44	0.58	2.02	-	4.74	6.55	24.1
3SN-2	3.69	0.58	4.27	-	4.92	8.40	20.0
3SN-3	5.71	0.58	6.29	-	5.20	10.0	9.9
4SN-1	1.44	1.16	2.60	-	5.10	7.8	47.7
4SN-2	3.69	1.16	4.85	-	5.09	9.03	29.0
4SN-3	5.71	1.16	6.87	-	5.30	10.2	12.1
1SNP-2	-	0.58	0.58	0.28	-	2.92	-
1SNP-3	-	1.16	1.16	0.19	-	4.69	-
1SNP-4	-	1.48	1.48	0.30	-	5.07	-
2SNP-1	1.80	-	1.80	0.23	-	3.25	-
2SNP-2	4.62	-	4.62	0.36	-	6.0	-
3SNP-1	1.80	0.58	2.38	0.17	-	5.15	58.5
3SNP-2	4.62	0.58	5.20	0.27	-	9.20	53.5
4SNP-1	1.80	1.16	2.96	0.26	-	6.56	101.8
4SNP-2	4.62	1.16	5.78	0.19	-	9.76	62.7
Lytag-sand Concrete							
1SL-1	-	-	-	-	3.30	3.30	-
1SL-2	-	1.61	1.61	-	4.91	6.55	98.5
2SL-1	1.44	-	1.44	-	3.46	5.70	-
2SL-2	3.69	-	3.69	-	4.18	6.91	-
2SL-3	5.71	-	5.71	-	4.18	7.28	-
3SL-1	1.44	1.61	3.05	-	6.0	8.69	52.5
3SL-2	3.69	1.61	6.20	-	5.82	9.37	35.6
1SLP-2	-	1.61	1.61	0.53	-	3.80	-
2SLP-1	1.80	-	1.80	0.45	-	3.12	-
2SLP-2	4.62	-	4.62	0.35	-	5.49	-
2SLP-3	7.14	-	7.14	0.28	-	6.90	-
3SLP-1	1.80	1.61	3.41	0.15	-	5.73	83.7
3SLP-2	4.62	1.61	6.23	0.30	-	8.48	54.5

* $r = A_s/bd$, where A_s = total area of stirrups crossing shear plane
bd = area of shear plane
fy = yield stress of stirrup

† σ_{cu} = post cracking tensile stength of fibre concrete

** detected visually

24.1%. The inclusion of 0.8% by volume brought about an increase of 12.1 to 53.7%. The influence of steel crimped fibres can be more clearly seen from Fig. 5.17(a). The inclusion of 0.4% by volume of fibres effected an average increase in the ultimate strength of 1.1 N/mm^2 for rf_y ranging from 0 to 5.71 N/mm^2. With 0.8% by volume inclusion, the average increase was 2.5 N/mm^2 for rf_y between 0 and 1.44 N/mm^2 and for rf_y greater than 1.44 N/mm^2, the magnitude of this increase decreased with increasing rf_y. This decrease was due probably to the fact that failure of the inclined struts between the diagonal tension cracks occurred before the stirrups were able to attain their yield strength.

The ultimate shear strength against the total shear reinforcement parameter for both the plain and fibre concrete specimens is shown in Fig. 5.18(a). In the same figure, some of the test results of Mattock (89) were also plotted. Linear regression analysis of the plain concrete results gave:

For initially uncracked plain gravel concrete,

$$v_u = 4.03 + 0.85\ (rf_y + \sigma_{cu}) \qquad (5.10)$$

where v_u = ultimate stress, N/mm^2

rf_y = conventional shear reinforcement parameter, N/mm^2

σ_{cu} = post-cracking tensile strength of fibre concrete, N/mm^2

The results of the fibre concrete were rather scattered but they did suggest an approximate linear relationship. A straight line parallel to equation (5.10) was fitted through all the points to obtain:

For initially uncracked fibre gravel concrete,

$$v_u = 5.1 + 0.85\ (rf_y + \sigma_{cu}) \qquad (5.11)$$

for $(rf_y + \sigma_{cu}) \geq 0.5\ N/mm^2$

Equations (5.10) and (5.11) are just convenient empirical relationships amd they have no theoretical basis. Mattock et al (90, 93) (see section 5.2.1) suggested a limiting ultimate shear transfer strength of plain gravel concrete of $0.3\ f_c'$ and this corresponds to about $10.0\ N/mm^2$ for the grade of concrete used in this investigation.

5.4.1.2 Initially Uncracked Lytag-sand Concrete

The results of all initially uncracked Lytag-sand concrete specimens are given in Table 5.3. It can be seen that the inclusion of 1.0% by volume of crimped fibres brought about an increase in the ultimate shear transfer strength of between 35.6 to 98.5%. This effect is more clearly seen in Fig. 5.17(b). The addition of 1% by volume of crimped fibres gave an average increase in the ultimate strength of about $3.0\ N/mm^2$ for rf_y ranging from 0 to $4.0\ N/mm^2$.

The ultimate shear transfer strength against the total shear reinforcement parameter for both the plain and fibre concrete specimens was plotted in Fig. 5.19(a). The relationship is clearly nonlinear for both cases. No attempt was made to derive any empirical equations to relate the ultimate strength to the total shear reinforcement parameter.

One interesting feature can be observed from Figs. 5.17(b) and 5.19(a). The ultimate strength of the plain concrete and that of the fibre concrete seemed to converge to different limits. The results, admittedly limited, suggested that the inclusion of steel fibres increased the limit of the ultimate shear transfer strength. This effect was less apparent in the

gravel concrete specimens. This may be due to the fact that the inclusion of steel fibres has a more pronounced effect on the failure envelope of Lytag-sand concrete subject to combined compressive and shear stresses than that of gravel concrete. The inclusion of steel fibres in Lytag-sand concrete seems to be more beneficial than in gravel concrete insofar as the ultimate shear transfer strength is concerned.

Finally the inclusion of steel fibres raised the limit of the ultimate shear transfer strength of Lytag-sand concrete to a value approaching that of gravel concrete.

5.4.1.3 Possible Explanation of the Influence of Steel Fibres on Initially Uncracked Specimens

The inclusion of steel fibres generally increased the shear load at the formation of the first diagonal tension cracks. See Table 5.3. This is to be expected since it is a well established fact that inclusion of steel fibres in concrete increases the tensile strength of the resulting composite. With the formation of these cracks, further shear caused rotation of the inclined struts between the cracks. But the fibres bridging the cracks and the higher deformation stiffness of fibre concrete reduced the magnitude of this rotation, a fact borne out by the generally lesser vertical and lateral displacements of fibre concrete specimens over those of corresponding plain concrete specimens at the same stress level. See Table 5.4. The net effect of all these was an increase in the ultimate shear transfer strength.

Table 5.4 Influence of Steel Fibres on the Deformation (in mm) of Initially Uncracked Specimens

		Shear Stress Level, N/mm^2				
		5.5	6.0	6.5	7.0	7.5
2SN-2 (0%)	Vert.Displ.	0.14	0.19	0.27	0.39	-
	Lat.Displ.	0.15	0.22	0.31	0.41	-
3SN-2 (o.4%)	Vert. Displ.	0.15	0.18	0.22	0.26	0.36
	Lat.Displ.	0.14	0.18	0.24	0.28	0.39
4SN-2 (o.8%)	Vert. Displ.	0.19	0.22	0.29	0.31	0.45
	Lat.Displ.	0.13	0.17	0.23	0.27	0.39
2SL-2 (o%)	Vert.Displ.	0.18	0.22	0.30	-	-
	Lat. Displ	0.20	0.25	0.35	-	-
3SL-2 (1.0%)	Vert. Displ.	0.13	0.17	0.20	0.24	0.27
	Lat.Displ.	0.05	0.11	0.13	0.16	0.18

5.4.1.4 Initially Cracked Gravel Concrete

The test results of all the initially cracked gravel concrete specimens are summarized in Table 5.3. The inclusion of 0.4 to 0.8% by volume of crimped fibres increased the ultimate shear transfer strength by 53.3 to 101.8%

Fig. 5.18(b) shows the relationship between the ultimate shear stress v_u and the total shear reinforcement parameter $(rf_y + \sigma_{cu})$ for both plain and fibre concrete specimens. Some of the results of Mattock (89) were also included. Linear regression analysis for both sets of results gave:

For initially cracked plain gravel concrete,

$$v_u = 1.82 + 0.91\ (rf_y + \sigma_{cu}) \qquad (5.12)$$

$$\text{for } (rf_y + \sigma_{cu}) \geq 0.5\ N/mm^2$$

For initially cracked fibre reinforced gravel concrete,

$$v_u = 2.78 + 1.22\ (rf_y + \sigma_{cu}) \qquad (5.13)$$

for $(rf_y + \sigma_{cu}) \geq 0.5\ N/mm^2$

Both equations (5.12) and (5.13) have some theoretical basis. They are modified forms of the famous Coulomb's Criterion (Eqn. (5.8)) which is applicable to a sliding type of failure. The total shear reinforcement parameter $(rf_y + \sigma_{cu})$ can be considered as the normal stress acting at the shear plane.

5.4.1.5 Initially cracked Lytag-sand Concrete

The test results of all initially cracked Lytag-sand concrete specimens are shown in Table 5.3. The addition of 1.0% by volume of crimped fibres caused an increase in the ultimate shear strength of 54.5 to 83.7%.

The relationships between the ultimate shear strength and the total shear reinforcement parameter for both plain and fibre concrete specimens are shown in Fig. 5.19(b). These can be approximated as :

For initially cracked plain Lytag-sand concrete

$$v_u = 1.80 + 0.74\ (rf_y + \sigma_{cu}) \qquad (5.14)$$

for $(rf_y + \sigma_{cu}) \geq 1.5 N/mm^2$

For initially cracked fibre Lytag-sand concrete,

$$v_u = 2.20 + 1.01\ (rf_y + \sigma_{cu}) \qquad (5.15)$$

for $(rf_y + \sigma_{cu}) \geq 1.5\ N/mm^2$

As for the previous case, equations (5.14) and (5.15) have some theoretical basis. Equations (5.12) and (5.14) revealed that the difference in the ultimate shear strength of

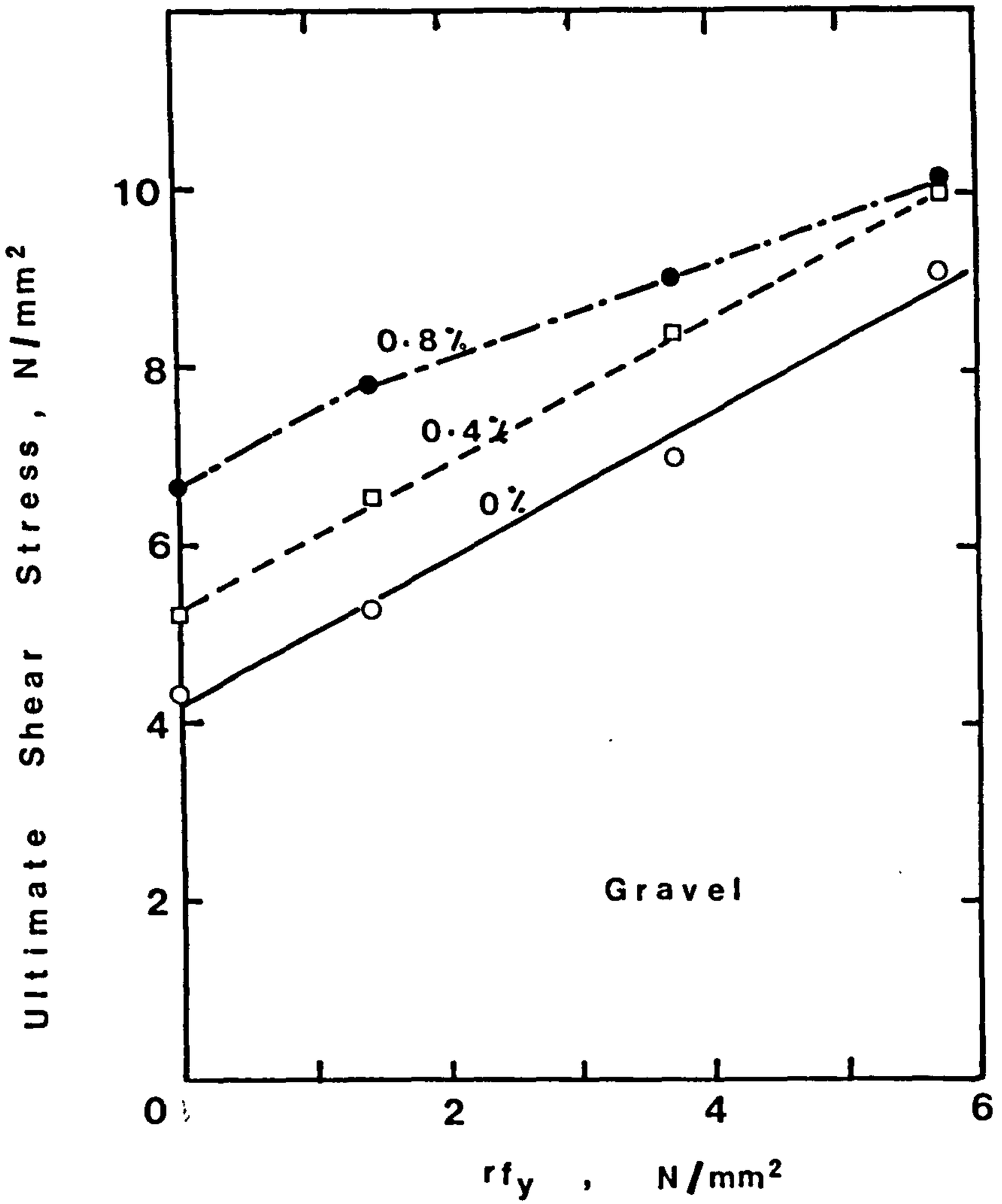

(a)

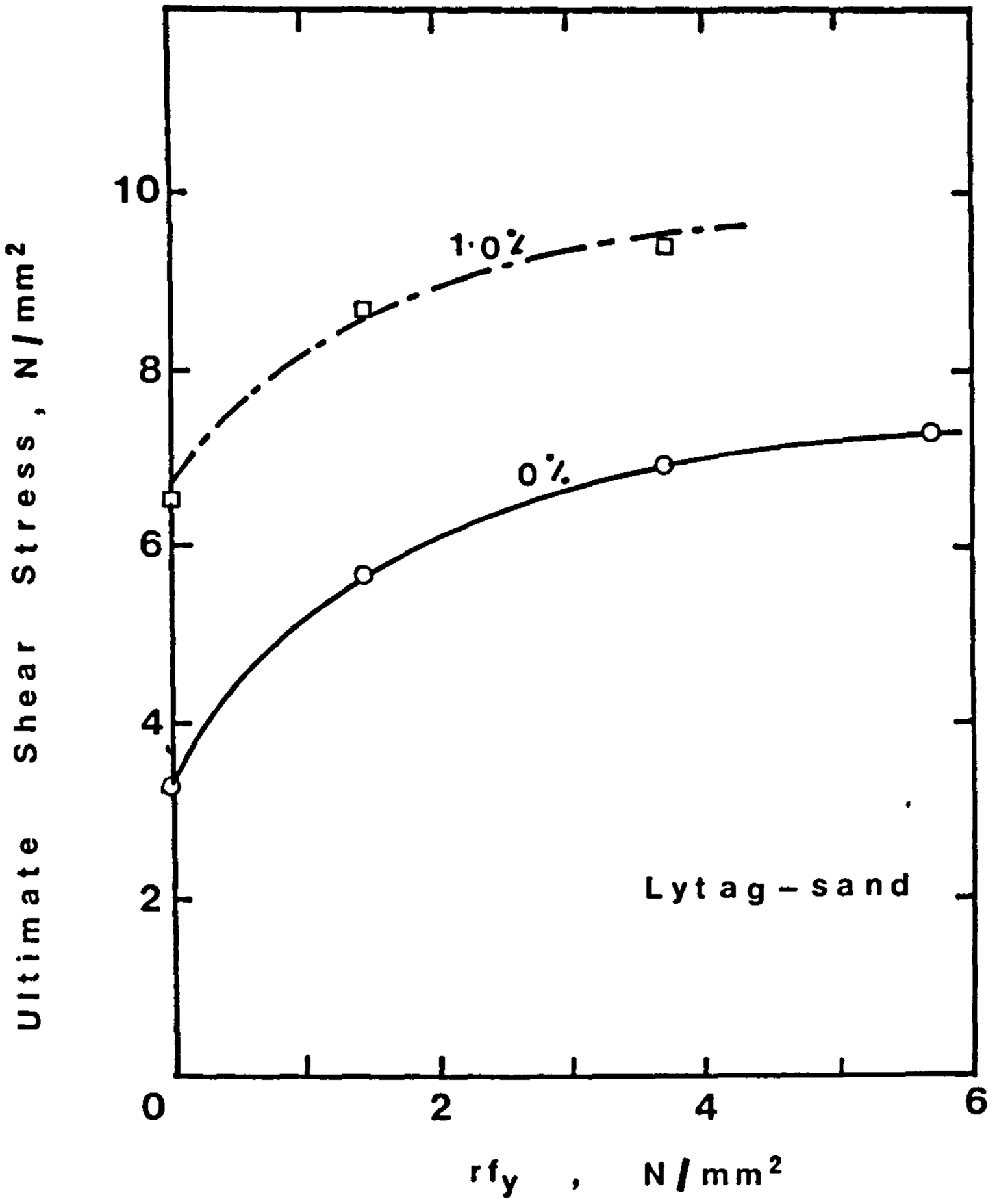

(b)

Fig. 5·17 Influence of Steel Fibres on the Ultimate Strength of Initially Uncracked Specimens

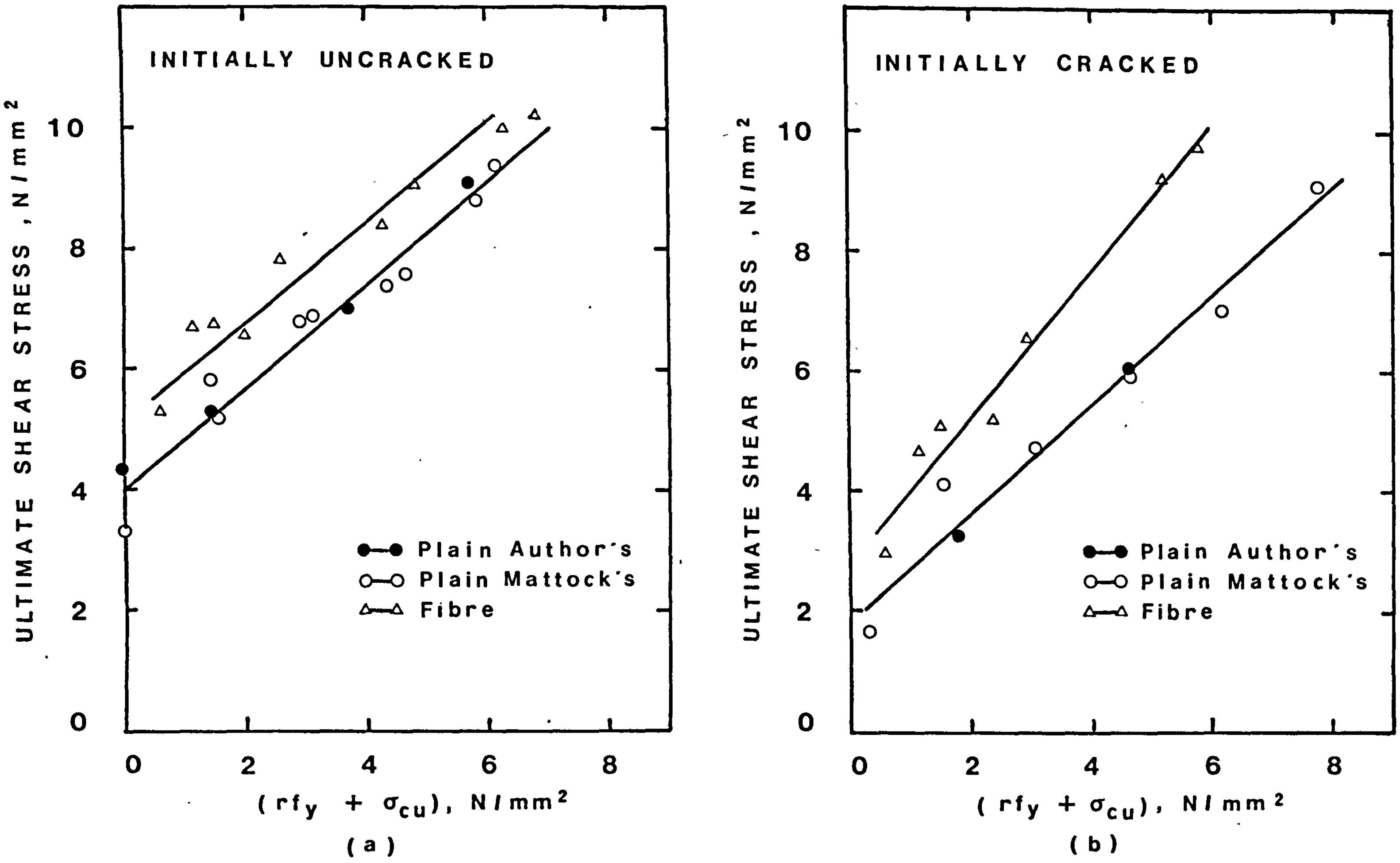

FIG 5·18 SHEAR TRANSFER STRENGTH OF GRAVEL CONCRETE

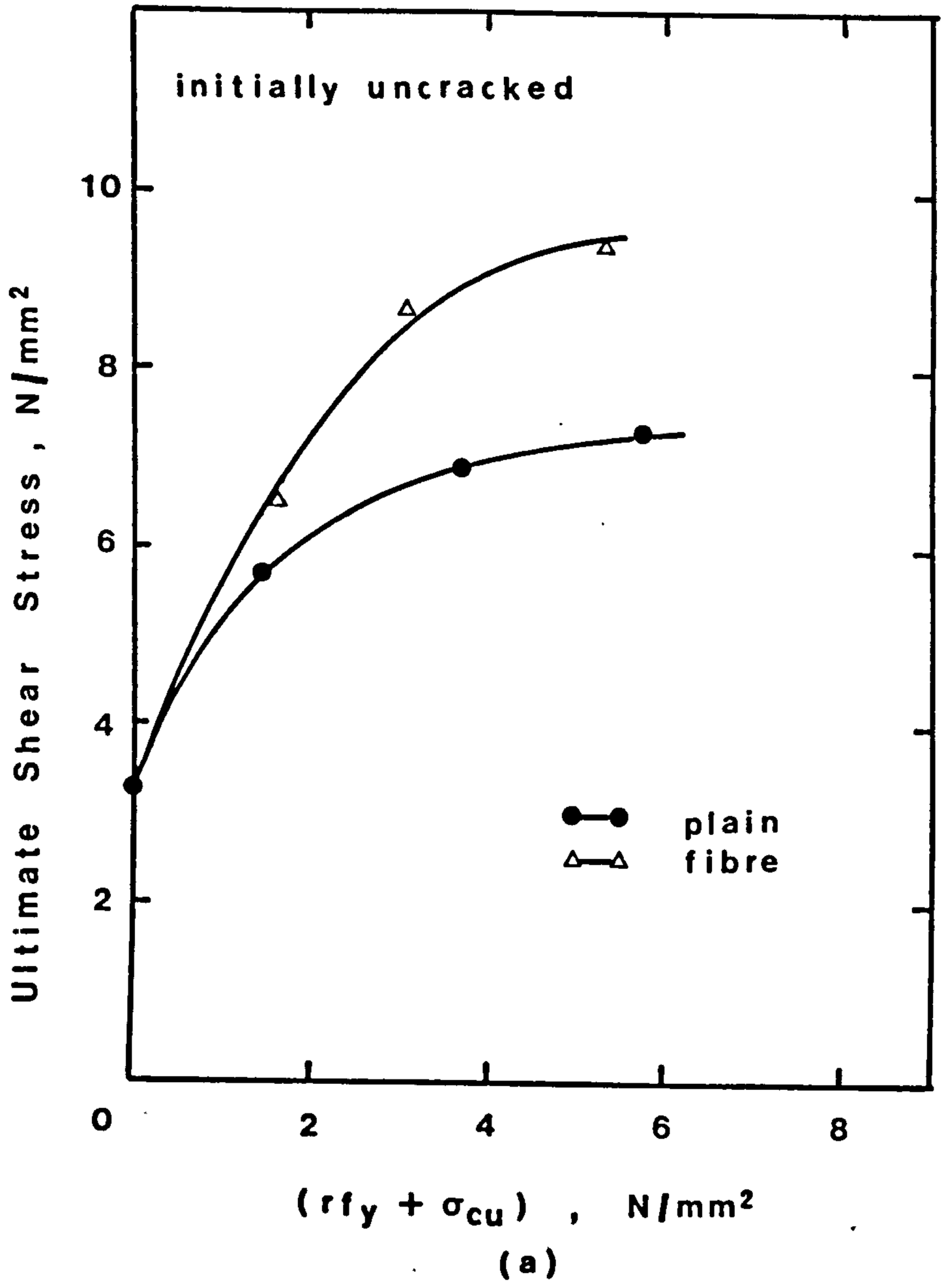

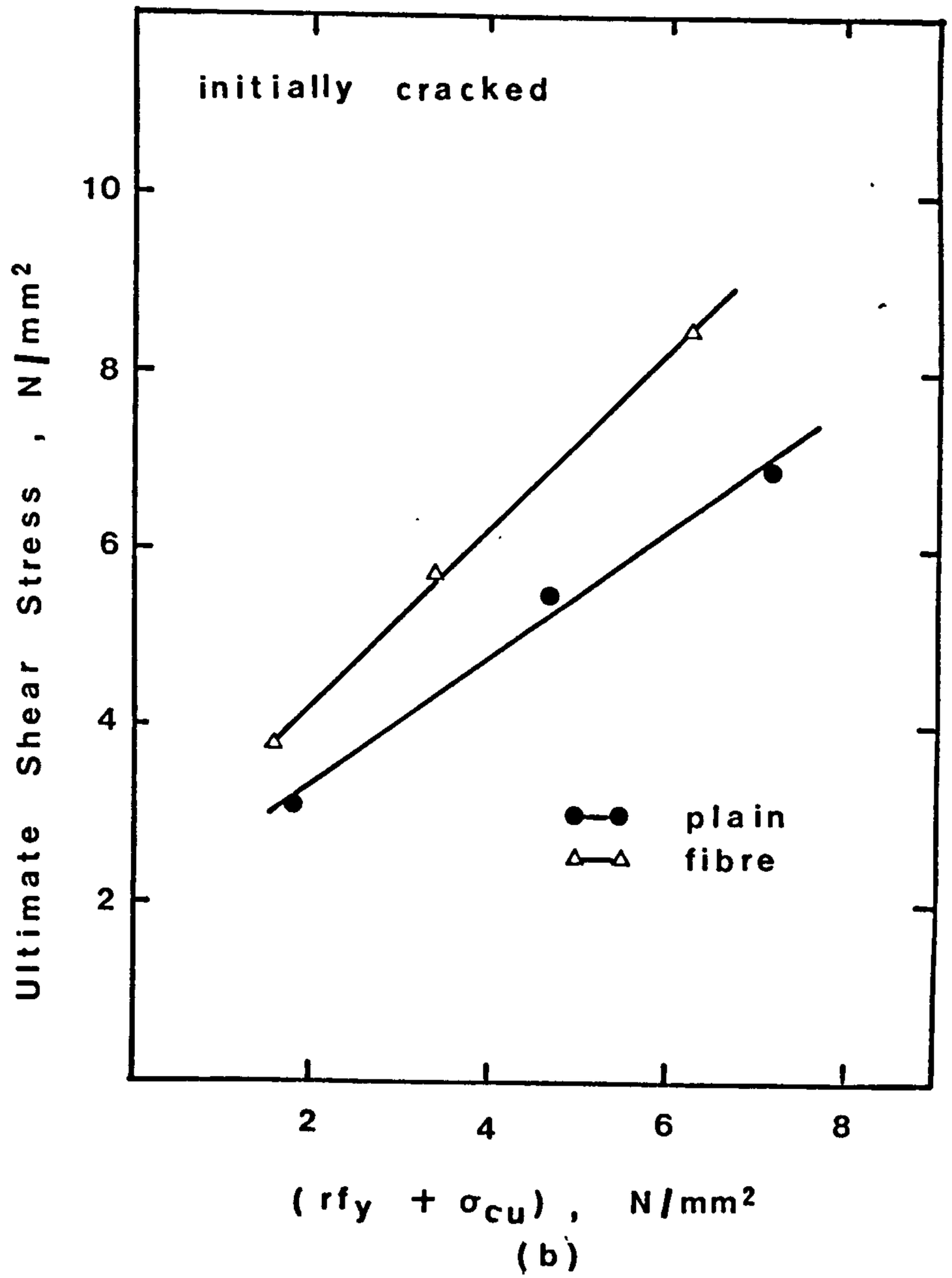

Fig.5·19 Shear Transfer Strength of Lytag-sand Concrete

gravel and Lytag-sand concrete specimens lies mainly in the coefficient of friction. Gravel concrete has a high coefficient of friction and this is also self-evident from Plate 5.1.

5.4.1.6 Possible Explanation of the Influence of Steel Fibres on Initially Cracked Specimens

The steel fibres bridging the preformed crack served two major purposes. Firstly, they provided clamping forces between the crack faces, which in turn developed shear resistance. Secondly, their dispersed existence enhanced the roughness of the crack faces. This can also be deduced from equations (5.12) to (5.15). Fibre concrete specimens had higher coefficients of friction than those of their plain concrete counterparts.

5.4.2 Load-Deformation Behaviour

5.4.2.1 Initially Uncracked Concrete

The influence of steel fibres on the load-displacement behaviour of initially uncracked concrete can be seen from the self explanatory graphs of Figs. 5.20 through 5.22. Fig. 20 shows the effect of the volume percentages of fibres on gravel concrete specimens not reinforced with conventional shear reinforcement (i.e., $rf_y = 0$) while Fig. 5.21 shows this effect on those reinforced with two R6 stirrups ($rf_y = 1.44\ N/mm^2$). Fig. 5.22 shows the influence of steel fibres on Lytag-sand concrete specimens not reinforced with conventional stirrups and those reinforced with two Y8 stirrups ($rf_y = 3.69\ N/mm^2$).

As can be observed from these figures and as mentioned in section 5.4.1.3, the inclusion of steel fibres generally decreased both the vertical and lateral displacements after the formation of diagonal tension cracks.

5.4.2.2 Initially Cracked Concrete

The self explanatory graphs of Figs. 5.23 through 5.25 show how steel fibres influence the load-deformation behaviour. Fig. 5.23 and Fig. 5.24 show the effect of the volume percentages of fibres on gravel concrete specimens not reinforced with conventional stirrups and those with two Y8 conventional stirrups (rf_y = 4.20 N/mm^2) respectively. Fig. 5.25 shows the influence of steel fibres on Lytag-sand concrete specimens. It can be seen that:

(1) The inclusion of steel fibres generally did not affect the initial slope of the shear stress-vertical (shear) displacement curves (or initial stiffness of shear transfer) for initial crack widths of about the same magnitude. Larger initial crack width resulted in a lower initial stiffness for both plain and fibre concrete.

(2) The inclusion of steel fibres increased the residual shear transfer strength and higher percentage by volume of fibres generally resulted in higher residual strength. Table 5.5 summarizes the residual strength of some of the specimens at a shear displacement of 3.0 mm.

(3) The inclusion of steel fibres prevented excessive opening of the preformed crack at failure.

5.4.3 Stiffness of Shear Transfer

It can be observed from Figs. 5.23 through 5.25 that the stiffness of shear transfer decreased with increasing shear load and that this decrease was a result of increasing lateral displacement (crack width). This suggests a relationship between the stiffness of shear transfer and the crack widths, an observation reported by other investigators (95,96). Accordingly,

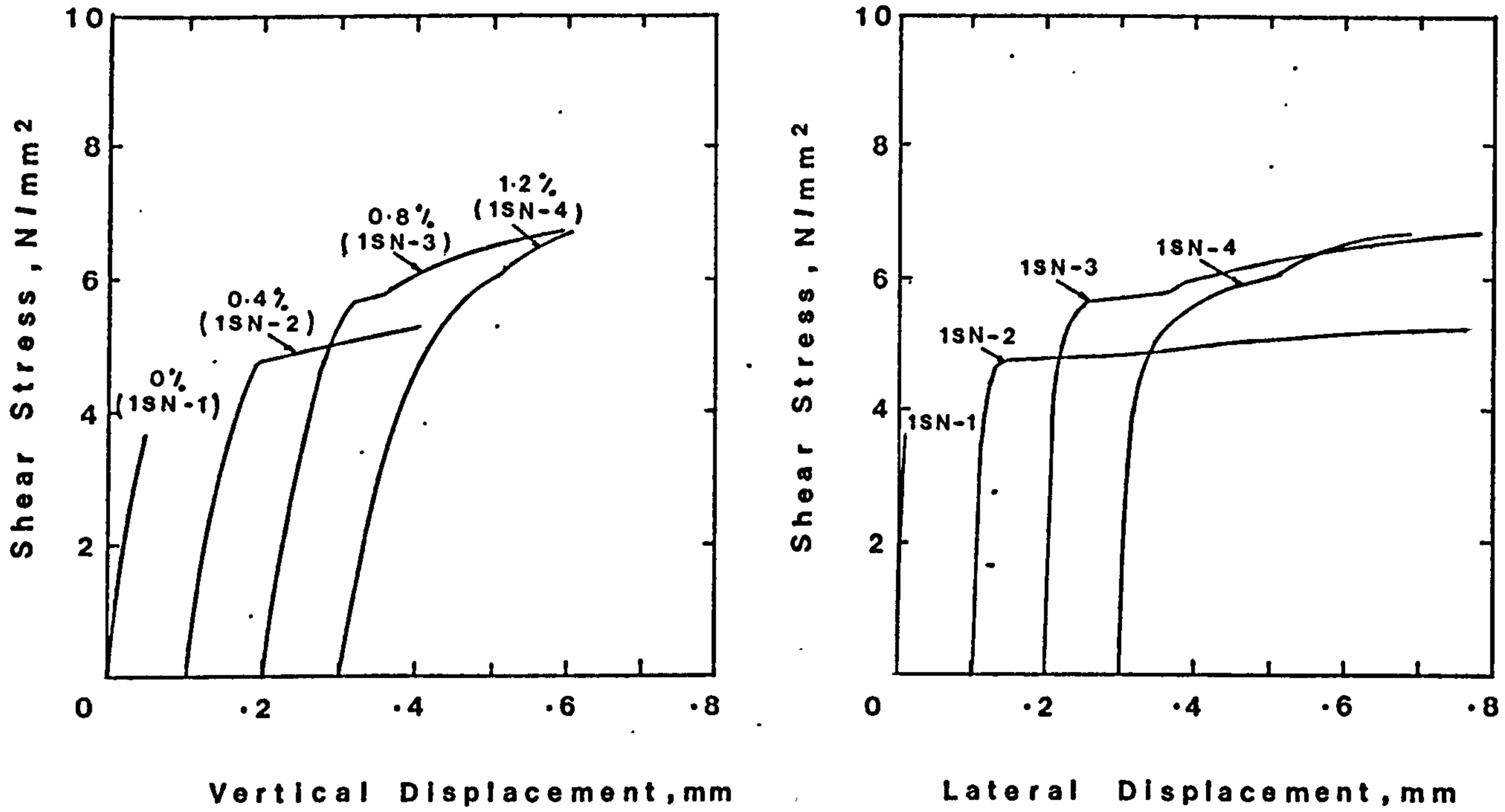

Fig. 5·20 Influence of Fibres on Load Deformation Behaviour of Initially Uncracked Gravel Concrete Specimens with $rf_y = 0\ N/mm^2$

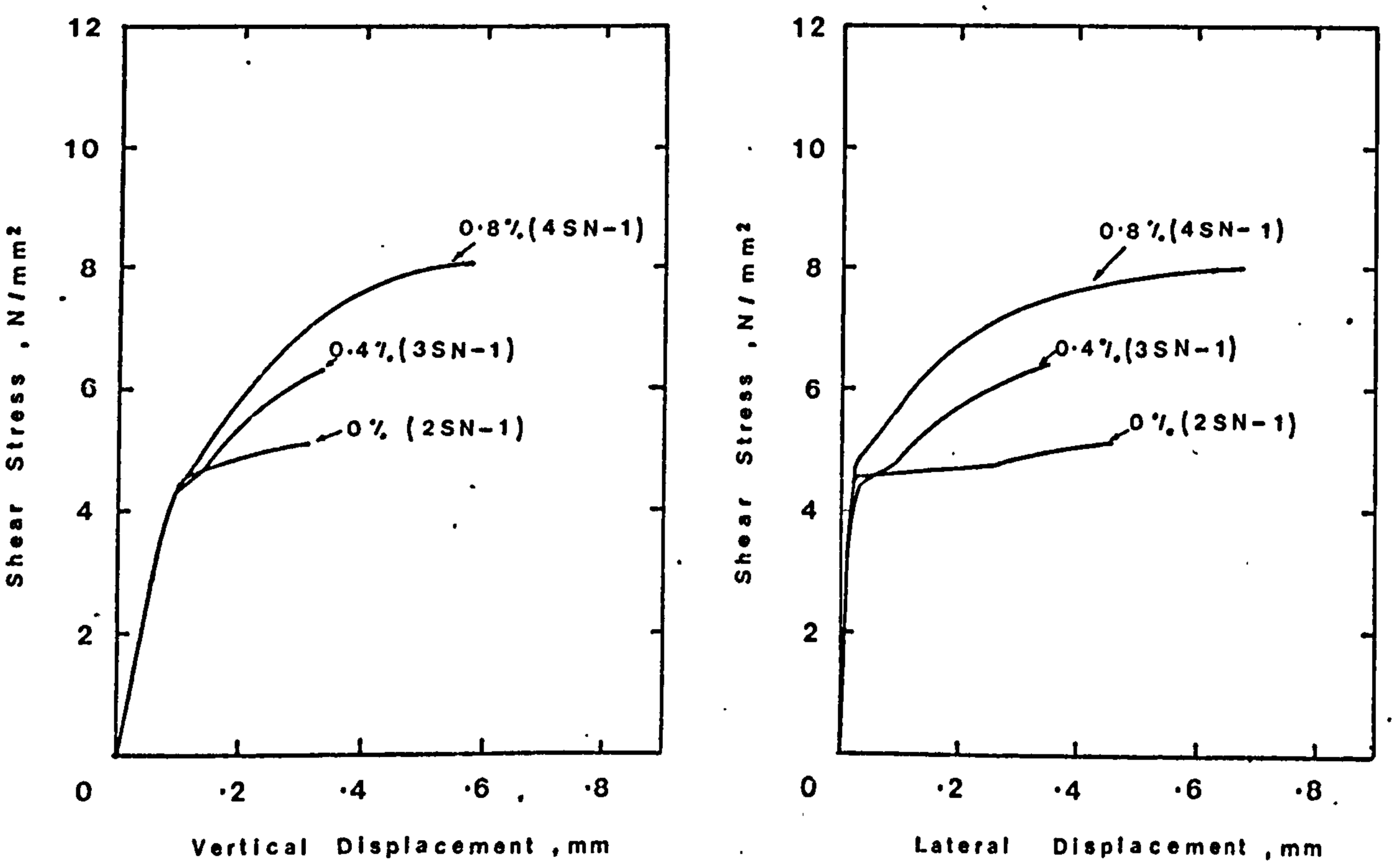

Fig. 5·21 Influence of Fibres on the Load Deformation Behaviour of Initially Uncracked Gravel Concrete Specimens with $rf_y = 1·44\ N/mm^2$

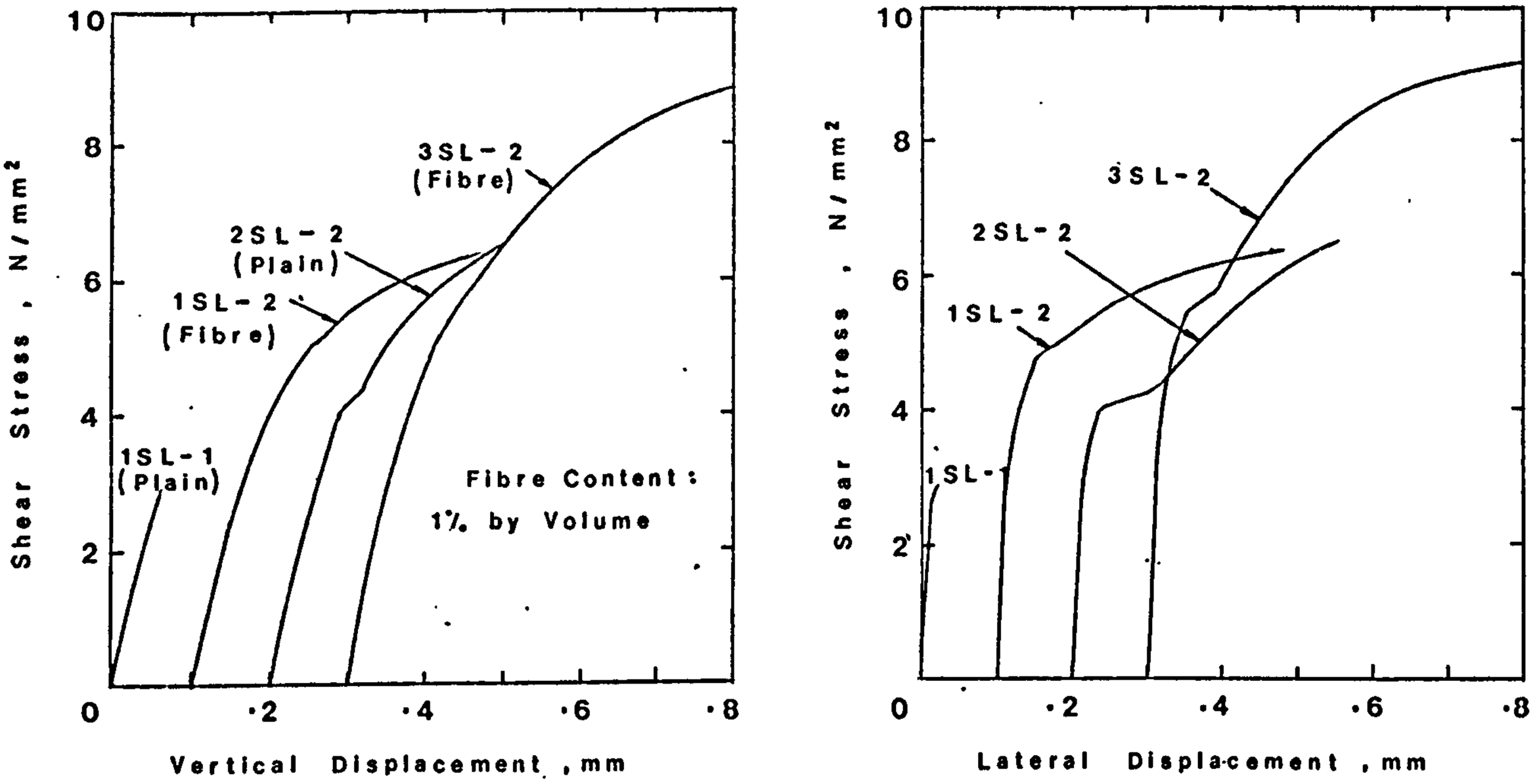

Fig. 5·22 Influence of Fibres on Load Deformation Behaviour of Initially Uncracked Lytag-Sand Concrete Specimens

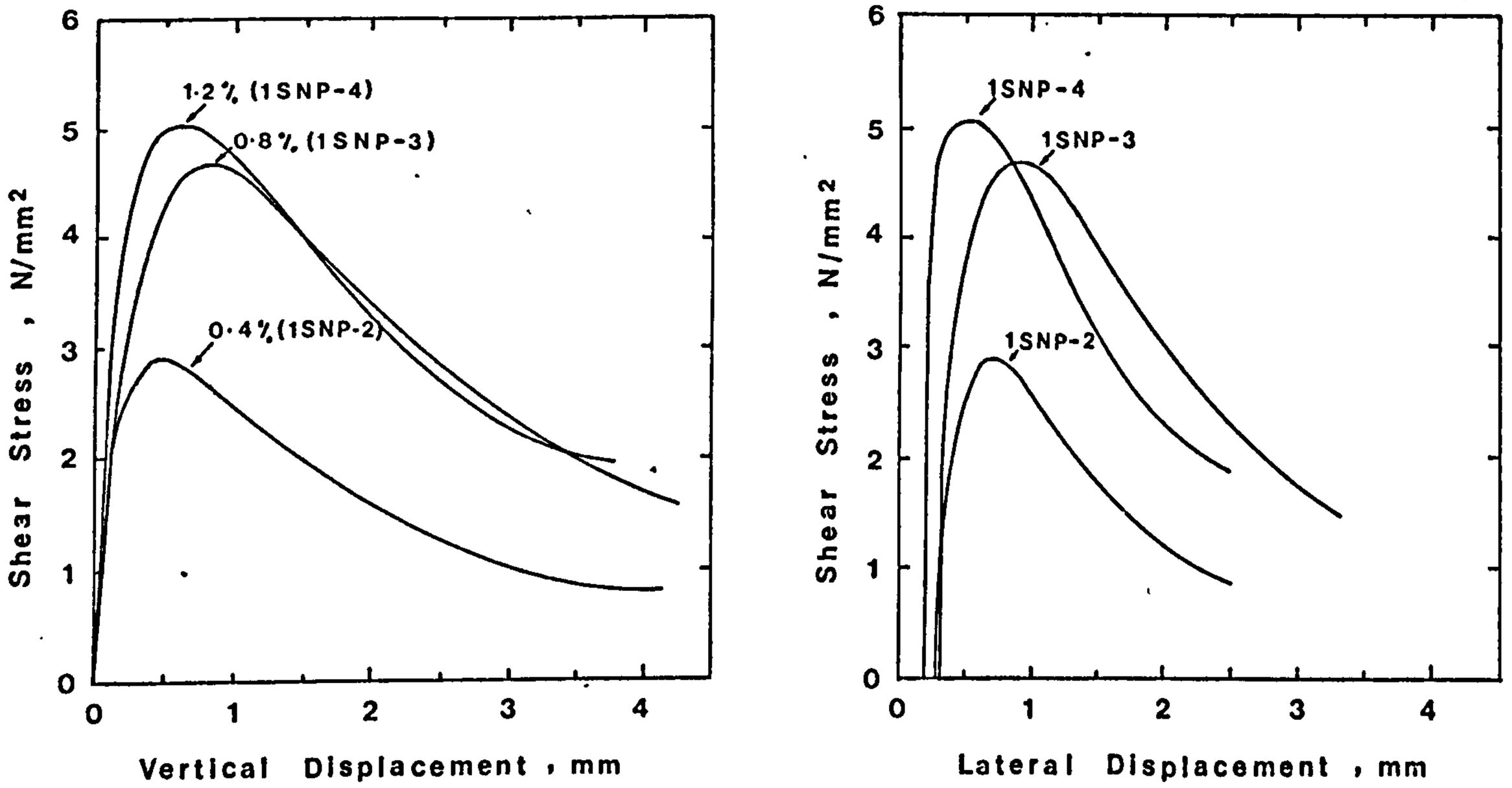

Fig. 5·23 Influence of Fibres on Load Deformation Behaviour of Initially Cracked Gravel Concrete Specimens With rf_y = 0 N/mm²

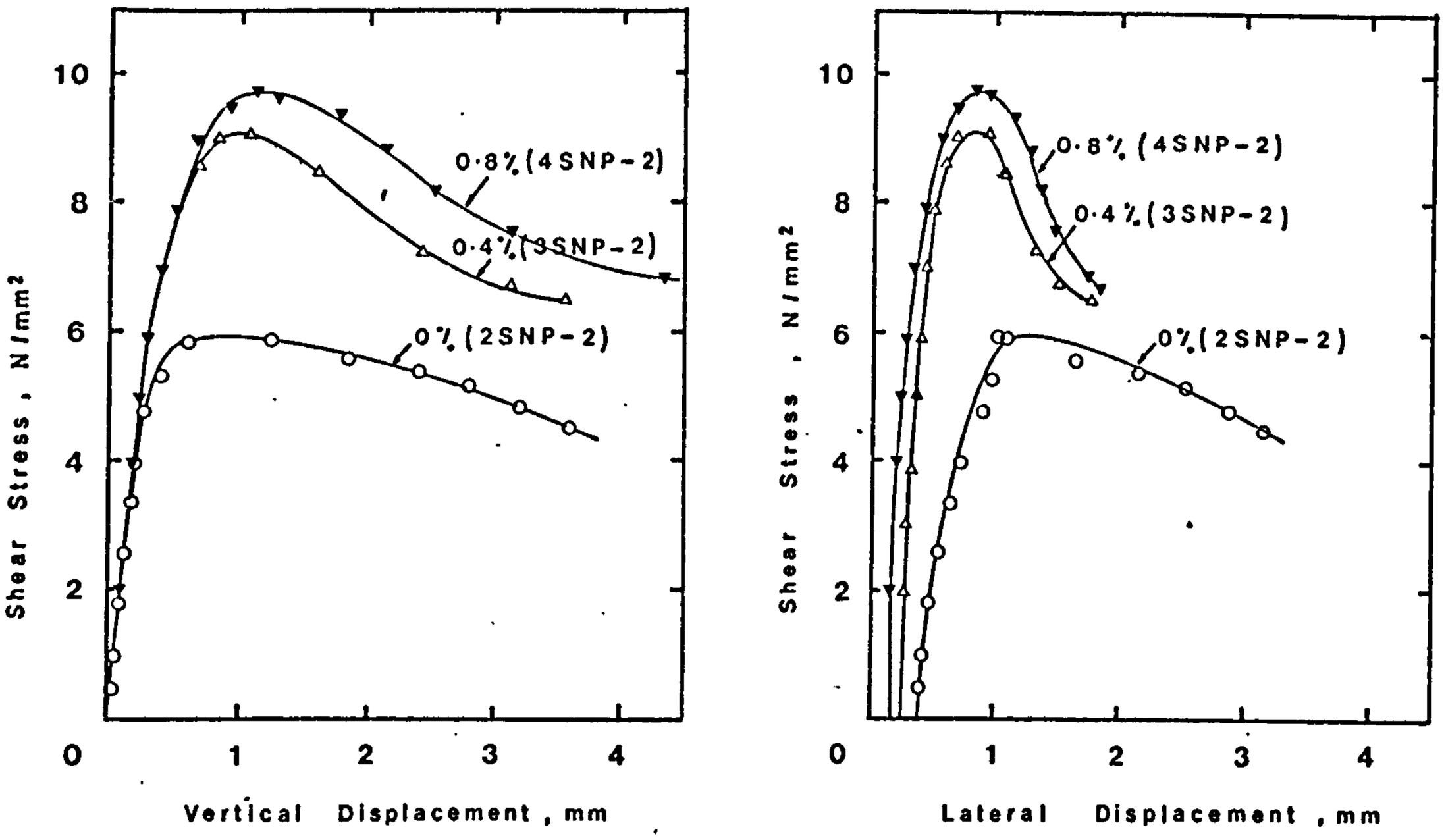

Fig. 5·24 Influence of Fibres on Load Deformation Behaviour of Initially Cracked Gravel Concrete Specimens with $rf_y = 4{\cdot}20$ N/mm²

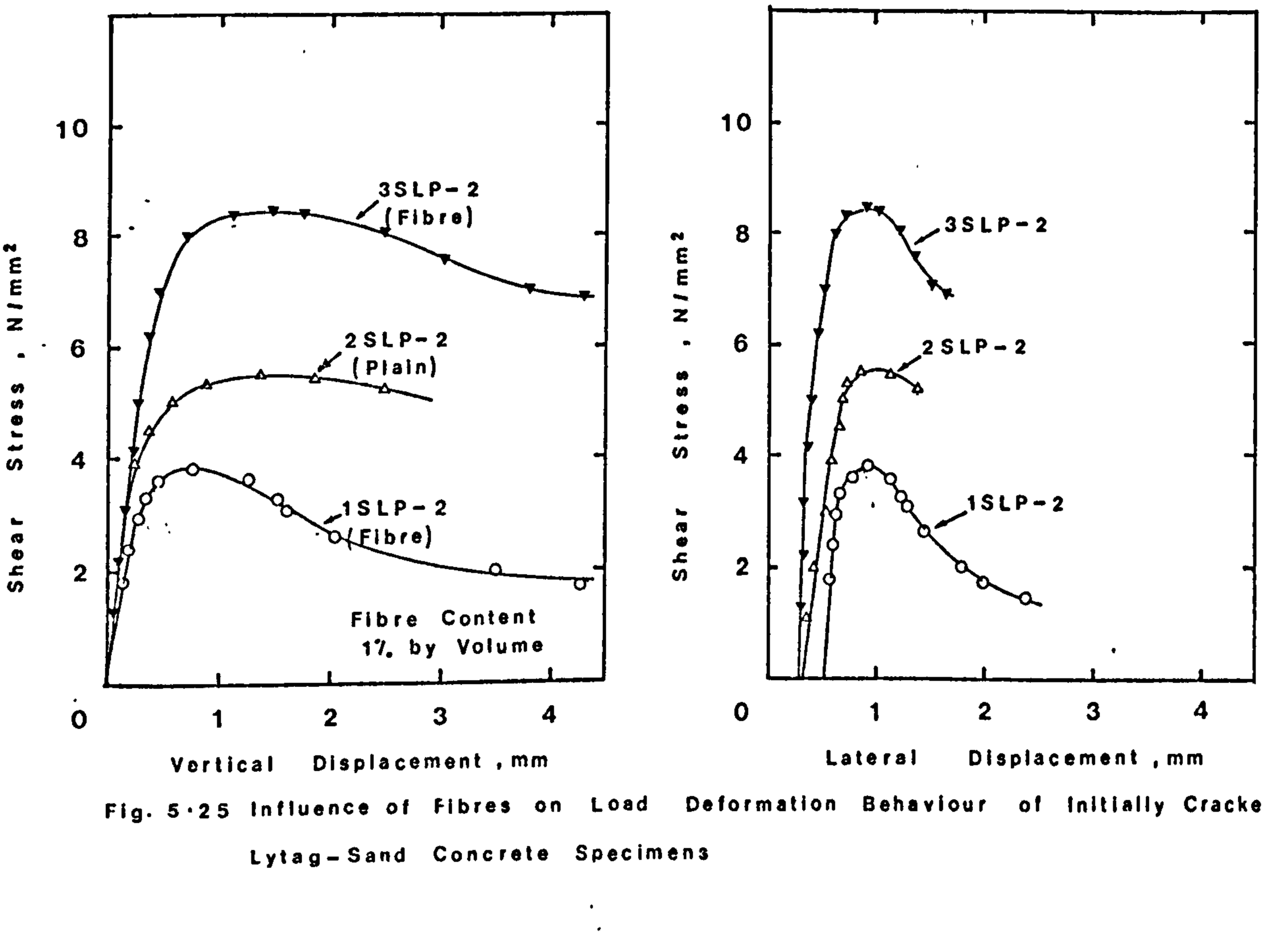

Fig. 5·25 Influence of Fibres on Load Deformation Behaviour of Initially Cracked Lytag-Sand Concrete Specimens

Table 5.5 Residual Strength of Initially Cracked Specimens at a Shear Displacement of 3.0mm.

Specimen No.	rf_y N/mm^2	Fibre Volume %	Residual Strength N/mm^2
2SNP-2	4.20	0	5.0
3SNP-2	4.20	0.4	6.7
4SNP-2	4.20	0.8	7.7
1SNP-2	-	0.4	1.1
1SNP-3	-	0.8	2.2
1SNP-4	-	1.2	2.4
1SLP-2	-	1.0	2.1
2SLP-2	4.20	0	5.0
3SLP-2	4.20	1.0	7.6

the secant modulus of the shear stress-vertical displacement curve for each of the initially cracked specimens was evaluated at increasing shear stress level and the corresponding crack width noted. Secant modulus was used instead of tangential stiffness for its ease and accuracy of evaluation and its convenience in representing the stiffness of the falling part of the load-displacement curve. The results for gravel concrete are shown in Fig. 5.26 while those for Lytag-sand concrete are shown in Fig. 5.27.

5.4.3.1 Gravel Concrete

From Fig. 5.26, it can be seen that at higher crack widths, the shear transfer stiffness of fibre concrete is generally slightly higher than that of plain concrete. Neglecting this, the shear transfer stiffness-crack width relationship for both plain and fibre concrete may be adequately represented by the equation:

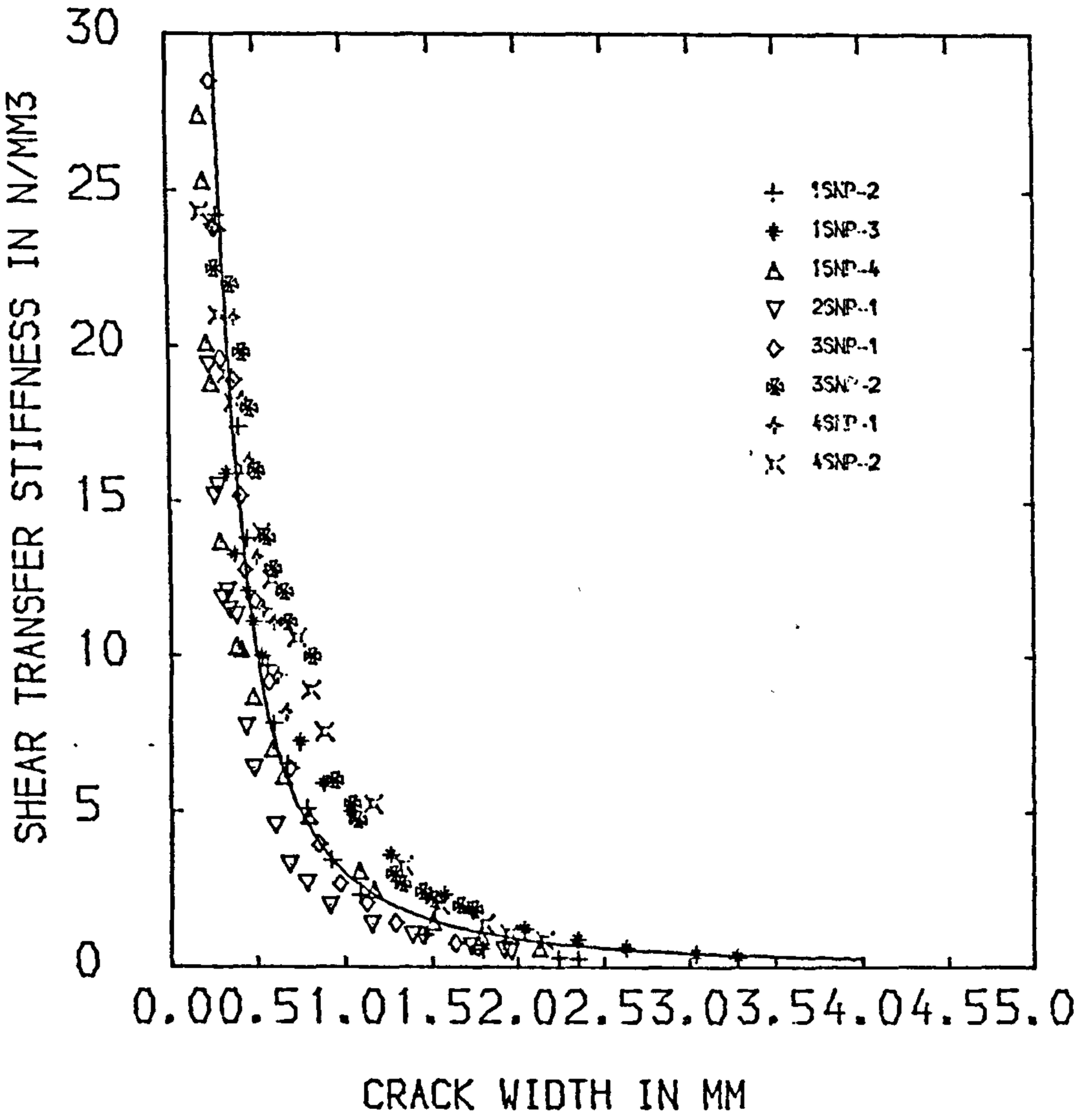

FIG.5.26 SHEAR TRANSFER STIFFNESS-CRACK WIDTH RELATIONSHIP OF GRAVEL CONCRETE

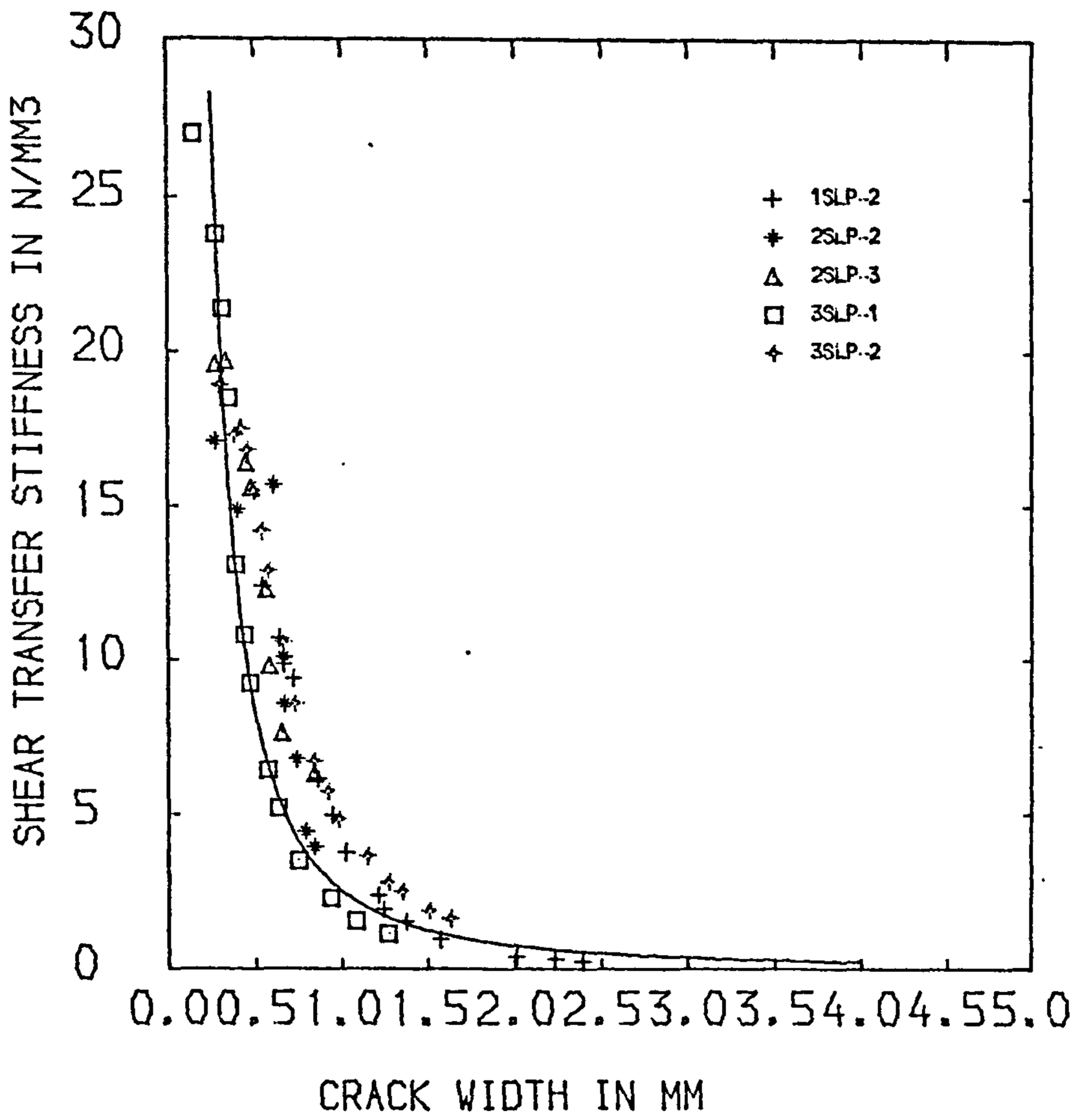

FIG.5.27 SHEAR TRANSFER STIFFNESS-CRACK WIDTH RELATIONSHIP OF LYTAG-SAND CONCRETE

$$G_s = 3.0 * (\frac{1}{w})^{1.75} \quad (5.16)$$

where G_s = shear transfer stiffness in N/mm^3

w = crack width in mm

5.4.3.2 Lytag-sand Concrete

The shear transfer stiffness-crack width relationship may be adequately represented by the equation

$$G_s = 2.5 (\frac{1}{w})^{1.75} \quad (5.17)$$

where G_s = shear trasnfer stiffness in N/mm^3

w = crack width in mm.

Comparison of equations (5.15) and (5.16) suggests that the rate of decrease of shear transfer with crack width in Lytag-sand concrete is faster than that in gravel concrete.

5.5 Conclusions

1. The shear transfer strength of initially cracked Lytag-sand concrete was generally lower than that of gravel concrete. This discrepancy was due to the higher degree of roughness in the fracture surface of gravel concrete.

2. In initially uncracked concrete the inclusion of crimped steel fibres reduced the amount of the rotation of the inclined struts after the formation of the diagonal tension cracks. This generally resulted in higher ultimate shear transfer strength.

3. In initially cracked concrete, steel fibres provided clamping forces across the crack faces and their random distribution across the shear plane seemed to enhance the roughness of the faces of the crack.

4. The inclusion of steel fibres seemed to raise the threshold of the ultimate shear transfer strength in Lytag-sand concrete. This effect was less apparent in gravel concrete. The inclusion of steel fibres raised the threshold of Lytag-sand concrete to a value approaching that of gravel concrete.

5. The ultimate shear transfer strength of both initially cracked plain and fibre concrete may be expressed on the basis of Coulomb's Criterion as:

$$v_u = c + \mu (rf_y + \sigma_{cu}) \qquad (5.18)$$

where v_u = ultimate shear transfer strength

c = constant depending on types of concrete

μ = coefficient of friction depending on types of concrete

rf_y = conventional shear reinforcement (stirrup) parameter

and σ_{cu} = post-cracking tensile strength of fibre concrete ($\sigma_{cu} = 0$ for plain concrete)

Values of c and μ for the various types of concrete used in this investion are tabulated in Table 5.6 below

Table 5.6 Values of c and μ of the Various Types of Concrete Used in this Investigation

Concrete Type	c N/mm^2	μ	Valid for $(rf_y + \sigma_{cu})$ >
plain gravel	1.82	0.91	0.5 N/mm^2
fibre gravel	2.78	1.22	0.5 N/mm^2
plain Lytag-sand	1.80	0.74	1.5 N/mm^2
fibre Lytag-sand	2.20	1.01	1.5 N/mm^2

6. The addition of steel fibres did not significantly affect the initial stiffness of shear transfer. Nevertheless, a higher initial crack width resulted in a lower initial

shear transfer stiffness in both plain and fibre concrete.

7. The use of steel fibres increased the residual shear transfer and a higher percentage by volume of fibres generally resulted in a higher residual strength.

8. Shear transfer stiffness may be adequately represented by the following expressions:

For the plain and fibre gravel concrete used in this investigation,

$$G_s = 3.0 \left(\frac{1}{w}\right)^{1.75}$$

and for the plain and fibre Lytag-sand concrete,

$$G_s = 2.5 \left(\frac{1}{w}\right)^{1.75}$$

where G_s = shear transfer stiffness in N/mm^3

and w = crack width in mm.

CHAPTER SIX

SHEAR RESISTANCE OF FIBRE CONCRETE BEAMS

6.1 Introduction

Recent investigations by several researchers have indicated favourably the potential of steel fibres as shear reinforcement in reinforced concrete beams. These investigations were carried out using normal weight concrete or mortar. As far as the author is aware, no reported investigation has been carried out using lightweight concrete. Because of its low tensile strength and modulus of of elasticity, the addition of a relatively high modulus fibre, such as steel, may bring about a more pronounced effect in flexure and shear than for normal weight concrete. The investigation reported in Chapter Five suggests that it is more beneficial to include steel fibres in lighweight concrete than in normal weight concrete insofar as the shear transfer strength is concerned.

The scope of the study reported in this Chapter was to investigate the effect of fibre reinforcement on the strength and deformation characteristics of lightweight reinforced concrete beams. This study forms a part of a wider investigation being carried out at Sheffield University into the use of steel fibres as shear reinforcement in lightweight reinforced and prestressed concrete members. Tests were carried out on beams with thin web as it is in such beams that conventional shear reinforcement will be difficult to place. Furthermore, a thin section ensures a more efficient fibre orientation to arrest the shear cracks.

The test programme is described in detail and then the test results are presented and discussed. The plain concrete beams are analysed using the methods given in several structural codes. A simple method based on the Standard Method of CEB-FIP

Model Code (5) is proposed to analyse the ultimate shear strength of fibre concrete beams. The proposed method is then applied to the fibre concrete beams of this investigation and to those of other investigations.

6.2 Experimental Programme

6.2.1 Details of Beams

A series of eighteen simply supported beams was tested under a symmetrical four point loading system. The general details of the test beams are shown in Fig. 6.1. Each beam had a compression flange of 295 x 52 mm, a tension flange of 115 x 87 mm and a thin web of 55 mm thickness. The smaller tension flange was provided to accommodate the longitudinal reinforcement. All beams had an effective depth of 265 mm. The beams were detailed to satisfy CP110 (68) requirements.

6.2.2 Parameters Investigated

Three major parameters which significantly affect the shear strength of reinforced concrete beams were considered:

(1) Amount of shear reinforcement in the form of steel fibres

(2) Amount of longitudinal tension reinforcement ρw

(3) Shear span/effective depth ratio $\frac{a_v}{d}$ - 2.0, 3.43 and 4.91.

6.2.3 Steel Fibres

The fibres used were 0.5 x 50 mm crimped steel fibres. The properties of these fibres are given in section 3.2.6. Percentages by volume of 0 and 1.0 were used.

6.2.4 Longitudinal Tension Reinforcement

These were in the form of 2Y12, 2Y16 and 2Y20 deformed bars (Tor Bar) giving steel values of 1.55, 2.76 and 4.31%

respectively. The properties and typical stress-strain curves of these bars are given in Table 3.2 and Fig. 3.2 respectively.

6.2.5 Concrete

Lytag-sand concrete was used for all the beams. The mix proportion is given in section 3.3.2

6.2.6 Manufacturing of Beams

Each beam was cast in a mould made with steel and wood. The formers and the base of the flange were fabricated out of wooden planks and the rest of the mould was fabricated out of standard steel channel and angle sections. The wooden planks were well varnished on all sides to ensure watertightness.

Because of the shape of the beam, the reinforcing cage had to be pushed into the mould from one of its ends. The concrete cover of 35 mm to centre of longitudinal bars was obtained by welding chairs to the reinforcement. The mould was oiled lightly beforehand.

Three 150 mm cubes, three 100 x 100 x 300 prisms and three 100 x 100 x 500 prisms were cast as control specimens for each beam.

The concrete was mixed in three batches using a 0.1 m^3 capacity horizontal pan-type mixer. The mixing procedure of each batch was as described in section 3.3.3. For plain concrete after mixing, each batch of the concrete was poured in a uniform layer into the mould and was compacted well by using a 25 mm diameter internal poker vibrator. For fibre concrete, a slightly different procedure of compaction was followed. After pouring the first batch of concrete into the mould, the fibre concrete was compacted well by using a vibrating table (3.0 x 1.20 m). This was to ensure proper compaction and proper fibre distribution

around the main steel. Subsequent batches of concrete were compacted well using the 25 mm diameter internal poker vibrator. The moulds of the control specimens were filled with concrete from the first and third batches and the concrete was compacted well using the internal poker vibrator. The surface of each of the specimens was levelled and finished using a steel trowel. The beam and control specimens were then covered with polythene sheets.

The specimens were demoulded three days after casting and stored in the uncontrolled laboratory atmosphere until testing. Testing of the specimens was carried out at 27 to 29 days after casting.

6.2.7 Test Measurements and Instrumentation

6.2.7.1 Deflection

Vertical deflection was measured at the centre of the span using a linear variable displacement transducer with a sensitivity of $\pm$ 0.003 mm and a 25 mm travel. The output voltage of the transducer was monitored by a portable 30 channel datalogger.

6.2.7.2 Concrete Strains

Concrete strains were measured using a 100 mm Demec gauge. For all the beams, concrete strains were measured at the section adjacent to each of the concentrated loads and at the mid section of the beams. The layout of the Demec points is shown in Fig. 6.2

In addition, for the beams tested at a shear/span effective depth ratio of 4.91, longitudinal concrete strains were also measured along the top surface at 300 cm centre to centre to obtain the top fibre strain profile.

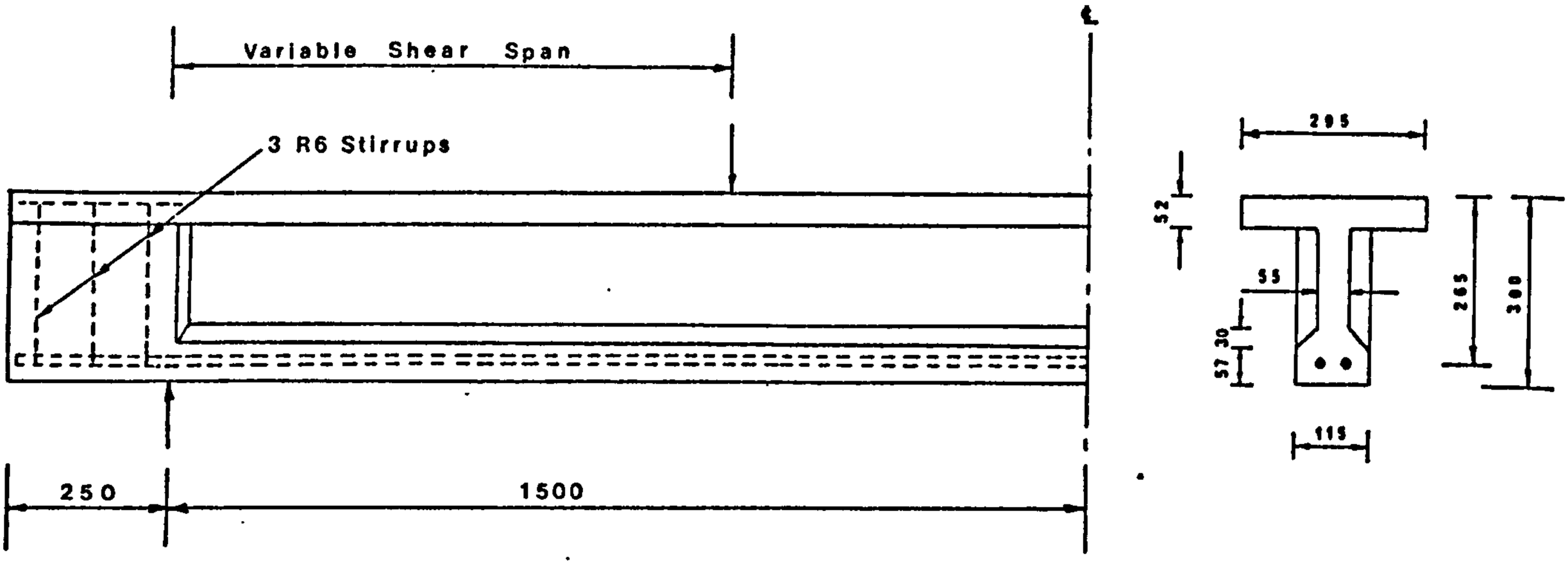

Note: All Dimensions Are In mm

Fig. 6·1 Longitudinal And Cross Sections Of Beams

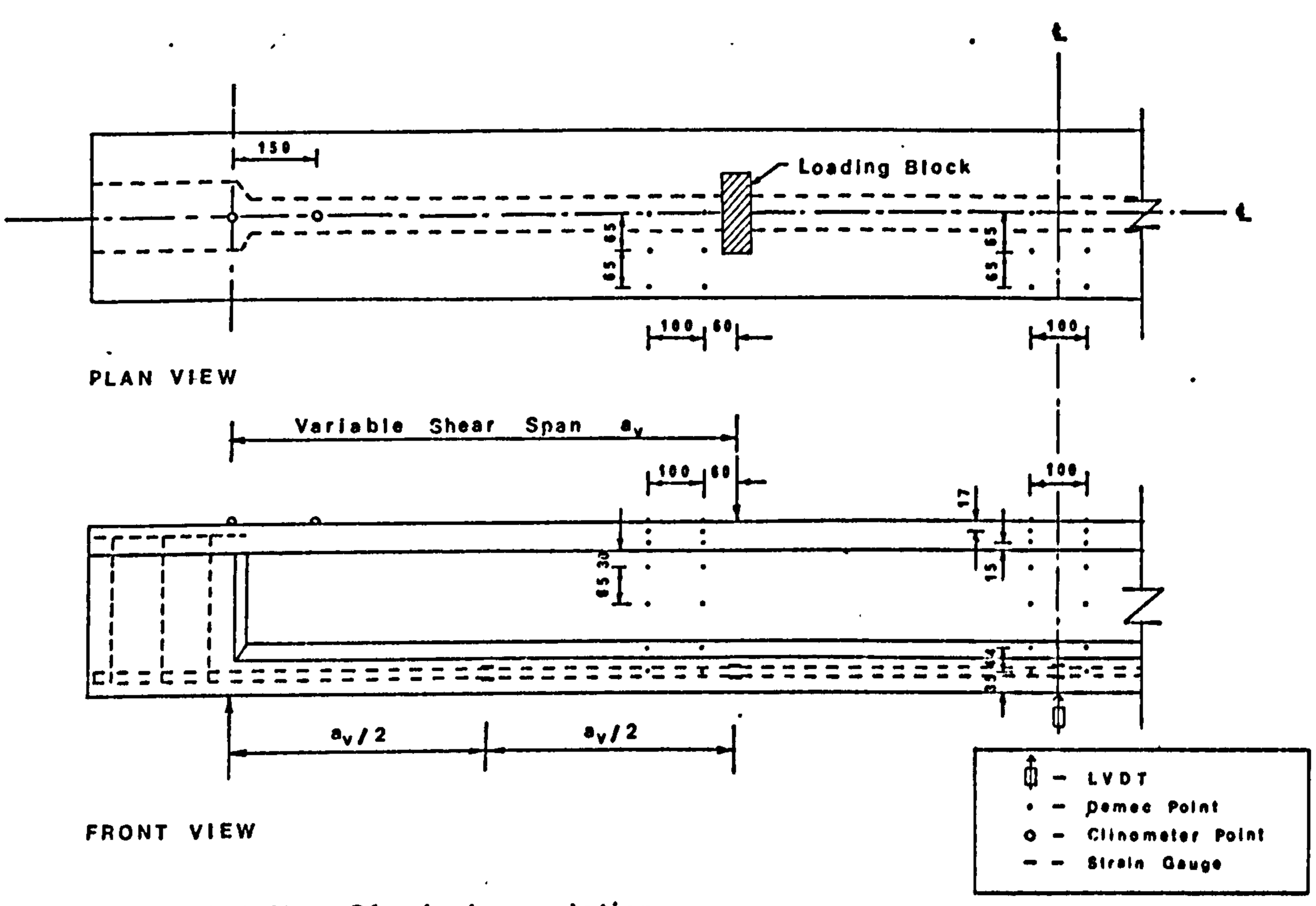

Fig. 6·2 Details Of Instrumentation

6.2.7.3 Steel Strains

The steel strains were measured at five locations along one of the main bars. See Fig. 6.2. These were at the mid section, under the point loads and in the middle of each shear span. At each location two 10 mm strain gauges (Kyowa, KFC-10-C1-11) were glued on vertical diametrically opposite sides of the bar to eliminate any bending strains due to local bending of the bar. The output voltages of the five strain gauge bridges were monitored by the 30 channel datalogger. All the strain gauges were protected with Kyowa's C-5 protective coating.

6.2.7.4 Rotations

The rotations were measured near to the supports of each beam. See Fig. 6.2. The rotation measurements were derived from slope changes using a Hilger and Watts clinometer, with an accuracy $\pm$ 30 seconds. Each pair of clinometer points consisted of 10 mm diameter steel balls glued to 10 mm washers, 150 mm centre to centre.

6.2.8 Testing Apparatus

A diagramatic layout of the test rig used is shown in Fig. 6.3. Loads were applied by means of a 500 kN maximum capacity loading machine through a hydraulic system connected to a 500 kN jack stroking downwards. The jack is connected to some counter weights to compensate for the weight of the piston.

The applied load was measured using a load cell with a sensitivity of $\pm$ 0.3 kN. The output voltage of the load cell was monitored by the portable datalogger. The load was applied incrementally according to the load scale of the machine. The readings from the load scale and the load cell were of the same order.

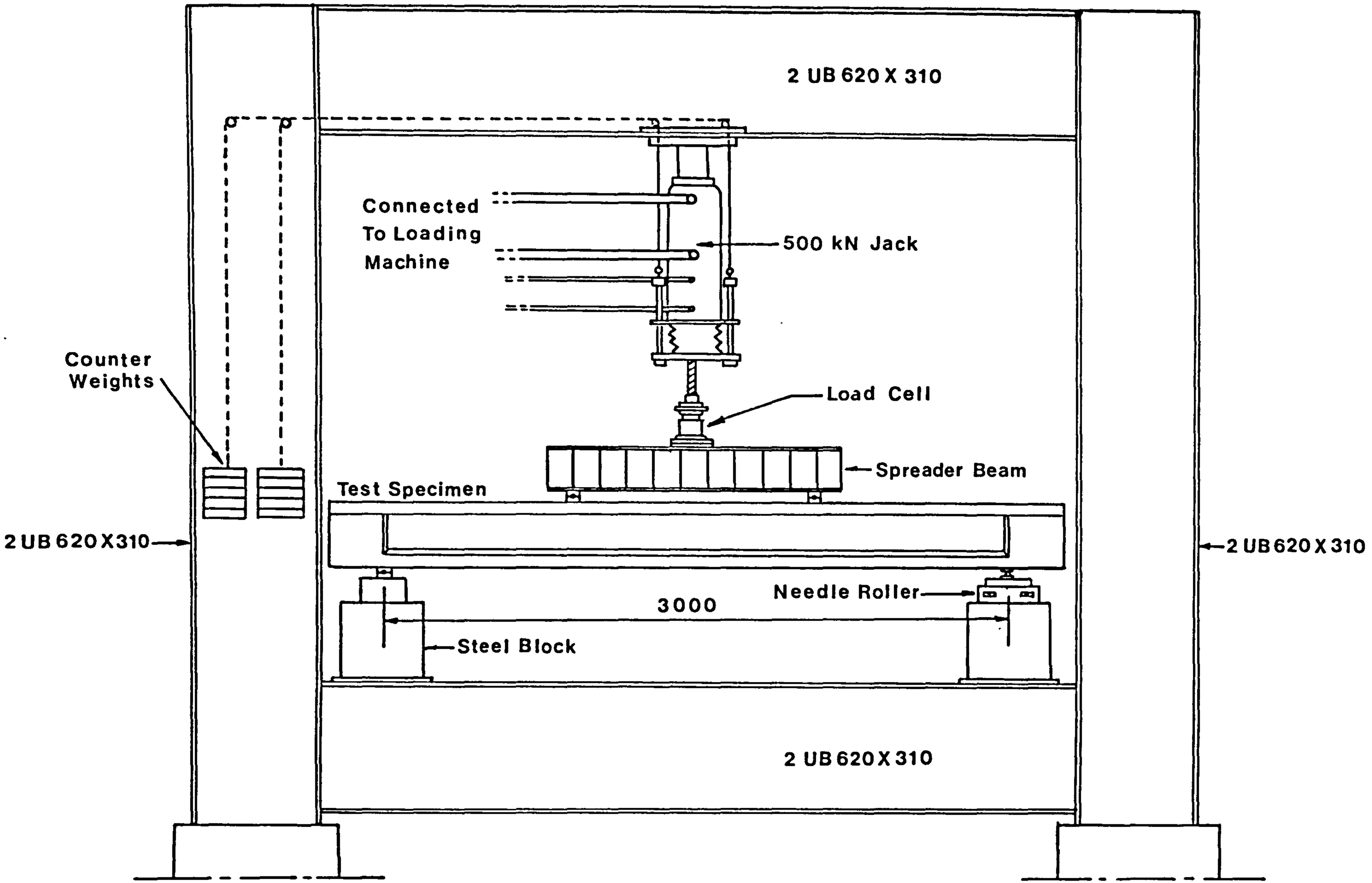

Fig. 6·3 Schematic Layout Of Test Rig

The load was applied to the test beam through a spreader beam. Three sizes of spreader beam were used in order to obtain the required shear span/effective depth ratios.

All the beams were simply supported with one end on a rocker and the other on a needle roller.

6.2.9 Testing Procedure

Before testing, a thin coat of whitewash was applied to the test beam to facilitate the location and study of the propagation of cracks.

The loading was applied in increments of 2.5, 5 or 10 kN, depending on the ultimate capacity of the beam tested. At each load increment, the concrete strains, end rotations, deflection and steel strains were taken. Then the developed crack patterns were marked by a felt pen on one face of the test beam and the load level (excluding the self-weight of the spreader beam) was written next to each crack.

Near to failure, no concrete strains or end rotation readings were taken. The datalogger was set to automatic scanning while the loading was slowly increased until failure occurred.

After failure,.the tested beam was photographed before being taken out of the test rig.

The control specimens of the tested beam were tested on the same day.

6.2.10 Beam Identification

Each beam was identified by alphanumeric characters. The first character identified the amount of main steel, 1 when it is 4.31%, 2 when it is 2.76% and 3 when it is 1.55%. The last character identifies the shear span/effective depth raio,

1 when it is 2.0, 2 when it is 3.43 and 3 when it is 4.91. The characters TL identify plain Lytag-sand concrete beams and TLF identify fibre Lytag-sand concrete beams. Thus 3TLF-3 identifies the fibre Lytag-sand concrete beam having 1.55% of main steel and tested at a a_v/d ratio of 4.91.

Table 6.1 gives the properties of all the beams tested in this investigation.

6.3 Discussion of Results

6.3.1 Deformation Characteristics

Extensive data on the deformation of the beams were obtained. Obviously it is not possible to present all of them and only the important and more relevant results are presented for discussion.

6.3.1.1 Load-Deflection Relationship

Figs. 6.4a through 6.4e compare the load-central deflection relations of both plain and fibre concrete beams. The modes of failure of the beams are also indicated. Shear-flexure failure was defined as the mode of shear failure which occurred after the main steel in the pure bending region had yielded.

It can be seen that the fibre concrete beams exhibited less deflection at all stress levels than their plain concrete counterparts. However, the decrease at the initial stages in most cases was marginal and this decrease can be attributed to the higher elastic modulus of fibre concrete (see section 3.3.5.5). With the formation of cracks, the role of the steel fibres in preserving the integrity of the cracked composite became clearly evident with larger decreases in deflection.

All the plain concrete beams failed in shear and the maximum deflection did not exceed 9.5 mm. All fibre concrete

Table 6.1 Properties of Test Beams

Beam Number	$\frac{a_v}{d}$	ρ_w (= $As/b_w d$) %	Volume Fibre Content %	Cube Strength f_{cu}' N/mm^2	M. O. R. N/mm^2		Elastic Modulus Ec kN/mm^2
					1st Crack	Ultimate	
1TL-1	2.0	4.31	0	44.3	3.60	3.60	19.4
1TLF-1	2.0	4.31	1.0	44.5	4.67	7.00	20.8
1TL-2	3.43	4.31	0	42.0	3.59	3.59	19.4
1TLF-2	3.43	4.31	1.0	51.1	4.96	7.35	22.0
1TL-3	4.91	4.31	0	42.6	3.44	3.44	19.6
1TLF-3	4.91	4.31	1.0	45.0	4.58	6.73	21.5
2TL-1	2.0	2.76	0	45.6	3.80	3.80	20.0
2TLF-1	2.0	2.76	1.0	47.2	4.93	7.00	21.6
2TL-2	3.43	2.76	0	41.7	3.56	3.56	19.3
2TLF-2	3.43	2.76	1.0	41.4	4.59	6.60	21.0
2TL-3	4.91	2.76	0	45.1	3.60	3.60	19.6
2TLF-3	4.91	2.76	1.0	44.9	4.60	6.90	21.4
3TL-1	2.0	1.55	0	46.7	3.76	3.76	20.2
3TLF-1	2.0	1.55	1.0	44.6	4.84	6.85	-
3TL-2	3.43	1.55	0	41.0	3.04	3.04	19.6
3TLF-2	3.43	1.55	1.0	43.1	4.56	7.73	-
3TL-3	4.91	1.55	0	42.3	3.36	3.36	18.7
3TLF-3	4.91	1.55	1.0	40.6	4.10	6.0	-

beams, on the other hand, failed at substantially higher deflection indicating the increased ductility imparted by the steel fibres. For those fibre concrete beams which failed in shear with yielding of the tension steel in the pure bending region and those which failed in flexure, the deflection at maximum load exceeded 21.0 mm.

Table 6.2 compares the deflection of the fibre concrete beams at working load level with the limits at serviceability limit state of CP110(68). The working load level was assumed to be $\frac{1}{\gamma_f}$ x maximum load and γ_f was taken to be 1.6 in accordance with CP110. It can be noted that none of the beams showed deflection (excluding deflection due to shrinkage and creep) at working load level greater than the limit of span/250 for final deflection. However, only those beams which failed in shear without the yielding of the main steel in the pure flexure region satisfied the more stringent limit of span/350.

6.3.1.2 Load-End Rotation Relation

Figs. 6.5a and 6.5b show the load-end rotation curves of some of the beams tested. The load-end rotation curves are very similar to the load-central deflection curves presented in section 6.3.1.1.

Again it can be observed that the inclusion of 1% crimped steel fibres resulted in a reduction in the end rotations and an increase in the rotational capacity at failure. Furthermore, beams which failed in flexure or shear-flexure exhibited greater rotational capacity than those that failed in shear.

6.3.1.3 Concrete Strains

Typical load-concrete strain curves are shown in Figs. 6.6a and 6.6c. The concrete strains were measured at the top fibre at midspan of the beams. Again, these curves showed

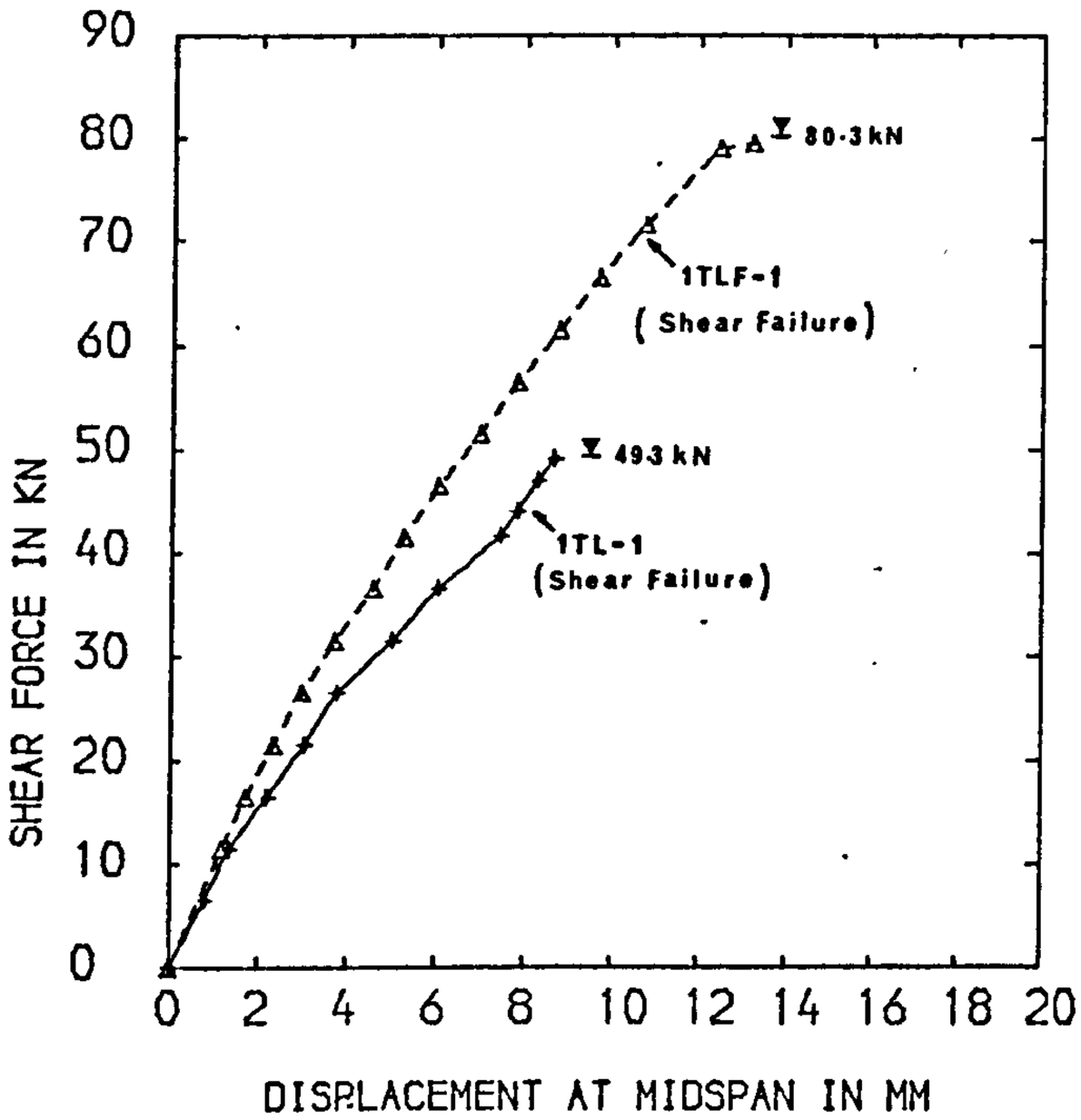

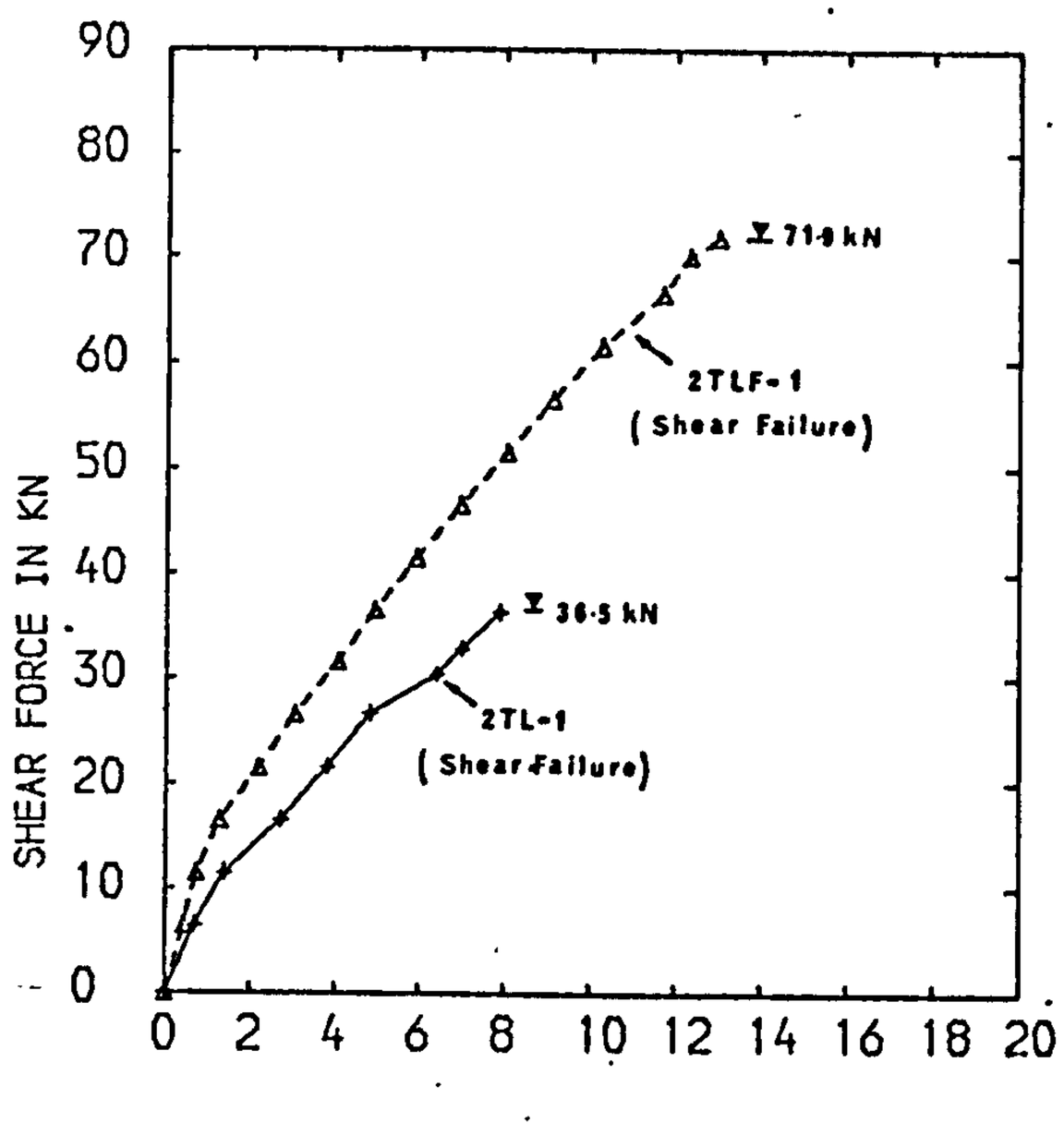

FIG.6.4(a) LOAD-MIDSPAN DISPLACEMENT CURVES

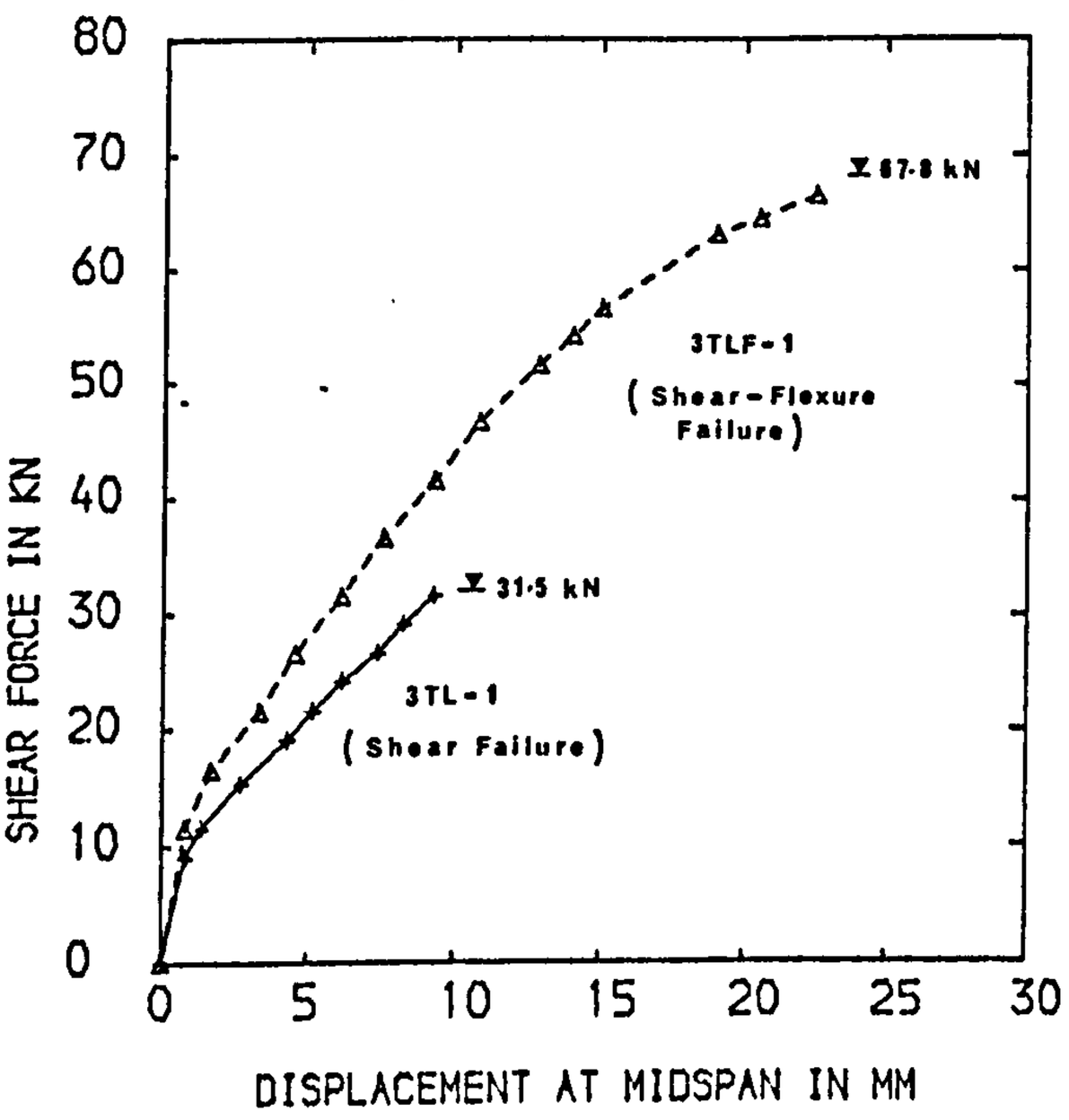

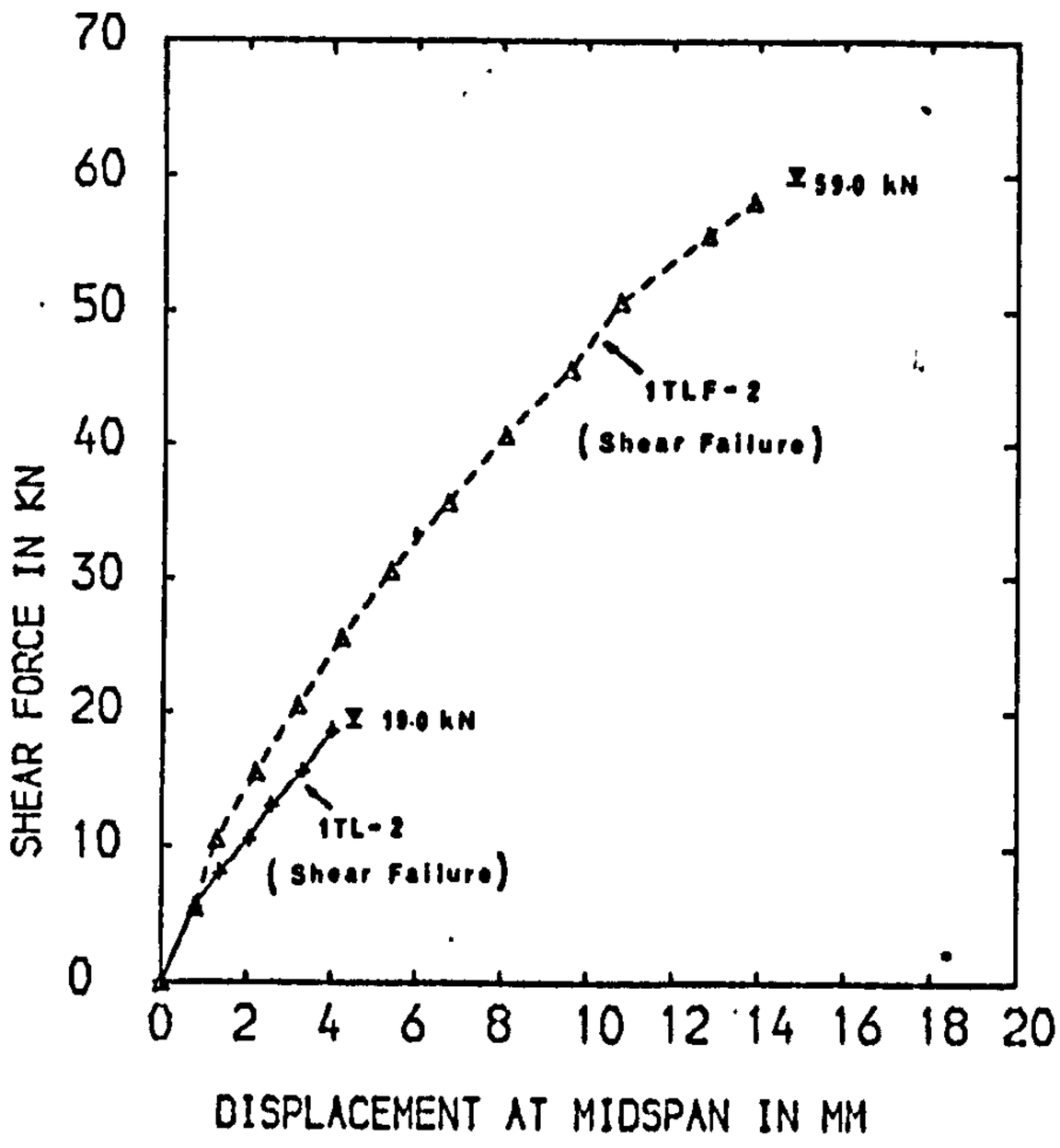

FIG.6.4(b) LOAD-MIDSPAN DISPLACEMENT CURVES

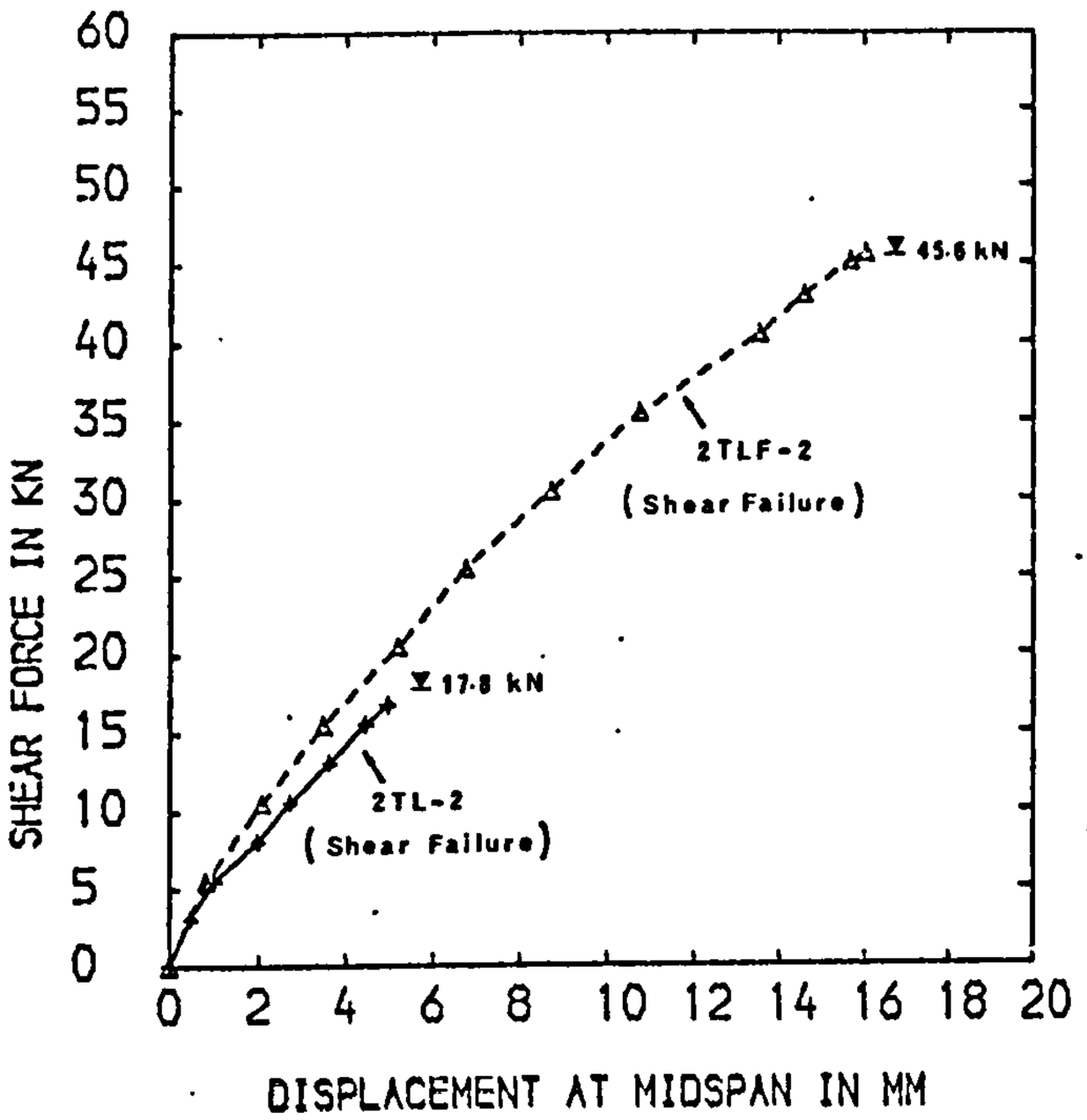

FIG.6.4(c) LOAD-MIDSPAN DISPLACEMENT CURVES

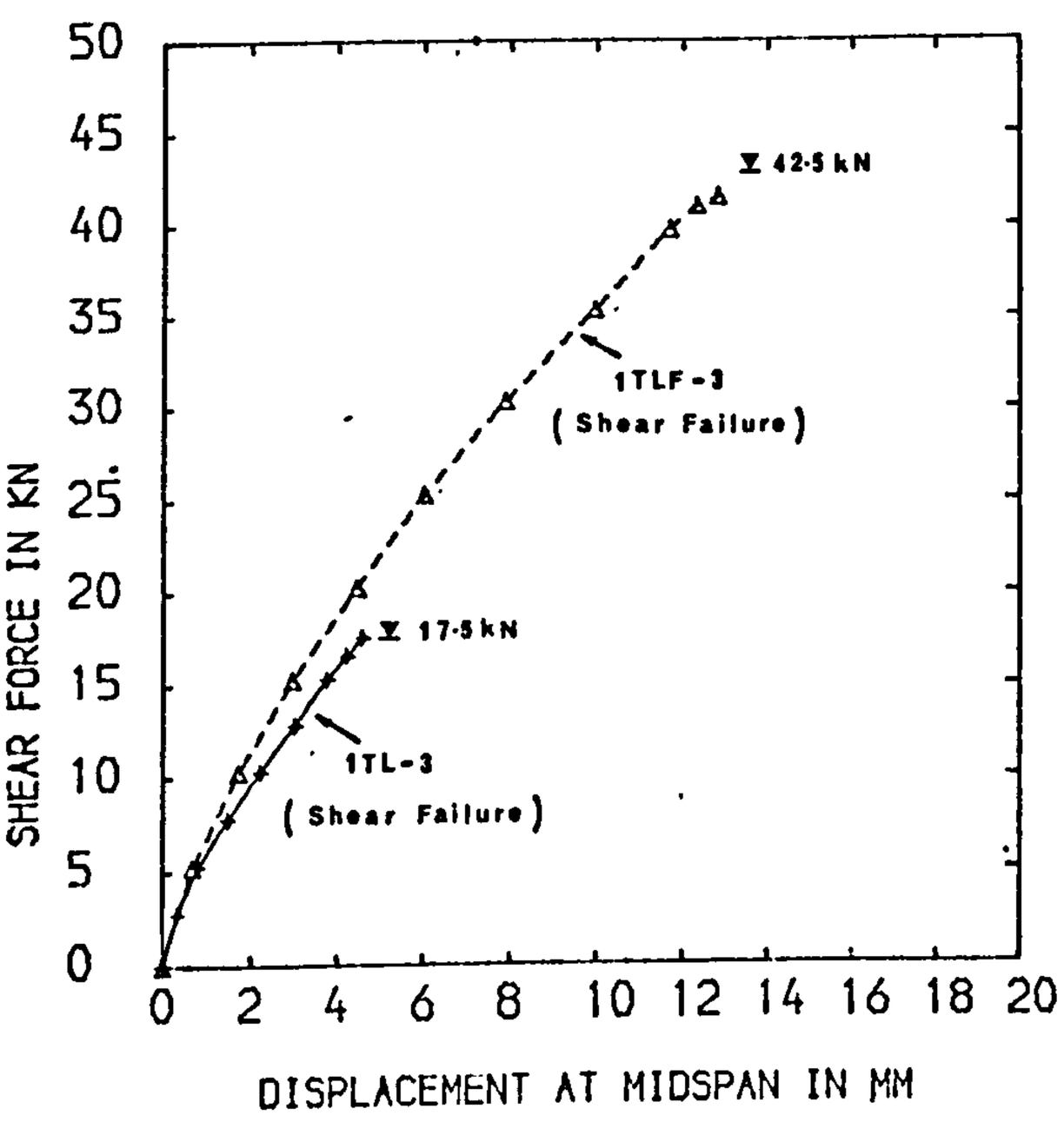

FIG.6.4(d) LOAD-MIDSPAN DISPLACEMENT CURVES

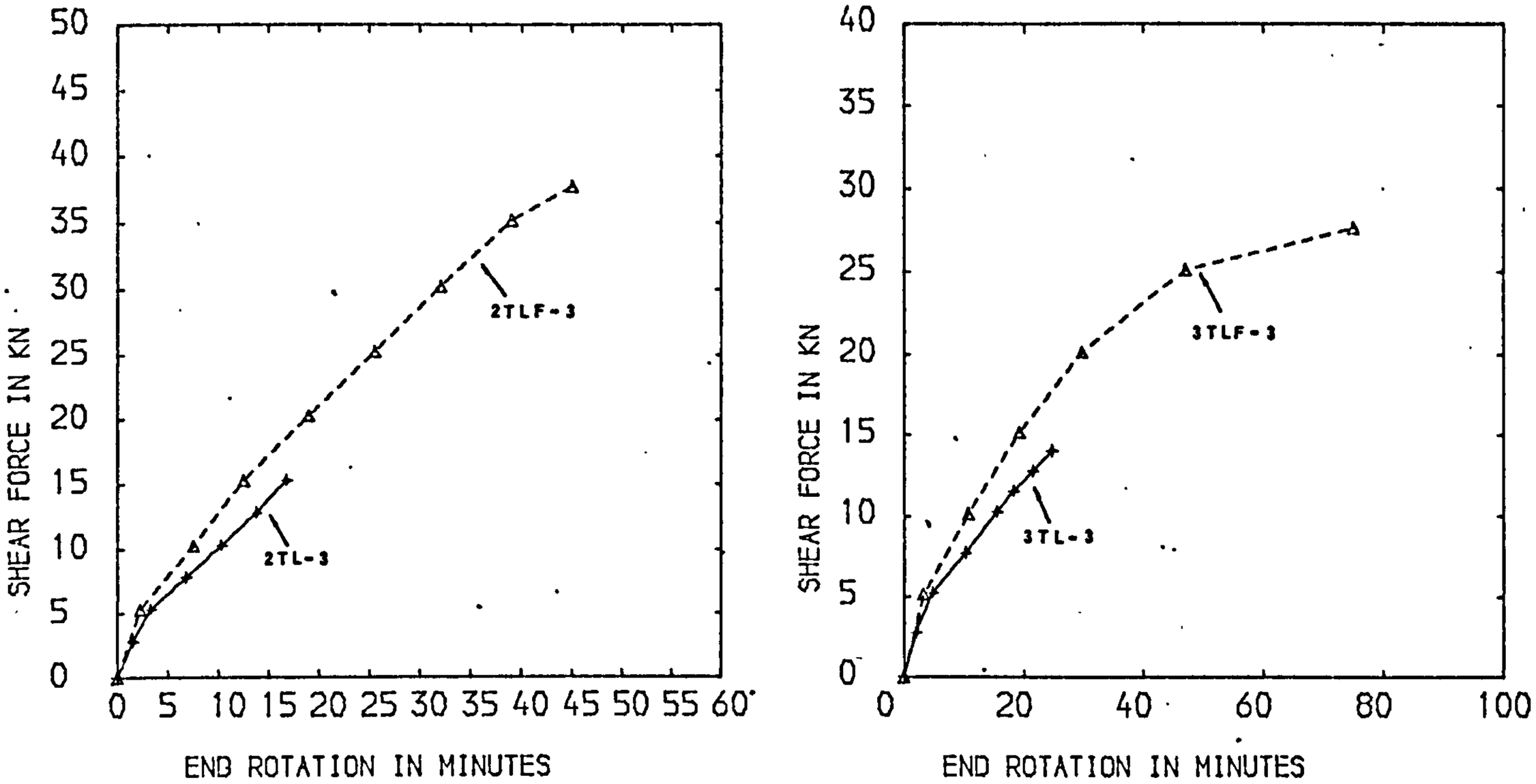

FIG.6.5(b) LOAD-END ROTATION CURVES

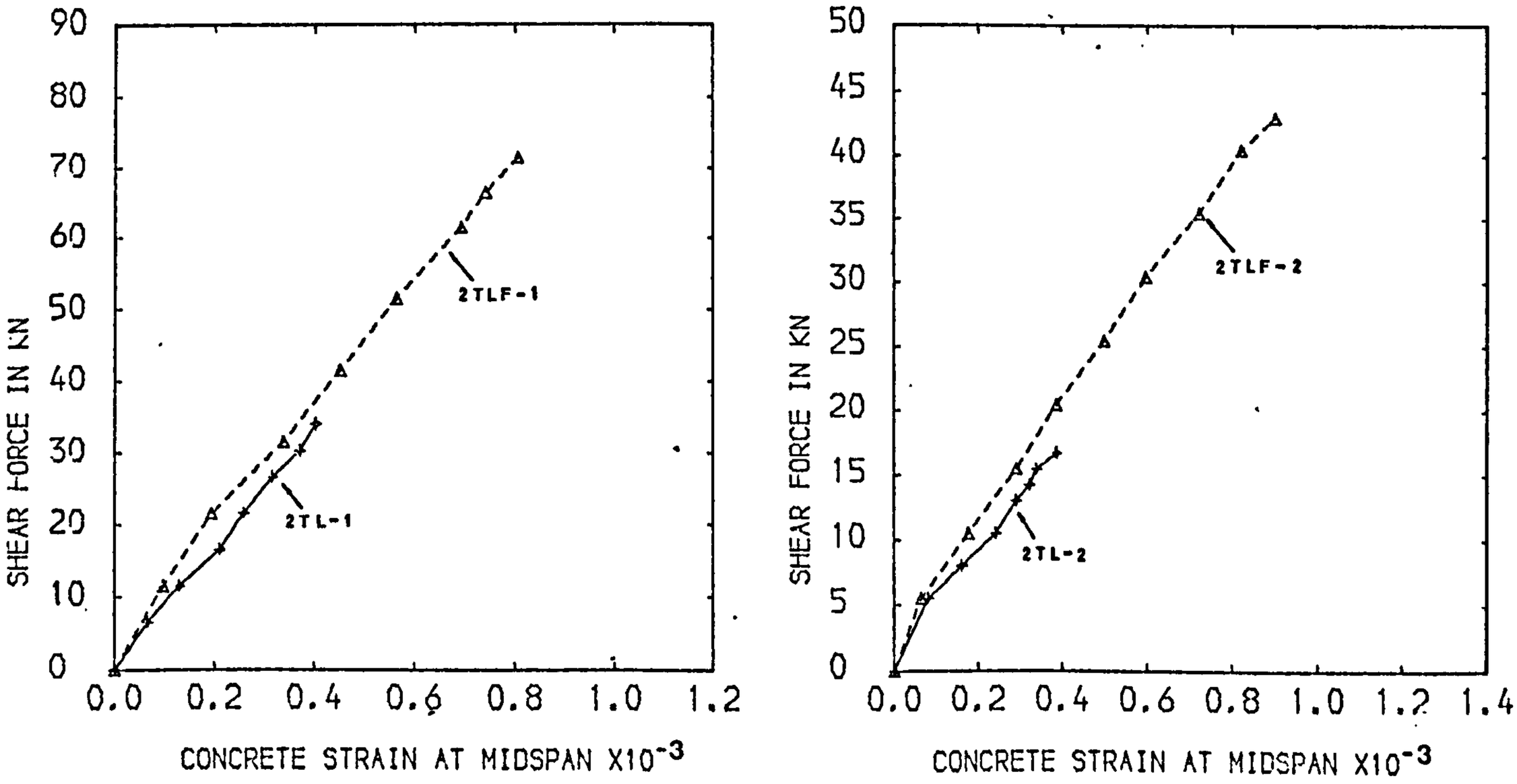

FIG.6.6(a) LOAD-CONCRETE STRAIN AT MIDSPAN CURVES

Table 6.2 Comparison of Deflection (in mm) of Fibre Concrete Beams with CP110's Allowable Values

Beam No.	Deflection at Max. Load	Deflection at 0.625 x Max. Load*	$\frac{\text{Span}}{350}$	$\frac{\text{Span}}{250}$	Failure Mode
1TLF-1	13.5	6.8	8.6	12.0	Shear
2TLF-1	13.2	6.8	8.6	12.0	Shear
3TLF-1	>22.0	9.5	8.6	12.0	Shear-Flexure
1TLF-2	14.5	7.2	8.6	12.0	Shear
2TLF-2	16.2	8.0	8.6	12.0	Shear
3TLF-2	>22.0	10.5	8.6	12.0	Flexure
1TLF-3	14.0	6.5	8.6	12.0	Shear
2TLF-3	>21.0	9.3	8.6	12.0	Shear-Flexure
3TLF-3	>32.0	8.7	8.6	12.0	Flexure

NOTE: Limit... L/250 for total deflection including deflection due to shrinkage and creep
L/350 deflection after construction of partition walls, laying floor finishes etc

* Excluding deflection due to shrinkage and creep

trends similar to the load-deflection curves. At any given load level, the concrete strains of fibre concrete beams were less than those of their plain concrete counterparts.

All the plain concrete beams failed at a maximum compressive strain not exceeding 600 microstrains. The fibre concrete beams sustained higher loads and showed a substantially higher maximum compressive strain at failure.

Fig. 6.7 represents the distribution of the longitudinal strains on top of the fibre concrete beams in which such strain measurements were taken. Beams 1TLF-3 and 2TLF-3 failed in shear and shear-flexure respectively and their strain profiles showed a diminishing compressive strains at sections towards the

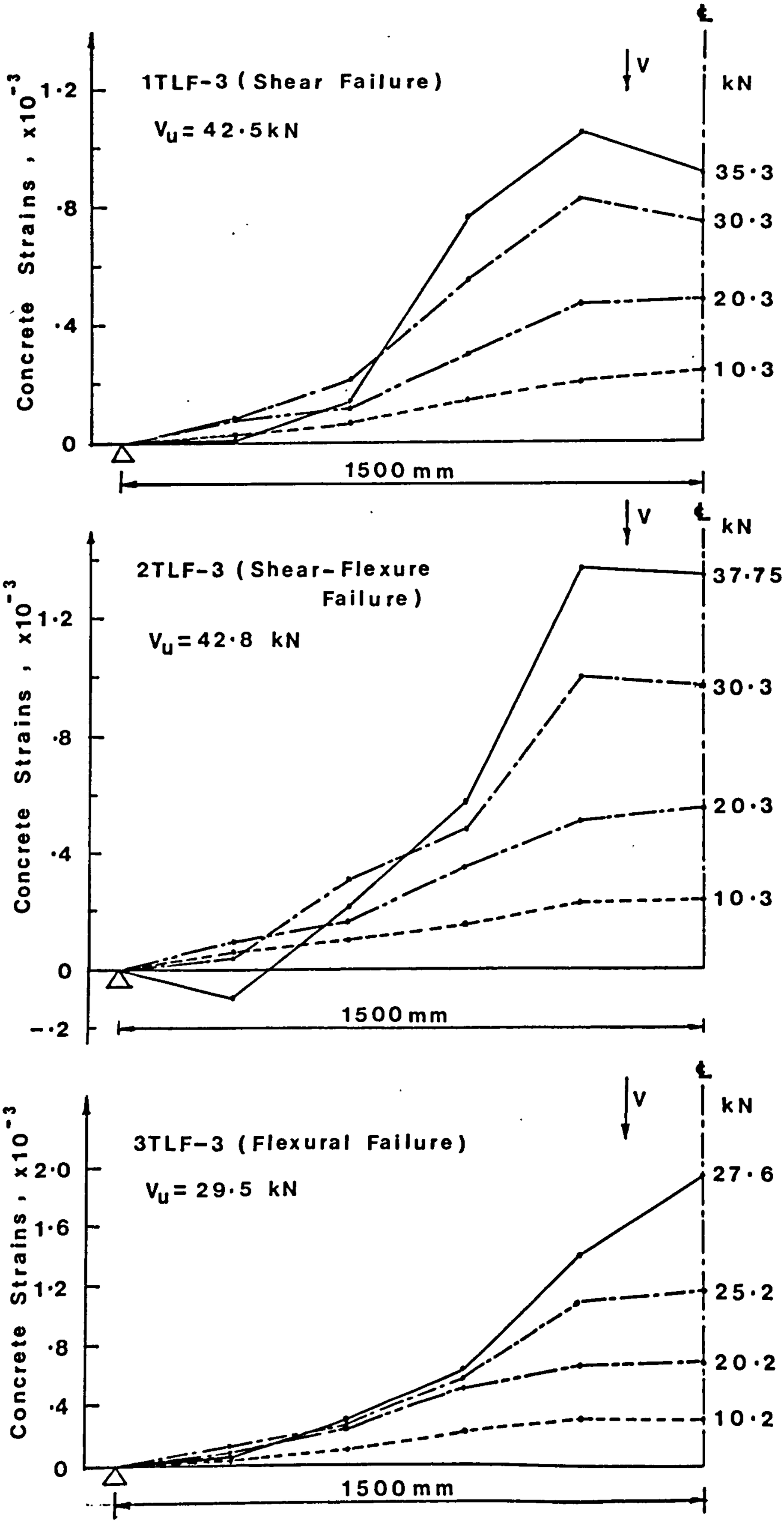

Fig.6·7 Top Fibre Strain Profiles

the support at increasing load level after the formation of shear cracks. These diminishing compressive strains became tensile at regions near the support prior to final failure. Muhidin (31, 99) and Leonhardt (100) reported similar observation. This implies that the resultant of the compression chord stresses must be inclined in this region (100). The strain profiles also showed that the top fibre strain adjacent to the point load was generally higher than that at the midspan after the formation of shear cracks. This could possibly be attributed to concentration of rotation and reduction in the neutral axis depth at the zone adjacent to the loading block.

Beam 3TLF-3 failed in flexure and this was reflected in the strain profile obtained.

Figs. 6.8a and 6.8b show the longitudinal strain variation on vertical sections at midspan and in the failure shear span adjacent to the loading block. The figures indicated that near to failure for the case of shear and shear-flexure failures, the neutral axis depth at the section near to the load point was much smaller than that at midspan.

6.3.1.4 Tensile Steel Strains

Typical load-tensile steel strain curves at midspan are shown in Figs. 6.9a and 6.9b. As expected, the inclusion of steel fibres reduced the tensile strains in the main steel. The reduction was more evident after the formation of cracks.

Table 6.3 gives the tensile strains near ultimate load at various locations along the main steel. The fibre concrete beams showed considerably higher tensile steel strains near failure than the corresponding plain concrete beams. Yielding of the main steel in the pure bending region occurred in all the fibre concrete beams with 1.55% of tension steel and the fibre

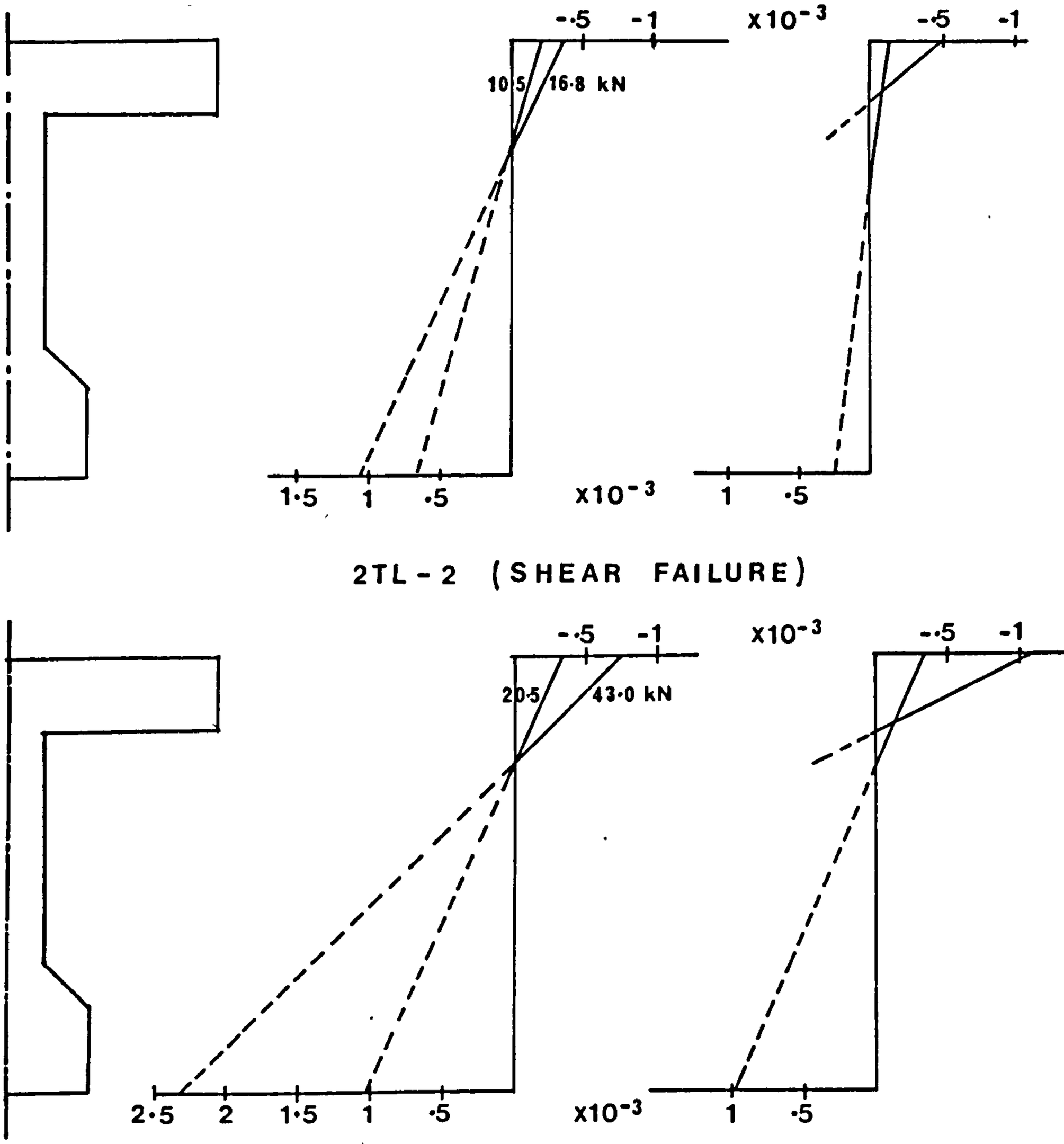

FIG·6·8(a) LONGITUDINAL STRAIN VARIATIONS ACROSS DEPTH OF SECTIONS

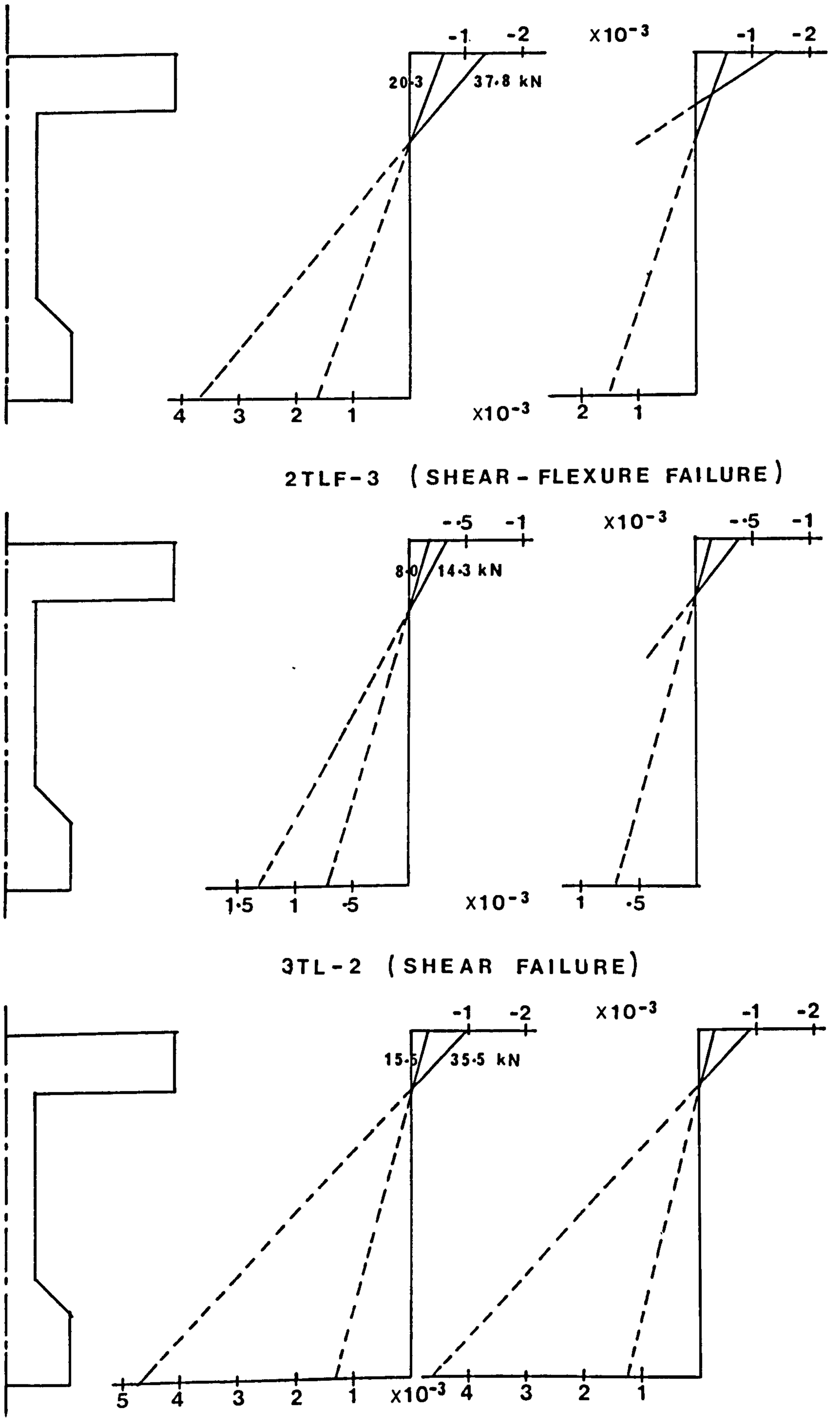

FIG 6 8(b) LONGITUDINAL STRAIN VARIATIONS ACROSS DEPTH OF SECTIONS

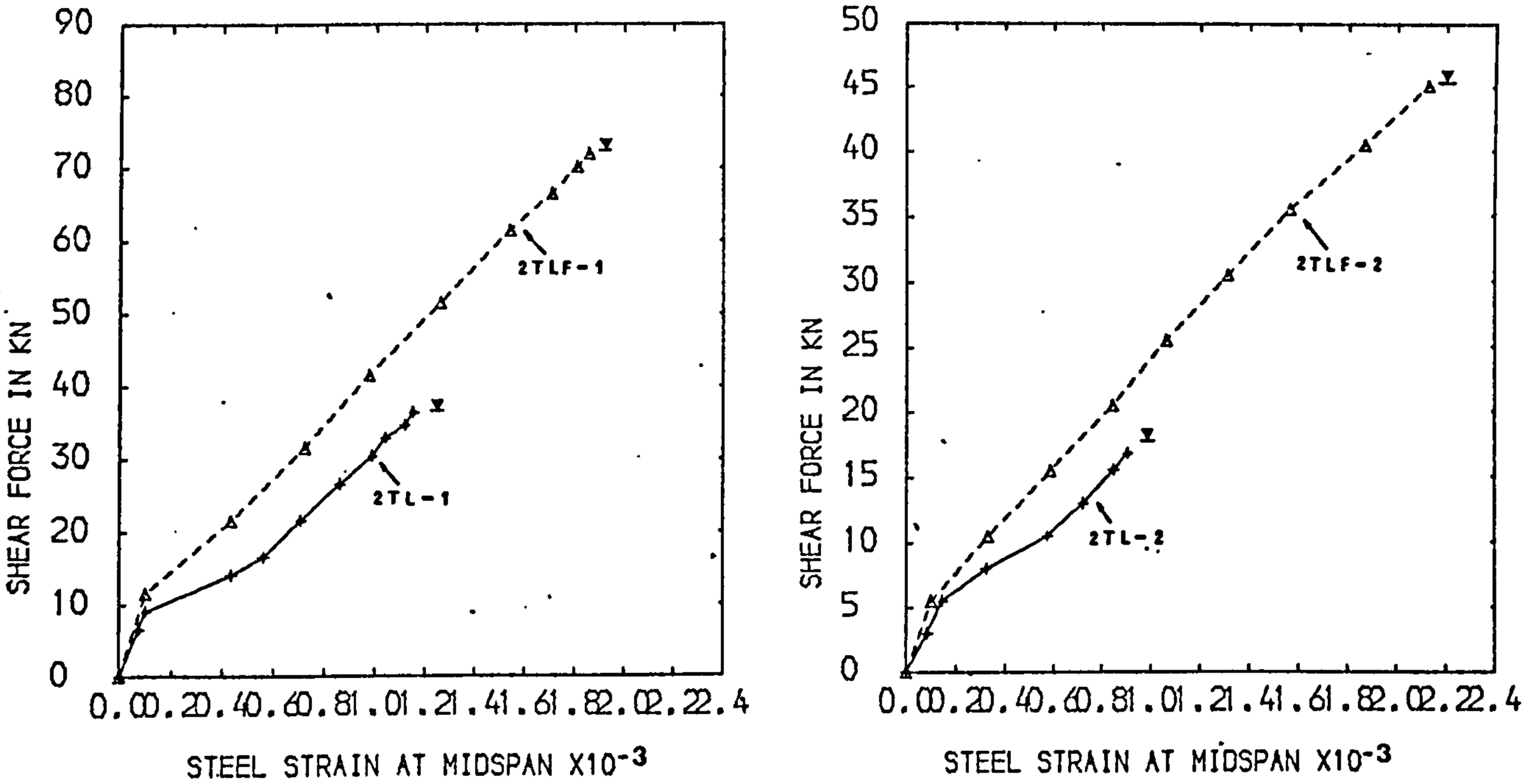

FIG.6.9(a) LOAD-MIDSPAN STEEL STRAIN CURVES

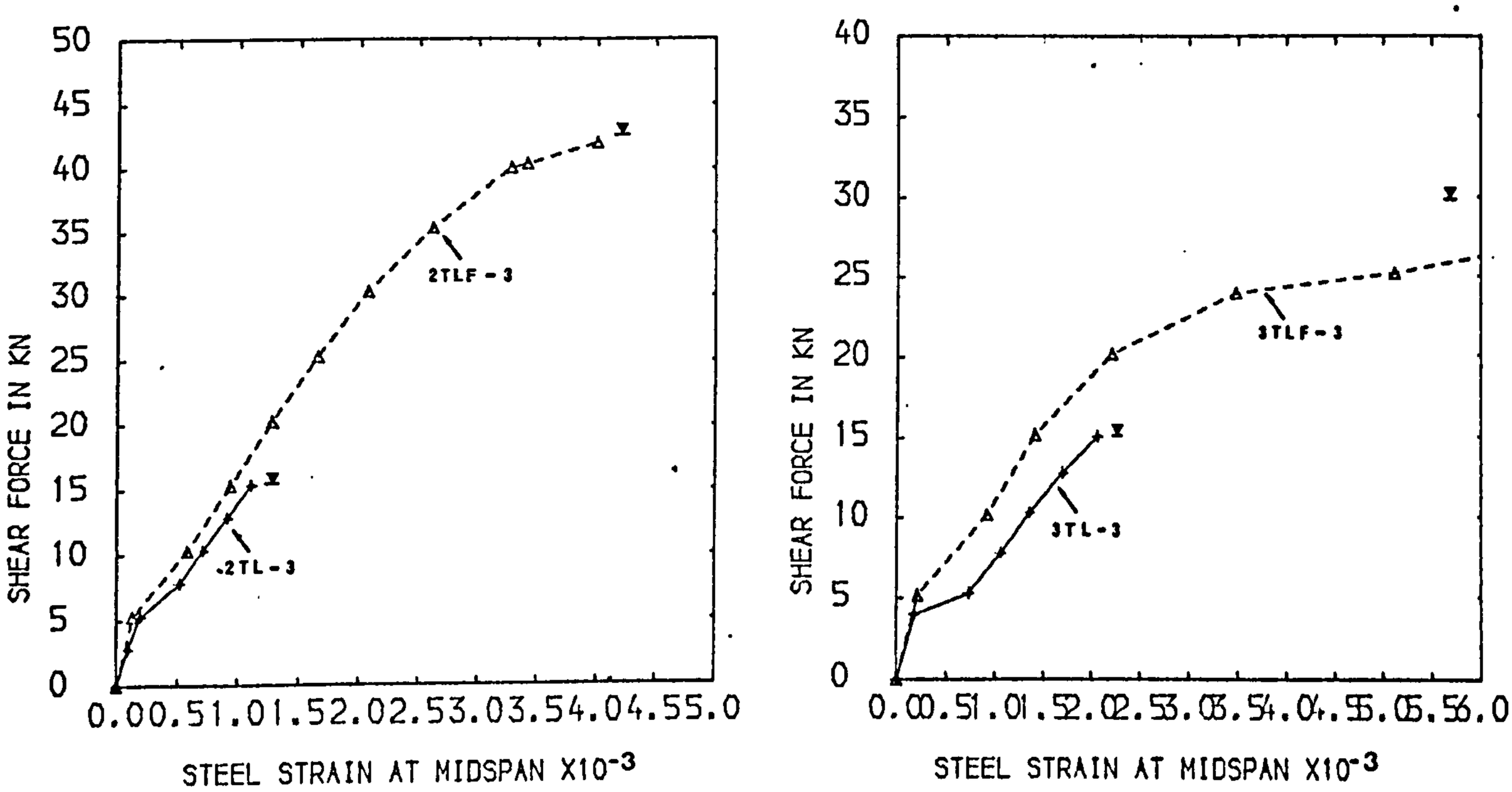

FIG.6.9(b) LOAD-MIDSPAN STEEL STRAIN CURVES

concrete beam with 2.76% of tension steel and tested under the highest a_v/d ratio. For beams with short shear spans, the tensile steel strains at the mid-shear span were about the same as those at the midspan or under the load point. This suggests arching action in such beams.

Table 6.3 Tensile Steel Strains Near Ultimate Load

Beam Number	Steel Strains x 10^{-6}			Beam Number	Steel Strains x 10^{-6}		
	Mid-Shear Span	Under Point Load	Mid-Span		Mid-Shear Span	Under Point Load	Mid-Span
1TL-1	930	1020	-	1TLF-1	1410	1260	1250
2TL-1	1040	1060	1150	2TLF-1	1610	1750	1860
3TL-1	1540	1530	1710	3TLF-1	2270	>4600	>5000
1TL-2	415	625	680	1TLF-2	1390	1770	1740
2TL-2	640	1020	950	2TLF-2	1620	2110	2130
3TL-2	765	1280	1170	3TLF-2	2030	>5000	>6000
1TL-3	600	905	960	1TLF-3	1060	1750	1770
2TL-3	770	1150	1120	2TLF-3	1890	>4500	>4500
3TL-3	1280	2050	-	3TLF-3	2280	>6500	>6500

NOTE: Average yield strain of main steel 4500 x 10^{-6}
(see Fig. 3.3)

6.3.2 Cracking and Modes of Failure

Table 6.4 gives the loads at first flexural and shear cracks for all the beams tested in this study. Plates 6.1 through 6.5 show some of the beams after failure. It should be pointed out again that the load levels written next to the cracks in the photographs did not include the self weight of the spreader beams. The loads shown in Table 6.4, however, took this into account.

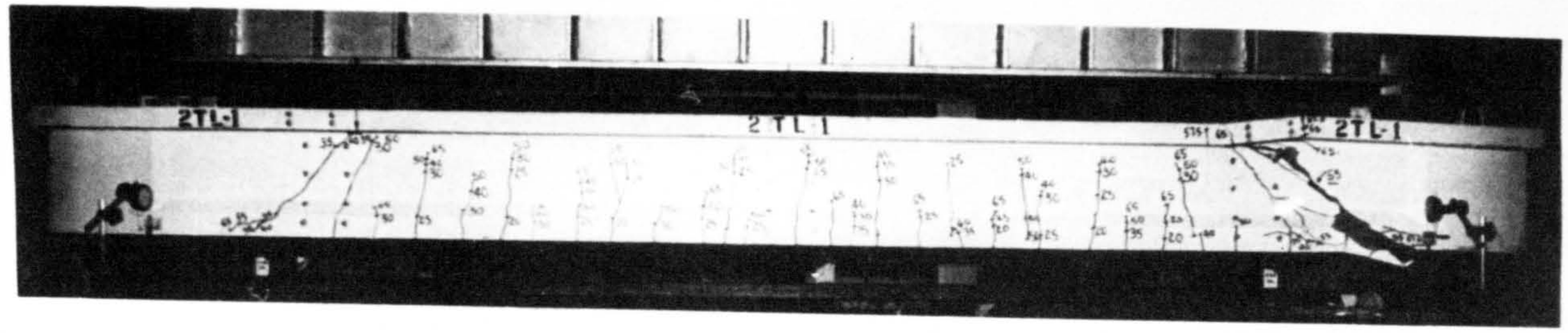

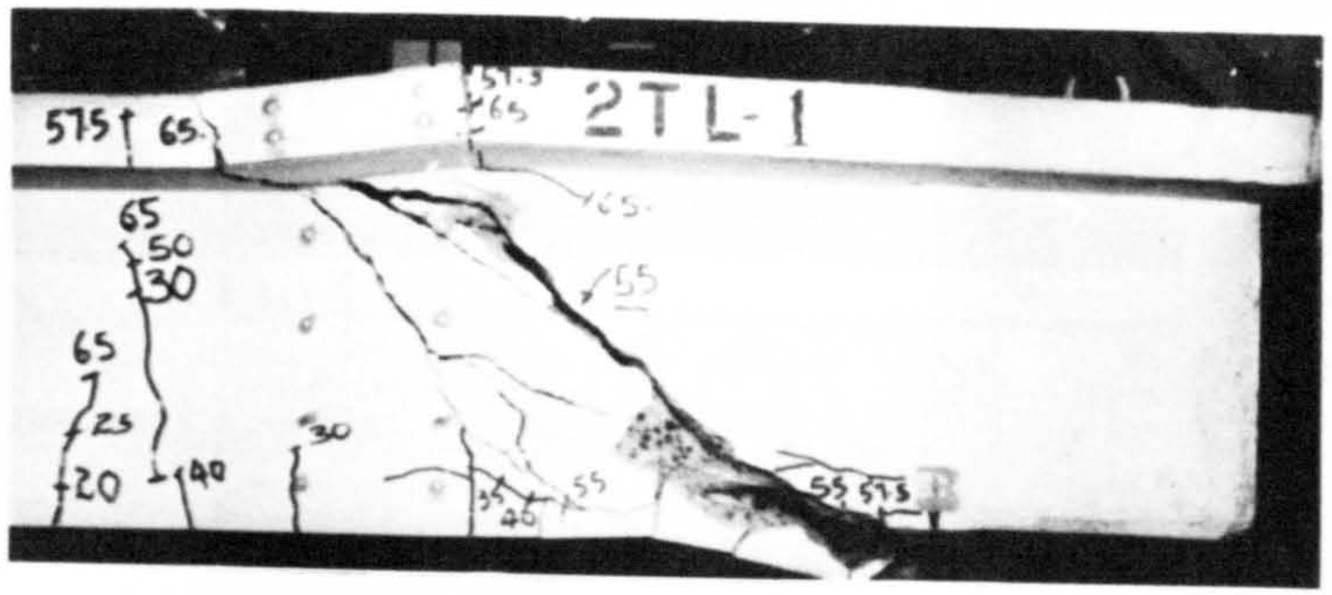

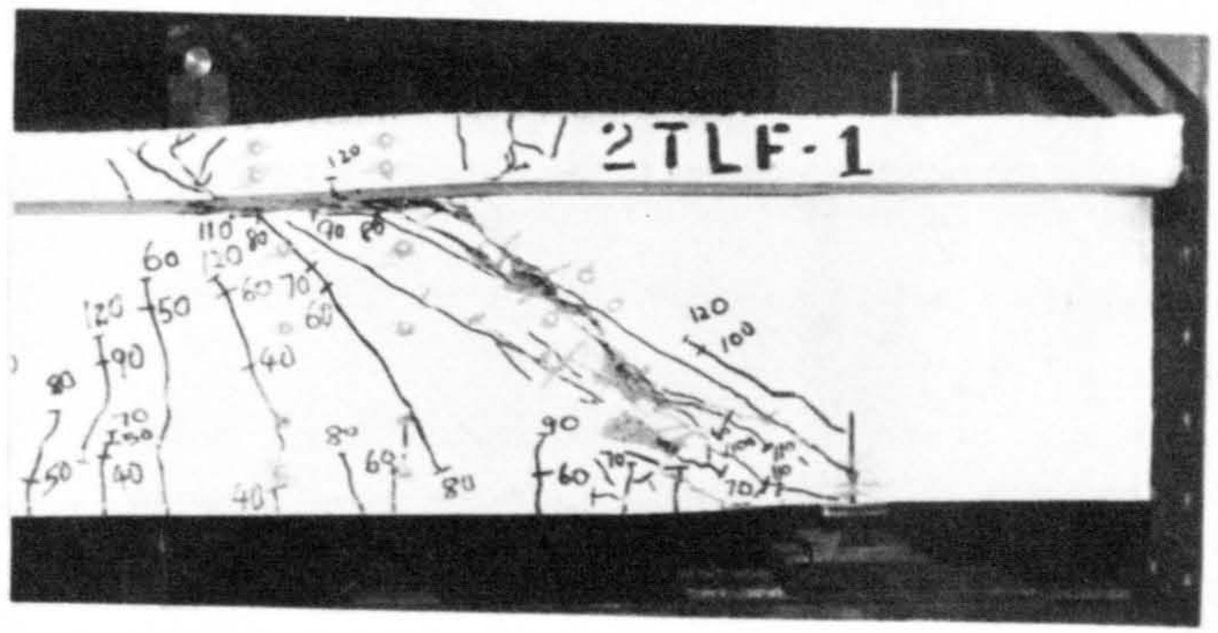

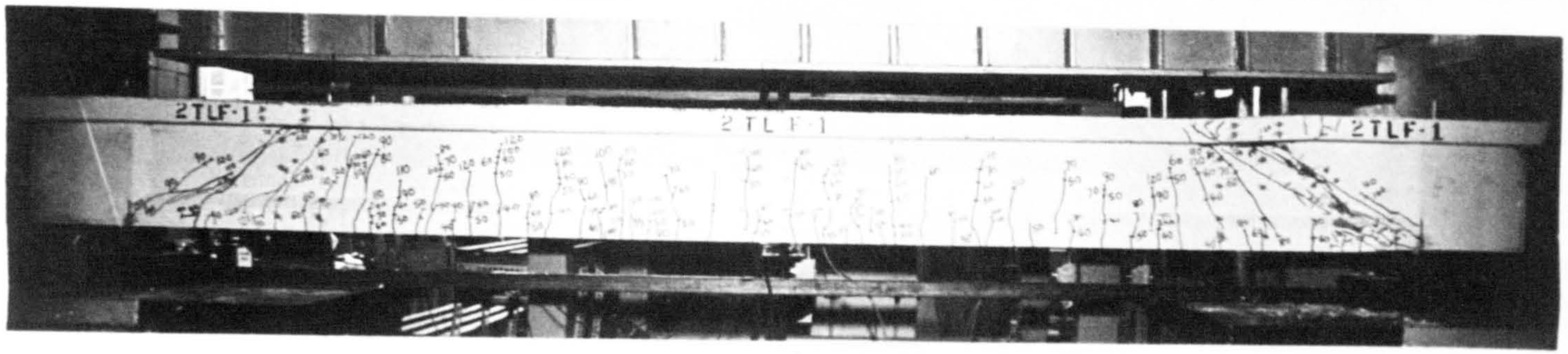

PLATE 6·1 Modes of failure of beams 2TL-1 and 2TLF-1

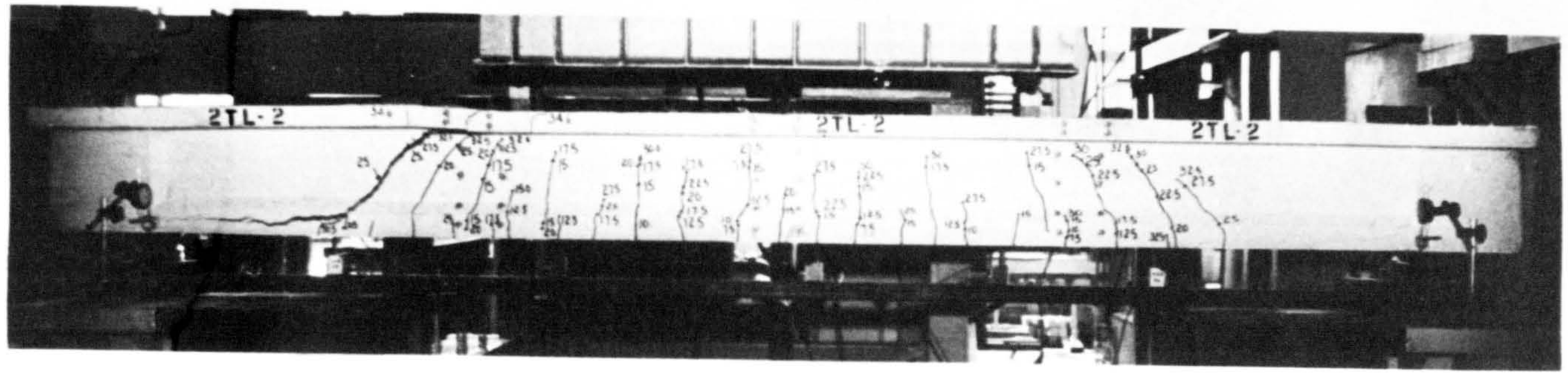

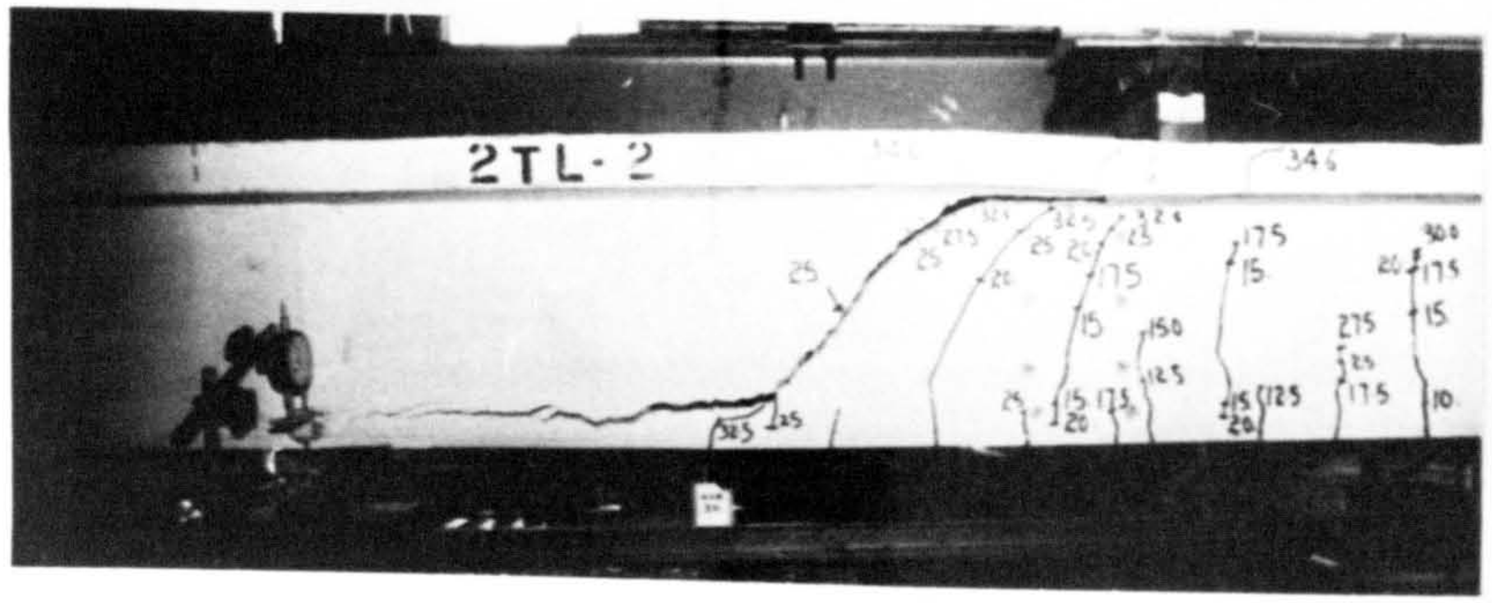

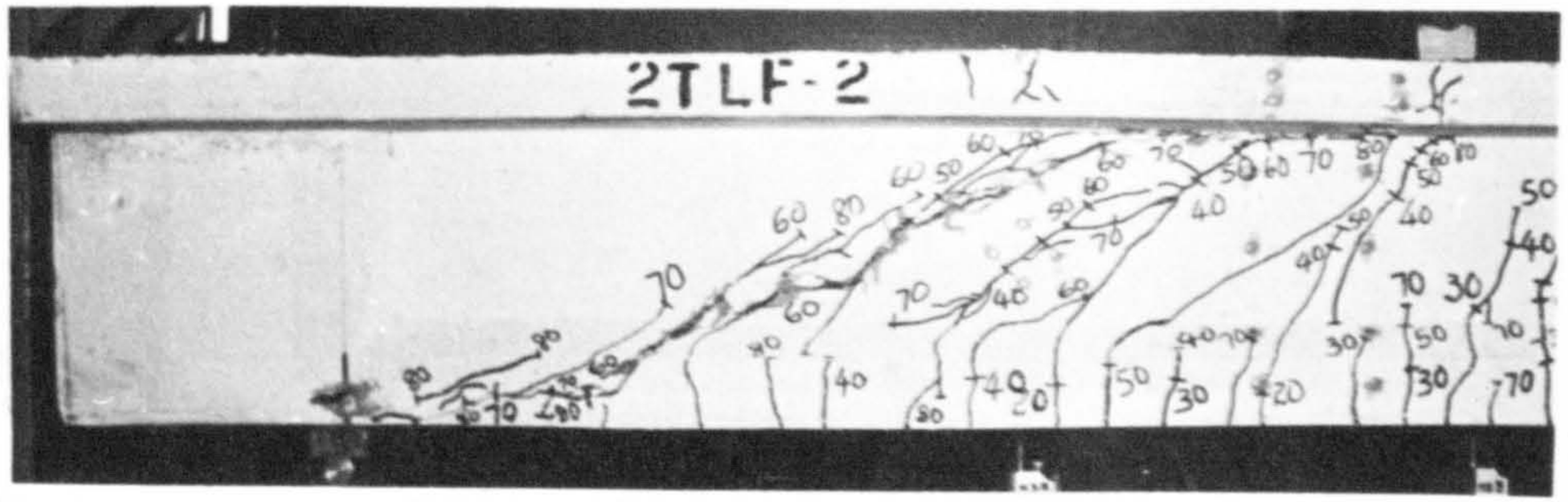

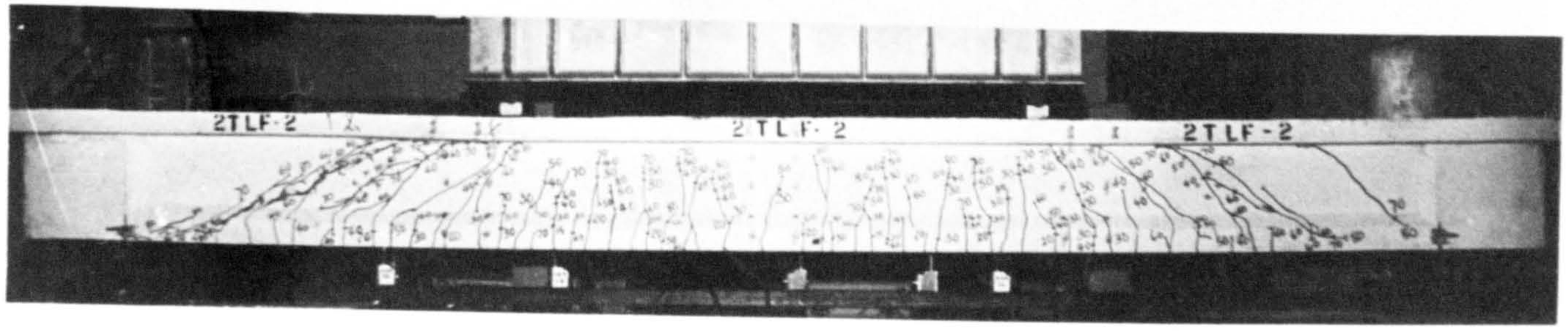

PLATE 6·2 Modes of failure of beams 2TL-2 and 2TLF-2

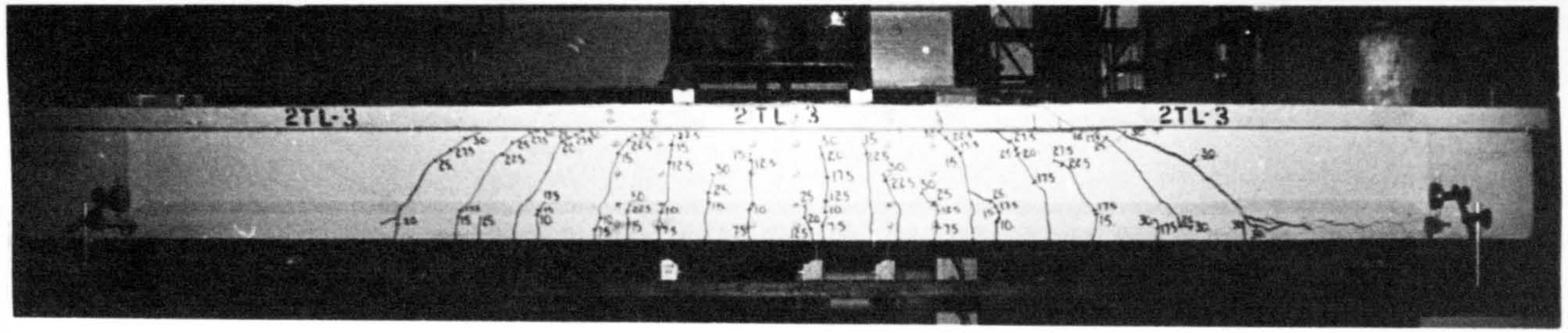

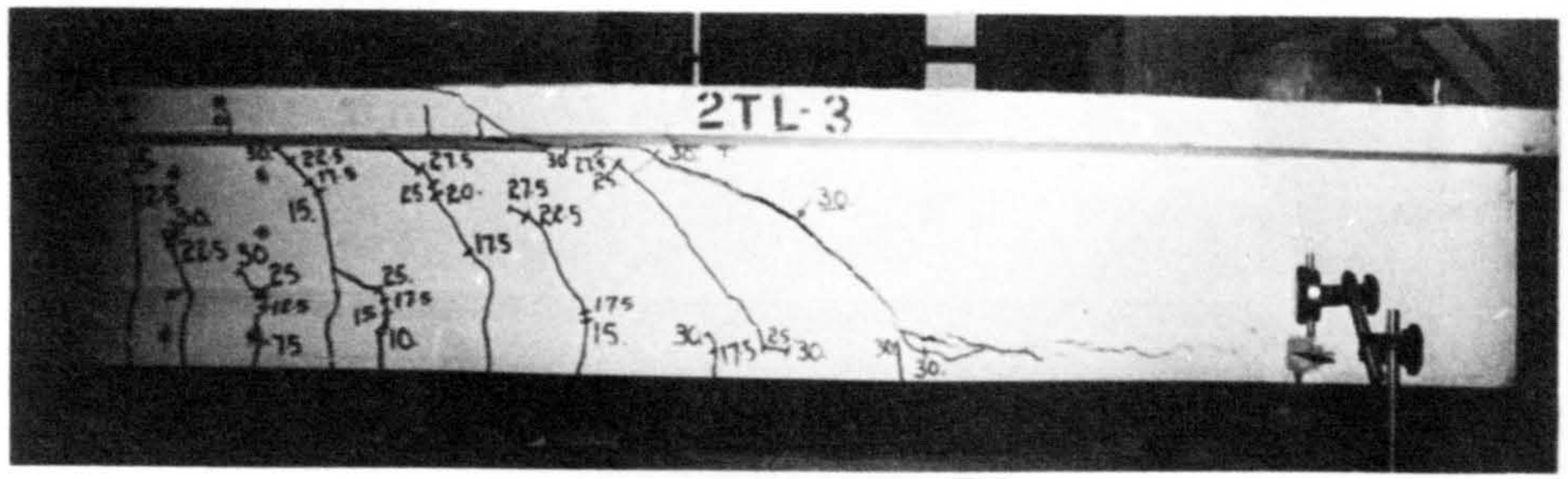

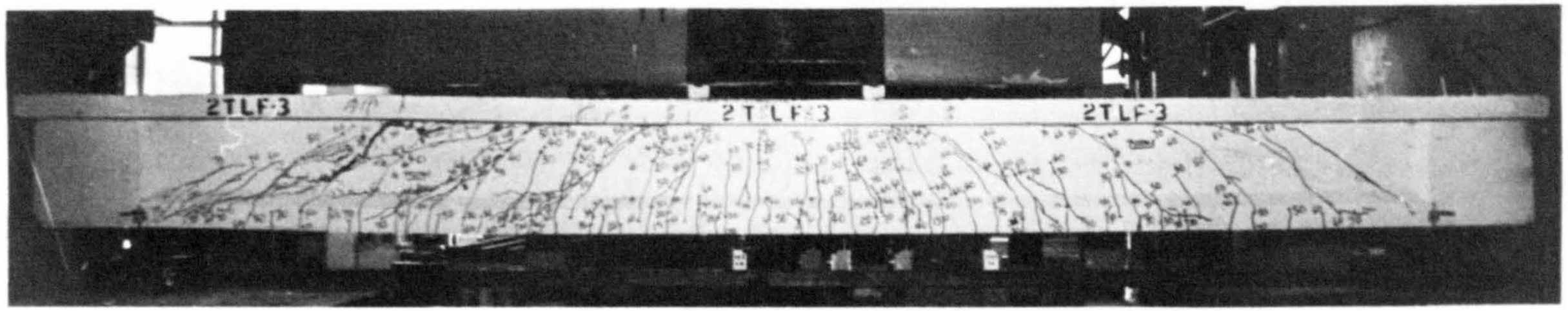

PLATE 6·3 Modes of failure of beams 2TL-3 and 2TLF-3

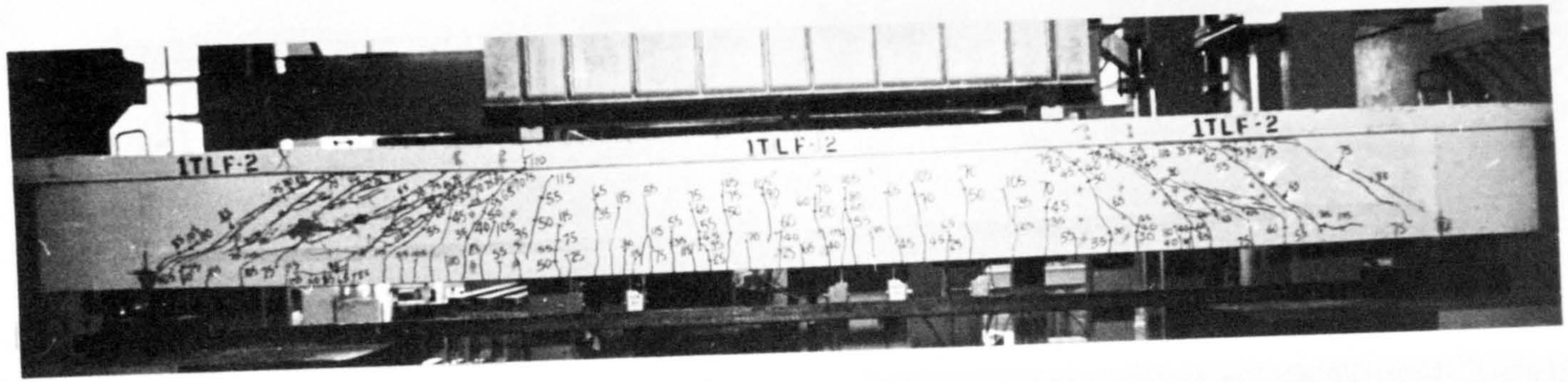

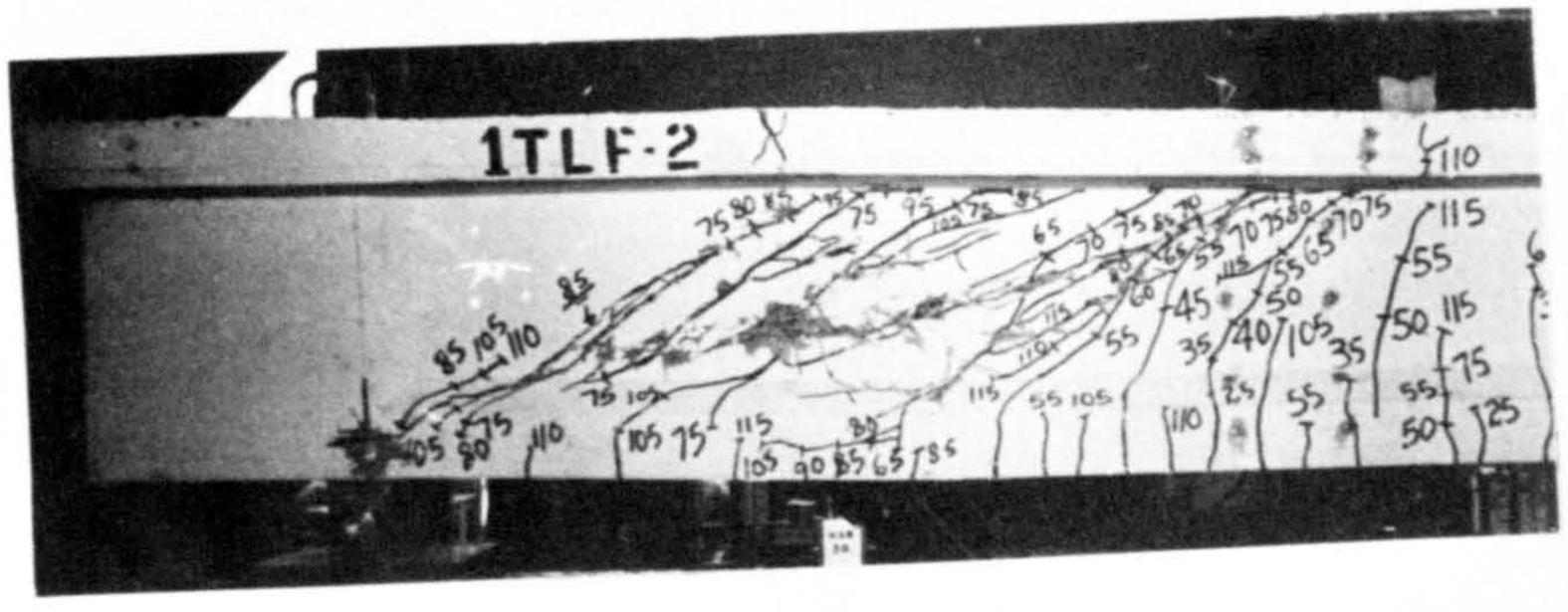

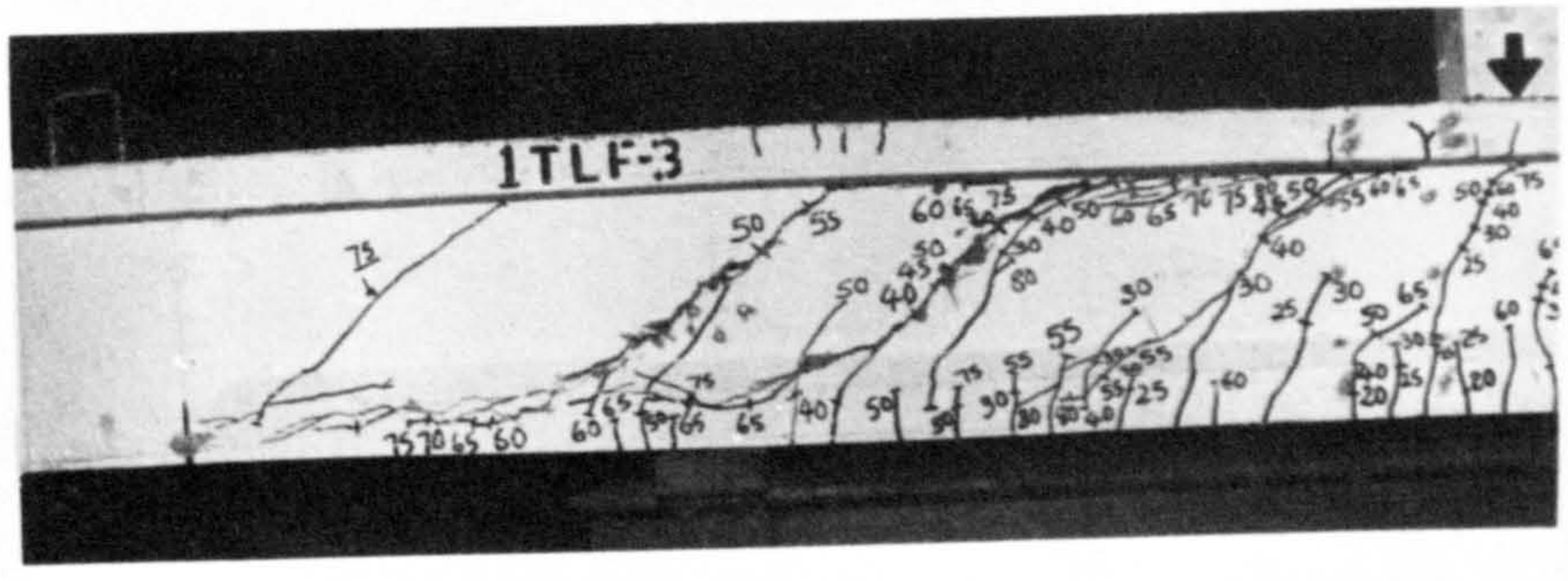

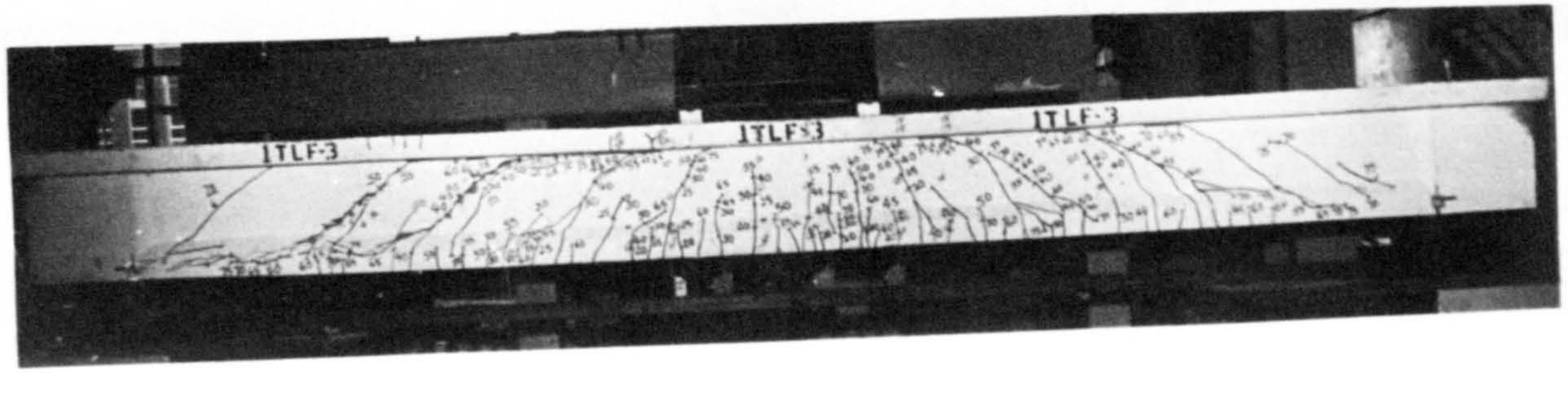

PLATE 6·4 Modes of failure of beams 1TLF-2 and 1TLF-3

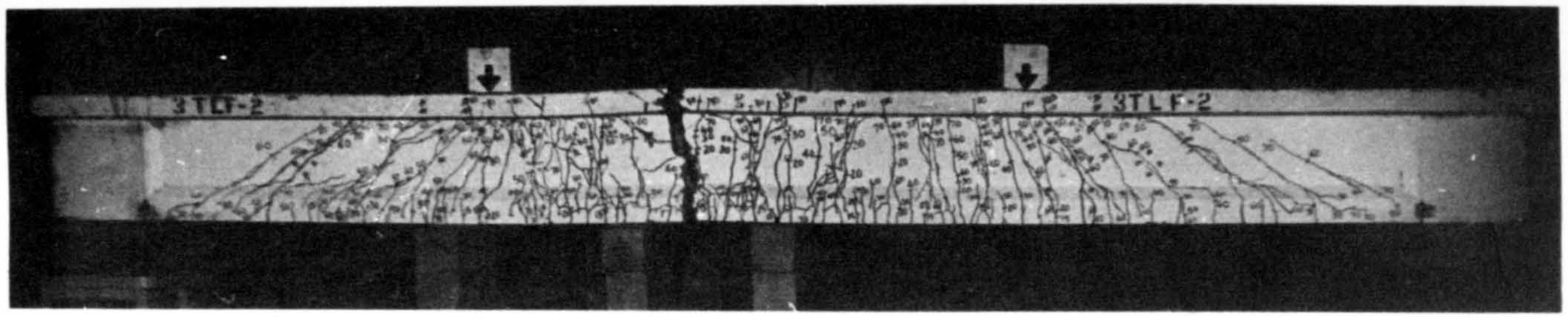

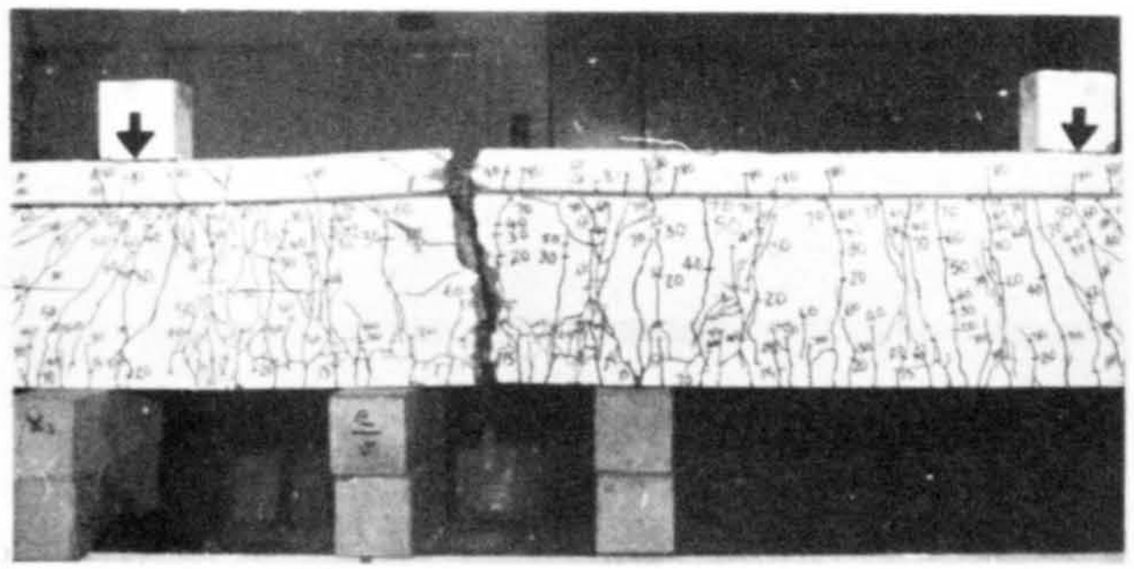

3TLF-2

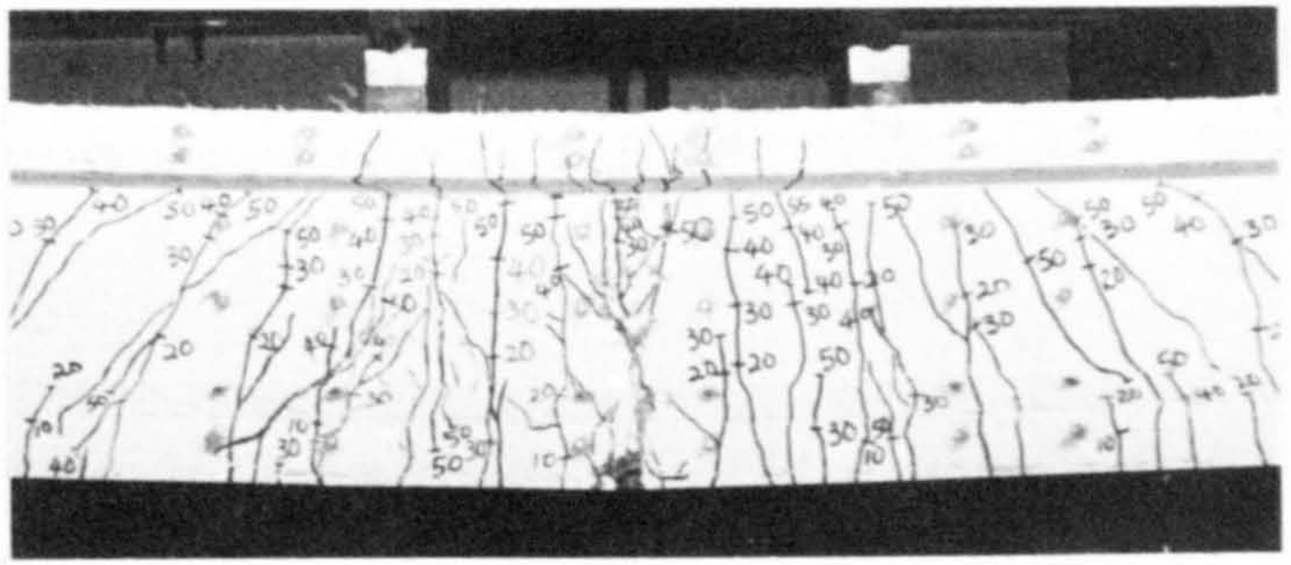

3TLF-3

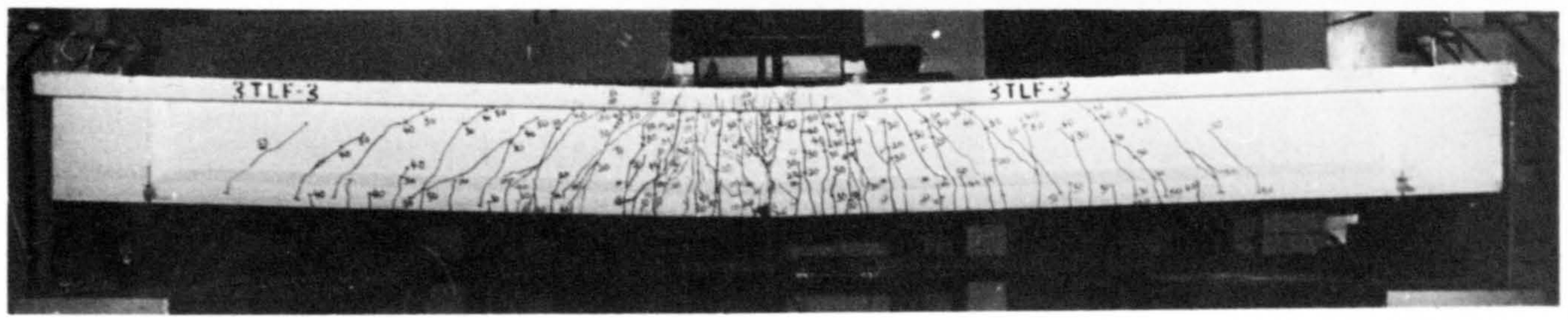

PLATE 6·5 Modes of failure of beams 3TLF-2 and 3TLF-3

Table 6.4 Test Results of Test Beams

Beam Number	Shear Force at V kN			Ult. Shear Stress v_u ($=V_u/b_w d$) N/mm^2	Mode of Failure
	1st Flex Crack	1st Shear Crack	Ultimate Load		
1TL-1	11.5	21.5	49.3	3.38	Shear
1TLF-1	11.5	36.5	80.3	5.51	Shear
1TL-2	5.3	15.5	19.0	1.30	Shear
1TLF-2	13.0	28.0	59.0	4.05	Shear
1TL-3	5.3	14.0	17.5	1.20	Shear
1TLF-3	10.3	21.5	42.5	2.92	Shear
2TL-1	9.0	19.0	36.5	2.50	Shear
2TLF-1	16.5	31.5	71.9	4.93	Shear
2TL-2	4.3	13.0	17.8	1.22	Shear
2TLF-2	8.0	20.5	45.6	3.13	Shear
2TL-3	4.0	12.8	15.5	1.06	Shear
2TLF-3	7.8	20.3	42.8	2.94	Shear-Flexure
3TL-1	9.0	19.0	31.5	2.16	Shear
3TLF-1	9.0	26.5	67.8	4.65	Shear-Flexure
3TL-2	5.5	14.3	15.0	1.03	Shear
3TLF-2	8.0	15.5	41.5	2.85	Flexure
3TL-3	4.0	14.0	15.1	1.04	Shear
3TLF-3	5.2	15.2	29.5	2.02	Flexure

NOTE: 1st flexural and shear cracks were detected visually.

The loads at first flexural and shear cracks were generally higher in the fibre concrete beams. This can be attributed to the higher tensile strength and the higher elastic modulus of fibre concrete.

The fibre concrete beams had more flexural and shear cracks at closer spacing than the plain concrete beams at ultimate load. The shear cracks also spread further towards the supports. In the case of the plain concrete beams having shear spans of 3.43 d and 4.91 d, a substantial portion of the beam at each end (well over half the shear span) remained free of any flexural or shear cracks. This clearly demonstrates the ability of steel fibres in mobilizing the tension zone to enable the beams to sustain higher loads.

In plain concrete beams, which had shear span of 3.43 d and 4.91 d, shear failure occurred generally soon after the appearance of web shear cracks. Final failure was characterized by tensile splitting along the level of the main reinforcement and simultaneous instability of the compression flange as the critical shear crack propagated to reach the soffit of the flange. This crack formed generally in the middle third of the shear span or slightly nearer the load point. It had an initial inclination of about 40^{o} - 45^{o} with the horizontal axis of the beam and this decreased to about 30^{o} before it reached the soffit of the compression flange.

For plain concrete beams having shear spans of 2.0 d, there was a substantial amount of shear resistance after the formation of the main shear cracks. The main shear crack formed in the middle third of the shear span and inclined at about 40^{o} to the horizontal axis of the beam. The crack propagated horizontally along the main steel towards the support and upwards

to the soffit of the compression flange then horizontally along the flange-web junction. At the same time progressive instability of the flange occurred and a vertical tension crack appeared at the top surface above the intersection of the shear crack with the soffit of the flange. Final failure was characterized by the destruction of the unstable portion of the compression flange and severe spalling where the shear crack met the main steel.

The fibre concrete beams with short shear spans all failed in shear though in the beam with the 1.55% of tension steel, shear failure occurred after the yielding of the main steel in the pure bending region. The mode of shear failure was basically similar to that of the corresponding plain concrete beams. However the steel fibres held the cracked compression flange in place and at failure reduced the spalling in the vicinity of the support.

Shear failures of the fibre concrete beams tested under high a_v/d ratios, generally involved more than one shear crack. These were generally at an inclination of about 45^o, and propagated upwards to the compression flange and then along the flange-web junction. Finally they triggered off instability of the portion of the flange above the horizontal part of the crack. Muhiddin(99) reported similar observations for fibre gravel concrete beams with thin web .

In beam 1TLF-2 (Plate 6.4), final failure occurred along an inclined crack running from the load point to the support and cutting across several active shear cracks. Splitting along the main steel was not significant. In beam 1TLF-3 (Plate 6.4), splitting along the main steel was substantial although the inclusion of steel fibres slowed down the propagation of the splitting cracks considerably. This was due to the

ability of steel fibres to hold the cracked concrete together around the main steel so that bond degeneration was delayed (see section 4.7.4.2). In beams 2TLF-2 (Plate 6.2) and 2TLF-3 (Plate 6.3) final failure was along an inclined crack running from the soffit of the compression flange below the flange tension cracks to the support. Splitting along the main steel again was not significant. Cracking along the tension flnage-web junction was readily seen in beam 2TLF-3. In addition, the main steel between the two point loads yielded before shear failure occurred.

The fibre concrete beams with 1.55% of tension steel and tested under high a_v/d ratios failed in flexural tension. See Plate 6.5. Some of the shear cracks in beam 3TLF-2 propagated some distance along the compression flange-web junction and multiple cracking especially at the main steel level was clearly evident in the pure bending region.

6.3.3 Ultimate Strength Characteristics

The ultimate shear strength and the ultimate shear stress of all the beams are summarized in Table 6.4. The ultimate shear strength was taken as the maximum shear force that the beams sustained and the ultimate shear stress was defined as the ultimate shear strength divided by $b_w d$, where b_w is the width of the web and d is the effective depth. The influence of steel fibres, amount of longitudinal steel and a_v/d ratio on the ultimate strength are discussed in the following sections.

6.3.3.1 Influence of Steel Fibres

Fig. 6.10 shows the influence of the inclusion of 1.0% of crimped steel fibres on the ultimate shear strength. The increase and percentage increase in ultimate shear strength of the fibre concrete beams over the corresponding plain concrete

beams are also shown on the same figure. It can be seen that the increase ranged from 1.72 to 2.75 N/mm^2 for beams failing in shear and shear-flexure and 0.98 to 1.82 N/mm^2 for beams failing in flexure. In terms of percentage increase, this increase ranged from 63.0 to 115.3% for beams with short shear spans, 143.3 to 211.5% for beams with larger shear spans and failing in shear or shear-flexure and 94.2 to 176.7% for beams failing in flexure.

6.3.3.2 Influence of a_v/d Ratio

The influence of a_v/d ratio on the ulitmate shear strength can be seen from Fig. 6.10.

As expected, both fibre and plain concrete beams with a_v/d ratio of 2.0 showed substantially higher shear strength and this can be attributed to arching action. For a_v/d equalled to or greater than 3.43, there was little difference in the ultimate shear strength for beams failing in shear or shear-flexure with the exception of beam 1TLF-2. The higher ultimate shear strength of beam 1TLF-2 was possibly due to the higher concrete strength (see Table 6.1) and a certain amount of arching action as the final failure plane was almost in the direction from the load point to the support (see Plate 6.4).

6.3.3.3 Influence of Main Steel

Fig. 6.11 shows the influence of percentage of main steel on the ultimate strength of both fibre and plain concrete beams. As can be seen from the figure, the influence of main steel was significant in beams with a_v/d ratio of 2.0. In these beams, the ultimate shear strength increased with increasing amount of main reinforcement. This increase was possibly due to the increasing contribution of dowel action of the main steel to

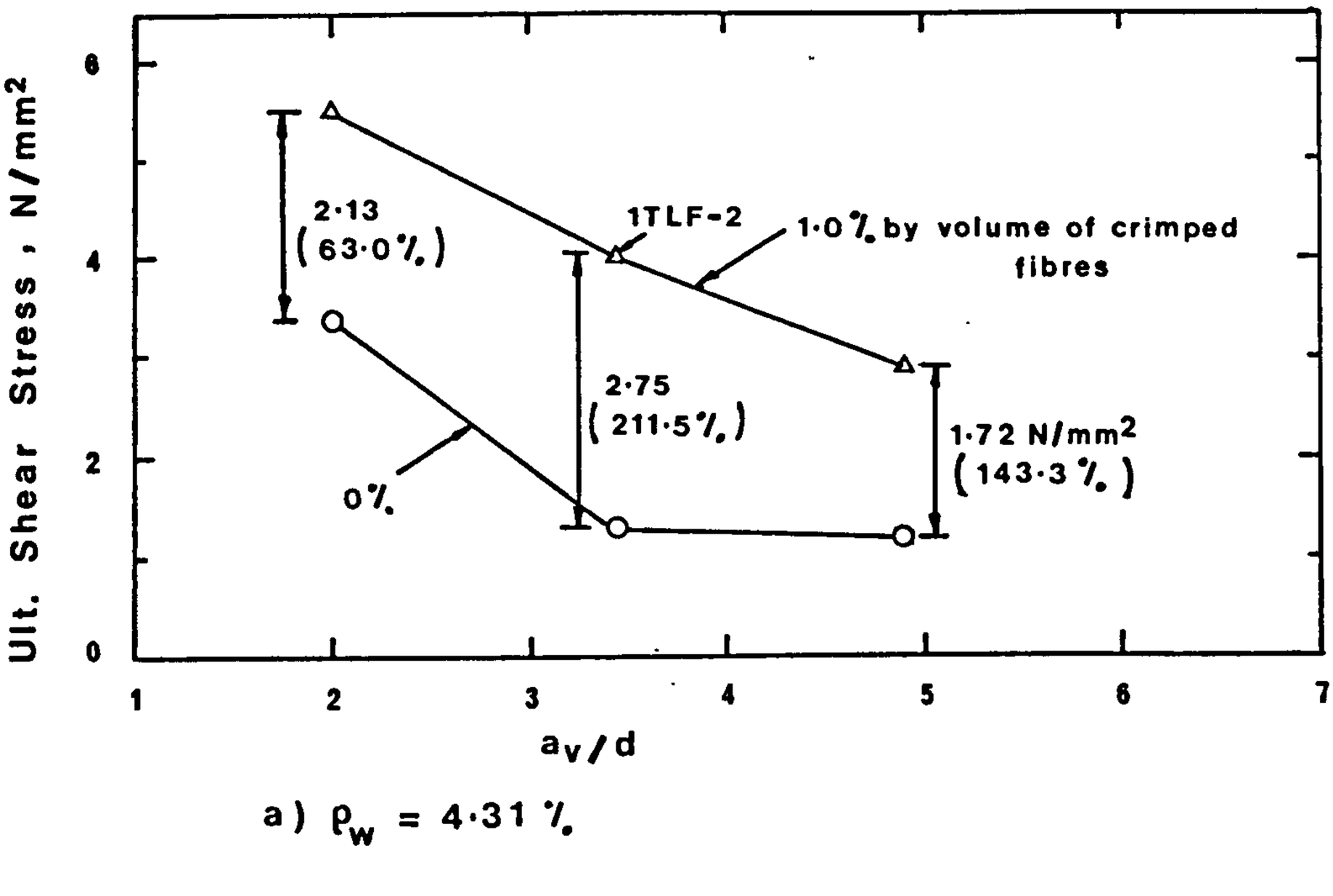

a) $\rho_w = 4{\cdot}31\ \%$

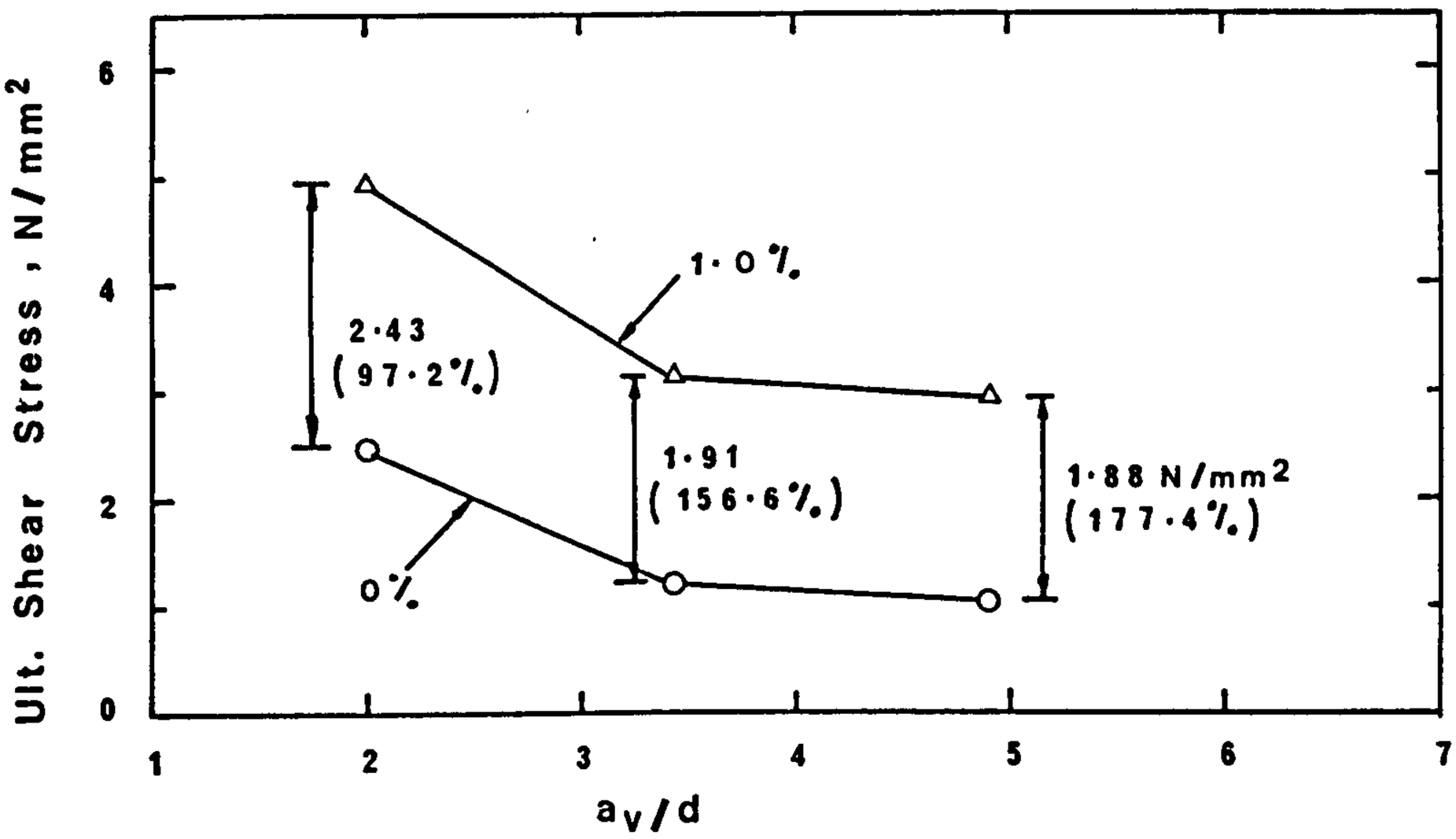

b) $\rho_w = 2{\cdot}76\ \%$

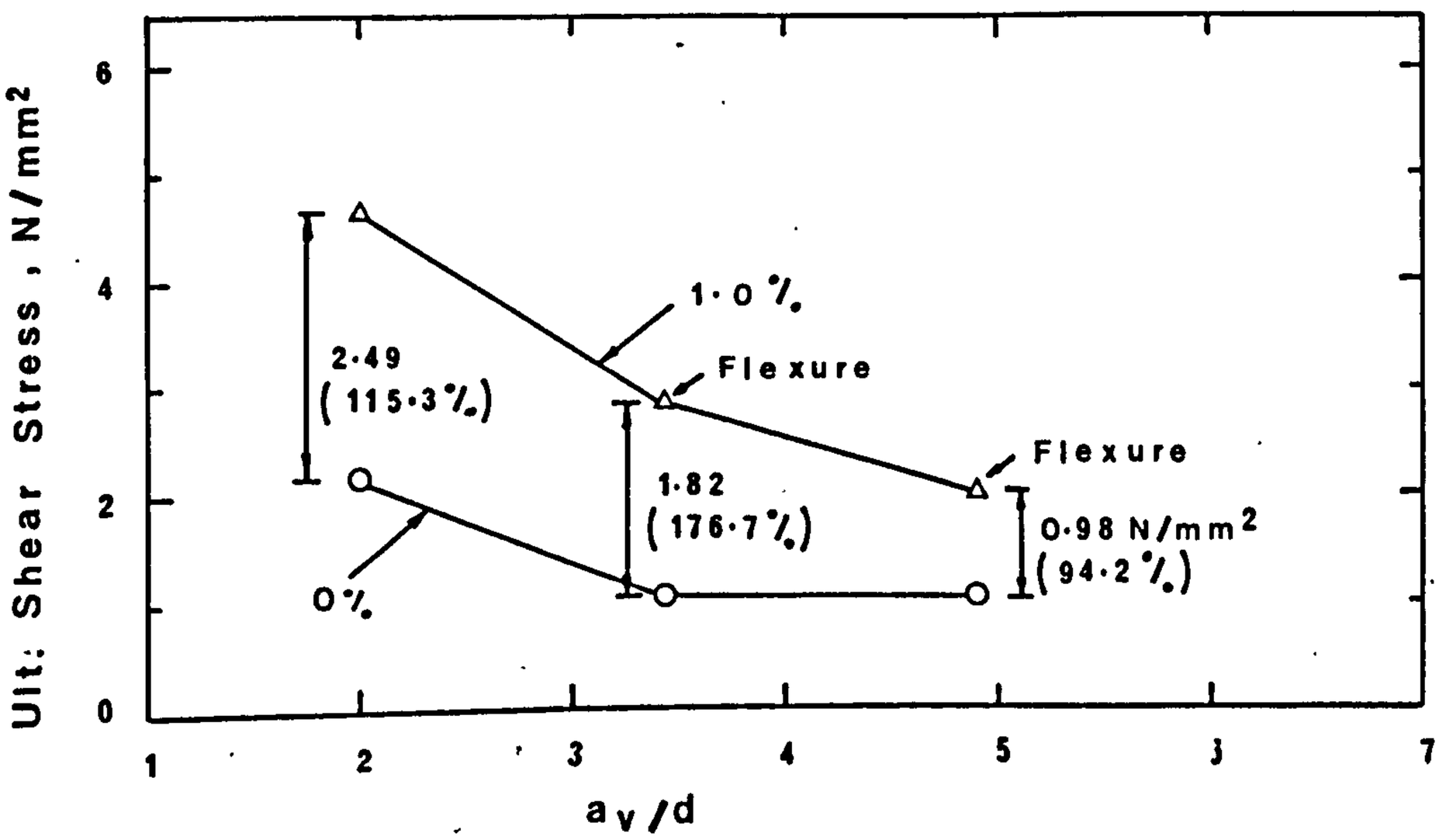

c) $\rho_w = 1{\cdot}55\ \%$

Fig·6·10 Influence Of Steel Fibres On Ultimate Shear Strength

shear resistance as the amount of main steel was increased.

For plain concrete beams with high a_v/d ratios, there was a slight increase in the ultimate shear strength with increasing amounts of main steel. The increase was marginally greater in beams with a_v/d ratio of 3.43 than those with a_v/d ratio of 4.91.

Excluding beam 1TLF-2, the influence of main steel on the ultimate strength of fibre concrete beams with high a_v/d ratios and failing in shear or shear-flexure seemed to be slight.

6.3.4 Comparison of Experiment Moment of Resistance with the Theoretical Flexural Capacity of Beams

The flexural capacity of all the beams was determined using CP110's (68) rectangular stress block for concrete in compression but with the average compressive stress taken as $0.6\ f_{cu}$ (i.e., $\gamma_m \times 0.4\ f_{cu}$) and the ultimate concrete compressive strain taken as 0.0035. The yield strength of the main steel used in the calculations was that given in Table 3.2 and the corresponding yield strain was read off from Fig. 3.3. The contribution of the steel fibres to the flexural capacity was neglected.

Table 6.5 compares the experimental moment of resistance with the flexural capacity of all the beams tested. The influence of steel fibres is self-evident from the table. The inclusion of 1% of steel crimped fibres by volume was sufficient to cause four of the beams to attain flexural capacity well beyond the theoretical value. This indicates the significant contribution of steel fibres to the flexural capacity of a beam.

Table 6.5 Comparison of Experimental Moment of Resistance With Flexural Capacity of Beams

Beam Number	Flexural Capacity M_F kN-m	Exp. Moment of Resist. M_{Exp} kN-m	$\frac{M_{Exp}}{M_F}$	Beam Number	Flexural Capacity M_F kN-m	Exp. Moment of Resist. M_{Exp} kN-m	$\frac{M_{Exp}}{M_F}$
1TL-1	70.62	26.13	0.37	1TLF-1	70.64	42.56	0.60
1TL-2	70.79	17.29	0.25	1TLF-2	71.31	53.69	0.75
1TL-3	70.41	22.75	0.32	1TLF-3	70.70	55.25	0.78
2TL-1	47.58	19.35	0.41	2TLF-1	47.64	38.11	0.80
2TL-2	47.36	16.20	0.34	2TLF-2	47.35	41.50	0.88
2TL-3	47.54	20.15	0.42	2TLF-3*	47.53	55.64	1.17
3TL-1	27.47	16.70	0.61	3TLF-1*	27.44	35.94	1.31
3TL-2	27.43	13.65	0.50	3TLF-2	27.41	37.77	1.38
3TL-3	27.40	19.63	0.72	3TLF-3	27.37	38.35	1.40

* Shear-Flexure Modes of Failure

6.4 Analytical Study of Ultimate Shear Strength of Test Beams

As a nonlinear 3-dimensional finite element anaylsis will be carried out later, it is considered adequate here just to analyse the beams using the various methods given in structural design codes or slightly modified versions of these methods.

6.4.1 Beams with No Shear Reinforcement

These beams were analysed using the methods given in CP110 (68), ACI-318-77 (101) and CEB-FIP Model Code (5).

Table 25 of CP110 gives the ultimate shear stress in lightweight aggregate concrete beams. The ultimate shear stress depends on the amount of tension reinforcement ρ_w and the grade of concrete. CP110 also stipulates that when the shear span a_v is less than 2.0d, the ultimate shear stress may be increased

by the factor $2d/a_v$.

ACI-318-77 gives two methods for calculating the design ultimate shear stress of lightweight aggregate concrete beams subject to shear and flexure only. These are:

(1) $$v_u = \frac{2f_{ct}}{6.7} \quad \text{(psi)} \qquad (6.1)$$

or $$v_u = 2K\sqrt{fc'} \quad \text{(psi)} \qquad (6.2)$$

where v_u = design ultimate shear stress in psi

f_{ct} = average splitting tensile strength in psi

fc' = cylinder compressive strength in psi

and K = constant, taking a value of 0.75 for "all lightweight concrete" and 0.85 for "sand-lightweight" concrete. Linear interpolation may be used when partial sand replacement is used.

(2) $$v_u = (1.9\frac{f_{ct}}{6.7} + 2500\rho_w \frac{Vd}{M}) \qquad (6.3)$$

or $$v_u = (1.9K\sqrt{fc'} + 2500\rho_w \frac{Vd}{M}) \qquad (6.4)$$

The quantity $\frac{Vd}{M}$ shall not be taken greater than 1.0 in computing v_u, where M is the moment occurring simultaneously with the shear force V at the section considered. v_u shall not exceed $3.5K\sqrt{fc'}$.

Equation (6.4) with K taken as 0.85 and fc' as 0.80 f_{cu} was adopted for the analysis of the test beams.

The CEB-FIP Model Code gives the following formula for calculating the design ultimate shear stress of lightweight aggregate concrete beams without significant longitudinal forces.

$$v_u = \tau_R(1 + 50\rho_w) \quad ; \qquad (6.5)$$

providing $\rho_w \nmid 0.02$

where τ_R depends on the concrete strength and is given in Table 6.6.

Table 6.6 Values of $\tau_R(5)$ in N/mm^2

fc'	12	16	20	25	30	35	40	45	50
τ_R	0.18	0.22	0.26	0.30	0.34	0.38	0.42	0.46	0.50

The design ultimate shear stress may be increased by the factor $2d/a_v$ for short shear spans where $a_v < 2d$. In the analysis fc' was taken to be $0.80\ f_{cu}$.

The design ultimate shear strength of the beams using the three codes is given in Table 6.7. The predicted failure shear strength was taken as the design ultimate shear strength multiplied by the appropriate safety factors of each of the codes. Finally Table 6.7 also gives the ratio of the predicted failure shear strength over the experimental failure shear strength using the three methods.

From Table 6.7, the following observations can be made:

(1) CEB-FIP Model Code generally gave marginally lower design ultimate shear strength and predicted failure shear strength than CP110. ACI-318-77 was less conservative with regards to the design ultimate shear strength but generally gave lower predicted failure shear strength when compared to the other two codes. ACI-318-77 uses a lower safety factor.

(2) For the beams with shear spans greater than or equal to 3.43d, the three codes all predicted the failure shear strength reasonably well. However, they all grossly underestimated the shear strength of the beams with shear spans of 2.0d. This underestimation was 64.3 to 65.9% for beams with 4.31% of tension steel and 50.8 to 55.9% for beams with

Table 6.7 Comparison of Codes' Design Ultimate and Predicted Failure Shear Strength (in kN) With Experimental Failure Shear Strength of Lytag-sand Concrete Beams

Beam Number	(1)	(2)	(3)	(4)	(5)	(6)	(7)			
	Exp.	CP110	ACI	CEB	CP110 x γ_m*	ACI x $\frac{1}{\gamma}$**	CEB x γ_m*	$\frac{(5)}{(1)}$	$\frac{(6)}{(1)}$	$\frac{(7)}{(1)}$
1TL-1	49.3	11.7	**14.5**	11.2	17.6	**17.1**	16.8	0.36	**0.35**	0.34
1TL-2	19.0	11.7	**12.3**	10.8	17.6	**14.5**	16.2	0.93	**0.77**	0.85
1TL-3	17.5	11.7	**11.6**	10.9	17.6	**13.6**	16.4	1.01	**0.78**	0.94
2TL-1	36.5	11.5	**13.0**	11.4	17.3	**15.3**	17.2	0.47	**0.42**	0.47
2TL-2	17.8	11.5	**11.6**	10.7	17.3	**13.6**	16.1	0.97	**0.77**	0.91
2TL-3	15.5	11.5	**11.2**	11.3	17.3	**13.2**	17.0	1.12	**0.85**	1.10
3TL-1	31.5	10.1	**11.8**	10.3	15.1	**13.9**	15.5	0.48	**0.44**	0.49
3TL-2	15.0	10.1	**10.5**	9.4	15.1	**12.3**	14.1	1.01	**0.82**	0.94
3TL-3	15.1	10.1	**10.4**	9.6	15.1	**12.2**	14.4	1.00	**0.81**	0.95
						Mean†		1.01	**0.80**	0.95
						Standard Deviation†		0.06	**0.03**	0.08

* γ_m = 1.5 ** γ = 0.85

† Excluding beamswith a/d = 2.0

1.55% of tension steel.

(3) None of the design ultimate shear strength exceeded the experimental failure shear strength.

It may be concluded that the three codes predict reasonably the failure shear strength of Lytag-sand concrete beams with no shear reinforcement for high $\frac{a_v}{d}$ ratios. They also give safe design ultimate shear strength for Lytag-sand concrete beams with no shear reinforcement although ACI-318-77 is the least conservative.

6.4.2 Fibre Concrete Beams Failing in Shear

A simple method based on the Standard Method of CEB-FIP Model Code (5) is hereby proposed for the analysis of these beams.

The reasoning behind the Standard Method is explained in depth in a paper by Leonhardt (100). It is based on a truss model with variable inclination of compression chord and of compression diagonals or struts. See Fig. 6.12. Basically the shear resistance consists of the components V_w and V_c. V_w is the contribution to shear from the shear reinforcement based on strut inclinations of 45^o in the web. V_w is given by the formula (5)

$$V_w = \frac{A_{sv}}{s} \; 0.9d \; f_y \; (1 + \cot\alpha) \sin \alpha \qquad (6.6)$$

where A_{sv} = area of shear reinforcement within a distance s

s = spacing of shear reinforcement in the direction parallel to longitudinal reinforcement

f_y = yield strength of shear reinforcement

and α = angle between inclined stirrups and longitudinal axis of member.

The Component V_c is the shear contribution from the inclined compression chord and also takes into account the reduction in tension forces in the web due to strut-inclinations

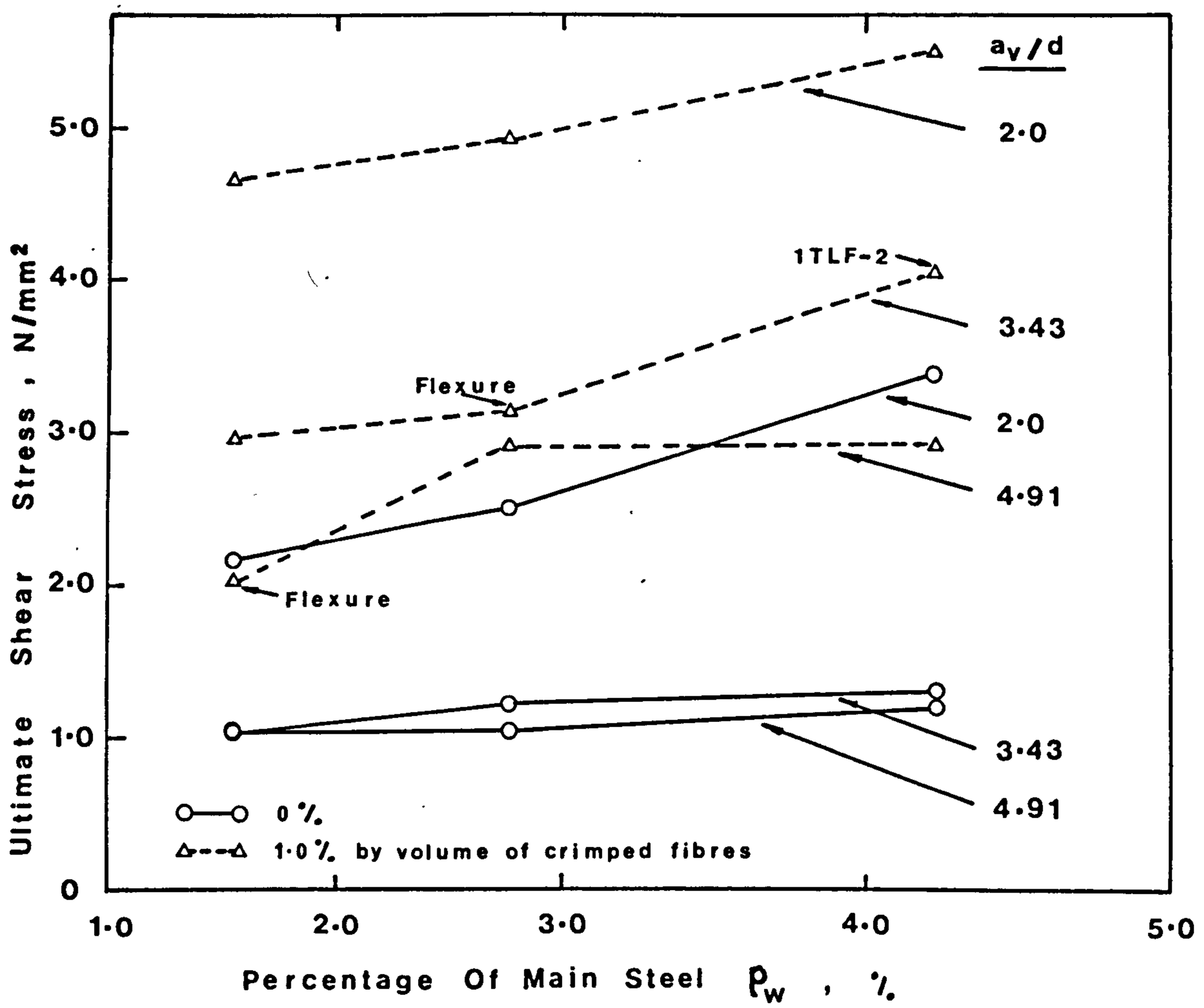

Fig. 6·11 Influence Of Percentage Of Main Steel On Ultimate Shear Strength

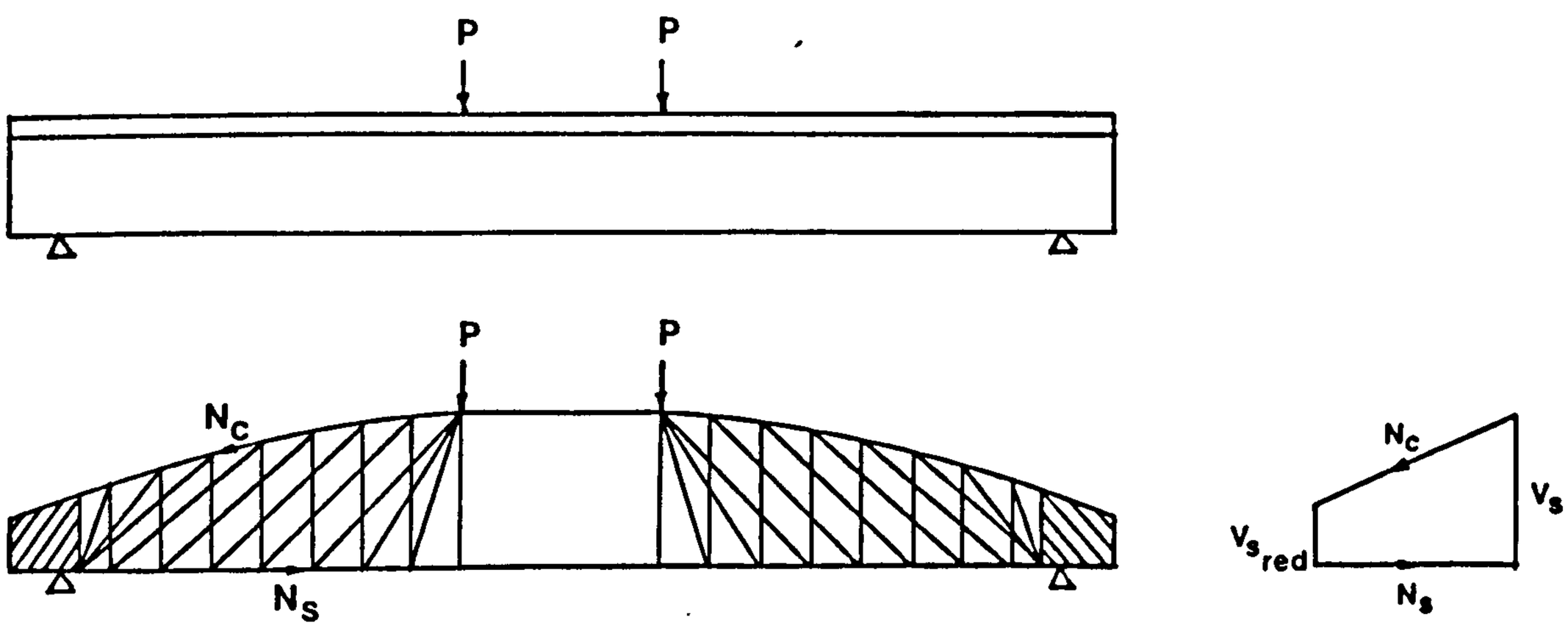

$V_{s_{red}}$ = shear in web members

Fig. 6·12 Generalised Truss Model With Variable Inclination Of Compression Chord And Of Struts(after Leonhardt (100))

smaller than 45^{o}. V_c is given by the formula (5):

$$V_c = 2.5\ \tau_R\ b_w\ d \qquad (6.7)$$

where τ_R is given in Table 6.6 above. For short spans, V_c may be increased by the factor $\frac{2d}{a_v}$.

The design ultimate shear force must not exceed $0.2fc'\ b_w\ d$ (5) with b_w taken as $(b_w - \frac{1}{2}\Sigma\phi)$ if the bar diameter $\phi > \frac{b_w}{8}$. This is to limit the compression in the inclined struts.

The experimental observations (see sections 6.3.1.3 and 6.3.2) seem to suggest that the above truss model can still be applied to fibre concrete beams with large shear spans.

V_c has been found to depend almost linearly on the compressive strength fc' of the concrete (100). However, in the design equation (6.7), V_c is related to the $^{2}/3$ power of the compressive strength as a matter of caution (100). Since the addition of steel fibres has little effect on the compressive strength of concrete, equation (6.7) is assumed to apply also to fibre concrete. The limit on the compression of the inclined struts as given above also still applies.

The problem now is to quantify the contribution of steel fibres to shear after the formation of the shear cracks. As in the case of conventional stirrups, this can be approximated by assuming strut inclinations of 45^{o} in the web. From Fig. 6.13, the design ultimate shear contribution of steel fibres, V_w, can be shown to be given by

$$V_w = 0.9\ \frac{\sigma_{cu}}{\gamma_m}\ b_w\ d \qquad (6.8)$$

where σ_{cu} = post-cracking tensile strength of fibre concrete

and γ_m = material safety factor (taken as 1.5)

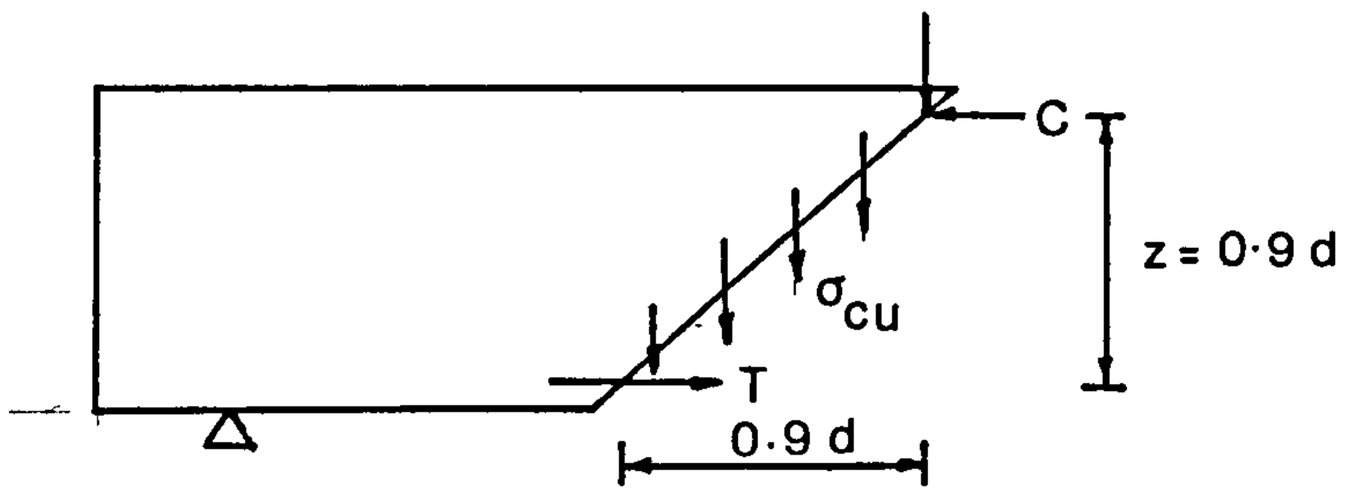

Fig. 6.13 Contribution of Steel Fibres to Shear

The post-cracking tensile strength may be calculated using the method given in Appendix A.

The shear failure loads of fibre concrete beams may be predicted using equations (6.7) and (6.8) with the safety factors removed as:

$$V_u = V_w + V_c \nmid 0.3\ fc'\ b_w\ d \qquad (6.9)$$

$$V_w = 0.9\ \sigma_{cu}\ b_w\ d \qquad (6.10)$$

$$V_c = 3.75\ \tau_R\ b_w\ d \qquad (6.11)$$

Table 6.8 compares the predicted failure shear strength and the experimental failure shear strength of all the fibre concrete beams. The post-cracking tensile stress of the fibre concrete beams was determined as shown in Appendix A using an average bond strength between the crimped fibres and Lytag-sand concrete of 4.04 N/mm^2 as determined in section 3.3.5.4. There is experimental evidence to suggest that the cylinder/cube strength ratio of fibre concrete is slightly higher than that of plain concrete. Al-Noori (88) reported an increase of 5.3% in the cylinder/cube strength with the inclusion of steel fibres.

By applying this increase of 5.3% to the cylinder/cube strength ratio 0.80 generally adopted for plain concrete, the resulting ratio for fibre concrete is 0.84. In the analysis, fc' was taken as 0.85 f_{cu} for fibre concrete.

It can be seen that the proposed method adequately predicted the failure shear strength of fibre reinforced Lytag-sand concrete beams with shear spans greater than or equal to 3.43 d but it underestimated the shear strength of fibre concrete beams with short shear spans by 35.4 - 45.6%

6.5 Application of Proposed Method of Analysis to Other Investigators' Test Results

To date, all reported experimental investigations on the use of steel fibres as shear reinforcement were carried out using normal weight reinforced concrete or mortar beams. The proposed method of analysis is still valid for such beams. However, the maximum allowable design ultimate shear strength of normal weight concretebeams can be increased to 0.30 fc' b_w d (5).

Thus the failure shear strength of fibre reinforced normal weight concrete beams may be predicted using:

$$V_u = V_w + V_d \nmid 0.45\ fc'\ b_w\ d \qquad (6.12)$$

$$V_w = 0.9\ \sigma_{cu}\ b_w\ d \qquad (6.10)$$

$$V_c = 3.75\ \tau_R\ b_w\ d \qquad (6.11)$$

6.5.1 Bahia's Test Results (6)

The comparison of the predicted and the actual failure shear strength of the T-beams is shown in Table 6.8.

The fibre type used was crimped steel. The average interfacial bond stress between the steel fibre and concrete (τ)

was determined from the flexural tensile strength of the control specimens using the approach given in section 3.3.5.4. It was found to be 5.12 N/mm^2. The post-cracking tensile strength σ_{cu} was determined using the approach shown in Appendix A.

With the exception of beam B54, the correlation between the predicted and experimental ultimate shear strength was satisfactory. The overestimation of the shear strength of beam B54 can be attributed to fibre balling with high percentage by volume of steel fibres.

6.5.2 Muhidin and Regan's Test Results (31)

The comparison of the predicted and the experimental failure shear strength of the I-beams is shown in Table 6.8. Duoform steel fibres were used in the investigation. Unfortunately, the flexural tensile strength was not given and hence the average interfacial shear stress between the steel fibre and concrete (τ) had to be approximated. Swamy and Mangat (20) have proposed a value of 4.15 N/mm^2 for plain steel fibres. The surface deformations of duoform fibres improve the bonding with the surrounding concrete. Therefore, a bond efficiency factor of 1.2 was applied to the basic value of 4.15 N/mm^2. Thus τ was taken as 4.98 N/mm^2 for duoform fibres. The post-cracking tensile strength of the fibre concrete σ_{cu} was then determined using the method given in Appendix A.

As evident from the table, the correlation between the predicted and experimental failure loads was satisfactory for fibre percentages by volume less than or equal to 1.5. For higher percentages, the proposed method generally overestimated the ultimate shear strength. Muhidin and Regan admitted that the practical fibre content was about 1.5% by volume (102).

Table 6.8 Comparison of Experimental and Predicted Ultimate Shear Strength of Fibre Concrete Beams Failing in Shear

Investigators	Beam No	Concrete Type	Fibre Type	$\frac{l_f}{d_f}$	% Fibre Volume	f_{cu} N/mm^2	σ_{cu} N/mm^2	V_w kN	V_c kN	$V_w + V_c$ kN	V_{Exp} kN	$\frac{V_w + V_c}{V_{Exp}}$
Author's	1TLF-1	Lytag-sand	Crimped	100	1.0	44.5	1.65	21.7	22.0	43.7	80.3	0.55
	1TLF-2			100	1.0	51.1	1.65	21.7	24.6	46.3	59.0	0.79
	1TLF-3			100	1.0	42.6	1.65	21.7	22.2	43.9	42.5	1.03
	2TLF-1			100	1.0	47.2	1.65	21.7	23.0	44.7	71.9	0.62
	2TLF-2			100	1.0	41.4	1.65	21.7	20.8	42.5	45.6	0.93
	2TLF-3			100	1.0	44.9	1.65	21.7	22.2	43.9	42.5	1.03
	3TLF-1			100	1.0	44.6	1.65	21.7	22.1	43.8	67.8	0.65
	* Excluding beams with a/d = 2.0									Mean*		0.95
										Standard Deviation*		0.11
Bahia's	B52	Gravel	Crimped	100	0.4	44.4	0.84	27.8	55.4	83.2	79.5	1.05
	B53			100	0.8	46.8	1.68	55.6	57.9	113.5	114.0	0.99
	B54			100	1.2	49.8	2.52	85.3	60.6	143.9	115.0	1.25
	B55			100	0.8	47.7	1.68	55.6	58.5	114.1	118.2	0.97
										Mean		1.07
										Standard Deviation		0.13

Investigators	Beam No	Concrete Type	Fibre Type	$\frac{l_f}{d_f}$	% Fibre Volume	f_{cu} N/mm^2	σ_{cu} N/mm^2	V_w kN	V_c kN	$V_w + V_c$ kN	V_{Exp} kN	$\frac{V_w + V_c}{V_{Exp}}$
Muhidin and Regan's	TF1	Gravel	Duoform	93.8	2.13	45.7	4.08	60.6	25.4	86.0	71.3	1.21
	TF2			62.5	2.25	49.8	2.87	42.6	27.2	69.8	81.0	0.86
	TF3			62.5	0.75	66.1	0.96	14.3	30.9	45.2	64.5	0.71
	TF4			62.5	1.50	54.1	1.91	28.4	29.1	57.5	61.0	0.94
	TF5			62.5	3.0	52.5	3.83	56.9	28.3	85.2	78.9	1.08
	TF6			80	2.25	42.5	3.67	54.5	24.0	78.5	59.6	1.32
	TF7			93.8	2.25	42.3	4.30	63.8	24.0	87.8	76.4	1.15
	TF8			80	1.50	52.2	2.45	35.4	27.9	64.3	65.0	0.99
	TF9			80	1.50	24.3	2.45	36.4	16.7	53.1	55.0	0.97
	TF10			80	1.50	76.3	2.45	36.4	30.9	67.3	69.5	0.97
	TF11			80	1.50	55.0	2.45	50.9	41.1	92.0	93.8	0.98
	TF12			80	1.50	55.0	2.45	21.8	17.6	39.4	55.4	0.71
	TFL1			80	1.50	61.1	2.45	35.3	30.0	65.3	62.4	1.05
	TFL2			80	1.50	49.0	2.45	40.8	30.1	70.9	81.4	0.87
	TFL3			80	0.30	49.1	0.49	7.1	26.0	33.1	36.9	0.90
	TFL4			80	0.75	42.1	1.22	17.6	23.2	40.8	45.0	0.91
	TFL5			80	1.13	52.8	1.84	26.5	27.6	54.1	57.4	0.94
	TFL6			80	2.25	54.1	3.67	52.8	28.1	80.9	60.6	1.35
	** Excluding beams with fibre content greater than 1.5% by volume									Mean**		0.91
										Standard Deviation**		0.11
LaFrauge et al's	1	Gravel	Plain	62.5	1.0	48.6	1.06	72.7	123.0	195.7	215.8	0.91
	2			100	1.0	57.6	1.70	116.6	140.5	257.1	191.4	1.34

6.5.3 LaFraugh and Moustafa's Test Results (30)

The fibre type used was plain wire. The interfacial shear stress between the fibre and concrete was taken as 4.15 N/mm^2. The comparison between the predicted and experimental failure shear strength of the T-beams is shown in Table 6.8.

6.6 Conclusions

1. The addition of 1% by volume of crimped steel fibres to Lytag-sand concrete beams without conventional shear reinforcement decreased the deflection, concrete strain at midspans, tension steel strains and end rotations at all stress levels. In all cases the reductions were small initially and were more pronounced after the formation of cracks.

2. The fibre concrete beams were more ductile and at failure, exhibited substantially greater deflection, concrete strain at midspan, tension steel strains and end rotations than their plain concrete counterparts.

3. None of the fibre concrete beams showed deflection (excluding deflection due to shrinkage and creep) at working load level greater than the CP110 limit of span/250 for final deflection.

4. The loads at first flexural and shear cracks were generally higher in the fibre concrete beams. The fibre concrete beams had more flexural and shear cracks and the latter were spread further towards the supports than in the corresponding plain concrete beams at failure.

5. Shear failure of plain concrete beams with large shear

spans generally occurred soon after the formation of the web shear cracks. Failure was by tensile splitting along the level of the main reinforcement and simultaneously instability of the compression flange above the shear crack.

6. Shear failure of fibre concrete beams with long shear spans involved the widening of more than one shear crack. The steel fibres slowed down the propagation of the shear cracks and final failure was triggered off by the instability of the compression zone above the active shear cracks.

7. The inclusion of steel fibres was generally sufficient to prevent significant tensile splitting along the level of the main reinforcement and when it did occur, the steel fibres were able to slow down its propagation considerably.

8. Both plain and fibre concrete beams with short shear spans showed more or less the same mode of shear failure. In the case where fibres were used however these held the cracked compression flange in place and reduced the spalling in the vicinity of the support as the failure load was approached.

9. The inclusion of 1% of crimped steel fibes by volume caused an increase in the ultimate strength ranging from 63 to 211.5% depending on the shear spans and modes of failure of the fibre concrete beams.

10. The influence of the amount of main steel on the ultimate shear strength was most important in beams with shear spans of 2.0 d. In these beams the ultimate shear strength increased with increasing amount of main reinforcement.

11. The methods given in CP110, ACI-318-77 and CEB-FIP Model Code

predicted the failure loads of the Lytag-sand concrete beams with no shear reinforcement with reasonable accuracy. However, they underestimated the shear strength of those beams with short shear spans by 50.8 - 65.9%. The various methods gave safe design ultimate shear strength for Lytag-sand concrete beams with no shear reinforcement although ACI-318-77 was less conservative than the other two codes.

12. The proposed method based on the Standard Method of CEB-FIP Model Code predicted ultimate shear strength of crimped steel fibre reinforced Lytag-sand concrete beams with large shear spans with adequate accuracy. The shear strength of beams with short shear spans were underestimated by 35.4 - 45.6%

    It predicted adequately the ultimate shear strength of steel fibre reinforced normal weight concrete beams.

CHAPTER SEVEN

FINITE ELEMENT MODEL

7.1 Introduction

The finite element method has undoubtedly become the most powerful tool of analysis and is applicable to a wide range of problems. It is an extension of the stiffness or displacement method of structural analysis and is essentially a product of the electronic digital computer age. A basic and practical introduction to the finite element method can be found in the text by Cheung and Yeo (103) and a more advanced and extensive coverage can be found in the texts by Zienkiewicz (104) and Desai and Abel (105).

Although it was developed primarily for the aircraft industry in the late fifties, its application rapidly extended to civil engineering problems. However, its use in the behaviour study of reinforced concrete is comparatively recent and was initiated by Ngo and Scordelis (106) about fifteen years ago. Since then finite element analysis of reinforced or prestressed concrete structures has been extensive and this has resulted in several state-of-the-art papers (107, 108, 109).

The scope of this analytical study was to develop a finite element model for plain and fibre reinforced concrete and to compare this model with the test results reported in Chapter 6 and those reported by Bahia (6). A three dimensional model was used as all practical cases of the structural systems are in reality three dimensional problems. Specifically, a flanged beam cannot be idealized as a planar structure.

7.2 Finite Element Approximations

Essentially there are three different models that are used to describe reinforced concrete (108). The first considers the components of concrete and steel reinforcement separately

using different elements. The steel reinforcement elements are connected to the concrete elements at the nodal points. Bond between both materials may be regarded as rigid or may be simulated by bond linkage elements. See Fig. 7.1a.

The discrete element model with and without bond linkage element has been used extensively in 2-dimensional anaysis of reinforced concrete beams (e.g. 106, 52, 110, 111, 112, 113). Hammad (51) adopted this model and assumed perfect bonding between steel and concrete in a 3-dimensional finite element study of the shear resistance of reinforced concrete T-beams.

The second model integrates concrete and steel into a single element with separate stress-strain relationships for concrete and steel reinforcement. This is achieved by one of the following ways (see Fig. 7.1b):

(1) A composite material matrix [D] is constructed by an appropriate combination of the material matrix of the reinforcement $[D_s]$ and that of the concrete $[D_c]$. This in effect smears the steel reinforcement through the 'parent' concrete element. Cervenka (114) studied the in-plane response of wall panels using this approach. Suidan and Schnobrich (115) also adopted this approach in a study of the behaviour of cracked beams.

(2) The stiffness matrix of the steel reinforcement and that of the 'parent' concrete element are determined separately. The stiffness matrix of the reinforced concrete element is then obtained by adding up the stiffness matrix of each material component. Sorensen (116) and Zienkiewicz et al (117, 118) applied this approach.

A third model considers reinforced concrete as a homogeneous

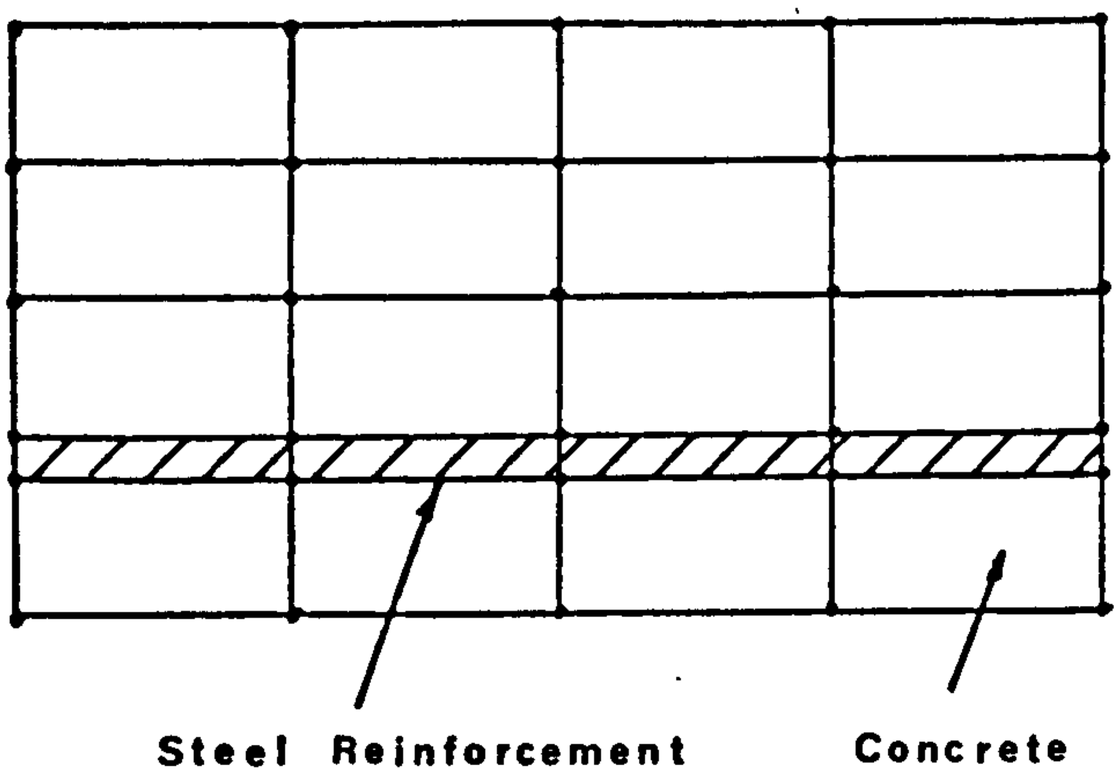

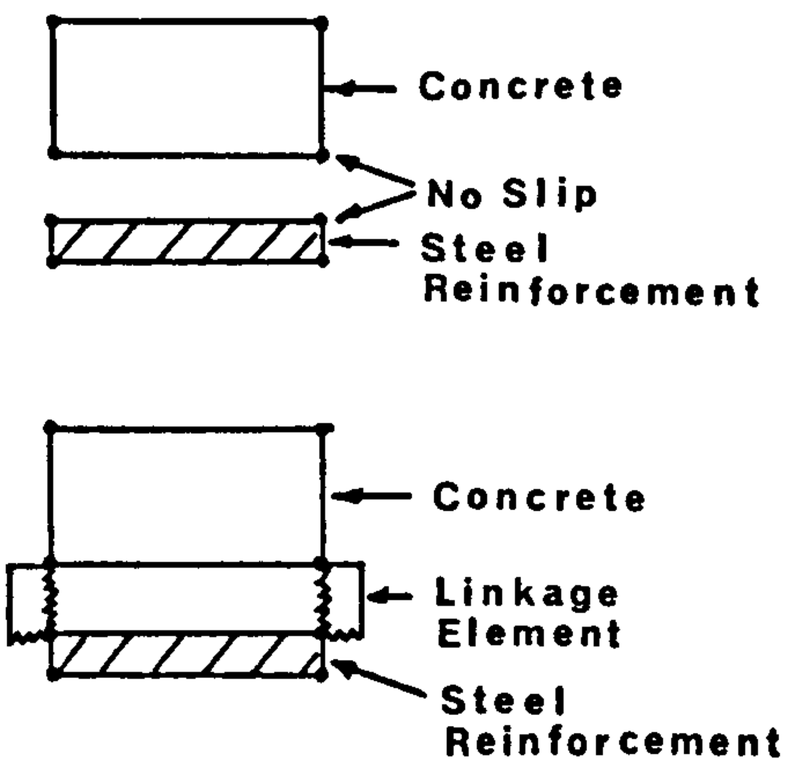

a) Concrete And Steel Using Different Elements

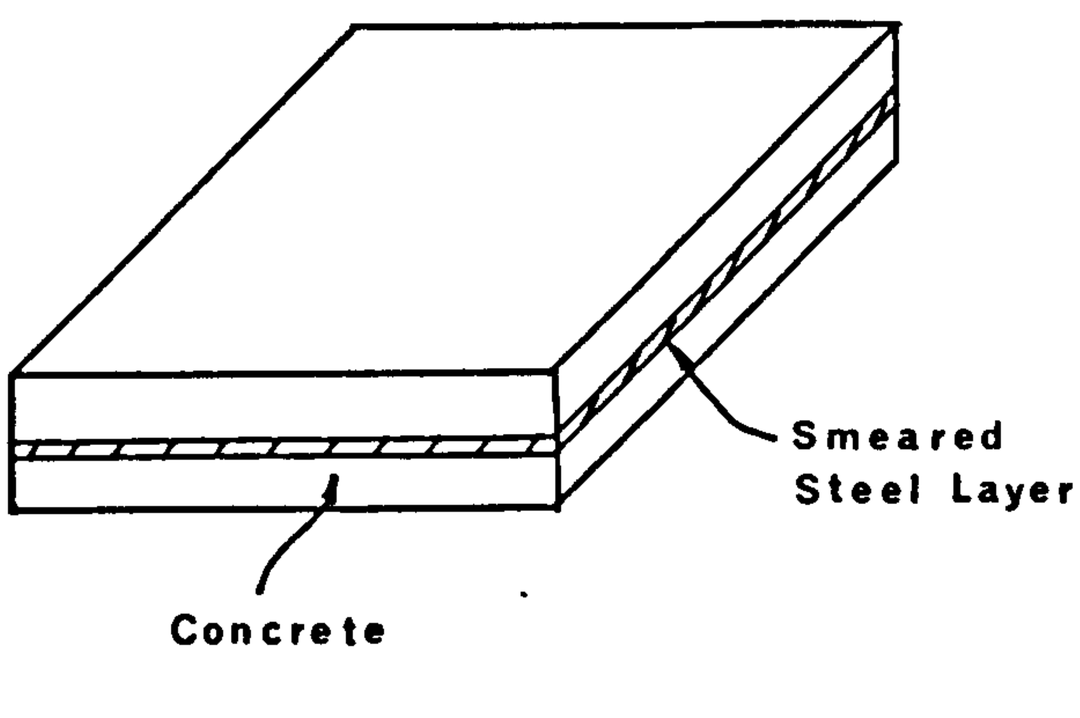

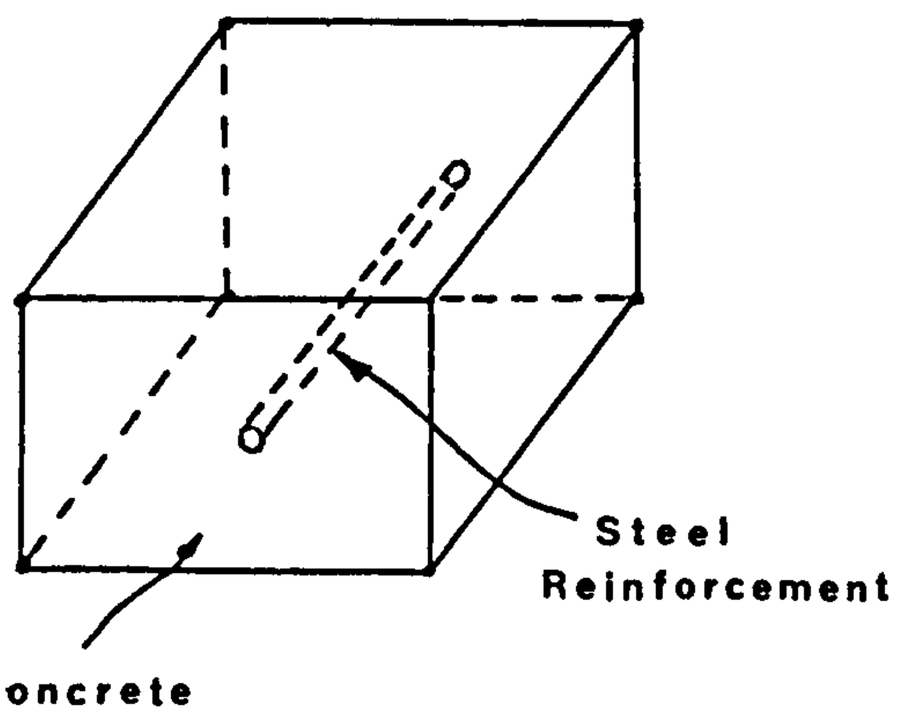

b) Concrete And Steel In One Element

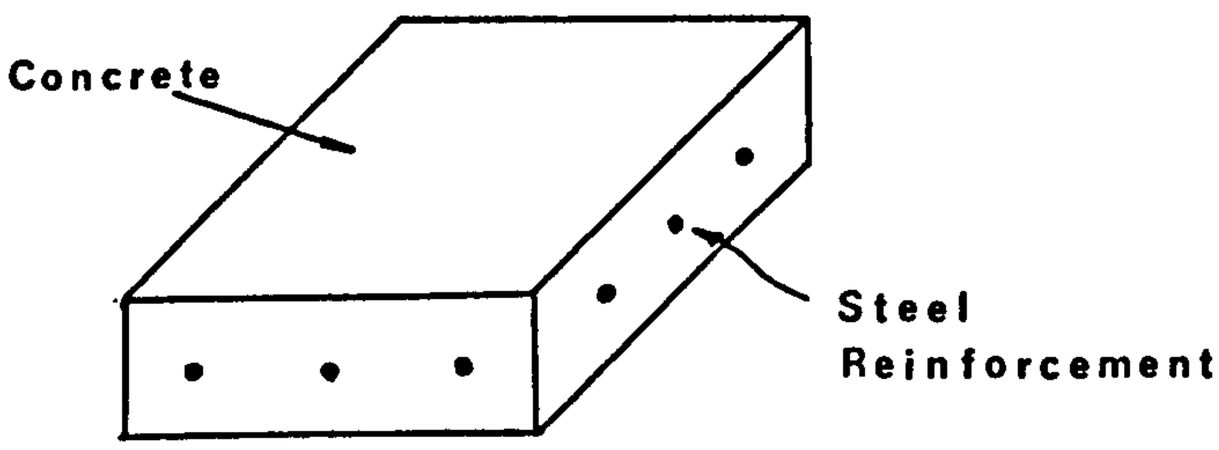

c) Reinforced Concrete With One Single Constitutive Law

Fig. 7-1 Reinforced Concrete Models

material with a single constitutive law. See Fig. 7.1c. Isenberg et al (119, 120) derived a single stress-strain relationship for reinforced concrete. Bond slip and dowel shear relations were incorporated into the model. The model is applicable to beams, beam columns and ring beams subjected to static and dynamic loading. Jofriet and McNiece (121) used a bilinear moment-curvature relation to study plate bending problems.

In the present study, the second model similar to that used by Sorensen and Ziekiewicz et al is adopted because of its flexibility for different arrangements of the reinforcement and its computational simplicity.

7.2.1 Three Dimensional Concrete Elements

7.2.1.1 General

The first major application of finite element in three dimensional stress analysis made use of simple tetrahedral and the refined ten node tetrahedral elements (122, 123). Such types of elements present difficulties of visualization and could easily lead to errors in inputing data and interpreting output results.

A significant advancement in three dimensional finite element analysis was achieved with the introduction of the isoparametric hexahedral elements by Ziekiewicz and his co-workers (104, 123, 124). The superiority of the isoparametric hexahedral elements over the tetrahedral elements in elastic solid analysis was demonstrated by Clough (125). He also recommended the simplest of the isoparametric hexahedra, i.e., the 8-node element with nodal points only at the corners for analysis of general elastic solids with flat surfaces. The superiority of the isoparametric elements in elastic-plastic analysis of two and three dimensional structures was pointed out by Nayak (126).

In the finite element analysis of reinforced concrete structures, Suidan and Schobrich (115) and Hammad (51) used the 20-node isoparametric hexahedron while Sorensen (116) adopted the 8-node isoparametric hexahedron.

The 8-node isoparametric hexahedron has been adopted in the present study.

7.2.1.2 Formulation of Element Stiffness Matrix $[K_e]$

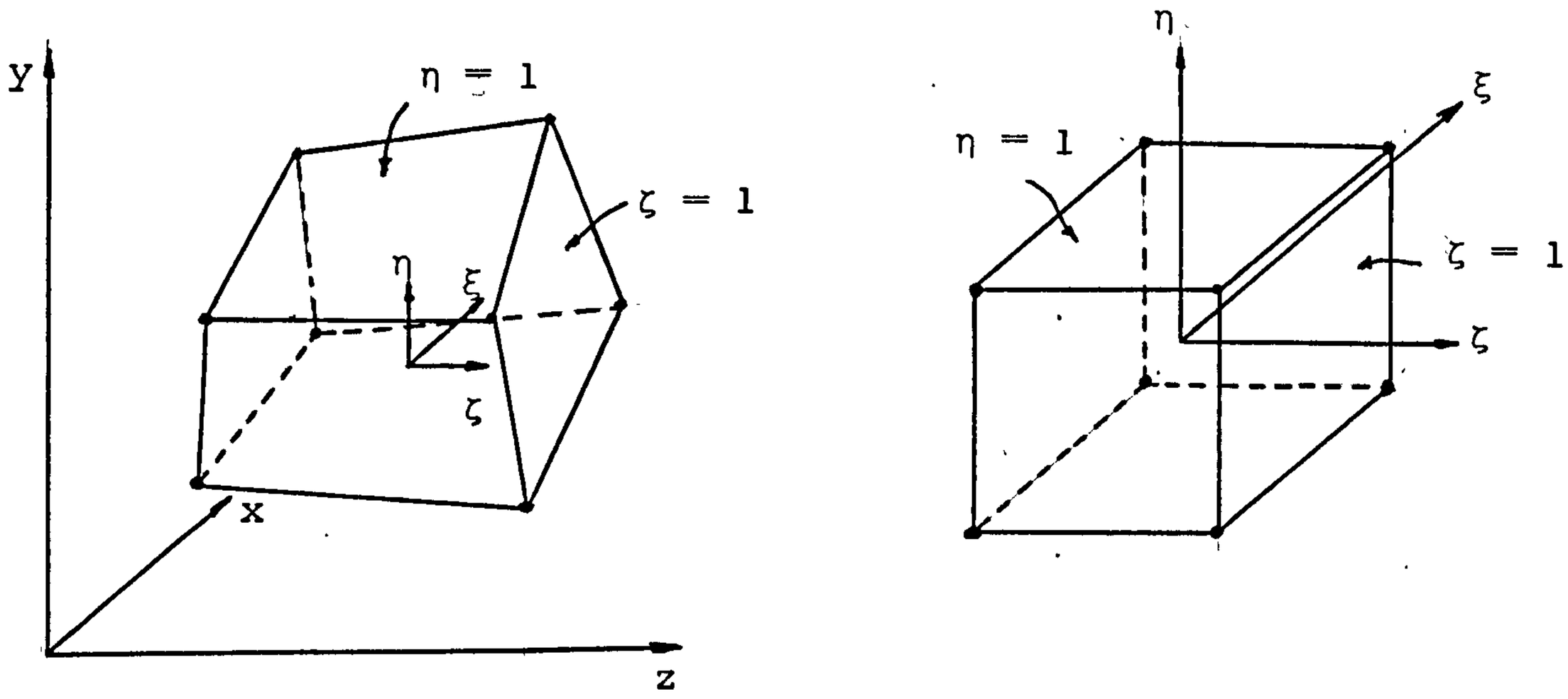

(a) Cartesian Co-ordinates (b) Local Co-ordinates

Fig. 7.2 8-node Isoparametric Hexahedron

The 8-node isoparametric hexahedron is shown in Fig. 7.2 in both local (ξ, η, ζ) and global cartesian (x, y, z) co-ordinate systems. The local co-ordinate system is arranged so that each of the axes is associated with a pair of opposing faces having co-ordinates of $\pm$ 1. Thus in the local co-ordinate system, the element is a cube. The element has 24 translational degrees of freedom, three at each nodal point.

The interpolation functions or shape functions (N_i) for the geometry and the internal displacement field of this element are given in Appendix B. The strain matrix [B] relates the strains to the nodal displacements and its derivation is also given in Appendix B.

The stiffness of the element can be derived using the equation (103, 104, 105):

$$[K_e] = \int_{-1}^{1} \int_{-1}^{1} \int_{-1}^{1} [B]^T [D_c] [B] \det [J] \, d\xi \, d\eta \, d\zeta \quad (7.1$$

where $[K_e]$ = element stiffness matrix

$[B]$ = strain matrix

$[D_c]$ = material matrix

and $[J]$ = Jacobian matrix

The material matrix $[D_c]$ relates the stresses to the strains and the Jacobian matrix [J] related the local derivatives of the shape functions N_i to the corresponding global cartesian derivatives. $[D_c]$ for an elastic, isotropic and homogeneous material and [J] are given in Appendix B.

7.2.1.3 Numerical Integration

Explicit integration of equation (7.1) is generally not possible and numerical integration has to be resorted to. Irons (127) has proved that the Gauss-Legendre quadrature is the most efficient approach for isoparametric elements. In this approach the integral I of equation (7.1) is approximated as

$$I = \int_{-1}^{1} \int_{-1}^{1} \int_{-1}^{1} f(\xi,\eta,\zeta) \, d\xi \, d\eta \, d\zeta$$

$$= \sum_{i=1}^{l} \sum_{j=1}^{m} \sum_{k=1}^{n} W_i W_j W_k f(\xi_i, \eta_j, \zeta_k) \quad (7.2)$$

where l, m and n are the number of Gauss integration or sampling

points in the ξ,η and ζ directions respectively, W_i, W_j, and W_k are the respective weighting coefficients and ξ_i, η_j and ζ_k are the co-ordinates of the Gauss points.

Table 7.1 shows the positions and weighting coefficients for 1 and 2 Gauss point integration as given in Ref (128).

Table 7.1 Abscissae and Weight Coefficients of the Gaussian Quadratic Formula

$$\int_{-1}^{1} f(x)\,dx = \sum_{i=1}^{n} W_i\, f(a_i)$$

± a	W
n = 1	
0	2.00000 00000 00000
n = 2	
0.57735 02691 89626	1.00000 00000 00000

The 8-node isoparametric hexahedron is a linear element and for exact integration requires 2 x 2 x 2 Gauss points (104). A preliminary elastic finite element analysis of beam 1TL-2 (see Table 6.1) was carried out using three discretization layouts as shown in Figs. 7.3a through 7.3c.and 2 x 2 x 2 Gauss point integration. The stresses were evaluated at each of the Gauss points as recommended by Irons (127). The primary objective of this preliminary study is to assess how well stresses are represented at the Gauss points using exact integration. The results of the analysis are summarized in Tables 7.2 and 7.3.

The normal stresses were consistent and conformed to what were expected. The shear stresses, however, deviated markedly from what were expected although the deviation decreased with increasing finer discretization. One expects the shear

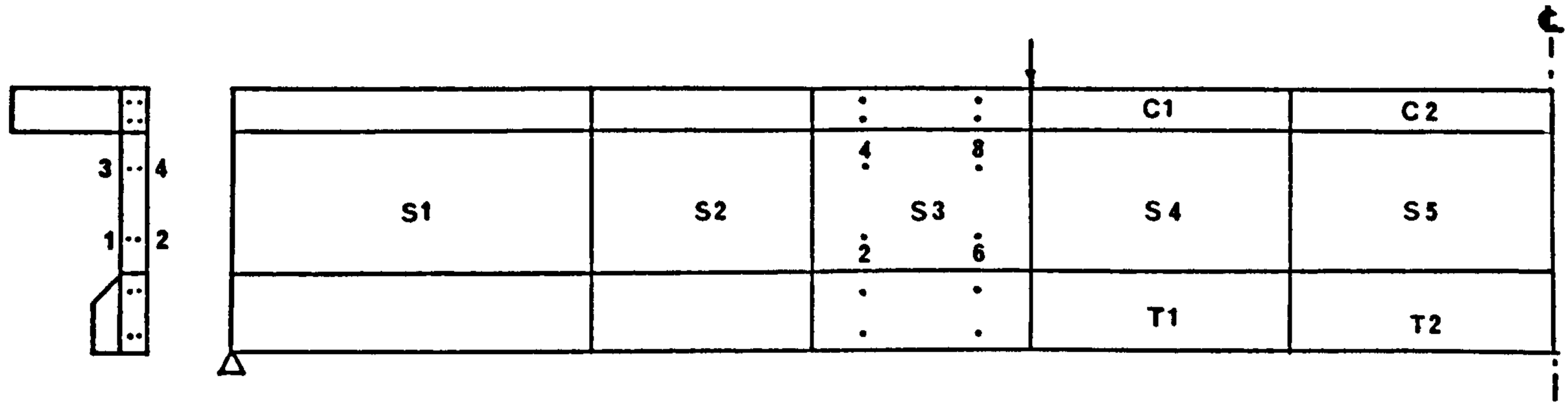

a) 5 x 5 Elements And 2x2x2 Gauss Point Integration

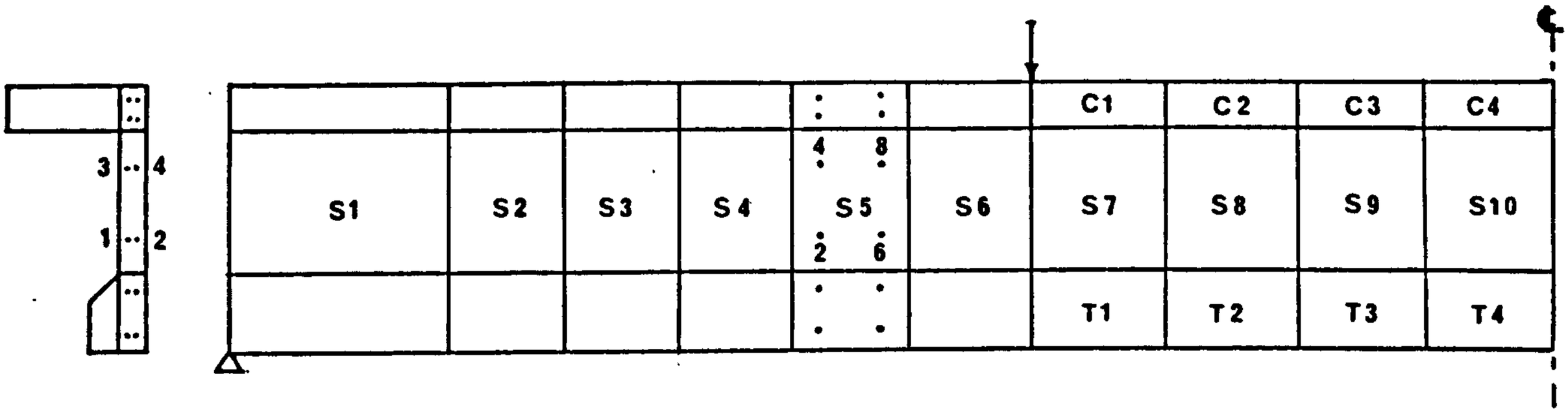

b) 5 x 10 Elements And 2x2x2 Gauss Point Integration

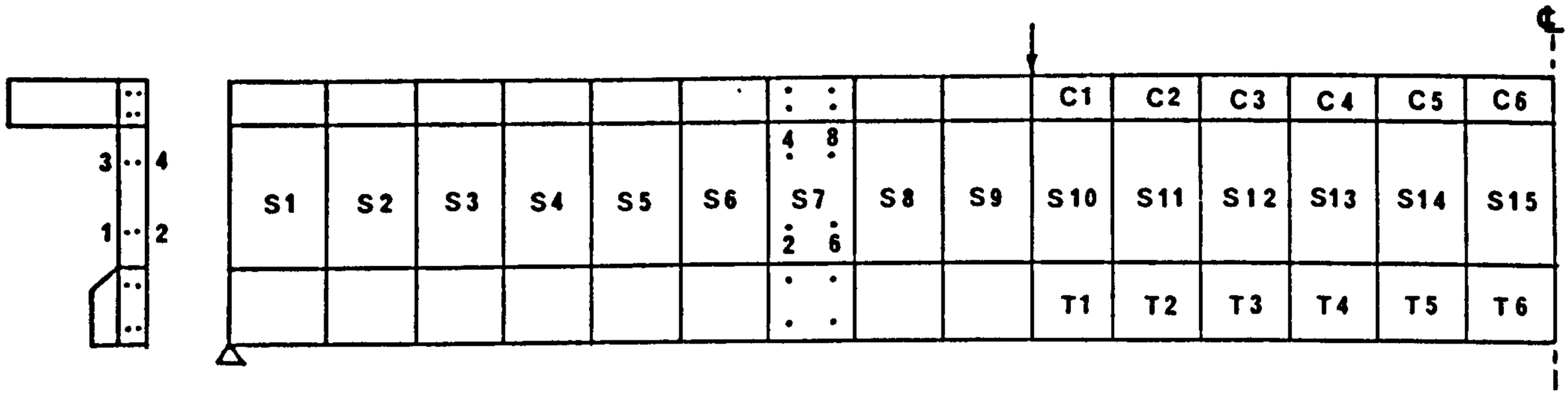

c) 5 x 15 Elements And 2x2x2 Gauss Point Integration

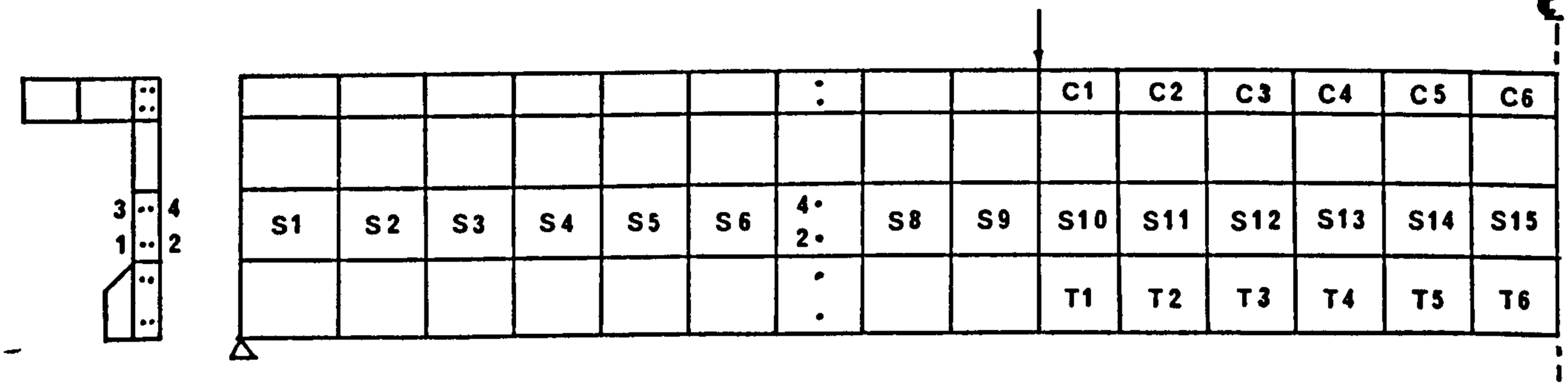

d) 7x15 Elements And 1x2x2 Gauss Point Integration

Note: 1 • – Gauss integration points

2 Steel reinforcement elements are not shown for clarity

Fig. 7.3 Element Details For Preliminary Determination Of Stresses

Table 7.2 Variation of Normal Stresses (σ_{xx}) in N/mm^2 With Number of Elements and Using 2 x 2 x 2 Gauss Point Integration

ELE-MENT No.	INTEGRATION POINTS 1	2	3	4	5	6	7	8	Applied Load N	Cal. Reaction N
	5 x 5 Elements									
C1	-1.14	-1.18	-1.56	-1.61	-1.11	-1.11	-1.50	-1.50		
C2	-1.13	-1.12	-1.47	-1.46	-1.14	-1.14	-1.49	-1.49	3500	3500
T1	1.67	1.66	1.03	1.03	1.67	1.67	1.04	1.04		
T2	1.55	1.56	0.96	0.96	1.56	1.56	0.96	0.96		
	5 x 10 Elements									
C1	-1.32	-1.42	-1.89	-2.0	-1.26	-1.27	-1.79	-1.80		
C2	-1.31	-1.29	-1.67	-1.66	-1.33	-1.33	-1.70	-1.70		
C3	-1.31	-1.32	-1.72	-1.73	-1.31	-1.31	-1.72	-1.72		
C4	-1.30	-1.30	-1.72	-1.72	-1.30	-1.31	-1.73	-1.73	3500	3500
T1	1.87	1.87	1.15	1.15	1.87	1.87	1.15	1.15		
T2	1.89	1.90	1.15	1.15	1.90	1.90	1.15	1.15		
T3	1.87	1.87	1.16	1.16	1.87	1.87	1.16	1.16		
T4	1.86	1.86	1.17	1.17	1.86	1.86	1.17	1.17		
	5 x 15 Elements									
C1	-1.35	-1.47	-2.03	-2.14	-1.27	-1.30	-1.90	-1.92		
C2	-1.35	-1.33	-1.71	-1.69	-1.37	-1.37	-1.73	-1.73		
C3	-1.35	-1.36	-1.76	-1.77	-1.35	-1.35	-1.76	-1.76		
C4	-1.35	-1.35	-1.77	-1.77	-1.35	-1.35	-1.78	-1.78		
C5	-1.35	-1.35	-1.77	-1.77	-1.35	-1.35	-1.77	-1.77		
C6	-1.35	-1.35	-1.80	-1.80	-1.35	-1.35	-1.80	-1.80	3500	3500
T1	1.93	1.93	1.17	1.17	1.92	1.92	1.17	1.18		
T2	1.95	1.95	1.18	1.18	1.96	1.96	1.18	1.18		
T3	1.94	1.94	1.18	1.18	1.94	1.94	1.18	1.18		
T4	1.92	1.92	1.20	1.20	1.92	1.92	1.20	1.20		
T5	1.92	1.92	1.21	1.21	1.92	1.92	1.21	1.21		
T6	1.93	1.93	1.20	1.20	1.93	1.93	1.20	1.20		

NOTE: For element notations, see Fig. 7.3

Table 7.3 Variation of Shear Stresses (τ_{xy}) in N/mm^2 With Number of Elements and Using 2 x 2 x 2 Gauss Point Integration

ELE-MENT NO.	INTEGRATION POINTS								Applied Load N	CAL. Reac-tion N
	1	2	3	4	5	6	7	8		
	5 x 5 Elements									
S1	-0.38	-0.37	-0.33	-0.31	-0.64	-0.62	-0.58	-0.57		
S2	-0.30	-0.29	-0.32	-0.30	-0.71	-0.70	-0.73	-0.71		
S3	-0.09	-0.07	-0.14	-0.12	-0.67	-0.66	-0.72	-0.71	3500	3500
S4	0.35	0.35	0.40	0.40	-0.46	-0.46	-0.41	-0.41		
S5	0.40	0.40	0.40	0.40	-0.40	-0.40	-0.40	-0.40		
	5 x 10 Elements									
S1	-0.48	-0.46	-0.39	-0.38	-0.63	-0.61	-0.54	-0.53		
S2	-0.48	-0.46	-0.49	-0.48	-0.63	-0.62	-0.65	-0.63		
S3	-0.41	-0.40	-0.43	-0.41	-0.62	-0.60	-0.64	-0.62		
S4	-0.40	-0.38	-0.39	-0.38	-0.65	-0.64	-0.65	-0.63		
S5	-0.34	-0.33	-0.38	-0.36	-0.66	-0.64	-0.69	-0.67	3500	3500
S6	-0.22	-0.20	-0.32	-0.30	-0.54	-0.54	-0.65	-0.64		
S7	0.12	0.12	0.22	0.22	-0.32	-0.32	-0.22	-0.22		
S8	0.22	0.22	0.24	0.24	-0.24	-0.24	-0.22	-0.22		
S9	0.24	0.24	0.24	0.24	-0.24	-0.24	-0.24	-0.24		
S10	0.24	0.24	0.24	0.24	-0.24	-0.24	-0.24	-0.24		
	5 x 15 Elements									
S1	-0.61	-0.58	-0.35	-0.33	-0.62	-0.58	-0.36	-0.34		
S2	-0.61	-0.59	-0.51	-0.50	-0.64	-0.63	-0.55	-0.53		
S3	-0.48	-0.46	-0.50	-0.48	-0.56	-0.55	-0.58	-0.56		
S4	-0.46	-0.45	-0.47	-0.45	-0.58	-0.57	-0.60	-0.58		
S5	-0.45	-0.43	-0.45	-0.43	-0.61	-0.60	-0.61	-0.59		
S6	-0.43	-0.42	-0.43	-0.42	-0.63	-0.61	-0.62	-0.61		
S7	-0.41	-0.39	-0.41	-0.39	-0.63	-0.62	-0.63	-0.62		
S8	-0.36	-0.34	-0.41	-0.40	-0.63	-0.61	-0.68	-0.67	3500	3500
S9	-0.25	-0.23	-0.37	-0.35	-0.53	-0.52	-0.65	-0.63		
S10	0.00	0.01	0.13	0.13	-0.29	-0.29	-0.16	-0.17		
S11	0.13	0.13	0.18	0.18	-0.19	-0.19	-0.14	-0.14		
S12	0.15	0.15	0.15	0.15	-0.17	-0.17	-0.17	-0.17		
S13	0.16	0.16	0.16	0.16	-0.16	-0.16	-0.16	-0.16		
S14	0.16	0.16	0.16	0.16	-0.16	-0.16	-0.17	-0.17		
S15	0.14	0.14	0.14	0.14	-0.15	-0.15	-0.15	-0.15		

NOTE: For element notations, see Fig. 7.3

stresses to be zero or near to zero in the pure bending regime and reasonably constant in the combined bending and shear regime except near the end support and the loading point, where stress concentration effects are present. The error in the shear stresses is due to the presence of what Zienkiewicz et al (129) termed 'parasitic' shear stresses. The inability of an element to follow the actual displacement mode, when subjected to bending, induced the 'parasitic' shear stresses. See Fig. 7.4. This has been observed in plane quadrilateral plate or shell element with linear displacement field (130) and isoparametric shell element with parabolic displacement field (129)

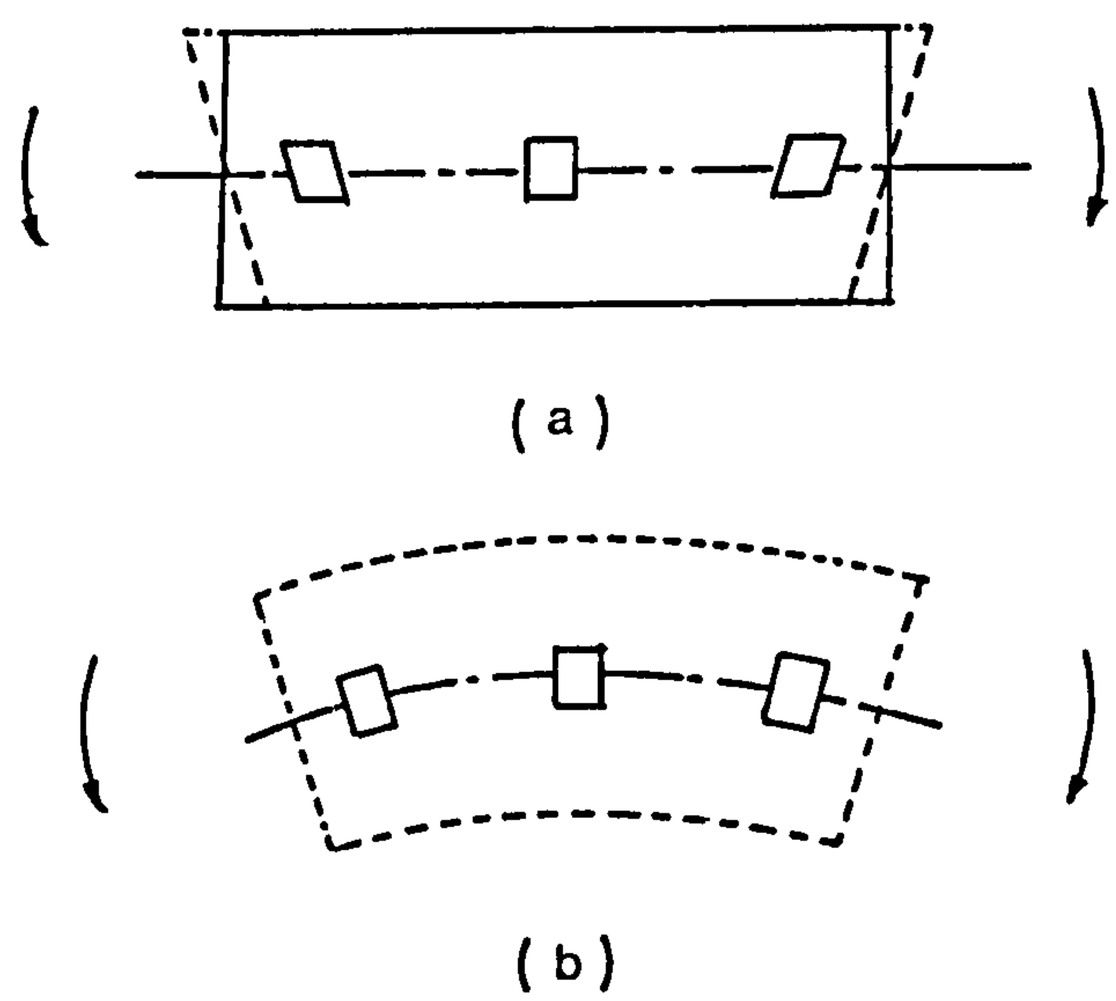

Fig. 7.4 'Parasitic' Shear Stresses Induced in a Linear Element Under Bending Mode (a) Constrained Mode; (b) True Mode (after ref. (129)

The obvious solution to the above problem is to refine the discretization further. However this is not economical as the computational time involved will increase dramatically. A better alternative is to reduce the order of integration as has been successfully done by Doherty et al (130) and Zienkiewicz et al (129). The reduced integration technique

not only reduces the computational time but it also gives a better solution as the errors due to discretization and due to inexact integration tend to cancel each other out (104).

For a linear element, a single-point integration is the minimum required to satisfy the convergence criterion. However in practice, it is generally not sufficient to ensure non-singularity of the global stiffness matrix [K] (104). Going back to Table 7.3, it can be observed that the average values of the shear stresses at integration points 1 and 5, 2 and 6, 3 and 7, and 4 and 8 give a better representation of the shear stresses. This suggests that a 1 x 2 x 2 Gauss point integration may be suitable.

An elastic analysis of beam 1TL-2 was again carried out using a discretization scheme as shown in Fig. 7.3d and 1 x 2 x 2 Gauss point integration. As before the stresses were calculated at the Gauss points. The results of the shear and normal stresses are given in Table 7.4. A far better stress representation was obtained this time.

Thus an 8-node isoparametric hexahedron with 1 x 2 x 2 Gauss point integration is selected for this study.

7.2.2 Bar Elements

7.2.2.1 General

To obtain a realistic representation of the stiffness properties of a reinforced concrete member, the steel reinforcement must be represented in the computational model. In the present study, the reinforcing bars are represented by separate 2-node bar elements and are allowed to lie within the isoparametric hexahedral elements along the lines of constant η and ζ. This has the advantage that new reinforcement can be easily added in an existing model without altering the original finite element

Table 7.4 Shear Stresses (τ_{xy}) and Normal Stresses (σ_{xx}) in N/mm^2
Using 7 x 15 Elements and 1 x 2 x 2 Gauss Point Integration

ELEMENT NO.	INTEGRATION POINTS				Applied Load N	CAL. REACTION N
	1	2	3	4		
	Shear Stresses τ_{xy}					
S1	-0.56	-0.51	-0.35	-0.33		
S2	-0.65	-0.65	-0.55	-0.54		
S3	-0.34	-0.35	-0.43	-0.43		
S4	-0.49	-0.48	-0.46	-0.45		
S5	-0.47	-0.47	-0.49	-0.49		
S6	-0.49	-0.48	-0.47	-0.45	3000	3000
S7	-0.49	-0.49	-0.51	-0.51		
S8	-0.47	-0.47	-0.49	-0.48		
S9	-0.34	-0.33	-0.36	-0.36		
S10	-0.15	-0.15	-0.13	-0.12		
S11	-0.02	-0.02	0.00	0.00		
S12	0.02	0.02	0.03	0.03		
S13	0.01	0.01	0.02	0.04		
S14	0.00	0.00	0.01	0.02		
S15	0.00	0.00	-0.01	-0.01		
	Normal Stresses σ_{xx}					
C1	-1.15	-1.24	-1.85	-1.93		
C2	-1.26	-1.22	-1.44	-1.40		
C3	-1.18	-1.20	-1.57	-1.59		
C4	-1.20	-1.20	-1.55	-1.54		
C5	-1.19	-1.20	-1.57	-1.58		
C6	-1.19	-1.19	-1.57	-1.56	3000	3000
T1	1.63	1.63	0.97	0.97		
T2	1.65	1.65	0.98	0.99		
T3	1.64	1.64	0.99	0.99		
T4	1.63	1.63	1.00	1.00		
T5	1.62	1.62	1.01	1.01		
T6	1.62	1.62	1.00	1.00		

NOTE: For element notations, see Fig. 7.3

topology. Furthermore, a large number of reinforcement can be prescribed by a relatively coarse element discretization.

7.2.2.2 Element Stiffness Matrix $[K^b]$

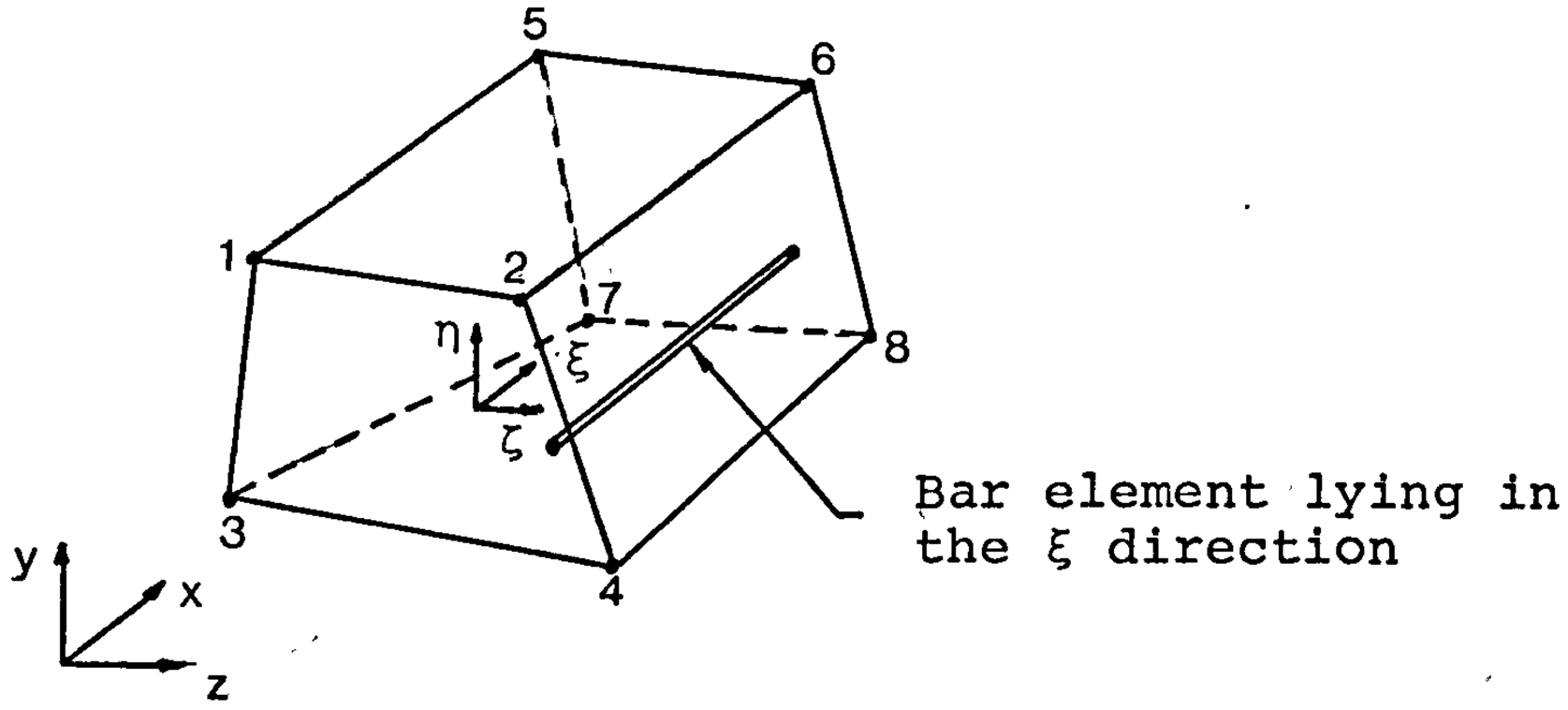

Fig. 7.5 Typical Bar Element Within a Hexahedron

Consider the 2-node bar element lying in the ξ direction within the 'parent' hexahedron as shown in Fig. 7.5. Since it is in a 3-dimensional space its nodes are defined by three co-ordinates and there are three components of displacements.

The interpolation functions or shape functions N_i for the geometry and the displacement field of the element are given in Appendix C.

The stiffness matrix of this element has been derived by Ergatoudis (123) and this derivation can also be found in Ref. (51). It takes the form of

$$[K^b] = \int_{-1}^{1} [B]^T E_s [B] \text{ (area) } \frac{ds}{d\xi} \, d\xi \qquad (7.3)$$

where $$B = a \left\{ [b] \frac{\partial N_1}{\partial \xi} \quad [b] \frac{\partial N_2}{\partial \xi} \right\} \qquad (7.4)$$

$$a = \frac{1}{\left(\frac{\partial x}{\partial \xi}\right)^2 + \left(\frac{\partial y}{\partial \xi}\right)^2 + \left(\frac{\partial z}{\partial \xi}\right)^2} \tag{7.5}$$

$$\frac{\partial x}{\partial \xi} = \sum_{i=1}^{2} \frac{\partial N_i}{\partial \xi} x_i \quad \text{etc} \tag{7.6}$$

$$[b] = \begin{bmatrix} \frac{\partial x}{\partial \xi} & \frac{\partial y}{\partial \xi} & \frac{\partial z}{\partial \xi} \end{bmatrix} \tag{7.7}$$

E_s = Young's modulus of elasticity of the bar

(area)= cross sectional area of the bar

$$\frac{ds}{d\xi} = \sqrt{\left(\frac{\partial x}{\partial \xi}\right)^2 + \left(\frac{\partial y}{\partial \xi}\right)^2 + \left(\frac{\partial z}{\partial \xi}\right)^2} \tag{7.8}$$

In the present study equation (7.3) was integrated numerically using 2 Gauss point integration.

7.2.2.3 Expansion of Bar Element Stiffness Matrix $[K^b]$ into Equivalent Hexahedron Stiffness Matrix $[K^{bh}]$

Since the bar element lies within the hexahedron, it is necessary to expand its [6 x 6] stiffness matrix (as given by equation (7.3)) to an equivalent [24 x 24] matrix associated with the degrees of freedom of the 8-node hexahedron before the assembly of the overall structural stiffness matrix.

Consider a 3-dimensional concrete element with a bar reinforcement as shown in Fig. 7.5. The global co-ordinates of the bar element ends are defined by the localization parameters a_1, b_1, a_2 and b_2 as shown in Fig. 7.6. Note that $0 \leq a_1, b_1, a_2, b_2 \leq 1$. It is shown in Appendix C that the equivalent hexahedron stiffness matrix $[K^{bh}]$ takes the form of

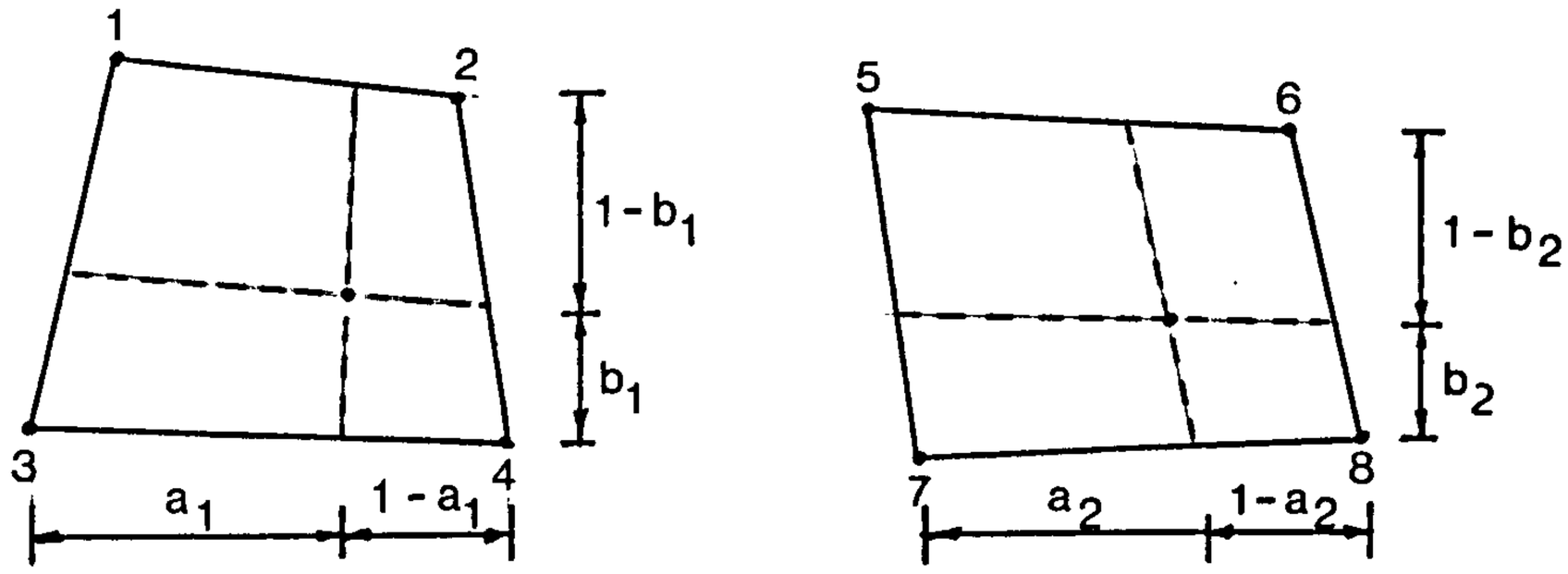

Fig. 7.6 Localization Parameters of Bar Element Ends

$$\begin{pmatrix} K_{11}^{bh} & K_{12}^{bh} & \cdots & K_{18}^{bh} \\ K_{21}^{bh} & K_{22}^{bh} & \cdots & K_{28}^{bh} \\ \vdots & & & \\ K_{81}^{bh} & K_{82}^{bh} & \cdots & K_{88}^{bh} \end{pmatrix} = \left(\begin{array}{c|c} [C_{11}]\, K_{11}^{b} & [C_{12}]\, K_{12}^{b} \\ \hline [C_{21}]\, K_{21}^{b} & [C_{22}]\, K_{22}^{b} \end{array}\right) \qquad (7.9)$$

where $[C_{mn}] = \begin{pmatrix} b_m b_n c_m c_n & a_n b_m b_n c_m & b_m c_m c_n d_n & a_n b_m c_m d_n \\ a_m b_m b_n c_n & a_m a_n b_m b_n & a_m b_m c_n d_n & a_m a_n b_m d_n \\ b_n c_m c_n d_m & a_n b_n c_m d_m & c_m c_n d_m d_n & a_n c_m d_m d_n \\ a_m b_n c_n d_m & a_m a_n b_n d_m & a_m c_n d_m d_n & a_m a_n d_m d_n \end{pmatrix}$

$$; \quad m, n = 1, 2 \qquad (7.10)$$

$$c_1 = (1 - a_1)\,, \; d_1 = (1 - b_1) \qquad (7.11)$$

$[K_{11}^{bh}]$ = [3 x 3] submatrix of $[K^{bh}]$, etc

$[K_{II}^{b}]$ = [3 x 3] submatrix of $[K^{b}]$, etc

$[C_{11}]$, $[C_{12}]$, $[C_{21}]$ and $[C_{22}]$ may be regarded as the expansion coefficient matrices. For most practical cases, the hexahedron will be regular. This implies $a_1 = a_2$, $b_1 = b_2$, $c_1 = c_2$ and $d_1 = d_2$ and it follows $[C_{11}] = [C_{12}] = [C_{21}] = [C_{22}]$. Note that the expanded equivalent stiffness matrix as given by equation (7.9) is symmetrical.

7.2.3 Bond Between Reinforcing Steel and Concrete

One of the aims of carrying out the bond tests reported in Chapter 4 was to provide information on the bond stress-slip characteristics in fibre concrete. Due to lack of time, this information is not made use of in the present finite element model. Instead a perfect bonding between steel and concrete is assumed. It will be demonstrated in Chapter 9 that the assumption of perfect bonding gives a reasonable prediction of the structural behaviour of reinforced concrete beams. However, it is to be expected that better prediction can be achieved if the bond stress-slip characteristics is incorporated into the model. One way of doing this is by allowing the bar elements to be connected to the concrete elements at the nodes through the use of linkage elements. The incorporation of bond stress-slip characteristics will invariably require greater computational efforts and hence greater computer time.

7.2.4 Assembly and Solution

The individual stiffness matrices of the concrete elements $[K_e]$ and the expanded equivalent matrices of the steel elements $[K^{bh}]$ are suitably assembled to form the global or structural stiffness matrix [K]. All applied loads are assembled in a global vector {R}. The overall equilibrium relations of the structure are given by

$$\{R\} = [K]\{\delta\} \qquad (7.12)$$

The system of linear equations represented by the above equation can be solved once the prescribed displacements have been substituted. In the present study, for zero displacements, a very large number (10^{25}) is added to the diagonal coefficients of the structural stiffness matrix corresponding to the prescribed variables. This in effect physically corresponds to 'earthing' the structure with a very stiff spring. For a rigid support a very small displacement instead of an absolute zero is obtained and the reaction for that support can be determined directly as

Reaction = -(Big spring stiffness) x (very small displacement)

Meyers (131, 132) has reviewed the state-of-the-art of solving linear equations. In the present study, the Gaussian elimination utilizing the symmetry and banded nature of the [K] matrix has been adopted to solve for the unknown displacements $\{\delta\}$ in equation (7.12). This method is computationally simple although care must be exercised in the numbering of the nodes so that a minimum band width is obtained.

After the evaluation of the displacements, strains and stresses at the integration points can be calculated by direct substitution into equations (B.6) and (B.9) respectively.

7.3 Mathematical Modeling of Concrete

7.3.1 Review of Material Model for Plain Concrete

Many models have been proposed in recent years to characterize the stress-strain and failure behaviour of concrete material. A brief review of some of these models is given below. A more extensive review can be found in Ref. (133).

7.3.1.1 Linear Elastic-Fracture Model

In this model, the basic stress-strain relations are those of linear elasticity which is described completely by two elastic constants, Poisson's ratio ν and Young's modulus E_c. The elastic limit envelope in general stress space is the same as that of the fracture envelope.

When the state of stress reaches a critical value as specified by a suitable fracture criterion, concrete will fail by fracturing. Two types of fracture depending on the stress states are distinguished: 'crushing' type of fracture if the principal stresses are in the compression-compression state and 'cracking' type of fracture if the principal stresses are in either tension-tension or tension-compression state.

Once concrete has fractured, the stiffness of the material is modified in accordance to the type of fracture. The manner in which this is done will be discussed later. The appropriate stresses are released and thrown back to the structure for distribution.

Overall, the structure is analysed by succession of transitions from one instantaneous elastic stiffness to another.

The model is applicable only to situations where reduction in the stiffness of the concrete is predominantly due to tensile cracking. Hammad (51) adopted this model.

7.3.1.2 Hypoelastic (Nonlinear) Model

This model has been applied extensively in 2-dimensional numerical analysis of reinforced concrete beams (52, 62, 110, 113, 134, 135). The basic concept is to treat the biaxial stress-strain behaviour of concrete as an equivalent uniaxial relation. In this approach, the strain increment in each principal direction is determined solely by the principal stress increment in the same

direction and the corresponding tangent stiffness which is a function of the principal stress ratio, accounts for Poisson's effect and microcrack confinement effect. Concrete is considered to be orthotropic with orthotropy direction coinciding with the principal stress direction.

The uniaxial stress-strain relation is nonlinear in compression but is generally assumed linear in tension.

'Cracking' fracture of concrete is taken care of as in the previous model.

A typical biaxial failure envelope for concrete is shown in Fig. 7.7.

7.3.1.3 Elastic-Perfectly Plastic-Fracture Model

This model assumes that concrete under multiaxial compression behaves as a classic elastic-plastic model for incremental stress-strain relations. The complete stress-strain relations are developed in three parts: (1) before yield; (2) during plastic flow; and (3) after fracture. The linear elastic stress-strain relationships before yield and after fracture are similar to those of the linear elastic-fracture model.

The Von Mises criterion, Druker-Prager criterion and Mohr-Coulomb criterion are some of the criteria used to define the condition of yield. To construct the stress-strain relations in the plastic range, the flow rule is generally employed. The flow rule requires the plastic deformation rate vector to be normal to the yield surface. A strain criterion for fracture is required to define the limit of concrete ultimate deformation capacity under compression states. This is usually developed by simply converting the yield criterion in stresses directly into strains.

Finally 'cracking' fracture under either tension-tension or tension-compression state is dealt with as in the linear

elastic-fracture model.

This model has been successfully employed in 2- and 3-dimensional numerical analysis of reinforced concrete structures (112, 114, 115, 137, 138).

7.3.1.4 Elastic-Strain Hardening Plastic and Fracture Model

This model proposed by Chen et al (139, 140), makes use of the strain hardening theory of plasticity and considers the nonlinear effects caused by the plasticity of concrete in compression and cracking of concrete in tension. Three loading surfaces are assumed and they are:

(1) The initial discontinuous surface which is defined as the limiting surface for elastic behaviour.

(2) The subsequent loading surface which is defined as the new subsequent discontinuous surface when the material is stressed beyond the initial discontinuous surface.

(3) The failure surface which is defined such that once the stress state reaches this surface the material will completely rupture and cannot resist any further loading.

Fig. 7.8 shows the initial discontinuous and failure surfaces.

Functions in terms of first stress invariant and second invariant of deviatoric stresses are then postulated to define these loading surfaces in the compression-compression region and tension-tension or tension-compression region. In addition the fracture surface is also defined in terms of strains. Thus a dual criteria is used to define the fracture surface of concrete.

The incremental elastic-plastic stress-strain relations are derived by using the classical theory of plasticity.

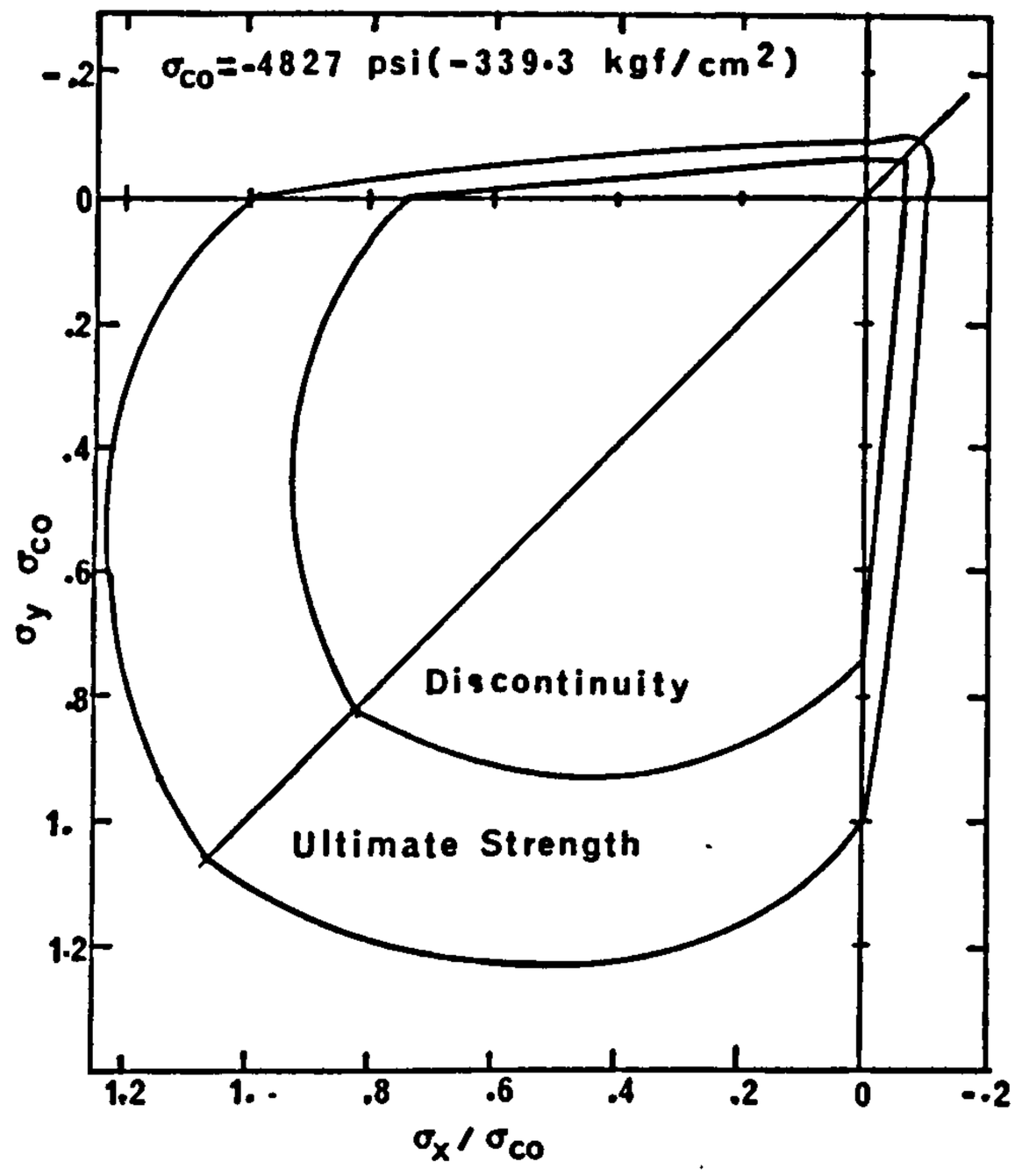

Fig.7.7 Biaxial Discontinuity And Ultimate Strength Envelopes Of Concrete (after Ref.(136))

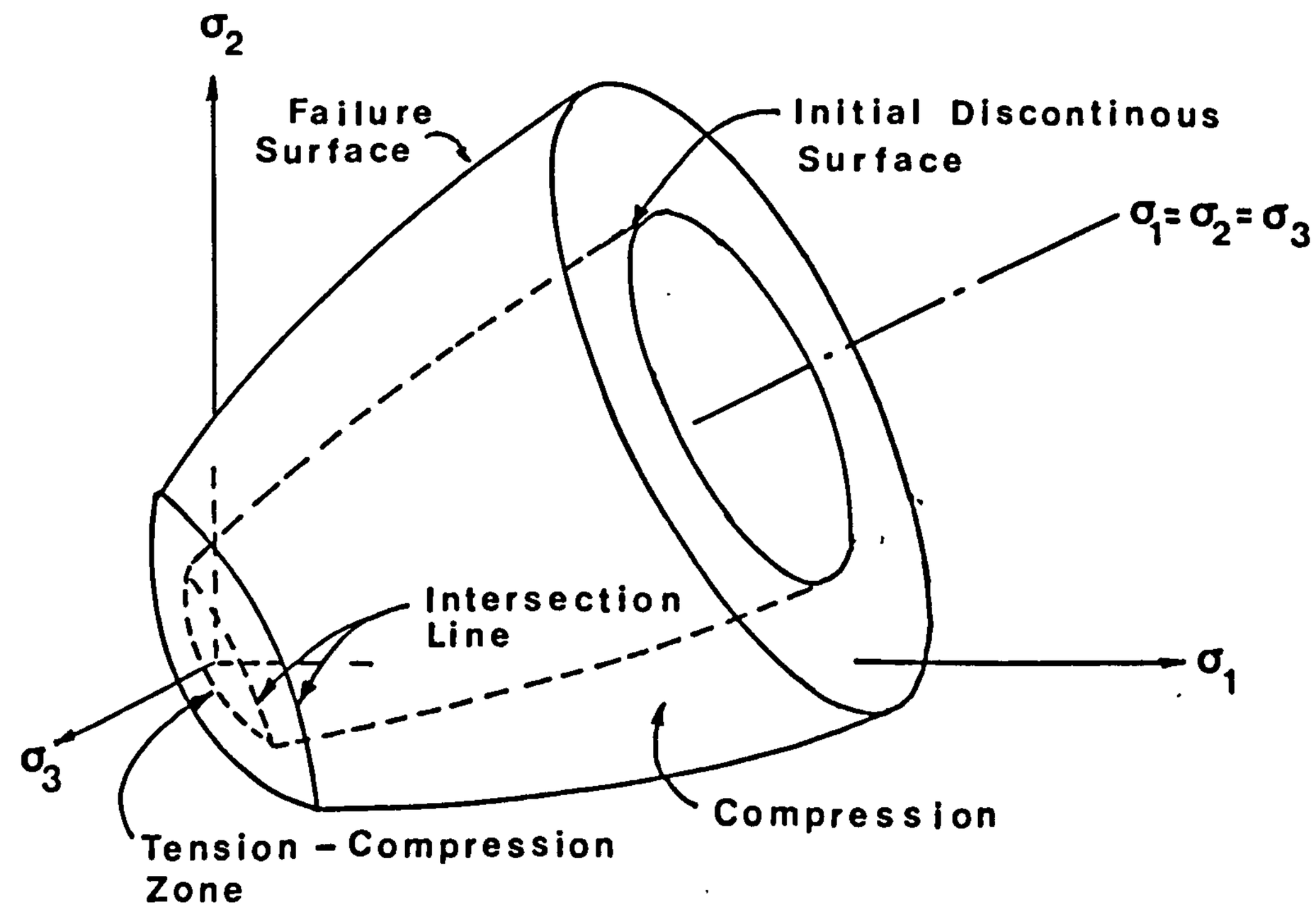

Fig.7.8 Failure And Initial Discontinous Surfaces In Principal Stress Space (after Ref.(139))

7.3.1.5 Endochronic Theory of Inelasticity for Behaviour of Concrete

The endochronic theory was developed by Valanis (141, 142) for the description of mechanical behaviour of metals. Bazant and Bhat (143) extended this theory to describe concrete behaviour. The endochronic model does not require the specific definition of yielding and hardening as in classical incremental flow theory of plasticity. Instead it employs a pseudo-time scale, the intrinsic time, to measure the extent of change (or damage) of the internal structure of the concrete material when it is subjected to deformation histories. The endochronic theory can be viewed as a generalization of the classical viscoelasticity to include not only the explicit time-history but also the permanent strain-history.(133).

The endochronic model appears to have the capability of characterizing a broad range of inelastic behaviour of concrete, including creep. It has been successfully applied by Sorensen (116) in a numerical analysis of reinforced concrete beams and slabs. However it should also be pointed out that some earlier versions of the endochronic theory have been shown to yield unstable and nonunique solutions (144).

7.3.2 Model Used in the Present Study

All the more refined material models for concrete were derived from experimental data obtained from biaxial or triaxial tests on plain normal weight concrete. The application of these models to plain lighweight concrete or fibre reinforced concrete is questionable. Therefore, the simpler elastic-perfectly plastic-fracture model is chosen for the present study.

7.3.2.1 Uniaxial Stress-Strain Relations

For plain concrete the stress-strain curve in compression

generally consists of two parts. See Fig. 7.9(a). In the ascending parts, the stress increases with strain at a decreasing rate up to a strain of around 0.25%. In the descending part, the stress decreases with strain until the concrete is completely disrupted.

For fibre concrete, the stress-strain relation for the ascending part is similar to that of plain concrete, the peak stress value and corresponding strain value being comparable to those of plain concrete. The descending part of the curve, however, exhibits a flatter slope, indicating a greater ultimate strain capacity.

In both cases, the stress-strain relation was idealized as elastic-perfectly plastic as shown in Fig. 7.9(b).

The uniaxial stress-strain curve in tension for plain concrete is nearly linear up to failure (145, 146). See Fig. 7.10(a). The maximum tensile strain does not usually exceed 0.02%. In this analytical study, the stress-strain relation was idealized as linear elastic up to failure. After failure the tensile stress is reduced to a negligible value. See Fig. 7.10(b).

Experimental data on uniaxial tension tests on fibre reinforced mortar and concrete (99, 147) suggest a stress-strain relation of the form shown in Fig. 11(a). The ascending part up to the cracking strength is nearly linear. After cracking, there is a drop in the stress and then followed by a gradual decrease in the stress with increasing strain. The stress-strain relation was idealized as linear elastic up to the cracking strength. After cracking, the tensile stress was reduced to a constant value, the post-cracking tensile strength of the composite σ_{cu}. See Fig. 7.11(b). Appendix A shows how this value can be calculated.

Al-Taan (62) ignored the post-cracking tensile strength of fibre concrete in his numerical analysis of fibre concrete

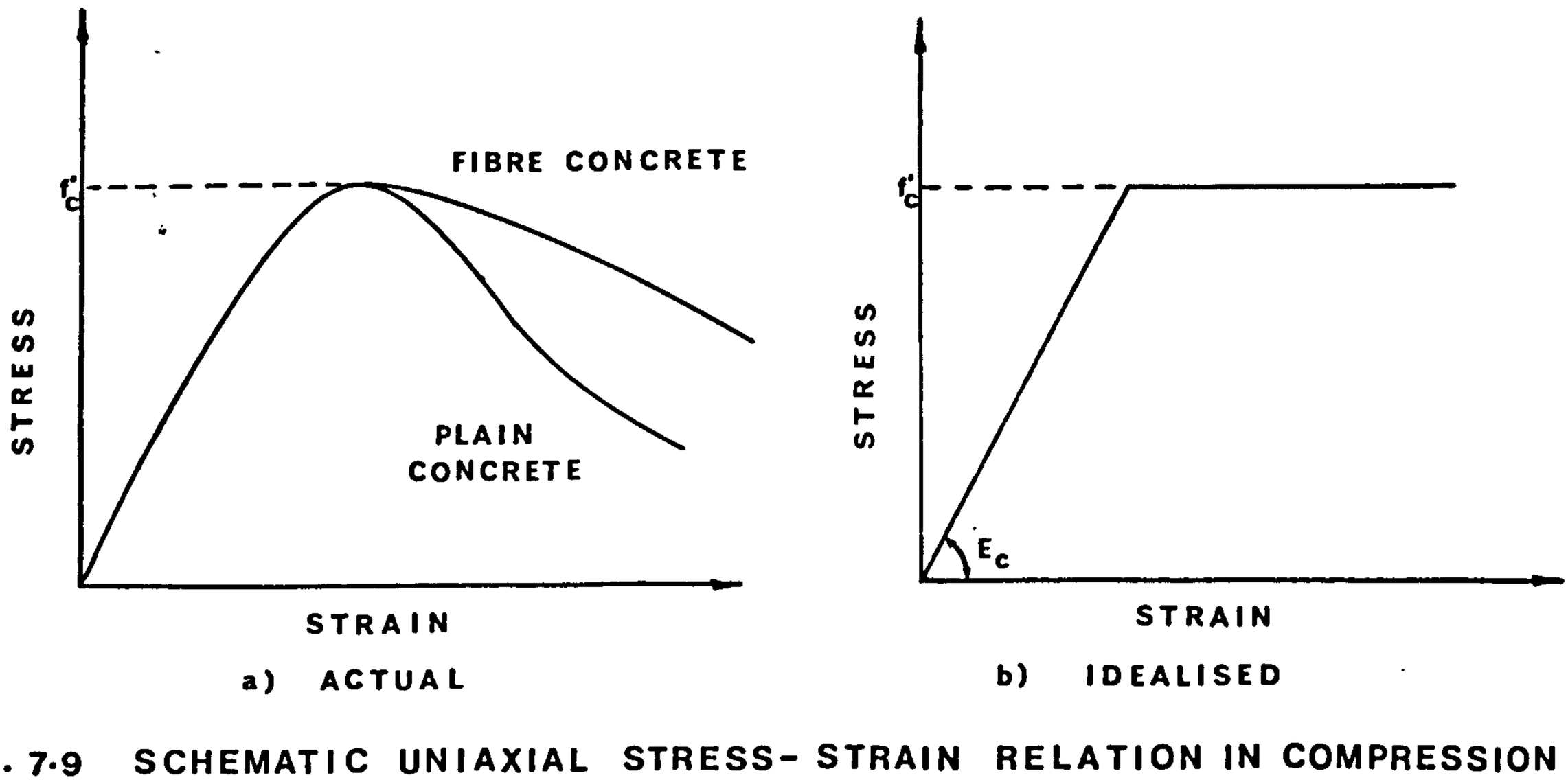

FIG. 7.9 SCHEMATIC UNIAXIAL STRESS- STRAIN RELATION IN COMPRESSION

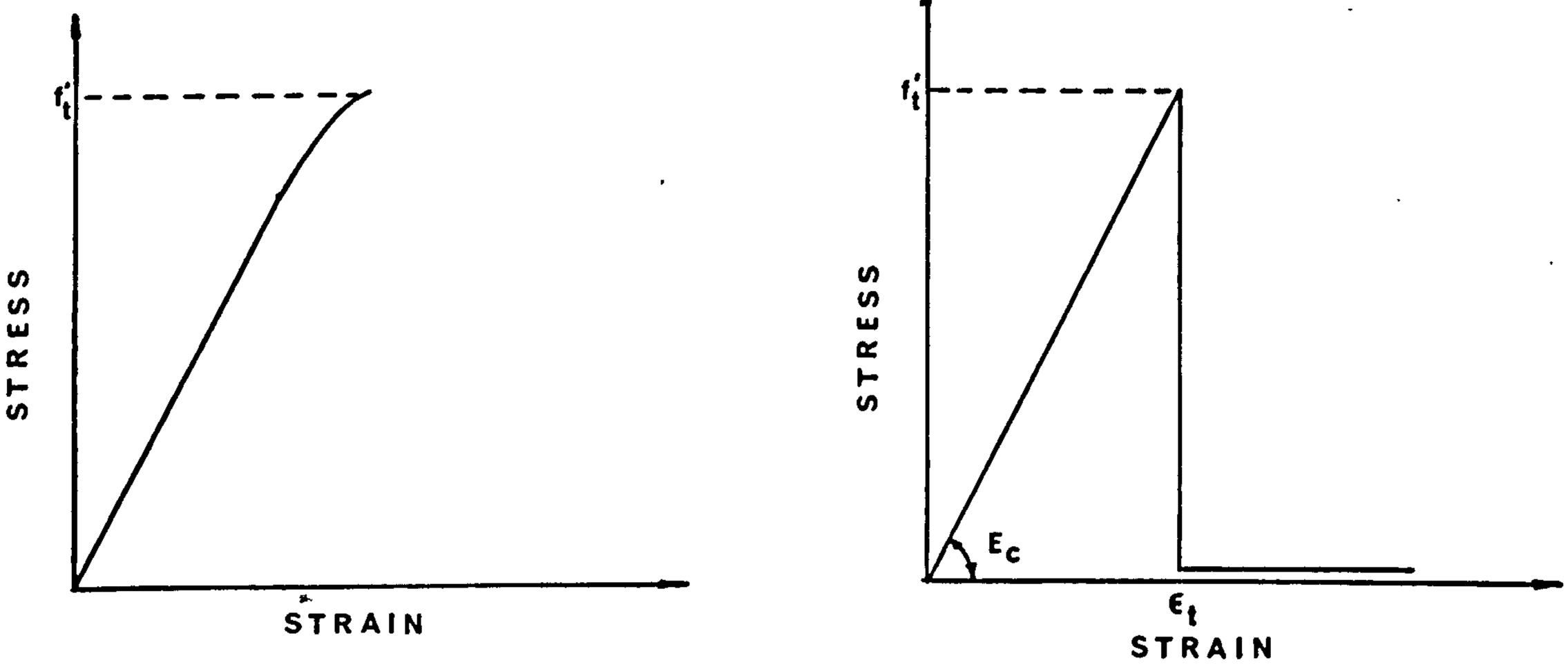

FIG. 7.10 SCHEMATIC UNIAXIAL STRESS-STRAIN RELATION IN TENSION (PLAIN CONCRETE)

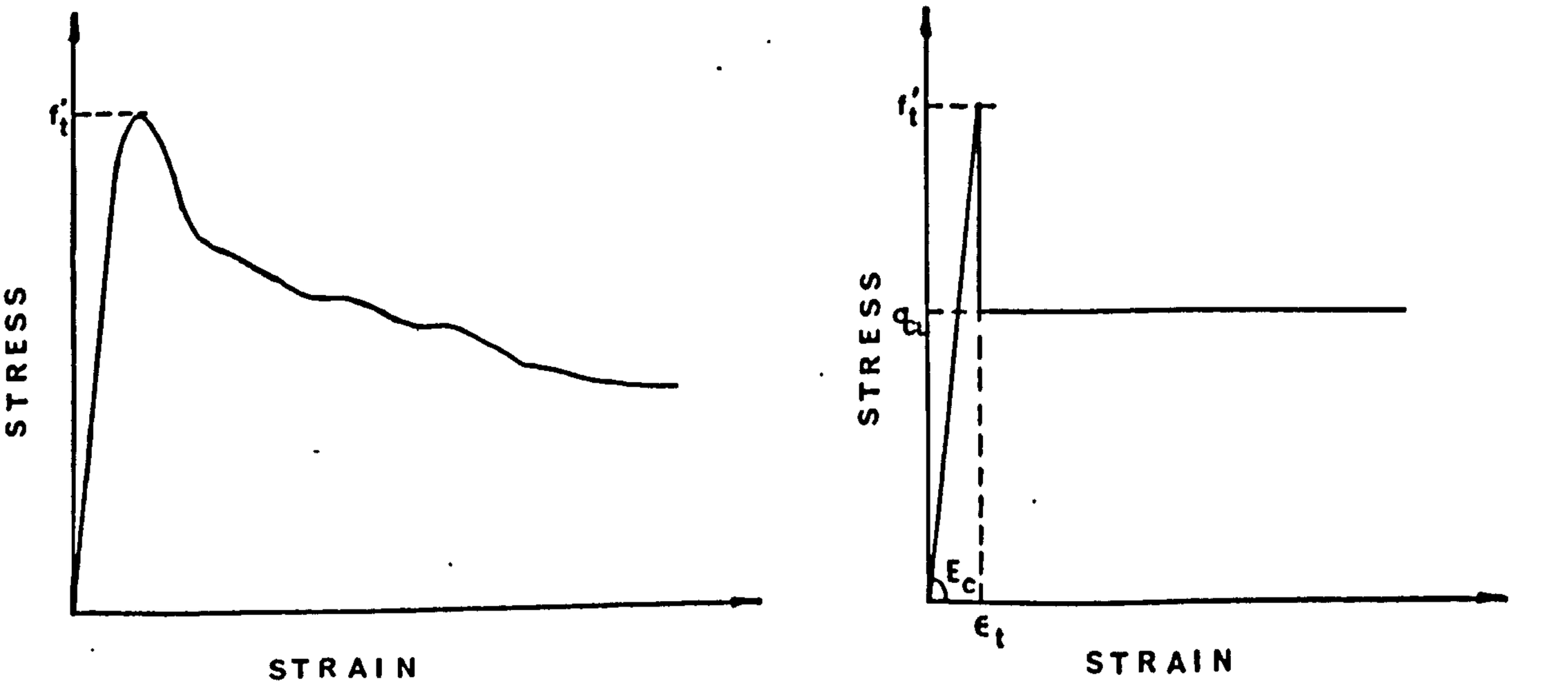

FIG. 7.11 SCHEMATIC UNIAXIAL STRESS- STRAIN RELATION IN TENSION (FIBRE CONCRETE)

beams. This led to significant underestimation of the load carrying capacity of the beams.

7.3.2.2 State of Stress at an Integration Point

Stresses and strains are evaluated at the integration points within the elements. These stresses and strains are referred to as the global reference frame. The principal stresses σ_1, σ_2 and σ_3 at an integration point can be determined from the six stress components in the x, y, z co-ordinates. This can be done by using the method given in Ref. (148).

The first stress invariant I_1 and the second invariant of deviatoric stresses J_2 are defined as follows:

$$I_1 = (\sigma_x + \sigma_y + \sigma_z) = (\sigma_1 + \sigma_2 + \sigma_3) \qquad (7.13)$$

$$J_2 = \frac{1}{6}[(\sigma_x - \sigma_y)^2 + (\sigma_y - \sigma_z)^2 + (\sigma_x - \sigma_x)^2 + 6\tau_{xy}^2 + 6\tau_{yz}^2 + 6\tau_{zx}^2]$$

$$= \frac{1}{6}[(\sigma_1 - \sigma_2)^2 + (\sigma_2 - \sigma_3)^2 + (\sigma_1 - \sigma_3)^2] \qquad (7.14)$$

The state of stress at an integration point is considered compression-compression if σ_1, σ_2 and σ_3 are all less than zero. It is regarded as tension-compression or tension-tension otherwise. In terms of stress invariants, Chen and Suzuki(140) have shown that the stress state is compression-compression if it satisfies the condition

$$J_2 \leq -\frac{1}{\sqrt{3}} I_1 \text{ and } I_1 \leq 0 \qquad (7.15)$$

Otherwise, it is tension-compression or tension-tension.

7.3.2.3 Incremental Elastic Constitutive Relations

Concrete is assumed to be linearly elastic and isotropic prior to cracking or yielding. Its elasticity or material matrix

$[D_c]$ is given by equation (B.8)

The incremental constitutive relations are given by

$$\{\Delta\sigma\} = [D_c]\{\Delta\varepsilon\} \tag{7.16}$$

7.4.2.4 Yield Criterion in Compression-Compression Zone

The Von Mises yield criterion has been adopted to approximate the yield surface of both plain and fibre reinforced concrete. This yield criterion has been used by several researchers in both 2-dimensional (11, 112, 138, 149) and 3-dimensional (115) numerical analysis of reinforced concrete structures. It is given by:

$$F(\{\sigma\}) = [\tfrac{1}{2}(\sigma_x - \sigma_y)^2 + \tfrac{1}{2}(\sigma_y - \sigma_z)^2 + \tfrac{1}{2}(\sigma_z - \sigma_x)^2 + 3\tau_{xy}^2 + 3\tau_{yz}^2 + 3\tau_{zx}^2]^{\frac{1}{2}} - f_c' \tag{7.17}$$

or in terms of J_2 as

$$F(\{\sigma\}) = \sqrt{3J_2} - f_c' \tag{7.18}$$

where f_c' is the uniaxial compressive strength.

The condition that F is less than, equal to or greater than zero establishes, respectively, the condition where the stress vector $\{\sigma\}$ is within the yield surface, on the yield surface or outside it.

The Von Mises yield criterion is shown in $(I_1, \sqrt{J_2})$ space om Fig. 7.12.

7.3.2.5 Incremental Elasto-Plastic Constitutive Relations

The incremental elasto-plastic constitutive relations are given by (150)

$$\{\Delta\sigma\} = [D_c]_{ep}\{\Delta\varepsilon\} \tag{7.19}$$

where $$[D_c]_{ep} = [D_c] - [D_c]\left\{\frac{\partial F}{\partial \{\sigma\}}\right\}\left\{\frac{\partial F}{\partial \{\sigma\}}\right\}^T$$

$$[D_c]\left[A + \left\{\frac{\partial F}{\partial \{\sigma\}}\right\}^T [D_c] \left\{\frac{\partial F}{\partial \{\sigma\}}\right\}\right]^{-1} \qquad (7.20)$$

$$A = \frac{\partial F}{\partial k} \Delta k \frac{1}{\lambda} \qquad (7.21)$$

k = hardening parameter

λ = proportionality constant

The elasto-plastic matrix $[D_c]_{ep}$ can be derived by assuming that the changes of strains during an infinitesimal increment of stress can be divided into an elastic and plastic parts, i.e.,

$$\{\Delta\varepsilon\} = \{\Delta\varepsilon\}_e + \{\Delta\varepsilon\}_p \qquad (7.22)$$

and adopting the associated flow rule or normality principle of plasticity, i.e.,

$$\{\Delta\varepsilon\}_p = \frac{\partial F}{\partial \{\sigma\}} \cdot \lambda \qquad (7.23)$$

$[D_c]_{ep}$ replaces the elasticity matrix $[D_c]$ in incremental analysis.

In the present study, F is given by equation (7.17). Ideal plasticity with no hardening is assumed and hence A is zero.

It should be pointed out that the inelasticity of concrete is caused not by actual plastic flow but by the cummulative effect of microcrack propagation. Therefore plasticity theory is not strictly applicable to concrete. However past experience has shown that it is sufficiently accurate for many applications notably the analysis of reinforced concrete beams and slabs. This is probably due to the fact that in such structures, other effects such as cracking and yielding of steel reinforcement are

more important. The addition of steel fibres improves the ductility of the composite and consequently the plasticity theory may be more appropriate to fibre concrete.

7.3.2.6 Fracture Criterion for Crushing of Concrete in Compression-Compression Zone

The fracture criterion adopted is analogous to the Von Mises yield criterion but in terms of strains. Lin and Scordelis (138) used similar approach. Thus crushing of concrete occurs if:

$$C(\varepsilon) = [\tfrac{1}{2}(\varepsilon_x - \varepsilon_y)^2 + \tfrac{1}{2}(\varepsilon_y - \varepsilon_z)^2 + \tfrac{1}{2}(\varepsilon_z - \varepsilon_x)^2 + \tfrac{3}{4}\gamma_{xy}^2 + \tfrac{3}{4}\gamma_{yz}^2 + \tfrac{3}{4}\gamma_{zx}^2]^{\frac{1}{2}} - \varepsilon_u' = 0 \quad (7.24)$$

where ε_u' = the ultimate strain in the uniaxial compression test

It is customary to take ε_u' to be 0.35% for plain concrete. The addition of steel fibres increases the ultimate strain (Fig. 7.9(a)) and an ultimate strain of 0.45% has been commonly used (64, 99). Therefore ε_u' is taken to be 0.45% for fibre concrete.

Once crushing has occurred, the concrete is assumed to lose all its stiffness. All terms in the material matrix are reduced to negligible values. The stresses prior to cracking are released completely for both plain and fibre concrete.

7.3.2.7 Fracture Criterion in Tension-Compression Domain For Plain Concrete

Calzona et al (151, 152, 153) carried out a comparative study of dense concrete and lightweight concrete under shear-compression or tension-compression state of stress. To date, this is probably the only major study on the behaviour of lightweight

aggregate concrete under such stress state.

The stress state was achieved by subjecting hollow cylinder specimens to compression and torsion. Thirty specimens were cast for each type of concrete. Each specimen had an outer diameter of 400 mm and an inner diameter of 300 mm, and an overall length of 800 mm. The specimens were tested under different ratios of torsional to axial load. The first crack and maximum torsional and compressional loads were recorded.

The main conclusion drawn was that lightweight concrete having equal uniaxial compressive strength showed lower values of first crack and failure stresses. Calzona et al attributed this to the fact that the "internal frictional effect" is less for the lightweight concrete than for the dense concrete.

Fig. 7.13 shows the test results of the lightweight concrete plotted in I_1, and $\sqrt{J_2}$ invariant stress space. The fracture surface has been approximated as

$$\sqrt{J_2} = c_o f_c' + c_1 I_1 + c_2 I_1^2 \qquad (7.25)$$

where $c_o \doteq \alpha = \frac{f_t'}{f_c'}$

$$c_1 = -\frac{(1 - \sqrt{3}\,\alpha)}{\sqrt{3}} \cdot \frac{6}{7}$$

$$c_2 = -\frac{c_1}{6 f_c'}$$

f_t' = uniaxial tensile strength

and f_c' = uniaxial compressive strength

Fig. 7.14 shows the test results of the dense concrete plotted in I_1 and $\sqrt{J_2}$ invariant stress space. The fracture surface has been approximated as

$$\sqrt{J_2} = c_o f_c' + c_1 I_1 \qquad (7.26)$$

where $c_o = \frac{f_t'}{f_c'} = \alpha$

and $c_1 = -\frac{(1 - \sqrt{3}\ \alpha)}{\sqrt{3}}$

The above criteria are adopted for the present finite element model. There are other fracture criteria for normal weight concrete subjected to tension-compression stress state (139, 154, 155) and the incorporation of any of these criteria into the present finite element model is straight forward. However, the accuracy of the various criteria has not been investigated in the present study.

7.3.2.8 Fracture Criteria in Tension-Tension Domain

There is at present no available information on the behaviour of lightweight aggregate concrete subject to multiaxial tensile stress state. In normal weight concrete, the most accepted failure theories for predicting cracking of concrete in tension are the maximum stress and maximum strain criteria. These theories state that if a principal tensile stress or strain reaches the uniaxial tensile strength of concrete then a crack is assumed to occur in a direction perpendicular to the offending principal stress or strain.

7.3.2.9 Simulation of Tensile Cracking

Essentially there are two main ways of simulating the effect of cracking in finite element models. The first allows the cracks to form between element boundaries. Ngo and Scordelis (106) predefined the crack pattern in accordance to previous experimental observation. Nilson (110) used an incremental solution to crack propagation. Cracking was simulated by allowing adjacent concrete elements to separate along their common boundaries, thus requiring repeated renumbering of the structure. Loov (156) used a similar

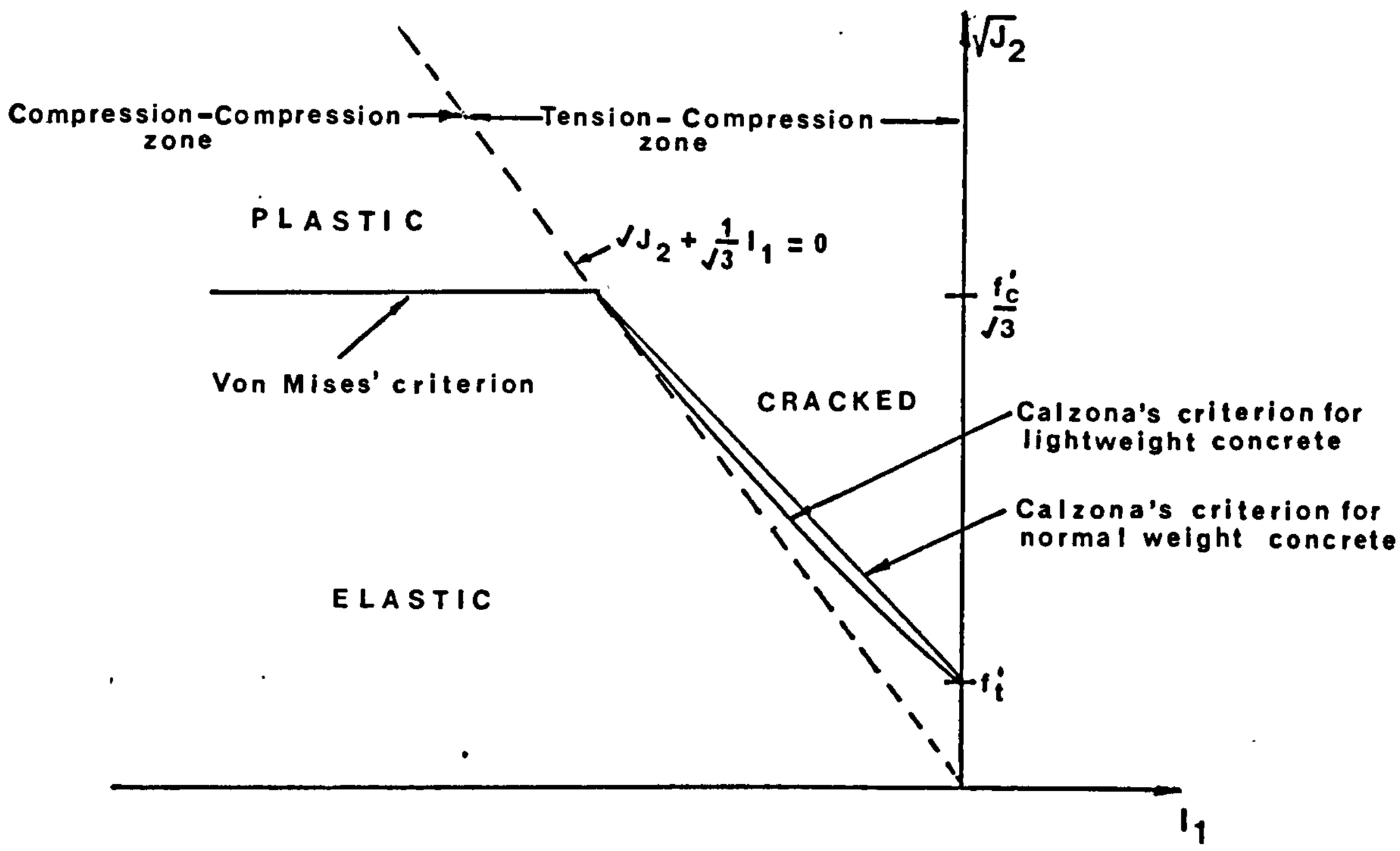

Fig. 7·12 Assummed Failure Surfaces Of Concrete In Compression-Compression And Tension-Compression Zones (I_1, $\sqrt{J_2}$ Space)

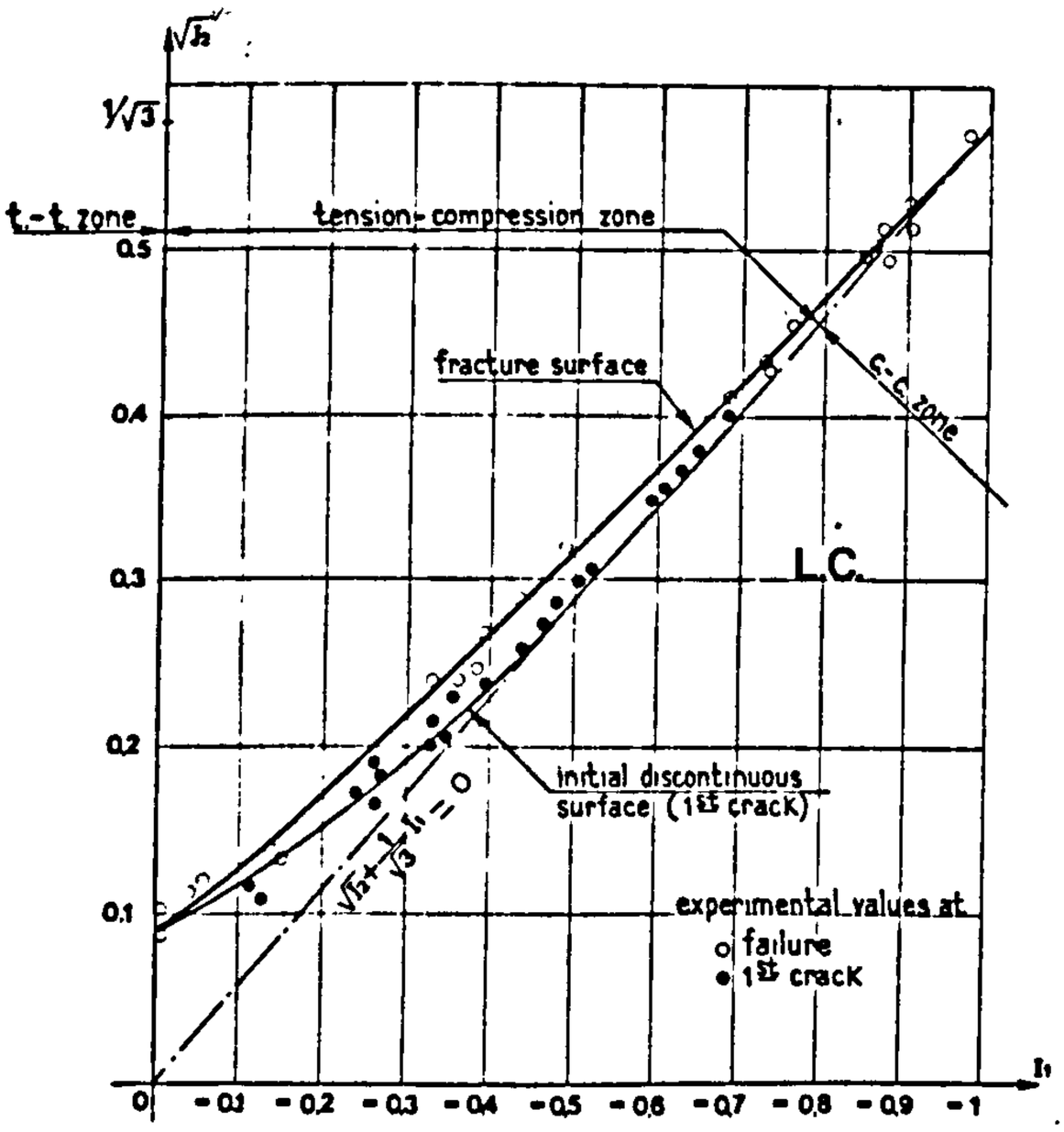

Note: I_1 & $\sqrt{J_2}$ are normalised w.r.t. f_c'

Fig.7·13 Test Results Of Lightweight Concrete Subjected Tension-Compression Stress State (I_1, $\sqrt{J_2}$ Space), After Ref. (153)

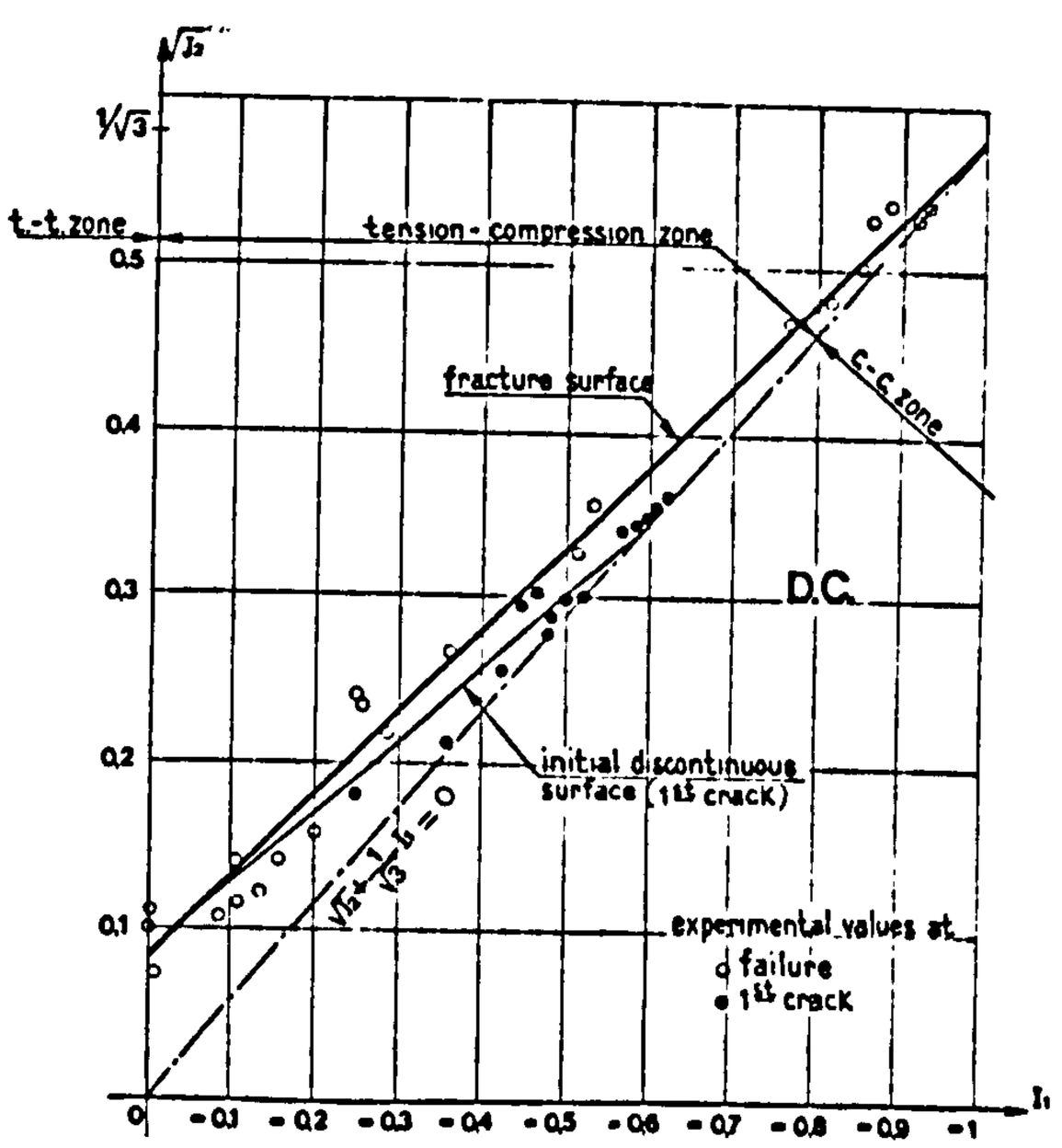

Fig. 7.14 Test Results Of Dense Concrete Subjected To Tension-Compression Stress State (I_1, $\sqrt{J_2}$ Space), After Ref. (153)

approach but he replaced the cracked element by four smaller elements, and separate nodes were redefined on both sides of the crack.

The limitations of the above technique are that cracks are artificially constrained to form along the element boundaries and the need to redefine the finite element mesh, which is computationally cumbersome. To overcome this, Sled (157) suggested the possibility of allowing cracks to occur within the elements themselves by modifying the element material matrices. The average properties of the cracked region are determined by this technique. Therefore a high accuracy in the crack pattern can only be obtained by using fine meshes. This method of simulating cracking in concrete has now been widely accepted.

7.3.2.10 Cracking in the Tension-Compression and Tension-Tension Zones

In the present study, the maximum principal tensile stress criterion is used to predict cracking in the tension-tension regime. A crack is assumed to open at an integration point when a principal tensile stress exceeds the uniaxial tensile strength f_t'. The plane of the crack is normal to the offending principal stress direction. Thus for cracking

$$\sigma_1 \geq f_t'$$

At the instant of the crack formation, the tensile stress normal to the plane of the crack is reduced to a negligible value in the case of plain concrete and to a constant value, the post-cracking tensile strength σ_{cu}, in the case of fibre concrete. See Figs. 7.10(b) and 7.11(b). The stress released is redistributed to other parts of the structure. In a direction parallel to the crack, the material is assumed to be capable of sustaining stresses

according to the biaxial stress state existing after cracking.

Cracking in the tension-compression zone is predicted by fracture criteria similar to those proposed by Calzona et al as described in section 7.3.2.10. The fracture suraces for both lightweight and normal weight concrete are shown in Fig. 7.12 in the invariant stress space. It is further assumed that the general form of equation (7.25) and equation (7.26) is applicable to fibre concrete. The validity of this assumption cannot be verified at the moment due to lack of experimental information. When the principal stresses at an integration point satisfy this criterion (i.e., when $\sqrt{J_2}$ is greater than or equal to the R.H.S. of equation (7.25) or equation (7.26)), fracture occurs. A single cleavage fracture orthogonal to the maximum principal stress is assumed irrespective of the tension to compression ratio.

7.3.2.11 Shear Retention Factor β

The shear retention factor β is introduced into the constitutive relations of cracked concrete. It represents a simple way to account for the effect of aggregate interlocking at a crack and dowel action of the reinforcement. Thus after cracking:

$$\tau^* = \beta G \gamma^* \qquad (7.27)$$

where G is the material shear modulus before cracking. βG may be considered as the effective cracked shear modulus.

Many researchers (e.g. 51, 62, 115, 116, 117, 138) have taken β to be a constant having value ranges from 0 to 1. This does not give a true representation as the cracked shear modulus in a real situation decreases with increasing crack width (as can be seen from the literature review and experimental study reported in Chapter 5). In order to give a closer representation to the physical phenomenon, Cedolin and Poli (52) allowed the cracked shear

modulus to decrease linearly with the fictitious tensile strain in the direction normal to the crack. Gogate and Bishara (158) considered the degradation of the cracked shear modulus as a function of the crack width.

From the experimental work on shear transfer reported in Chapter 5, it has been concluded that the shear transfer stiffness (equivalent to the cracked shear modulus) of plain and fibre reinforced concrete can be adequately expressed as:

For Lytag-sand concrete,

$$G_s = 2.5 \left(\frac{1}{w}\right)^{1.75} \tag{7.28}$$

For gravel concrete,

$$G_s = 3.0 \left(\frac{1}{w}\right)^{1.75} \tag{7.29}$$

G_s is the shear stransfer stiffness in N/mm^2 and w is the crack width in mm.

In the present study, in order to avoid excessive computational time, no attempt is made to calculate the crack widths. β is chosen instead to vary with the fictitious tensile strain in the direction normal to the crack according to the following relation:

$$\beta = \alpha \left(\frac{\varepsilon_t}{\varepsilon_1}\right)^{1.75} \tag{7.30}$$

where α = constant

ε_t = limiting uniaxial tensile strain

and ε_1 = fictitious tensile strain in the direction normal to the crack.

An α value of 0.5 has been found to give satisfactory results with regards to the deformation and ultimate strength of both plain and

fibre reinforced Lytag-sand and gravel concrete beams.

In order to make a comparative study, a constant β of 0.1 has also been used.

7.3.2.12 Incremental Constitutive Relations of Cracked Concrete

Before cracking, the incremental constitutive relations can be written as

$$\begin{Bmatrix} \Delta\sigma_x \\ \Delta\sigma_y \\ \Delta\sigma_z \\ \tau_{xy} \\ \tau_{yz} \\ \tau_{zx} \end{Bmatrix} = \begin{bmatrix} D_{c11} & D_{c12} & D_{c13} & 0 & 0 & 0 \\ & D_{c22} & D_{c23} & 0 & 0 & 0 \\ & & D_{c33} & 0 & 0 & 0 \\ & & & D_{c44} & 0 & 0 \\ & \text{symmetric} & & & D_{c55} & 0 \\ & & & & & D_{c66} \end{bmatrix} \begin{Bmatrix} \Delta\varepsilon_x \\ \Delta\varepsilon_y \\ \Delta\varepsilon_z \\ \Delta\gamma_{xy} \\ \Delta\gamma_{yz} \\ \Delta\gamma_{zx} \end{Bmatrix} \quad (7.31)$$

$$\{\Delta\sigma\} = [D_c]\{\Delta\varepsilon\} \quad (7.32)$$

The elements D_{cij} can be identified from equation (7.11). The matrix $[D_c]$ is isotropic and hence equation (7.31) is applicable in any rectangular reference frame.

After cracking, orthotropic conditions are introduced and the material matrix $[D_c]$ is modified to $[D_c]^*$ to reflect that the concrete exhibits no resistance against further loading in the direction perpendicular to the crack. $[D_c]^*$ is given by

$$[D_c]^* = \begin{bmatrix} 0 & 0 & 0 & 0 & 0 & 0 \\ & \left(D_{c22}-\frac{D_{c12}^2}{D_{c11}}\right) & \left(D_{c23}-\frac{D_{c13}D_{c12}}{D_{c11}}\right) & 0 & 0 & 0 \\ & & \left(D_{c33}-\frac{D_{c13}^2}{D_{c11}}\right) & 0 & 0 & 0 \\ & & & \beta D_{c44} & 0 & 0 \\ & \text{Symmetric} & & & D_{c55} & 0 \\ & & & & & \beta D_{c66} \end{bmatrix} \quad (7.33)$$

in which β is the shear retention factor as discussed in the previous section.

As the constitutive relationships are still elastic after cracking, the material matrix $[D_c]^*$ represents a sudden change from one elastic state to another. Thus, the crack propagation is solved by a series of transitions from one instantaneous elastic stiffness to another.

Since the modified material matrix $[D_c]^*$ is referred to the principal stress co-ordinate system, it is essential to transform it back to the global co-ordinate system for stiffness calculations. This can be done through the use of a transformation matrix as follows:

$$[D_c] = [T]^T [D_c]^* [T] \tag{7.33}$$

where the transformation matrix [T]has the following form

$$[T] = \begin{pmatrix} a_{11}^2 & a_{21}^2 & a_{31}^2 & a_{11}a_{21} & a_{21}a_{31} & a_{11}a_{31} \\ a_{12}^2 & a_{22}^2 & a_{32}^2 & a_{12}a_{22} & a_{22}a_{32} & a_{12}a_{32} \\ a_{13}^2 & a_{23}^2 & a_{33}^2 & a_{13}a_{23} & a_{23}a_{33} & a_{13}a_{33} \\ 2a_{11}a_{12} & 2a_{21}a_{22} & 2a_{31}a_{32} & a_{11}a_{22}+a_{12}a_{21} & a_{21}a_{32}+a_{22}a_{31} & a_{11}a_{32}+a_{12}a_{31} \\ 2a_{12}a_{13} & 2a_{22}2_{23} & 2a_{32}a_{33} & a_{12}a_{23}+a_{13}a_{22} & a_{22}a_{33}+a_{23}a_{32} & a_{12}a_{33}+a_{13}a_{32} \\ 2a_{11}a_{13} & 2a_{21}a_{23} & 2a_{31}a_{33} & a_{11}a_{23}+a_{13}a_{21} & a_{21}a_{33}+a_{23}a_{31} & a_{11}a_{33}+a_{13}a_{31} \end{pmatrix} \tag{7.34}$$

where a_{ij} are the terms from the normalized modal matrix [A]

$$[A] = \begin{pmatrix} a_{11} & a_{12} & a_{13} \\ a_{21} & a_{22} & a_{23} \\ a_{31} & a_{32} & a_{33} \end{pmatrix} \qquad (7.35)$$

in which a_{11} = direction cosine of the major principal stress axis to the global x-axis

a_{21} = direction cosine of the major principal stress axis to the global y-axis

a_{31} = direction cosine of the major principal stress axis to the global z-axis

A method for calculating matrix [A] is given in references(148) and (51).

7.4 Mathematical Modelling of Steel Reinforcement

Steel reinforcement can be assumed to be stressed uniaxially. The material property of steel is very well defined. A typical uniaxial stress-strain curve for high yield steel is shown in Fig. 7.15. In the present study, it is idealized as elastic-plastic as shown in the same figure. The Young's modulus of steel, E_s, is taken as 200 kN/mm^2 and the yield stress from Table 3.2.

7.5 Nonlinear Solution Procedure

7.5.1 General

In the present analytical study, only time independent material nonlinearity due to monotonically increasing loading is considered. Geometrical nonlinearity, creep and shrinkage effects and cyclic loadings are beyond the scope of this work.

The nonlinear solution is carried out by using a combined

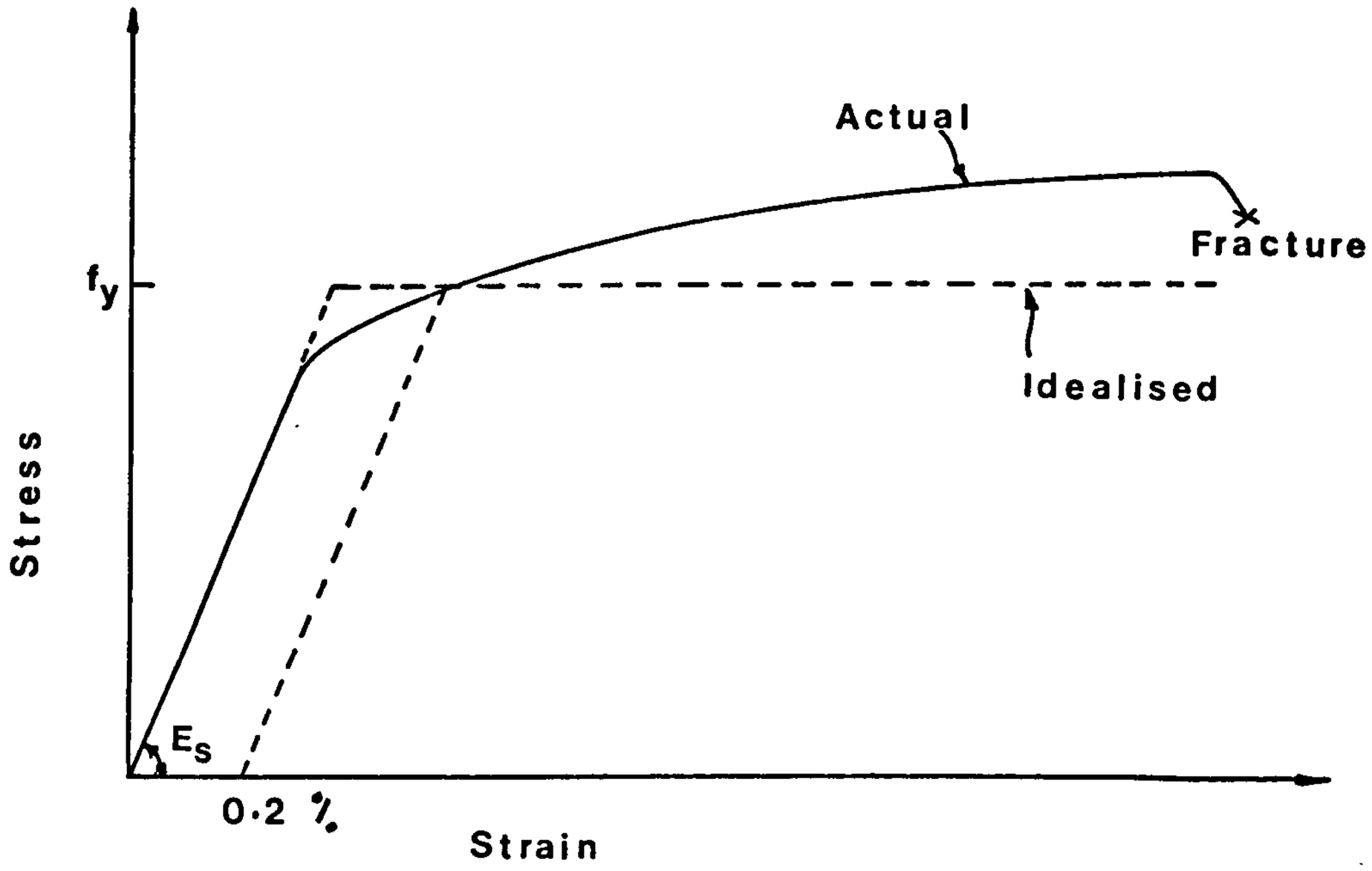

Fig. 7·15 Uniaxial Stress-Strain Curve For High Yield Steel

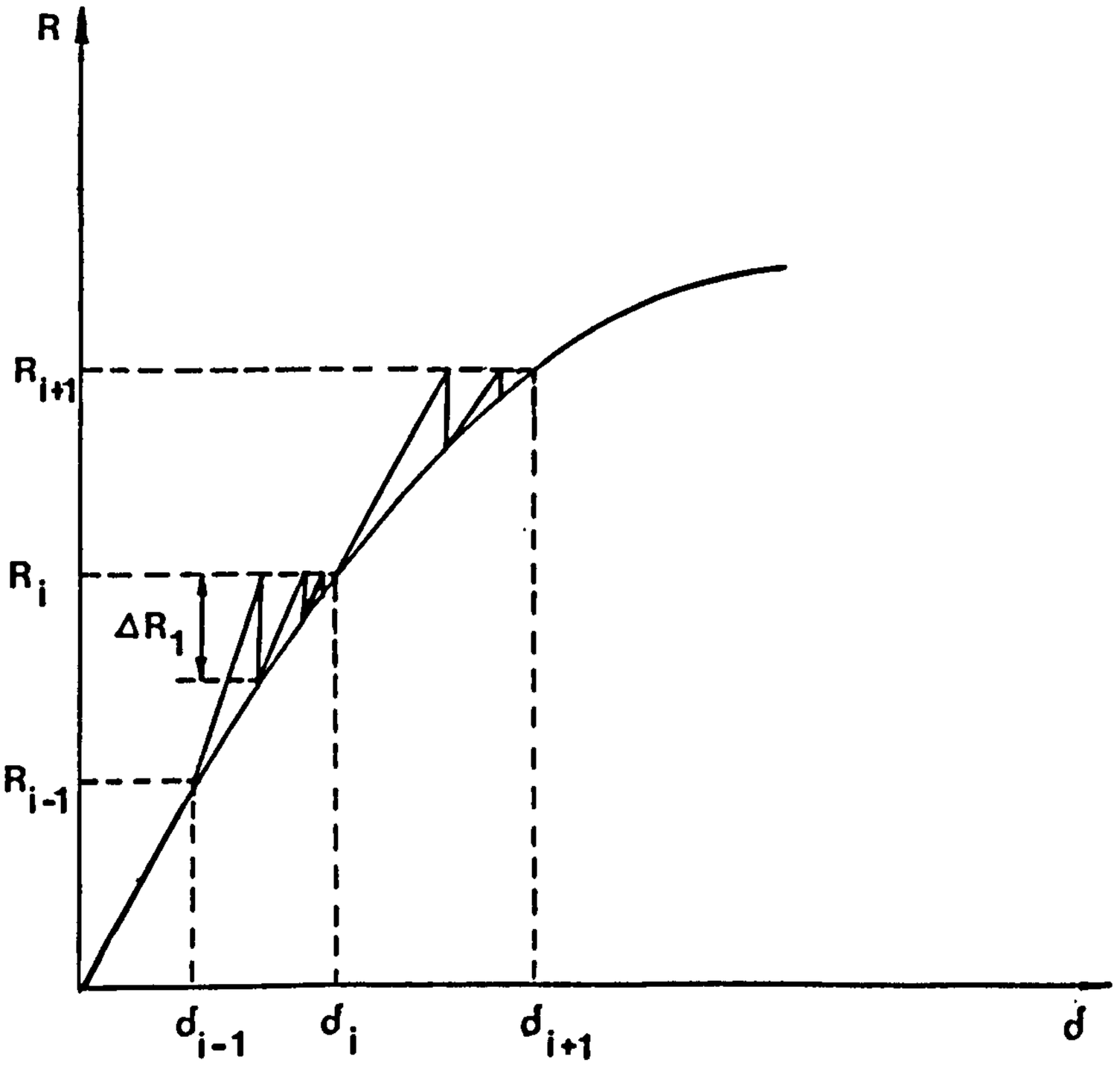

Fig. 7·16 Combined Incremental And Iterative Procedure

incremental and iterative scheme as shown in Fig. 7.16. The loading is applied incrementally. For each increment of loading, iterations are performed until the equilibrium and constitutive relations are satisfied within a tolerable limit. The structural stiffness matrix is updated after every iteration and the structure is reanalysed for the unbalanced nodal forces $\{\Delta R_1\}$ resulted from the previous iteration.

7.5.2 Computational Procedure

The essential steps for a typical load increment are as follows:

1. The load increment is applied and a first estimate of the nodal displacements $\{\Delta\delta\}_1$ is computed using the updated global stiffness matrix existing at the end of the iteration for the previous load increment. The elastic increments of the strains $\{\Delta\varepsilon\}_1$ and stresses $\{\Delta\sigma^1\}_1$ are then computed using the material properties used in forming the current structural stiffness matrix.

2. These increments are added to the existing values at the start of the load increment to obtain the current total displacements, strains and stresses

$$\{\delta_i\} = \{\delta_{i-1}\} + \{\Delta\delta\}_1 \qquad (7.36)$$

$$\{\varepsilon_i\} = \{\varepsilon_{i-1}\} + \{\Delta\varepsilon\}_1 \qquad (7.37)$$

$$\{\sigma_i^1\} = \{\sigma_{i-1}\} + \{\Delta\sigma^1\}_1 \qquad (7.38)$$

3. The stress vector $\{\sigma_i^1\}$ is checked against the Von Mises yield criterion, F. If F $(\{\sigma_i^1\}) < 0$, then only elastic strains have occurred. Proceed to step 5.

If $F(\{\sigma_i^1\}) > 0$ but $F(\{\sigma_{i-1}\}) < 0$ (i.e yielding for the first time), determine the intermediate stress value at which yielding begins using the r factor method (159) described in Appendix D. Compute increment $\{\Delta\sigma_1\}$ using equation (7.19) starting from that point

$$\{\Delta\sigma\}_1 = (1 - r)\ [D_c]_{ep}\ \{\Delta\varepsilon\}_1 \qquad (7.39)$$

with $[D_c]_{ep}$ computed from equation (7.20) with stresses (σ_i^1). The updated stress vector is

$$\{\sigma_i\} = \{\sigma_{i-1}\} + r\{\Delta\sigma^1\}_1 + \{\Delta\sigma\}_1 \qquad (7.40)$$

If yielding at the integration point has occurred at the start of increment, find$\{\Delta\sigma\}_1$ using equation (7.19).

$$\{\Delta\sigma\}_1 = [D_c]_{ep}\ \{\Delta\varepsilon\}_1 \qquad (7.41)$$

The updated stress vector is given by

$$\{\sigma_i\} = \{\sigma_{i-1}\} + \{\Delta\sigma\}_1 \qquad (7.42)$$

The stresses released due to plastic yielding are thus given by

$$\{\Delta\sigma_p\} = (\{\sigma_i^1\}_1 - \{\sigma_i\}) \qquad (7.43)$$

These stresses are converted to unbalanced nodal forces for the element through propert integration.

$$\{\Delta R_1\}_p = \int [B]^T \{\Delta\sigma_p\}\ d\ (vol) \qquad (7.44)$$

4. The strain vector $\{\varepsilon_i\}$ is checked against the crushing criterion of concrete (equation (7.24)). If the latter is satisfied, crushing occurs and the stress vector $\{\sigma_i\}$ is converted entirely into unbalanced nodal forces by

$$\{\Delta R_1\}_c = \int [B]^T \{\sigma_i\}\ d\ (vol) \qquad (7.45)$$

The terms in the material matrix are all set to a negligible value.

5. The principal stresses are checked against the appropriate fracture criterion for cracking. If it is satisfied, cracking occurs and the material matrix $[D_c]$ is modified appropriately. For the case of no previous cracking at the integration point, the stresses over and above the allowable tensile strength after cracking, $\{\sigma_t\}^*$, are released. The allowable tensile strength after cracking is zero for plain concrete and σ_{cu} for fibre concrete. These released stresses are referred to as the principal stress co-ordinate system and hence they are transformed to the global reference frame as follows:

$$\{\sigma_t\} = [T]^T \{\sigma_t\}^* \qquad (7.46)$$

where [T] is given by equation (7.34).

The stress vector $\{\sigma_t\}$ is then converted to an equivalent unbalanced nodal force vector $\{\Delta R_l\}_t$.

$$\{\Delta R_l\}_t = \int [B]^T \{\sigma_t\} \, d\,(vol) \qquad (7.47)$$

The updated stress vector at the cracked integration point is given by

$$\{\sigma_i\} = \{\sigma_i{}^1\} - \{\sigma_t\} \qquad (7.48)$$

If cracking has occurred previously at the point, then the stresses released are those due to the degradation of the cracked shear modulus, βG. These stresses are given by

$$\{\Delta\tau_a\}^* = (\beta_{i-1} - \beta_i)G\{\Delta\gamma\}^* \qquad (7.49)$$

where $\{\Delta\gamma\}^*$ are the incremental shear strains in the plane of the crack. $\{\Delta\tau_a\}^*$ are then transformed back to the global

reference frame as $\{\Delta\sigma_a\}$. Thus the unbalanced nodal forces are given by

$$\{\Delta R_1\}_a = \int [B]^T \{\Delta\sigma_a\} \, d(\text{vol}) \tag{7.50}$$

and the updated stress vector is given by

$$\{\sigma_i\} = \{\sigma_i{}^1\} - \{\Delta\sigma_a\} \tag{7.51}$$

Obviously if a constant β is used there will be no residual stresses.

6. Check for yielding of the steel reinforcement. If yielding occurs, the force over and above the yield force of the steel element is converted directly to equivalent nodal forces of the parent element, $\{\Delta R_1\}_r$, by simple linear interpolation. The stiffness of the steel element is then reduced to a negligible value and the stress in the steel element updated to the yield stress.

7. The equivalent unbalanced nodal force vector for the whole structure is evaluated as

$$\{\Delta R_1\} = \sum^{\text{all conc. elements}} (\{\Delta R_1\}_p + \{\Delta R_1\}_c + \{\Delta R_1\}_t + \{\Delta R_1\}_a + \{\Delta R_1\}_r) \tag{7.52}$$

8. Form new structural stiffness matrix and analyse for the unbalanced nodal forces to obtain the increments of nodal displacements $\{\Delta\delta\}_2$. Hence compute $\{\Delta\varepsilon\}_2$ and $\{\Delta\sigma^1\}_2$.

9. Repeat steps 2 - 7.

10. Check the displacement increments for convergence. If they have converged or the number of iterations has exceeded the

prescribed limit, proceed to step 1 for the next load increment. Convergence is assumed if

$\{\Delta\delta\}_2 - \{\Delta\delta\}_1 \leq$ a prescribed constant.

CHAPTER EIGHT

COMPUTER PROGRAM

8.1 Introduction

This chapter describes in some detail the computer program developed for the present study. In the present form, the program can analyse plain or fibre reinforced lightweight and normal weight concrete beams of any arbitrary shape but of uniform cross-section throughout.

The program is coded in Fortran IV language for Prime 750 computers.

A three dimensional finite element analysis is generally costly in terms of computational time. Steps should be taken to ensure that wastage in computational time is minimized. The present program allows the user to terminate the analysis temporarily after a specified number of load increments so that a check of the results obtained so far can be carried out. If the results are reasonable, the analysis is resumed with a further number of load increments. Otherwise, the analysis is discontinued. This procedure does not require an advanced knowledge of the expected failure load of the beam.

Finally four temporary files (designated F1, F2, F3, F4) are used to relieve the core-store requirements and to enable the program to be written in as efficient a form as possible. To implement the above stop-check-and-continue solution procedure, another temporary file (F5) is used.

8.2 Structure of the Program

The program consists of a set of subroutines which perform the basic computations and a master segment which controls the order in which the subroutines are called.

A flow chart for the main operations in the program for

a specified number of load increments is shown in Fig. 8.1. Note that for the first load increment, an exact elastic analysis is carried out.

8.2.1 Master Segment

In addition to controlling the order in which the subroutines are called, the master segment also does the following:

(1) It reads the current load increment number, the number of load increments and the control for the type of shear retention factor to be used. It updates the load increment number by one after every load increment.

(2) It evaluates the differences in the current displacements in the x, y and z directions and the corresponding displacements in the previous iteration for every node of the structure. It then compares them with the convergence criteria given below

$$u_i - u_{i-1} \leq 0.01$$

$$v_i - v_{i-1} \leq 0.05$$

$$w_i - w_{i-1} \leq 0.01$$

The next load increment is applied if the criteria are satisfied or if the number of iteration exceeds 5.

8.2.2 Subroutine GDATA

This subroutine reads the material properties, the local co-ordinates of the element nodes and integration points, the boundary nodes and the boundary conditions.

8.2.3 Subroutine DATGEN

Based on input information for the first set of elements in the yz plane and the number and sizes of the discretization

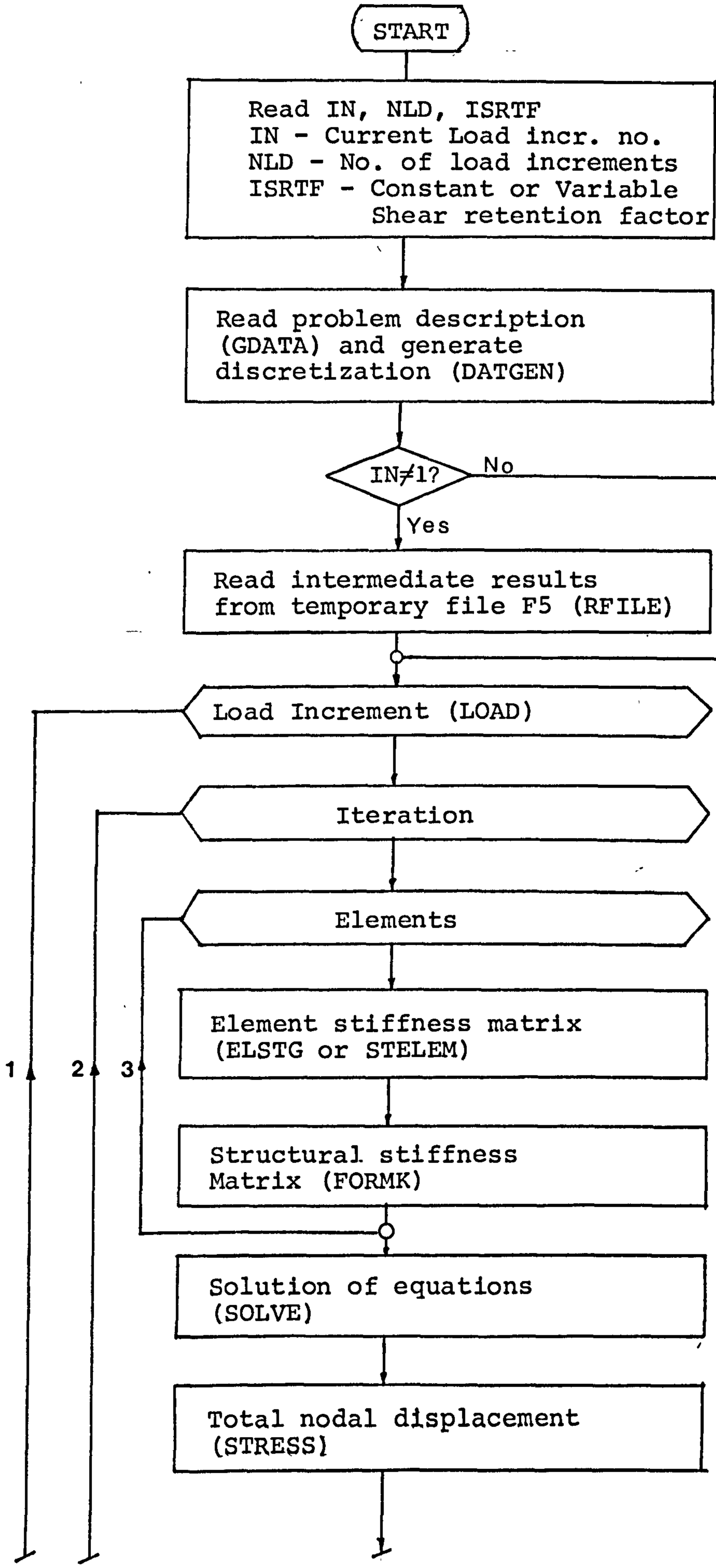
START
Read IN, NLD, ISRTF
IN - Current Load incr. no.
NLD - No. of load increments
ISRTF - Constant or Variable
Shear retention factor
Read problem description
(GDATA) and generate
discretization (DATGEN)
IN≠1?
No
Yes
Read intermediate results
from temporary file F5 (RFILE)
Load Increment (LOAD)
Iteration
Elements
Element stiffness matrix
(ELSTG or STELEM)
Structural stiffness
Matrix (FORMK)
Solution of equations
(SOLVE)
Total nodal displacement
(STRESS)
1
2
3

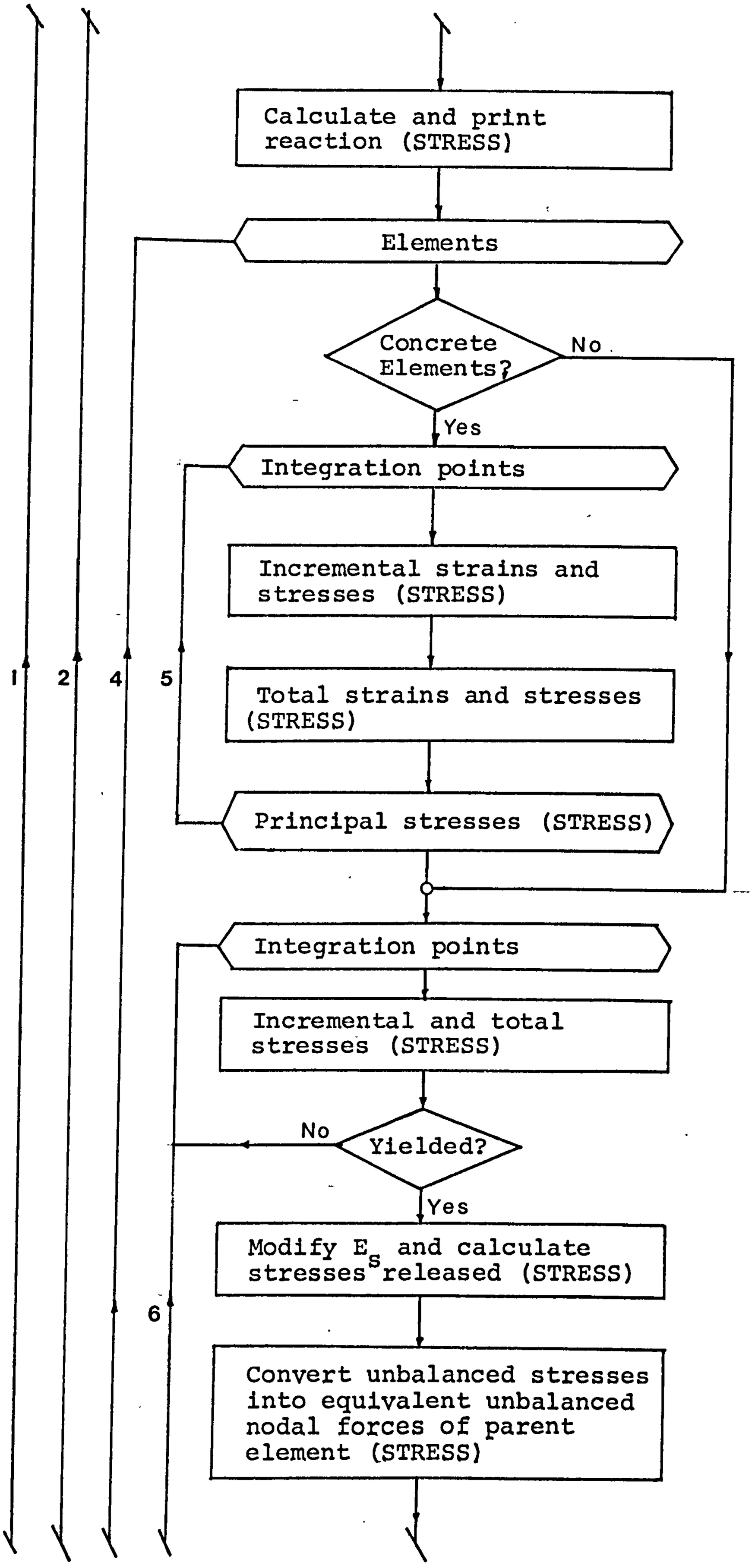
Calculate and print reaction (STRESS)
Elements
Concrete Elements?
No
Yes
Integration points
Incremental strains and stresses (STRESS)
Total strains and stresses (STRESS)
Principal stresses (STRESS)
Integration points
Incremental and total stresses (STRESS)
No
Yielded?
Yes
Modify E_s and calculate stresses released (STRESS)
Convert unbalanced stresses into equivalent unbalanced nodal forces of parent element (STRESS)
1
2
4
5
6

4

6

Update total stresses (STRESS)

Concrete elements

Integration points

No

Failure criteria (FCRACK)

Yes

Transformation matrix (T) (FCRACK)

Modify material matrix (FCRACK or FYIELD)

Calculate stresses released (FCRACK or FYIELD)

1

2

7

8

Calculate crack direction (FCRACK)

Transform modified material matrix to global axes (FCRACK)

Transform the unbalanced stresses to the global axes (FCRACK)

Update total stresses (FCRACK or FYIELD)

Calculate unbalanced nodal forces (ANODF)

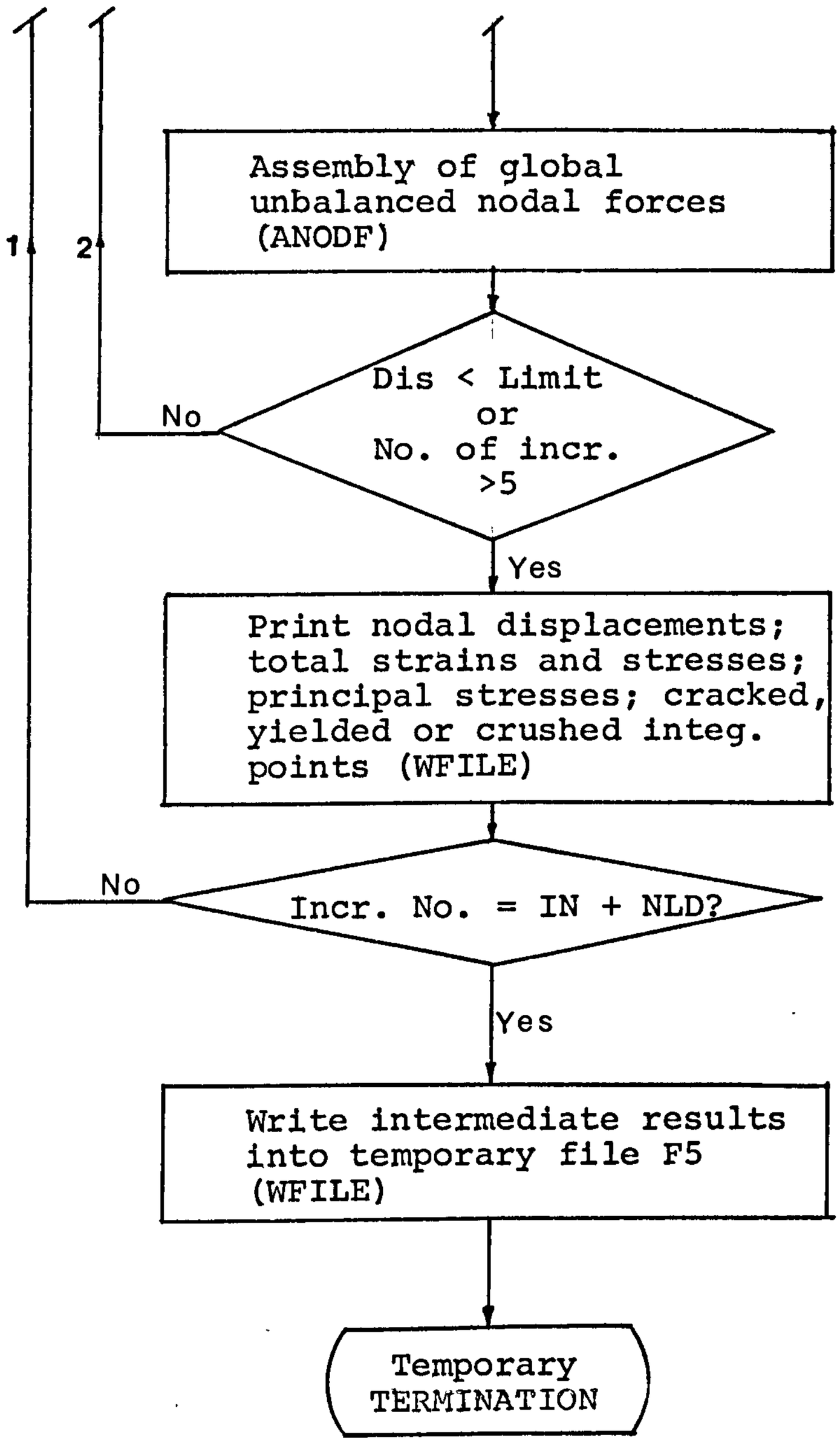

Fig. 8.1 Flow Diagram for the Main Operations of the Computer Program for a Specified Number of Load Increments.

along the x-axis (i.e. the beam axis), DATGEN automatically generates the x, y, z co-ordinates of the rest of the nodes and assigns appropriate node number to the rest of the concrete elements.

The steel element data is read directly.

8.2.4 Subroutine Load

This subroutine reads the incremental external load values and assembles the global load vector.

8.2.5 Subroutine ANODF

This subroutine converts the residual (or released) stresses of each concrete element into unbalanced nodal forces associated with the element. It then assembles these forces and those resulting from the steel elements into the global unbalanced force vector.

8.2.6 Subroutine ELSTG

This subroutine evaluates the stiffness matrix of each of the concrete elements. It contains the main loop for the integration rule. The operations involved are summarized in the self-explanatory flow chart shown in Fig. 8.2

8.2.7 Subroutine SFRI

In this subroutine the shape functions and their first derivations are computed.

8.2.8 Subroutine JACOB

First this subroutine evaluates the (3 x 3) Jacobian matrix from the first derivatives of the shape functions and the x, y, z nodal co-ordinates. Then it determines the determinant of this matrix. If this value is negative or very small, the solution is terminated and an error message is printed to

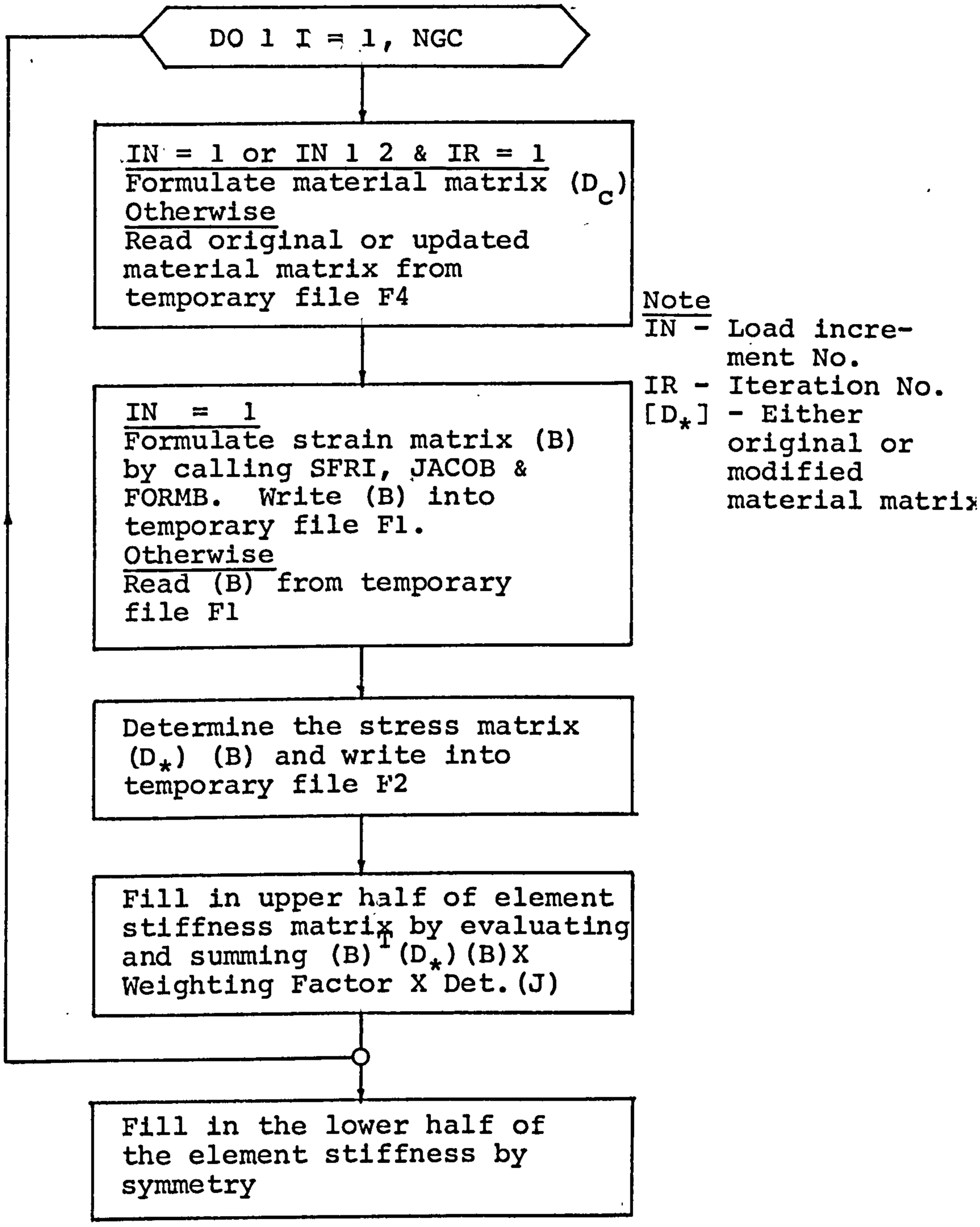

Fig. 8.2 Flow Chart of Subroutine ELSTG

identify the element in which this occurred. Finally the inverse of the Jacobian matrix is formulated.

8.2.9 Subroutine FORMB

This subroutine evaluates the terms of the strain matrix from the inverse of the Jacobian matrix and the first derivatives of the shape functions. It then arranges these terms in the correct-location in the (6 x 24) strain matrix. The strain matrix is written into temporary file F1.

8.2.10 Subroutine STELEM

This subroutine is called to calculate the stiffness of each of the bar elements. It evaluates the shape functions and their first derivatives at the integration points and then using these together with the nodal x, y,z co-ordinates to calculate the strain vector. The stress vector is determined and stored in temporary file F3. The (6 x 6) bar element stiffness matrix is formulated by summing the contribution of stiffnesses at each integration point.

The (6 x 6) stiffness matrix is then expanded into an equivalent (24 x 24) stiffness matrix, associating with the degrees of freedom of the concrete element in which the bar is located.

8.2.11 Subroutine FORMK

This subroutine assembles the global or structural stiffness matrix. After every element stiffness matrix is evaluated, the terms of the matrix are transferred to the structural stiffness matrix none-by-node. The stiffness contribution of the current element to a node is added to the existing stiffness value at that node. The concrete element stiffness matrices are assembled first and then the expanded equivalent

steel element stiffness matrices. As the structural stiffness matrix is banded and symmetrical, only the upper half of the band is formed and then stored in a rectangular array.

Boundary conditions are inserted after completion of the assembly. Each degree of freedom is examined and if it is restrained then a big spring stiffness (10^{25}) is added to the corresponding diagonal term in the structural stiffness matrix.

8.2.12 Subroutine SOLVE

This subroutine is called to solve the governing set of simultaneous equations using Gaussian elimination but taking advantage of the half band width nature of the structural stiffness matrix. The solution gives the global or structural displacement vector associated with the global load vector or the global unbalanced nodal force vector.

8.2.13 Subroutine STRESS

The following operations are executed:

(1) The current incremental nodal displacements are added to the existing nodal displacements to get the total nodal displacements.

(2) The reaction of the support is calculated.

(3) The strain and stress matrices evaluated previously are reread from the temporary files F1 and F2 respectively. These together with the incremental nodal displacements are used to calculate the current increments in the strains and stresses at the integration points. These are then added to the existing stresses and strains to get the total strains and stresses.

(4) The principal stresses are calculated at the integration

points of each concrete element from the total stresses evaluated above.

(5) Increments of the nodal displacements of the bar elements are evaluated by linear interpolation from those of the parent elements. The stress matrices of the bar elements calculated previously are reread from temporary file F3. The increments of the stresses in the bar elements are evaluated at the integration points and these are then added to the existing stresses to give the total stresses.

(6) The total stresses in the bar elements are then checked against the yield stress of the steel reinforcement. If yielding occurs, the Young's modulus E_s is reduced to a negligible value and the total stress over and above the yield stress is released and converted to unbalanced nodal forces associated with the parent element. The total stress is then updated to the yield stress.

8.2.14 Subroutine FCRACK

At each integration point of the concrete elements, the following operations are carried out:

(1) Calculate the principal stress directions and hence the transformation matrix (T).

(2) Check the stress state against the appropriate failure criteria (i.e., tensile cracking, yielding or crushing). Modify the material matrix and determine the stresses released.

(3) Calculate the cracks' directions.

(4) Transform the modified material matrix to the global

directions and write the transformed material matrix into temporary file F4.

(5) Transform the unbalanced stresses into the global directions and then update the total stresses.

8.2.15 Subroutine FYIELD

The call to this routine is issued from subroutine FCRACK. It is called to calculate the plastic stress increment at a yielded integration point. It also checks the total strains of yielded concrete against the crushing criterion. The stresses released due to yielding or crushing are evaluated. The total stresses are then updated and the elasto-plastic or crushed material matrices are written into temporary file F4.

8.2.16 Subroutine WFILE

This subroutine is called to print out the relevant results at the end of each load increment. If it is required to terminate the execution after a certain number of load increments, WFILE writes the intermediate results that are necessary to resume running of the program into temporary file F5.

8.2.17 Subroutine RFILE

This subroutine is called when resuming the run of a program that has been temporarily terminated. It reads back the intermediate results which were stored in the temporary file F5.

8.3 Output of Program

At the end of every load increment, the following results are printed out:

(1) Total displacements at all nodes of the structure.

(2) Reaction at support.

(3) The six components of the total stresses and strains and the principal stresses at each integration point of the concrete elements.

(4) The directions of the cracks with respect to the global axes.

(5) The cracked, yielded or crushed integration points of the concrete elements.

(6) The total stresses at the integration points of the bar elements.

8.4 Concluding Remarks

The program developed was based on an earlier version written by Hammad (51) for the analysis of normal reinforced concrete T beams. He used a 20-node isoparametric element and allowed the steel bar elements to be connected to the concrete elements at the nodes. He adopted a linear elastic-fracture material model for concrete and assumed a linear elastic uniaxial stress-strain curve for the steel reinforcement. He chose an incremental-direct iterative scheme, whereby at each load increment, iterations are carried out using an updated stiffness matrix but using the same load increment every time. No facilities were provided to allow for temporary termination of the execution of the program.

Extensive modifications to the original program had to be made in order to implement the present finite element model and nonlinear solution scheme. The original subroutines FORMK and SOLVE were replaced by more concise and efficient ones. Furthermore, the maximum order of dimension blocks was reduced from 5-dimensional to 3-dimensional. The efficiency of a program improves with the use of lower order dimension blocks.

The form of the present program is very general and it can easily be modified to incorporate higher order isoparametric hexadedral elements and other failure criteria for concrete.

CHAPTER NINE

COMPARISON OF FINITE ELEMENT ANALYTICAL RESULTS WITH TEST DATA

9.1 Introduction

First, the finite element program described in Chapter 8 is used to analyse some of the test beams reported in Chapter 6. The objective is to examine the accuracy of the finite element model developed in Chapter 7 in predicting the behaviour of the plain and fibre reinforced Lytag-sand concrete beams. In particular, the load-displacement behaviour, the load-tensile steel strain relations, the crack patterns and the ultimate strength are compared with the experimental data.

Both constant and variable shear retention factors are used in the numerical analysis. Their effects on the analytical results are presented.

Finally, the finite element program is used to analyse four of the plain and fibre reinforced gravel concrete beams tested by Bahia (6).

9.2 Comparison Using Test Data from Present Investigation

9.2.1 Beam Discrétization

Due to symmetry, only one quarter of the beam needs to be solved analytically. This quarter is formed by the two planes of symmetry, namely, the midspan plane and the longitudinal plane through the middle of the beam.

Each beam was idealized as shown in Fig. 9.1. The dimension of the discretization in the x-direction depends on the shear span/effective depth raio of the beam. A fine discretization was used in order to give a better simulation of the cracking of concrete.

All boundary nodes located on the midspan were constrained horizontally in the x-direction and free to move in the y and z

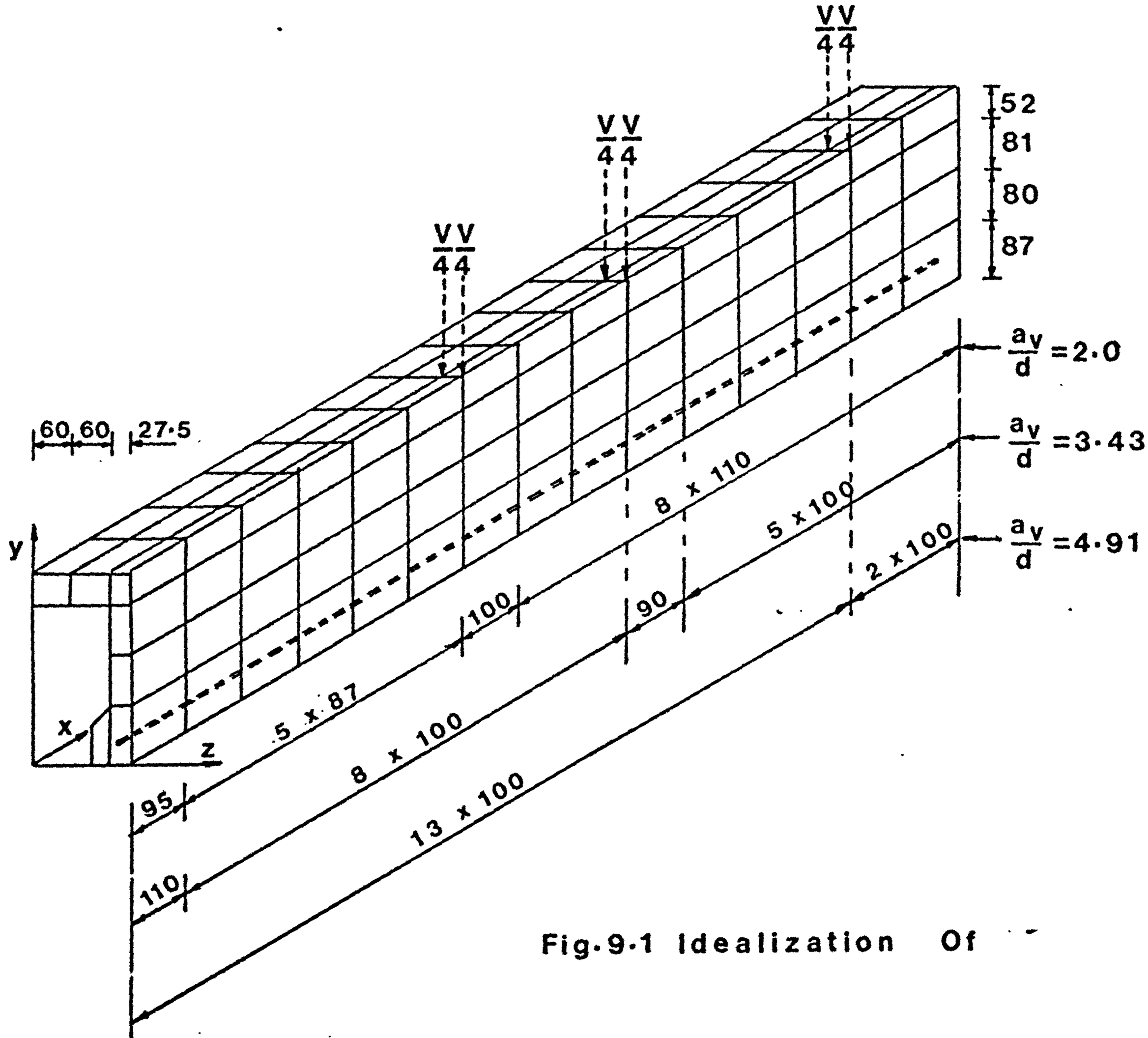

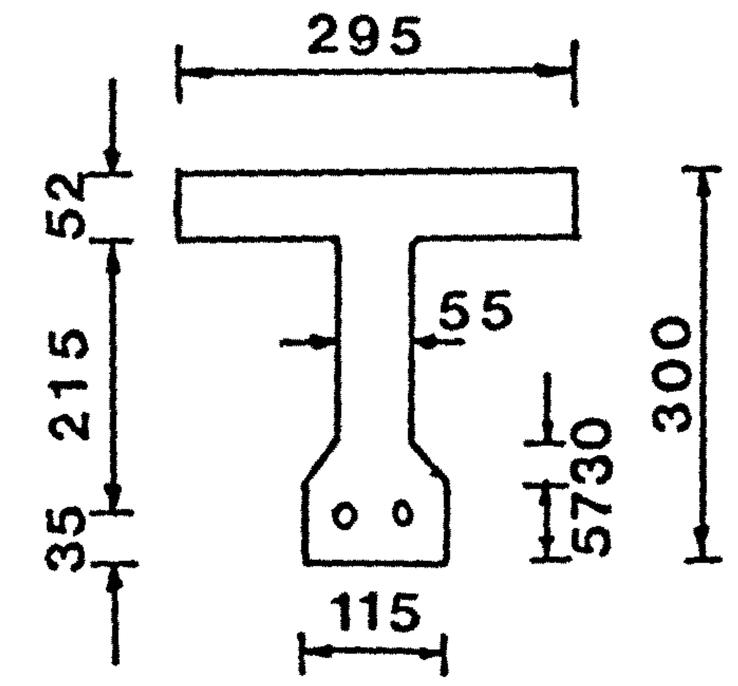

Beam Cross-Section

Fig·9·1 Idealization Of

directions. Boundary nodes located on the longitudinal plane of symmetry were constrained in the z-direction and free to translate in the x and y directions. The nodes at the support were restrained in the y and z direction and free in the x direction.

The applied concentrated load V acting on each shear span was represented by the nodal loads, each of the magnitude $\frac{V}{4}$.

9.2.2 Concrete Material Properties

The material properties were determined from the control specimens cast along with the beams.

9.2.2.1 Uniaxial Compressive Strength

This was taken as 0.8 f_{cu} for plain concrete and 0.85 f_{cu} for fibre concrete.

9.2.2.2 Uniaxial Tensile Strength f_t'

The uniaxial tensile strength f_t' can be approximated from the flexural tensile strength f_{tm} using equation (2.3) of CEB-FIP Model Code (5).

$$\frac{f_{tm}}{f_t'} = 0.6 + \frac{0.4}{\sqrt{h}} \leq 1 \qquad (9.1)$$

where h denotes the height of the element in metres. The control specimens for flexural tensile strength were 100 x 100 x 500 prisms. Thus h = 0.1 m and from the above equation $f_t' = 0.76\ f_{tm}$.

In the numerical analysis f_t' was taken as 0.75 f_{tm} and this corresponds to 2.6 N/mm^2 and 3.5 N/mm^2 for plain and fibre concrete respectively.

The post-cracking tensile strength of fibre concrete was taken as 1.65 N/mm^2 as given in Appendix A.

9.2.2.3 Elastic Modulus E_c

The average elastic modulus as determined from the control specimens was 19.5 kN/mm^2 for plain concrete and 21.3 kN/mm^2 for fibre concrete (section 3.3.5.5)

9.2.2.4 Poisson's Ratio

This was taken as 0.19 for plain concrete and 0.18 for fibre concrete.

9.2.3 Steel Material Properties

The elastic modulus was taken as 200 kN/mm^2 and the Poisson's ratio as 0.33. The yield stresses for the various diameter steel bars are tabulated in Table 3.2

9.2.4 Load-Midspan Displacement Relations

Figs. 9.2(a) through 9.2(e) compare the analytical and experimental load-midspan deflection relations of five plain and five fibre concrete beams. The correlation was reasonable although the stiffness of the fibre concrete beams were generally overestimated in the later stages of loading. This is possibly due to the assumption of a constant post-cracking tensile stress. In reality the tensile post-cracking stress decreases as the crack widens due to increasing fibre pull-out.

The effect of the type of shear retention factor became evident only at the later stages of loading. The constant shear retention factor gave higher deformation stiffnesses than the varying shear retention factor. However, the difference was not very significant and the greater computational effort in adopting a varying shear retention may not be justified.

9.2.5 Steel Strains or Stresses

Figs. 9.3(a) through 9.3(d) show the load-steel strain

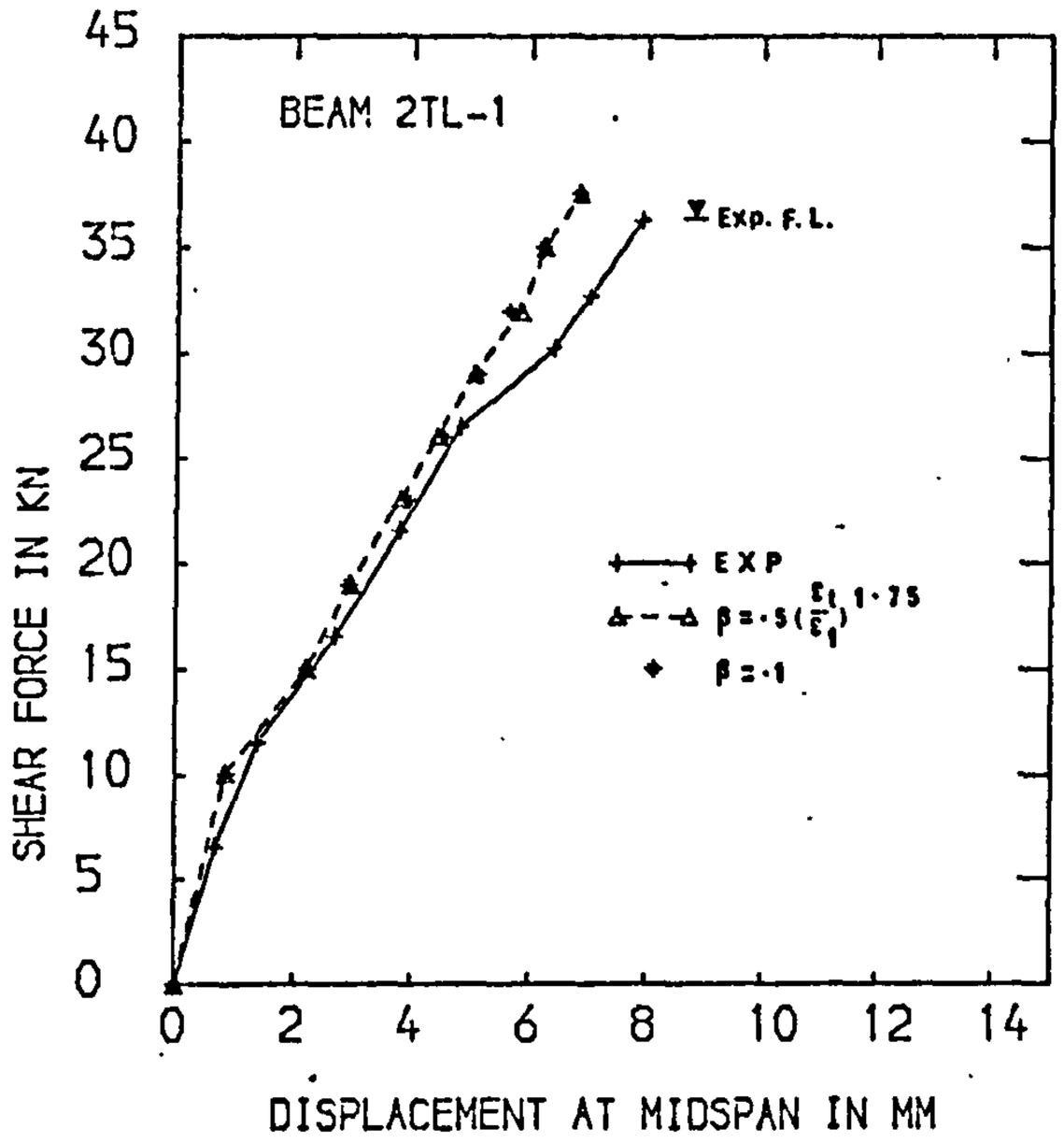

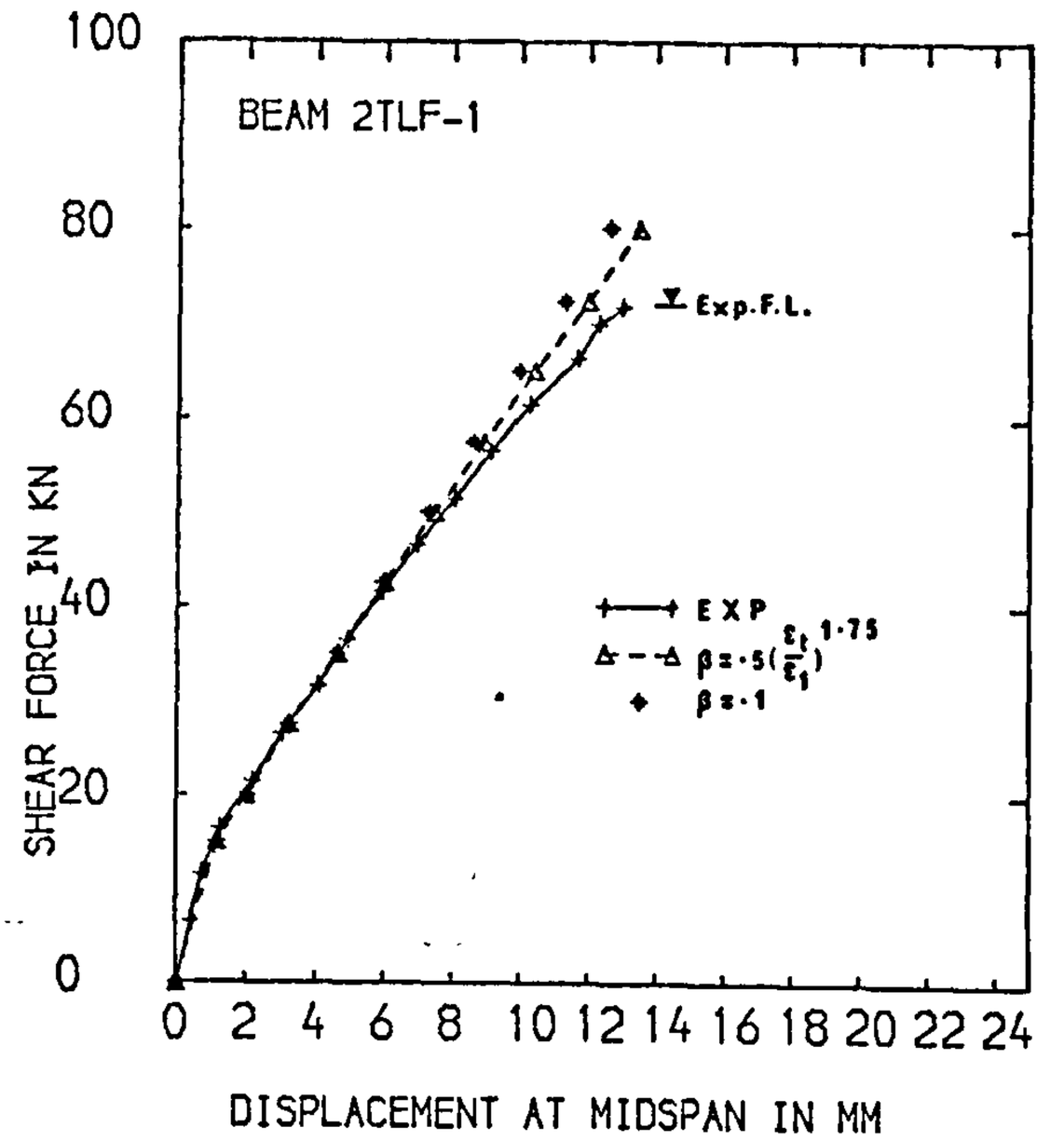

FIG.9.2(a) LOAD-MIDSPAN DISPLACEMENT CURVES

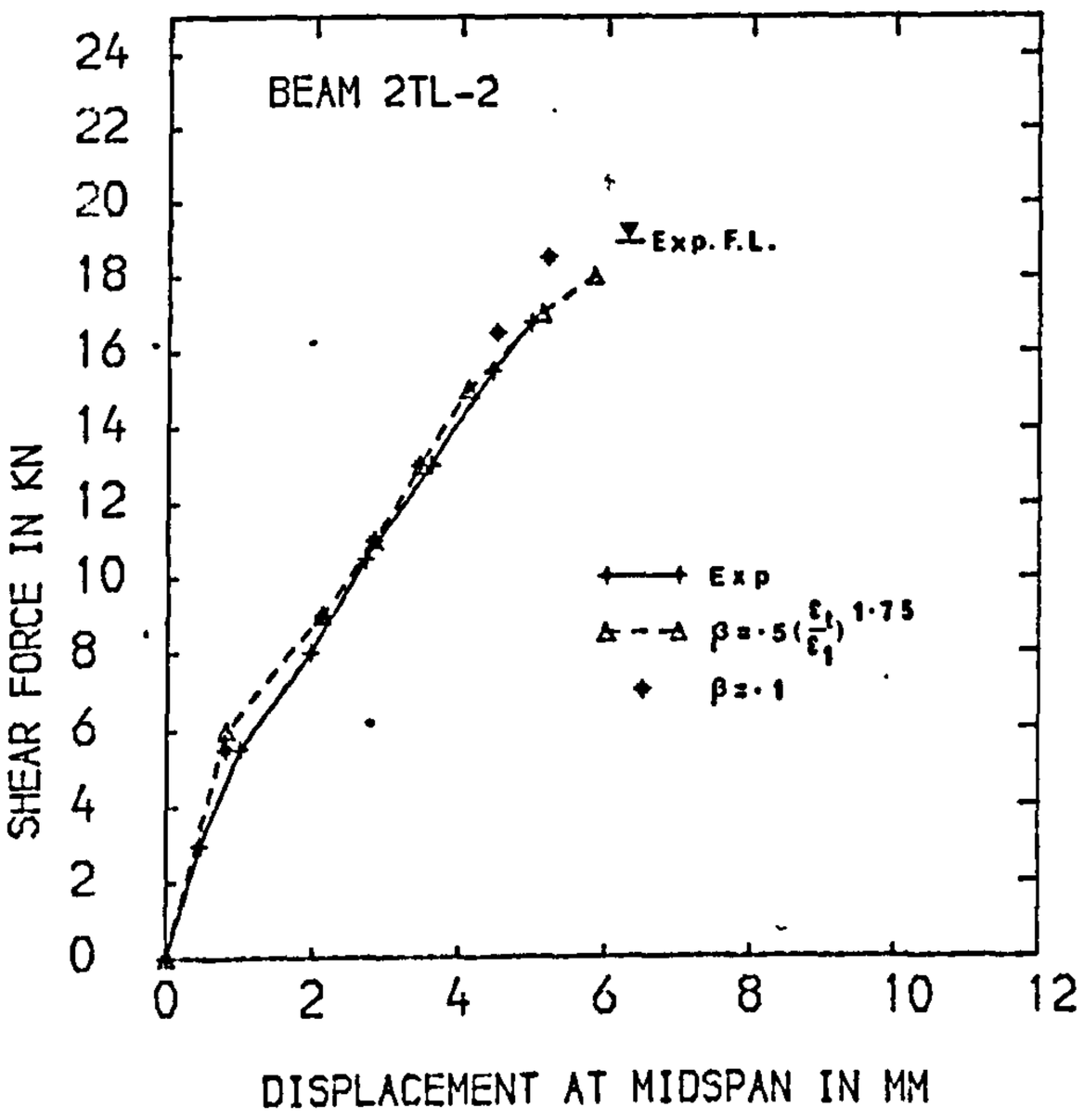

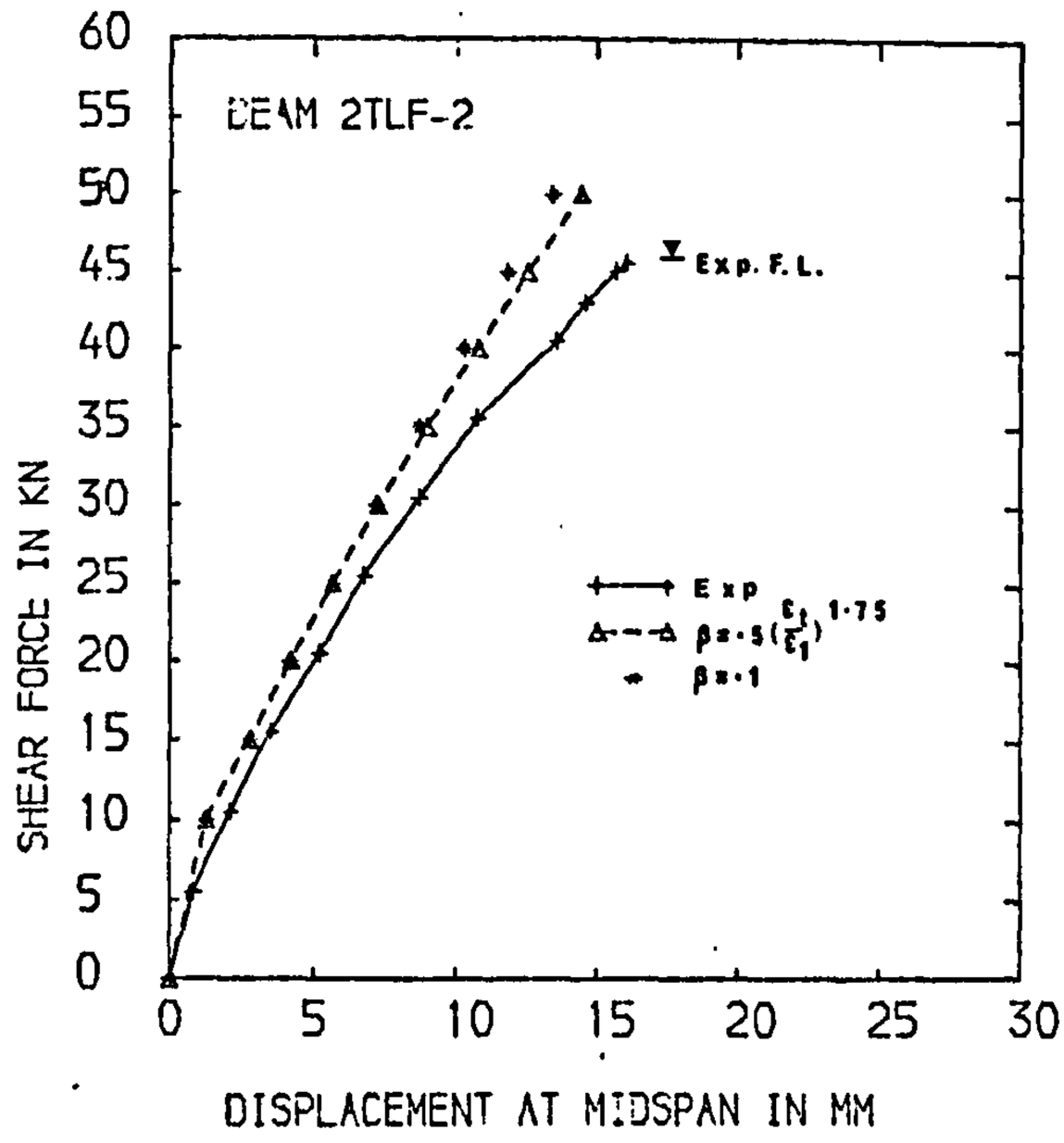

FIG.9.2(b) LOAD-MIDSPAN DISPLACEMENT CURVES

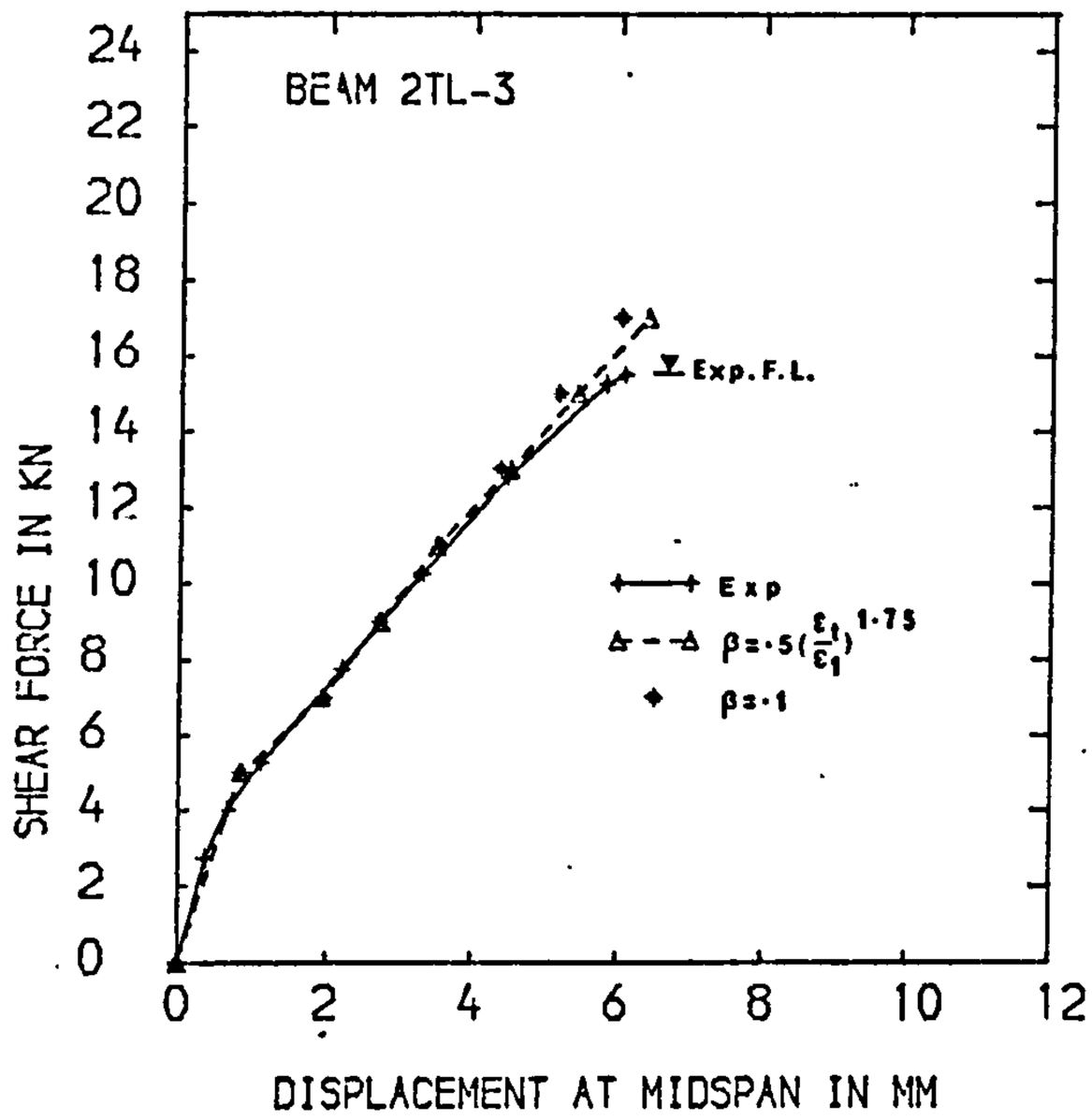

FIG.9.2(c) LOAD-MIDSPAN DISPLACEMENT CURVES

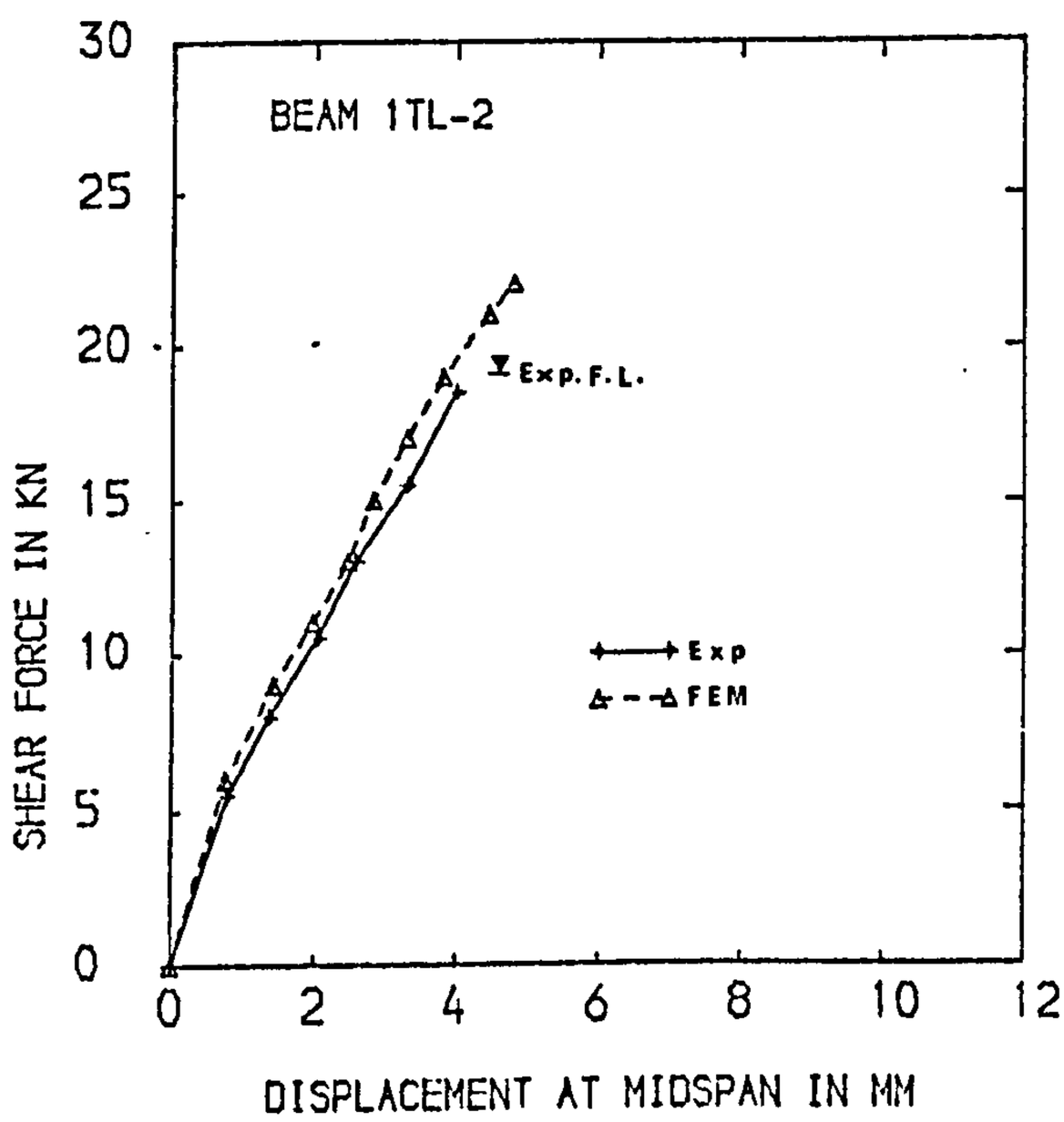

FIG.9.2(d) LOAD-MIDSPAN DISPLACEMENT CURVES

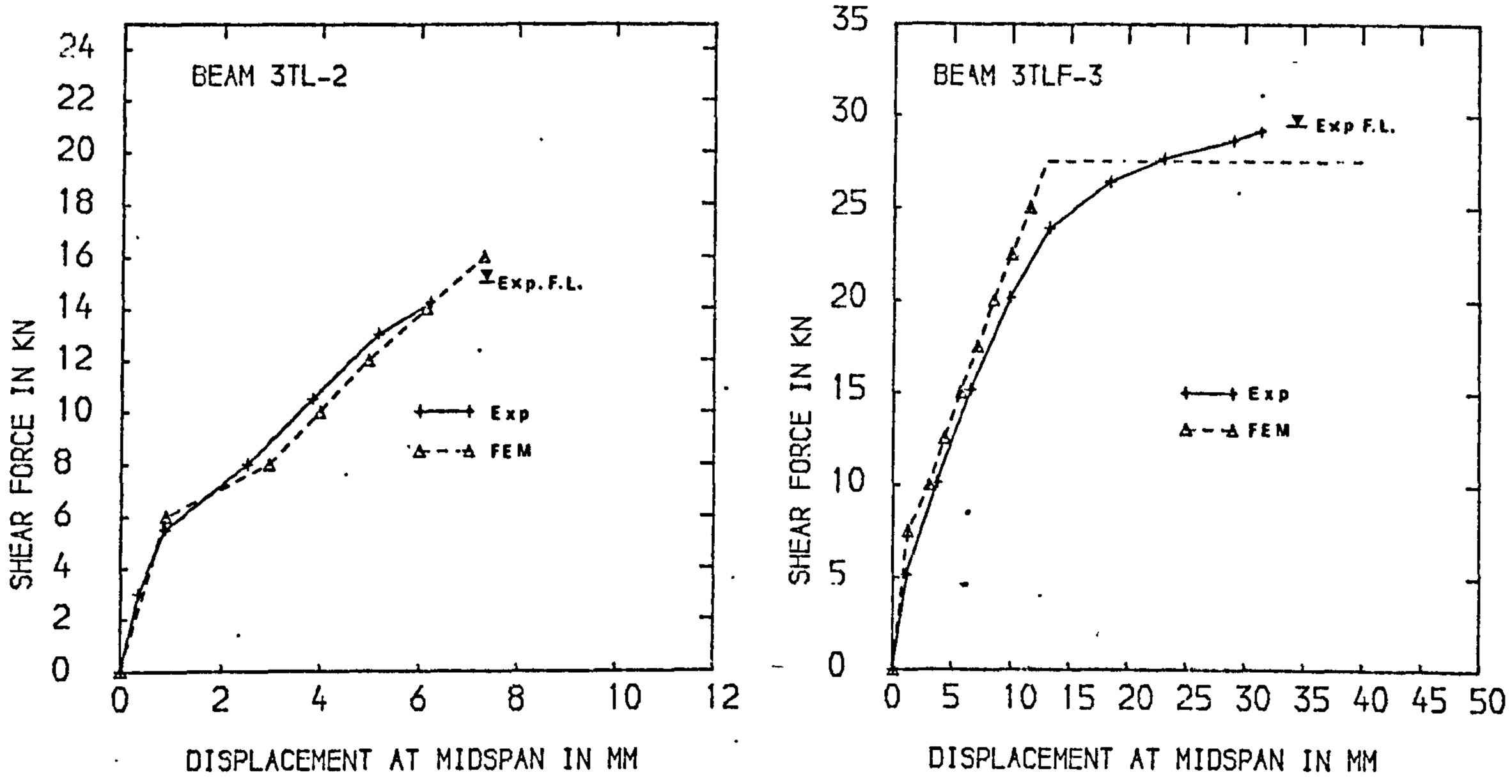

FIG.9.2(e) LOAD-MIDSPAN DISPLACEMENT CURVES

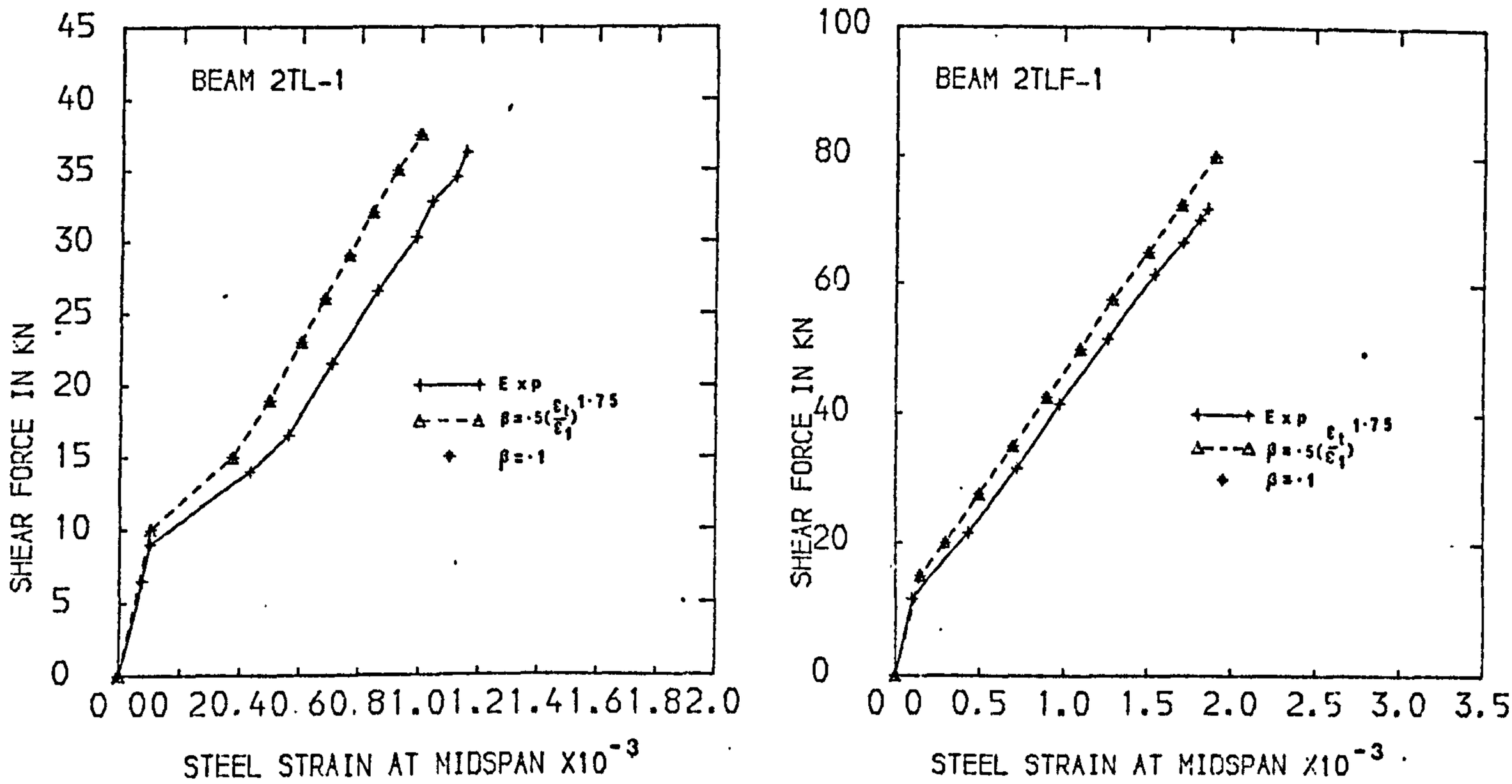

FIG.9.3(a) LOAD-MIDSPAN STEEL STRAIN CURVES

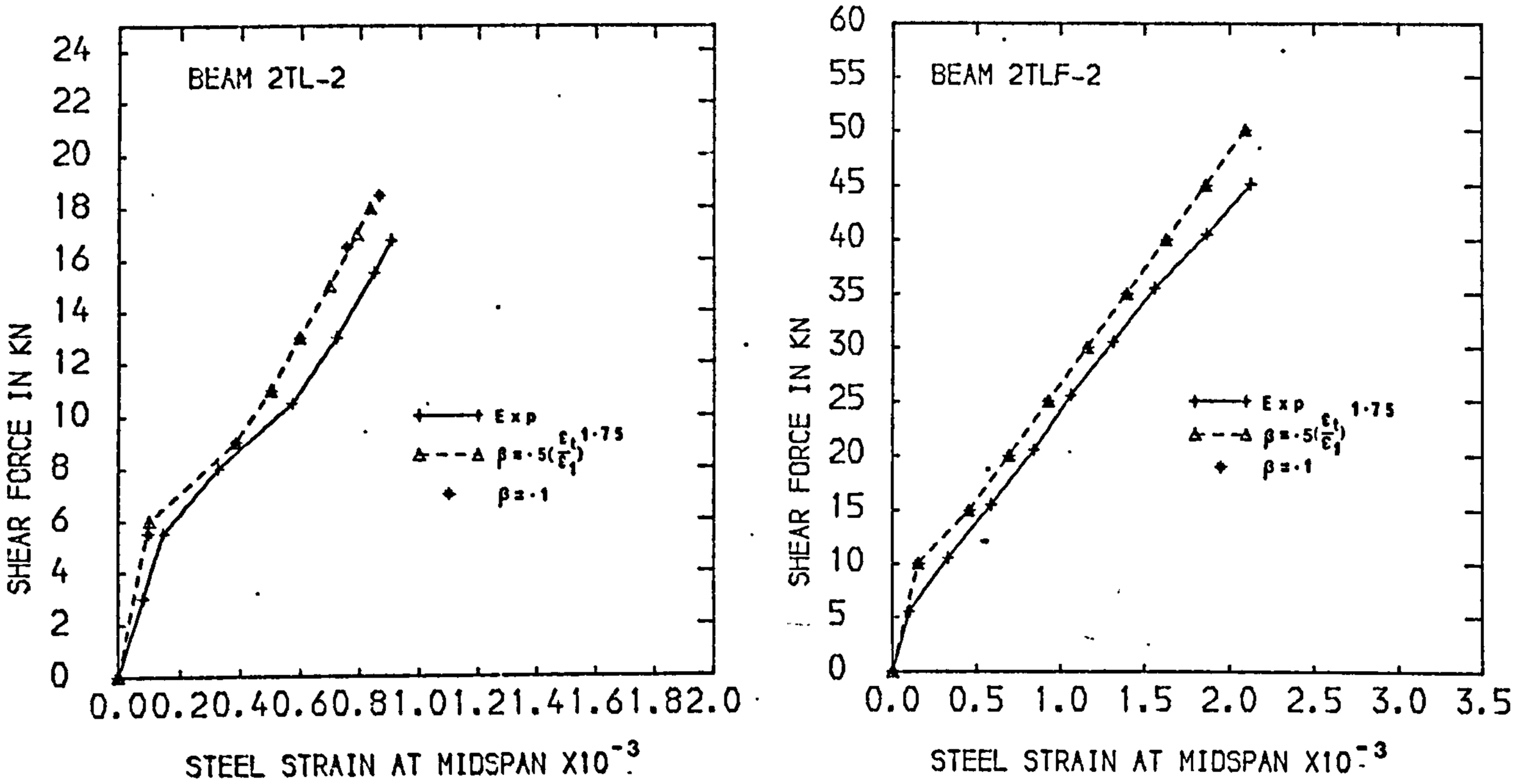

FIG.9.3(b) LOAD-MIDSPAN STEEL STRAIN CURVES

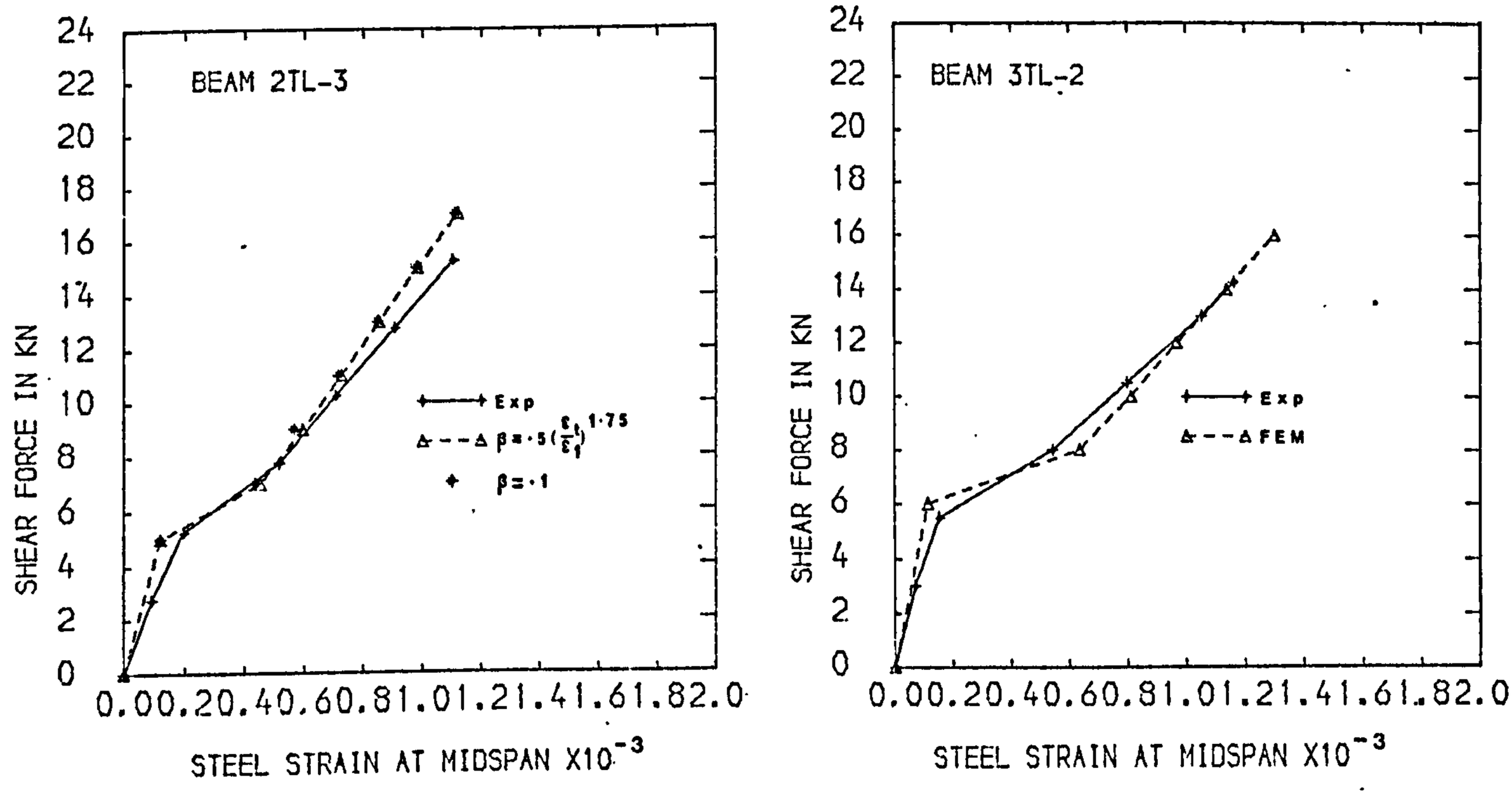

FIG.9.3(c) LOAD-MIDSPAN STEEL STRAIN CURVES

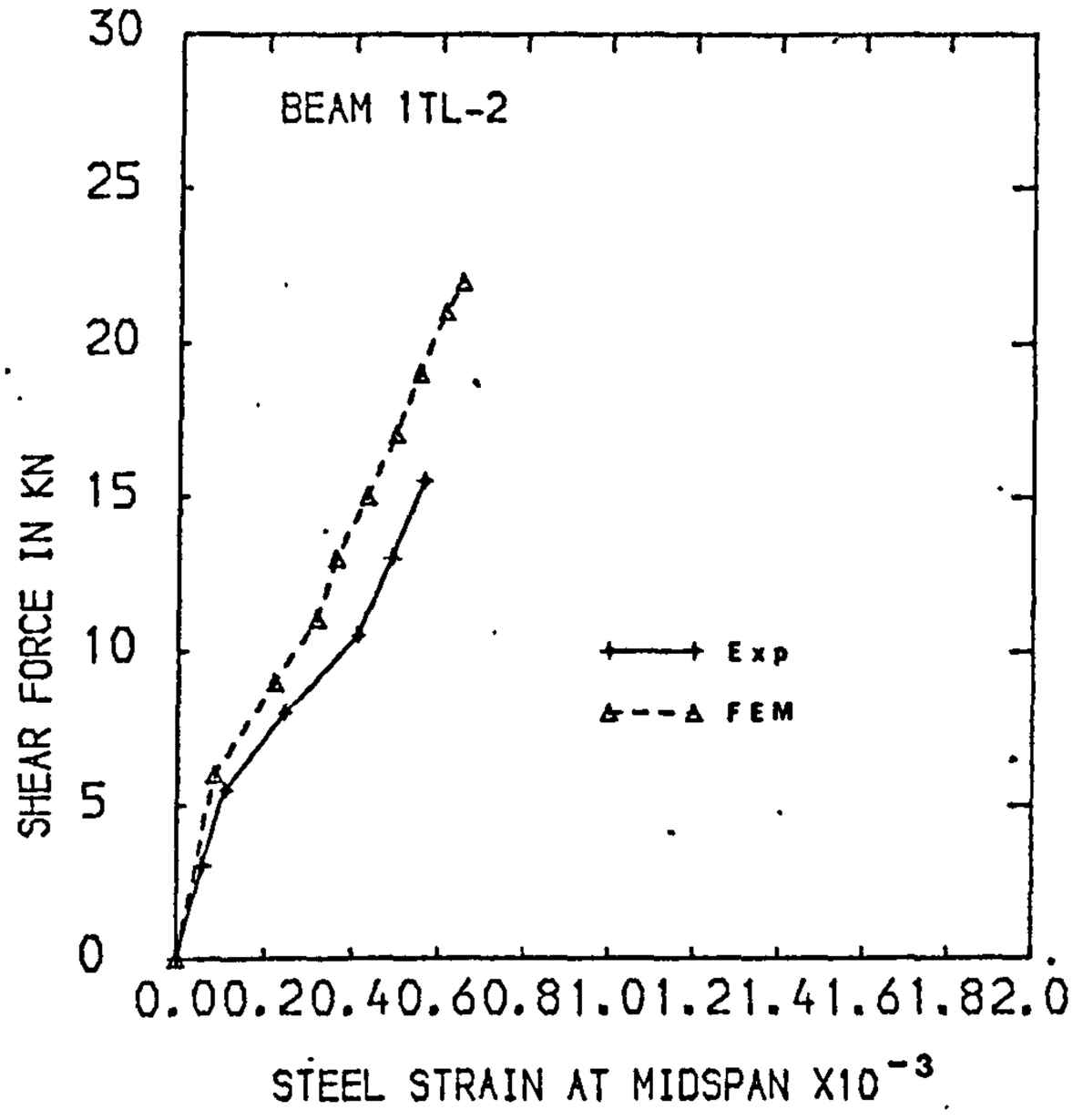

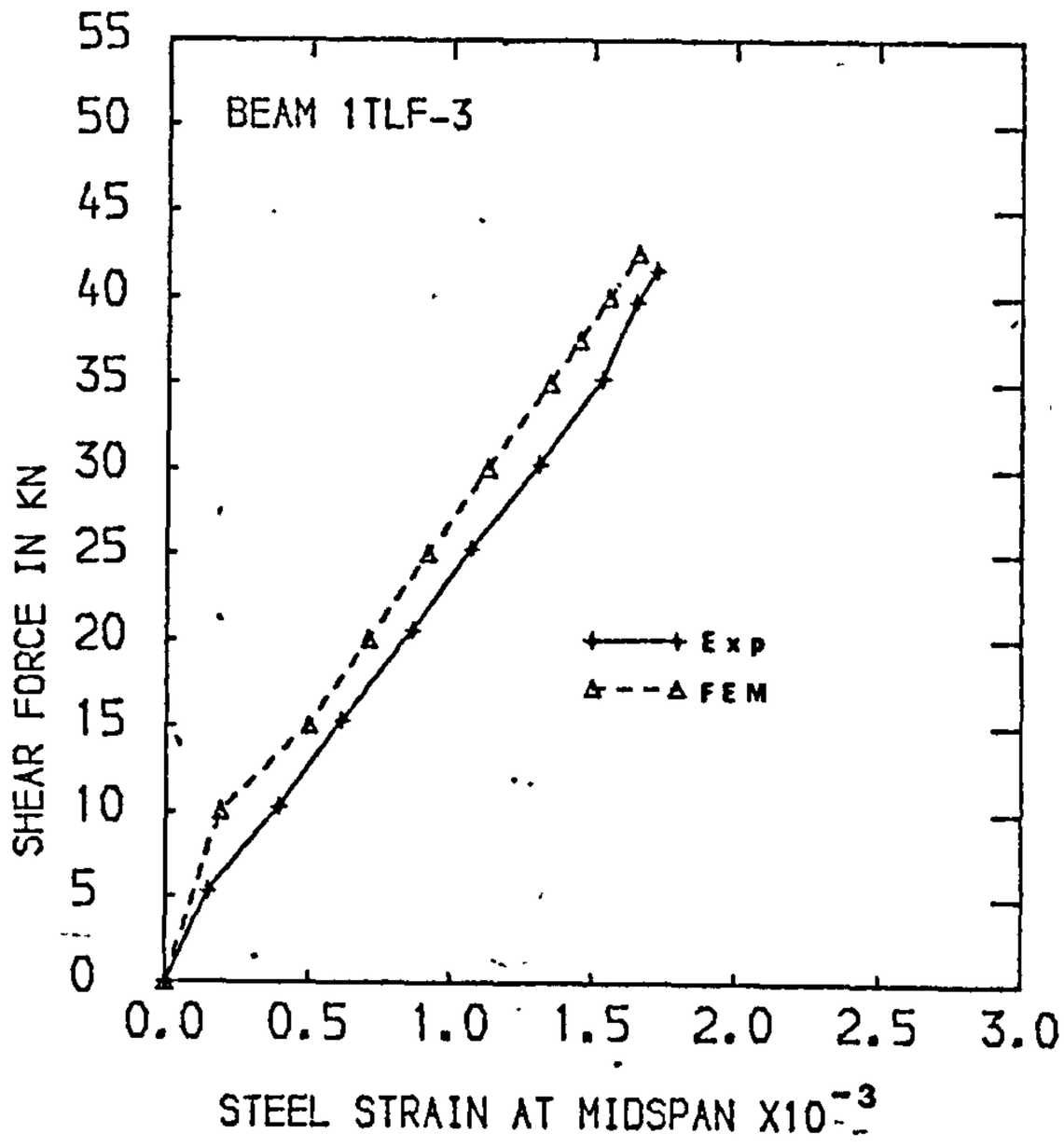

FIG.9.3(d) LOAD-MIDSPAN STEEL STRAIN CURVES

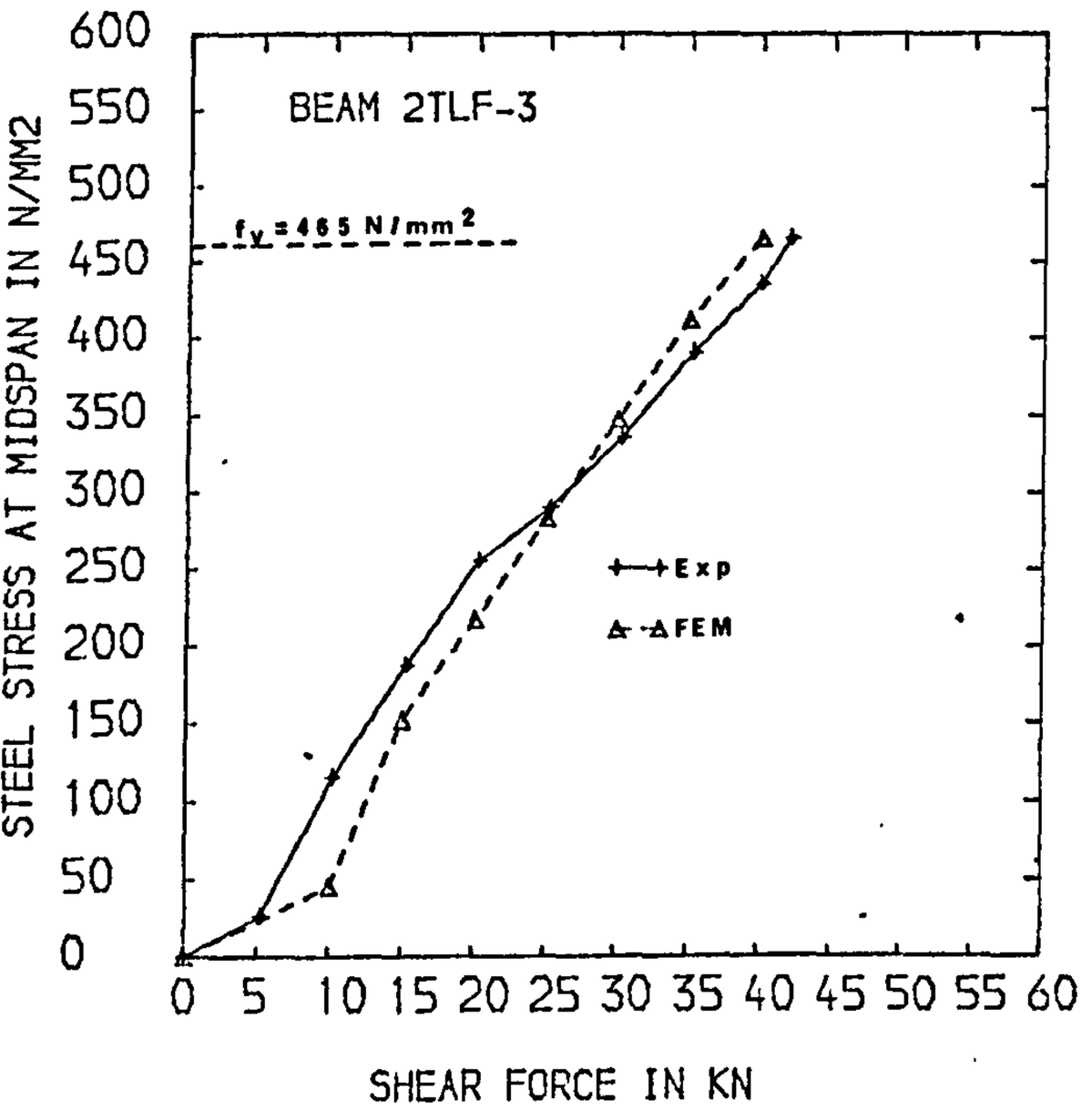

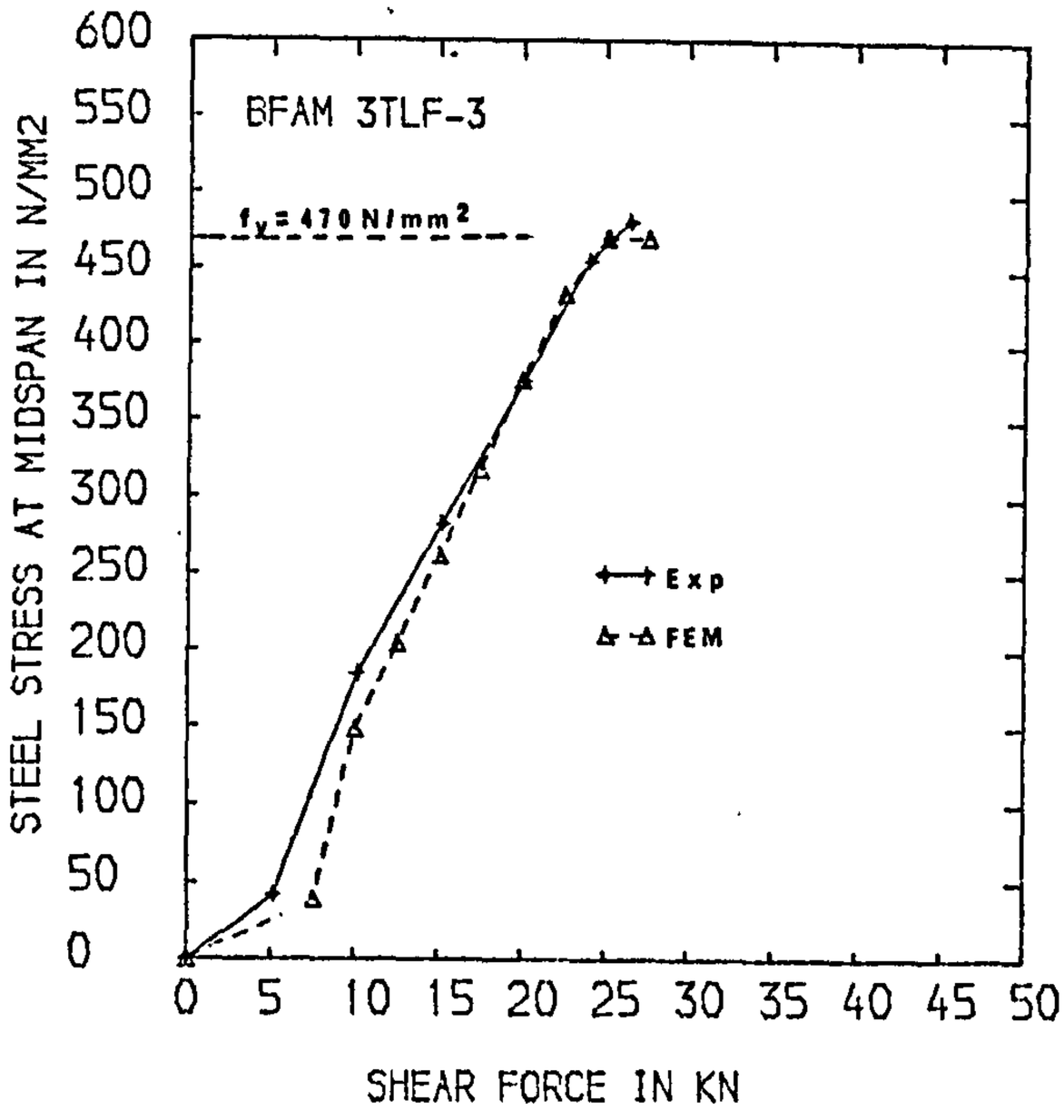

FIG.9.4 MIDSPAN STEEL STRESS-LOAD CURVES

curves at midspan for the beams failing in shear without yielding of the main reinforcement. The numerical analysis generally underestimated the steel strain. This may be attributed to the assumption of perfect bonding between steel and concrete.

Beam 2TLF-3 failed in shear with yielding of the main reinforcement and beam 3TLF-3 failed in flexural tension. Fig. 9.4 shows the good agreement between the analytical and experimental steel stress-load curves at midspan for these two beams.

The type of shear retention factor had negligible influence on the load-steel strain relations.

9.2.6 Crack Patterns

The analytical patterns of beams 2TL-2 and 2TLF-2 at various load levels are shown in Fig. 9.5 and Fig. 9.6 respectively. The analytical crack patterns near failure of the other beams are shown in Figs. 9.7 through 9.10. The actual crack patterns of these beams are also shown in the respective figures.

When comparing the crack pattern, it must be remembered that the finite element analysis provides only a qualitative description. In view of this limitation, it can be seen that the analytical crack patterns represented the modes of failure of the beams adequately.

9.2.7 Longitudinal Strain Profile Near Top Surface

The longitudinal distributions of concrete strain at 10 mm from the top surface of beams 2TLF-2, 2TLF-3 and 1TLF-3, resulting from analysis, are shown in Fig. 9.11. Two features can be observed from the figure. The longitudinal strain was tensile near the support. In the case of beam 1TLF-3 where the strain profile shown was that prior to failure, the tensile strain spread over a distance of 270 mm (equivalent to 1.01 x effective depth) from the support. The longitudinal strain adjacent to the

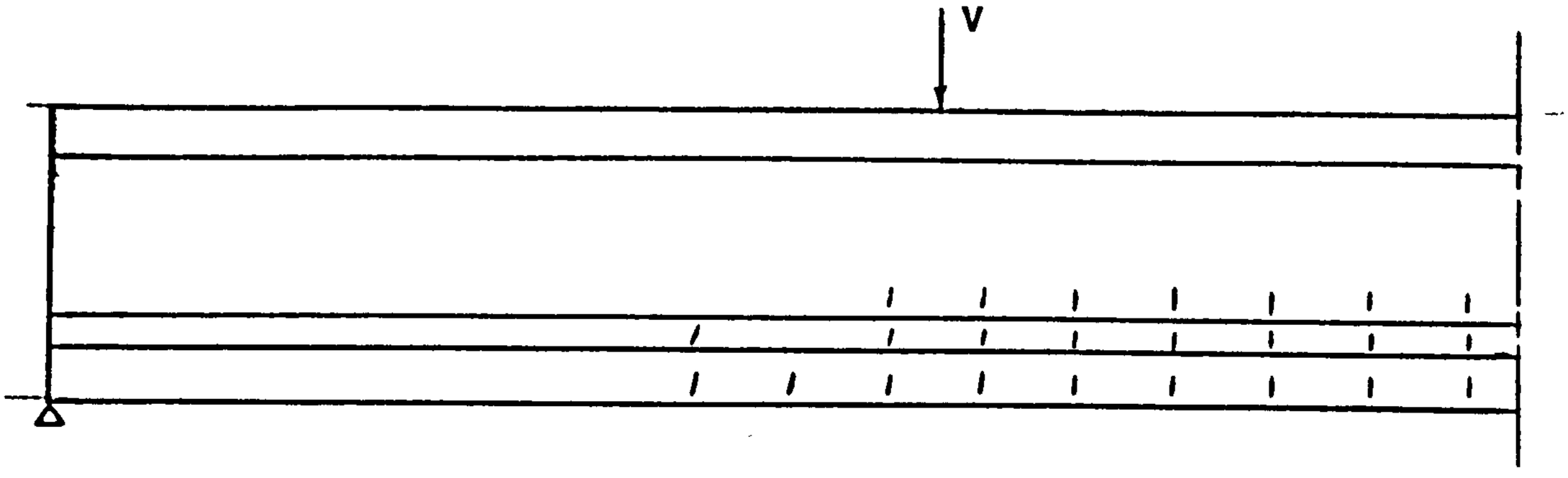

V = 9·0 kN

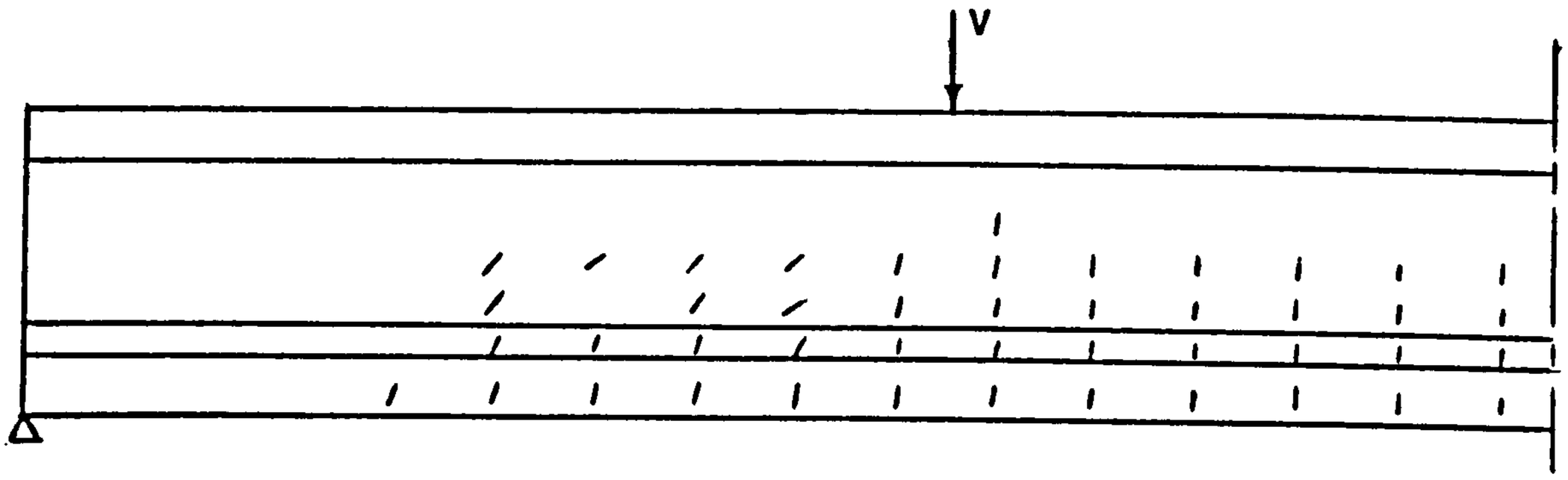

V = 13·0 kN

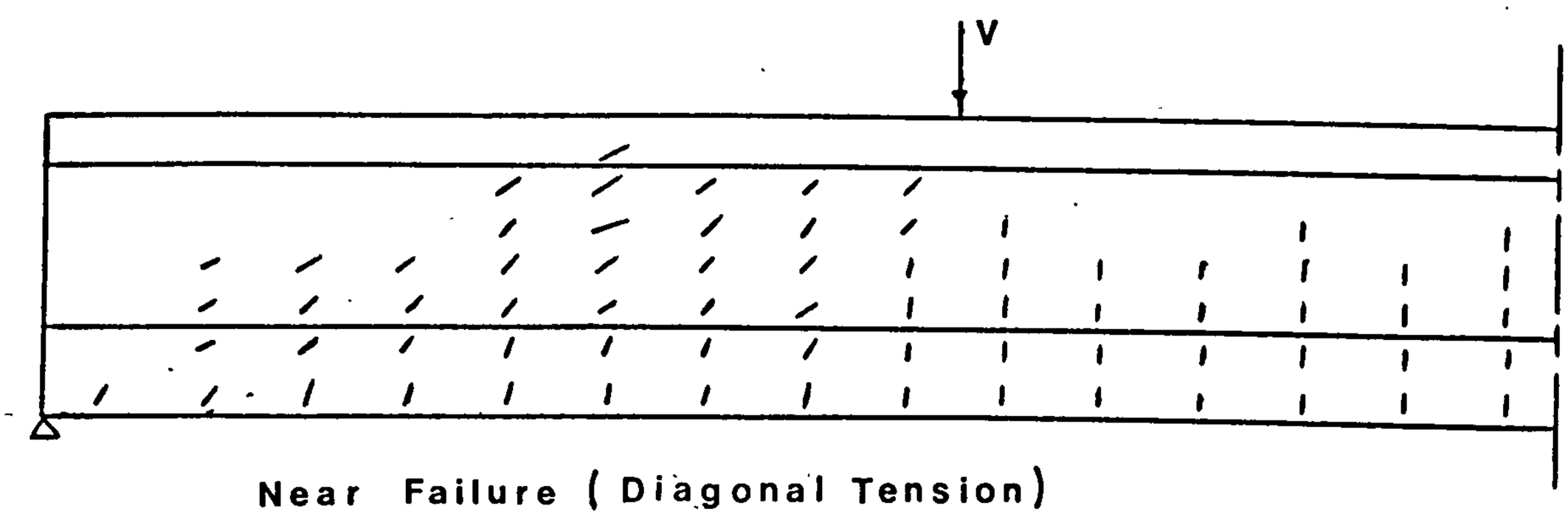

Near Failure (Diagonal Tension)

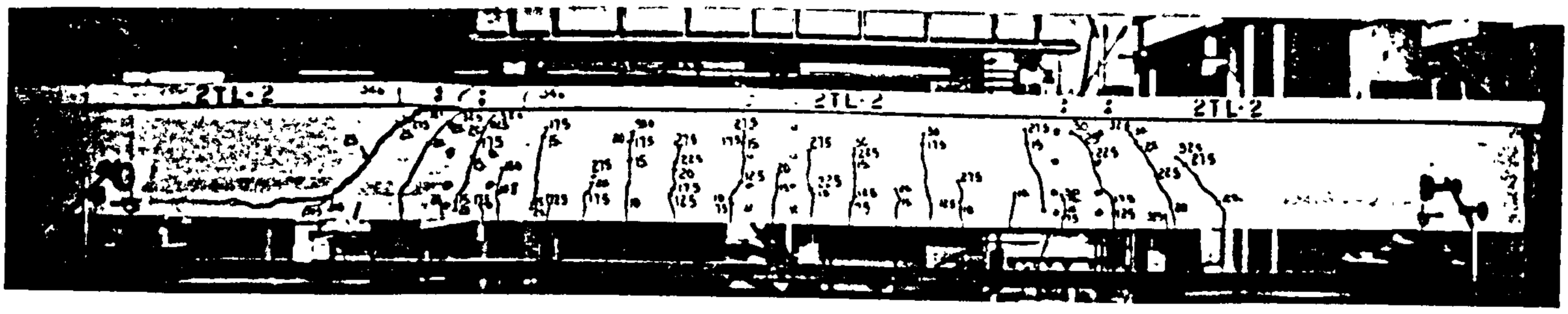

Actual Crack Patterns (Loads indicated are total loads excluding s.w. of spreader beam)

Fig.9·5 Crack Patterns Of Beam 2TL-2 plain At Various Load Levels

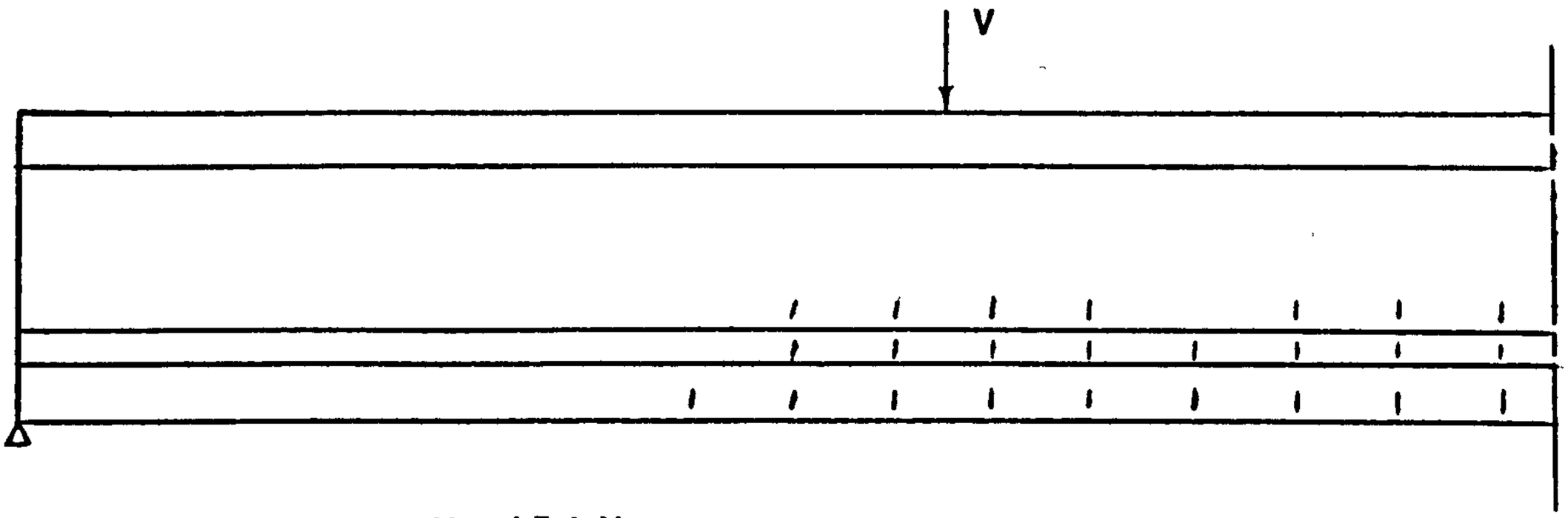

V = 15 kN

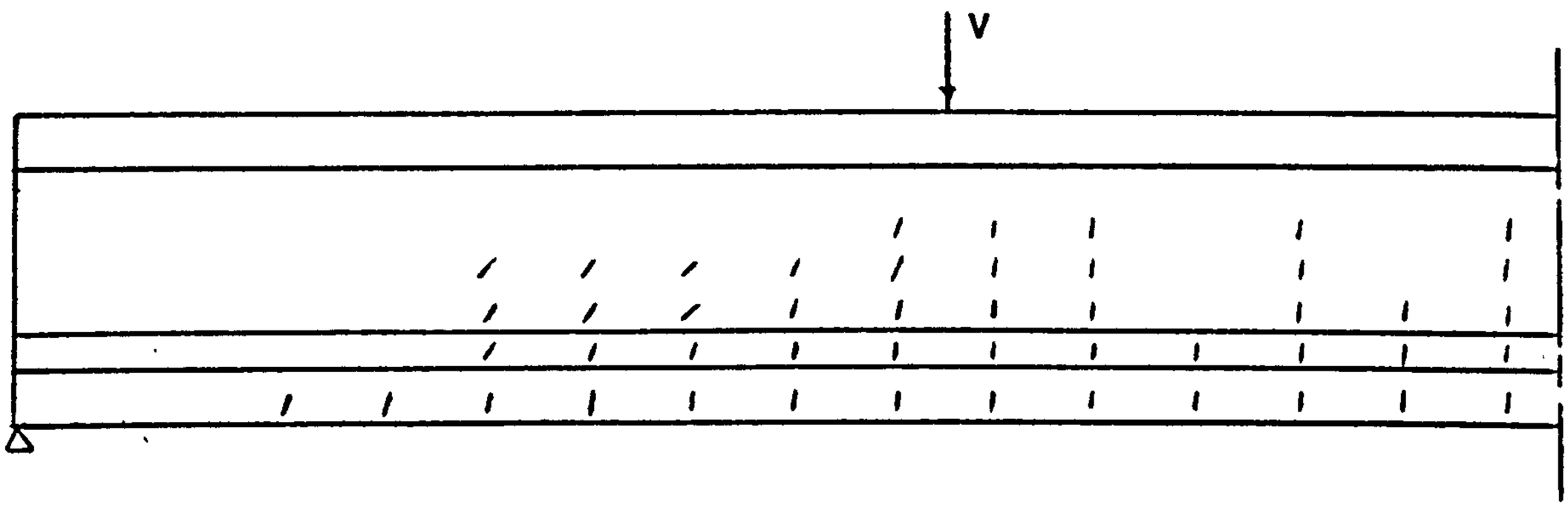

V = 25 kN

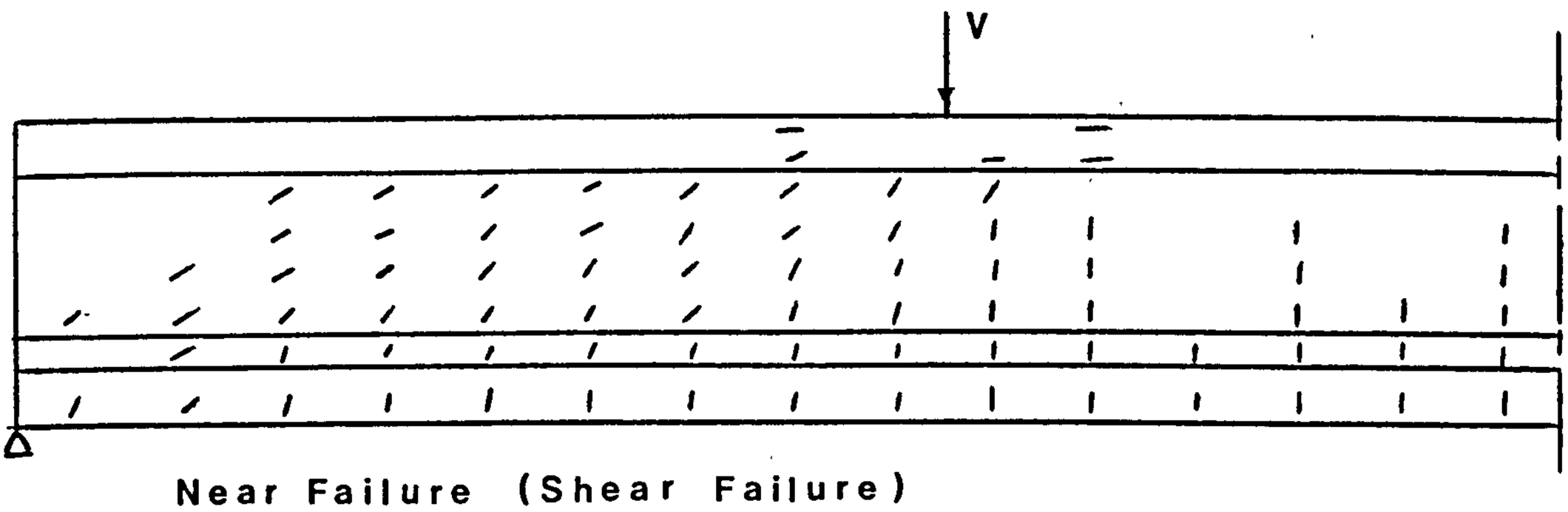

Near Failure (Shear Failure)

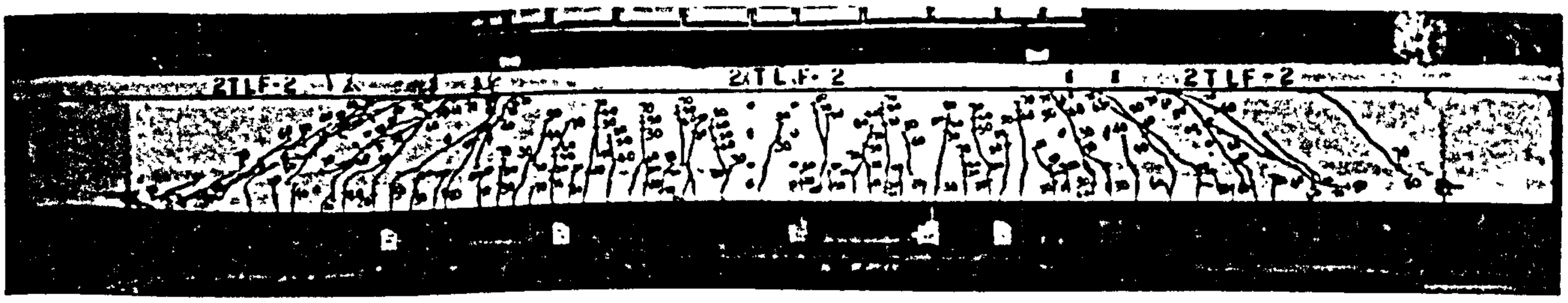

Actual Crack Pattern (Loads indicated are total loads excluding s.w. of spreader beam)

Fig.9.6 Crack Patterns Of Beam 2TLF-2 At Various Load Levels

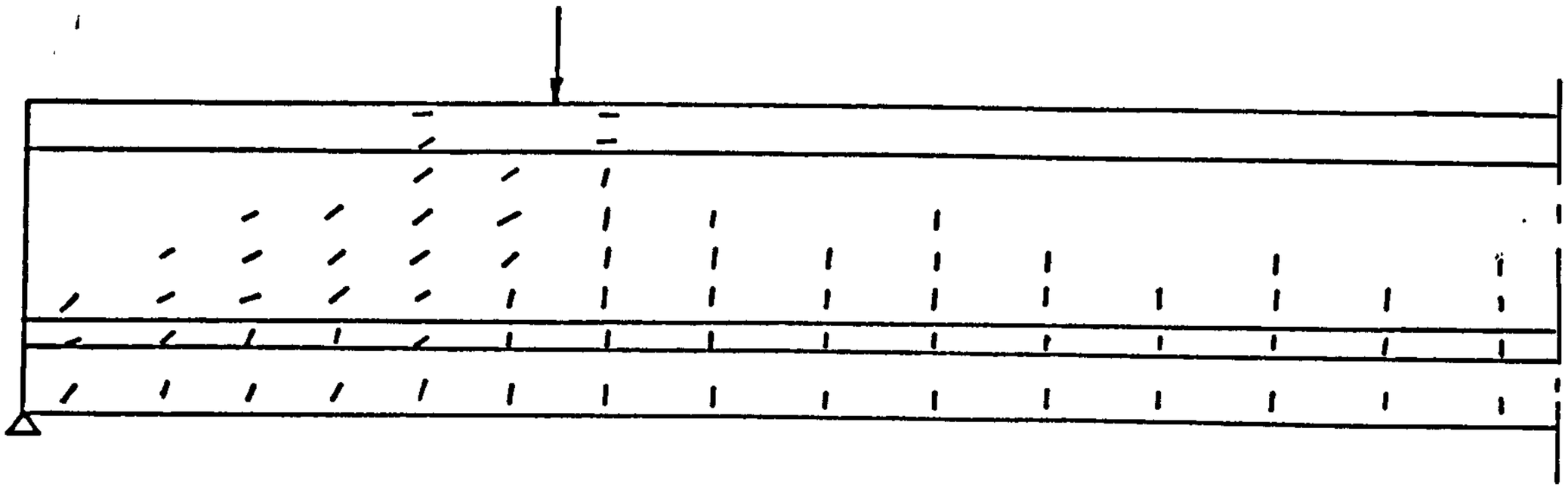

2TL-1 (Plain) Shear Failure

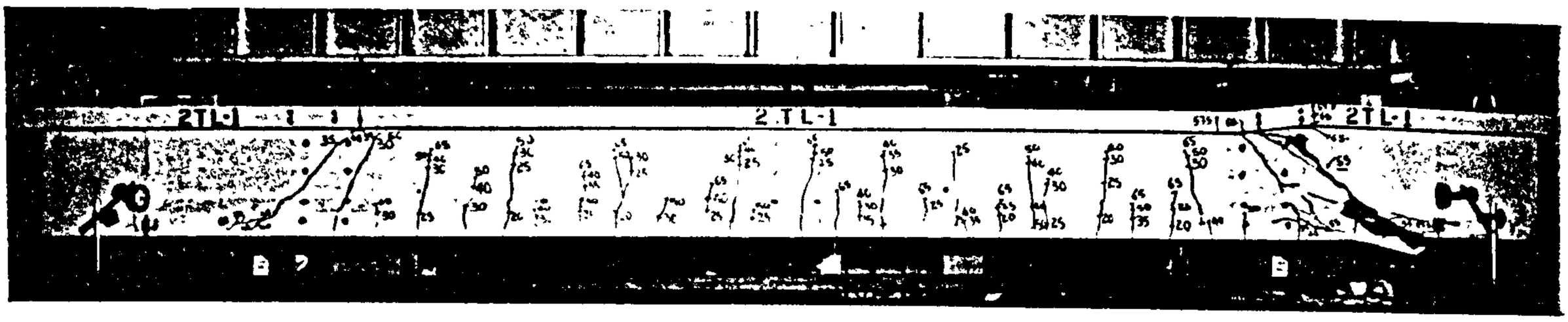

Actual Crack Pattern Of 2TL-1

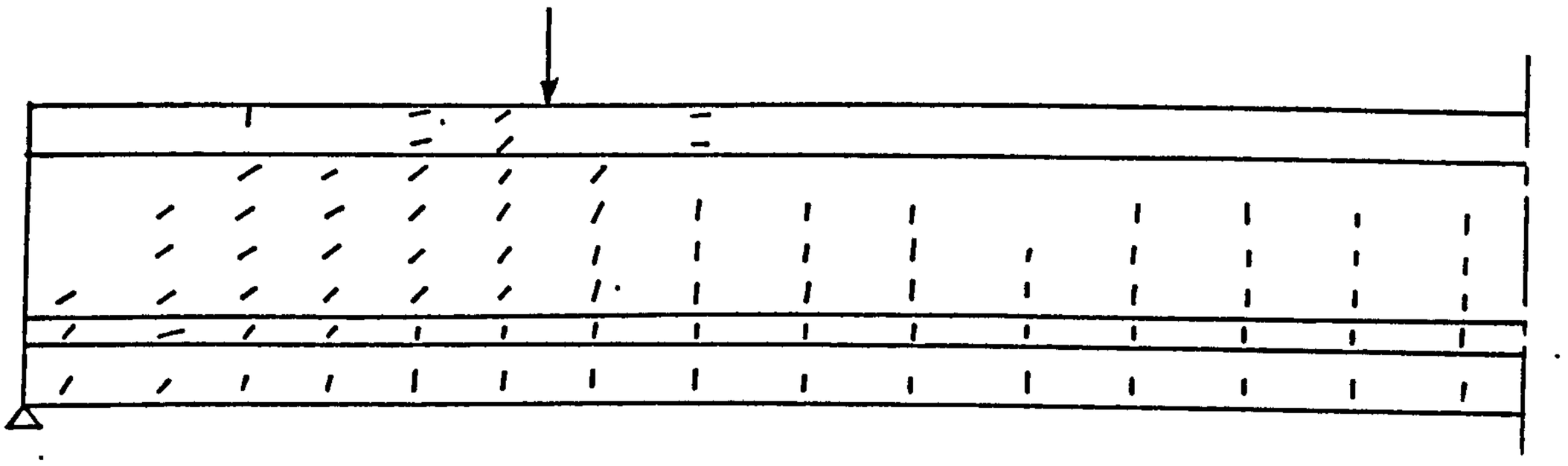

2TLF-1 (Fibre) Shear Failure

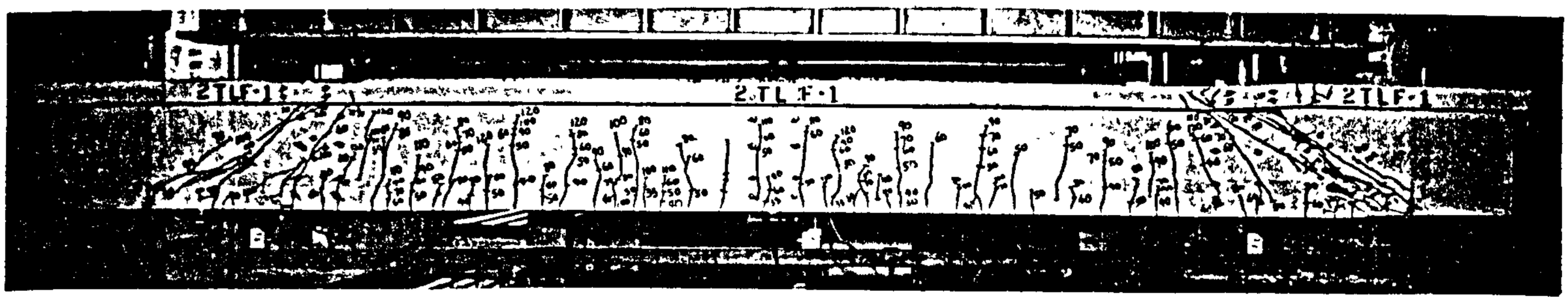

Actual Crack Patterns Of 2TLF-1

Fig.9·7 Crack Patterns Of Beams 2TL-1 and 2TLF-1 Near Failure

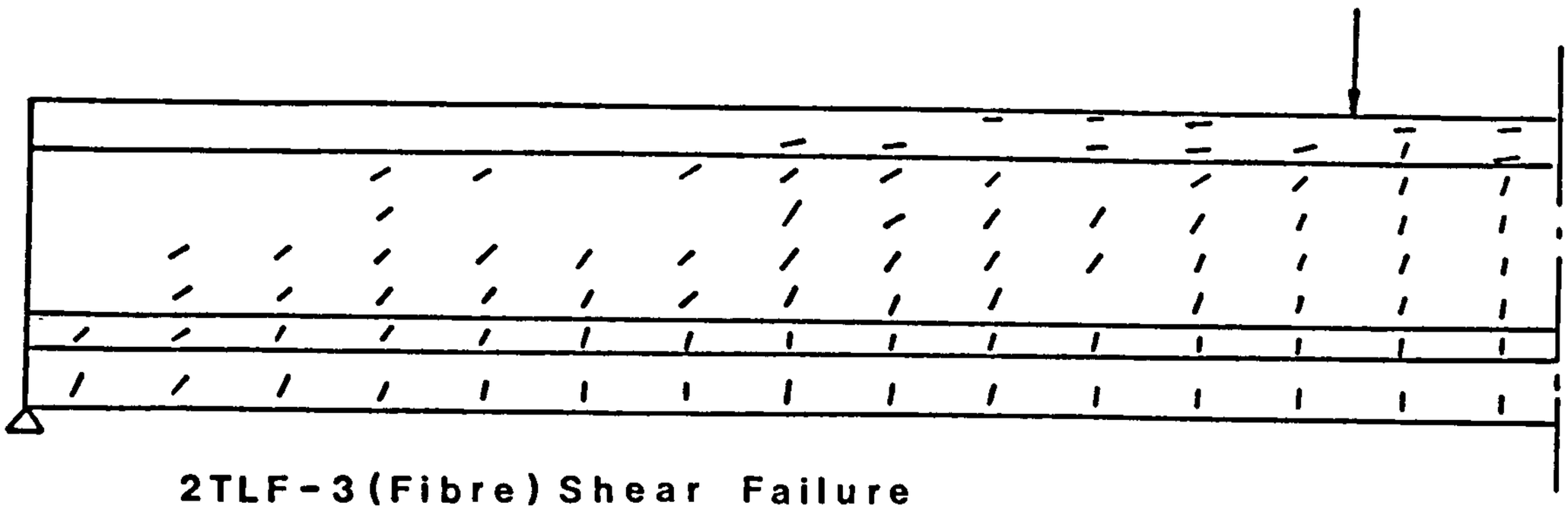

2TLF-3 (Fibre) Shear Failure

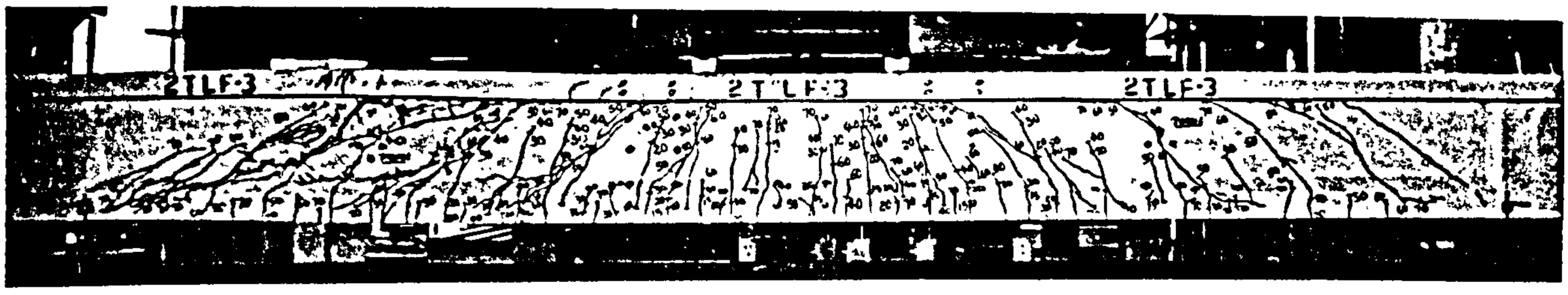

Actual Crack Patterns Of 2TLF-3

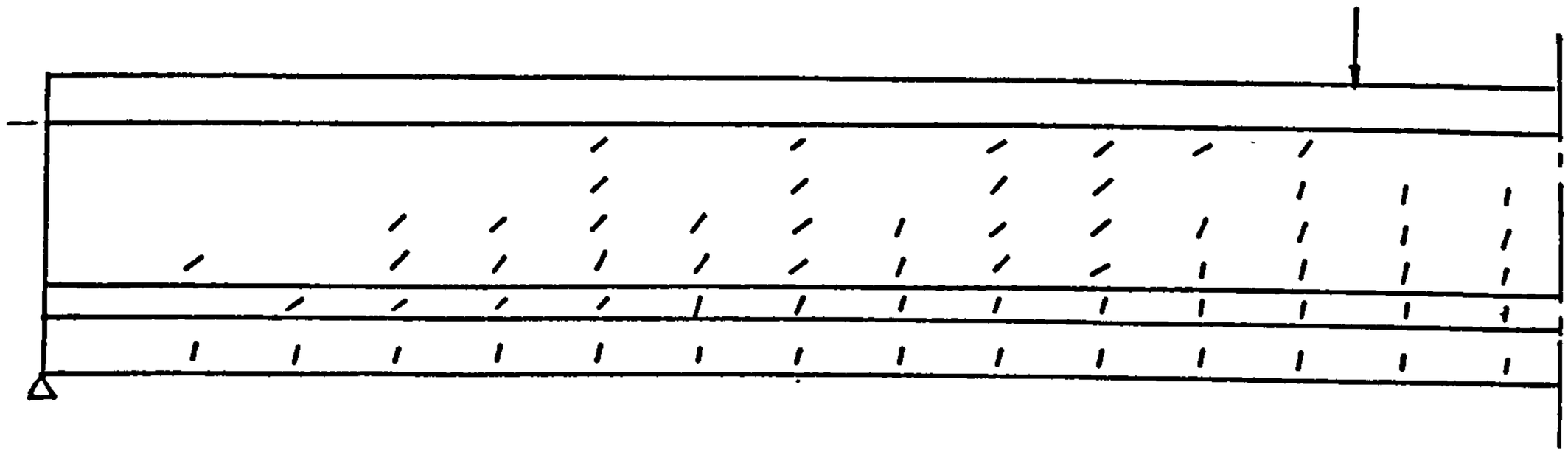

2TL-3 (Plain) Diagonal Tension Failure

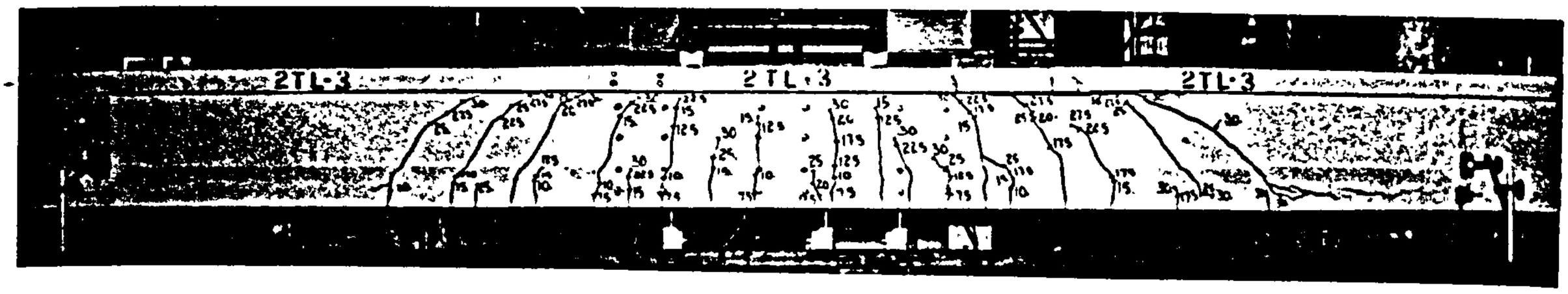

Actual Crack Patterns Of 2TL-3

Fig. 9·8 Crack Patterns Of Beams 2TL-3 and 2TLF-3 Near Failure

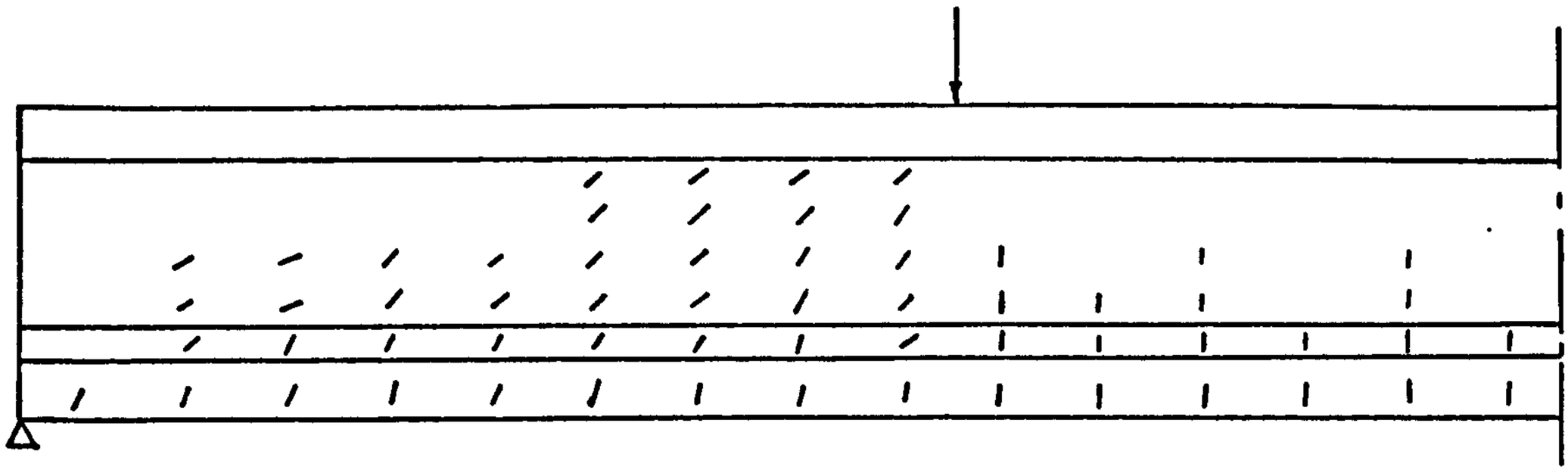

1TL- 2 (Plain) Diagonal Tension Failure

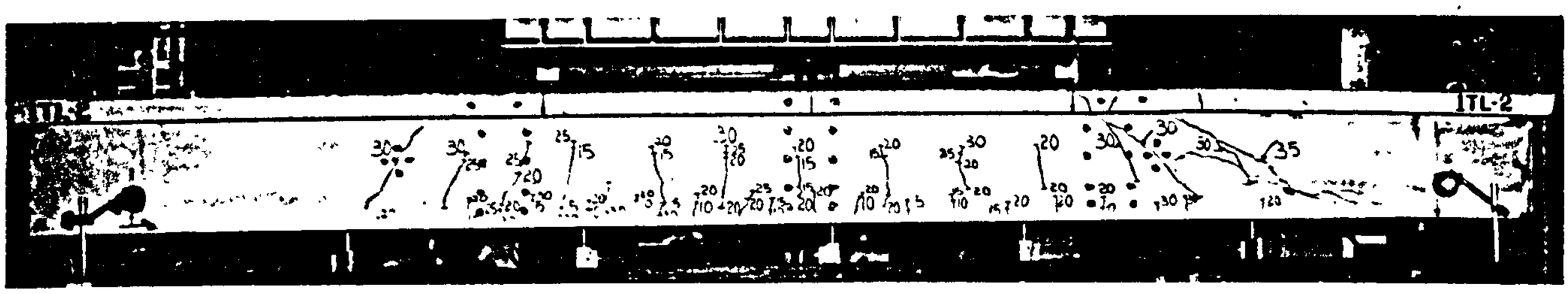

Actual Crack Patterns Of 1TL-2

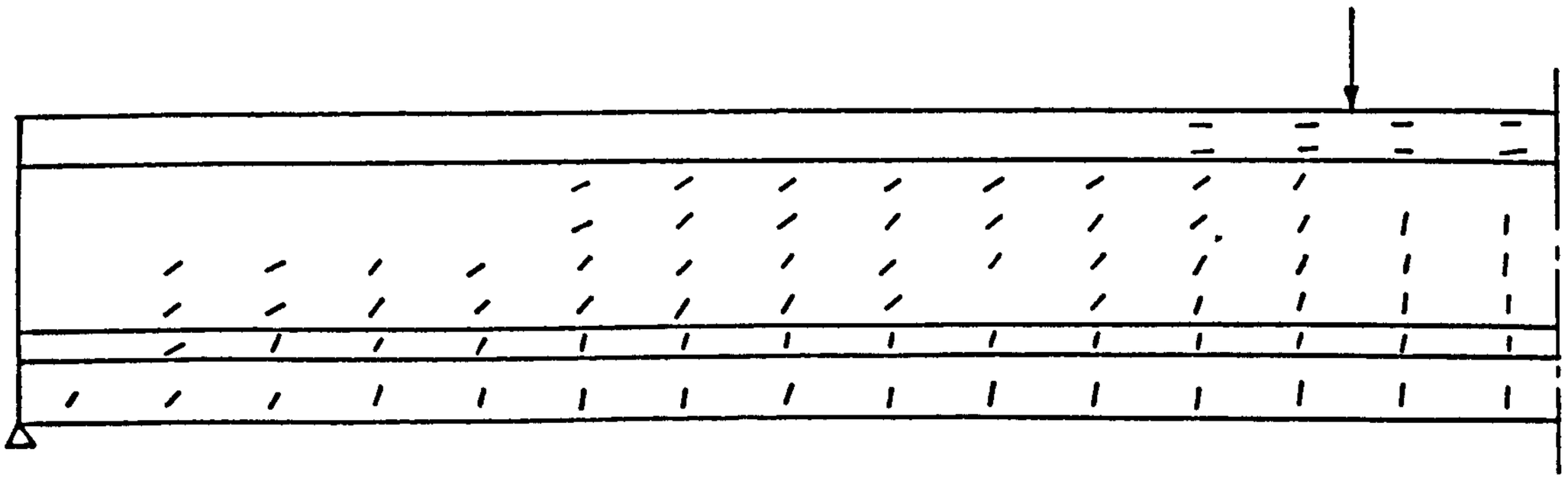

1TLF-3 (Fibre) Shear Failure

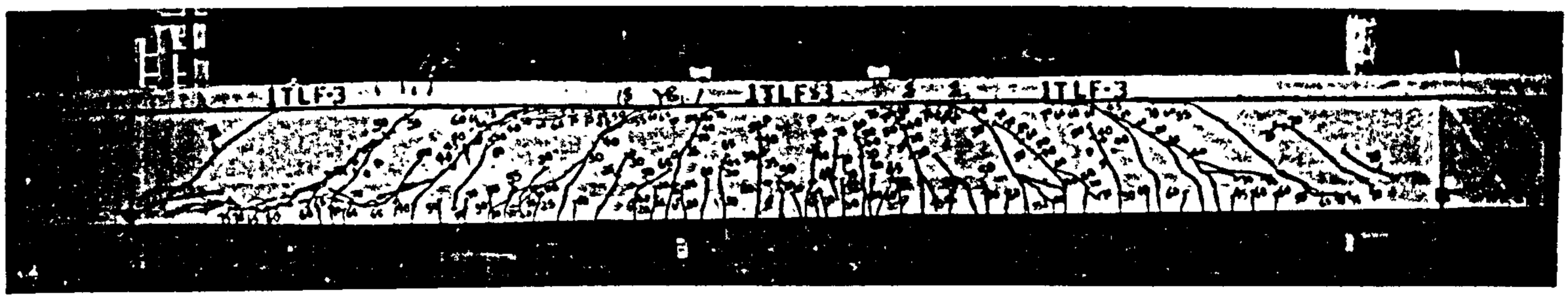

Actual Crack Patterns Of 1TLF-3

Fig.9.9 Crack Patterns Of Beams 1TL-2 and 1TLF-3 Near Failure

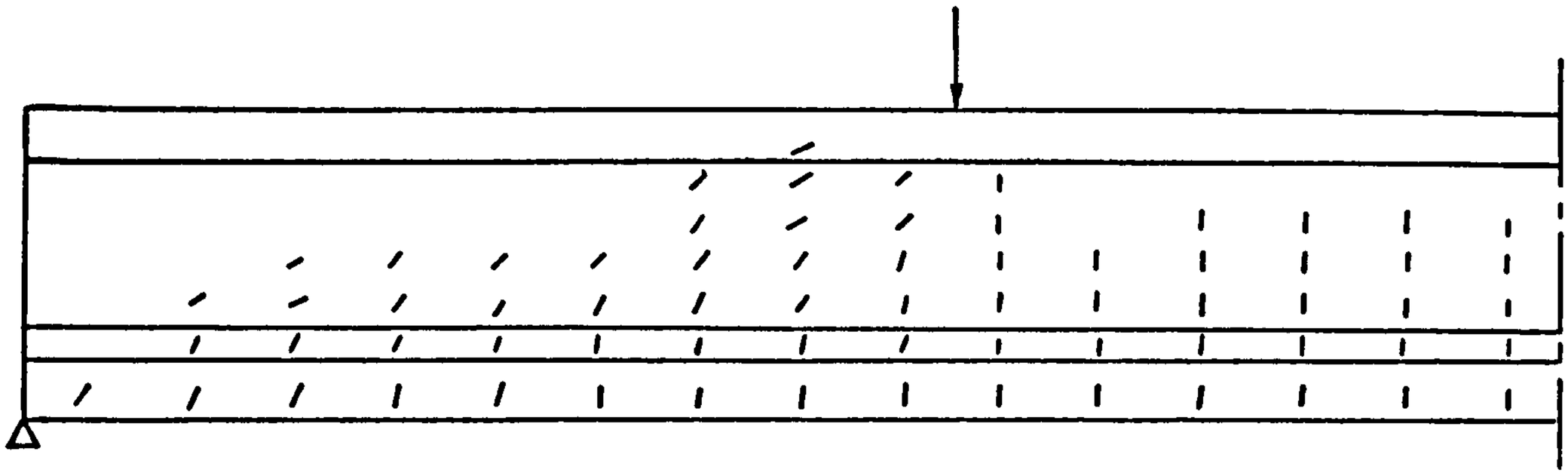

3TL-2 (Plain) Diagonal Tension Failure

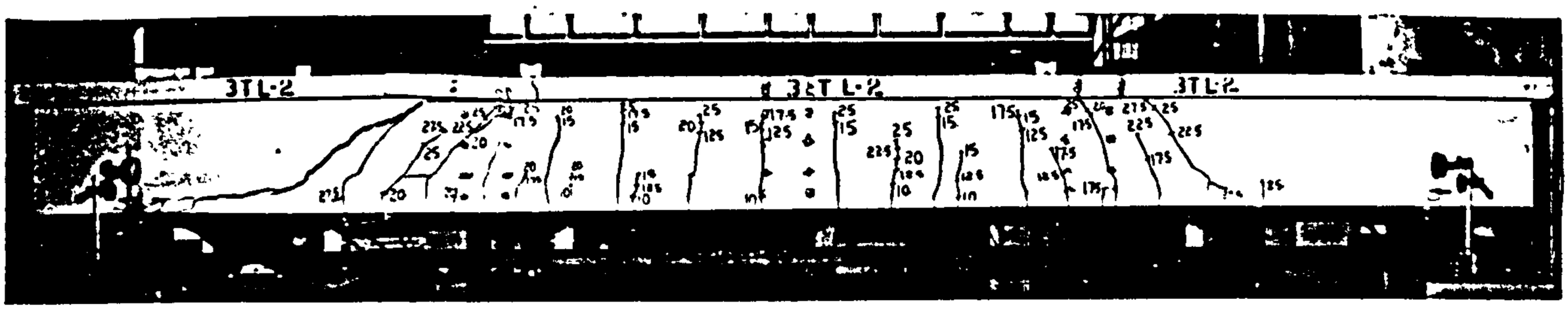

Actual Crack Patterns Of 3TL-2

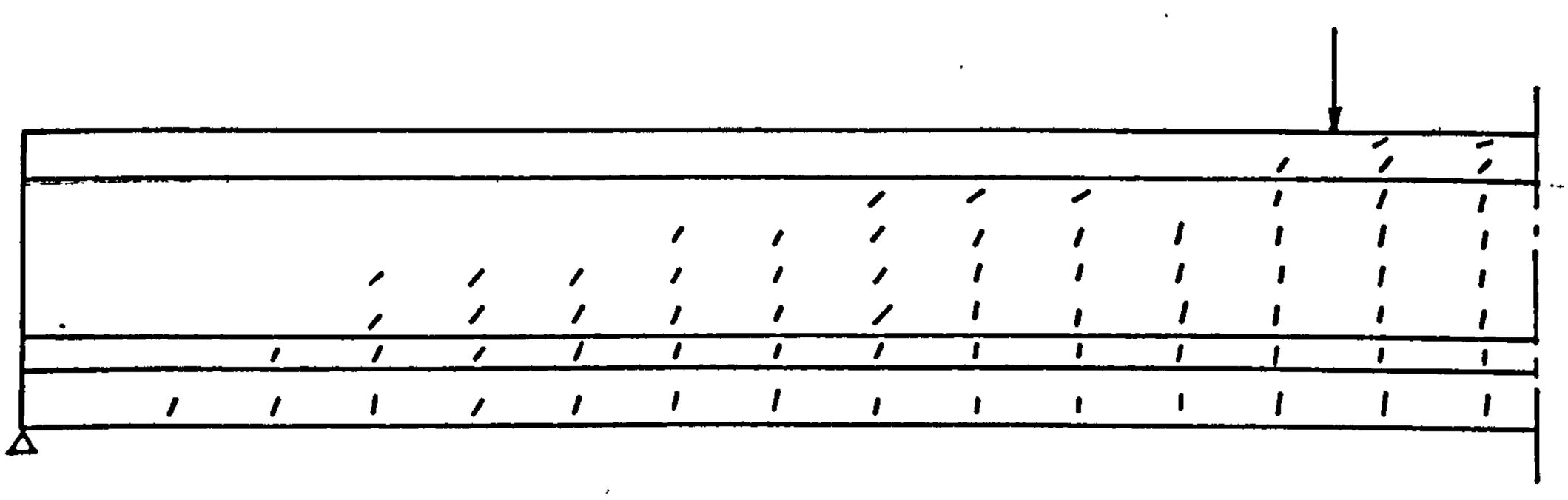

3TLF-3 (Fibre) Flexure-Tension Failure

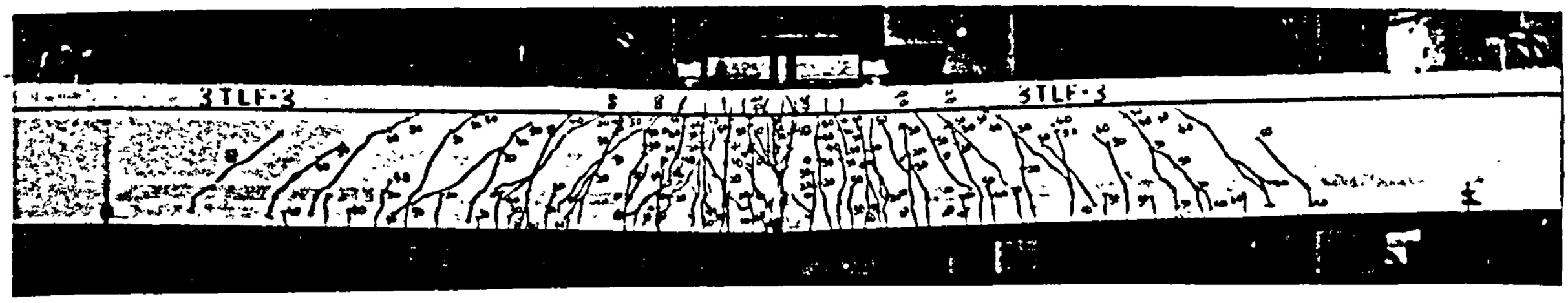

Actual Crack Patterns Of 3TLF-3

Fig.9·10 Crack Patterns Of Beams 3TL-2 and 3TL-3 Near Failure

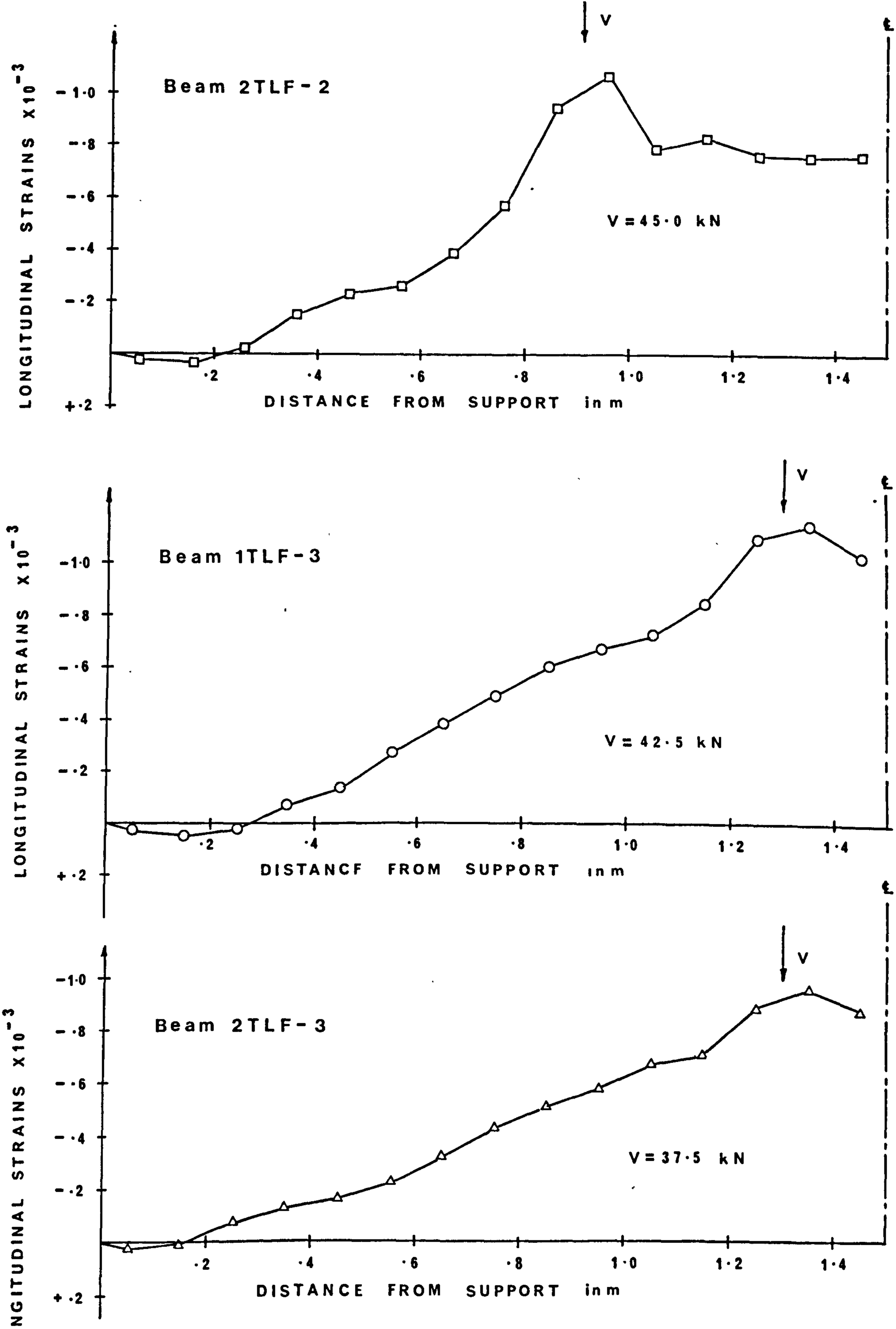

Fig.9.11 Variation Along Span Of Concrete Longitudinal Strain Near the Top Surface

applied load was greater than that in the pure bending region. These features have been observed and discussed in the experimental study reported in Chapter 6. The experimental strain profiles of beam 1TLF-3 and 2TLF-3 are shown in Fig. 6.7.

9.2.8 Ultimate Strength of Beams

Table 9.1 compares the analytical and experimental strength of the beams at failure. In the analysis, for plain concrete beams failing in diagonal tension, failure was deemed to have occurred when cracking reached the soffit of the compression flange and the vicinity of the support. For beams failing in shear other than diagonal tension and in flexure, failure was considered to have taken place when cracking reached the top of the flange. In addition, in the case of beams with reinforcement yielding near failure, final failure was characterized by a large increase in the displacement.

As can be seen from the table, the correlation was reasonable. Again the type of shear retention factor had negligible influence on the ultimate strength.

Table 9.1 Comparison of Analytical and Experimental Ultimate Strength

Beam No.	% Fibre by Voume	f_{cu} N/mm^2	Ult. Strength V, kN			$\frac{V_{analy}}{V_{Exp}}$	Mode of Failure
			Analytical		Exp.		
			Constant S.R.F.	Varying S.R.F.			
1TL-2	0	42.0	-	22.0	19.0	1.16	DT
1TLF-3	1.0	45.0	-	42.5	42.5	1.00	S
2TL-1	0	45.6	37.5	37.5	36.5	1.03	S
2TLF-1	1.0	47.1	72.5	72.5	71.9	1.01	S
2TL-2	0	41.7	17.0	16.0	17.8	0.90	ST
2TLF-2	1.0	41.4	50.0	50.0	45.6	1.10	s
2TL-3	0	45.1	17.0	17.0	15.5	1.10	DT
2TLF-3	1.0	44.9	-	40.0	42.8	0.94	S-FT
3TL-2	0	41.0	-	16.0	15.0	1.07	DT
3TLF-3	1.0	40.6	-	27.5	29.5	0.93	FT

NOTE; S.R.F. - shear retention factor
DT - diagonal tension
S - shear
FT - flexural tension

9.3 Comparison With Test Data from Bahia's Investigation

Four of the normal weight concrete beams tested by Bahia (6) have been chosen for this study. Two of the beams have rectangular cross-section and two have T cross-section. The beams are either without shear reinforcement or with shear reinforcement in the form of 0.8% by volume of crimped steel fibres.

9.3.1 Beam Idealization

The rectangular beams were idealized as shown in Fig. 9.12. Half of each beam was considered in the x-direction and free to translate in the y- and z-directions. The nodes at the support were constrained in the y- and z-directions but were free in the x-direction. The applied load V was idealized as two nodal loads each of magnitude $\frac{V}{2}$.

The T-beams were idealized as shown in Fig. 9.13. One quarter of each beam was considered and the boundary conditions were similar to those applied to the author's I-beams (section 9.2.1). The applied load V was idealized as two nodal loads each of magnitude $\frac{V}{4}$.

9.3.2 Material Properties

The Young modulus of concrete (E_c) was taken as 24.0 kN/mm^2 for plain concrete and 28.0 kN/mm^2 for fibre concrete. These are the values reported by Bahia. The respective Poisson's ratios were taken as 0.19 and 0.18.

The uniaxial compressive strength f_c' was taken as 0.80 f_{cu} and 0.85 f_{cu} for plain and fibre concretes respectively.

The uniaxial tensile strength f_t was assumed to be 0.75 times the flexural tensile strength f_{tm}'. This corresponded to 3.57 N/mm^2 for plain concrete and 4.13 N/mm^2 for fibre concrete. A value of 1.68 N/mm^2 was used for the post-cracking tensile

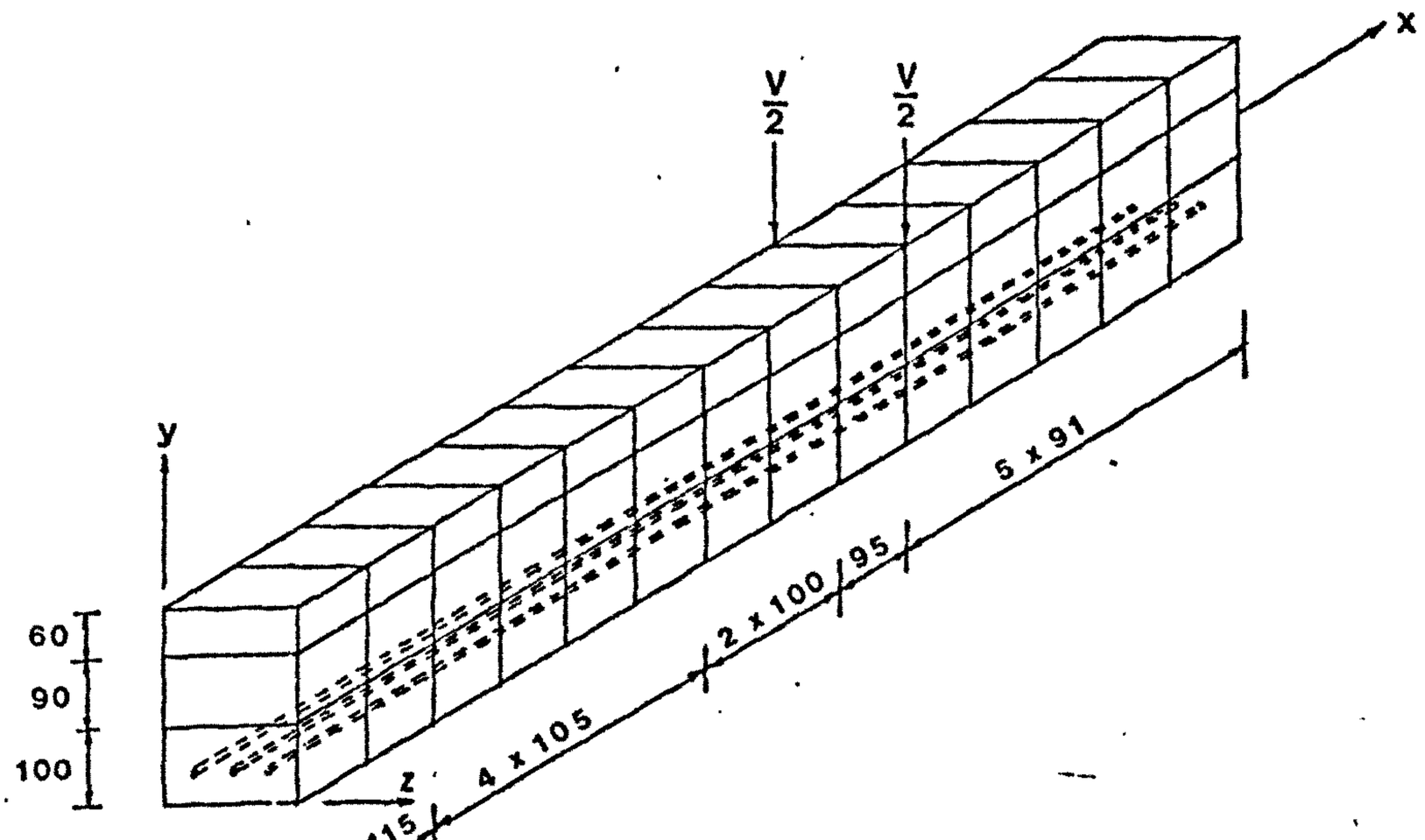

Beam Cross-Sec

Fig.9·12 Idealization Of Bahia's Rectangular Beams

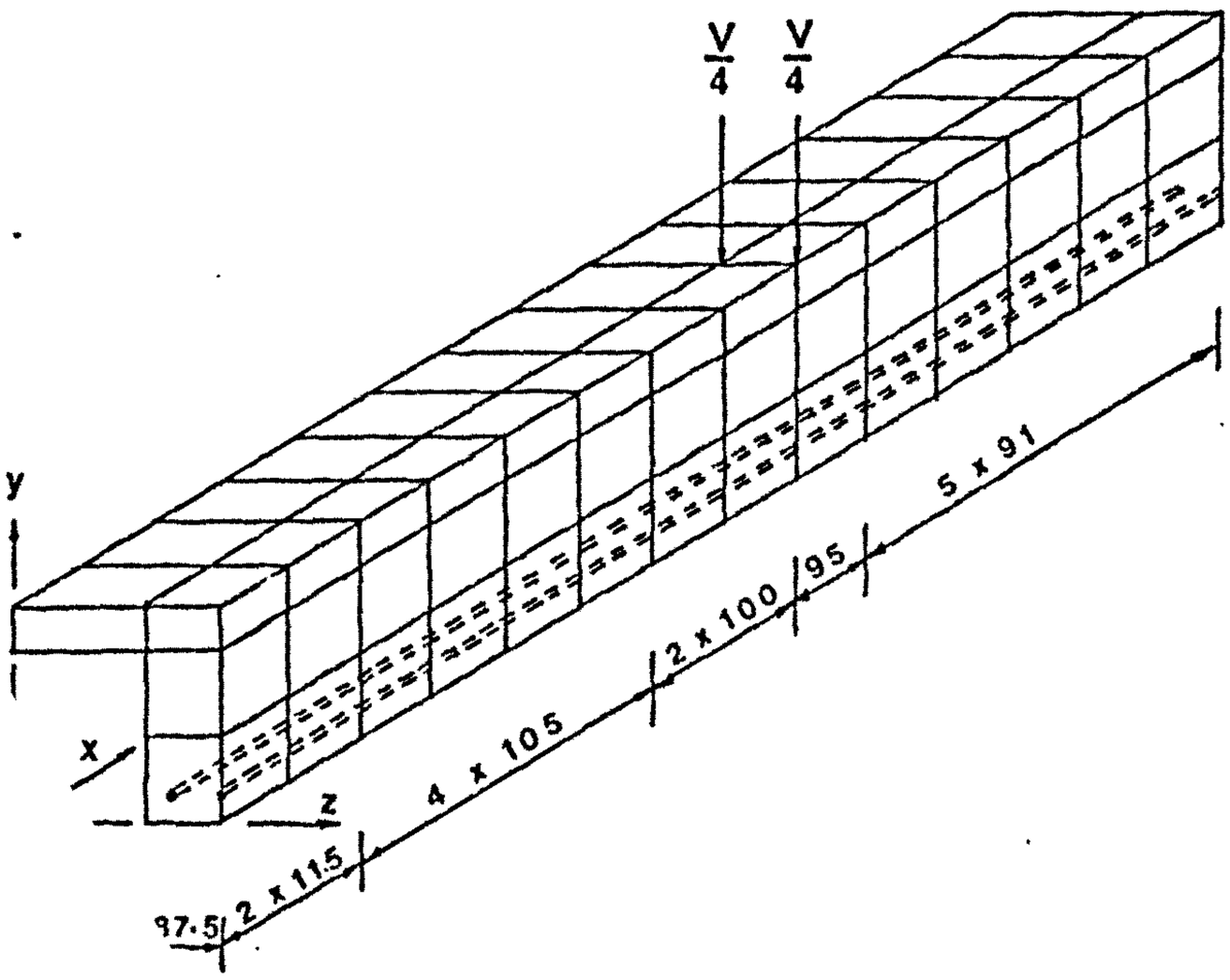

Beam Cross-Section

Idealization Of Bahia's T-Beams

strength of fibre concrete (see section 6.5.1).

The Young modulus of steel reinforcement (E_s) was taken as 200 kN/mm^2 and the yield stresses were taken as 445, 460 and 465 N/mm^2 for bars of 25, 20 and 16 mm diameter respectively.

The shear retention factors used were similar to those used for lighweight concrete.

9.3.3 Analytical Results Versus Experimental Observations

Fig. 9.14 shows the load-deflection curves of the rectangular beams while Fig. 9.15 shows the load-deflection curves of the T-beams. The analytical solutions of the plain concrete beams were in good agreement with the experimental observations. For fibre concrete beams, the deformation stiffnesses were overestimated. This is possibly due to overestimation of the uniaxial tensile strength f_t' and the assumption of a constant post-cracking tensile stress.

The load-steel strain curves at midspan of beams B61R, B51 and B53 are shown in Figs. 9.16 and 9.18. The analytical curves were in close agreement with the experimental curves. The analytical and experimental midspan steel stress-load curves of beam B63R are shown in Fig. 9.17. The analytical curve indicated that the reinforcement had yielded at failure and the experimental curve seemed to suggest likewise too. The overall correspondence was good.

The crack patterns of the beams near failure are shown in Figs. 9.19 and 9.20. Beam B61R failed in diagonal tension and the analytical crack pattern indicated this type of failure. Beam B63R failed in flexural compression and its analytical results indicated yielding of the concrete near failure. Instability of the analytical solution occurred with crushing of concrete at the 'yielded' integration points. Beam B51 failed

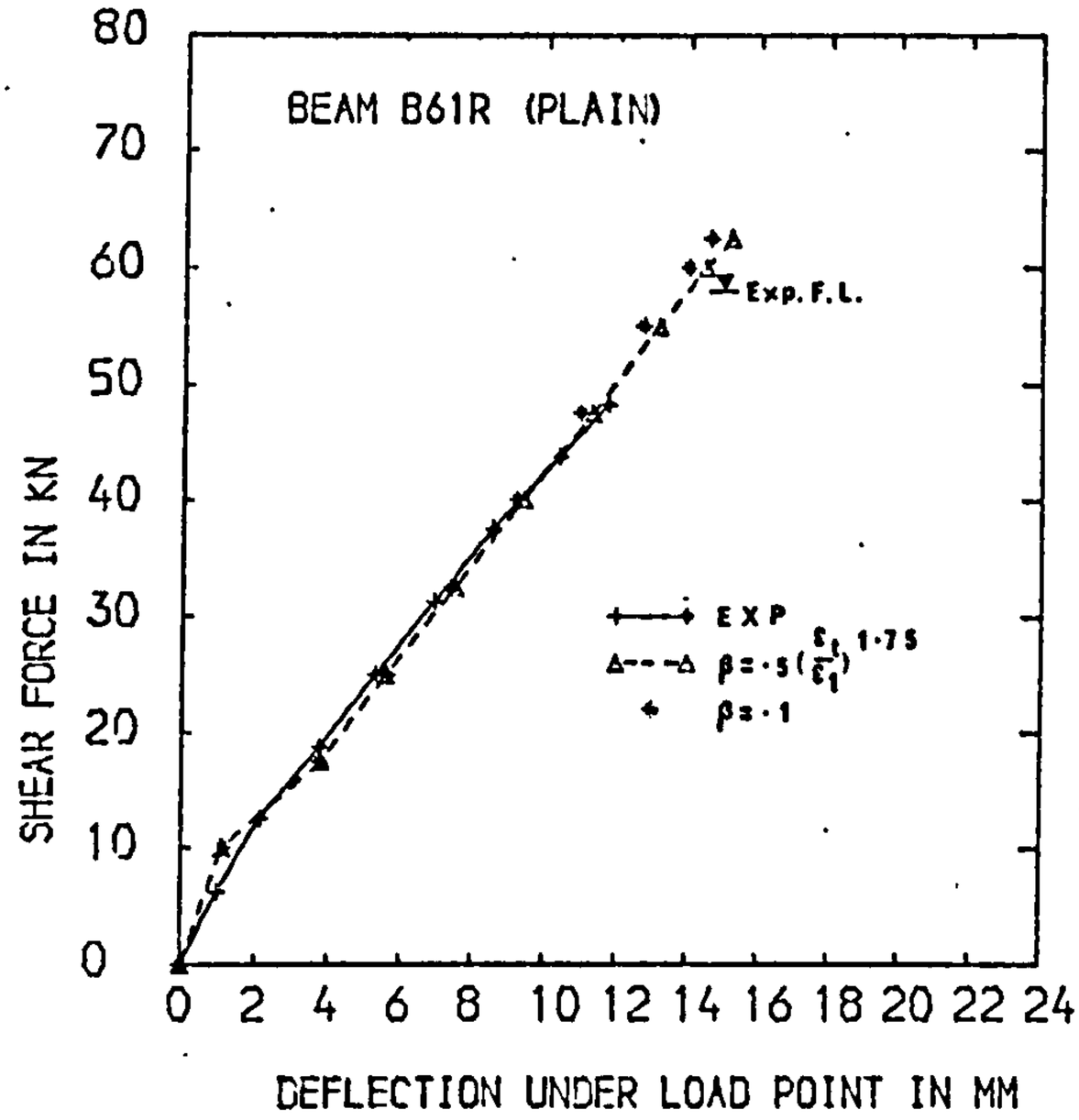

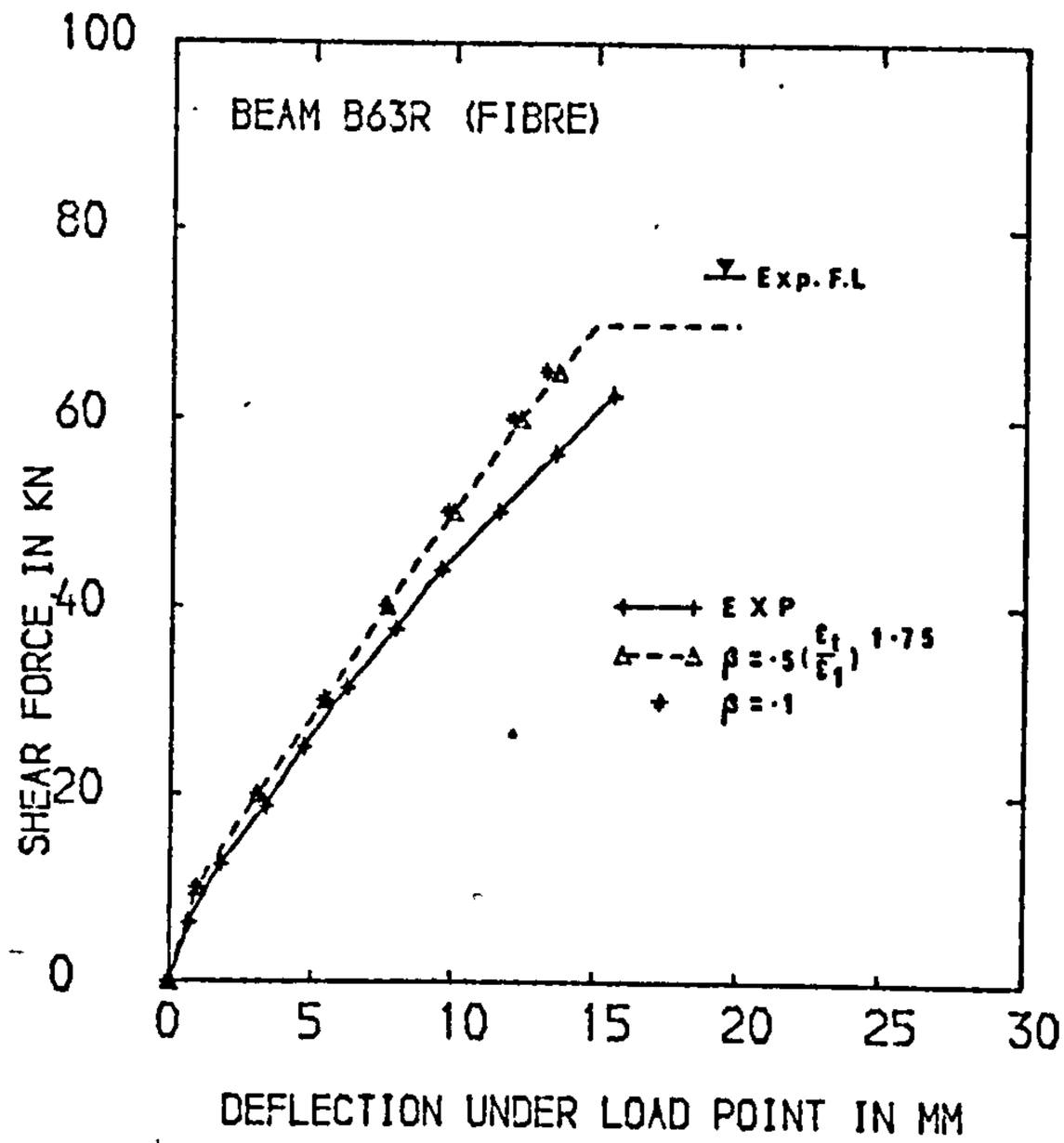

FIG.9.14 LOAD-DEFLECTION CURVES OF BAHIA'S RECTANGULAR BEAMS

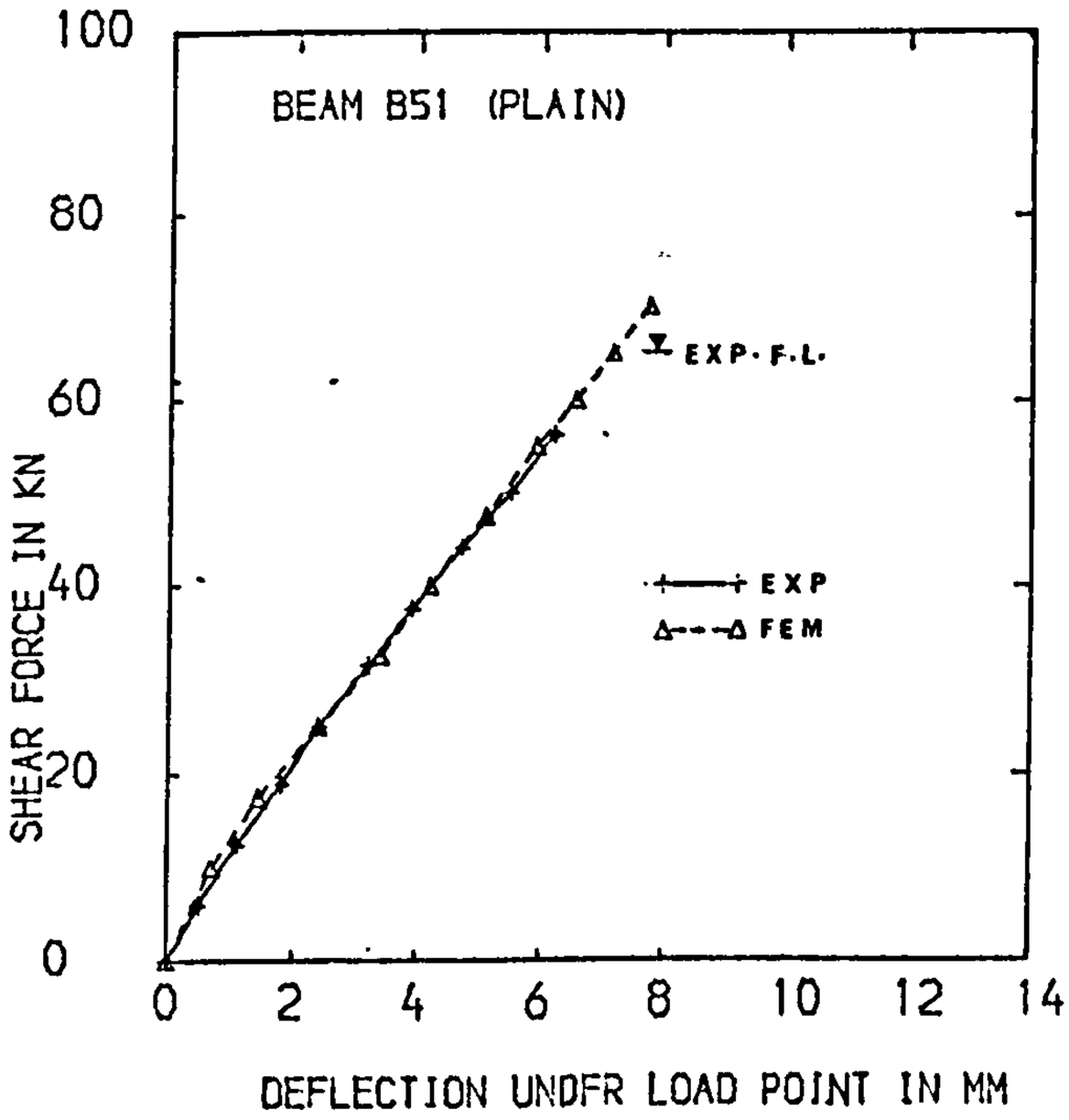

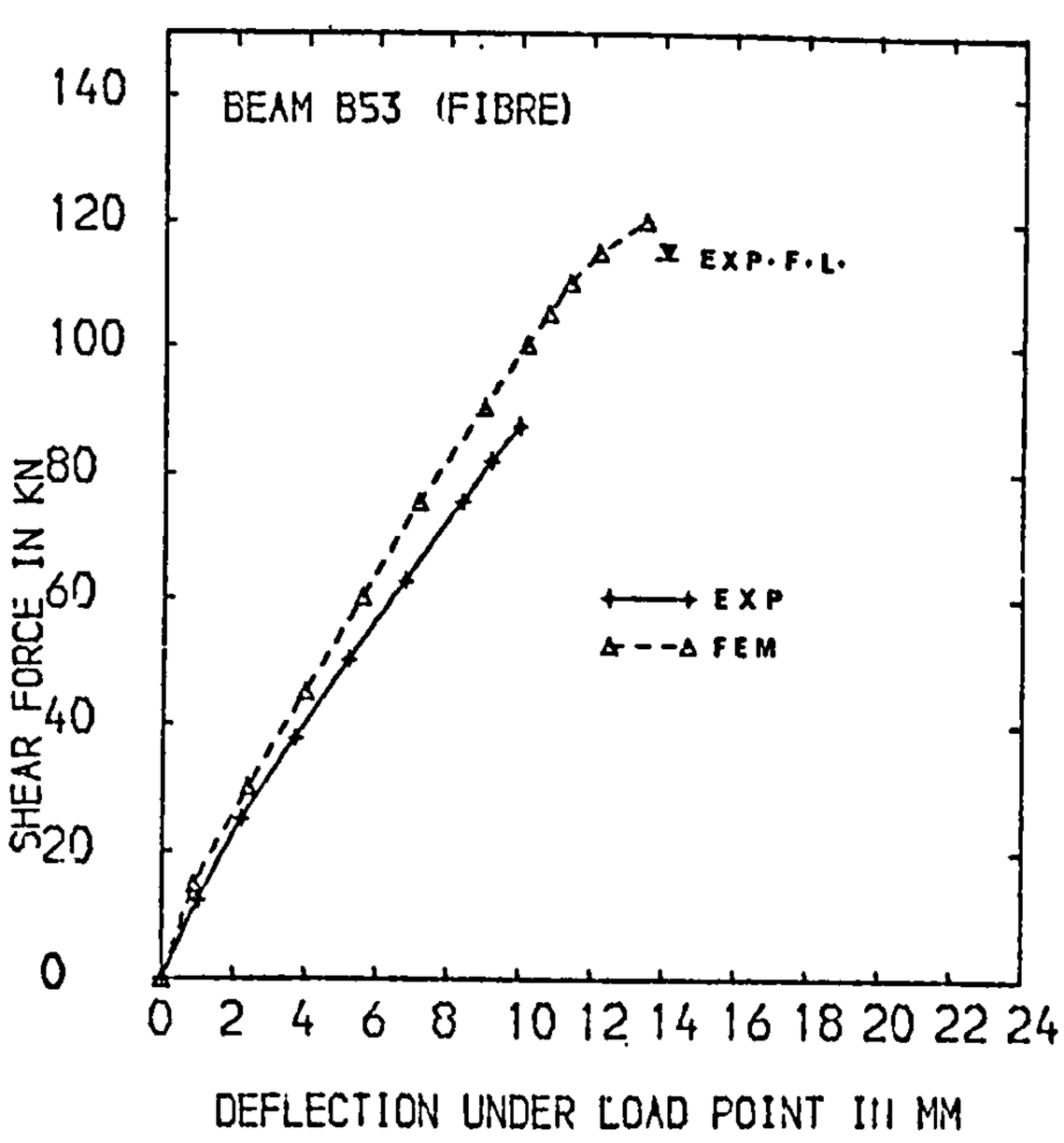

FIG.9.15 LOAD-DEFLECTION CURVES OF BAHIA'S T-BEAMS

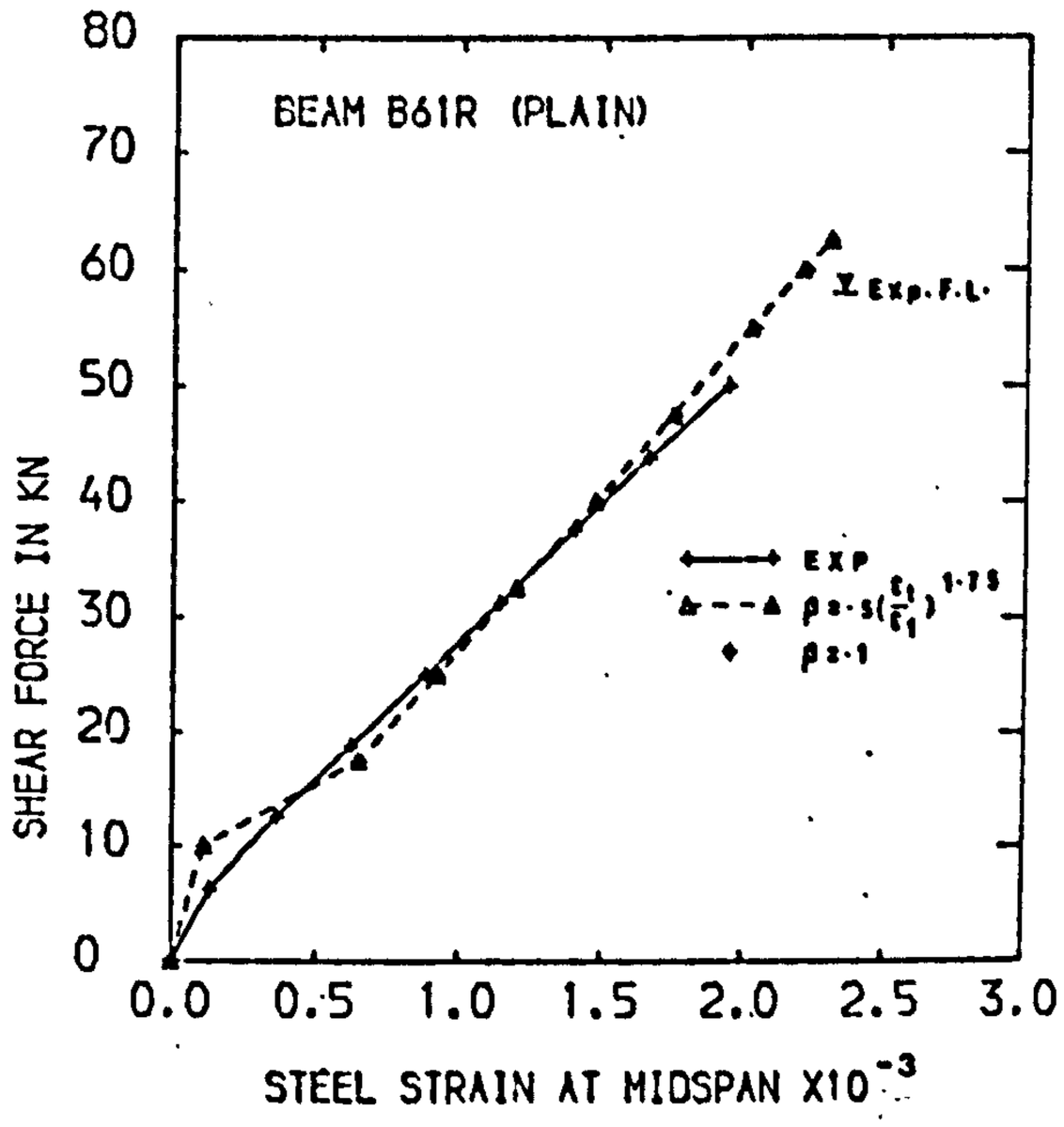

FIG.9.16 LOAD-STEEL STRAIN CURVES OF B61R

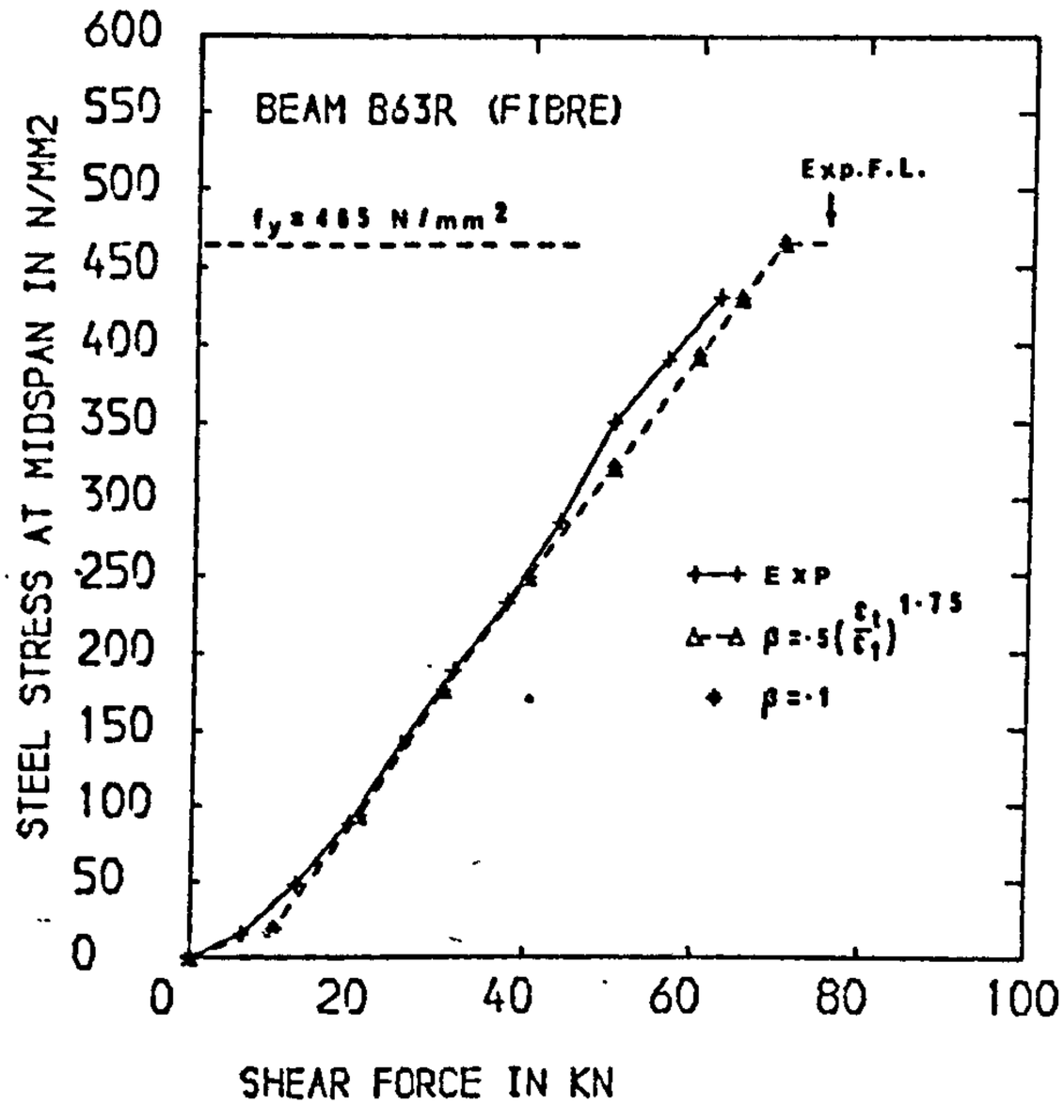

FIG.9.17 STEEL STRESS-LOAD CURVES OF B63R

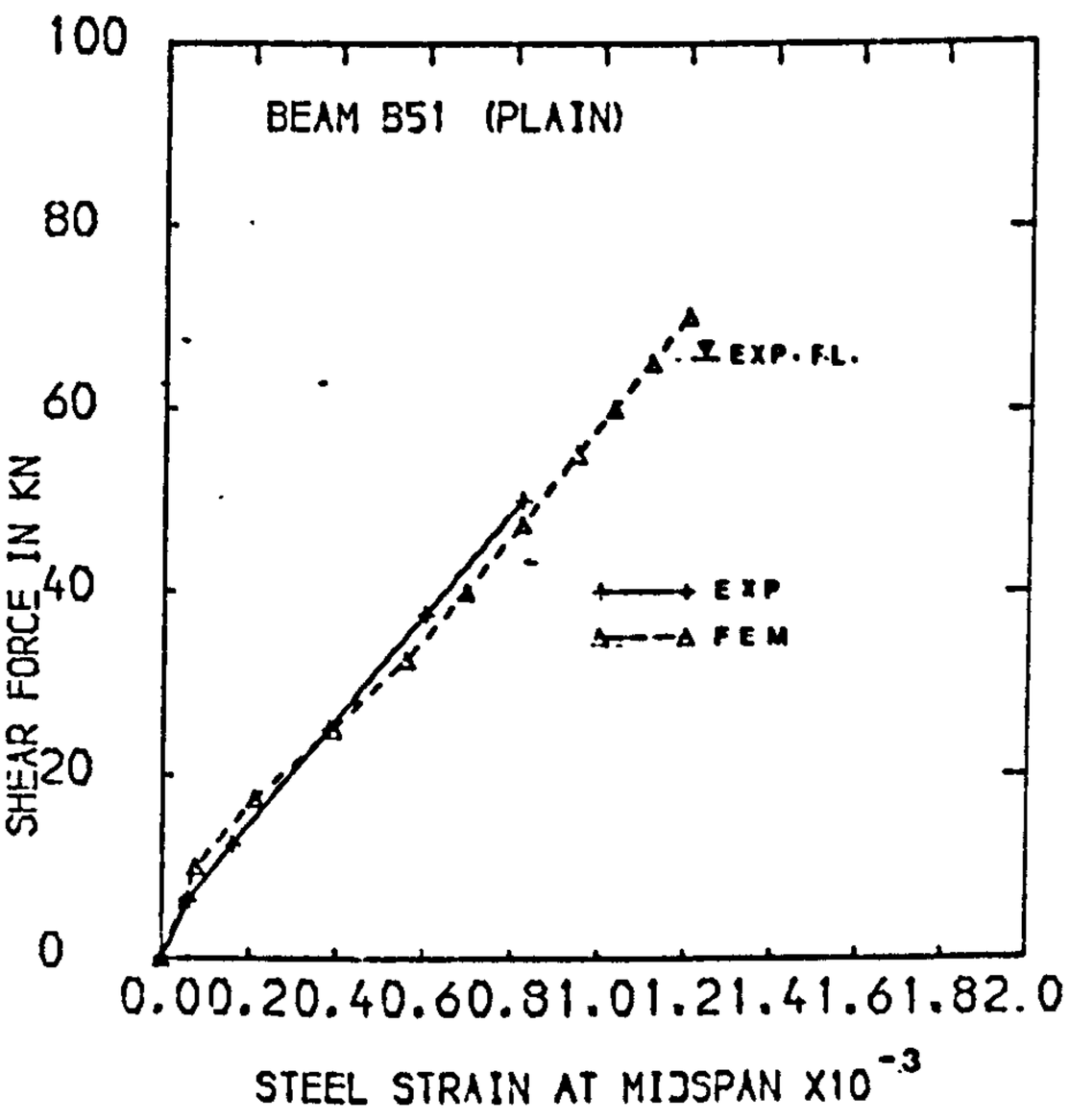

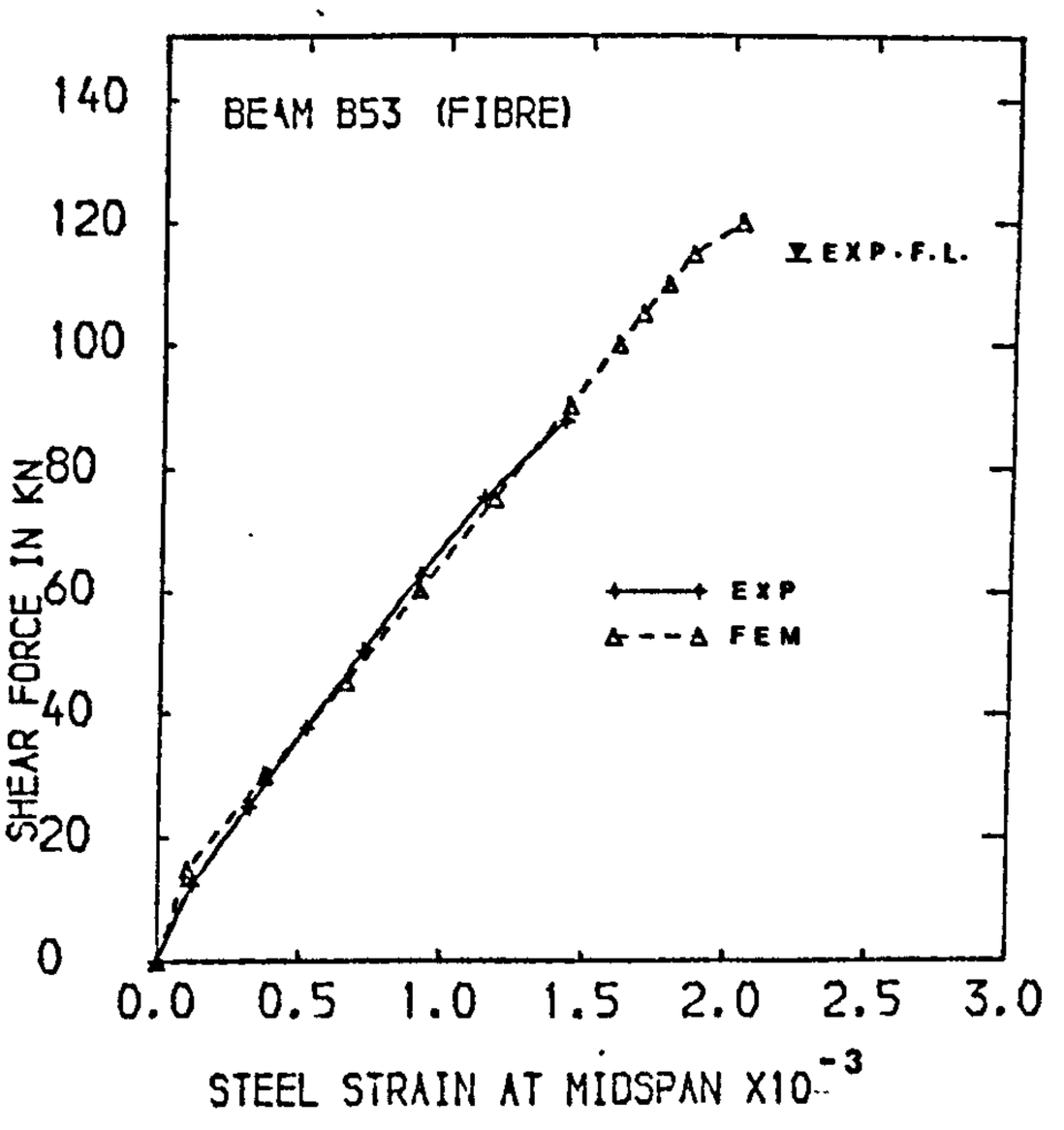

FIG.9.18 LOAD-STEEL STRAIN CURVES OF BAHIA'S T-BEAMS

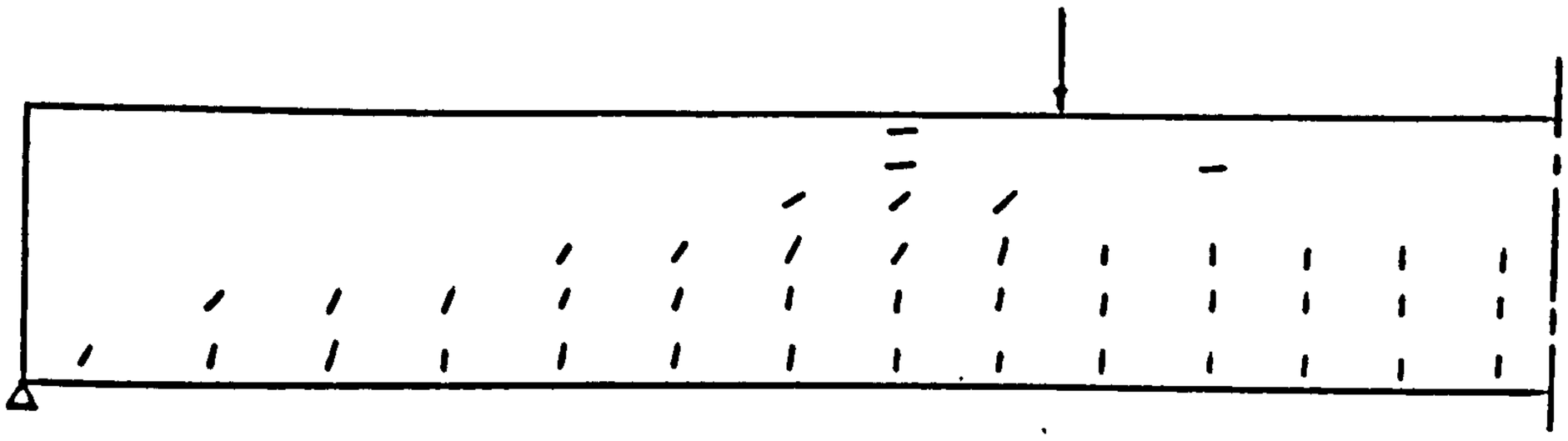

a) Beam B61R (Plain) Diagonal Tension

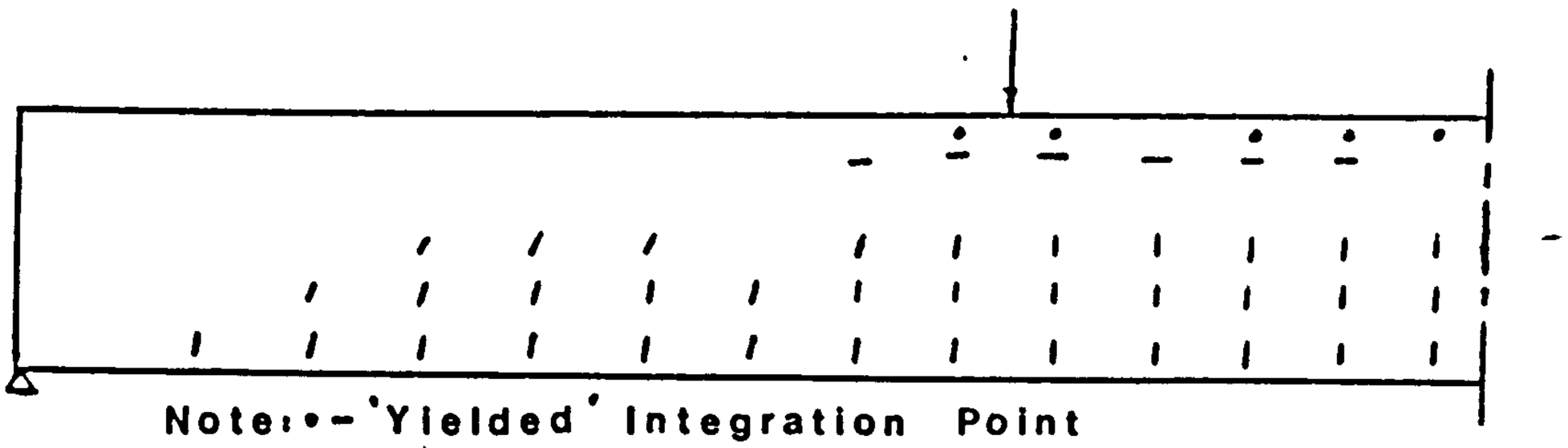

Note: • - 'Yielded' Integration Point

b) Beam B63R (Fibre) Flexural Compression

Fig. 9·19 Crack Patterns Of Bahia's Rectangular Beams Near Failure

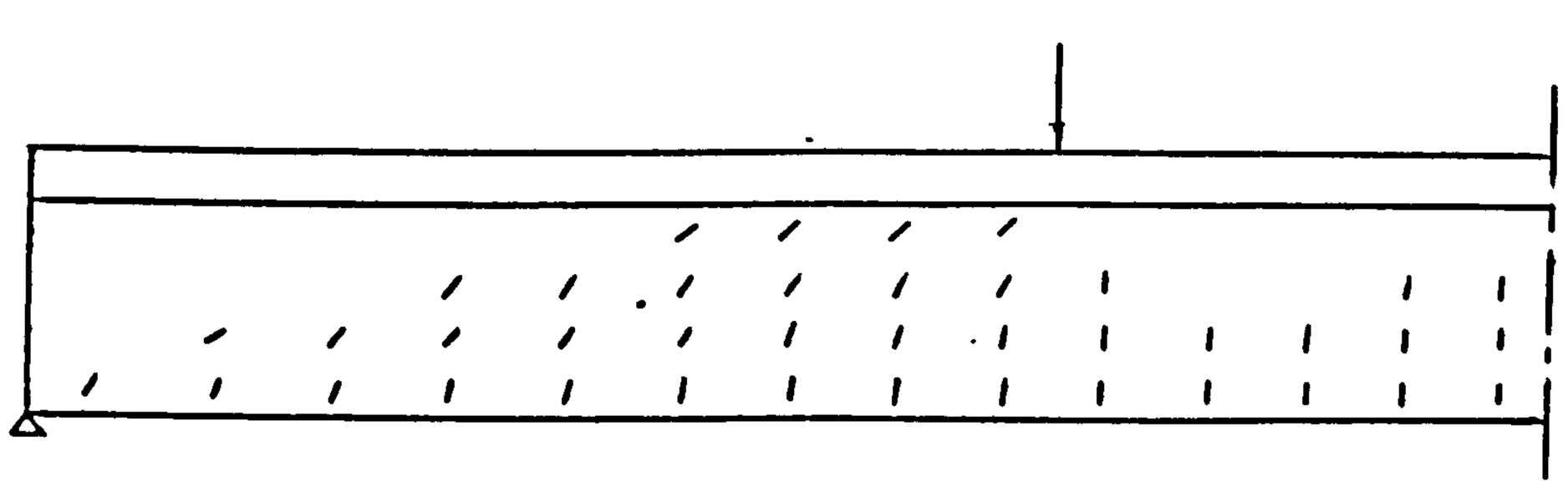

a) Beam B51 (Plain) Diagonal Tension

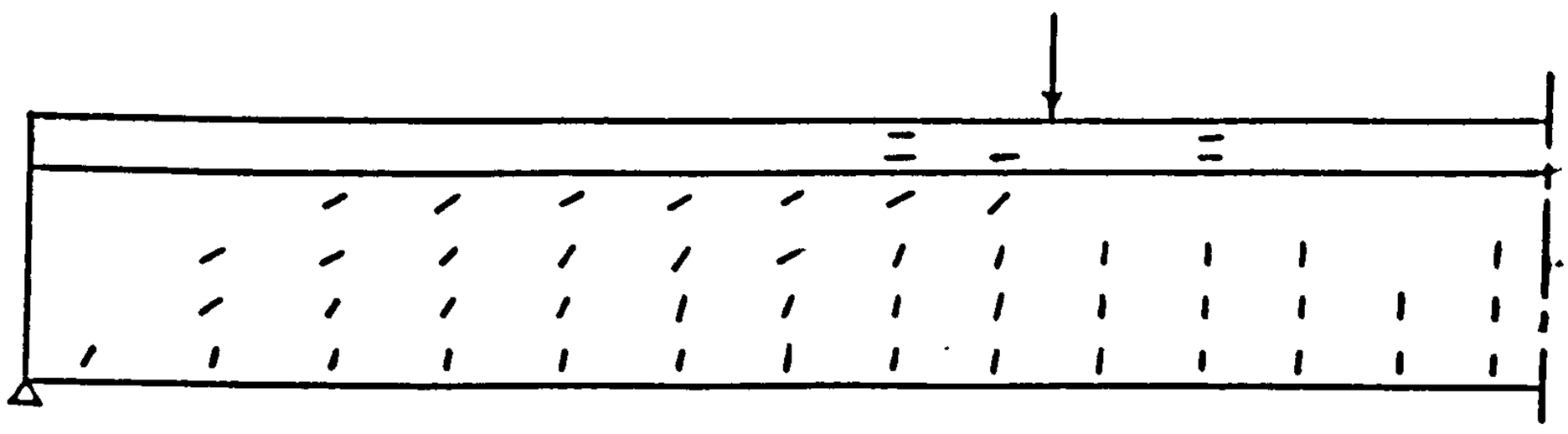

b) Beam B53 (Fibre) Shear Failure

Fig. 9·20 Crack Patterns Of Bahia's T-Beams Near Failure

in diagonal tension and final failure in beam B53 occurred by the destruction of the flange adjacent to the loading block. The analytical crack patterns indicated qualitatively the associated modes of failure of these beams.

Table 9.2 compares the analytical and experimental ultimate strength of the beams. The correlation was reasonable.

Table 9.2 Comparison of Analytical and Experimental Ultimate Strength Using Bahia's Test Data

Beam No.	% Fibre by Volume	f_{cu} N/mm^2	Ultimate Strength, V, kN			$\frac{V_{analy.}}{V_{Exp}}$	Mode of Failure
			Analytical				
			Constant S.R.F.	Varying S.R.F	Exp.		
B51	0	47.5	-	70.0	65.0	1.08	DT
B53	0.8	46.8	-	120.0	114.0	1.05	S
B61R	0	53.7	62.5	62.5	57.9	1.08	DT
B63R	0.8	43.9	70.0	70.0	75.5	0.93	FC

NOTE: S.R.F. - shear retention factor
DT - diagonal tension
FC - flexural compression
S - shear

Finally as in the lightweight concrete, the type of shear retention factor had a small influence on the load-displacement relations but had negligible influence on the load-steel strain relations and the ultimate strength of the beams.

9.4 Conclusion

From the analytical study, the following main conclusion may be drawn:

1. The finite element model of the present study predicts adequately the behaviour of plain and fibre reinforced

lightweight and normal weight concrete beams failing in shear or flexure.

2. A constant shear retention factor generally gives marginally higher deformation stiffnesses than a varying shear retention factor at high load levels. However, the type of shear retention factor has no appreciable influence on the load-steel strain relations and the ultimate strength of reinforced concrete beams.

CHAPTER TEN

LIMITATIONS, CONCLUSIONS AND SUGGESTIONS FOR FUTURE WORK

10.1 Limitations of the Present Work

The present work has provided some useful information on the use of steel fibres as shear reinforcement in reinforced concrete beams. Although the information from the subsidiary experimental tests was not fully made use of in the present finite element analytical study ,
it is suggested that such information will be useful for future analytical studies of reinforced concrete members.

The main limitations of the present work can be summarized as follows:

Experimental Studies

1. Ordinary Portland Cement with partial replacement by pulverized fuel ash (PFA) was used.

2. Only one grade of concrete (28-day cube strength of about 40 N/mm^2 was used throughout the investigation.

3. Where lightweight aggregates were used, these were restricted to only Lytag aggregates.

4. Crimped steel fibres with an aspect ratio of 100 were the main type of fibres used.

5. Cold worked deformed steel bars (Tor Bar) with specified yield stress ranging from 425 to 460 N/mm^2 and plain mild steel bars with specified yield stress of 350 N/mm^2 were used.

6. All test specimens were air-cured in the uncontrolled laboratory atmosphere and tested at 27 to 29 days after casting.

7. The size of the test beams was of full laboratory scale.

8. The number of tests carried out and parameters studied were limited.

Finite Element Model

9. Perfect bonding between steel and concrete is assumed.

10. Combined aggregate interlock and dowel action are considered through the use of either a constant or varying shear retention factor. For the latter, the shear retention factor is assumed to vary with the fictitious tensile strain perpendicular to the crack.

11. 8-node isoparametric hexahedra with 1 x 2 x 2 integration points are used to represent the concrete continuum.

12. Concrete in compression-compression zone is assumed to be elastic-plastic, obeying Von Mises's yield criterion and the associated flow rule of plasticity.

13. The uniaxial tensile stress-strain curve of plain concrete is assumed to be linearly elastic up to the tensile strength of the concrete. Once the tensile strength is exceeded, cracking occurs and the tensile stress is reduced instantly to zero. For fibre concrete, it is assumed to be linearly elastic up to the formation of the first crack and after cracking, the tensile stress is reduced to a constant value equalled to the post-cracking tensile strength of fibre concrete.

14. The tension reinforcement, represented by bar elements, is assumed to have an elastic-plastic stress-strain relationship.

10.2 Conclusions

From the present work, the following main conclusions can be drawn:

Material Properties

1. PFA replacement of cement and sand can be successfully carried out to obtain Lytag-sand concrete mixes of good early strength.

   Fibres can be introduced and successfully incorporated in both gravel and Lytag-sand concrete mixes.

2. Inclusion of crimped steel fibres effected a small increase of between 2.8 and 10.1% in the 28-day compressive cube strength for both the gravel and Lytag-sand concretes.
   In the gravel concrete, the addition of 0.4 to 1.2% by volume of fibres increased the 28-day ultimate modulus of rupture by 31.3 to 78.2% whereas in the Lytag-sand concrete the inclusion of 1.0% by volume of fibres caused an increase of between 92.6 and 95.5%. Inclusion of 1.0% by volume of fibres caused a 9.7% increase in the static elastic modulus and a 6.6% decrease in the Poisson's ratio of Lytag-sand concrete.

3. The increase of compressive strength and ultimate modulus of rupture of the plain Lytag-sand concrete from 28 days to 180 days were 8.8% and 44.1% respectively. The corresponding increases in the fibre reinforced Lytag-sand concrete were 13.6% and 0.2% respectively.

Pull-out Tests

4. Steel fibres slowed down the propagation and opening of the longitudinal and transverse cracks. This ability to contain

the splitting cracks transformed a sudden bond failure to a gradual one.

5. The maximum bond stress was not significantly affected by the inclusion of steel fibres. The addition of steel fibres effected an increase of between 2.2 and 10.1% for both gravel and Lytag-sand concrete.

   The inclusion of steel fibres had no appreciable effect on the average initial slope (slip modulus) of the bond stress-slip relationship.

6. The post-cracking characteristics of fibre concrete is reflected in the bond stress-slip relations. The fibres were able to hold the split specimens so that the bond stress could be maintained at more or less the maximum value over a considerable amount of slip. The bond stress-slip relations can be idealized as elastic-plastic.

Shear Transfer Tests

7. In initially uncracked concrete, the inclusion of crimped steel fibres reduced the amount of rotation of the inclined struts after the formation of the diagonal tension cracks. This generally resulted in higher ultimate shear transfer strength.

   In initially cracked concrete, steel fibres provided clamping forces across the crack faces and their random distribution across the shear plane seemed to enhance the roughness of the faces of the crack.

8. The inclusion of steel fibres seemed to raise the threshold of the ultimate shear transfer strength of Lytag-sand concrete. This effect was less apparent in gravel concrete.

9. The ultimate shear transfer strength (v_u) of the initially cracked plain and fibre concrete used in this investigation may be expressed as:

For the gravel concrete without steel fibre inclusion,

$$v_u = 1.82 + 0.91\, r f_y$$

for $r f_y \geq 0.5$ N/mm^2

For the gravel concrete with steel fibre inclusion,

$$v_u = 2.78 + 1.32\, (r f_y + \sigma_{cu})$$

for $(r f_y + \sigma_{cu}) \geq 0.5$ N/mm^2

For the Lytag-sand concrete without steel fibre inclusion,

$$v_u = 1.96 + 0.71\, r f_y$$

for $r f_y \geq 1.5$ N/mm^2

For Lytag-sand concrete with steel fibre inclusion,

$$v_u = 2.22 + 1.01\, (r f_y + \sigma_{cu})$$

for $(r f_y + \sigma_{cu}) \geq 1.5$ N/mm^2

$r f_y$ is the conventional shear reinforcement parameter and σ_{cu} is the post-cracking tensile strength of fibre concrete.

10. Shear transfer stiffness may be represented by:

For the plain and fibre reinforced gravel concrete,

$$G_s = 3.0\, (\frac{1}{w})^{1.75}$$

For the plain and fibre reinforced Lytag-sand concrete,

$$G_s = 2.5\, (\frac{1}{w})^{1.75}$$

G_s is the shear transfer stiffness in N/mm^3 and w is the crack width in mm.

Beam Tests

11. The addition of 1% by volume of crimped steel fibres to Lytag-sand concrete beams without conventional shear reinforcement decreased the deflection, concrete strain at midspan, tension steel strains and end rotations at all stress levels. The reductions were small initially and were more pronounced after the formation of cracks. At failure, fibre concrete beams showed greater ductility than their plain concrete counterparts.

12. The loads at first flexural and shear cracks were generally higher in the fibre concrete beams. The fibre concrete beams had more flexural and shear cracks and the latter were spread further towards the supports than in the corresponding plain concrete beams at failure.

13. Shear failure of plain concrete beams with large shear spans generally occurred soon after the formation of the web shear cracks. Failure was by tensile splitting along the level of the main reinforcement and simultaneous instability of the compression flange above the shear crack.

14. Shear failure of fibre concrete beams with long shear spans involved the widening of more than one shear crack. The steel fibres slowed down the propagation of the shear cracks and final failure was triggered off by the instability of the compression zone above the active shear cracks.

15. The inclusion of steel fibres was generally sufficient to prevent significant tensile splitting along the level of the main reinforcement and when it did occur, the steel fibres were able to slow down its propagation considerably.

16. The inclusion of 1% by volume of crimped steel fibres caused an increase in the ultimate strength ranging from 63 to 211.5% depending on the shear spans and modes of failure of the fibre concrete beams.

17. The methods given in CP110, CI-318-77 and CEB-FIP Model Code predicted the failure loads of the Lytag-sand concrete beams with no shear reinforcement and with large shear spans with reasonable accuracy. However they underestimated the shear strength of those beams with short shear spans by 50.8 - 65.9%

18. The proposed method based on the Standard Method of CEB-FIP Model Code predicted the ultimate shear strength of crimped steel fibre reinforced Lytag-sand concrete beams with large shear spans with adequate accuracy. The shear strength of beams with short shear spans was underestimated by 35.4 - 45.6%. It predicted adequately the ultimate shear strength of steel fibre reinforced normal weight concrete beams .

Finite Element Analytical Study

19. The finite element model of the present study predicts adequately the behaviour of plain and fibre reinforced lightweight and normal weight concrete beams subjected to short term monotonically increasing loading.

20. A constant shear retention factor generally gives marginally higher deformation stiffnesses than a varying shear retention factor at high load levels. However, the type of shear retention factor has no appreciable influence on the load-steel strain relations and the ultimate strength of reinforced concrete beams.

10.3 Suggestions for Future Work

Experimental Studies

1. More tests on the use of steel fibres as shear reinforcement in lightweight concrete beams are needed. Useful parameters for study include the type of lightweight aggregate, the grade of concrete and the type of steel fibres.

2. Studies are needed on the effect of size of specimen in fibre reinforced concrete beams.

3. The possibility of using steel fibres in conjunction with a limited amount of conventional stirrups relatively large spacing in concrete beams needs to be investigated.

4. Failure criteria of fibre concrete under combined stresses are needed for a more accurate analytical study of fibre reinforced concrete members.

Possible Improvements of the Present Finite Element Model and Computer Program

These include:

1. The incorporation of bond stress-slip characteristics, for example, through the use of linkage elements.

2. The incorporation of more appropriate failure criteria for fibre concrete subjected to multiaxial stress states when they become available.

3. The use of a more exact uniaxial tensile stress-strain curve for fibre concrete.

4. Extension of the model to allow the consideration of conventional stirrups.

5. The incorporation of material nonlinearities due to shrinkage and creep of concrete.

6. Increasing the flexibility of the program by allowing the use of other higher order isoparametric hexahedral elements to represent the concrete.

7. The use of standard graph plotting routines to output important results graphically, for example, the propagation of cracking after each load increment.

List of References

1. Swamy, R. N., Mangat, P. S. and Rao, C.V.S.K., "The Mechanics of Fibre Reinforcement of Cement Matrices", Fibre Reinforced Concrete, ACI Special Publication, SP-44, 1974, pp 1 - 28.

2. ACI Committee 408, "Bond Stress - The State of the Art", ACI Journal, Proceedings, V. 63, No. 11, 1966, pp 1161 - 1188.

3. Birkeland, P. W. and Birkeland, H.W., "Connections in Precast Concrete Construction", ACI Journal, Proceedings, V. 63, No. 3, March, 1966, pp 345 - 368.

4. Mast, R. F., "Auxilliary Reinforcement in Concrete Connections", Journal of Structural Division, ASCE, Vol. 94, ST6, June, 1968, pp 1485 - 1504.

5. CEB-FIP, "Model Code for Concrete Structures", International System of Unified Standard Codes of Practice for Structures, Vol. II, Bulletin D'information N.124/125 - E, 1978.

6. Bahia, H. M., "Shear Transfer of Fibre Reinforced Concrete". Ph.D Thesis, University of Sheffield, 1976.

7. ACI Committee 544, "State-of-the-art Report on Fibre Reinforced Concrete", Fibre Reinforced Concrete, ACI Special Publication, SP-44, 1974, pp 535-550.

8. Swamy, R. N., "The Technology of Steel Fibre Reinforced Concrete for Practical Applications", Proc. Inst. of Civil Engrs., V. 56, Part 1, May, 1974, pp 143 - 159.

9. Edgington, J., Hannant, D. J. and Williams, R. I., "Steel Fibre Reinforced Concrete", Building Research Establishment Current Paper CP 69 (74, July, 1974).

10. Romualdo, J. P. and Mandel, J. A., "Tensile Strength of Concrete affected by Uniformly Distributed and Closely Spaced Short Lengths of Wire Reinforcement", ACI Journal, Proceedings, V.61, No. 6, June, 1964, pp 657 - 671.

11. Cox, H. L., "The Elasticity and Strength of Paper and Other Fibrous Materials", British Journal of Applied Physics, Vol. 3, March, 1952, pp 72 - 79.

12. Krenchel, H., "Fibre Reinforcement", Copenhagen:Akademisk Forlag, 1964.

13. Laws, V., "The Efficiency of Fibrous Reinforcement of Brittle Matrices", Journal of Applied Physics, Vol. 4, 1971, pp 1737 - 1746.

14. Swamy, R. N., "Fibre Reinforcement of Cement and Concrete", RILEM Materials and Structures, Vol. 8, No. 45, 1975 pp 235 - 254.

15. Maage, M., "Fibre Bond and Friction in Cement and Concrete", Proceedings of Symposium on Testing and Test Methods of Fibre Cement Composites, Sheffield, 5 - 7 April, 1978.

16. Gray, R. J. and Johnston, C. D., "The Measurement of Fibre-Matrix Interfacial Bond Strength in Steel Fibre Reinforced Cementitious Composite", Proceedings of Symposium on Testing and Test Methods of Fibre Cement Composites, Sheffield, 5 - 7 April, 1978.

17. Tattersall, G. H. and Urbanowicz, C. R., "Bond Strength in Steel Fibre Reinforced Concrete", Magazine of Concrete Research, Vo. 26, No. 87, June, 1974, pp 105 - 113.

18. Hughes, B. P. and Fattuhi, N. I. "Fibre Bond Strengths in Cement and Concrete", Magazine of Concrete Research, Vol. 27, No. 92, September, 1975, pp 161 - 166.

19. Aveston, J., Mercer, R. A. and Sillwood, J. M., "Fibre Reinforced Cements - Scientific Foundations for Specifications", Proceedings of Conference on Composites - Standards, Testing and Design, National Physical Laboratory, 1974, pp 93 - 103.

20. Swamy, R. N. and Mangat, P. S.,"A Theory for the Flexural Strength of Steel Fibre Reinforced Concrete", Cement and Concrete Research, Vol. 4., January, 1974, pp 313 - 325.

21. Swamy, R. N. and Mangat, P. S., "The Interfacial Bond Stress in Steel fibre Cement Composites", Cement and Concrete Research, Vo. 6, 1976, pp 641 - 650.

22. Romualdi, J. P. and Batson, G. B., "Behaviour of Reinforced Concrete Beams with Closely Spaced Reinforcement", ACI Journal, Proceedings, Vol. 60, June, 1963, pp 775 - 789.

23. Romualdi, J. P. and Batson, G. B.,"Mechanics of Crack Arrest in Concrete", J. of the Engineering Mechanics Division, ASCE, Vol. 89, No. EM3, June, 1963, pp 147 - 168.

24. Kar, J. N. and Pal, A. K., "Strength of Fibre-Reinforced Concrete". J. of the Structural Division, ASCE, Vol. 98, No. ST5, May, 1972, pp 1053 - 1068.

25. Shah, S. P. and Rangan, B. V., "Fibre Reinforced Concrete Properties", ACI Journal, Proceedings, Vol. 68, No. 2., February, 1971.

26. Edgington, J., "Economic Fibrous Concrete", Fibre Reinforced Materials: Design and Engineering Applications, Inst. of Civil Engineers, London, 1977, pp 129 - 140.

27. Majumdar, A. J., "Fibre Cement and Concrete - a Review", Building Research Establishment Current Paper CP26/75, 1975.

28. Batson, G, Jenkins, E. and Spatney, R., "Steel Fibres as Shear Reinforcement in Beams", ACI Journal, Proceedings, V. 69, No. 10, Oct., 1972, pp 640 - 644.

29. Williamson, G. R. and Knab, L. I., "Full scale Fibre Concrete Beam Tests", RILEM Symposium on Fibre Reinforced Cement and Concrete, London, 1975, Construction Press, pp 209 - 214.

30. LaFraugh, R. W. and Moustafa, S. E., "Experimental Investigation of the Use of Steel Fibres for Shear Reinforcement", Report, Concrete Technology Associates, Tacoma, Washington, 1975.

31. Muhidin, N. A. and Regan, P. E., "Chopped Steel Fibres as Shear Reinforcement in Concrete Beams", Fibre Reinforced Materials: Design Engineering Applications, Inst. of Civil Engrs., London, 1977, pp 149 - 163.

32. Bresler, B. and MacGregor, J. G., "Review of Concrete Beams Failing in Shear", Jl. of Strucutural Division, ASCE, Vol. 93, No. ST1, Feb., 1967 pp 343 - 372.

33. Shear Study Group, "The Shear Strength of Reinforced Concrete Beams", Inst. of Structural Engineers, London, 1969.

34. ASCE-ACI Committee 426, "The Shear Strength of Reinforced Concrete Members", Jl. of Structural Division, ASCE, Vol. 99, No. ST6, June, 1973, pp 1091 - 1187.

35. CEB Commission V, "Shear and Torsion", Explanatory and Viewpoint Papers on Model Code Chapters 11 and 12, Bulletin D'information No. 126, June, 1978.

36. Taylor, H. P. J., "Basic Behaviour in Shear and the Model Code Provisions for Members Without Shear Reinforcement", Shear and Torsion, CEB Bulletin D'information N. 126, June, 1978, pp 126 - 140.

37. Leonhardt, F. and Walther, R., "The Stuttgart Shear Tests, 1961", Translation No. 111, Cement and Concrete Association, London.

38. Kani, G. N. J., "How Safe are Our Large Concrete Beams?", Jl. of ACI, Proceedings, V. 64, Mar., 1967, pp 128 - 141.

39. Taylor, H. P. J., "The Shear Strength of Large Beams", Jl. of Structural Division, ASCE, Vol. 98, No. ST11, Nov., 1972, pp 2473 - 2490.

40. Kani, G. N. J., "The Riddle of Shear Failure and Its Solution", Jl. of ACI, Proceedings, V. 63, June 1966, pp 441 - 467.

41. Fenwick, R. C. and Paulay, T., "Mechanisms of Shear Resistance of Concrete Beams", Jl. of Structural Dvision, ASCE, Vol. 94, No. ST10, Oct., 1968, pp 2325 - 2350.

42. Rabbat, B. G. and Collins, M. P., "A Variable Angle-Space Truss Model for Structural Concrete Members Subjected to Complete Loadings", Douglas McHenry International Symposium on Concrete and Concrete Structures, Detroit, 1978, ACI SP-55, pp 547 - 587.

43. Grab, J. and Thurlimann, B., "Ultimate Strength and Design of Reinforced Concrete Beams Under Bending and Shear", IABSE Pubications, Vo. 36, No. II, 1976, pp 105 - 120.

44. Swamy, R. N. and Qureshi, S. A., "An Ultimate Shear Strength Theory for Reinforced Concrete T-beams Without Web Reinforcement", Materiaux Et Constructions, Vol. 7, No. 39, 1974, pp 181 - 189.

45. Swamy, R. N. and Qureshi, S. A., "An Ultimate Shear Strength Theory for Reinforced Concrete T-beams With Web Reinforcement", Proc. Inst. of Civil Engrs. Part 2, Vol. 57, Mar., 1974, pp 21 - 34.

46. Zsulty, T. C., "Beam Shear Strength Prediction by Analysis of Existing Data", Jl of ACI, Proceedings, V. 65, Nov., 1968, pp 943 - 951.

47. Nielsen, M. P. and Braestrup, M. W., "Plastic Shear Strength of Reinforced Concrete Beams", Bygningsstatiske Meddelelser, Vo. 46, No. 3, 1975, pp 61 - 99.

48. Braestrup, M. W., "Effect of Main Steel Strength on the Shear Capacity of Reinforced Concrete Beams With Stirrups", Rapport NR.R 110, 1979, Structural Research Laboratory, Technical University of Denmark.

49. Scordelis, A. C., Ngo, D. and Franklin, H. A., "Finite Element Study of Reinforced Concrete Beams With Diagonal Tension Cracks", ACI Special Publications SP 42-4, Vol. 1, 1974, pp 79 - 102.

50. Houde, J. and Mirza, M. S. , "A Finite Element Analysis of Shear Strength of Reinforced Concrete Beams", ACI Special Publications SO 42-4, Vol I, 1974, pp 103 - 129.

51. Hammad, Y. M. H., "Influence of the Flange on the Ultimate Shear Capacity pf Reinforced Concrete T-beams", Ph.D Thesis, University of Sheffield, 1978.

52. Cedolin, L. and Doli, S. D., "Finite Element Studies of Shear-Critical R/C Beams", Jl. of Engineering Mechanics Division, ASCE, Vol. 103, No. EM3, June, 1977, pp 395 - 410.

53. British Standards Institute, B.S. 12: 1978, "Ordinary and Rapid-Hardening Portland Cement".

54. British Standards Institute, B.S. 3892, 1965, "PFA for Use in Concrete", Metric Units.

55. British Standards Institute, B.S. 882, 1201: Part 2: 1973, "Specification for Aggregates from Natural Sources for Concrete" with amendment slip (1975).

56. British Standards Institute, B.S. 3797: Part 2: 1976, "Specification for Lightweight Aggregates for Concrete",

57. Swamy, R. N., and Stavrides, H., 1975, "Some Properties of High Workability Steel Fibre Concrete", Fibre Reinforced Cement and Concrete, RILEM Symposium, Sept. 1975, pp 197 - 208.

58. Ali, S. A. R., "Effect of Fibre Reinforcement on the Punching Shear of Flat Plates", Ph.D Thesis, University of Sheffield, April, 1979.

59. Jackson, A. J. and Goodridge, W. F., "A New Approach to PFA Concrete", The Contract Journal, March, 1961, pp 1284 - 1286.

60. Lambert, G. H. Private Communication, University of Sheffield

61. British Standards Institute, B.S. 1881 : 1970, "Method of Testing Concrete", Parts 4 and 5.

62. Al-Ta'an, S. A., "Structural Behaviour of Conventionally Reinforced Concrete Beams with Steel Fibres", Ph.D Thesis, University of Sheffield, July, 1978.

63. Sittampalan, K., "Flexural Behaviour of Limited Prestressed Lightweight (Lytag) Concrete Beams With and Without Fibre Reinforcement", M.Eng. Thesis, University of Sheffield, 1979.

64. Theodorakopoulos, D., "Punching Shear Strength of Steel Fibre Reinforced Lightweight Concrete Slabs", Ph.D Thesis University of Sheffield, September, 1980.

65. Swamy, R. N. and Stavrides, H., "Influence of the Method of Fabrication on Strength Properties of Steel Fibre Concrete", RILEM Material and Structures, Vol. 9, No. 52, July - August, 1976, pp 243 - 253.

66. Teychenne, D. C. "Structural Concrete Made With Light-weight Aggregate Concrete", Concrete, Vol. 1, No. 4, April. 1967, pp 111 - 122.

67. Ritche, A. G. B. and Al-Kayyali, O. A., "The Effects of Fibre Reinforcement on Lightweight Aggregate Concrete, RILEM Symposium on Fibre Reinforced Cement and Concrete, London, 1975, pp 247 - 256.

68. CP110 Part 1 : 1972, "The Structural Use of Concrete - Design, Materials and Workmanship".

69. Neville, A. M., "Properties of Concrete", 3rd Edition, Pitman Publishing Limited, London, 1981.

70. Lutz, L. A. and Gergely, P., "Mechanics of Bond and Slip of Deformed Bars in Concrete", Jl. of ACI, Proceedings, V. 64, No. 11, Nov., 1967, pp 711 - 721.

71. Rehm, G., "The Basic Principles of the Bond Between Steel and Concrete", Cement and Concrete Association Trans-lation No. 134, 1961.

72. Broms, B. and Lutz, L. A., "Effect of Arrangement of Reinforcement on Crack Width and Spacing in Reinforced Concrete Members", Jl. of ACI, Proceedings, V. 62, No. 11, Nov., 1965, pp 1395 - 1409.

73. Bresler, B. and Bertero, V., "Behaviour of Reinforced Concrete Under Repeated Load", Jl. of the Structural Division, ASCE, Vol. 94, ST6, June, 1968, pp 1567 - 1590.

74. Goto, Y, "Cracks Formed in Concrete Around Deformed

Tension Bars", Jl. of ACI, Proceedings, V. 68, No. 6, April 1971, pp 244 - 251.

75. Watstein, D., "Distribution of Bond Stress in Concrete Pullout Specimens", Jl. of ACI, Proceedings, Vol. 43, No. 5, May, 1947, pp 1041 - 1052.

76. Mains, R. M., "Measurement of the Distribution of Tensile and Bond Stresses Along Reinforcing Bars", ACI Journal, Proceedings, V. 48, No. 11, Nov., 1951, pp 225 - 252.

77. Perry, E. S. and Thompson, J. N., "Bond Stress Distribution on Reinforcing Steel in Beams and Pullout Specimens", ACI Journal, Proceedings, V. 63, No. 8, Aug., 1966, pp 865 - 974.

78. Nilson, A. H., "Bond Stress-Slip Relations in Reinforced Concrete", Report No. 345, Department of Structural Engineering, Cornell University, New York, 1971.

79. Stavrides, H., "Ma terial Properties and Structural Behaviour of Fibre Reinforced Cement Composites", Ph.D Thesis, University of Sheffield, June, 1978.

80. Evans, R. H. and Robinson, G. W., "Bond Stresses in Prestressed Concrete from X-Ray Photographs", Proc. Inst. of Civil Engrs., Part 1, Vol. 4, No. 2, March, 1955, pp 212 - 235.

81. Wahla, M. I., Scott, N. P. and Nilson, A. H., "Direct Measurement of Bond-Slip in Reinforced Concrete", Proceedings of American Society of Agricultural Engineers, 1969, paper 69 - 921.

82. Edwards, A. D. and Picard, A., "Bonding Properties of ½in Diameter Strand", ACI Journal, Proceedings, V. 69, No. 11, Nov., 1972, pp 684 - 689.

83. Edwards, A. D. and Yannopoulos, P. J., "Local Bond-Stress to Slip Relationships for Hot Rolled Deformed Bars and Mild Steel Plain Bars", ACI Journal, Proceedings, V. 76, No. 3, March, 1979, pp 405 - 420.

84. Nilson, A. H., "Nonlinear Analysis of Reinforced Concrete by the Finite Element Method", ACI Journal, Proceedings, V. 65, No. 9, Sept., 1968, pp 757 - 766.

85. Bresler, B., and Bertero, V., "Influence of Load History on Cracking in Reinforced Concrete", Report to California Division of Highways, Department of Civil Engineering, Division of Structural Engineering and Structural Mechanics, University of California (Berkeley), 1966.

86. Tepfers, R., "Cracking of Concrete Cover Along Anchored Deformed Reinforcing Bars", Magazine of Concrete Research, Vol. 31, No. 106, March, 1979, pp 3 - 12.

87. Reinforced Steel Services, "Tor Bar", Publication No. 61, 3rd Edition, Feb., 1980.

88. Al-Noori, N. A., "Flexural Behaviour of Conventionally Reinforced Fibre Concrete Beams", Ph.D. Thesis, University of Sheffield, 1974.

89. Hofbeck, J. A., Ibrahim, I. O. and Mattock, A. H., "Shear Transfer in Reinforced Concrete", ACI Journal, Proceedings, V. 66, No. 2, Feb., 1969, pp 119 - 128.

90. Mattock, A. H. and Hawkins, N. W., "Shear Transfer in Reinforced Concrete - Recent Research", Journal of Prestressed Concrete Institute, Vol. 17, No. 2, 1972, pp 55 - 75.

91. Mattock, A. H., Li, W. K. and Wang, T. C., "Shear Transfer in Lightweight Reinforced Concrete", Journal of Prestressed Concrete Institute, Vol. 21, No. 2, 1976, pp 20 - 39.

92. Taylor, H. P. J., "Investigation of the Forces Carried Across Cracks in Reinforced Concrete Beams in Shear by Interlock of Aggregate", Cement and Concrete Association, Technical Report TRA 42.448, No., 1970, London.

93. Mattock, A. H., "Shear Transfer in Concrete Having Reinforcement at an Angle to the Shear Plane", Shear in Reinforced Concrete, ACI publication, SP-42, 1974, pp 17 - 42.

94. Paulay, T., and Leober, P. J., "Shear Transfer by Aggregate Interlock", Shear in Reinforced Concrete, ACI publication, SP - 42, 1974, pp 1 - 15.

95. Houde, J. and Mirza, M. S., "A Finite Element Analysis of Shear Strength of Reinforced Concrete Beams", Shear in Reinforced Concrete, ACI publication, SP - 42, 1974, pp 103 - 128.

96. Hamadi, Y. D., "Force Transfer Across Cracks in Concrete Structures", Ph. D Thesis, Polytechnic of Central London, 1976.

97. Walraven, J. C., Vos, E. and Reinhardt, H. W., "Experiments on Shear Transfer in Cracked Concrete", Nonlinear Behaviour of Reinforced Concrete Spatial Structures, Vol. 1, 1978, IASS Symposium 1978, Darmstadt, pp 61 - 73.

98. Criswell, M. E., "Shear in Fibre Reinforced Concrete", Dept. of Civil Engineering, Colorado State University, 1976.

99. Muhidin, N. A., "Design Criteria for Fibre Reinforced Concrete", Ph.D Thesis, Polytechnic of Central London, 1977.

100. Leonhardt, F., "Shear in Concrete Structures", CEB Bulletin D'information N. 126, Shear and Torsion, June, 1978, pp 67 - 124.

101. ACI Building Code, "Building Code Requirements for Reinforced Concrete", ACI-318-77, 1977.

102. Discussion on Ref. (31), "Fibre Reinforced Material: Design and Engineering Applications, Inst. of Civil Engrs., London, 1977.

103. Cheung, Y. K. and Yeo, M. F., "A Practical Introduction to Finite Element Analysis", Pitman, 1979.

104. Zienkiewicz, O. C., "The Finite Element Method", 3rd Edition, McGraw-Hill, London, 1977.

105. Desai, C. S. and Abel, J. F., "Introduction to the Finite Element Method", Van Nostrand Reinhold, New York, 1972.

106. Ngo, D. and Scordelis, A. C. "Finite Element Analysis of Reinforced Concrete Beams", ACI Journal, Proceedings, V. 64, No. 3, March, 1967, pp 152 - 163.

107. Scordelis, A. C., "Finite Element Analysis of Reinforced Concrete Structures", Proc. Specialty Conference on the Finite Element Method in Civil Engineering, McGill University, Montreal, Canada, June, 1972, pp 71 - 113.

108. Wegner, R., "Finite Element Models for Reinforced Concrete", Proc. US-German Symposium on Formulation and Computational Alogorithms in Finite Element Analysis, MIT, Boston, 1976, pp 393 - 439.

109. Chen, W. F., "Constitutive Equations for Concrete", Plasticity in Reinforced Concrete, Introductory Report, IABSE Colloquium, Copenhagen, 1979, pp 11 - 34.

110. Nilson, A. H., "Nonlinear Analysis of Reinforced Concrete by the Finite Element Method", ACI Journal, Proceedings, Vol. 65, No. 9, Sept., 1968, pp 757 - 766.

111. Nam, C. H. and Salmon, C. G., "Finite Element Analysis of Concrete Beams", Journal of the Structural Division, ASCE, Vol. 100, No. ST12, Dec., 1974, pp 2419 - 2432.

112. Valliappan, S. and Doolan, T. F., "Nonlinear Stress Analysis of Reinforced Concrete", Journal of the Structural Division, ASCE, Vol. 98, St. ST4, April, 1972, pp 885 - 897.

113. Robins, P. J. and Kong, F. K., "Modified Finite Element Method Applied to RC Deep Beams", Civil Engineering and Public Works Review, Nov, 1973, pp 963 - 966.

114. Cervenka, V., "Inelastic Finite Element Analysis of Reinforced Concrete Panels Under Inplane Loads", Ph.D Thesis, University of Colorado, 1970.

115. Suidan, M and Schnobroch, W. C., "Finite Element Analysis of Reinforced Concrete", Journal of the Structural Division, ASCE, Vol. 99, No. ST10, Oct., 1973, pp 2109 - 2122.

116. Sorensen,S.I., "Endochronic Theory in Nonlinear Finite Element Analysis of Reinforced Concrete", Report No. 78-1, Division of Structural Mechanics, The Norwegian Institute of Technology, The University of Trondheim, 1978.

117. Zienkiewicz, O. C., Owen, D. R. J. Philips, D. V., and Nayak, G. C., "Finite Element Methods in the Analysis of Reactor Vessels", Nuclear Engineering and Design, Vol. 20, No. 2, 1972, pp 507 - 541.

118. Zienkiewicz, O. C., Philips, D. V. and Owen, D. R. J., "Finite Element Analysis of Some Concrete Nonlinearities - Theory and Examples", Seminar on Concrete Structures Subjected to Triaxial Stresses, ISMES - Bergamo, Italy, May, 1974, pp 1 - 21.

119. Isenberg, J. and Adhams, S., "Analysis of Orthotropic Reinforced Concrete Structures", Journal of the Structural Division, ASCE, Vol. 96, ST12, Dec., 1970, pp 2607 - 2624.

120. Adham, S., Bhaumik, A., and Isenberg, J., "Reinforced Concrete Constitutive Relations", AFWL-TR-74-72, Air Force Weapons Laboratory, Feb., 1975.

121. Jofret, J. C. and McNiece, G.M., "Finite Element Analysis of Reinforced Concrete Slabs", Journal of the Structural Division, ASCE, Vol. 97, No. ST3, March, 1971, pp 785 - 806.

122. Argyris, J. H., "Three Dimensional Anisotropic and Inhomogeneous Elastic Media", Matrix Analysis of Small and Large Displacements, Proceedings 11th International Congress Applied Mechanics, Munich, 1964.

123. Argyris, J. H., "Matrix Analysis of 3-Dimensional Media - Small and Large Displacements", AIAA Journal, Vol. 3, No. 1, 1965, pp 45 - 51.

124. Ergatoudis, I., Irons, B. M. and Zienkiewicz, O. C., "Curved Isoparametric, Quadrilateral Elements for Finite Element Analysis", Journal of Solids Structures, Vol. 4, 1968, pp 31 - 42.

125. Clough, R. W., "Comparison of Three-Dimensional Finite Elements", Proceedings Symposium on Applications of Finite Element Methods in Civil Engineering, Vanderbilt University, Tennessee, 1969, pp 1 - 26.

126. Nayak, C. H., "Plasticity and Large Deformation Problems by Finite Element Method", Ph.D Thesis, University of Wales, 1971.

127. Irons, B. M., "Engineering Applications of Numerical Integration in Stiffness Methods", AIAA Journal, Vol. 4, Part 2, Nov., 1966, pp 2053 - 2037.

128. Kopal, Z. "Numerical Analysis", 2nd Editition, Chapman & Hall, London, 1961.

129. Zienkiewicz, O. C., Taylor, R. L. and Too, J. M., "Reduced Integration Technique in General Analysis of Plates and Shells", Int'l Journal Numerical Methods in Engineering,, Vol. 3,1971, pp 275 - 290

130. Doherty, W. P., Wilson, E. L., and Taylor, R. L., "Stress Analysis of Axisymmetric Solids Utilizing Higher Order Quadrilateral Finite Elements", Structural Engineering Laboratory, University of California, Berkeley, California, 1969.

131. Meyer, C., "Solution of Linear Equations - State-of-the-Art", Journal of the Structural Division, ASCE, Vol. 99, No. ST7, July, 1973, pp 1507 - 1526.

132. Meyer, C., "Special Problems Related to Linear Equation Solvers", Journal of the Structural Division, ASCE, Vol. 101, No. ST4, April, 1975, pp 869 - 890.

133. Chen, W. F. and Ting, E. C., "Constitutive Models for Concrete Structures", Journal of the Engineering Mechanics Division, ASCE, Vol. 106, No. EM1, Feb., 1980, pp 1 - 19.

134. Krishnamoorthy, C. S. and Panneerselvam, A., "A Finite Element Model for Non-linear Analysis of Reinforced Concrete Frame Structures", The Structural Engineer, Vol. 55, No. 8, Aug., 1972, pp 331 - 338.

135. Nixon, C. D., Manuel, R. F. and Bowes, W. H., " A Finite Element Analysis of a Diagonal Cracking Behaviour in Reinforced Concrete", The Engineering Journal, Transactions of the Engineering Institute of Canada, Vol. 16, No. A-5, July, 1973, pp I - V.

136. Tasuji, M. E., Slate, F. O. and Nilson, A. H., "Stress -Strain Response and Fracture of Concrete in Biaxial Loading", ACI Journal, Proceedings, V.75, No. 7, July, 1978, pp 306 - 312.

137. Buyukoztürk, O., "Nonlinear Analysis of Reinforced Concrete Structures", Computers and Structures, Vol. 7, 1977, pp 149 - 156.

138. Lin, C. S. and Scordelis, A. C., "Nonlinear Analysis of RC Shells of General Form", Journal of the Structural Division, ASCE, Vol . 101, No. ST3, March, 1975, pp 523 - 438.

139. Chen, A. C. T. and Chen, W. F., "Constitutive Relations for Concrete", Journal of the Engineering Mechanics Division, ASCE, Vol. 101, No. EM4, Aug., 1975, pp 465 - 481.

140. Chen, W. F. and Suzuki, H., "Constitutive Models for Concrete", Computers and Structures, Vol. 12, 1980, pp 23 - 32.

141. Valanis, K. C., "A Theory of Viscoplasticity Without a Yield Surface, Part I, General Theory", Archives of Mechanics, Vol. 23, No. 4, 1971, pp 517 - 534.

142. Valanis, K. C., "A Theory of Viscoplasticity Without a Yield Surface, Part II, Application to Mechanical Behaviour of Metals". Archives of Mechanics, Vol. 23, No. 4, 1971, pp 535 - 551.

143. Bazant, Z. P. and Bhat, P. D., "Endochronic Theory of Inelasticity and Failure of Concrete", Journal of the Engineering Mechanics Division, ASCE, Vol. 102, No. EM4, Aug., 1976, pp 701 - 722.

144. Sandler, I. S., "On the Uniqueness and Stability of Endochronic Theories of Material Behaviour", Journal of Applied Mechanics, Vol. 45, No. 2, June, 1978, pp 263 - 266

145. Lydon, F. D. and Balendran, R. V., "Some Properties of Higher Strength Lightweight Concrete Under Short-Term Tensile Stress", The International Journal of LIghtweight Concrete, Vol. 2, No. 3, Sept., 1980, pp 125 - 139.

146. Hughes, B. P. and Chapman, G. P. , "The Complete Stress-Strain Curve for Concrete in Direct Tension", RILEM Bulletin No. 30, March, 1966, pp 95 - 98.

147. Johnston, C. D. and Coleman, R. A., "Strength and Deformation of Steel Fibre Reinforced Mortar in Uniaxial Tension", Fibre Reinforced Concrete, ACI Publication, SO-44, 1974, pp 177 - 193.

148. Smith, G. N., "An Introduction to Matrix and Finite Element Methods in Civil Engineering", Applied Science, London, 1971.

149. Arnesen, A., Sorensen, S. I. and Bergan, P. G., "Nonlinear Analysis of Reinforced Concrete", Computers and Structures, Vol. 12, 1980, pp 571 - 579.

150. Zienkiewicz, O. C., Valliappan, S. and King, I. P., "Elasto-Plastic Solutions of Engineering Problems - Initial-Stress, Finite Element Approach", Int'l Jl. for Numerical Methods in Engineering, Vol. 1, 1969, pp 75 - 100.

151. Calzona, R., "Behaviour of Dense and Lighweight Concrete Under Multiaxial Stresses", Istituto di Scienza della Construzione Report II - 222. Preeented at the 8th Int'l Congress of the F.I.P., London, April 30 - May 5, 1978, pp 31 - 43.

152. Calzona, R. and Persia, P., "Fracture Criteria in Tension-Compression Domain for Dense and Lightweight Concrete", Instituto di Scienza della Construzioni Report II-24L, 1979.

153. Calzona, R., "Fracture Criteria for Marine Structures - Lightweight versus Dense Concrete". The Int'l Jl. of Lightweight Concrete, Vol. 2, No. 2, June 1980, pp 105 - 113.

154. Mahmood, N. and Hannant, D. J., "The Strength of Concrete Subjected to Compression- Compression-Tension Stress Systems", Jl. of Testing and Evaluation, Vol. 3, No. 2, March, 1975, pp 107 - 112.

155. Cedolin, L., Crutzen, Y. R. J. and Poli, S. D., "Stress-Strain Relationship and Ultimate Strength of Concrete Under Triaxial Loading Conditions", Construzioni in Cemento Armato, Politechnio di Milana, Italiementi, 1976, pp 123 - 137.

156. Loov, R. E., "Finite Element Analysis of Concrete Members Considering the Effect of Cracking and the Inclusion of Reinforcement", Ph.D Thesis, University of Cambridge, 1972.

157. Sled, J. J. "Discussion of "Nonlinear Analysis of Reinforced Concrete by the Finite Element Method" by Nilson, A. H.", ACI Journal, Proceedings, V. 66, No. 3., March, 1969, p 27.

158. Gogate, A. B. and Bishara, A. G., "Finite Element Analysis of Deep Concrete Beams". Indian Concrete Journal, December, 1980, pp 326 - 334.

159. Nayak, G. C. amd Zienkiewicz, O. C., "Elasto-Plastic Stress Analysis - A Generalization for Various Constitutive Relations Including Strain Softening", Int'l Jl. for Numerical Methods in Engineering, Vol. 5, 1972, pp 113 - 135.

160. Timenshenko, S. and Goodier, J., "Theory of Elasticity", McGraw-Hill, London, 1951.

161. Ergatoudis, I., "Isoparametric Elements in Two and Three Dimensional Analysis", Ph.D Thesis, University of Wales, 1968.

APPENDIX A

POST-CRACKING TENSILE STRENGTH OF FIBRE REINFORCED CONCRETE

The post-cracking tensile strength of fibre reinforced concrete has generally been estimated by neglecting the contribution of the matrix. It is based on the argument that after cracking, the quantities which will determine the ultimate tensile strength are the forces in the individual fibres spanning the cracks. The post-cracking tensile strength can be considered as the force per unit area of a section carried by the fibres. It is given by:

$$\sigma_{cu} = \eta_o \eta_L \sigma_{fu} V_f \qquad (A.1)$$

where σ_{cu} - post-cracking tensile strength

η_o - orientation factor

η_L - length efficiency factor

σ_{fu} - fibre fracture stress

and V_f - volume percentage of fibres.

Equation (A.1) is obtained from the composite mixture rule for discontinuous fibre composite (see section 2.2.3) but neglecting the contribution of the matrix.

The orientation factor can be taken as 0.41 (see section 2.2.2.2). In members with thin webs, this factor may be greater than 0.41 but this possible increase was neglected in the present investigation.

Law's expressions for the length efficiency factor (see section 2.2.2.3) can be adopted (64). These are given by:

For $l_f < l_c$

$$\eta_L = \frac{\tau}{\sigma_{fu}} \frac{l_f}{d_f} \qquad (A.2)$$

For $l_f > l_c$

$$\eta_L = 1 - \frac{\sigma_{fu}}{4\tau} \frac{d_f}{l_f} \quad (A.3)$$

Thus the post-cracking tensile strength of fibre concrete is given by:

For $l_f < l_c$

$$\sigma_{cu} = 0.41 \tau \frac{l_f}{d_f} V_f \quad (A.4)$$

For $l_f > l_c$

$$\sigma_{cu} = 0.41 \left(1 - \frac{\sigma_{fu}}{4\tau} \frac{d_f}{l_f} \right) \sigma_{fu} V_f \quad (A.5)$$

The post-cracking tensile strength of the fibre reinforced concretes used in the experimental studies are tabulated in Table A.1. The interfacial bond stresses (τ) used were as determined in section 3.3.5.4.

Table A.1 Post-cracking Tensile Strength of the Fibre Reinforced Concretes Used in the Present Investigation

Concrete	Method of Vibration	% Fibre Volume	l_c mm	Bond Stresses, τ N/mm^2	σ_{cu} N/mm^2
gravel	External	0.4	111	3.55	0.58
gravel	External	0.8	111	3.54	1.16
gravel	External	1.2	131	3.00	1.48
Lytag	External	1.0	100	3.92	1.61
Lytag	Internal	1.0	97	4.04	1.65

NOTE (1) All fibres were 0.5 x 50 crimped steel fibres

(2) σ_{fu} was taken as 1570 N/mm^2 (see section 3.2.6)

APPENDIX B

8-Node Isoparametric lement

B.1 Shape Function N_i

The displacement yield for the element is linear and is given by

$$\begin{Bmatrix} u \\ v \\ w \end{Bmatrix} = \sum_{i=1}^{8} N_i \begin{Bmatrix} u_i \\ v_i \\ w_i \end{Bmatrix} \qquad (B.1)$$

where u_i, v_i and w_i are the nodal displacements and N_i are the interpolation functions or shape functions. N_i are expressed in terms of the local co-ordinates (ξ, η, ζ) as (105):

$$N_i = \tfrac{1}{8}(1 + \xi_o) (1 + \eta_o) (1 + \zeta_o) \qquad (B.2)$$

where $\xi_o = \xi\xi_i$, $\eta_o = \eta\,\eta_i$ and $\zeta_o = \zeta\zeta_i$.

The isoparametric concept makes use of the same shape functions which describe the displacement yield to describe the geometry of the element. This has the form:

$$\begin{Bmatrix} x \\ y \\ z \end{Bmatrix} = \sum_{i=1}^{8} N_i \begin{Bmatrix} x_i \\ y_i \\ z_i \end{Bmatrix} \qquad (B.3)$$

where x_i, y_i and z_i are the nodal co-ordinates in the cartesian system.

B.2 Element Strains and Stresses

The strain displacement relationships can be obtained by differentiating equation (B.3) w.r.t. the (x, y , z) - co-ordinates. It is given by

$$\begin{Bmatrix} \varepsilon_x \\ \varepsilon_y \\ \varepsilon_z \\ \gamma_{xy} \\ \gamma_{yz} \\ \gamma_{zx} \end{Bmatrix} = \begin{Bmatrix} \frac{\partial u}{\partial x} \\ \frac{\partial v}{\partial y} \\ \frac{\partial w}{\partial z} \\ \frac{\partial u}{\partial y} + \frac{\partial v}{\partial x} \\ \frac{\partial v}{\partial z} + \frac{\partial w}{\partial y} \\ \frac{\partial w}{\partial x} + \frac{\partial u}{\partial z} \end{Bmatrix} = \begin{bmatrix} \frac{\partial N_1}{\partial x} & 0 & 0 \cdots & \frac{\partial N_8}{\partial x} & 0 & 0 \\ 0 & \frac{\partial N_1}{\partial y} & 0 \cdots & 0 & \frac{\partial N_8}{\partial y} & 0 \\ 0 & 0 & \frac{\partial N_1}{\partial z} \cdots & 0 & 0 & \frac{\partial N_8}{\partial z} \\ \frac{\partial N_1}{\partial y} & \frac{\partial N_1}{\partial x} & 0 \cdots & \frac{\partial N_8}{\partial y} & \frac{\partial N_8}{\partial x} & 0 \\ 0 & \frac{\partial N_1}{\partial z} & \frac{\partial N_1}{\partial y} \cdots & 0 & \frac{\partial N_8}{\partial z} & \frac{\partial N_8}{\partial y} \\ \frac{\partial N_1}{\partial z} & 0 & \frac{\partial N_1}{\partial x} \cdots & \frac{\partial N_8}{\partial z} & 0 & \frac{\partial N_8}{\partial x} \end{bmatrix} \begin{Bmatrix} u_1 \\ v_1 \\ w_1 \\ \vdots \\ v_8 \\ w_8 \end{Bmatrix} \qquad \text{(B.4)}$$

This can be written in the form

$$\{\varepsilon\} = [B]\{\delta\} \qquad \text{(B.5)}$$

As the shape functions N_i are given in terms of local co-ordinates, it is necessary to express the global cartesian derivatives in terms of local derivatives. This is done through the use of the normal chain rule of partial differentiation. This yields

$$\begin{Bmatrix} \frac{\partial N_i}{\partial x} \\ \frac{\partial N_i}{\partial y} \\ \frac{\partial N_i}{\partial z} \end{Bmatrix} = [J]^{-1} \begin{Bmatrix} \frac{\partial N_i}{\partial \xi} \\ \frac{\partial N_i}{\partial \eta} \\ \frac{\partial N_i}{\partial \zeta} \end{Bmatrix} \qquad \text{(B.6}$$

where [J] is known as the Jacobian matrix. It is defined by

$$[J] = \begin{pmatrix} \frac{\partial N_1}{\partial \xi} & \frac{\partial N_2}{\partial \xi} & \cdots & \frac{\partial N_8}{\partial \xi} \\ \frac{\partial N_1}{\partial \eta} & \frac{\partial N_2}{\partial \eta} & \cdots & \frac{\partial N_8}{\partial \eta} \\ \frac{\partial N_1}{\partial \zeta} & \frac{\partial N_2}{\partial \zeta} & \cdots & \frac{\partial N_8}{\partial \zeta} \end{pmatrix} \begin{pmatrix} x_1 & y_1 & z_1 \\ x_2 & y_2 & z_2 \\ \vdots & \vdots & \vdots \\ x_8 & y_8 & z_8 \end{pmatrix} \qquad \text{(B.7)}$$

For an elastic, isotropic and homogeneous material, the stress-strain relations are given by (160):

$$\begin{Bmatrix} \sigma_x \\ \sigma_y \\ \sigma_z \\ \tau_{xy} \\ \tau_{yz} \\ \tau_{zx} \end{Bmatrix} = \frac{E}{(1+\nu)(1-2\nu)} \begin{bmatrix} 1-\nu & \nu & \nu & 0 & 0 & 0 \\ & 1-\nu & \nu & 0 & 0 & 0 \\ & & 1-\nu & 0 & 0 & 0 \\ & & & \frac{1-2\nu}{2} & 0 & 0 \\ & \text{symmetrical} & & & \frac{1-2\nu}{2} & 0 \\ & & & & & \frac{1-2\nu}{2} \end{bmatrix} \begin{Bmatrix} \varepsilon_x \\ \varepsilon_y \\ \varepsilon_z \\ \gamma_{xy} \\ \gamma_{yx} \\ \gamma_{zx} \end{Bmatrix} \qquad \text{(B.8)}$$

where E is the elastic modulus and ν is the Poisson's ratio.

Equation (B.8) can be written in the form

$$\{\sigma\} = [D_c] \{\varepsilon\} \qquad \text{(B.9)}$$

where $[D_c]$ is the elasticity or material matrix.

APPENDIX C

BAR ELEMENT

C.1 Shape Function

The interpolation formulae for displacements and co-ordinates of a 2-node bar element lying in the ξ direction within a 'parent' hexahedron as shown in Fig. 7.5 are given by equation (C.1) and (C.2) respectively.

$$\begin{Bmatrix} u \\ v \\ w \end{Bmatrix} = \sum_{i=1}^{2} N_i \begin{Bmatrix} u_i \\ v_i \\ x_i \end{Bmatrix} \qquad (C.1)$$

$$\begin{Bmatrix} x \\ y \\ z \end{Bmatrix} = \sum_{i=1}^{2} N_i \begin{Bmatrix} x_i \\ y_i \\ z_i \end{Bmatrix} \qquad (C.2)$$

N_i are the shape functions and are given by (160):

$$N_i = \frac{1 - \xi}{2}$$

$$N_2 = \frac{1 + \xi}{2} \qquad (C.3)$$

This element has linear vaiation of displacement and constant stream along the bar ξ is the local dimensionless variable taking value between +1 and -1.

C.2 Expansion of Bar Element Stiffness Matrix to Equivalent Hexahedron Stiffness Matrix

The general expansion procedure due to Sorensen (116) was adapted to derive the required expansion coefficient matrices for the case shown in Fig. 7.5.

The stiffness relation for the bar is

$$[K^b]\{\delta\}^b = \{R^b\} \tag{C.4}$$

where $[K^b]$ = bar element (6 x 6) stiffness matrix and $\{\delta^b\}$, $\{R^b\}$ = bar nodal displacement and force vectors respectively.

The stiffness relation of equation (C.4) may also be expressed by

$$[K^{bh}]\{\delta^{bh}\} = \{R^{bh}\} \tag{C.5}$$

where $[K^{bh}]$ = equivalent, expanded (24 x 24) stiffness matrix associated with the degrees of freedom of the hexahedron

and $\{\delta^{bh}\}$, $\{R^{bh}\}$ = nodal displacement and equivalent force vectors of the hexahedron.

However equations (C.4) and (C.5) are equivalent if and only if the virtual work done by the equivalent nodal forces at the bar and the hexahedron is equal, i.e.,

$$\Delta\{\delta^b\}^T \{R^b\} = \Delta\{\delta^{bh}\}^T \{R^{bh}\} \tag{C.6}$$

where Δ denotes a virtual quantity.

Equations (C.4) and (C.5) can be split into 3 x 3 submatrices as

$$\left[\begin{array}{c|c} K_{11}^b & K_{12}^b \\ \hline K_{21}^b & K_{22}^b \end{array}\right] \left\{\begin{array}{c} \delta_1^b \\ \\ \delta_2^b \end{array}\right\} = \left\{\begin{array}{c} R_1^b \\ \\ R_2^b \end{array}\right\} \tag{C.7}$$

and

$$\begin{bmatrix} K_{11}^{bh} & K_{12}^{bh} & \cdots & K_{18}^{bh} \\ K_{21}^{bh} & K_{22}^{bh} & \cdots & K_{28}^{bh} \\ \vdots & & & \\ K_{81}^{bh} & K_{82}^{bh} & \cdots & K_{88}^{bh} \end{bmatrix} \begin{Bmatrix} \delta_1^{bh} \\ \delta_2^{bh} \\ \vdots \\ \delta_8^{bh} \end{Bmatrix} = \begin{Bmatrix} R_1^{bh} \\ R_2^{bh} \\ \vdots \\ R_8^{bh} \end{Bmatrix} \tag{C.8}$$

The nodal displacements of the bar element can be obtained by linear interpolation between the nodal displacements of the enclosing concrete element. This approach assumes complete comparability between steel reinforcement and concrete, i.e., without any 'bond slip'. Using this approach and defining the global co-ordinates of the bar element ends by the localization parameters a, b, a_2 and b_2 as shown in Fig. 7.6, the relations between the nodal displacement vectors $\{\delta^b\}$ and $\{\delta^{bh}\}$ can be established as:

$$\begin{aligned}
\delta_1^b &= b_1c_1\delta_1^{bh} + a_1b_1\delta_2^{bh} + c_1d_1\delta_3^{bh} + \\
&\quad a_1d_1\delta_4^{bh} \\
\delta_2^b &= b_2c_2\delta_5^{bh} + a_2b_2\delta_6^{bh} + c_2d_2\delta_7^{bh} + \\
&\quad a_2d_2\delta_8^{bh}
\end{aligned} \tag{C.9}$$

where $c_1 = (1 - a_1),\ d_1 = (1 - b_1)$ (C.10)

$c_2 = (1 - a_2),\ d_2 = (1 - b_2)$

Combining equations (C.6), (C.7) and (C.8) and omitting Δ for convenience to get

$$(\delta_1^b)^T K_{11}^b \delta_1^b + (\delta_1^b)^T K_{12}^b \delta_2^b + (\delta_2^b)^T K_{21}^b \delta_1^b + (\delta_2^b)^T K_{22}^b \delta_2^b$$

$$= (\delta_1^{bh})^T K_{11}^{bh} \delta_1^{bh} + (\delta_1^{bh})^T K_{12}^{bh} \delta_2^{bh} + \ldots + (\delta_1^{bh})^T K_{18}^{bh} \delta_8^{bh}$$

$$+ (\delta_2^{bh})^T K_{21}^{bh} \delta_1^{bh} + (\delta_2^{bh})^T K_{22}^{bh} \delta_2^{bh} + \ldots + (\delta_2^{bh})^T K_{28}^{bh} \delta_8^{bh}$$

$$+ (\delta_8^{bh})^T K_{81}^{bh} \delta_1^{bh} + (\delta_8^{bh})^T K_{82}^{bh} \delta_2^{bh} + \ldots + (\delta_8^{bh})^T K_{88}^{bh} \delta_8^{bh} \tag{C.11}$$

Expanding the L.H.S. of equation (C.11) after substituting

equation (C.9) and then comparing coefficient gives:

$$\begin{pmatrix} K_{11}^{bh} & k_{12}^{bh} & \cdots & K_{18}^{bh} \\ K_{21}^{bh} & K_{22}^{bh} & \cdots & K_{28}^{bh} \\ \vdots & & & \\ K_{81}^{bh} & K_{82}^{bh} & \cdots & K_{88}^{bh} \end{pmatrix} = \left(\begin{array}{c|c} [C11]K_{11}^{b} & [C12]\,K_{12}^{b} \\ \hline [C21]K_{21}^{b} & [C22]\,K_{22}^{b} \end{array}\right)$$

where

$$[Cmn] = \begin{pmatrix} b_m b_n c_m c_n & a_n b_m b_n c_m & b_m c_m c_n d_n & a_n b_m c_m d_n \\ a_m b_m b_n c_n & a_m a_n b_m b_n & a_m b_m c_n d_n & a_m a_n b_m d_n \\ b_n c_m c_n d_m & a_n b_n c_m d_m & c_m c_n d_m d_n & a_n c_m d_m d_n \\ a_m b_n c_n d_m & a_m a_n b_n d_m & a_m c_n d_m d_n & a_m a_n d_m d_n \end{pmatrix}$$

$$m;\ n = 1, 2 \qquad (C.13)$$

APPENDIX D

Determination of Plastic Stress Increments

During transition from elastic to plastic conditions it is necessary to determine the stress vector at which yield begins. This can be done as follows:

Let $\{\sigma_{i-1}\}$ represent the initial elastic conditions and $\{\Delta\varepsilon\}_1$ be the strain increment with corresponding elastic stress change $\{\Delta\sigma^1\}_1$.

If plasticity is encountered in the increment, then the following conditions must be satisfied

$$F\ (\ \{\sigma_{i-1}\}\ )\ =\ F_o < 0$$

$$F\ (\ \{\sigma_{i-1}\} + \{\Delta\sigma^1\}_1\ )\ =\ F_1 > 0$$

The objective is to determine r such that

$$F\ (\ \{\sigma_{i-1}\} + r\{\Delta\sigma^1\ _1\ )\ =\ 0$$

The factor r can be determined by linear interpolation (159) as

$$r\ =\ -\ \frac{F_o}{F_1\ -\ F_o} \qquad D.1$$

The plastic increment is given by

$$\{\Delta\sigma\}_1\ =\ (1\ -\ r)\ [D_c]_{ep}\ \{\Delta\varepsilon\}_1 \qquad D.2$$

The above procedure is applicable for small load increments.